

**Interaction between Biogenic and Anthropogenic VOCs in  
Mixtures Investigated by a Combination of Novel and  
Conventional Analytical Techniques in an Atmospheric  
Simulation Chamber**

A thesis submitted to The University of Manchester for the degree of

**Doctor of Philosophy**

in the Faculty of Science and Engineering.

**Mao Du**

**School of Natural Sciences**

**Department of Earth and Environmental Sciences**

**2022**

[BLANK PAGE]

# Contents

|  |           |
|--|-----------|
| <b>Abstract.....</b>   | <b>6</b>  |
| <b>Declaration.....</b>  | <b>8</b>  |
| <b>Copyright.....</b>  | <b>10</b> |
| <b>Acknowledgements .....</b>  | <b>11</b> |
| <b>Chapter 1. Introduction.....</b>  | <b>15</b> |
| <b>1.1 Introduction .....</b>  | <b>15</b> |
| <b>1.2 Outline of the thesis.....</b>  | <b>17</b> |
| <b>References .....</b>  | <b>19</b> |
| <b>Chapter 2. Review of the current state-of-the-science and motivation.....</b>     | <b>24</b> |
| <b>2.1 Gas-phase chemistry .....</b>   | <b>24</b> |
| 2.1.1 Oxidants.....  | 24        |
| 2.1.2 VOCs degradation .....   | 26        |
| <b>2.2 Gas-particle partitioning .....</b>   | <b>31</b> |
| <b>2.3 Instruments application to measure SOA components.....</b>                    | <b>33</b> |
| <b>2.4 Laboratory studies .....</b>  | <b>37</b> |
| <b>2.5 Mixtures studies.....</b>   | <b>39</b> |
| <b>2.6 Aim and objectives .....</b>  | <b>41</b> |
| <b>References .....</b>  | <b>42</b> |
| <b>Chapter 3. Methodology and Instrumentation .....</b>                              | <b>56</b> |
| <b>3.1 Chamber description and experimental design.....</b>                          | <b>56</b> |
| 3.1.1 Chamber description.....   | 56        |
| 3.1.2 Experimental design .....  | 57        |
| 3.1.3 Experimental procedure.....  | 58        |
| <b>3.2 Instrumentation .....</b>   | <b>60</b> |
| 3.2.1 TOF-CIMS and FIGAERO.....  | 60        |
| 3.2.2 LC-Orbitrap MS.....  | 63        |
| 3.2.3 Other instruments.....   | 65        |
| <b>3.3 Data processing.....</b>  | <b>66</b> |
| <b>References .....</b>  | <b>67</b> |
| <b>Chapter 4. Results.....</b>   | <b>71</b> |
| <b>4.1 Paper 1: Characterisation of the Manchester Aerosol Chamber facility.....</b> | <b>71</b> |

|  |            |
|--|------------|
| 4.1.1 Paper introduction.....  | 71         |
| 4.1.2 Contribution to the joint authorship.....  | 71         |
| 4.1.3 Supplemental information .....   | 71         |
| <b>4.2 Paper 2: Chamber investigation of the formation and transformation of secondary organic aerosol in mixtures of biogenic and anthropogenic volatile organic compounds.....</b> | <b>93</b>  |
| 4.2.1 Paper introduction.....  | 93         |
| 4.2.2 Contribution to the joint authorship.....  | 93         |
| 4.2.3 Supplemental information .....   | 93         |
| <b>4.3 Paper 3: Combined application of Online FIGAERO-CIMS and Offline LC-Orbitrap MS to Characterize the Chemical Composition of SOA in Smog Chamber Studies.....</b>              | <b>151</b> |
| 4.3.1 Paper introduction.....  | 151        |
| 4.3.2 Contribution to the joint authorship.....  | 151        |
| 4.3.3 Supplemental information .....   | 152        |
| <b>4.4 Paper 4: Chemical characterization and clustering behaviour of oxidation products generated from the mixed anthropogenic and biogenic VOCs in chamber studies.....</b>        | <b>196</b> |
| 4.4.1 Paper introduction.....  | 196        |
| 4.4.2 Contribution to the joint authorship.....  | 196        |
| 4.4.3 Supplemental information .....   | 197        |
| <b>4. Discussion .....</b>   | <b>228</b> |
| <b>Chapter 5. Conclusions and Perspectives .....</b>   | <b>246</b> |
| <b>5.1 Conclusions .....</b>   | <b>246</b> |
| <b>5.2 Future work .....</b>   | <b>248</b> |
| <b>Appendices.....</b>   | <b>252</b> |
| <b>Supplementary Information for Paper 1.....</b>  | <b>252</b> |
| <b>Supplementary Information for Paper 2.....</b>  | <b>254</b> |
| <b>Supplementary Information for paper 3.....</b>  | <b>259</b> |
| <b>Supplementary Information for paper 4.....</b>  | <b>276</b> |

Total number of words: 89,589



[BLANK PAGE]

## Abstract

Secondary organic aerosol (SOA) contributes significantly to the total organic aerosol mass in the atmosphere. Understanding the SOA formation is crucial in order to estimate its impact on the air quality, climate and human health. SOA is typically produced from the oxidation of anthropogenic volatile organic compounds (AVOCs) or biogenic volatile organic compounds (BVOCs) by the oxidants such as OH radical, O<sub>3</sub>, or NO<sub>3</sub> radical. SOA formation from single BVOCs or AVOCs has been widely investigated, while there are limited studies of the SOA formation from VOCs mixtures. There are many uncertainties in the physicochemical properties of SOA formed in the mixed VOC precursors.

This work designed a series of experiments to explore SOA formation from the mixed AVOC (*o*-cresol) and BVOCs ( $\alpha$ -pinene and isoprene) under the presence of NO<sub>x</sub> in the Manchester Aerosol Chamber. The online and offline analytical techniques were applied to investigate the chemical and physical properties of SOA. The gas- and particle-phase oxidation products were monitored by the near real-time online iodide chemical ionization mass spectrometry (CIMS) coupled with Filter Inlet for Gases and AEROsols (FIGAERO). The collected filter at the end of each experiment was characterised by the offline liquid chromatography orbitrap mass spectrometry (LC-Orbitrap MS) to investigate particle-phase chemical components. This study found that the chemical components of SOA formed from various VOCs systems showed big differences. In the  $\alpha$ -pinene and  $\alpha$ -pinene/isoprene mixture, the products with carbon, hydrogen and oxygen (CHO group) dominated the signals in the particle phase, broadly consistent with the LC-Orbitrap MS negative mode analysis which was able to better identify the sulphur-containing fraction. By contrast, *o*-cresol containing systems were dominated by the CHON signal fraction (>60%) from offline negative mode analysis. More compounds with high carbon numbers ( $nC \geq 16$ ) were detected by the LC-Orbitrap MS positive ionisation mode, which indicated a fraction missed by the negative mode and CIMS measurements. Additionally, unique-to-the-mixture products were observed in the mixture, suggesting molecular interactions in the mixture systems. This work brought an insight into the SOA chemical composition from the mixed volatile precursors by the combination of online FIGAERO-CIMS and offline LC-Orbitrap MS analytical techniques and highlighted the importance of SOA studies in the mixed volatile precursors.

[BLANK PAGE]

## **Declaration**

I declare that part of the work referred to in the thesis (Papers 1 and 2) has joint authorship, which might be included in a thesis submitted by other students to this university or any other university or other institutes of learning.

[BLANK PAGE]

## Copyright

The author of this thesis (including any appendices and/or schedules to this thesis) owns certain copyright or related rights in it (the “Copyright”) and he has given The University of Manchester certain rights to use such Copyright, including for administrative purposes.

Copies of this thesis, either in full or in extracts and whether in hard or electronic copy, may be made only in accordance with the Copyright, Designs and Patents Act 1988 (as amended) and regulations issued under it or, where appropriate, in accordance with licensing agreements which the University has from time to time. This page must form part of any such copies made.

The ownership of certain Copyright, patents, designs, trademarks and other intellectual property (the “Intellectual Property”) and any reproductions of copyright works in the thesis, for example, graphs and tables (“Reproductions”), which may be described in this thesis, may not be owned by the author and may be owned by third parties. Such Intellectual Property and Reproductions cannot and must not be made available for use without the prior written permission of the owner(s) of the relevant Intellectual Property and/or Reproductions.

Further information on the conditions under which disclosure, publication and commercialization of this thesis, the Copyright and any Intellectual Property and/or Reproductions described in it may take place is available in the University IP Policy (see <http://documents.manchester.ac.uk/DocuInfo.aspx?DocID=2442>), in any relevant Thesis restriction declarations deposited in the University Library, The University Library’s regulations and in The University’s policy on Presentation of Theses (see <http://documents.manchester.ac.uk/display.aspx?DocID=7420>).

[BLANK PAGE]

## Acknowledgements

This project is funded by the President's Doctoral Scholar Award from the University of Manchester. I sincerely appreciate the University of Manchester for providing financial support throughout my PhD study.

I would like to express my deepest gratitude to my supervisors, Prof Gordon McFiggans and Dr M. Rami. Alfarra. Both of them are knowledgeable and passionate about research, giving me very professional academic guidance and inspiration during my PhD. Rami, I much appreciate your attention to details that make our chamber goes a lot smoother. Gordon, I much appreciate you providing me with the opportunities to build a network in the atmospheric science community with the Manchester aerosol group, the Jülich and the Gothenburg groups. I much appreciate your encouragement for stepping outside my comfort zone, supporting me to join the mass spectrometry training in Germany and summer school in Brazil. I much appreciate your always help, support and understanding whenever I need it during my PhD.

I would like to express my special thanks to the chamber group members Dr Yu Wang, Dr Yunqi Shao and Dr Aristeidis Voliotis for our pleasant cooperation in the experimental campaigns and discussions on all things. Many thanks to Thomas J. Bannan, Kelly Louise Pereira, Michael. Flynn, Simon.O. Meara, Dr Zainab Bibi, Dr Dawei Hu, Dr Rongrong Wu, Dr Huihui Wu, Dr Kaiyue Xing, Dr Xing Li, Dr Jiaming Wang, Dr Huaxiang Yan, Dr Linhua He, Dr Cong Yao, Dr Kangpei Meng, Dr Janis Castins, Dr Fatemeh Shahbazi, Dr Muhammad Omer, Dr Mojgan Hadi Mosleh, and Dr Majid Sedighi. Their help, support and friendship make me enjoy this fruitful PhD journey. Many thanks to Bruno Bakes Meller, Hemraj Bhattarai, Sishir Dahal, Jie Gao, Shuting Zhai, Yuying Wang, Liang Mian, who gave me many great memories of my time in Brazil. Many thanks to all my friends now scattered among countries and continents - without all of you this journey would have been much harder.

Finally, I must express my massive thanks to my beloved parents and husband Tian Chen for their always selfless love, understanding, support and motivation. I love you so much. Especially thanks to my husband Tian Chen for his always unconditional support and massive care over the hundred miles PhD journey. I even can't get through this entire journey without his support, love and thoughtfulness.

I would say no regrets when looking backwards. Everyone I met, everything I experienced no matter happiness or pain in the past 3.5 years would be the most precious



memories. All those are worth being cherished. Time flies. I would optimistically believe the future will be much expected.

[BLANK PAGE]

# Chapter 1. Introduction

## 1.1 Introduction

Atmospheric aerosol is a suspension of liquid or solid particles in the air, which is known to play an important role in many environmental processes (Poschl, 2005; Hallquist et al., 2009). Their presence in the atmosphere has a significant effect on air quality, global climate (Ipcc, 2013), and human health (Who, 2016). First, aerosols directly or indirectly affect the earth's radiation budget and light absorption by scattering and absorbing solar and terrestrial radiation (Haywood and Boucher, 2000). Second, aerosols can alter the formation and properties of clouds and participation via impacting the abundance and distribution of atmospheric gases and chemistry (Haywood and Boucher, 2000; Hallquist et al., 2009). Their presence can reduce the horizontal visibility of a region (An et al., 2019). Furthermore, aerosols can involve in the spread of biological organisms and pathogens (e.g., pollen, bacteria and viruses) and have the possibility to be inhaled by human beings when these aerosols disperse in the atmosphere, resulting in severe health problems, such as respiratory, pneumonia, allergic diseases and cardiovascular (Pope and Dockery, 2006; Nel, 2005; Bernstein et al., 2004).

Atmospheric aerosols are strikingly and spatially variable in concentration, size, structure and chemical composition. In the lower atmosphere, the mass concentration ranges from 1 to 100  $\mu\text{g m}^{-3}$  or even greater in polluted areas (Yang et al., 2011; Monkkonen, 2004). The total particle number concentration varies from  $10^2$  and  $10^5 \text{ cm}^{-3}$  (Poschl, 2005). The diameter of particles varies and the particles can be divided into four modes based on their distribution of diameter: nucleation mode (with diameter less than 10nm), Aitken mode (diameter between 10 nm and 0.1 $\mu\text{m}$ ), accumulation mode (diameter with the range of 0.1  $\mu\text{m}$  and 1  $\mu\text{m}$ ) and coarse mode (diameter more than 1  $\mu\text{m}$ ) (Willeke and Whitby, 1975; Spurny, 1998). Aerosols from the accumulation mode and coarse mode are the main contributors to the atmosphere (Kim et al., 2001). Aerosols with diameters of 2.5  $\mu\text{m}$  or less than 2.5  $\mu\text{m}$  are called fine particles (defined as Particulate Matter, 2.5  $\mu\text{m}$ , PM 2.5).

Atmospheric aerosols can be produced from various sources. Primary aerosols are directly emitted from natural sources, such as marine layers (Fitzgerald, 1991), biogenic sources, and biomass burning (Guo et al., 2012; Fine et al., 2004). In contrast, secondary

aerosols are generated from the oxidation of organic or inorganic precursors via a series of physical and chemical processes in the atmosphere. Further, based on their constituents, aerosols can be split into inorganic aerosols (e.g.,  $\text{NO}_3^-$ ,  $\text{NH}_4^+$ ,  $\text{SO}_4^{2-}$  etc) and organic aerosols (Kang et al., 2010; Li et al., 2013; Jimenez et al., 2009). Studies show that a large fraction (20%-50%, up to 90% in tropical forested areas) of atmospheric aerosols is made up of organic compounds (Kroll and Seinfeld, 2008; M. Kanakidou et al., 2005). Based on the source of organic aerosols, it can be divided into a primary organic aerosol (POA) which emits primarily from both natural (vegetation and micro-organisms) and anthropogenic sources such as combustion of fossil fuels and biofuels, and biomass burning (forest fire) (Hodzic et al., 2010; Turpin and Huntzicker, 1995) and secondary organic aerosol (SOA). SOA is formed from a variety of organic compounds over a series of oxidation processes. It makes a greater contribution to the total organic aerosol burden (Kroll and Seinfeld, 2008).

The global SOA budget has been estimated through two distinct approaches using global models: bottom-up estimation and top-down estimation. The bottom-up estimation method combined global models with SOA formation data from laboratory studies, giving a conservative global SOA formation of 12–70 Tg/yr (Henze and Seinfeld, 2006; M. Kanakidou et al., 2005). A relatively smaller contribution of anthropogenic SOA is estimated in the range of 2-12 Tg/yr (D.K.Henze, 2008). In contrast, the top-down estimation leads to a higher SOA budget estimation, with a broad range of 120 –1820 Tg /yr SOA formation (Spracklen et al., 2011). Although there are still many uncertainties between bottom-up models and top-down approaches, the large difference lies in the two methods which illustrate that there are many uncertainties in the SOA precursor sources such as intermediate volatile organic compounds (IVOCs) (Hallquist et al., 2009; Robinson et al., 2007; Goldstein and Galbally, 2007; Spracklen et al., 2011; Ehn et al., 2014). The estimated global SOA contributes around 71% - 85% to the total OA from the Global Model of Aerosol Processes (GLOMAP) global aerosol model (Spracklen et al., 2011).

Generally, SOA is considered to be produced from the oxidation of a series of volatile organic compounds (VOCs) in the atmosphere. There are 10 000 to 100 000 different organic compounds measured in the atmosphere (Goldstein and Galbally, 2007). Certain classes of VOCs have a high possibility to form SOA by virtue of their high reactivity with oxidants. According to different locations, times and specific source regions, two main types of VOCs

are involved in SOA formation: anthropogenic VOCs (AVOCs) and biogenic VOCs (BVOCs) (M. Hallquist et al., 2009). The previous study shows that BVOCs have an estimated flux of around 1150 Tg C/ yr, while the flux of AVOCs accounts for about 140 Tg C/yr (Eddingsaas et al., 2012). BVOCs are mainly generated from vegetation. The BVOC emissions from the vegetation are related to the plant species (Vivaldo et al., 2017), its surrounding ecosystem (Abis et al., 2020) and environmental conditions (Zhao et al., 2017). Generally, the terpenoids are considered as the most abundant class of BVOCs, which consist of typically C<sub>5</sub> units including hemiterpenes (C<sub>5</sub>, such as isoprene), monoterpenes (C<sub>10</sub>, e.g., pinenes, limonene) and sesquiterpenes (C<sub>15</sub>, e.g., caryophyllene). Isoprene (C<sub>5</sub>H<sub>8</sub>) produced from deciduous plants is one of the most abundant BVOCs, accounting for 70% of the total mass of VOCs. Monoterpenes are the second abundant species, around 11%, which are a class of terpenes, consisting of two isoprene units with the molecular formula C<sub>10</sub>H<sub>16</sub> (S. Kim, 2010; J. D. Fuentes, 2000). BVOCs are considered the most abundant precursors to the production of SOA.

SOA formation from AVOCs has also been attracting considerable interest since industrial revolution times. AVOCs (e.g, alkanes, alkenes and aromatics compounds) originate from human activities, such as vehicle exhaust, solvent uses, cooking, etc. On regional scales, AVOCs emissions can exceed BVOCs, especially in urban areas. Locally and regionally anthropogenic emissions vary significantly. Among all VOCs in the urban atmosphere, aromatic hydrocarbons which contain one or more benzene rings make up an important fraction, accounting for 20%-30% (Tu et al., 2016) and have been proved to contribute to SOA formation by a series of oxidation processes. Benzene (C<sub>6</sub>H<sub>6</sub>), Toluene (C<sub>7</sub>H<sub>8</sub>), C<sub>8</sub> (ethylbenzene and xylenes) and C<sub>9</sub> (ethyltoluenes and trimethylbenzenes) are the most important aromatic hydrocarbons in the atmosphere (Lu Hu et al., 2014; C. L. Heald et al., 2008; Ng et al., 2007).

## **1.2 Outline of the thesis**

This thesis delivers the results about the SOA formation from the mixed anthropogenic and biogenic VOCs experiments in the Manchester Aerosol Chamber. This work focuses on the exploration of chemical composition in the gas and particle-phase oxidation products formed from the mixture and individual systems. Chapter 2 gives a detailed literature review on the progress of the SOA formation mechanisms (including the gas-phase chemistry and gas-to-particle partitioning), the development of analytical techniques in the observation of SOA

chemical composition, laboratory studies in the SOA formation and mixture studies. Finally, the aim and objectives of this work are proposed.

Chapter 3 presents the detailed methodology to guide this work and provides the core instruments utilized in this work. The contents in this chapter include the chamber facilities description, the theory behind the experimental design, description of analytical techniques and data analysis processing.

Chapter 4 presents the results of the work, including two co-first author papers and two individual papers. Paper 1 focuses on the systematic chamber characterization in order to ensure the reliable and reproducible results conducted in this chamber. This paper is to solve the first objective of the project. Paper 2 provides an overview of the experimental design for mixture studies and the overview of SOA yields in the mixed systems and refers to the chemical composition, volatility and other physical properties. This paper aims to address the second objective of the project. Paper 3 assesses the advantages of the combination of online FIGAERO-CIMS and offline LC-Orbitrap MS in chamber studies, which is to answer the third objective of the project. Paper 4 explores the chemical composition of SOA from the photooxidation of anthropogenic and biogenic VOCs mixtures. This paper aims to address the fourth objective of the project.

Chapter 5 is the conclusions and perspectives of this thesis.

## References

- Abis, L., Loubet, B., Ciuraru, R., Lafouge, F., Houot, S., Nowak, V., Tripied, J., Dequiedt, S., Maron, P. A., and Sadet-Bourgeteau, S.: Reduced microbial diversity induces larger volatile organic compound emissions from soils, *Sci Rep*, 10, 6104, 10.1038/s41598-020-63091-8, 2020.
- An, Z., Huang, R. J., Zhang, R., Tie, X., Li, G., Cao, J., Zhou, W., Shi, Z., Han, Y., Gu, Z., and Ji, Y.: Severe haze in northern China: A synergy of anthropogenic emissions and atmospheric processes, *Proc Natl Acad Sci U S A*, 116, 8657-8666, 10.1073/pnas.1900125116, 2019.
- Bernstein, J. A., Alexis, N., Barnes, C., Bernstein, I. L., Bernstein, J. A., Nel, A., Peden, D., Diaz-Sanchez, D., Tarlo, S. M., and Williams, P. B.: Health effects of air pollution, *J Allergy Clin Immunol*, 114, 1116-1123, 10.1016/j.jaci.2004.08.030, 2004.
- C. L. Heald, A. H. G., J. D. Allan, A. C. Aiken, E. Apel, E. L. Atlas, A. K. Baker, T. S. Bates, A. J. Beyersdorf, D. R. B. T. Campos, H. Coe, J. D. Crouse, P. F. DeCarlo, J. A. de Gouw, E. J. Dunlea, F. M. Flocke, A. F. P. G., R. J. Griffin, S. C. Herndon, J. S. Holloway, R. Holzinger, J. L. Jimenez, W. J. W. C. Kuster, A. C. Lewis, S. Meinardi, D. B. Millet, T. Onasch, A. Polidori, P. K. Q., D. D. Riemer, J. M. Roberts, D. Salcedo, B. Sive, A. L. Swanson, R. Talbot, C. Warneke, R. J. W., P. Weibring, P. O. Wennberg, D. R. Worsnop, A. E. Wittig, R. Zhang, and J. Zheng, W. Z.: Total observed organic carbon (TOOC) in the atmosphere: a synthesis of North American observations, *Atmos. Chem. Phys*, 8, 2007–2025, 2008.
- D.K.Henze, J. H. S., N. L. Ng, J. H. Kroll, T.-M. Fu, D. J. Jacob, C. L. Heald: Global modeling of secondary organic aerosol formation from aromatic hydrocarbons: high- vs. low-yield pathways, *Atmos. Chem. Phys*, 8, 2405-2421, 2008.
- Eddingsaas, N. C., Loza, C. L., Yee, L. D., Seinfeld, J. H., and Wennberg, P. O.: alpha;-pinene photooxidation under controlled chemical conditions – Part 1: Gas-phase composition in low- and high-NO<sub>x</sub> environments, *Atmospheric Chemistry and Physics Discussions*, 12, 6447-6483, 10.5194/acpd-12-6447-2012, 2012.
- Ehn, M., Thornton, J. A., Kleist, E., Sipila, M., Junninen, H., Pullinen, I., Springer, M., Rubach, F., Tillmann, R., Lee, B., Lopez-Hilfiker, F., Andres, S., Acir, I. H., Rissanen, M., Jokinen, T., Schobesberger, S., Kangasluoma, J., Kontkanen, J., Nieminen, T., Kurten, T., Nielsen, L. B., Jorgensen, S., Kjaergaard, H. G., Canagaratna, M., Maso, M. D., Berndt, T., Petaja, T., Wahner, A., Kerminen, V. M., Kulmala, M., Worsnop, D. R., Wildt, J., and Mentel, T. F.: A large source of low-volatility secondary organic aerosol, *Nature*, 506, 476-479, 10.1038/nature13032, 2014.
- Fine, P. M., Cass, G. R., and Simoneit, B. R. T.: Chemical Characterization of Fine Particle Emissions from the Fireplace Combustion of Wood Types Grown in the Midwestern and Western United States, *Environmental Engineering Science*, 21, 387-409, 10.1089/109287504323067021, 2004.
- Fitzgerald, J. W.: Marine aerosols: A review, *Atmospheric Environment. Part A. General Topics*, 25, 533-545, 10.1016/0960-1686(91)90050-h, 1991.
- Goldstein, A. H. and Galbally, I. E.: Known and unknown organic constituents in the Earth's

atmosphere, *Environ Sci Technol*, 41, 1514-1521, 10.1021/es072476p, 2007.

Guo, S., Hu, M., Guo, Q., Zhang, X., Zheng, M., Zheng, J., Chang, C. C., Schauer, J. J., and Zhang, R.: Primary sources and secondary formation of organic aerosols in Beijing, China, *Environ Sci Technol*, 46, 9846-9853, 10.1021/es2042564, 2012.

Hallquist, M., Wenger, J. C., Baltensperger, U., Rudich, Y., Simpson, D., Claeys, M., Dommen, J., Donahue, N. M., George, C., Goldstein, A. H., Hamilton, J. F., Herrmann, H., Hoffmann, T., Iinuma, Y., Jang, M., Jenkin, M. E., Jimenez, J. L., Kiendler-Scharr, A., Maenhaut, W., McFiggans, G., Mentel, T. F., Monod, A., Prévôt, A. S. H., Seinfeld, J. H., Surratt, J. D., Szmigielski, R., and Wildt, J.: The formation, properties and impact of secondary organic aerosol: current and emerging issues, *Atmospheric Chemistry and Physics*, 9, 5155-5236, 10.5194/acp-9-5155-2009, 2009.

Haywood, J. and Boucher, O.: Estimates of the direct and indirect radiative forcing due to tropospheric aerosols: A review, *Reviews of Geophysics*, 38, 513-543, 10.1029/1999rg000078, 2000.

Henze, D. K. and Seinfeld, J. H.: Global secondary organic aerosol from isoprene oxidation, *Geophysical Research Letters*, 33, 10.1029/2006gl025976, 2006.

Hodzic, A., Jimenez, J. L., Madronich, S., Canagaratna, M. R., DeCarlo, P. F., Kleinman, L., and Fast, J.: Modeling organic aerosols in a megacity: potential contribution of semi-volatile and intermediate volatility primary organic compounds to secondary organic aerosol formation, *Atmospheric Chemistry and Physics*, 10, 5491-5514, 10.5194/acp-10-5491-2010, 2010.

IPCC: Climate Change 2013: The Physical Science Basis. Contribution of Working Group I to the Fifth Assessment Report of the Intergovernmental Panel on Climate Change, Cambridge University Press, Cambridge, United Kingdom and New York, NY, USA, 2013.

J. D. Fuentes, M. L., B. Lamb, C. Geron, R. Atkinson, D. Balducchi, J. W. Bottenheim, P. Ciccioli, L. Gu, A. Guenther, T. D. Sharkey, and W. Stockwell: Biogenic Hydrocarbons in the atmospheric boundary layer: a review.pdf, *Bulletin of the American Meteorological Society*, 81, 1537-1576, 2000.

Jimenez, J. L., Canagaratna, M. R., Donahue, N. M., Prevot, A. S., Zhang, Q., Kroll, J. H., DeCarlo, P. F., Allan, J. D., Coe, H., Ng, N. L., Aiken, A. C., Docherty, K. S., Ulbrich, I. M., Grieshop, A. P., Robinson, A. L., Duplissy, J., Smith, J. D., Wilson, K. R., Lanz, V. A., Hueglin, C., Sun, Y. L., Tian, J., Laaksonen, A., Raatikainen, T., Rautiainen, J., Vaattovaara, P., Ehn, M., Kulmala, M., Tomlinson, J. M., Collins, D. R., Cubison, M. J., Dunlea, E. J., Huffman, J. A., Onasch, T. B., Alfarra, M. R., Williams, P. I., Bower, K., Kondo, Y., Schneider, J., Drewnick, F., Borrmann, S., Weimer, S., Demerjian, K., Salcedo, D., Cottrell, L., Griffin, R., Takami, A., Miyoshi, T., Hatakeyama, S., Shimono, A., Sun, J. Y., Zhang, Y. M., Dzepina, K., Kimmel, J. R., Sueper, D., Jayne, J. T., Herndon, S. C., Trimborn, A. M., Williams, L. R., Wood, E. C., Middlebrook, A. M., Kolb, C. E., Baltensperger, U., and Worsnop, D. R.: Evolution of organic aerosols in the atmosphere, *Science*, 326, 1525-1529, 10.1126/science.1180353, 2009.

Kang, J., Cho, B. C., and Lee, C. B.: Atmospheric transport of water-soluble ions (NO<sub>3</sub><sup>-</sup>, NH<sub>4</sub><sup>+</sup> and nss-SO<sub>4</sub><sup>2-</sup>) to the southern East Sea (Sea of Japan), *Sci Total Environ*, 408,



2369-2377, 10.1016/j.scitotenv.2010.02.022, 2010.

Kim, S., Jaques, P. A., Chang, M., Froines, J. R., and Sioutas, C.: Versatile aerosol concentration enrichment system (VACES) for simultaneous in vivo and in vitro evaluation of toxic effects of ultrafine, fine and coarse ambient particles Part I: Development and laboratory characterization, *Journal of Aerosol Science*, 32, 1281-1297, 10.1016/s0021-8502(01)00057-x, 2001.

Kroll, J. H. and Seinfeld, J. H.: Chemistry of secondary organic aerosol: Formation and evolution of low-volatility organics in the atmosphere, *Atmospheric Environment*, 42, 3593-3624, 10.1016/j.atmosenv.2008.01.003, 2008.

Li, Y. J., Lee, B. Y. L., Yu, J. Z., Ng, N. L., and Chan, C. K.: Evaluating the degree of oxygenation of organic aerosol during foggy and hazy days in Hong Kong using high-resolution time-of-flight aerosol mass spectrometry (HR-ToF-AMS), *Atmospheric Chemistry and Physics*, 13, 8739-8753, 10.5194/acp-13-8739-2013, 2013.

Lu Hu, D. B. M., Munkhbayar Baasandorj, Timothy J. Griffis, Katherine R. Travis,, Christopher W. Tessum, J. D. M., Wesley F. Reinhart, Tomas Mikoviny, Markus Müller,, and Armin Wisthaler, M. G., Carsten Warneke, Joost de Gouw: Emissions of C6–C8 aromatic compounds in the United States: Constraints from tall tower and aircraft measurements, *Journal of Geophysical Research: Atmospheres*, 120, 826-842, 10.1002/2014JD022627, 2014.

M. Hallquist, J. C. W., U. Baltensperger, Y. Rudich, D. Simpson, M. Claeys, J. Dommen,, N. M. Donahue, C. G., A. H. Goldstein, J. F. Hamilton, H. Herrmann, T. Hoffmann, Y. Iinuma,, M. Jang, M. E. J., J. L. Jimenez, A. Kiendler-Scharr, W. Maenhaut, G. McFiggans, Th. F. Mentel,, and A. Monod, A. S. H. P. e. o., J. H. Seinfeld, J. D. Surratt, R. Szmigielski, J. Wildt: The formation, properties and impact of secondary organic aerosol: current and emerging issues, *Atmos. Chem. Phys*, 9, 5155-5236, 2009.

M. Kanakidou, J. H. S., S. N. Pandis, I. Barnes, F. J. Dentener, M. C. Facchini, R. Van Dingenen,, B. Ervens, A. N., C. J. Nielsen, E. Swietlicki, J. P. Putaud, Y. Balkanski, S. Fuzzi, J. Horth,, and G. K. Moortgat, R. W., C. E. L. Myhre, K. Tsigaridis, E. Vignati, E. G. Stephanou, J. Wilson: Organic aerosol and global climate modelling: a review *Atmos. Chem. Phys*, 5, 1053–1123, 2005.

Monkkonen, P.: Relationship and variations of aerosol number and PM10 mass concentrations in a highly polluted urban environment? New Delhi, India, *Atmospheric Environment*, 38, 425-433, 10.1016/j.atmosenv.2003.09.071, 2004.

Nel, A.: Atmosphere. Air pollution-related illness: effects of particles, *Science*, 308, 804-806, 10.1126/science.1108752, 2005.

Ng, N. L., Kroll, J. H., Chan, A. W. H., Chhabra, P. S., Flagan, R. C., and Seinfeld, J. H.: Secondary organic aerosol formation from <i>m</i>-xylene, toluene, and benzene, *Atmospheric Chemistry and Physics*, 7, 3909-3922, 10.5194/acp-7-3909-2007, 2007.

Pope, C. A., 3rd and Dockery, D. W.: Health effects of fine particulate air pollution: lines that connect, *J Air Waste Manag Assoc*, 56, 709-742, 10.1080/10473289.2006.10464485, 2006.

- Poschl, U.: Atmospheric aerosols: composition, transformation, climate and health effects, *Angew Chem Int Ed Engl*, 44, 7520-7540, 10.1002/anie.200501122, 2005.
- Robinson, A. L., Donahue, N. M., Shrivastava, M. K., Weitkamp, E. A., Sage, A. M., Grieshop, A. P., Lane, T. E., Pierce, J. R., and Pandis, S. N.: Rethinking organic aerosols: semivolatile emissions and photochemical aging, *Science*, 315, 1259-1262, 10.1126/science.1133061, 2007.
- S. Kim, T. K., A. Guenther, G. Tyndall, J. Orlando, P. Harley, R. Rasmussen, and E. Apel: Emissions and ambient distributions of biogenic volatile organic compounds in a ponderosa pine ecosystem interpretation of PTR-MS mass spectra *Atmospheric Chemistry and Physics*, 10, 1759–1771, 2010.
- Spracklen, D. V., Jimenez, J. L., Carslaw, K. S., Worsnop, D. R., Evans, M. J., Mann, G. W., Zhang, Q., Canagaratna, M. R., Allan, J., Coe, H., McFiggans, G., Rap, A., and Forster, P.: Aerosol mass spectrometer constraint on the global secondary organic aerosol budget, *Atmospheric Chemistry and Physics*, 11, 12109-12136, 10.5194/acp-11-12109-2011, 2011.
- Spurny, K.: On the physics, chemistry and toxicology of ultrafine anthropogenic, atmospheric aerosols (UAAA): new advances, *Toxicology Letters*, 96-97, 253-261, 10.1016/s0378-4274(98)00080-0, 1998.
- Tu, P., Hall, W. A. t., and Johnston, M. V.: Characterization of Highly Oxidized Molecules in Fresh and Aged Biogenic Secondary Organic Aerosol, *Anal Chem*, 88, 4495-4501, 10.1021/acs.analchem.6b00378, 2016.
- Turpin, B. J. and Huntzicker, J. J.: Identification of secondary organic aerosol episodes and quantitation of primary and secondary organic aerosol concentrations during SCAQS, *Atmospheric Environment*, 29, 3527-3544, 10.1016/1352-2310(94)00276-q, 1995.
- Vivaldo, G., Masi, E., Taiti, C., Caldarelli, G., and Mancuso, S.: The network of plants volatile organic compounds, *Sci Rep*, 7, 11050, 10.1038/s41598-017-10975-x, 2017.
- WHO, W. H. O.: *Ambient air pollution: A global assessment of exposure and burden of disease*, 2016.
- Willeke, K. and Whitby, K. T.: Atmospheric Aerosols: Size Distribution Interpretation, *Journal of the Air Pollution Control Association*, 25, 529-534, 10.1080/00022470.1975.10470110, 1975.
- Yang, F., Tan, J., Zhao, Q., Du, Z., He, K., Ma, Y., Duan, F., Chen, G., and Zhao, Q.: Characteristics of PM<sub>2.5</sub> speciation in representative megacities and across China, *Atmospheric Chemistry and Physics*, 11, 5207-5219, 10.5194/acp-11-5207-2011, 2011.
- Zhao, D. F., Buchholz, A., Tillmann, R., Kleist, E., Wu, C., Rubach, F., Kiendler-Scharr, A., Rudich, Y., Wildt, J., and Mentel, T. F.: Environmental conditions regulate the impact of plants on cloud formation, *Nat Commun*, 8, 14067, 10.1038/ncomms14067, 2017.

[BLANK PAGE]

## Chapter 2. Review of the current state-of-the-science and motivation

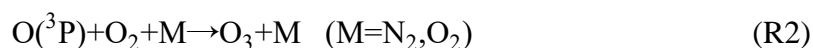
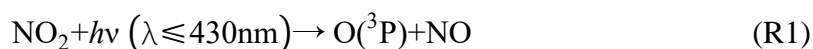
This section aims to review recent advances in our understanding of SOA studies. It includes mechanisms of SOA formation (Sections 2.1 and 2.2), developments of analytical techniques in SOA chemical composition measurements (Section 2.3), advances in laboratory studies (Section 2.4) and the advances of mixture studies (Section 2.5). Subsequently, the research aim and objectives are proposed in Section 2.6.

### 2.1 Gas-phase chemistry

#### 2.1.1 Oxidants

VOCs undergo numerous physical and chemical processes, resulting in their transformation in the atmosphere or removal from the atmosphere. Some VOCs can deposit on the surfaces of existing objects, which will be removed by dry deposition or wet deposition with the rain. It is estimated that around 23% of the gas-phase VOCs are likely removed by wet deposition, while insufficient information can be provided for the estimated fraction of dry deposition of gas-phase VOCs (Goldstein and Galbally, 2007). In contrast, the majority of VOCs can be removed by the chemical processes which are initiated by  $O_3$ , OH and  $NO_3$  radicals (Atkinson and Carter, 2002; Atkinson and Arey, 2003) or chlorine atoms (Cl) under certain conditions, e.g., marine environments (Young et al., 2014; Cai and Griffin, 2006). Those chemical processes will lead to the formation of ozone and SOA.

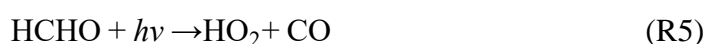
In the troposphere,  $O_3$  is considered a primary atmospheric oxidant during nighttime and greenhouse gas (Jacob, 2000). Generally, two crucial means can produce ozone in the troposphere. One is transported from the ozone layer of the stratosphere, reaching the atmosphere directly. Another is from photochemical reactions in atmospheric conditions. In the atmosphere,  $O_3$  can be produced by photolysis of  $NO_2$  at wavelengths below 430nm. It can be seen in polluted areas, the  $O_3$  concentration will be higher as a result of the high concentration of  $NO_x$  ( $NO_x = NO + NO_2$ ) which is emitted from combustion processes such as vehicle exhaust and fossil fuel power plants (Alex Guenther, 2000).



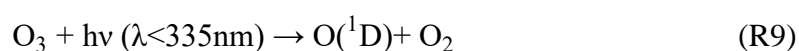
The NO can be quickly oxidized back to NO<sub>2</sub> via O<sub>3</sub>,



Ideally, R1, R2 and R3 can achieve a balance among O<sub>3</sub>, NO<sub>2</sub> and NO, resulting in a steady concentration of O<sub>3</sub> in the troposphere. However, the existence of VOCs breaks this balance. The degradation reactions of VOCs generate intermediate peroxy radicals (RO<sub>2</sub><sup>•</sup>) in the presence of NO<sub>x</sub>, which can convert NO to NO<sub>2</sub> (see R4). Additionally, some carbonyl compounds (RCHO) go through photolysis to produce HO<sub>2</sub>, which can also compete with O<sub>3</sub>, oxidizing NO to NO<sub>2</sub>, as in the case of HCHO (R5 and R6). Even though the loss of O<sub>3</sub> exists (see R7 and R8), there is still a net production of O<sub>3</sub> formation in the troposphere (Robert C. Chapleski Jr., 2016; Yu, 2018).

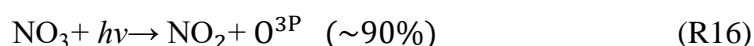
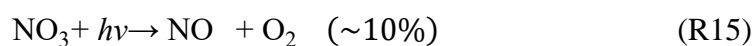


OH radicals are considered as the critical oxidant during the daytime. The dominant source of OH is produced from the photolysis of O<sub>3</sub> in the presence of water vapour in “clean” air. The excited oxygen, O(<sup>1</sup>D), is formed from O<sub>3</sub> at wavelengths below 335nm, which can react with water vapour to produce OH when the atmospheric relative humidity is around 50%. Therefore, some regions with higher humidity and sufficient sunlight irradiation have higher OH concentrations. In polluted regions, the OH radicals can be generated from the photolysis of nitrous acid (HONO) and hydrogen peroxide (H<sub>2</sub>O<sub>2</sub>) (F. Rohrer1, 2005). Additionally, the intermediate HO<sub>2</sub> radicals from VOCs degradation can react with NO to produce NO<sub>2</sub> and recycle OH (see R6). Finally, other compounds such as formaldehyde and carbonyls in the presence of NO<sub>x</sub> also contribute to the production of OH radicals (Woojin Lee 2005; Kroll and Seinfeld, 2008). The detailed chemical reactions are shown below:

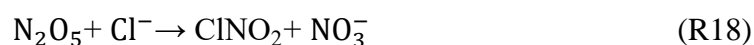
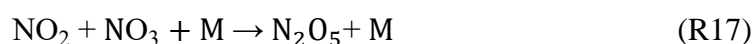




The third important atmospheric oxidant is  $\text{NO}_3$  during nighttime. In the troposphere, the main source of  $\text{NO}_3$  is the chain reactions in the presence of  $\text{NO}$  (R13 and R14).  $\text{NO}_3$ -initiated oxidation can be important at night because the rapid photolysis of  $\text{NO}_3$  radical under sunlight results in a  $\text{NO}_3$  lifetime of  $\sim 5$ s and a negligible concentration at daytime (Atkinson, 2000), although the presence of  $\text{NO}_2$  from natural and anthropogenic sources can lead to the production of  $\text{NO}_3$  (see R15).



Additionally, in marine environments, the Cl-atom is a potential oxidant of VOCs. Cl-atoms are primarily from the source of  $\text{ClNO}_2$  in the polluted marine boundary layer, though  $\text{HCl}$  and  $\text{NH}_4\text{Cl}$  are other commonly measured sources (Riedel et al., 2012). Those species usually exist in form of aerosol particles. Thus, the particulate  $\text{ClNO}_2$  needs to react with nitrogen oxides and then be photolyzed to form Cl-atoms, as shown below. Nitrogen oxides and aerosol chloride sources coexist, such as urban areas and ship engine exhaust plumes (Osthoff et al., 2008).

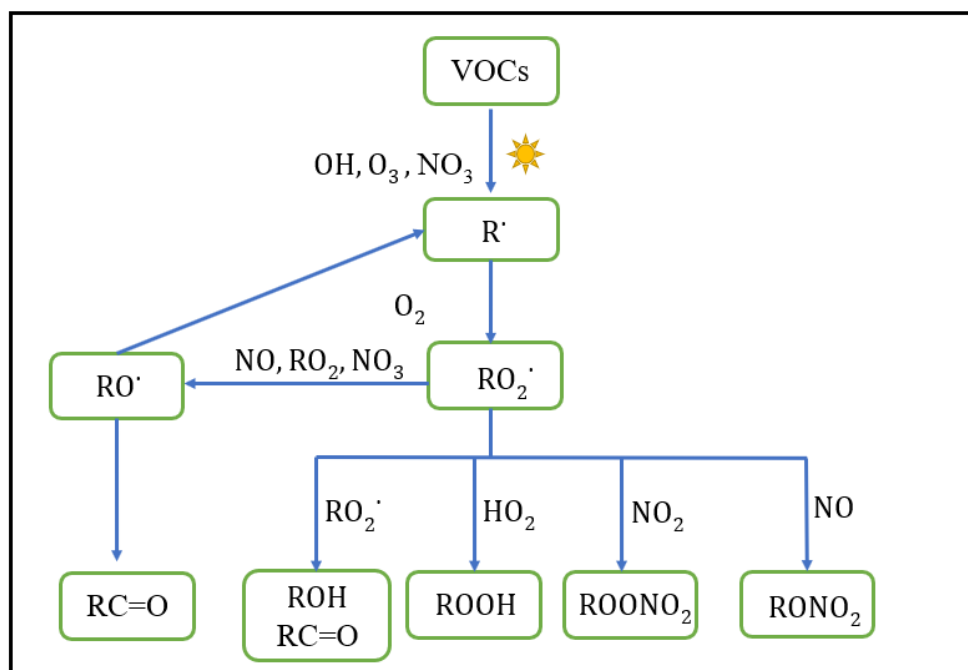


### 2.1.2 VOCs degradation

VOCs can be oxidized by these oxidants in different orders of magnitude due to their different reactivities toward each oxidant, leading to the formation of lower volatility compounds. The reactivity of the VOC toward oxidants presents their atmospheric lifetimes. For example, the most abundant monoterpene  $\alpha$ -pinene shows a 2.6 h atmospheric lifetime with OH, 5 mins with  $\text{NO}_3$  and 4.6 h with  $\text{O}_3$  (Atkinson, 2000). Commonly, OH and  $\text{NO}_3$  can react

with most VOCs whilst  $O_3$  can only react with alkenes and other VOCs with C=C bonds. Thus, terpenes can react with OH,  $O_3$  and  $NO_3$  due to the double carbon bond easily attacked, while most aromatics can only react with OH on the atmospherically relevant timescales. It is worth mentioning that the exceptions or variations exist in the broad assumptions here. The reaction mechanism starts with the reaction of a VOC and radicals (OH,  $O_3$ ,  $NO_3$ , or Cl.), initiating oxidation from H-abstraction of a hydrogen atom to generate an alkyl or substituted alkyl radical ( $R^\cdot$ ). Subsequently, the peroxy radical ( $RO_2^\cdot$ ) is formed from  $R^\cdot$  through  $O_2$  addition. The fate of  $RO_2^\cdot$  is dependent on the structure of the radical, atmospheric conditions such as  $NO_x$  concentration, the concentration of  $HO_2$  radicals, etc (Assaf et al., 2018; Berndt et al., 2018b). A generalized tropospheric degradation scheme that is applicable for the majority of VOCs is displayed in Figure 2.1.

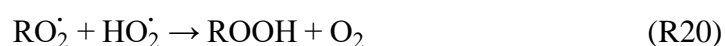
Additionally, the reactions of VOCs with ozone may generate Criegee intermediates (CI) (Johnson and Marston, 2008; Hasson et al., 2003). The fate of activated CI depends on the competition between collisional stabilisation and prompt unimolecular reactions (Vereecken and Francisco, 2012). Usually, the CI with small carbon numbers (e.g.  $CH_2OO$ ) will not be stabilized at the atmospheric pressure, whereas the CI with large carbon numbers will be stabilized (SCI thereafter) (Vereecken and Francisco, 2012). The CI can either be stabilized or decompose to produce OH and other fragments which will further react with  $O_2$  to form  $RO_2$  radicals (Lester and Klippenstein, 2018; Johnson and Marston, 2008). The SCI may undergo either decomposition or bimolecular reactions with water to generate carboxylic acids or hydroxyalkyl hydroperoxides, or react with  $NO_2$  to generate  $NO_3$  and coproducts (Caravan et al., 2017; Sarwar et al., 2013), or react with  $SO_2$  to the production of sulfuric acid (Percival et al., 2013; Mauldin et al., 2012).



**Figure 2.1.** The simplified chemical reaction mechanism for the majority of VOCs in the atmosphere is adapted from Kroll and Seinfeld (2008).

Under lower NO<sub>x</sub> conditions, the reactions of RO<sub>2</sub>· with HO<sub>2</sub> and RO<sub>2</sub>· become competitive. RO<sub>2</sub>· reacting with HO<sub>2</sub> to form hydroperoxide products (ROOH) is the dominant termination channel (Atkinson and Arey, 2003). Meanwhile, part of RO<sub>2</sub>· may propagate the reactions by reacting with self RO<sub>2</sub>· to generate alkoxy radicals RO·, ending in carbonyls hydroxycarbonyls, alcohol or carbonyl products. As a result, VOC degradation at very low-level NO<sub>x</sub> leads to the production of hydroperoxides, carbonyls, hydroxycarbonyls and alcohols. If the organic species contain oxygenated functional groups initially, which can also be retained in the products. In this case, percarboxylic acid (RC(O)OOH) and carboxylic acid (RC(O)OH) products can be generated by peroxyacyl radicals via RC(O)O<sub>2</sub> reacting with HO<sub>2</sub> and the RO<sub>2</sub>·. The terminated channels of RO<sub>2</sub>· are shown below (Hallquist et al., 2009; Pullinen, 2017):

Hydroperoxy channel:

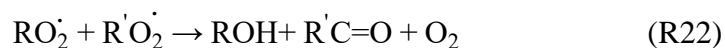


Carbonyl and alcohol channel:

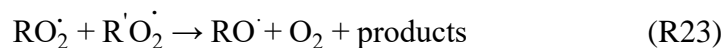




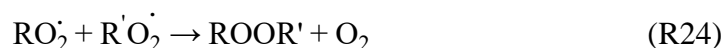
Hydroxy channel:



Alkoxy channel:



Isomerization way:



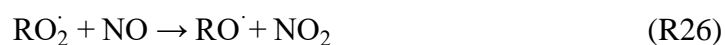
Where  $\text{RO}_2\dot{\phantom{O}}$  and  $\text{R}'\text{O}_2\dot{\phantom{O}}$  can be the same or different peroxy radicals.

At the high- $\text{NO}_x$  level,  $\text{NO}_x$  can compete with  $\text{HO}_2$  to alter the termination pathway of  $\text{RO}_2\dot{\phantom{O}}$ . First,  $\text{RO}_2\dot{\phantom{O}}$  can react with  $\text{NO}_2$  and is terminated by the generation of peroxyxynitrate ( $\text{ROONO}_2$ ) (see R27) which are only temporary reservoirs for  $\text{RO}_2$  and  $\text{NO}_x$  due to a very short lifetime (less than 1 s for alkyl peroxyxynitrates) (Hallquist et al., 2009). The peroxyacyl nitrates (PANs) are generally formed from peroxyacyl radicals of generic formula  $\text{RC}(\text{O})\text{O}_2$ . Another termination channel is to react with  $\text{NO}$  to produce  $\text{RO}\dot{\phantom{O}}$  which may typically react with  $\text{O}_2$  to form carbonyl product and  $\text{HO}_2$ , leading to decomposition into a smaller carbonyl product or an organic radical or ultimately to a hydroxy carbonyl product. The reaction with  $\text{NO}$  can also be terminated by forming nitrate product ( $\text{RONO}_2$ ) directly. As a result, VOC degradation under high- $\text{NO}_x$  conditions generates a product distribution that is dominated by carbonyls, hydroxycarbonyls, organic nitrates and PANs. However, if the organic species initially contain oxygenated functional groups, they may be retained in the products. The detailed termination channel is shown below.

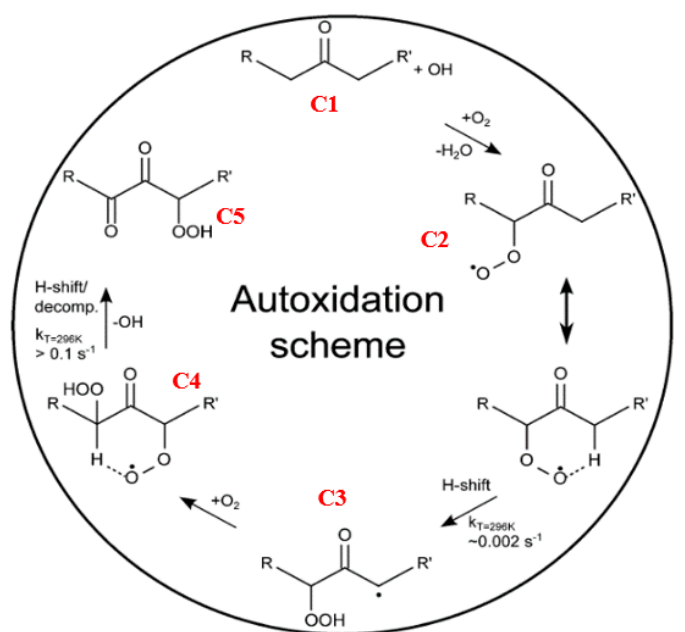
Peroxyxynitrates channel:



Reactions with  $\text{NO}$  pathway:



Recently, researchers found that some products cannot be explained by the traditional formation mechanisms such as using mechanisms in the Master Chemical Mechanism (MCM) (Mehra et al., 2020; Zhang et al., 2017; Bianchi et al., 2019). Some molecules are highly oxidised with extremely low volatility (Ehn et al., 2014) and generated from newly found auto-oxidation pathways (Crouse et al., 2013). Bianchi et al. (2019) very specifically defined this type of molecule as a highly oxygenated molecule (HOM) if it is satisfied the following three requirements: 1) typically contains six or more than six oxygen atoms; 2) are formed via autoxidation processes and 3) are formed in the gas phase under atmospherically relevant conditions. Currently, studies assume that HOMs can condense on pre-existing particles irreversibly, which are highly suspected to contribute to the formation of SOA. The general mechanism of HOMs formation from the autoxidation is shown in Figure 2.2 (Crouse et al., 2013). A parent  $RO_2$  undergoes an intramolecular hydrogen-atom shift (H-shift), leading to a hydroperoxide functionality formation and a  $R'$  formation. A new more oxidized peroxy radical is rapidly formed through the subsequent addition of  $O_2$ . The new peroxy radical reacts with either  $NO$ ,  $HO_2$ , or other peroxy radicals, ending with  $OH$  loss and highly oxidized molecules formation. Nevertheless, there are limited studies to be conducted to assess the contribution of these pathways, since there is limited understanding of gas-phase oxidation for many VOCs and the capability to measure relevant heterogeneous chemistry processes (Bianchi et al., 2019; Steimer et al., 2018).



**Figure 2.2.** An example of autoxidation in OH-initiated oxidation of ketones (Crouse et al., 2013). Carbonyl compound C1 forms a peroxy radical (C2) which undergoes H abstraction, resulting in the formation of C3 with a radical center on the carbon atom. Subsequently, C3 goes through rapid addition of O<sub>2</sub>, generating a new peroxy radical (C4), which undergoes another H-shift and terminates the autoxidation via loss of an OH radical, leading to a formation of dicarbonyl hydroperoxide. The process between C2 and C4 is called autoxidation (Crouse et al., 2013).

## 2.2 Gas-particle partitioning

Although gas-phase chemistry is complicated due to around 10,000 to 100,000 organic compounds in the atmosphere (Goldstein and Galbally, 2007), it is still widely believed the gas-phase oxidation reactions of some VOCs play an important role in the SOA formation, as semi-volatile compounds can be formed in the processes. Then those gaseous semi-volatile compounds can partition into particles under certain conditions. The gas-particle partitioning of SOA is generally described as a theory based on organic aerosol phase partitioning developed by Pankow (Pankow, 1994) and further developed by Odum to SOA formation (Odum et al., 1996a). Partitioning of a compound is described by an equilibrium partitioning coefficient  $K_{p,i}$  ( $\text{m}^3 \mu\text{g}^{-1}$ ) or its inverse. The absorptive partitioning co-efficient ( $K_p$ ,  $\text{m}^3 \mu\text{g}^{-1}$ ) is described in Eq. 1 and the saturation vapour concentration  $C_i^*$  ( $\mu\text{g m}^{-3}$ ) is shown in Eq. 2 (Donahue et al., 2006). However, it should be noted that some fraction of a given semivolatile compound can partition into particle phase as long as the absorbing mass exists, even though the gas phase concentration is blow its  $C^*$ . Thus, Eq. 3 proposed the fraction  $F_i$  of a semivolatile compound in the particle phase (Hallquist et al., 2009).

$$K_{p,i} = \frac{P_i}{MG_i} = \frac{760RT}{10^6 MW_{om} \zeta_i P_{Li}^o} \quad \text{Eq 1}$$

$$C_i^* = \frac{Coa \times C_i^p}{C_i^g} = \frac{10^6 M \zeta_i P_{Li}^o}{760RT} \quad \text{Eq 2}$$

$$F_i = \frac{C_i^p}{C_i^g + C_i^p} = \frac{Coa \times K_{p,i}}{1 + Coa \times K_{p,i}} = \frac{1}{1 + C_i^*/Coa} \quad \text{Eq 3}$$

In Eq. 1,  $P_i$  is the mass concentration of semi-volatile species,  $i$ , in the particle phase ( $\mu\text{g m}^{-3}$ ).  $G_i$  is the mass concentration of semi-volatile species in the gas phase ( $\mu\text{g m}^{-3}$ ).  $M$  is the mass concentration of the total absorbing particulate phase ( $\mu\text{g m}^{-3}$ ).  $T$  is the temperature (K).  $R$  is the ideal gas constant ( $8.206 \times 10^{-5} \text{ m}^3 \text{ mol}^{-1} \text{ K}^{-1}$ ),  $MW_{om}$  is the average molecular weight of the absorbing phase ( $\text{g mol}^{-1}$ ).  $P_{Li}^o$  is the vapour pressure of the absorbing semi-volatile

species as a liquid (Torr), and  $\zeta$  is the activity co-efficient of the semi-volatile species in the particulate phase.

In Eq.2 and Eq.3,  $C_i^g$  is the mass concentration of species  $i$  per unit volume of air in the gas phase ( $\mu\text{g m}^{-3}$ ),  $C_i^p$  is the mass concentration per unit volume of air in the particle phase ( $\mu\text{g m}^{-3}$ ), and  $C_{oa}$  is the mass concentration per unit volume of air of the total absorbing particle phase ( $\mu\text{g m}^{-3}$ ).  $K_{p,i}$  represent mass yield partitioning coefficient of compound  $i$ , respectively, which can be theoretically derived from the saturation vapour pressure of the pure compounds if its activity coefficient in the absorbing phase can be determined (Chang and Pankow, 2006; Donahue et al., 2006).

As SOA consists of thousands of components, it is not practical to measure the vapour pressure for all components. In order to simplify the gas-particle partition method, the volatility basis set (VBS) has been developed to clarify the relationships between different species and their saturation vapour concentrations ( $C^*$ ). This VBS method was utilized in a one-dimensional VBS (1D-VBS) to quantify the SOA products from  $\alpha$ -pinene + ozone using the measured O:C of the observed molecular composition (Donahue et al., 2006; Donahue et al., 2009). Later, this model was further extended into a two-dimensional VBS (2D-VBS) to improve the ability to predict the thermodynamics, including organic mixing and polarity, and ultimately to coherently describe oxidation chemistry (Donahue et al., 2011). The bulk parameters used in these methods simplify the complexity of organic aerosol mixtures by considering the interactions of carbon-carbon bond, oxygen-oxygen bond and carbon-oxygen bond. Generally, the VBS consists of several bins, each of which is separated by one order of magnitude in  $C^*$ . The detailed classification of atmospheric compounds based on their volatility is shown below:

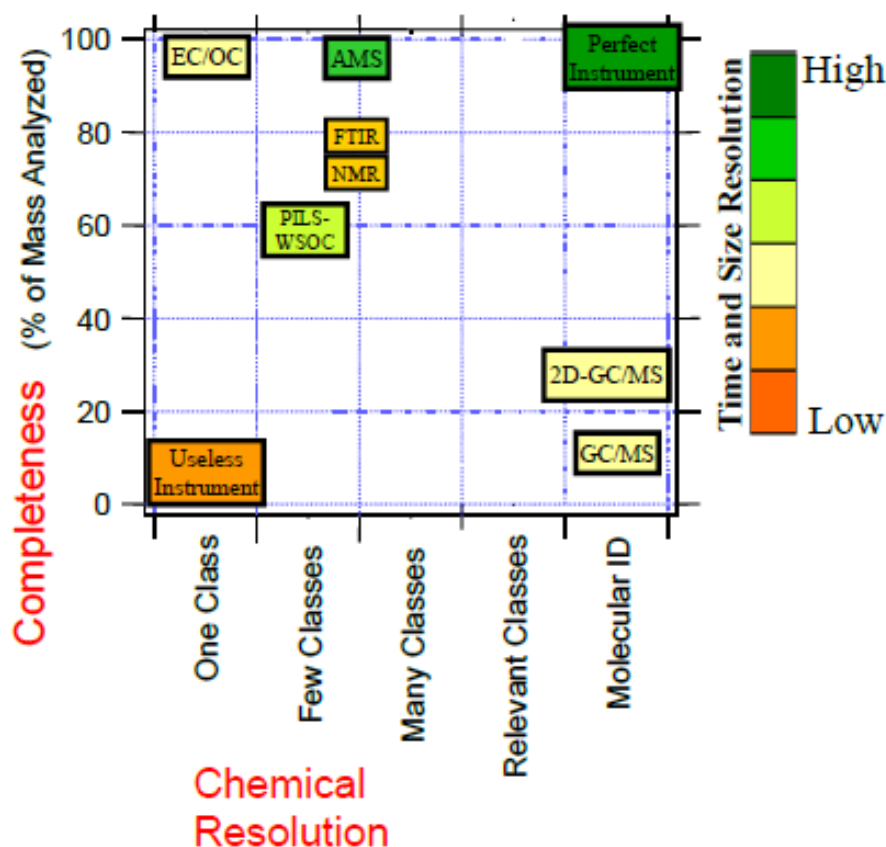
- Volatile organic compounds: VOC with  $C^* > 1 \times 10^6 \mu\text{g m}^{-3}$ ; This type of VOC plays a dominant role in the gas phase oxidation chemistry and is an important SOA precursor.
- Intermediate volatility organic compounds: IVOC,  $1 \times 10^3 < C^* < 1 \times 10^6 \mu\text{g m}^{-3}$ ; This type of VOC appears almost exclusively in the gas phase under atmospheric conditions despite relatively low vapour pressures (Robinson et al., 2007; Donahue et al., 2009)

- Semi-volatile organic compounds: SVOC,  $1 < C^* < 1 \times 10^3 \mu\text{g m}^{-3}$ ; This type of VOC can exist in both gas and particle phases, playing a primary role in the SOA formation and growth by absorptive partitioning (Pankow, 1994).
- Low volatility organic compounds: LVOC,  $1 \times 10^{-2} < C^* < 1 \mu\text{g m}^{-3}$ ; This type of VOC will condense easily onto pre-existing particles and primarily exist in the particle phase.
- Extremely low volatility organic compounds: ELVOC,  $C^* < 1 \times 10^{-2} \mu\text{g m}^{-3}$ ; This type of VOC can condense readily onto pre-existing particles and almost exclusively exists in the particle phase.

It can be seen volatility impacts on the gas phase partitioning into particle phase for a compound. And each type of VOC plays different roles in SOA formation and SOA growth. For example, HOMs are usually the ELVOC and LVOC, except for some exceptions in SVOCs (Bianchi et al., 2019), and are thus expected to contribute to SOA formation and growth. Furthermore, laboratory and modelling studies show that the experimental SOA yield from  $\alpha$ -pinene and ozone reaction can be fitted to the VBS well (Presto and Donahue, 2006; Pathak et al., 2007).

### **2.3 Instruments application to measure SOA components**

In the last decades, the chemical composition of SOA has been extensively studied by researchers. The development of a wide range of new analytical techniques in field measurements and laboratory studies has been driven by scientific questions addressing the atmospheric aerosols' formation, evolution and physicochemical properties (McMurry, 2000; Laj et al., 2009). However, no perfect instrument is capable of providing detailed SOA components in the atmosphere, as shown in Figure 2.3 (Hallquist et al., 2009). Thus, numerous analytical instruments are required to be combined or redesigned to investigate the chemical composition of SOA. Generally, many of the advanced instruments are mass spectrometry-based (McCluckey and Wells, 2001). And these mass spectrometric techniques can be broadly divided into offline and online analytical techniques. Offline instruments can provide detailed information on the individual chemical species or functional groups of SOA.



**Figure 2.3.** Visualization of analytical techniques utilized to characterize the organic components. It shows that the different sizes and time resolution and chemical resolution can be achieved in different instruments. EC/OC: thermal optical elemental carbon/organic carbon analyser. PILS-WSOC: particle into liquid sampler combined with analysis for water-soluble organic compounds. FTIR: Fourier Transform Infra-Red spectroscopy. NMR: nuclear magnetic resonance. GC/MS: gas chromatography-mass spectrometry. 2D-GC/MS: two-dimensional GC/MS. This figure is from Hallquist et al. (2009).

Advanced off-line instruments have been employed to investigate SOA composition either in fields or laboratory studies in recent years. Chromatographic approaches such as liquid chromatography (LC) or gas chromatographic (GC) have been applied for separating individual compounds in a solvent flow or a gas flow before detection. GC and LC are usually combined with other spares to characterize the SOA composition. For example, two-dimensional GC in conjunction with MS or a combination of LC-GC-MS and TD-GC-MS (Thermal desorption gas chromatography-mass spectrometry) is used to investigate the polycyclic aromatics hydrocarbons (PAHs), oxygenated PAHs and other components from fine particles (Hays and Lavrich, 2007; Ho et al., 2011; Kallio et al., 2003). High-performance liquid chromatography-electrospray ionization tandem mass spectrometry (HPLC-ESI-MS/MS) is presented for the identification of acidic products from terpene oxidation such as pinic acid, pinonic acid, etc, in the atmospheric particle samples (Warnke et al., 2006). The structural elucidation of

organosulfates or HOMs is carried out via one- or two-dimensional high-performance liquid chromatography (1D/2D-HPLC) simultaneously coupled to ESI-Time-of-flight MS (ESI-TOFMS) or ESI-ITMS (electrospray ionization-ion trap mass spectrometry), providing new information on chemical heterogeneous reactions involved in SOA formation and growth (Yoshiteru Iinuma, 2007; De Vijlder et al., 2018; Mutzel et al., 2015). Additionally, other off-line techniques such as LDI-MS (laser desorption ionization mass spectrometry), FTIR (Fourier Transform Infra-Red spectroscopy) and NMR (nuclear magnetic resonance) are used to identify the polymers of atmospheric organic aerosols, strengthening the qualitative and quantitative understanding of SOA polymers formation (Stefano Decesari, 2007; M. Kalberer et al., 2004).

Molecular speciation can be obtained via offline GC/MS or LC/MS due to their high mass resolution, although it only can characterize a small part of the SOA in the samples owing to the limitation of calibration standards. During the process, the offline analysis method requires the collected samples in the field or the laboratory studies, after which those samples are extracted by solvents or thermal desorption to release the semivolatile species (Claeys et al., 2009; Gautier et al., 2016; Hernandez et al., 2005). This process may result in the contamination of the sample on the filters. To minimize limitations or disadvantages of off-line techniques such as potential samples' contamination during storage and transportation, and sampling time integrating, nearly real-time analytical techniques which enable to collect of samples online and analyzed samples simultaneously have been developed to characterize the chemical components of SOA (Lopez-Hilfiker et al., 2014; Alfarra et al., 2006; Ng et al., 2006; Rosati et al., 2019).

Online GC-MS has been proven very useful to identify the gas-phase speciated information on the organic fraction. GC-MS has been utilized for the identification and quantification of parent VOCs and tracers from anthropogenic VOCs chemical reactions (Vivanco et al., 2011; Aragon et al., 2013; Xu et al., 2006). Additionally, online aerosol mass spectrometry (AMS) has been developed for atmospheric particles composition analysis and temporal evolution of chemical composition (Alfarra et al., 2006; Allan et al., 2003; Drewnick et al., 2005). New information on non-refractory aerosol mass concentrations, chemical speciated mass distribution and single-particle information can be attained from this technique. The latest version, named high-resolution Time-of-Flight Aerosol Mass Spectrometer (HR-

TOF-AMS) with higher resolution and relatively higher sensitivity, is a combination of the previous well-characterized quadrupole mass spectrometer-based Aerodyne AMS (Drewnick et al., 2005; Lee et al., 2013; Quéléver et al., 2019). Aerosols organic species such as carboxylic acids based on the fragments' signals and organic-mass-to-organic-carbon ratios (OM/OC) and oxygen-to-carbon (O/C) ratios can be observed by researchers using HR-TOF-AMS (Chen et al., 2020; Xu et al., 2017; Li et al., 2013; Aiken et al., 2008).

More recently, chemical ionization mass spectrometry (CIMS) has become an increasingly useful method for the measurement of a wide range of atmospheric trace gases (Huey, 2007). Modifications and developments have been made for the CIMS to measure the aerosol species recently. Such optimization like TD-CIMS (thermal desorption CIMS) and high-resolution time-of-flight (TOF-CIMS) are employed to observe the organic acids, peroxides and aldehydes (Zhao et al., 2012; Lee et al., 2014). Organosulfates, nitroxy organosulfates are observed utilizing a novel method, HR-TOF-CIMS coupling to Filter Inlet for Gas and Aerosol (HR-TOF-FIGAERO), which enables measurements of both gas-phase components and particles by a high-resolution mass spectrometer via multi-port inlets (Lopez-Hilfiker et al., 2014). Besides, Nitrate Atmospheric Pressure Interface Time-Of-Flight Mass Spectrometer (CI-API-TOF) and Nitrate TOF-CIMS FIGAERO have been proved to greatly improve the detection and quantification and aid to investigate of HOMs formation pathway (Bianchi et al., 2019; Pye et al., 2019; Tu et al., 2016). As the result of the complexity of SOA components, a series of offline analytical techniques and online analytical techniques are usually combined to investigate the samples, allowing to providing comprehensive information on the chemical composition and structure of individual species (Zhang et al., 2017; Isaacman-Vanwertz et al., 2017; Berndt et al., 2018a).



**Table 1.** advantages and disadvantages of various analytical methods for the detection of aerosols.

| Analytical technique | Advantages   | Disadvantages   |
|----------------------|--|---|
| GC-MS                | Enable to identify molecular structure; Online and offline measurement availability;<br>Quantificational and quantitative                                      | Standards needed;<br>Expensive equipment;   |
| LC-MS                | Enable to identify molecular structure;<br>High resolution;<br>Quantificational and quantitative   | Sample collection and preparation needed;<br>Expensive equipment;<br>Standards needed;                              |
| AMS                  | Can obtain organic mass and chemical properties for nonrefractory species  | Cannot provide molecular composition information;   |
| CIMS                 | Near real-time analysis,<br>Time-saving;<br>Multiple reagent ions can be used;<br>Can couple with FIGAERO to measure the gas and particle phase simultaneously | Cannot separate isomers and cannot provide molecular structural information;<br>Reagent ions needed                 |
| FTIR                 | Traditional method;<br>cheap equipment   | Lower resolution  |
| NMR                  | Non-destructive;<br>Structural details can be obtained;<br>Easy sample preparation;  | Expensive;<br>Signal overlapping in complex samples;<br>Lower resolution than MS;<br>Requires larger samples volume |

## 2.4 Laboratory studies

Laboratory studies, as one of the “three-legged stools”, play a critical role in the understanding of atmospheric chemistry, delivering a mechanistic understanding of atmospheric chemistry at a molecular level and helping better understanding of SOA formation from VOCs oxidation (Burkholder et al., 2017). The majority of studies have been carried out in the outdoor or indoor simulation chambers with a volume ranging from 1-270 m<sup>3</sup> (Carter et al., 2005; Cocker et al., 2001; Babar et al., 2017; Wang et al., 2011; Zador et al., 2005; Shao et al., 2021; Rohrer et al., 2005; Jonsson et al., 2007), and other studies have been performed in aerosol flow reactors (Schild et al., 1999; Mcfiggans et al., 2019; Lambe et al., 2011; Wiles

and Watts, 2012). Generally, the smog chambers are utilized to mimic the atmospherically relevant conditions. The smog chamber experiments are usually conducted in a batch mode (Chuang and Donahue, 2017; Shao et al., 2021) but sometimes in a continuous flow mode (Zhang et al., 2018; Seinfeld et al., 2003). The flow reactors are usually designed to separate reactions to further explore the specific chemical mechanisms.

Traditionally, the atmospheric chemistry about the rates and mechanisms of some important gas-phase reactions has been explored via laboratory studies (Wang et al., 2014; Carter, 2007; Atkinson et al., 1980). Recent studies have transformed the laboratory studies into more atmospherically related about the VOCs oxidation to the aerosol particles formation and its physical-chemistry properties. This shows more connections between fundamental knowledge obtained in laboratory studies and real atmospheric behaviors of organic compounds. For example, the gas-phase chemistry of the largest source of biogenic VOCs isoprene emitted from the vegetation has been demonstrated via chamber experiments (Paulot et al., 2009; Kroll et al., 2005). Surratt et al. (2010) have been further validated it is an important SOA precursor in the atmosphere. The new findings highly oxidized molecules (HOMs) with the extremely low volatility generated from the autooxidation reaction have been investigated in some VOCs oxidation such as  $\alpha$ -pinene and isoprene (Crouse et al., 2013; Wang et al., 2018; Zhang et al., 2017; Steimer et al., 2018). The HOMs are generally believed to the production of SOA in the atmosphere, although little is known about those highly oxidized multifunctional reactions in the terms of subsequent gas-phase and particle-phase reactivity, photochemistry and light-absorbing properties. It requires more effort in future work.

SOA yields from biogenic and anthropogenic VOCs can be obtained via laboratory studies. The most common way to calculate the SOA yield has been defined as  $Y = \Delta M / \Delta \text{VOCs}$ , where  $\Delta M$  ( $\mu\text{g m}^{-3}$ ) is the changes in aerosol mass concentration and  $\Delta \text{VOCs}$  represent the changes in the amount of VOC precursor concentration (Odum et al., 1996b). Generally, an effective density of  $1.4 \text{ g cm}^{-3}$  has been utilized for SOA in the chamber studies (Dommen et al., 2006; Ng et al., 2007; Presto et al., 2005; Fry et al., 2014; Eddingsaas et al., 2012b), although there are many uncertainties in the influence of experimental conditions and other parameters on the SOA density. SOA yields for a precursor in the chamber studies are affected by some factors, such as  $\text{NO}_x$  levels, seed conditions, etc. For example, the same aromatic compounds displayed different SOA yields under high- $\text{NO}_x$  and low- $\text{NO}_x$  conditions

(Ng et al., 2007; Odum et al., 1996a). Another important development is that Mcfiggans et al. (2019) recently found that the SOA yields in the mixture shows lower than the sum of the SOA yields in the individual precursor due to the interactions in the oxidation products between VOCs.

Nevertheless, more effort in laboratory studies is needed to better understand the atmospheric chemistry and SOA formation from organic compounds, such as how does the chemistry affect the formation of cloud and how the transformation of oxidation products occurred in the atmosphere. Much work is also required to connect the laboratory studies with field measurements activities and modelling. Additionally, the comprehensive characteristics of the smog chambers remain some uncertainties, such as the chamber materials, volume, mode of operation etc. Those differences may lead to different gas and particle loss rates, oxidation concentration, etc, resulting in difficulty in the interpretation and comparison of the experimental results across chambers. Thus, it is essential to carry out the systematic characterization of the chamber before experimental campaigns.

## **2.5 Mixtures studies**

SOA formation from individual VOCs precursor has been extensively explored since the early 1980s (Jennifer E. Stern, 1987; Joseph A. Leone, 1985). BVOCs, such as  $\alpha$ -pinene (Ehn et al., 2012; Eddingsaas et al., 2012a; Eddingsaas et al., 2012b) and isoprene (Claeys et al., 2004; Ng et al., 2008; Safi Shalamzari et al., 2013), and AVOCs, such as benzene (Sato et al., 2012; Borrás and Tortajada-Genaro, 2012), toluene (Ng et al., 2007; Sato et al., 2007), etc, are widely studied in their SOA formation. Although there is some progress in the SOA formation mixtures, it remains uncertain on the SOA formation mechanisms and physicochemical properties. And it is still sparse in the exploration of SOA formation from the mixtures of anthropogenic and biogenic emissions, although this area has been attracted more attention in recent years.

Observations showed that possible interactions exist in the SOA particle formation between VOCs emissions and anthropogenic activities (Kiendler-Scharr et al., 2009; Kanawade et al., 2011), which may influence the SOA budget in the atmosphere (Spracklen et al., 2011). Studies illustrated that isoprene can suppress new particle formations of natural biogenic VOC emissions (Kiendler-Scharr et al., 2009; Kanawade et al., 2011). Weber et al.

(2007) investigated that SOA formation is spatially and strongly correlated with anthropogenic emissions such as CO and anthropogenic VOCs according to the measured organic water-soluble compounds in the southeastern United States, suggesting that biogenic SOA formations may be enhanced in polluted areas. The CARES campaign conducted in the vicinity of Sacramento, California showed that SOA production is higher under the high frequency of anthropogenic activities and NO<sub>x</sub> concentrations have a significant influence on the enhancement of SOA formation from isoprene (Shilling et al., 2013). Hoyle et al. (2011) and De Gouw et al. (2005) provided evidence that anthropogenic emissions have a significant effect on the formation of biogenic SOA. The possible mechanisms of anthropogenic emission enhancement may be the results of gas-particle partitioning, accretion reactions, or new particle formation (Ahlberg et al., 2017; Hoyle et al., 2011). As for gas-particle partitioning, we assume all organic particles are well-mixed and stay in a single particle phase state (Hoyle et al., 2011). It shows that a well-mixed single-phase organic aerosol can absorb greater amounts of semi-volatile species but few experiments exist on the phase distribution of particles (Asa-Awuku et al., 2009), and thus more efforts are needed to convince this theory on the enhancement effect. Second, irreversible condensed-phase accretion reactions may play a critical role in particle-phase production, such as esterification, oligomerization, hemiacetal formation and Criegee intermediate adduct reactions (Kroll and Seinfeld, 2008; Bianchi et al., 2019). Besides, another potential effect on BSOA would be an increase in the number of aerosol particles through a modification of new particle formation by heteromolecular homogeneous nucleation (Kanakidou et al., 2000). However, more efforts are needed to evaluate those theories on the enhancement effect.

A series of experiments have been carried out to study the SOA yield impacted in the anthropogenic and biogenic mixtures. Vivanco et al. (2011) provided evidence that the SOA formation can be enhanced in anthropogenic mixtures in the addition of SO<sub>2</sub> but ambiguous conclusions for biogenic VOCs mixtures (Vivanco et al., 2011). Emanuelsson et al. (2013) illustrated that the presence of anthropogenic VOCs can enhance the biogenic SOA yield. However, Loza et al. (2013) and Hildebrandt et al. (2011) found that the SOA yield in mixtures depends on the sequence of addition of the SOA precursors. Adding the biogenic VOC ( $\alpha$ -pinene) into anthropogenic VOC (toluene as representative) can increase the volatility of SOA, resulting in the SOA yield decreased, while adding anthropogenic VOC into biogenic VOC can decrease the volatility of SOA, leading to the SOA yield increased. Another interesting

research area is the role of isoprene on new particle formation. It has been proved that the higher concentration of isoprene emitted by deciduous plants can suppress the nucleation of new particles in the isoprene-dominated forests (Kiendler-Scharr et al., 2009; Kanawade et al., 2011; Lee et al., 2016). However, there are fewer studies to get insights into the interaction mechanisms. Mcfiggans et al. (2019) revealed the suppression mechanism in the presence of isoprene. The study found that isoprene can scavenge hydroxyl radicals (oxidant scavenging) reactions and the products from isoprene such as peroxy radicals (product scavenging) can also inhibit the formation of highly oxygenated molecules from  $\alpha$ -pinene. The suppression effect can significantly decrease the SOA yields of  $\alpha$ -pinene in the  $\alpha$ -pinene and isoprene mixed system. The study further demonstrated that SOA yields and net SOA mass are not a linear sum of yields from individual VOCs. However, there is a lack of studies to illustrate the role of isoprene in the anthropogenic VOCs and other monoterpenes.

## 2.6 Aim and objectives

Based on the current knowledge mentioned above, this work aims to design experiments to explore SOA formation and properties from the mixtures of anthropogenic VOC and biogenic VOCs. The representative anthropogenic VOCs ortho-cresol (o-cresol thereafter), which is generated from the oxidation of toluene, particularly in anthropogenic polluted areas (Seinfeld and Pandis, 2016), and the abundant biogenic VOCs,  $\alpha$ -pinene and isoprene, (Guenther et al., 2012) are chosen as the VOC precursors. Experiments have been conducted in the Manchester Aerosol Chamber (MAC) to explore the SOA yields and chemical composition in the mixtures using online and offline analytical techniques.

The main objectives of this work are set, as shown below:

(1) To characterize the MAC and ensure the chamber is well characterized to conduct the SOA formation experiments;

(2) To find out the rational way to design the mixture experiments (binary systems:  $\alpha$ -pinene/ isoprene system,  $\alpha$ -pinene/o-cresol system, and o-cresol/isoprene system; ternary system:  $\alpha$ -pinene, isoprene and o-cresol) and explore SOA yields and other physicochemical properties in the mixed systems;

(3) To assess the advantages of the combinational offline LC-Orbitrap MS and online FIGAERO-CIMS measurements in terms of characterization chemical properties of SOA oxidation products in chamber studies;

(4) To identify the chemical composition in gas and particle phases in the mixed systems and evaluate the time-series behaviours of oxidation products in the mixed systems.

## References

Ahlberg, E., Falk, J., Eriksson, A., Holst, T., Brune, W. H., Kristensson, A., Roldin, P., and Svenningsson, B.: Secondary organic aerosol from VOC mixtures in an oxidation flow reactor, *Atmospheric Environment*, 161, 210-220, 10.1016/j.atmosenv.2017.05.005, 2017.

Aiken, A. C., Decarlo, P. F., Kroll, J. H., Worsnop, D. R., Huffman, J. A., Docherty, K. S., Ulbrich, I. M., Mohr, C., Kimmel, J. R., Sueper, D., Sun, Y., Zhang, Q., Trimborn, A., Northway, M., Ziemann, P. J., Canagaratna, M. R., Onasch, T. B., Alfarra, M. R., Prevot, A. S., Dommen, J., Duplissy, J., Metzger, A., Baltensperger, U., and Jimenez, J. L.: O/C and OM/OC ratios of primary, secondary, and ambient organic aerosols with high-resolution time-of-flight aerosol mass spectrometry, *Environ Sci Technol*, 42, 4478-4485, 10.1021/es703009q, 2008.

Alex Guenther, C. G., Tom Pierce, Brian Lamb, Peter Harley, Ray Fall: Natural emissions of non-methane volatile organic compounds, carbon monoxide, and oxides of nitrogen from North America, *atmospheric Environment*, 34, 2205-2230, 2000.

Alfarra, M. R., Paulsen, D., Gysel, M., Garforth, A. A., Dommen, J., Prévôt, A. S. H., Worsnop, D. R., Baltensperger, U., and Coe, H.: A mass spectrometric study of secondary organic aerosols formed from the photooxidation of anthropogenic and biogenic precursors in a reaction chamber, *Atmospheric Chemistry and Physics*, 6, 5279-5293, 10.5194/acp-6-5279-2006, 2006.

Allan, J. D., Jimenez, J. L., Williams, P. I., Alfarra, M. R., Bower, K. N., Jayne, J. T., Coe, H., and Worsnop, D. R.: Quantitative sampling using an Aerodyne aerosol mass spectrometer 1. Techniques of data interpretation and error analysis, *Journal of Geophysical Research: Atmospheres*, 108, n/a-n/a, 10.1029/2002jd002358, 2003.

Aragon, M., Marce, R. M., and Borrull, F.: Determination of N-nitrosamines and nicotine in air particulate matter samples by pressurised liquid extraction and gas chromatography-ion trap tandem mass spectrometry, *Talanta*, 115, 896-901, 10.1016/j.talanta.2013.07.010, 2013.

Asa-Awuku, A., Miracolo, M. A., Kroll, J. H., Robinson, A. L., and Donahue, N. M.: Mixing and phase partitioning of primary and secondary organic aerosols, *Geophysical Research Letters*, 36, n/a-n/a, 10.1029/2009gl039301, 2009.

Assaf, E., Schoemaeker, C., Vereecken, L., and Fittschen, C.: Experimental and theoretical investigation of the reaction of RO<sub>2</sub>radicals with OH radicals: Dependence of the HO<sub>2</sub>yield on the size of the alkyl group, *International Journal of Chemical Kinetics*, 50, 670-680,

10.1002/kin.21191, 2018.

Atkinson, R.: Atmospheric chemistry of VOCs and NO<sub>x</sub>, *Atmospheric Environment*, 34, 2063-2101, 10.1016/s1352-2310(99)00460-4, 2000.

Atkinson, R. and Arey, J.: Gas-phase tropospheric chemistry of biogenic volatile organic compounds: a review, *Atmospheric Environment*, 37, 197-219, 10.1016/s1352-2310(03)00391-1, 2003.

Atkinson, R. and Carter, W. P. L.: Kinetics and mechanisms of the gas-phase reactions of ozone with organic compounds under atmospheric conditions, *Chemical Reviews*, 84, 437-470, 10.1021/cr00063a002, 2002.

Atkinson, R., Carter, W. P. L., Darnall, K. R., Winer, A. M., and Pitts, J. N.: A smog chamber and modeling study of the gas phase NO<sub>x</sub>-air photooxidation of toluene and the cresols, *International Journal of Chemical Kinetics*, 12, 779-836, 10.1002/kin.550121102, 1980.

Babar, Z. B., Park, J.-H., Kang, J., and Lim, H.-J.: Characterization of a Smog Chamber for Studying Formation and Physicochemical Properties of Secondary Organic Aerosol, *Aerosol and Air Quality Research*, 16, 3102-3113, 10.4209/aaqr.2015.10.0580, 2017.

Berndt, T., Mentler, B., Scholz, W., Fischer, L., Herrmann, H., Kulmala, M., and Hansel, A.: Accretion Product Formation from Ozonolysis and OH Radical Reaction of alpha-Pinene: Mechanistic Insight and the Influence of Isoprene and Ethylene, *Environ Sci Technol*, 52, 11069-11077, 10.1021/acs.est.8b02210, 2018a.

Berndt, T., Scholz, W., Mentler, B., Fischer, L., Herrmann, H., Kulmala, M., and Hansel, A.: Accretion Product Formation from Self- and Cross-Reactions of RO<sub>2</sub> Radicals in the Atmosphere, *Angew Chem Int Ed Engl*, 57, 3820-3824, 10.1002/anie.201710989, 2018b.

Bianchi, F., Kurten, T., Riva, M., Mohr, C., Rissanen, M. P., Roldin, P., Berndt, T., Crouse, J. D., Wennberg, P. O., Mentel, T. F., Wildt, J., Junninen, H., Jokinen, T., Kulmala, M., Worsnop, D. R., Thornton, J. A., Donahue, N., Kjaergaard, H. G., and Ehn, M.: Highly Oxygenated Organic Molecules (HOM) from Gas-Phase Autoxidation Involving Peroxy Radicals: A Key Contributor to Atmospheric Aerosol, *Chem Rev*, 119, 3472-3509, 10.1021/acs.chemrev.8b00395, 2019.

Borrás, E. and Tortajada-Genaro, L. A.: Secondary organic aerosol formation from the photooxidation of benzene, *Atmospheric Environment*, 47, 154-163, 10.1016/j.atmosenv.2011.11.020, 2012.

Burkholder, J. B., Abbatt, J. P., Barnes, I., Roberts, J. M., Melamed, M. L., Ammann, M., Bertram, A. K., Cappa, C. D., Carlton, A. G., Carpenter, L. J., Crowley, J. N., Dubowski, Y., George, C., Heard, D. E., Herrmann, H., Keutsch, F. N., Kroll, J. H., McNeill, V. F., Ng, N. L., Nizkorodov, S. A., Orlando, J. J., Percival, C. J., Picquet-Varrault, B., Rudich, Y., Seakins, P. W., Surratt, J. D., Tanimoto, H., Thornton, J. A., Tong, Z., Tyndall, G. S., Wahner, A., Weschler, C. J., Wilson, K. R., and Ziemann, P. J.: The Essential Role for Laboratory Studies in Atmospheric Chemistry, *Environ Sci Technol*, 51, 2519-2528, 10.1021/acs.est.6b04947, 2017.

Cai, X. and Griffin, R. J.: Secondary aerosol formation from the oxidation of biogenic hydrocarbons by chlorine atoms, *Journal of Geophysical Research*, 111, 10.1029/2005jd006857, 2006.

Caravan, R. L., Khan, M. A. H., Rotavera, B., Papajak, E., Antonov, I. O., Chen, M. W., Au, K., Chao, W., Osborn, D. L., Lin, J. J., Percival, C. J., Shallcross, D. E., and Taatjes, C. A.: Products of Criegee intermediate reactions with NO<sub>2</sub>: experimental measurements and tropospheric implications, *Faraday Discuss*, 200, 313-330, 10.1039/c7fd00007c, 2017.

Carter, W.: A detailed mechanism for the gas-phase atmospheric reactions of organic compounds, *Atmospheric Environment*, 41, 80-117, 10.1016/j.atmosenv.2007.10.061, 2007.

Carter, W., Cockeriii, D., Fitz, D., Malkina, I., Bumiller, K., Sauer, C., Pisano, J., Bufalino, C., and Song, C.: A new environmental chamber for evaluation of gas-phase chemical mechanisms and secondary aerosol formation, *Atmospheric Environment*, 39, 7768-7788, 10.1016/j.atmosenv.2005.08.040, 2005.

Chang, E. I. and Pankow, J. F.: Prediction of activity coefficients in liquid aerosol particles containing organic compounds, dissolved inorganic salts, and water—Part 2: Consideration of phase separation effects by an X-UNIFAC model, *Atmospheric Environment*, 40, 6422-6436, 10.1016/j.atmosenv.2006.04.031, 2006.

Chen, Y., Takeuchi, M., Nah, T., Xu, L., Canagaratna, M. R., Stark, H., Baumann, K., Canonaco, F., Prévôt, A. S. H., Huey, L. G., Weber, R. J., and Ng, N. L.: Chemical characterization of secondary organic aerosol at a rural site in the southeastern US: insights from simultaneous high-resolution time-of-flight aerosol mass spectrometer (HR-ToF-AMS) and FIGAERO chemical ionization mass spectrometer (CIMS) measurements, *Atmospheric Chemistry and Physics*, 20, 8421-8440, 10.5194/acp-20-8421-2020, 2020.

Chuang, W. K. and Donahue, N. M.: Dynamic consideration of smog chamber experiments, *Atmospheric Chemistry and Physics*, 17, 10019-10036, 10.5194/acp-17-10019-2017, 2017.

Claeys, M., Graham, B., Vas, G., Wang, W., Vermeylen, R., Pashynska, V., Cafmeyer, J., Guyon, P., Andreae, M. O., Artaxo, P., and Maenhaut, W.: Formation of secondary organic aerosols through photooxidation of isoprene, *Science*, 303, 1173-1176, 10.1126/science.1092805, 2004.

Claeys, M., Iinuma, Y., Szmigielski, R., Surratt, J. D., Blockhuys, F., Van Alsenoy, C., Boge, O., Sierau, B., Gomez-Gonzalez, Y., Vermeylen, R., Van der Veken, P., Shahgholi, M., Chan, A. W., Herrmann, H., Seinfeld, J. H., and Maenhaut, W.: Terpenylic acid and related compounds from the oxidation of alpha-pinene: implications for new particle formation and growth above forests, *Environ Sci Technol*, 43, 6976-6982, 10.1021/es9007596, 2009.

Cocker, D. R., 3rd, Flagan, R. C., and Seinfeld, J. H.: State-of-the-art chamber facility for studying atmospheric aerosol chemistry, *Environ Sci Technol*, 35, 2594-2601, 10.1021/es0019169, 2001.

Crouse, J. D., Nielsen, L. B., Jørgensen, S., Kjaergaard, H. G., and Wennberg, P. O.: Autoxidation of Organic Compounds in the Atmosphere, *The Journal of Physical Chemistry Letters*, 4, 3513-3520, 10.1021/jz4019207, 2013.



De Gouw, J. A. A. M. M., C. Warneke, P. D. Goldan, W. C. Kuster., J. M. Roberts, F. C. F., D. R. Worsnop, M. R. Canagaratna., and A. A. P. Pszenny, W. C. K., M. Marchewka, S. B. Bertman, T. S. Bates: Budget of organic carbon in a polluted atmosphere: Results from the New England Air Quality Study in 2002, *Journal of Geophysical Research*, 110, 10.1029/2004jd005623, 2005.

De Vijlder, T., Valkenburg, D., Lemièr, F., Romijn, E. P., Laukens, K., and Cuyckens, F.: A tutorial in small molecule identification via electrospray ionization-mass spectrometry: The practical art of structural elucidation, *Mass Spectrom Rev*, 37, 607-629, 10.1002/mas.21551, 2018.

Dommen, J., Metzger, A., Duplissy, J., Kalberer, M., Alfarra, M. R., Gascho, A., Weingartner, E., Prevot, A. S. H., Verheggen, B., and Baltensperger, U.: Laboratory observation of oligomers in the aerosol from isoprene/NO<sub>x</sub>photooxidation, *Geophysical Research Letters*, 33, 10.1029/2006gl026523, 2006.

Donahue, N. M., Robinson, A. L., and Pandis, S. N.: Atmospheric organic particulate matter: From smoke to secondary organic aerosol, *Atmospheric Environment*, 43, 94-106, 10.1016/j.atmosenv.2008.09.055, 2009.

Donahue, N. M., Epstein, S. A., Pandis, S. N., and Robinson, A. L.: A two-dimensional volatility basis set: 1. organic-aerosol mixing thermodynamics, *Atmospheric Chemistry and Physics*, 11, 3303-3318, 10.5194/acp-11-3303-2011, 2011.

Donahue, N. M., Robinson, A. L., Stanier, C. O., and Pandis, S. N.: Coupled partitioning, dilution, and chemical aging of semivolatile organics, *Environ Sci Technol*, 40, 2635-2643, 10.1021/es052297c, 2006.

Drewnick, F., Hings, S. S., DeCarlo, P., Jayne, J. T., Gonin, M., Fuhrer, K., Weimer, S., Jimenez, J. L., Demerjian, K. L., Borrmann, S., and Worsnop, D. R.: A New Time-of-Flight Aerosol Mass Spectrometer (TOF-AMS)—Instrument Description and First Field Deployment, *Aerosol Science and Technology*, 39, 637-658, 10.1080/02786820500182040, 2005.

Eddingsaas, N. C., Loza, C. L., Yee, L. D., Seinfeld, J. H., and Wennberg, P. O.:  $\alpha$ -pinene photooxidation under controlled chemical conditions – Part 1: Gas-phase composition in low- and high-NO<sub>x</sub> environments, *Atmospheric Chemistry and Physics*, 12, 6489-6504, 10.5194/acp-12-6489-2012, 2012a.

Eddingsaas, N. C., Loza, C. L., Yee, L. D., Chan, M., Schilling, K. A., Chhabra, P. S., Seinfeld, J. H., and Wennberg, P. O.:  $\alpha$ -pinene photooxidation under controlled chemical conditions – Part 2: SOA yield and composition in low- and high-NO<sub>x</sub> environments, *Atmospheric Chemistry and Physics*, 12, 7413-7427, 10.5194/acp-12-7413-2012, 2012b.

Ehn, M., Kleist, E., Junninen, H., Petäjä, T., Lönn, G., Schobesberger, S., Dal Maso, M., Trimborn, A., Kulmala, M., Worsnop, D. R., Wahner, A., Wildt, J., and Mentel, T. F.: Gas phase formation of extremely oxidized pinene reaction products in chamber and ambient air, *Atmospheric Chemistry and Physics*, 12, 5113-5127, 10.5194/acp-12-5113-2012, 2012.

Ehn, M., Thornton, J. A., Kleist, E., Sipila, M., Junninen, H., Pullinen, I., Springer, M., Rubach,

F., Tillmann, R., Lee, B., Lopez-Hilfiker, F., Andres, S., Acir, I. H., Rissanen, M., Jokinen, T., Schobesberger, S., Kangasluoma, J., Kontkanen, J., Nieminen, T., Kurten, T., Nielsen, L. B., Jorgensen, S., Kjaergaard, H. G., Canagaratna, M., Maso, M. D., Berndt, T., Petaja, T., Wahner, A., Kerminen, V. M., Kulmala, M., Worsnop, D. R., Wildt, J., and Mentel, T. F.: A large source of low-volatility secondary organic aerosol, *Nature*, 506, 476-479, 10.1038/nature13032, 2014.

Emanuelsson, E. U., Hallquist, M., Kristensen, K., Glasius, M., Bohn, B., Fuchs, H., Kammer, B., Kiendler-Scharr, A., Nehr, S., Rubach, F., Tillmann, R., Wahner, A., Wu, H. C., and Mentel, T. F.: Formation of anthropogenic secondary organic aerosol (SOA) and its influence on biogenic SOA properties, *Atmospheric Chemistry and Physics*, 13, 2837-2855, 10.5194/acp-13-2837-2013, 2013.

F. Rohrer<sup>1</sup>, B. B., T. Brauers<sup>1</sup>, D. Bruning, Chemie und Dynamik der Geosph, F.J. Johnen, J. Kleffmann: Characterisation of the photolytic HONO-source in the atmosphere simulation chamber SAPHIR, *Atmos. Chem. Phys*, 5, 2189-2201, 2005.

Fry, J. L., Draper, D. C., Barsanti, K. C., Smith, J. N., Ortega, J., Winkler, P. M., Lawler, M. J., Brown, S. S., Edwards, P. M., Cohen, R. C., and Lee, L.: Secondary organic aerosol formation and organic nitrate yield from NO<sub>3</sub> oxidation of biogenic hydrocarbons, *Environ Sci Technol*, 48, 11944-11953, 10.1021/es502204x, 2014.

Gautier, T., Schmitz-Afonso, I., Touboul, D., Szopa, C., Buch, A., and Carrasco, N.: Development of HPLC-Orbitrap method for identification of N-bearing molecules in complex organic material relevant to planetary environments, *Icarus*, 275, 259-266, 10.1016/j.icarus.2016.03.007, 2016.

Goldstein, A. H. and Galbally, I. E.: Known and unknown organic constituents in the Earth's atmosphere, *Environ Sci Technol*, 41, 1514-1521, 10.1021/es072476p, 2007.

Guenther, A. B., Jiang, X., Heald, C. L., Sakulyanontvittaya, T., Duhl, T., Emmons, L. K., and Wang, X.: The Model of Emissions of Gases and Aerosols from Nature version 2.1 (MEGAN2.1): an extended and updated framework for modeling biogenic emissions, *Geoscientific Model Development*, 5, 1471-1492, 10.5194/gmd-5-1471-2012, 2012.

Hallquist, M., Wenger, J. C., Baltensperger, U., Rudich, Y., Simpson, D., Claeys, M., Dommen, J., Donahue, N. M., George, C., Goldstein, A. H., Hamilton, J. F., Herrmann, H., Hoffmann, T., Iinuma, Y., Jang, M., Jenkin, M. E., Jimenez, J. L., Kiendler-Scharr, A., Maenhaut, W., McFiggans, G., Mentel, T. F., Monod, A., Prévôt, A. S. H., Seinfeld, J. H., Surratt, J. D., Szmigielski, R., and Wildt, J.: The formation, properties and impact of secondary organic aerosol: current and emerging issues, *Atmospheric Chemistry and Physics*, 9, 5155-5236, 10.5194/acp-9-5155-2009, 2009.

Hasson, A. S., Chung, M. Y., Kuwata, K. T., Converse, A. D., Krohn, D., and Paulson, S. E.: Reaction of Criegee Intermediates with Water Vapor: An Additional Source of OH Radicals in Alkene Ozonolysis?, *The Journal of Physical Chemistry A*, 107, 6176-6182, 10.1021/jp0346007, 2003.

Hays, M. D. and Lavrich, R. J.: Developments in direct thermal extraction gas chromatography-mass spectrometry of fine aerosols, *TrAC Trends in Analytical Chemistry*, 26, 88-102, 10.1016/j.trac.2006.08.007, 2007.

Hernandez, F., Sancho, J. V., and Pozo, O. J.: Critical review of the application of liquid chromatography/mass spectrometry to the determination of pesticide residues in biological samples, *Anal Bioanal Chem*, 382, 934-946, 10.1007/s00216-005-3185-5, 2005.

Hildebrandt, L., Henry, K. M., Kroll, J. H., Worsnop, D. R., Pandis, S. N., and Donahue, N. M.: Evaluating the mixing of organic aerosol components using high-resolution aerosol mass spectrometry, *Environ Sci Technol*, 45, 6329-6335, 10.1021/es200825g, 2011.

Ho, S. S. H., Chow, J. C., Watson, J. G., Ting Ng, L. P., Kwok, Y., Ho, K. F., and Cao, J.: Precautions for in-injection port thermal desorption-gas chromatography/mass spectrometry (TD-GC/MS) as applied to aerosol filter samples, *Atmospheric Environment*, 45, 1491-1496, 10.1016/j.atmosenv.2010.12.038, 2011.

Hoyle, C. R., Boy, M., Donahue, N. M., Fry, J. L., Glasius, M., Guenther, A., Hallar, A. G., Huff Hartz, K., Petters, M. D., Petäjä, T., Rosenoern, T., and Sullivan, A. P.: A review of the anthropogenic influence on biogenic secondary organic aerosol, *Atmospheric Chemistry and Physics*, 11, 321-343, 10.5194/acp-11-321-2011, 2011.

Huey, L. G.: Measurement of trace atmospheric species by chemical ionization mass spectrometry: speciation of reactive nitrogen and future directions, *Mass Spectrom Rev*, 26, 166-184, 10.1002/mas.20118, 2007.

Isaacman-VanWertz, G., Massoli, P., O'Brien, R. E., Nowak, J. B., Canagaratna, M. R., Jayne, J. T., Worsnop, D. R., Su, L., Knopf, D. A., Misztal, P. K., Arata, C., Goldstein, A. H., and Kroll, J. H.: Using advanced mass spectrometry techniques to fully characterize atmospheric organic carbon: current capabilities and remaining gaps, *Faraday Discuss*, 200, 579-598, 10.1039/c7fd00021a, 2017.

Jacob, D. J.: Heterogeneous chemistry and tropospheric ozone, *Atmospheric Environment* 34, 2131-2159, 2000.

Jennifer E. Stern, R. C. P., Daniel Grosjean, John H. Seinfeld: Aerosol Formation and Growth in Atmospheric Aromatic Hydrocarbon Photooxidation, *Environ. Sci. Technol.* , 21, 1224-1231, 1987.

Johnson, D. and Marston, G.: The gas-phase ozonolysis of unsaturated volatile organic compounds in the troposphere, *Chem Soc Rev*, 37, 699-716, 10.1039/b704260b, 2008.

Jonsson, Å. M., Hallquist, M., and Saathoff, H.: Volatility of secondary organic aerosols from the ozone initiated oxidation of  $\alpha$ -pinene and limonene, *Journal of Aerosol Science*, 38, 843-852, 10.1016/j.jaerosci.2007.06.008, 2007.

Joseph A. Leone, R. C. F., Daniel Grosjean, John H. Seinfeld: An Outdoor Smog Chamber and Modeling Study of Toluene-NO, Photooxidation *International Journal of Chemical Kinetics*, 17, 177-216, 1985.

Kallio, M., Hyötyläinen, T., Lehtonen, M., Jussila, M., Hartonen, K., Shimmo, M., and Riekkola, M.-L.: Comprehensive two-dimensional gas chromatography in the analysis of urban aerosols, *Journal of Chromatography A*, 1019, 251-260, 10.1016/s0021-9673(03)01238-x, 2003.

Kanakidou, M., Tsigaridis, K., Dentener, F. J., and Crutzen, P. J.: Human-activity-enhanced formation of organic aerosols by biogenic hydrocarbon oxidation, *Journal of Geophysical Research: Atmospheres*, 105, 9243-9354, 10.1029/1999jd901148, 2000.

Kanawade, V. P., Jobson, B. T., Guenther, A. B., Erupe, M. E., Pressley, S. N., Tripathi, S. N., and Lee, S. H.: Isoprene suppression of new particle formation in a mixed deciduous forest, *Atmospheric Chemistry and Physics*, 11, 6013-6027, 10.5194/acp-11-6013-2011, 2011.

Kiendler-Scharr, A., Wildt, J., Dal Maso, M., Hohaus, T., Kleist, E., Mentel, T. F., Tillmann, R., Uerlings, R., Schurr, U., and Wahner, A.: New particle formation in forests inhibited by isoprene emissions, *Nature*, 461, 381-384, 10.1038/nature08292, 2009.

Kroll, J. H. and Seinfeld, J. H.: Chemistry of secondary organic aerosol: Formation and evolution of low-volatility organics in the atmosphere, *Atmospheric Environment*, 42, 3593-3624, 10.1016/j.atmosenv.2008.01.003, 2008.

Kroll, J. H., Ng, N. L., Murphy, S. M., Flagan, R. C., and Seinfeld, J. H.: Secondary organic aerosol formation from isoprene photooxidation under high-NO<sub>x</sub> conditions, *Geophysical Research Letters*, 32, n/a-n/a, 10.1029/2005gl023637, 2005.

Laj, P., Klausen, J., Bilde, M., Plaß-Duelmer, C., Pappalardo, G., Clerbaux, C., Baltensperger, U., Hjorth, J., Simpson, D., Reimann, S., Coheur, P. F., Richter, A., De Mazière, M., Rudich, Y., McFiggans, G., Tørseth, K., Wiedensohler, A., Morin, S., Schulz, M., Allan, J. D., Attié, J. L., Barnes, I., Birmili, W., Cammas, J. P., Dommen, J., Dorn, H. P., Fowler, D., Fuzzi, S., Glasius, M., Granier, C., Hermann, M., Isaksen, I. S. A., Kinne, S., Koren, I., Madonna, F., Maione, M., Massling, A., Moehler, O., Mona, L., Monks, P. S., Müller, D., Müller, T., Orphal, J., Peuch, V. H., Stratmann, F., Tanré, D., Tyndall, G., Abo Rizeq, A., Van Roozendaal, M., Villani, P., Wehner, B., Wex, H., and Zardini, A. A.: Measuring atmospheric composition change, *Atmospheric Environment*, 43, 5351-5414, 10.1016/j.atmosenv.2009.08.020, 2009.

Lambe, A. T., Ahern, A. T., Williams, L. R., Slowik, J. G., Wong, J. P. S., Abbatt, J. P. D., Brune, W. H., Ng, N. L., Wright, J. P., Croasdale, D. R., Worsnop, D. R., Davidovits, P., and Onasch, T. B.: Characterization of aerosol photooxidation flow reactors: heterogeneous oxidation, secondary organic aerosol formation and cloud condensation nuclei activity measurements, *Atmospheric Measurement Techniques*, 4, 445-461, 10.5194/amt-4-445-2011, 2011.

Lee, B. H., Lopez-Hilfiker, F. D., Mohr, C., Kurten, T., Worsnop, D. R., and Thornton, J. A.: An iodide-adduct high-resolution time-of-flight chemical-ionization mass spectrometer: application to atmospheric inorganic and organic compounds, *Environ Sci Technol*, 48, 6309-6317, 10.1021/es500362a, 2014.

Lee, B. P., Li, Y. J., Yu, J. Z., Louie, P. K. K., and Chan, C. K.: Physical and chemical characterization of ambient aerosol by HR-ToF-AMS at a suburban site in Hong Kong during springtime 2011, *Journal of Geophysical Research: Atmospheres*, 118, 8625-8639, 10.1002/jgrd.50658, 2013.

Lee, S.-H., J. U., Alex B. Guenther, Alex B. Nadykto, J. H., Nga L. Ng., Karsten Baumann, V. P. K., and Kevin Olsen, A. G., Qi Ouyang: Isoprene suppression of new particle formation Potential mechanisms and implications, *Journal of Geophysical Research: Atmospheres*, 121,

14,621-614,635, 10.1002/2016JD024844., 2016.

Lester, M. I. and Klippenstein, S. J.: Unimolecular Decay of Criegee Intermediates to OH Radical Products: Prompt and Thermal Decay Processes, *Acc Chem Res*, 51, 978-985, 10.1021/acs.accounts.8b00077, 2018.

Li, Y. J., Lee, B. Y. L., Yu, J. Z., Ng, N. L., and Chan, C. K.: Evaluating the degree of oxygenation of organic aerosol during foggy and hazy days in Hong Kong using high-resolution time-of-flight aerosol mass spectrometry (HR-ToF-AMS), *Atmospheric Chemistry and Physics*, 13, 8739-8753, 10.5194/acp-13-8739-2013, 2013.

Lopez-Hilfiker, F. D., Mohr, C., Ehn, M., Rubach, F., Kleist, E., Wildt, J., Mentel, T. F., Lutz, A., Hallquist, M., Worsnop, D., and Thornton, J. A.: A novel method for online analysis of gas and particle composition: description and evaluation of a Filter Inlet for Gases and AEROSols (FIGAERO), *Atmospheric Measurement Techniques*, 7, 983-1001, 10.5194/amt-7-983-2014, 2014.

Loza, C. L., Coggon, M. M., Nguyen, T. B., Zuend, A., Flagan, R. C., and Seinfeld, J. H.: On the mixing and evaporation of secondary organic aerosol components, *Environ Sci Technol*, 47, 6173-6180, 10.1021/es400979k, 2013.

M. Kalberer, D. P., M. Sax, M. Steinbacher, J. Dommen, A. S. H. P., R. Fisseha, E. Weingartner, and V. Frankevich, R. Z., U. Baltensperger: Identification of Polymers as Major Components of Atmospheric Organic Aerosols, *science report*, 303, 1659-1662, 2004.

Mauldin, R. L., 3rd, Berndt, T., Sipila, M., Paasonen, P., Petaja, T., Kim, S., Kurten, T., Stratmann, F., Kerminen, V. M., and Kulmala, M.: A new atmospherically relevant oxidant of sulphur dioxide, *Nature*, 488, 193-196, 10.1038/nature11278, 2012.

McFiggans, G., Mentel, T. F., Wildt, J., Pullinen, I., Kang, S., Kleist, E., Schmitt, S., Springer, M., Tillmann, R., Wu, C., Zhao, D., Hallquist, M., Faxon, C., Le Breton, M., Hallquist, A. M., Simpson, D., Bergstrom, R., Jenkin, M. E., Ehn, M., Thornton, J. A., Alfarra, M. R., Bannan, T. J., Percival, C. J., Priestley, M., Topping, D., and Kiendler-Scharr, A.: Secondary organic aerosol reduced by mixture of atmospheric vapours, *Nature*, 565, 587-593, 10.1038/s41586-018-0871-y, 2019.

McLuckey, S. A. and Wells, J. M.: Mass analysis at the advent of the 21st century, *Chem Rev*, 101, 571-606, 10.1021/cr990087a, 2001.

McMurry, P.: A review of atmospheric aerosol measurements, *Atmospheric Environment*, 34, 1959-1999, 10.1016/s1352-2310(99)00455-0, 2000.

Mehra, A., Wang, Y., Krechmer, J. E., Lambe, A., Majluf, F., Morris, M. A., Priestley, M., Bannan, T. J., Bryant, D. J., Pereira, K. L., Hamilton, J. F., Rickard, A. R., Newland, M. J., Stark, H., Croteau, P., Jayne, J. T., Worsnop, D. R., Canagaratna, M. R., Wang, L., and Coe, H.: Evaluation of the chemical composition of gas- and particle-phase products of aromatic oxidation, *Atmospheric Chemistry and Physics*, 20, 9783-9803, 10.5194/acp-20-9783-2020, 2020.

Mutzel, A., Poulain, L., Berndt, T., Iinuma, Y., Rodigast, M., Boge, O., Richters, S., Spindler,

G., Sipila, M., Jokinen, T., Kulmala, M., and Herrmann, H.: Highly Oxidized Multifunctional Organic Compounds Observed in Tropospheric Particles: A Field and Laboratory Study, *Environ Sci Technol*, 49, 7754-7761, 10.1021/acs.est.5b00885, 2015.

Ng, N. L., Kroll, J. H., Chan, A. W. H., Chhabra, P. S., Flagan, R. C., and Seinfeld, J. H.: Secondary organic aerosol formation from  $\alpha$ -xylene, toluene, and benzene, *Atmospheric Chemistry and Physics*, 7, 3909-3922, 10.5194/acp-7-3909-2007, 2007.

Ng, N. L., Kroll, J. H., Keywood, M. D., Bahreini, R., Varutbangkul, V., Flagan, R. C., Seinfeld, J. H., Lee, A., and Goldstein, A. H.: Contribution of first- versus second-generation products to secondary organic aerosols formed in the oxidation of biogenic hydrocarbons, *Environ Sci Technol*, 40, 2283-2297, 10.1021/es052269u, 2006.

Ng, N. L., Kwan, A. J., Surratt, J. D., Chan, A. W. H., Chhabra, P. S., Sorooshian, A., Pye, H. O. T., Crouse, J. D., Wennberg, P. O., Flagan, R. C., and Seinfeld, J. H.: Secondary organic aerosol (SOA) formation from reaction of isoprene with nitrate radicals ( $\text{NO}_3$ ), *Atmospheric Chemistry and Physics*, 8, 4117-4140, 10.5194/acp-8-4117-2008, 2008.

Odum, Thorsten Hoffmann, Frank Bowman, Don Collins, and Richard C. Flagan, a. J. H. S.: Gas/Particle Partitioning and Secondary Organic Aerosol Yields, *Environ. Sci. Technol*, 30, 2580-2585, <https://doi-org.manchester.idm.oclc.org/10.1021/es950943+>, 1996a.

Odum, Thorsten Hoffmann, Frank Bowman, Don Collins, Richard C. Flagan, and Seinfeld, J. H.: Gas/Particle Partitioning and Secondary Organic Aerosol Yields, *Environ. Sci. Technol*, 30, 2580-2585, <https://doi-org.manchester.idm.oclc.org/10.1021/es950943+>, 1996b.

Osthoff, H. D., Roberts, J. M., Ravishankara, A. R., Williams, E. J., Lerner, B. M., Sommariva, R., Bates, T. S., Coffman, D., Quinn, P. K., Dibb, J. E., Stark, H., Burkholder, J. B., Talukdar, R. K., Meagher, J., Fehsenfeld, F. C., and Brown, S. S.: High levels of nitryl chloride in the polluted subtropical marine boundary layer, *Nature Geoscience*, 1, 324-328, 10.1038/ngeo177, 2008.

Pankow, J. F.: An absorption model of the gas/aerosol partitioning involved in the formation of secondary organic aerosol, *Atmospheric Environment*, 28, 189-193, 10.1016/1352-2310(94)90094-9, 1994.

Pathak, R. K., Presto, A. A., Lane, T. E., Stanier, C. O., Donahue, N. M., and Pandis, S. N.: Ozonolysis of  $\alpha$ -pinene: parameterization of secondary organic aerosol mass fraction, *Atmospheric Chemistry and Physics*, 7, 3811-3821, 10.5194/acp-7-3811-2007, 2007.

Paulot, F., Crouse, J. D., Kjaergaard, H. G., Kurten, A., St Clair, J. M., Seinfeld, J. H., and Wennberg, P. O.: Unexpected epoxide formation in the gas-phase photooxidation of isoprene, *Science*, 325, 730-733, 10.1126/science.1172910, 2009.

Percival, C. J., Welz, O., Eskola, A. J., Savee, J. D., Osborn, D. L., Topping, D. O., Lowe, D., Utembe, S. R., Bacak, A., McFiggans, G., Cooke, M. C., Xiao, P., Archibald, A. T., Jenkin, M. E., Derwent, R. G., Riipinen, I., Mok, D. W., Lee, E. P., Dyke, J. M., Taatjes, C. A., and Shallcross, D. E.: Regional and global impacts of Criegee intermediates on atmospheric sulphuric acid concentrations and first steps of aerosol formation, *Faraday Discuss*, 165, 45-73,

10.1039/c3fd00048f, 2013.

Presto, A. A. and Donahue, N. M.: Investigation of alpha-pinene + ozone secondary organic aerosol formation at low total aerosol mass, *Environ Sci Technol*, 40, 3536-3543, 10.1021/es052203z, 2006.

Presto, A. A., Hartz, K. E., and Donahue, N. M.: Secondary organic aerosol production from terpene ozonolysis. 2. Effect of NO<sub>x</sub> concentration, *Environ Sci Technol*, 39, 7046-7054, 10.1021/es050400s, 2005.

Pullinen, L. I. M.: Photochemistry of Highly Oxidized Multifunctional Organic Molecules a Chamber Study Institute of Energy and Climate Research  
*Troposphere*, 2017.

Pye, H. O. T., D'Ambro, E. L., Lee, B. H., Schobesberger, S., Takeuchi, M., Zhao, Y., Lopez-Hilfiker, F., Liu, J., Shilling, J. E., Xing, J., Mathur, R., Middlebrook, A. M., Liao, J., Welti, A., Graus, M., Warneke, C., de Gouw, J. A., Holloway, J. S., Ryerson, T. B., Pollack, I. B., and Thornton, J. A.: Anthropogenic enhancements to production of highly oxygenated molecules from autoxidation, *Proc Natl Acad Sci U S A*, 116, 6641-6646, 10.1073/pnas.1810774116, 2019.

Quéléver, L. L. J., Kristensen, K., Normann Jensen, L., Rosati, B., Teiwes, R., Daellenbach, K. R., Peräkylä, O., Roldin, P., Bossi, R., Pedersen, H. B., Glasius, M., Bilde, M., and Ehn, M.: Effect of temperature on the formation of highly oxygenated organic molecules (HOMs) from alpha-pinene ozonolysis, *Atmospheric Chemistry and Physics*, 19, 7609-7625, 10.5194/acp-19-7609-2019, 2019.

Riedel, T. P., Bertram, T. H., Crisp, T. A., Williams, E. J., Lerner, B. M., Vlasenko, A., Li, S. M., Gilman, J., de Gouw, J., Bon, D. M., Wagner, N. L., Brown, S. S., and Thornton, J. A.: Nitryl chloride and molecular chlorine in the coastal marine boundary layer, *Environ Sci Technol*, 46, 10463-10470, 10.1021/es204632r, 2012.

Robert C. Chapleski Jr., Y. Z., Diego Troya, John R. Morris: Heterogeneous chemistry and reaction dynamics of the atmospheric oxidants, O<sub>3</sub>, NO<sub>3</sub>, and OH, on organic surfaces, *Chem. Soc. Rev* 2016.

Rohrer, F., Bohn, B., Brauers, T., Brüning, D., Johnen, F. J., Wahner, A., and Kleffmann, J.: Characterisation of the photolytic HONO-source in the atmosphere simulation chamber SAPHIR, *Atmospheric Chemistry and Physics*, 5, 2189-2201, 10.5194/acp-5-2189-2005, 2005.

Rosati, B., Teiwes, R., Kristensen, K., Bossi, R., Skov, H., Glasius, M., Pedersen, H. B., and Bilde, M.: Factor analysis of chemical ionization experiments: Numerical simulations and an experimental case study of the ozonolysis of  $\alpha$ -pinene using a PTR-ToF-MS, *Atmospheric Environment*, 199, 15-31, 10.1016/j.atmosenv.2018.11.012, 2019.

Safi Shalamzari, M., Ryabtsova, O., Kahnt, A., Vermeylen, R., Herent, M. F., Quetin-Leclercq, J., Van der Veken, P., Maenhaut, W., and Claeys, M.: Mass spectrometric characterization of organosulfates related to secondary organic aerosol from isoprene, *Rapid Commun Mass Spectrom*, 27, 784-794, 10.1002/rcm.6511, 2013.

Sarwar, G., Fahey, K., Kwok, R., Gilliam, R. C., Roselle, S. J., Mathur, R., Xue, J., Yu, J., and Carter, W. P. L.: Potential impacts of two SO<sub>2</sub> oxidation pathways on regional sulfate concentrations: Aqueous-phase oxidation by NO<sub>2</sub> and gas-phase oxidation by Stabilized Criegee Intermediates, *Atmospheric Environment*, 68, 186-197, 10.1016/j.atmosenv.2012.11.036, 2013.

Sato, K., Hatakeyama, S., and Imamura, T.: Secondary organic aerosol formation during the photooxidation of toluene: NO<sub>x</sub> dependence of chemical composition, *J Phys Chem A*, 111, 9796-9808, 10.1021/jp071419f, 2007.

Sato, K., Takami, A., Kato, Y., Seta, T., Fujitani, Y., Hikida, T., Shimono, A., and Imamura, T.: AMS and LC/MS analyses of SOA from the photooxidation of benzene and 1,3,5-trimethylbenzene in the presence of NO<sub>x</sub>: effects of chemical structure on SOA aging, *Atmospheric Chemistry and Physics*, 12, 4667-4682, 10.5194/acp-12-4667-2012, 2012.

Schild, A., Gutsch, A., Mühlenweg, H., and Pratsinis, S. E.: <Schild1999\_Article\_SimulationOfNanoparticleProduc.pdf>, *Journal of Nanoparticle Research*, 1, 305-315, 10.1023/a:1010025121980, 1999.

Seinfeld, J. H. and Pandis, S. N.: *Atmospheric chemistry and physics : from air pollution to climate change*, Third edition., John Wiley & Sons, Hoboken, New Jersey 2016.

Seinfeld, J. H., Kleindienst, T. E., Edney, E. O., and Cohen, J. B.: Aerosol Growth in a Steady-State, Continuous Flow Chamber: Application to Studies of Secondary Aerosol Formation, *Aerosol Science and Technology*, 37, 728-734, 10.1080/02786820300915, 2003.

Shao, Y., Wang, Y., Du, M., Voliotis, A., Alfarra, M. R., Turner, S. F., and McFiggans, G.: Characterisation of the Manchester Aerosol Chamber facility, *Atmospheric measurement techniques*, 10.5194/amt-2021-147, 2021.

Shilling, J. E., Zaveri, R. A., Fast, J. D., Kleinman, L., Alexander, M. L., Canagaratna, M. R., Fortner, E., Hubbe, J. M., Jayne, J. T., Sedlacek, A., Setyan, A., Springston, S., Worsnop, D. R., and Zhang, Q.: Enhanced SOA formation from mixed anthropogenic and biogenic emissions during the CARES campaign, *Atmospheric Chemistry and Physics*, 13, 2091-2113, 10.5194/acp-13-2091-2013, 2013.

Spracklen, D. V., Jimenez, J. L., Carslaw, K. S., Worsnop, D. R., Evans, M. J., Mann, G. W., Zhang, Q., Canagaratna, M. R., Allan, J., Coe, H., McFiggans, G., Rap, A., and Forster, P.: Aerosol mass spectrometer constraint on the global secondary organic aerosol budget, *Atmospheric Chemistry and Physics*, 11, 12109-12136, 10.5194/acp-11-12109-2011, 2011.

Stefano Decesari, M. M., Fabrizia Cavalli, Sandro Fuzzi, Fabio Moretti, Emilio Tagliavini, Maria Cristina Facchini Source Attribution of Water-Soluble Organic Aerosol by Nuclear Magnetic Resonance Spectroscopy, *Environ. Sci. Technol.*, 41, 2479-2484, 2007.

Steimer, S. S., Delvaux, A., Campbell, S. J., Gallimore, P. J., Grice, P., Howe, D. J., Pitton, D., Claeys, M., Hoffmann, T., and Kalberer, M.: Synthesis and characterisation of peroxydic acids as proxies for highly oxygenated molecules (HOMs) in secondary organic aerosol, *Atmospheric Chemistry and Physics*, 18, 10973-10983, 10.5194/acp-18-10973-2018, 2018.



Surratt, J. D., Chan, A. W., Eddingsaas, N. C., Chan, M., Loza, C. L., Kwan, A. J., Hersey, S. P., Flagan, R. C., Wennberg, P. O., and Seinfeld, J. H.: Reactive intermediates revealed in secondary organic aerosol formation from isoprene, *Proc Natl Acad Sci U S A*, 107, 6640-6645, 10.1073/pnas.0911114107, 2010.

Tu, P., Hall, W. A. t., and Johnston, M. V.: Characterization of Highly Oxidized Molecules in Fresh and Aged Biogenic Secondary Organic Aerosol, *Anal Chem*, 88, 4495-4501, 10.1021/acs.analchem.6b00378, 2016.

Vereecken, L. and Francisco, J. S.: Theoretical studies of atmospheric reaction mechanisms in the troposphere, *Chem Soc Rev*, 41, 6259-6293, 10.1039/c2cs35070j, 2012.

Vivanco, M. G., Santiago, M., Martínez-Tarifa, A., Borrás, E., Ródenas, M., García-Diego, C., and Sánchez, M.: SOA formation in a photoreactor from a mixture of organic gases and HONO for different experimental conditions, *Atmospheric Environment*, 45, 708-715, 10.1016/j.atmosenv.2010.09.059, 2011.

Wang, J., Doussin, J. F., Perrier, S., Perraudin, E., Katrib, Y., Pangui, E., and Picquet-Varrault, B.: Design of a new multi-phase experimental simulation chamber for atmospheric photo-smog, aerosol and cloud chemistry research, *Atmospheric Measurement Techniques*, 4, 2465-2494, 10.5194/amt-4-2465-2011, 2011.

Wang, S., Riva, M., Yan, C., Ehn, M., and Wang, L.: Primary Formation of Highly Oxidized Multifunctional Products in the OH-Initiated Oxidation of Isoprene: A Combined Theoretical and Experimental Study, *Environ Sci Technol*, 52, 12255-12264, 10.1021/acs.est.8b02783, 2018.

Wang, X., Liu, T., Bernard, F., Ding, X., Wen, S., Zhang, Y., Zhang, Z., He, Q., Lü, S., Chen, J., Saunders, S., and Yu, J.: Design and characterization of a smog chamber for studying gas-phase chemical mechanisms and aerosol formation, *Atmospheric Measurement Techniques*, 7, 301-313, 10.5194/amt-7-301-2014, 2014.

Warnke, J., Bandur, R., and Hoffmann, T.: Capillary-HPLC-ESI-MS/MS method for the determination of acidic products from the oxidation of monoterpenes in atmospheric aerosol samples, *Analytical and bioanalytical chemistry*, 385, 34-45, 10.1007/s00216-006-0340-6, 2006.

Weber, R. J., Sullivan, A. P., Peltier, R. E., Russell, A., Yan, B., Zheng, M., de Gouw, J., Warneke, C., Brock, C., Holloway, J. S., Atlas, E. L., and Edgerton, E.: A study of secondary organic aerosol formation in the anthropogenic-influenced southeastern United States, *Journal of Geophysical Research: Atmospheres*, 112, 10.1029/2007jd008408, 2007.

Wiles, C. and Watts, P.: Continuous flow reactors: a perspective, *Green Chem.*, 14, 38-54, 10.1039/c1gc16022b, 2012.

Woojin Lee, M. B., Philips. Stevens, Ronald. Hites Monitoring OH-Initiated Oxidation Kinetics of Isoprene and Its Products Using Online Mass Spectrometry, *Environ. Sci. Technol*, 39, 1030-1036, 2005.

Xu, L., Guo, H., Weber, R. J., and Ng, N. L.: Chemical Characterization of Water-Soluble

Organic Aerosol in Contrasting Rural and Urban Environments in the Southeastern United States, *Environ Sci Technol*, 51, 78-88, 10.1021/acs.est.6b05002, 2017.

Xu, Y., Jia, L., Ge, M., Du, L., Wang, G., and Wang, D.: A kinetic study of the reaction of ozone with ethylene in a smog chamber under atmospheric conditions, *Chinese Science Bulletin*, 51, 2839-2843, 10.1007/s11434-006-2180-3, 2006.

Yoshiteru Iinuma, T. B., Olaf Boge, Magda Claeys, Hartmut Herrmann: Evidence for the Existence of Organosulfates from  $\alpha$ -Pinene Ozonolysis in Ambient Secondary Organic Aerosol, *Environ.Sci.Technol*, 41, 6678-6683, 10.1021/es070938t 2007.

Young, C. J., Washenfelder, R. A., Edwards, P. M., Parrish, D. D., Gilman, J. B., Kuster, W. C., Mielke, L. H., Osthoff, H. D., Tsai, C., Pikel'naya, O., Stutz, J., Veres, P. R., Roberts, J. M., Griffith, S., Dusanter, S., Stevens, P. S., Flynn, J., Grossberg, N., Lefer, B., Holloway, J. S., Peischl, J., Ryerson, T. B., Atlas, E. L., Blake, D. R., and Brown, S. S.: Chlorine as a primary radical: evaluation of methods to understand its role in initiation of oxidative cycles, *Atmospheric Chemistry and Physics*, 14, 3427-3440, 10.5194/acp-14-3427-2014, 2014.

Yu, Z.: Chamber study of biogenic volatile organic compounds plant emission, oxidation products and their OH reactivity 2018, 2018.

Zador, J., Wagner, V., Wirtz, K., and Pilling, M.: Quantitative assessment of uncertainties for a model of tropospheric ethene oxidation using the European Photoreactor (EUPHORE), *Atmospheric Environment*, 39, 2805-2817, 10.1016/j.atmosenv.2004.06.052, 2005.

Zhang, X., Ortega, J., Huang, Y., Shertz, S., Tyndall, G. S., and Orlando, J. J.: A steady-state continuous flow chamber for the study of daytime and nighttime chemistry under atmospherically relevant NO levels, *Atmospheric Measurement Techniques*, 11, 2537-2551, 10.5194/amt-11-2537-2018, 2018.

Zhang, X., Lambe, A. T., Upshur, M. A., Brooks, W. A., Gray Be, A., Thomson, R. J., Geiger, F. M., Surratt, J. D., Zhang, Z., Gold, A., Graf, S., Cubison, M. J., Groessl, M., Jayne, J. T., Worsnop, D. R., and Canagaratna, M. R.: Highly Oxygenated Multifunctional Compounds in  $\alpha$ -Pinene Secondary Organic Aerosol, *Environ Sci Technol*, 51, 5932-5940, 10.1021/acs.est.6b06588, 2017.

Zhao, R., Lee, A. K., and Abbatt, J. P.: Investigation of aqueous-phase photooxidation of glyoxal and methylglyoxal by aerosol chemical ionization mass spectrometry: observation of hydroxyhydroperoxide formation, *The journal of physical chemistry. A*, 116, 6253-6263, 10.1021/jp211528d, 2012.

[BLANK PAGE]

## Chapter 3. Methodology and Instrumentation

### 3.1 Chamber description and experimental design

#### 3.1.1 Chamber description

The Manchester Aerosol Chamber (MAC) is located at the University of Manchester. The MAC is operated as a batch reactor with a 18m<sup>3</sup> (3L × 2W × 3H) FEP Teflon bag. The MAC is detailed in the first paper, see Section 4.1. Briefly, the MAC is housed in a rectangular enclosure with an extruded aluminum framework. Four pieces of Teflon films are installed in three frames with one central fixed frame and two movable upper and down frames. The upper and down frames are counter-weighted to enable the bag to expand and collapse when sample air is introduced and extracted in the process of fill/flush cycles and sampling. There are two 6 kW arc Xenon lamps (XBO 6000 W/HSLA OFR, Osram) installed on the bottom-left and the top-right of the chamber housing with 112 halogen lamps (7 rows of 16 bulbs each row, Solux 50W/4700K, Solux MR16, USA). Usually, the combination of 5 rows bulbs and 2 arc Xenon lamps are deployed to mimic the solar light spectra over the wavelength range of 290-800 nm (Alfarra et al., 2012). An air conditioning unit, a circulating water system in front of the Xenon lamps and a chiller are utilized to remove the unwanted heat energy from the irradiation sources and to keep a stable temperature in the chamber.

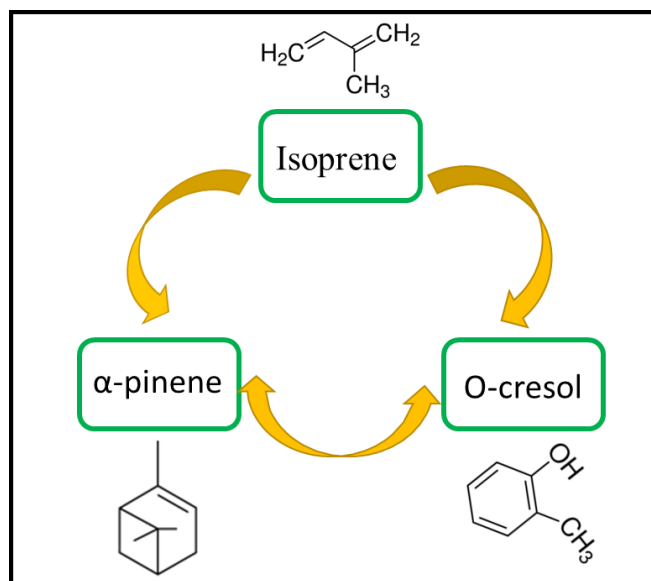
A custom-built automatic control system was designed to regulate the chamber operational procedures and devices conveniently, repeatably and precisely, such as fill/flush cycles, injection procedure, VOC bulb heating, humidifier, seed injection and ozoniser operation. All component switches are controlled from a home-built PLC board, with all control signals processed using ladder logic and communicating with a graphical front end in Visual Basic. All components are controlled by the Programmable Logic Controller (PLC). This is detailed in Section 4.1 of paper 1. The experimental conditions of the chamber are under control during the experiments, such as the relative humidity, temperature, the gaseous and seed particle concentrations. A batch of analytical techniques is equipped to measure the gas- and particle phase in the chamber. The simplified schematic of MAC is shown in Figure 1 of Paper 1.

### 3.1.2 Experimental design

In this project, the whole overview of the rational theory behind the experimental design is illustrated in Paper 2, see Section 4.2. Briefly,  $\alpha$ -pinene (Sigma-Aldrich,  $\geq 99.99\%$ ) is regarded as the representative of biogenic VOCs from monoterpenes due to the highest emissions in the atmosphere (Presto and Donahue, 2006). Isoprene (Sigma-Aldrich,  $\geq 99.99\%$ ) is chosen to represent terpenoids emission (Kroll et al., 2005). Ortho-cresol (o-cresol thereafter, Sigma-Aldrich,  $\geq 99.99\%$ ) which is generated from the oxidation of toluene, particularly in anthropogenic polluted areas is considered as representative anthropogenic VOCs (Seinfeld and Pandis, 2016). The reasons for choosing the o-cresol are i) the oxidation of toluene can produce four first-generation products which will make the processes more complicated if toluene was chosen as the representative of anthropogenic VOCs. O-cresol as the major contributor of aromatic compounds to the oxidation of toluene was chosen to act as the representative of anthropogenic VOCs; ii) most of the studies have been focused on the toluene rather than o-cresol, thus, there are many uncertainties on the research of o-cresol and o-cresol mixed systems.

Generally, the OH oxidant is produced from the photolysis of  $\text{NO}_2$  in our experiments and is considered as the main oxidant under our photooxidation conditions. The  $\alpha$ -pinene and isoprene will react with ozone to generate appreciable SOA products due to the carbon-carbon double bond, while the o-cresol is unable to react with ozone. Therefore, the initial concentrations of individual VOC and mixtures are decided according to the same reaction reactivity with OH radicals compared with isoprene to the OH oxidant concentrations (call it iso-reactivity in this study). This design can ensure the three VOCs produce a comparable amount of oxidation products at the beginning of experiments. The rate coefficients of OH-initiated chemical reactions are shown in Table 3.1, which refers to the values from IUPAC (<https://iupac-aeris.ipsl.fr/>). Additionally, appreciable aerosol mass is required in the chamber in order to perform the offline data analysis at the end of each experiment. Based on the two principles, the higher reactivity of VOC precursors with OH, the less will be injected into the chamber. As a result, the targeted initial concentrations of o-cresol were 400 ppb, 200 ppb and 133 ppb for the single experiment, binary system and ternary systems, respectively. The corresponding targeted initial concentrations of isoprene concentration were designed to 164 ppb, 82 ppb and 55 ppb in the single experiment, binary system and ternary systems,

respectively.. 309 ppb, 155 ppb and 103 ppb of initial targeted  $\alpha$ -pinene concentration were used for a single experiment, binary system and ternary systems, respectively.



**Figure 3.2.** Structure of  $\alpha$ -pinene, isoprene and o-cresol and experiments designed according to this scheme.

**Table 3.1.** Rate coefficients of  $\alpha$ -pinene, isoprene and o-cresol reacting with OH at 298K

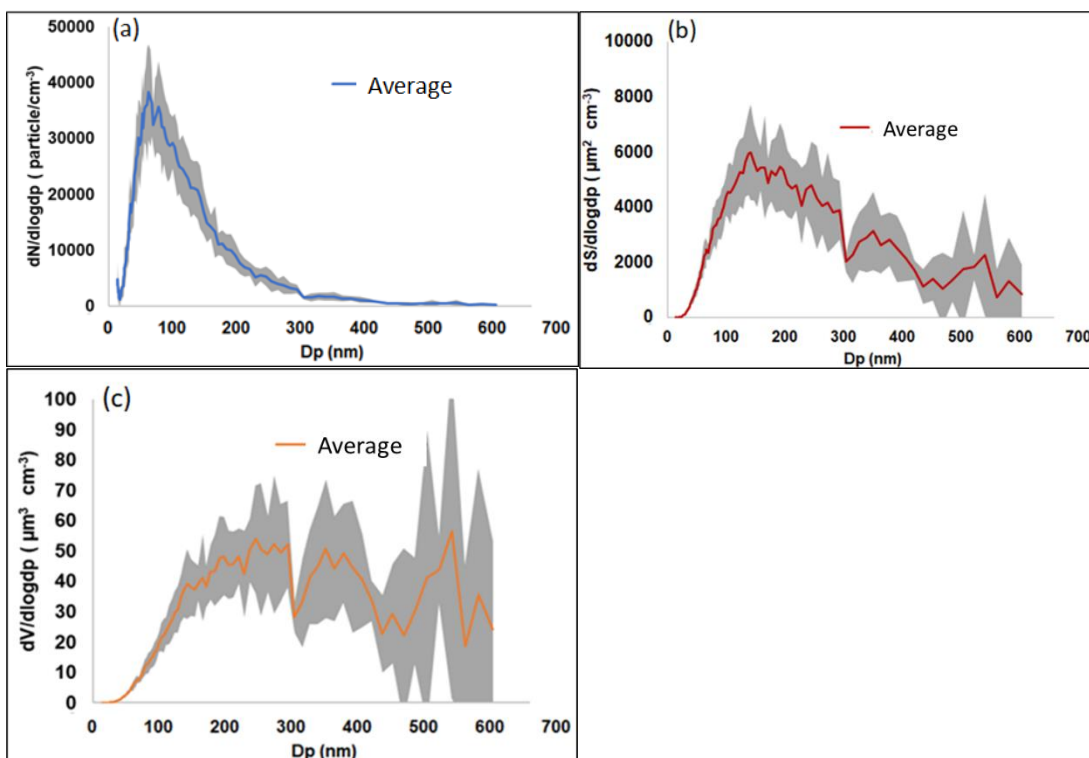
| VOCs             | Oxidant | Rate coefficient at 298K ( $\text{k}/\text{cm}^3 \text{molecule}^{-1} \text{s}^{-1}$ ) |
|------------------|---------|--|
| $\alpha$ -pinene | OH      | $5.3 \times 10e^{-11}$   |
| isoprene         | OH      | $1.0 \times 10e^{-10}$   |
| o-cresol         | OH      | $4.1 \times 10e^{-11}$   |

### 3.1.3 Experimental procedure

A series of experiments are designed and conducted to observe the photooxidation reactions in individual  $\alpha$ -pinene, isoprene and o-cresol and their mixtures (including binary and ternary systems) under moderate  $\text{NO}_x$  conditions in the presence of ammonia sulphate (AS) seed particles. The experimental procedures are shown below. First, the chamber was cleaned by several fill/flush cycles (including cleaning the VOCs bulbs) with purified air through three filters (the first canister containing Purafil/charcoal, the second containing activated charcoal, and the third with a Hepa filter to remove the  $\text{NO}_x$ , volatile organic compounds and particles) at a high flow rate of  $3 \text{ m}^3 \text{ min}^{-1}$  for  $\sim 1.5 \text{ h}$  before each experiment. At end of each experiment,  $\sim 1$ -hour post-experiments was conducted to clean the chamber and then a high concentration

of O<sub>3</sub> (more than 700ppb) was fed into the chamber to further oxidize the potential contaminants in the chamber overnight. Additionally, harsh cleaning was carried out weekly, with high ozone concentration (~1ppm) inside the chamber and at least 4-hour photooxidation reactions under strong irradiation. Those procedures ensured a very lower chamber background before each experiment (particle concentrations <15 # cm<sup>-3</sup>, particle mass concentration ~0 μg m<sup>-3</sup>, O<sub>3</sub> concentrations ~0ppb and NO<sub>x</sub> concentration < 10ppb (NO < 8ppb and NO<sub>2</sub>< 2ppb).

The concentrations of liquid parent VOCs were injected into the heated gaseous injection port (preheating the bulb for 15min to a maximum of 80°C) and flushed into the chamber by ECD grade N<sub>2</sub> (N4.8; purity 99.998%; N<sub>2</sub>) at a flow 0.5bar. NO<sub>x</sub> (custom-made cylinder: 10% v/v NO<sub>2</sub> and 90% v/v N<sub>2</sub>) was added to the chamber and flushed into the chamber with the ECD grade N<sub>2</sub> as the carrier gas. The mixing ratio of NO<sub>2</sub> was controlled via a mass flow controller. Ammonium sulfate (AS, 1g AS dissolving in 100ml deionized water) acted as seeds were introduced into the chamber via the atomizer (Topaz model ATM 230) subsequently. The size distribution of AS seeds and the experimental repeatability of size distribution is shown in Figure 3.3, which shows consistent size distributions of injected AS seeds aerosols across experiments. Relative humidity of the chamber was controlled by the custom-built humidifier which comprises a 50L tank fed with ultra-pure water (resistivity ≥18.2 MΩ-cm), producing water vapour using an immersion heater. The temperature in the chamber was controlled by the cooling systems (air conditioner, water circulation systems and a chiller). All experiments were conducted at room temperature (around 25 °C) and relative humidity of ~50 %. Before initiating the photooxidation reactions, a ~1-hour dark equilibration period with the clean air in the chamber was conducted to measure the chamber background. Another 1-hour dark equilibration period with the precursors and seeds in the chamber was requested to measure the background of seeds and VOC concentrations. Each experiment was performed under replication of the atmospheric actinic spectrum and kept constant for 6-hour photooxidation reactions. The initial VOCs/NO<sub>x</sub> ranges from 4 to 12, and the initial conditions of the experiments are summarized in Table 1 of Paper 2.



**Figure 3.3.** (a) the size distribution of seeds aerosols (mean  $\pm 1\sigma$ ,  $n=6$ ) before photooxidation experiments initiated ( $t=0$ ). The surface area ( $dS/d\log dp$ ) (b) and volume ( $dV/d\log dp$ ) (c) size distributions were calculated assuming spherical particles.

## 3.2 Instrumentation

### 3.2.1 TOF-CIMS and FIGAERO

A Time-of-Flight Chemical Ionization Mass Spectrometer (TOF-CIMS) developed by Aerodyne Research Inc. and ToFwerk is widely deployed in the atmospheric science community. This technique is made of five important sections and is described in detail by Lee et al. (2014). In this project, the iodide reagent ions are used.

The real-time TOF-CIMS measurement uses the chemical ionization method to measure the gas-phase oxidation products. Here, the chamber air is sampled through a critical orifice at 1slm via a 0.5 m  $\frac{1}{4}$ " I.D. PFA tubing into the ion molecular reactor (IMR) chamber (Fig 3.4, S1). The IMR chamber is pumped by a dry scroll pump (Varian SH-110) at  $100 \text{ L min}^{-1}$ , which is typically throttled down to achieve a sampling pressure of 100 mbar. In this application, reagent iodide ions ( $I^-$ ) are formed by passing trace  $\text{CH}_3\text{I}$  in ultra-high purity (UHP) nitrogen ( $\text{N}_2$ , 99.9995 %) through a commercial  $^{210}\text{Po}$  alpha emitter (NRD, P-2021 EOL Ionizer). The



entire IMR chamber, including the ionizer, is electrically isolated and biased to -100V to facilitate the efficient transport of ions to the entrance aperture of the second pumping stage.

The molecules with iodide adduct then go through the short segmented quadrupole (SSQ) and big segmented quadrupole (BSQ) (Fig 3.4, S2 and S3 respectively). Direct current and radio frequency are applied in the two rods of the two quadrupoles. The function of the SSQ and BSQ is to dissociate or preserve weakly bound molecular clusters according to the electrical field strength. The iodide adducts will be a beam with energetically homogenize (Fig 3.4, S4) and then those ions enter into the ToF path by the extractor. This pulse accelerates all ions through the flight tube simultaneously, thus separating purely based on their mass to charge ratio by the equation:

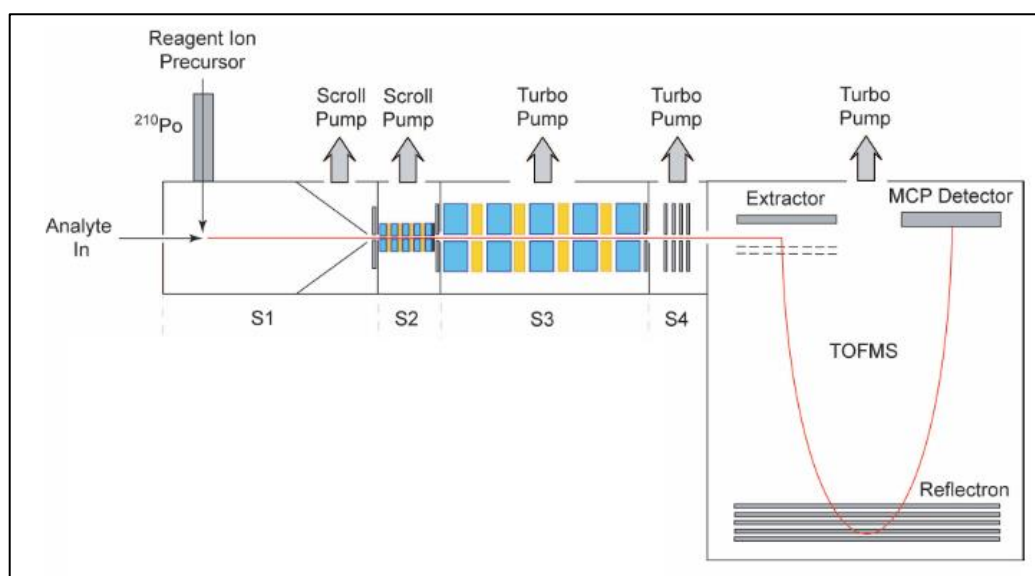
$$t = \sqrt{\left(\frac{m}{q}\right) \cdot \frac{d}{\sqrt{2V}}}$$

where  $t$  is time to reach the detector,  $m$  is mass,  $q$  is the charge,  $d$  is the constant distance to the detector and  $V$  is a constant voltage applied.

Time-of-flight mass spectrometry was used to separate the ions in the TOF-CIMS measurement. Ions with smaller mass-to-charge ratios will be detected earlier as they have higher movement velocities at the same kinetic energy. The detector can be configured to monitor either positive or negative ions. These ions can travel through the ToF either with a single reflectron (V-mode), which offers higher sensitivity, or a double reflectron (W-mode), which offers higher mass resolution (Yatavelli et al., 2012). The reflectron provides a constant electrostatic field to reflect the ion beam to the detector, with more energetic ions penetrating deeper into the reflectron and thus taking a longer path to the detector, and less energetic ions a shorter path. The TOF-MS resolution of online measurement was set around 4000 Th/Th in this study. Analyte ions are finally detected at the microchannel plate (MCP).

The possibility of ions detected by the detector is heavily dependent on the ionization probability of neutral molecules and the probability of detection of formed ions. The ionization process largely relies on the nature of parent ions. Theoretically, the neutral molecules can form strong bound clusters with reagent ions (e.g., iodides, acetic acid and nitrates) at the collision limit in the ion molecular reactor (IMR). Chemical properties of different reagent ions (e.g.,

$\text{NH}_4^+$ ,  $\text{NO}_3^-$ ,  $\text{H}_3\text{O}^+$ , etc) have been studied computationally in recent years and successfully reproduced in several observations (Hyttinen et al., 2015; Hyttinen et al., 2018). The issue of the I-clusters is that they have weak bound strength which may undergo declustering in the process of transmission to the detector, reducing the possibility of ions being detected by the detector (Riva et al., 2019). Additionally, Lee et al. (2014) found that iodide adducts can cause molecules to fragment (e.g. peroxy acids decomposing to carboxylate anions). Both declustering and fragmentations processes reduce the detector's sensitivity to ions. The solution for this issue remains challenging even though some researchers have been proposed approaches to solve it, such as voltage scans (Lopez-Hilfiker et al., 2016b; Lopez-Hilfiker et al., 2016a).

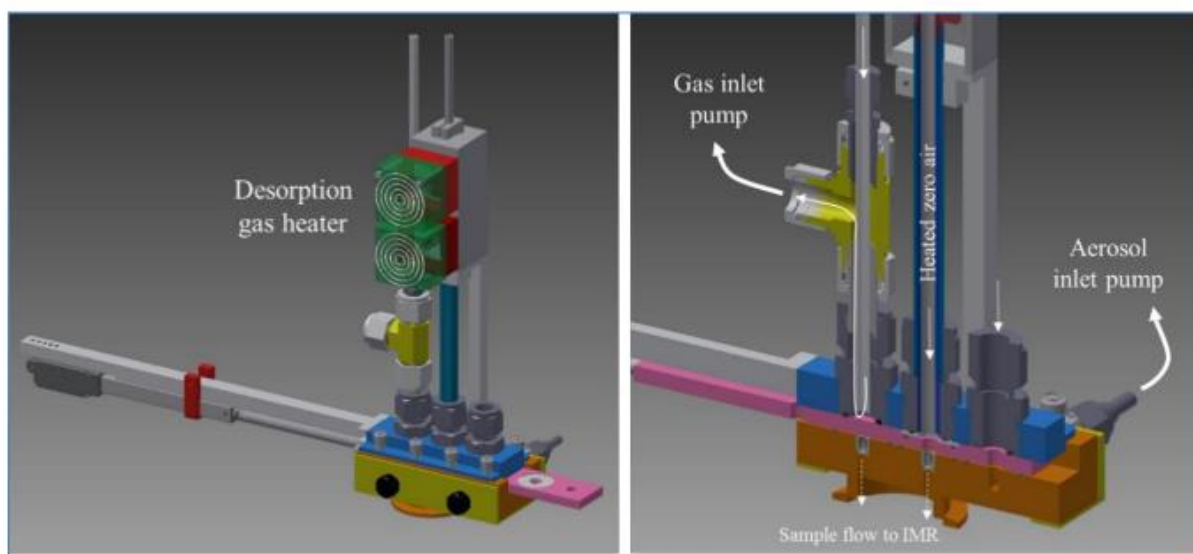


**Figure 3.4.** Schematic of the chemical ionization source and four stages (S1–S4) differentially pumped interface coupled to the time-of-flight mass spectrometer. The figure is from the study of Bertram et al (Bertram et al., 2011).

### The filter inlet for gases and aerosols (FIGAERO)

The filter inlet for gases and aerosols (FIGAERO) (see Fig 3.5) is developed to couple with TOF-CIMS to detect the oxidation products in the particle phase (Lopez-Hilfiker et al., 2014). Since this is combined with gaseous interfaces, various reagent ions can also be used to measure the particle phase (Ng et al., 2017; Lee et al., 2014; Zhang et al., 2018; Reyes-Villegas et al., 2018). The sampling was much simpler for online FIGAERO-CIMS measurement, which was directly sampled from the chamber onto a Teflon filter for a while and subsequently the collected samples were thermally desorbed by heated  $\text{N}_2$  to the chemical ionization reactor. In

our cases, aerosols were collected simultaneously in a separate inlet of the FIGAERO on a PTFE filter (Zeflour, 2.0  $\mu\text{m}$  pore size), after which the filter underwent thermal desorption (15-min temperature ramp to 200  $^{\circ}\text{C}$ , 10 mins holding time and 8 mins cooling down to room temperature) with 2SLM temperature-controlled nitrogen flow through it, allowing the desorbed vapours to the IMR. During the experiments, chamber air was drawn at 1 SLM from the chamber centre via a 0.5 m  $\frac{1}{4}$ " I.D. PFA tubing to sample the gas phase. 1SLM particle sample flow was set to collect the aerosols onto the filter. The authentic sample flow is monitored by a mass flow meter to track the total volume over the collection period.



**Figure 3.5.** Schematic of the FIGAERO from Bannan et al. (2019). The panel on the left shows the full assembly with a mechanical actuator that controls gas sampling/aerosol collection or aerosol desorption operating modes. The panel on the right is a cross-sectional view that shows flows for both gas and particle sampling mode and the two apertures that connect with the IMR. In this view, the FIGAERO slide is positioned in the aerosol desorption mode and the gas sample flow into the IMR is closed (Lopez-Hilfiker et al., 2014).

### 3.2.2 LC-Orbitrap MS

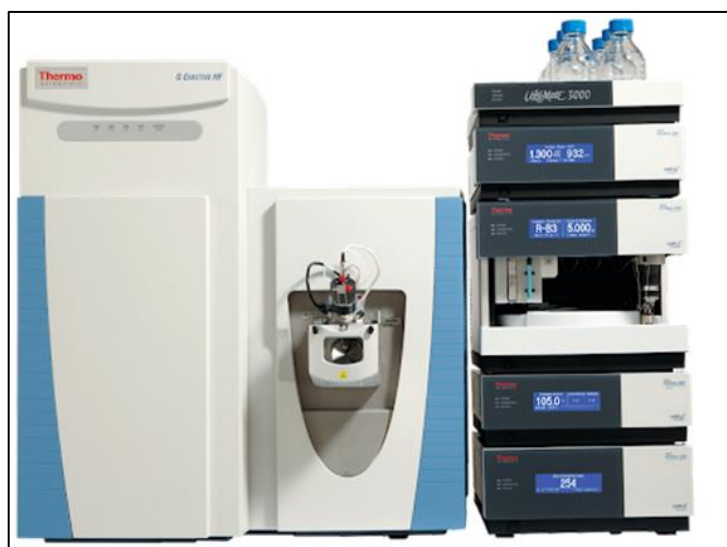
Liquid chromatography ultra-high resolution orbitrap mass spectrometry (LC-Orbitrap MS) is an analytical technique to characterize organics extracted from aerosol particles (Parshintsev and Hyotylainen, 2015). It has high resolution which is beneficial to the identification of unknown compounds (Lin et al., 2018). Generally, there are three important parts for the LC-Orbitrap MS: liquid chromatography, electrospray ionization (ESI) and high-resolution orbitrap mass spectrometry. The reverse phase liquid chromatography (RP-LC) made of a polar mobile phase and a less polar stationary phase

(C18 alkyl chains bonded to a silica surface) allows separating polar and non-polar compounds. The ESI converts compounds separated from the LC mobile phase into gaseous ions, allowing the detection of those species by mass spectrometry (Kearle and Verkerk, 2009). ESI is regarded as a soft ionisation technique and well suited for the analysis of small polar compounds. The fragmentation of species during ionisation will be subsequently detected by techniques such as mass spectrometry, offering the structural elucidation of species through fragmentation (Yasmeen et al., 2012). Ions trap mass spectrometry enables the separation of the ions and fragments several times in succession before the final mass spectrum is obtained based on their  $m/z$  values, resulting in good separations compared to other mass analysers (Pitt, 2009). The method of sample preparation described in Bryant et al. (2020) was slightly modified to be more applicable to our conditions. Briefly, half of the filter was cut into small pieces and transferred into a clean and dry extraction vial. 4ml methanol was then added to the vial and left at room temperature for 2h. Subsequently, the samples were sonicated for 30 mins. The extracted solution was then filtered via a 0.22  $\mu\text{m}$  filter (Thermo Fisher Scientific) by a syringe (1 $\mu\text{m}$ , BD PLASTIC PAK, STERILE) into another sample vial, which was evaporated to dryness using a vacuum solvent evaporator (Biotage, Sweden), and then the dried sample was reconstituted in 1ml of 10:90 methanol (B): water (A) (optima LC-Orbitrap MS grade, Thermo Fisher Scientific) solution.

The prepared samples were analyzed by the ultra-performance liquid chromatography ultra-high resolution orbitrap mass spectrometry (Dionex 3000, Orbitrap QExactive, ThermoFisher Scientific). Compound separation was achieved using a reverse-phase C18 column (Accucore, ThermoFisher Scientific) with the following dimensions: 100 mm (length)  $\times$  2.1 mm (width) and 2.6  $\mu\text{m}$  particle size. The column was heated to 40  $^{\circ}\text{C}$  during analysis. The solvent composition consisted of water (A) and methanol (B) (optima LC-MS grade, ThermoFisher Scientific). Gradient elution was used, starting at 90 % (A) with a 1-minute post-injection hold, decreasing to 10 % (A) at 26 minutes, returning to the starting mobile phase conditions at 28 minutes, with a 2-minute hold to re-equilibrate the column (total run time = 30 minutes). The flow rate was set to 0.3 ml/min with a sample injection volume of 2  $\mu\text{l}$ . Samples were stored in a temperature-controlled autosampler tray during analysis which was set to 4  $^{\circ}\text{C}$ . The mass spectrometer was operated in negative and positive ionization mode with a scan range of  $m/z$  85 to 750. Heated electrospray ionization was used, with the following parameters: capillary and auxiliary gas temperature of 320  $^{\circ}\text{C}$ , sheath gas flow rate of 70 (arb.)

and auxiliary gas flow rate of 3 (arb.). Tandem mass spectrometry was performed using higher-energy collision dissociation with a normalized collision energy of 65, 115.

Electrospray ionization (ESI) was deployed in the LC-Orbitrap MS method, which was comprehensively investigated by Banerjee and Mazumdar (Banerjee and Mazumdar, 2012). Briefly, the spray nozzle was kept at positive potential or negative potential by switching the electric field and produced protonated ions ((M+H)<sup>+</sup> or less possibility of (M+Na)<sup>+</sup>) and deprotonated ions (M-H)<sup>-</sup> of the analytes. Some ions can be further fragmented during ionization. Many factors can affect ionization efficiencies, such as sample components and ESI source parameters (Kruve et al., 2014). In this paper, we do not discuss those factors in detail. However, it is noteworthy that either the iodide chemical ionization or ESI method has different sensitivities to different species, such as ESI negative mode in favour of polar compounds with an acid functional group (Laj et al., 2009). Figure 3.6 displays the appearance of the LC-Orbitrap MS.



**Figure 3.6.** the LC-Orbitrap MS.

### 3.2.3 Other instruments

Additional fundamental analytical techniques were employed to measure other chemistry or physical parameters during our experiments (e.g., temperature, humidity, concentrations of trace gases and particles, organic mass). Condensation Particle Counters (CPC: TSI; 3776), both water and butanol based as working fluid, are employed to achieve the goal of observing of chamber particles total number online and roughly tell whether the chamber is clean before

one experiment and whether the condensation happens when injecting the parent VOCs. The injection, production and consumption of O<sub>3</sub> and NO<sub>x</sub> can be read directly from the O<sub>3</sub> analyser (Thermo; 49C) and NO<sub>x</sub> analyzer (Thermo; 42i), respectively. It is important to keep a similar range of VOCs/NO<sub>x</sub> ratios during experiments, thus an accurate NO<sub>x</sub> analyser record plays a critical role in maintaining the required VOCs/NO<sub>x</sub> ratios. Also, a custom-built Differential Mobility Particle Sizer (DMPS) and the Scanning mobility particle sizer (SMPS, TSI; 3081) are an approach to measure the submicron aerosol size distributions, which can detect particles down to 10 nm and is sensitive to the variations in particle shape. Non-refractory PM1 composition and SOA mass are measured using a high-resolution time-of-flight aerosol mass spectrometer (HR-ToF-AMS; Aerodyne). Additionally, the gas chromatography coupled to a mass spectrometer (GC-MS) was deployed to measure the VOCs concentrations. The detailed information about those instruments is listed in Paper 2.

### **3.3 Data processing**

Data analysis processes for online FIGAERO-CIMS and offline LC-orbitrap MS can be found in detail in the Methodology Section of paper 3.

## References

Alfarra, M. R., Hamilton, J. F., Wyche, K. P., Good, N., Ward, M. W., Carr, T., Barley, M. H., Monks, P. S., Jenkin, M. E., Lewis, A. C., and McFiggans, G. B.: The effect of photochemical ageing and initial precursor concentration on the composition and hygroscopic properties of  $\beta$ -caryophyllene secondary organic aerosol, *Atmospheric Chemistry and Physics*, 12, 6417-6436, 10.5194/acp-12-6417-2012, 2012.

Banerjee, S. and Mazumdar, S.: Electrospray ionization mass spectrometry: a technique to access the information beyond the molecular weight of the analyte, *Int J Anal Chem*, 2012, 282574, 10.1155/2012/282574, 2012.

Bertram, T. H., Kimmel, J. R., Crisp, T. A., Ryder, O. S., Yatavelli, R. L. N., Thornton, J. A., Cubison, M. J., Gonin, M., and Worsnop, D. R.: A field-deployable, chemical ionization time-of-flight mass spectrometer, *Atmospheric Measurement Techniques*, 4, 1471-1479, 10.5194/amt-4-1471-2011, 2011.

Bryant, D. J., Dixon, W. J., Hopkins, J. R., Dunmore, R. E., Pereira, K. L., Shaw, M., Squires, F. A., Bannan, T. J., Mehra, A., Worrall, S. D., Bacak, A., Coe, H., Percival, C. J., Whalley, L. K., Heard, D. E., Slater, E. J., Ouyang, B., Cui, T., Surratt, J. D., Liu, D., Shi, Z., Harrison, R., Sun, Y., Xu, W., Lewis, A. C., Lee, J. D., Rickard, A. R., and Hamilton, J. F.: Strong anthropogenic control of secondary organic aerosol formation from isoprene in Beijing, *Atmospheric Chemistry and Physics*, 20, 7531-7552, 10.5194/acp-20-7531-2020, 2020.

Hyttinen, N., Kupiainen-Maatta, O., Rissanen, M. P., Muuronen, M., Ehn, M., and Kurten, T.: Modeling the Charging of Highly Oxidized Cyclohexene Ozonolysis Products Using Nitrate-Based Chemical Ionization, *J Phys Chem A*, 119, 6339-6345, 10.1021/acs.jpca.5b01818, 2015.

Hyttinen, N., Otkjaer, R. V., Iyer, S., Kjaergaard, H. G., Rissanen, M. P., Wennberg, P. O., and Kurten, T.: Computational Comparison of Different Reagent Ions in the Chemical Ionization of Oxidized Multifunctional Compounds, *J Phys Chem A*, 122, 269-279, 10.1021/acs.jpca.7b10015, 2018.

Kebarle, P. and Verkerk, U. H.: Electrospray: from ions in solution to ions in the gas phase, what we know now, *Mass Spectrom Rev*, 28, 898-917, 10.1002/mas.20247, 2009.

Kroll, J. H., Ng, N. L., Murphy, S. M., Flagan, R. C., and Seinfeld, J. H.: Secondary organic aerosol formation from isoprene photooxidation under high-NO<sub>x</sub> conditions, *Geophysical Research Letters*, 32, n/a-n/a, 10.1029/2005gl023637, 2005.

Kruve, A., Kaupmees, K., Liigand, J., and Leito, I.: Negative electrospray ionization via deprotonation: predicting the ionization efficiency, *Anal Chem*, 86, 4822-4830, 10.1021/ac404066v, 2014.

Laj, P., Klausen, J., Bilde, M., Plaß-Duelmer, C., Pappalardo, G., Clerbaux, C., Baltensperger, U., Hjorth, J., Simpson, D., Reimann, S., Coheur, P. F., Richter, A., De Mazière, M., Rudich, Y., McFiggans, G., Torseth, K., Wiedensohler, A., Morin, S., Schulz, M., Allan, J. D., Attié, J. L., Barnes, I., Birmili, W., Cammas, J. P., Dommen, J., Dorn, H. P., Fowler, D., Fuzzi, S., Glasius, M., Granier, C., Hermann, M., Isaksen, I. S. A., Kinne, S., Koren, I., Madonna, F.,

Maione, M., Massling, A., Moehler, O., Mona, L., Monks, P. S., Müller, D., Müller, T., Orphal, J., Peuch, V. H., Stratmann, F., Tanré, D., Tyndall, G., Abo Riziq, A., Van Roozendael, M., Villani, P., Wehner, B., Wex, H., and Zardini, A. A.: Measuring atmospheric composition change, *Atmospheric Environment*, 43, 5351-5414, 10.1016/j.atmosenv.2009.08.020, 2009.

Lee, B. H., Lopez-Hilfiker, F. D., Mohr, C., Kurten, T., Worsnop, D. R., and Thornton, J. A.: An iodide-adduct high-resolution time-of-flight chemical-ionization mass spectrometer: application to atmospheric inorganic and organic compounds, *Environ Sci Technol*, 48, 6309-6317, 10.1021/es500362a, 2014.

Lin, P., Fleming, L. T., Nizkorodov, S. A., Laskin, J., and Laskin, A.: Comprehensive Molecular Characterization of Atmospheric Brown Carbon by High Resolution Mass Spectrometry with Electrospray and Atmospheric Pressure Photoionization, *Anal Chem*, 90, 12493-12502, 10.1021/acs.analchem.8b02177, 2018.

Lopez-Hilfiker, F. D., Iyer, S., Mohr, C., Lee, B. H., and Ambro, E. L., Kurtén, T., and Thornton, J. A.: Constraining the sensitivity of iodide adduct chemical ionization mass spectrometry to multifunctional organic molecules using the collision limit and thermodynamic stability of iodide ion adducts, *Atmospheric Measurement Techniques*, 9, 1505-1512, 10.5194/amt-9-1505-2016, 2016a.

Lopez-Hilfiker, F. D., Mohr, C., Ehn, M., Rubach, F., Kleist, E., Wildt, J., Mentel, T. F., Lutz, A., Hallquist, M., Worsnop, D., and Thornton, J. A.: A novel method for online analysis of gas and particle composition: description and evaluation of a Filter Inlet for Gases and AEROSols (FIGAERO), *Atmospheric Measurement Techniques*, 7, 983-1001, 10.5194/amt-7-983-2014, 2014.

Lopez-Hilfiker, F. D., Mohr, C., D'Ambro, E. L., Lutz, A., Riedel, T. P., Gaston, C. J., Iyer, S., Zhang, Z., Gold, A., Surratt, J. D., Lee, B. H., Kurten, T., Hu, W. W., Jimenez, J., Hallquist, M., and Thornton, J. A.: Molecular Composition and Volatility of Organic Aerosol in the Southeastern U.S.: Implications for IEPOX Derived SOA, *Environ Sci Technol*, 50, 2200-2209, 10.1021/acs.est.5b04769, 2016b.

Ng, N. L., Brown, S. S., Archibald, A. T., Atlas, E., Cohen, R. C., Crowley, J. N., Day, D. A., Donahue, N. M., Fry, J. L., Fuchs, H., Griffin, R. J., Guzman, M. I., Herrmann, H., Hodzic, A., Inuma, Y., Jimenez, J. L., Kiendler-Scharr, A., Lee, B. H., Luecken, D. J., Mao, J., McLaren, R., Mutzel, A., Osthoff, H. D., Ouyang, B., Picquet-Varrault, B., Platt, U., Pye, H. O. T., Rudich, Y., Schwantes, R. H., Shiraiwa, M., Stutz, J., Thornton, J. A., Tilgner, A., Williams, B. J., and Zaveri, R. A.: Nitrate radicals and biogenic volatile organic compounds: oxidation, mechanisms, and organic aerosol, *Atmos Chem Phys*, 17, 2103-2162, 10.5194/acp-17-2103-2017, 2017.

Parshintsev, J. and Hyotylainen, T.: Methods for characterization of organic compounds in atmospheric aerosol particles, *Anal Bioanal Chem*, 407, 5877-5897, 10.1007/s00216-014-8394-3, 2015.

Pitt, J. J.: Principles and Applications of Liquid Chromatography Mass Spectrometry in Clinical Biochemistry, *Clin Biochem Rev* 30, 2009.

Presto, A. A. and Donahue, N. M.: Investigation of alpha-pinene + ozone secondary organic



aerosol formation at low total aerosol mass, *Environ Sci Technol*, 40, 3536-3543, 10.1021/es052203z, 2006.

Reyes-Villegas, E., Bannan, T., Le Breton, M., Mehra, A., Priestley, M., Percival, C., Coe, H., and Allan, J. D.: Online Chemical Characterization of Food-Cooking Organic Aerosols: Implications for Source Apportionment, *Environ Sci Technol*, 52, 5308-5318, 10.1021/acs.est.7b06278, 2018.

Riva, M., Rantala, P., Krechmer, J. E., Peräkylä, O., Zhang, Y., Heikkinen, L., Garmash, O., Yan, C., Kulmala, M., Worsnop, D., and Ehn, M.: Evaluating the performance of five different chemical ionization techniques for detecting gaseous oxygenated organic species, *Atmospheric Measurement Techniques*, 12, 2403-2421, 10.5194/amt-12-2403-2019, 2019.

Seinfeld, J. H. and Pandis, S. N.: *Atmospheric chemistry and physics : from air pollution to climate change*, Third edition., John Wiley & Sons, Hoboken, New Jersey 2016.

Yasmeen, F., Vermeylen, R., Maurin, N., Perraudin, E., Doussin, J.-F., and Claeys, M.: Characterisation of tracers for aging of  $\alpha$ -pinene secondary organic aerosol using liquid chromatography/negative ion electrospray ionisation mass spectrometry, *Environmental Chemistry*, 9, 10.1071/en11148, 2012.

Zhang, H., Yee, L. D., Lee, B. H., Curtis, M. P., Worton, D. R., Isaacman-VanWertz, G., Offenberg, J. H., Lewandowski, M., Kleindienst, T. E., Beaver, M. R., Holder, A. L., Lonneman, W. A., Docherty, K. S., Jaoui, M., Pye, H. O. T., Hu, W., Day, D. A., Campuzano-Jost, P., Jimenez, J. L., Guo, H., Weber, R. J., de Gouw, J., Koss, A. R., Edgerton, E. S., Brune, W., Mohr, C., Lopez-Hilfiker, F. D., Lutz, A., Kreisberg, N. M., Spielman, S. R., Hering, S. V., Wilson, K. R., Thornton, J. A., and Goldstein, A. H.: Monoterpenes are the largest source of summertime organic aerosol in the southeastern United States, *Proc Natl Acad Sci U S A*, 115, 2038-2043, 10.1073/pnas.1717513115, 2018.

[BLANK PAGE]

## Chapter 4. Results

### 4.1 Paper 1: Characterisation of the Manchester Aerosol Chamber facility

This paper is accepted by the journal of “*Atmospheric Measurement Techniques*” and waiting for publication. It can be found on <https://amt.copernicus.org/preprints/amt-2021-147/>.

#### 4.1.1 Paper introduction

This paper aimed to provide detailed information about the Manchester Aerosol Chamber (MAC) and comprehensive characterization of the MAC to ensure reproducible and reliable results from the chamber. This paper can solve the 1<sup>st</sup> objective of this project.

It was found that the potential to conduct experiments can be controlled at temperatures 15-35 °C and relative humidity of 25-80 % under simulated solar radiation or dark conditions. The NO<sub>2</sub> photolysis, gases and particles wall loss rates can be affected by the usage history of the chamber bag, such as the frequency of bag usage, experimental types performed in the bag etc. Also, the wall loss correction methods would impact the particle mass in the chamber. The results of those parameters are shown in this paper.

#### 4.1.2 Contribution to the joint authorship

The author has contributed the following:

I together with other co-first authors was responsible for the design and conduction of experiments. I was mainly responsible for the writing of the section about the results from fundamental instruments (such as NO<sub>x</sub>, RH, T and the description of the chamber and mode of operation etc) and the discussion section. I also acted as one of the editors to ensure fluency and consistency among sections and grammar checking.

#### 4.1.3 Supplemental information

The paper is presented below.



# Characterisation of the Manchester Aerosol Chamber facility

Yunqi Shao<sup>1,★</sup>, Yu Wang<sup>1,★</sup>, Mao Du<sup>1,★</sup>, Aristeidis Voliotis<sup>1,★</sup>, M. Rami Alfarra<sup>1,2,a</sup>, Simon P. O'Meara<sup>1,2</sup>, S. Fiona Turner<sup>1,b</sup>, and Gordon McFiggans<sup>1</sup>

<sup>1</sup>Centre for Atmospheric Science, Department of Earth and Environmental Sciences, School of Natural Sciences, University of Manchester, Manchester, M13 9PL, UK

<sup>2</sup>National Centre for Atmospheric Science (NCAS), University of Manchester, Manchester, M13 9PL, UK

<sup>a</sup>now at: Environment & Sustainability Center, Qatar Environment & Energy Research Institute, 34110, Doha, Qatar

<sup>b</sup>now at: AMETEK Land, Dronfield, Derbyshire, S18 1DJ, UK

★These authors contributed equally to this work.

**Correspondence:** Gordon McFiggans (gordon.b.mcfiggans@manchester.ac.uk)

Received: 20 May 2021 – Discussion started: 14 June 2021

Revised: 14 October 2021 – Accepted: 11 November 2021 – Published: 31 January 2022

**Abstract.** This study describes the design of the Manchester Aerosol Chamber (MAC), initially developed in 2005 and presents for the first time its comprehensive characterisation. The MAC is designed to investigate multi-phase chemistry and the evolution of aerosol physico-chemical properties from the real-world emissions (e.g. diesel engine, plants) or of secondary organic aerosol (SOA) produced from pure volatile organic compounds (VOCs). Additionally, the generated aerosol particles in the MAC can be transferred to the Manchester Ice Cloud Chamber (MICC), which enables investigation of cloud formation in warm, mixed-phase, and fully glaciated conditions (with temperature,  $T$ , as low as  $-55^{\circ}\text{C}$ ). The MAC is an  $18\text{ m}^3$  fluorinated ethylene propylene (FEP) Teflon chamber with the potential to conduct experiments at controlled temperature ( $15\text{--}35^{\circ}\text{C}$ ) and relative humidity (RH;  $25\text{--}80\%$ ) under simulated solar radiation or dark conditions. Detailed characterisations were conducted at common experimental conditions ( $25^{\circ}\text{C}$ ,  $50\%$  RH) for actinometry and determination of background contamination, wall losses of gases ( $\text{NO}_2$ ,  $\text{O}_3$ , and selected VOCs), aerosol particles at different sizes, chamber wall reactivity, and aerosol formation. In addition, the influences of chamber contamination on the wall loss rate of gases and particles and the photolysis of  $\text{NO}_2$  were estimated.

## 1 Introduction

Atmospheric aerosols have significant effects on air quality, regional to global climate, and human health (Lohmann and Feichter, 2005; Pope et al., 2002; Katsouyanni et al., 1997). Aerosol particles range from a few nanometres to several tens of micrometres in diameter. Their composition is complex, comprising inorganic and organic compounds, dependent on their sources, which may be either primary (e.g. sea salt, dust, wildfires) or secondary, from the oxidation of gaseous precursors (Seinfeld and Pandis, 2016). Organic compounds contribute 20 % to 90 % of the mass of submicron aerosols in the Northern Hemisphere (Jimenez et al., 2009; Zhang et al., 2007), and of an estimated 10 000 to 100 000 atmospheric organic compounds (Goldstein and Galbally, 2007), only around 10 % have been identified, such as alkanes, carbonyls, alcohols, esters, and acids (Hallquist et al., 2009; Goldstein and Galbally, 2007). Owing to this complexity, their chemical reaction pathways and properties lead to substantial outstanding challenges to the understanding of organic aerosol (OA) formation, transformation, fate, and impacts (Hallquist et al., 2009). Such an inadequate understanding of aerosol particles and particularly the organic fraction leads to large uncertainties in understanding their role in air quality and global climate (McFiggans et al., 2006). Processes relating to organic-containing particles have consequently been a primary focus of studies in our chamber.

Over the last several decades, numerous field measurements have been conducted globally to characterise OA in the atmosphere (Gray et al., 1986; Hoffman and Duce, 1977; Turpin and Huntzicker, 1991, 1995; Hallquist et al., 2009; Jimenez et al., 2009; Zhang et al., 2007). However, isolation of chemical and microphysical processes from meteorology and other atmospheric processes can be challenging in ambient measurements (Becker, 2006). To better understand the sources, physico-chemical properties, and ageing processes influencing atmospheric aerosols, simulation chamber facilities have been developed across the globe since the 1960s (Karl et al., 2004; Cocker et al., 2001a; Carter et al., 2005; Paulsen et al., 2005; Saathoff et al., 2009; Wang et al., 2011, 2014; Platt et al., 2013; Schnitzhofer et al., 2014; Leskinen et al., 2015; Babar et al., 2016; Gallimore et al., 2017; Leone et al., 1985). In principle, a simulation chamber is a controlled system to elucidate processes that occur in the real atmosphere (Barnes and Rudzinski, 2006), gas-phase reactions and chemical pathways (Carter and Lurmann, 1991; Seakins, 2010; Atkinson et al., 1992; Paulot et al., 2009; Surratt et al., 2010; Ehn et al., 2012; Bianchi et al., 2019; Thornton et al., 2020), secondary organic aerosol (SOA) production (Hallquist et al., 2009; Carlton et al., 2009; McFiggans et al., 2019), new particle formation (Smith, 2016; Wang et al., 2020; Wagner et al., 2017; Dunne et al., 2016), cloud processes (Wang et al., 2011; Frey et al., 2018; Wagner et al., 2006), transformations and properties of real-world emissions (from vehicles; e.g. Liu et al., 2017, biomass burning; e.g. Hennigan et al., 2011, plants; e.g. Hohaus et al., 2016), and health effects (Tong et al., 2018; Taylor et al., 2000).

The design of simulation chambers varies widely with respect to the light sources, chamber sizes, materials, and operation conditions to address varied lines of research (Barnes and Rudzinski, 2006). The size of chamber facilities ranges from  $\sim 1$  to  $\sim 300\text{ m}^3$  and are variously constructed from pyrex or quartz, aluminium, stainless steel, and fluorinated ethylene propylene (FEP) Teflon. The light sources of chambers include artificial and natural solar radiation, leading to a convenient classification into indoor and outdoor chambers (Barnes and Rudzinski, 2006). Pyrex or quartz is widely used for chambers with a volume of less than  $1\text{ m}^3$ , with a few that are larger, such as the JPAC (Jülich Plant Atmosphere Chamber;  $1.45\text{ m}^3$ ) (Ehn et al., 2014), Bayreuth chambers ( $2.4\text{ m}^3$ ) (Behnke et al., 1988), and the quartz-glass reaction chamber ( $> 1\text{ m}^3$ ) (Barnes et al., 1994). Owing to its reasonably inert nature and transparency towards short-wavelength lights, pyrex and quartz chambers enable ready access to radical generation studies. Also, pyrex and quartz chambers can enable temperature-dependent studies with the use of a cooling or heating bath. Metal chambers are usually built with a volume of 1 to  $6\text{ m}^3$ , with exceptions such as the AIDA (Aerosol Interactions and Dynamics in the Atmosphere) chamber ( $85\text{ m}^3$ ) (Wagner et al., 2006), the MICC (Manchester Ice Cloud Chamber;  $10\text{ m}^3$ ) (Connolly et al., 2012), and the CERN (Eu-

ropean Organization for Nuclear Research) cloud chamber ( $26\text{ m}^3$ ) (Schnitzhofer et al., 2014). The largest advantage of the rigid metal chambers is the ability to conduct experiments under varying temperatures, enabling simulation of free-tropospheric conditions (Wagner et al., 2006; Schnitzhofer et al., 2014) and warm, mixed-phase, and fully glaciated clouds. FEP Teflon is widely used in medium to large chambers, such as FORTH-ASC (Foundation for Research and Technology Hellas Atmospheric Simulation Chamber;  $10\text{ m}^3$ ) (Kostenidou et al., 2013), the Manchester Aerosol Chamber (MAC) ( $18\text{ m}^3$ ), LEAK-LACIS (Leipziger Aerosolkammer Leipziger Aerosol and Cloud Interaction Simulator;  $19\text{ m}^3$ ) (Mutzel et al., 2015; Niedermeier et al., 2020), IASC (Irish Atmospheric Simulation Chamber;  $27\text{ m}^3$ ), Caltech dual chambers (both  $28\text{ m}^3$ ; Cocker et al., 2001b), the University of California at Riverside dual chambers (both  $90\text{ m}^3$ ) (Carter et al., 2005), PSI (Paul Scherrer Institute) chamber ( $27\text{ m}^3$ ) (Paulsen et al., 2005), ILMARI (Aerosol Physics, Chemistry and Toxicology Research Unit;  $29\text{ m}^3$ ) (Leskinen et al., 2015), HELIOS (Outdoor Atmospheric Simulation Chamber of Orleans;  $90\text{ m}^3$ ) (Ren et al., 2017), SAPHIR (Simulation of Atmospheric Photochemistry In a Large Reaction Chamber;  $270\text{ m}^3$ ) (Karl et al., 2004), and EUPHORE (European PhotoReactor;  $2 \times 200\text{ m}^3$ ) (Bloss et al., 2005; Dunne et al., 2016). The transparency of Teflon enables its widespread use in both indoor and outdoor chambers, enabling transmission across the solar spectrum.

All chambers have limitations. A universal challenge is the presence of chamber walls that can act as a sink of the reacting gases and aerosol particles (McMurry and Grosjean, 1985) and as a surface on which they can react. Consequently, experimental results relating to gas-particle partitioning, aerosol formation rate, and yield, for example, require careful interpretation (McMurry and Grosjean, 1985; Matsunaga and Ziemann, 2010; Zhang et al., 2014; Ye et al., 2016; Wang et al., 2018). Similarly, photochemistry experiments in indoor chambers using artificial lights require consideration of the wavelength dependence of the irradiance (Barnes and Rudzinski, 2006). Outdoor chambers, particularly the larger ones, are challenged by control of relative humidity (RH) and temperature ( $T$ ) due to the ambient diurnal variation, which may introduce some uncertainty (Barnes and Rudzinski, 2006). In addition, gases and particles as well as the intermediate reactants can interact with and partition into chamber walls (so-called memory effect), which can affect repeatability and reliability of the results (Carter and Lurmann, 1991; Wang et al., 2011, 2014; Schnitzhofer et al., 2014). This artefact due to the memory effect necessitates a clear and detailed characterisation of chamber behaviour and history.

This paper provides a description and characterisation of a novel indoor simulation chamber, the Manchester Aerosol Chamber (MAC), located at the University of Manchester. The MAC has been well developed and predominantly used since 2005 to understand the chemical and physical prop-

erties of aerosols from different sources (e.g. engines, real-plant emissions, biogenic or anthropogenic volatile organic compounds (VOCs)). But all these studies have not required the quantification of aerosol amount; therefore the mixing or wall effect had not been characterised at the time of many previous experiments. Recently, in order to understand the SOA formation (e.g. yield) from mixed precursors (e.g. Voliotis et al., 2021; Wang et al., 2021), a full characterisation of the chamber was implemented to ensure the reliability of the studies. Equipped with state-of-the-science instruments, the MAC has been used to explore the aerosol formation and ageing (Hamilton et al., 2011; Alfarra et al., 2012), physico-chemical properties of multi-component aerosol particles (Alfarra et al., 2013; Wang et al., 2021; Voliotis et al., 2021), gas–particle partitioning (Voliotis et al., 2021), aerosol formation, and properties and transformations from plant emissions (Wyche et al., 2014) and from engine emissions (Pereira et al., 2018; Liu et al., 2017). Additionally, the entire contents of the MAC can be transferred directly to the MICC (Manchester Ice Cloud Chamber) to investigate the warm, mixed-phase, and fully glaciated cloud formation on the aerosol particles that will act as cloud condensation nuclei (CCN) and ice nuclei (IN). A detailed description of the coupling between the facilities and its use can be found in Connolly et al. (2012) and Frey et al. (2018) and is not discussed here.

## 2 Description of the MAC

The MAC is operated as a batch reactor where the composition of the gaseous precursors, pre-existing seed, oxidising environment, relative humidity, and temperature are controlled throughout a typical experimental duration of several hours. It is equipped with a variable combination of gas-phase and particle-phase analytical instruments as listed in Table 1. The MAC consists of an 18 m<sup>3</sup> FEP Teflon bag suspended from a frame comprising a central fixed-frame member and two moving members, all contained within an RH- and temperature-controlled enclosure. Along with the light sources, cooling systems, and air purification system, the MAC is shown in the schematic in Fig. 1.

### 2.1 Enclosure and environmental control

The rectangular enclosure comprises an extruded aluminium framework supporting two access sides, each with two bi-fold doors, and two fixed sides, within which the lamp enclosures and air conditioning (AC) ducts are situated. The inner walls and the ceiling of the enclosure and the floor are fully coated with a reflective space blanket to approximate an integrating sphere to maximise the chamber irradiance and provide even light intensity. The temperature and relative humidity between the chamber and the enclosure walls are controlled by the AC, allowing a temperature within the range of

15–35 °C and RH between 25 % and 80 %. The inlet duct is positioned aloft at one end of the chamber, and the outlet duct is at the bottom of the other such that conditioned air at 3 m<sup>3</sup> s<sup>-1</sup> continually passes through the 50 cm space between the bag and enclosure, agitating and mixing the air in the bag as it does so. The RH set points are chosen to match the dew point of the chamber air at the desired temperature. Temperature and dew point are measured at two points in the chamber (at the middle and on the side) using a dew point hygrometer and two thermocouples to choose the set point.

### 2.2 Teflon reactor

The reactor comprises four sections of FEP Teflon film (50 µm, AdTech Polymer Engineering Ltd.). FEP Teflon film is chosen since it is chemically inert and more transparent than polyvinyl fluoride (PVF) and polytetrafluoroethylene (PTFE), having better light transmission between 290 and 800 nm, and it has lower rates of hydrocarbon off-gassing (Finlayson-Pitts and Pitts, 2000). A weakness of the FEP film is the accumulation of electrostatic charge, which can significantly increase the wall loss rates for particles with a diameter smaller than 500 nm (McMurry and Rader, 1985; Charan et al., 2018). The chamber is suspended in the enclosure, and joints between three pairs of edges of the Teflon film are made by compression-sealing between the three pairs of rectangular extruded aluminium frames. The edges of the top and bottom Teflon webs are clamped by stainless steel clips installed on the aluminium frames with expanded foam strips relieving between the frame and Teflon to ensure even compression between the Teflon sheets. This approach avoids additional contamination from glue or tapes. The central rigid frame is fixed, with the upper and lower frames free to move vertically. They are counter-weighted to enable the bag to expand and collapse when sample air is introduced and extracted in the process of fill–flush cycles and sampling. This reduces the possibility of the chamber operating under negative pressure, minimising instrumental sampling problems and contamination from laboratory air. In normal practice, around 80 % of the chamber air can be extracted from the chamber within ~ 5 min at a flow rate of 3 m<sup>3</sup> min<sup>-1</sup> in each flush cycle; after that the purified air can be filled into the chamber at the same flow rate. A low background condition is achieved in around 2 h of continuous automated fill–flush cycles. This relatively rapid cleaning improves the duty cycle and efficiency of the chamber preparation process. The central fixed-frame pair supports three inlet and sampling manifolds constructed of solid Teflon, one in each of the two long sides and one in the short side of the bag, as well as mirrors and optical fibre mounting for a two-pass broadband differential optical absorption spectroscopy (DOAS) system for retrieval of aerosol optical properties along the long axis of the chamber. One manifold is connected to the air purification system (described in Sect. 2.4) for injection of purified air, VOC precursor, NO<sub>x</sub>, O<sub>3</sub>, and seed aerosols and transfer of

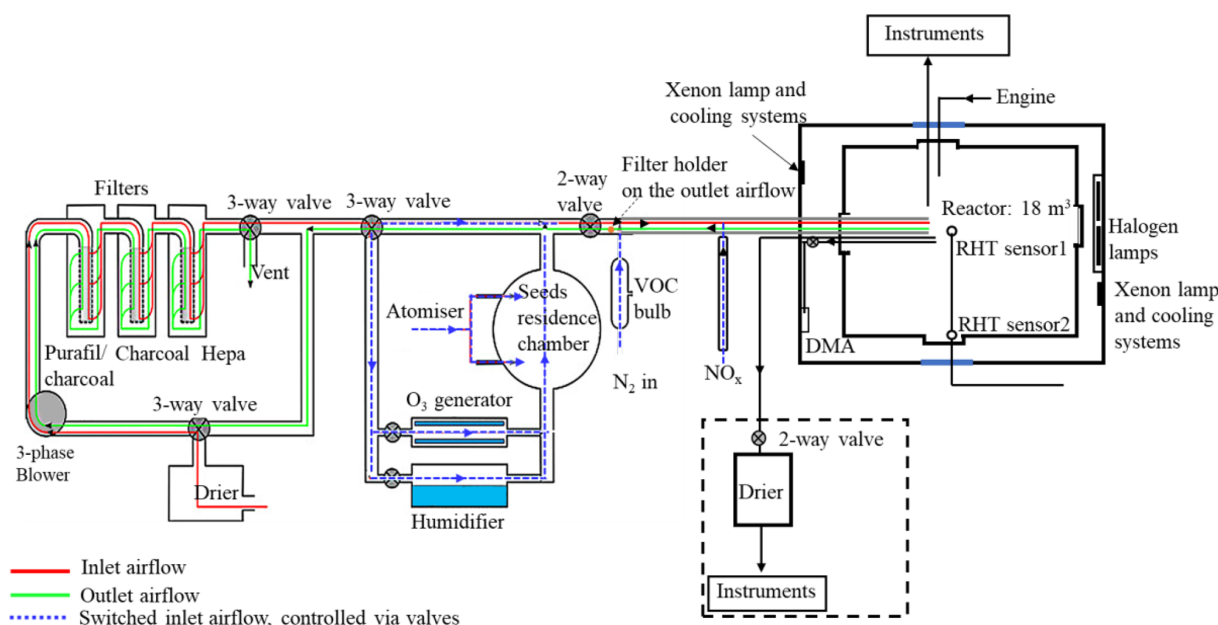
**Table 1.** List of the available instrumentation at the MAC.

| Instrument  | Model                                     | Measured parameter                                  | Limit of detection (LOD) or range   |
|---|---|---|---|
| Core instrumentation  |   |   |   |
| Dew point hygrometer  | Edgetech; DM-C1-DS2-MH-13                 | Dew point   | $-20-90 \pm 0.2$ °C   |
| Sensirion capacitance sensor  | Sensirion; SHT75                          | Temperature, relative humidity                      | $-40$ to $+125$ , $\pm 0.3$ °C; $0-100$ , $\pm 1.8$ %                       |
| NO <sub>x</sub> analyser  | Thermo; 42i                               | NO, NO <sub>2</sub>                                 | 0.5 to 1000 ppb   |
| O <sub>3</sub> analyser   | Thermo; 49C                               | O <sub>3</sub>                                      | 0–0.05 to 200 ppm   |
| CO analyser   | Thermo; 48i                               | CO  | $> 0.04$ ppm  |
| Water-based condensation particle counter, wCPC                         | TSI; 3785, 3786                           | Particle number                                     | $< 10^7$ pcc <sup>-1</sup>  |
| Differential mobility particle sizer                                    | Custom-built <sup>a</sup>                 | Particle size                                       | 40–600 nm   |
| Filter collector  | Custom-built <sup>b</sup>                 | Particle collection for offline analysis            |   |
| Additional instrumentation  |   |   |   |
| Condensation particle counter, CPC                                      | TSI; 3776                                 | Particle number                                     | $< 10^7$ pcc <sup>-1</sup>  |
| Scanning mobility particle sizer, SMPS                                  | TSI; 3081                                 | Particle size                                       | 10–1000 nm  |
| Aerodynamic Aerosol Classifier, AAC                                     | Cambustion                                | Selection of particles by size                      | 25–5000 nm  |
| Centrifugal Particle Mass Analyser                                      | Cambustion                                | Selection of particles by mass                      | Mass accuracy: 5 %  |
| High-resolution time-of-flight aerosol mass spectrometer, HR-ToF-AMS    | Aerodyne                                  | PM <sub>1</sub> non-refractory particle composition | $> 0.05$ µg m <sup>-3</sup>   |
| Iodide chemical ionisation mass spectrometer, I <sup>-</sup> -CIMS      | Aerodyne/Tofware                          | Oxygenated VOC                                      | LOD $> 60$ ppt; Mass resolution 4000 ThTh <sup>-1</sup>                     |
| Filter Inlet for Gases and AEROSols, FIGAERO                            | Aerodyne/Tofware                          | Particle composition                                | $> 10^2$ ng   |
| Semi-continuous organic carbon/elemental carbon aerosol analyser, OC/EC | Sunset Laboratory; Model 4                | Organic/elemental carbon concentration              | $> 0.5$ µg C m <sup>-3</sup>  |
| Hygroscopicity tandem differential mobility analyser, HTDMA             | Custom-built <sup>c</sup>                 | Hygroscopicity                                      | 20–350 nm   |
| Cloud condensation nuclei counter, CCNc                                 | Droplet Measurement Technologies; CCN-100 | CCN activity  | $> 6 \times 10^3$ particles cm <sup>-3</sup> at supersaturation (SS): 0.2 % |
| Thermal denuder   | Custom-built <sup>d</sup>                 | Volatility  | Temperature range: ambient–200 °C   |
| Three-wavelength photoacoustic spectrometer, PAS                        | Droplet measurement Tech                  | BC  | 0–100 000 M m <sup>-1</sup>   |
| Single Particle Soot Photometer, SP2                                    | Droplet measurement Tech                  | light absorbing property of soot                    | $> 10$ ng m <sup>-3</sup>   |

<sup>a</sup> Alfara et al. (2012), <sup>b</sup> Hamilton et al. (2011), <sup>c</sup> Good et al. (2010), <sup>d</sup> Voliotis et al. (2021).

sample to selected instrumentation in the upper-floor laboratory. A second manifold is used for sampling gas and particulate material from the chamber to online instrumentation next to the chamber throughout each experiment. A second port in this manifold can be used to couple the chamber to emission

sources, such as engines or plant chambers, and has been discussed elsewhere (Wyche et al., 2014; Pereira et al., 2018). The third manifold houses sensors to monitor the RH and  $T$  inside the chamber and at the chamber walls.



**Figure 1.** Schematic of the Manchester Aerosol Chamber (MAC).

### 2.3 Chamber illumination

The irradiation source, consisting of two xenon arc lamps and a bank of halogen bulbs, is mounted inside the enclosure and is used to approximate the atmospheric actinic spectrum. Two 6 kW arc xenon lamps (XBO 6000 W/HSLA OFR, Osram) are installed on the bottom left and the top right of the chamber housing, respectively. Quartz plates with optical polish (PI-KEM Ltd) of 4 mm thickness in front of each arc lamp filter out unwanted UV light. The bank of 112 halogen lights, 7 rows of 16 bulbs each (Solux 50 W, 4700 K, Solux MR16, USA), is mounted on the same enclosure wall as the bottom xenon arc lamp, facing the inlet.

The unwanted heat generated from the irradiation source is removed by the cooling system, which includes the air conditioning (AC) unit and a water tank in front of each arc lamp, with a circulating water system. The chiller water circulates through aluminium bars, cooling the halogen bulb holders, and through tanks in front of each arc lamp faced by the quartz filter plates in order to dissipate heat produced by absorption of unwanted infrared (IR) light by water vapour.

### 2.4 Chamber air purification, conditioning, and injection system

Purified dry air is supplied by passing laboratory air at up to  $3 \text{ m}^3 \text{ min}^{-1}$  using a three-phase blower (Nash Elmo, model G200) through a drier (ML180, Munters) and three filters (the first canister containing Purafil and charcoal, the second containing activated charcoal and the third with a HEPA filter to remove the  $\text{NO}_x$ , volatile organic compounds, and particles). This typically results in particle concentrations <

$15 \text{ particles cm}^{-3}$ , particle mass concentration  $\sim 0 \mu\text{g m}^{-3}$ ,  $\text{O}_3$  concentrations  $\sim 0 \text{ ppb}$ , and  $\text{NO}_x$  concentration  $< 10 \text{ ppb}$  ( $\text{NO} < 8 \text{ ppb}$  and  $\text{NO}_2 < 2 \text{ ppb}$ ).

The clean air can be conditioned by passing through the humidifier, ozoniser, and aerosol mixing tank before entering the chamber. The ozoniser (OZV30, Waterth) generates ozone using two mercury lamps. The custom-built humidifier comprises a 50 L tank fed with ultra-pure water (resistivity  $\geq 18.2 \text{ M}\Omega \text{ cm}$ ), producing water vapour using an immersion heater that heats the water to  $\sim 80^\circ\text{C}$ . VOCs are added to the chamber by injecting the desired liquid amount into a gently heated glass bulb (to  $\sim 80^\circ\text{C}$ ) and transferred using the electron capture device (ECD)-grade nitrogen ( $\text{N}_4.8$ , purity 99.998 %,  $\text{N}_2$ ) as the carrier gas.  $\text{NO}_x$  ( $\text{NO}$  and  $\text{NO}_2$ ) is added to the chamber using custom-made cylinders at 10 %  $v/v$  and a mass flow controller and transferred with ECD-grade  $\text{N}_2$  as the carrier gas. Seed particles are generated by an atomiser (Topaz model ATM 230) and pass through a  $0.12 \text{ m}^3$  stainless steel aerosol residence chamber before being flushed into the chamber. All components are connected with large-bore (50 mm) stainless steel pipes apart from the diversion lines for the seed, humidifier, and ozoniser, which have a 25 mm bore. The flow path is controlled by several two- and three-way electro-pneumatic valves along the inlet system. As shown in Fig. 1, the purified lab air that is used to fill the chamber can be directed through the humidifier, the ozoniser, and aerosol residence chamber and carry any of their components to the chamber while filling at a high flow rate ( $3 \text{ m}^3 \text{ min}^{-1}$ ), ensuring rapid mixing (see Sect. 3.2).



## 2.5 Control system

To regulate the chamber operational procedures and devices (fill–flush cycles, injection procedure, humidification, VOC bulb heating, ozoniser operation) conveniently, repeatedly, and precisely, a bespoke automated control system is used. All component switches are controlled from a home-built PLC (programmable logic controller) board, with all control signals processed using ladder logic and communicating with a graphical front end in Visual Basic. All components (including the two- and three-way valves) shown in Fig. 1 are controlled by the PLC. Selection of the valve position controls whether clean air is injected into the chamber or the chamber contents are flushed to exhaust. Cycles of filling and flushing are programmed to enable unsupervised operation during cleaning cycles. The humidifier and ozoniser can be bypassed by controlling the diversion line valves during the fill part of the cycle. Relative humidity and temperature of the chamber were continuously measured via the EdgeTech and Sensirion sensors that are also PLC-controlled. All control data are saved automatically. Three pre-programmed operations (pre-experiment, post-experiment, and fill–flush cycle) are provided in the control system to enable manual or automated operation. More details about these operational procedures are provided in Sect. 2.7.

## 2.6 Modes of operation

The MAC generally operates as a batch reactor that provides a closed system without the continuous flow of reactants or dilution flow of clean air. There have been several modes of operation used. The most straightforward mode is the heated-bulb injection of commercial pure-VOC precursors to investigate

The most straightforward mode is using the heated bulb injection of commercial pure VOC precursors to investigate the SOA formation and transformation in either sole- or mixed-VOC systems (Hamilton et al., 2011; Jenkin et al., 2012). The MAC has additionally been coupled to whole combustion process and biogenic emission sources. A dynamometer, diesel engine, and oxidising catalyst unit can be connected to the chamber directly, allowing controlled exhaust dilutions by controlled injection timing of exhaust fumes into the chamber under selected loads and speeds. For example, Pereira et al. (2018) reported the effect of different engine conditions and emission control devices on unregulated diesel exhaust gas emissions. The MAC has been coupled with a custom-built plant chamber to investigate the SOA formation from the real plants under controlled conditions. Wyche et al. (2014) deployed the chamber to investigate SOA formation from biogenic VOC precursors emitted from the silver birch and three Southeast Asian tropical plant species. Also, the MAC infrastructure was recently successfully extended to continuously generate  $\text{NO}_3$  radicals using

synthesised  $\text{N}_2\text{O}_5$  to enable studies of SOA formation and transformation under nighttime conditions.

## 2.7 Experimental procedures

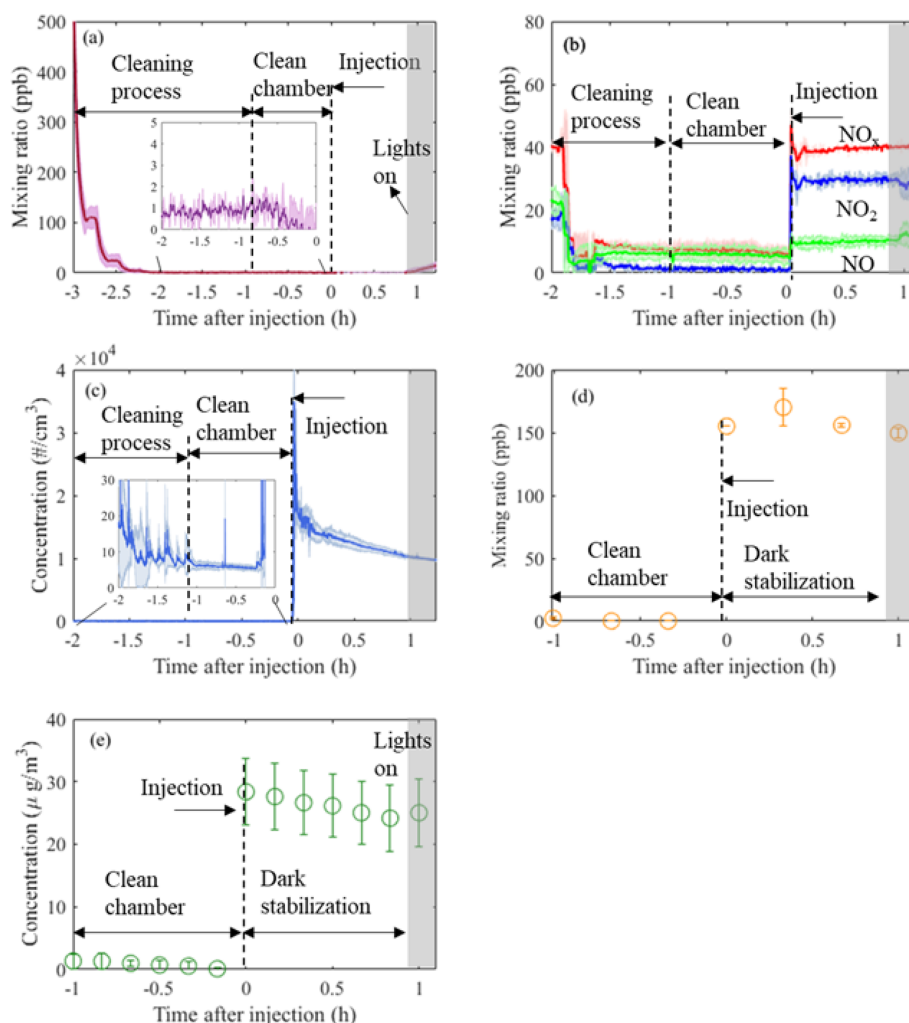
To ensure reliable and reproducible control of experimental conditions, three specific experimental procedures have been programmed to be sequenced and implemented automatically or manually to ensure a lower chamber background. The first, designated the pre-experiment procedure, includes several fill–flush cycles of the chamber with clean air at a high flow rate of  $3 \text{ m}^3 \text{ min}^{-1}$  for  $\sim 1.5 \text{ h}$ . The VOC glass bulb is also cleaned in the course of the pre-experiment procedure using ECD-grade  $\text{N}_2$ .

The second, conducted at the end of each experiment, is the post-experiment procedure. Again, this consists of several fill–flush cycles of the chamber with clean air at a high flow rate of  $3 \text{ m}^3 \text{ min}^{-1}$  for  $\sim 1.5 \text{ h}$ , followed by a fill with a high concentration of  $\text{O}_3$  ( $\sim 1 \text{ ppm}$ ) to soak the chamber overnight to oxidise the residual  $\text{O}_3$ -reacting volatile species. The third, a more aggressive “harsh cleaning” procedure, is carried out weekly during experimental campaigns. In this procedure a high concentration of  $\text{O}_3$  ( $\sim 1 \text{ ppm}$ ) is filled into the chamber with illumination, undergoing several hours of photo-oxidation at high relative humidity ( $\sim 80 \%$ ).

These procedures ensure a clean environment is provided in the MAC prior to SOA experiments. Gaseous and particle time series before and after injection of reactants in three  $\alpha$ -pinene photo-oxidation experiments in the presence of ammonium sulfate (AS) seeds are shown in Fig. 2. As can be observed from Fig. 2a and b, during the cleaning cycle the mixing ratios of  $\text{NO}_x$  and  $\text{O}_3$  are sharply decreasing from  $\sim 40$  and  $\sim 500 \text{ ppb}$ , respectively, down to  $< 10$  and  $< 1 \text{ ppb}$ , respectively, during our automated filling cycle in less than an hour. Similarly, the particle number and mass concentration decreases down to  $< 10 \text{ particles cm}^{-3}$  and  $0 \mu\text{g m}^{-3}$ , respectively, prior to the injection of the reactants to chamber (Fig. 2c and e); the mixing ratio of a selected VOC ( $\alpha$ -pinene) also decreases to  $0 \text{ ppb}$  (Fig. 2d). Furthermore, after  $\sim 3 \text{ h}$  of illumination in our cleaned bag (i.e. clean air plus light experiments) the particle number and mass concentrations remain at the background levels (see Fig. S1 in the Supplement). This shows that our overall chamber gas-phase background is sufficiently low to prevent the formation of particles in the presence of light and in the absence of reactants. Overall, before the addition of the reactants to the MAC, our automated cleaning procedure ensures rapid cleaning that results in repeatedly low background concentrations.

## 2.8 Instrumentation

A range of instruments can be used to measure the physical and chemical properties of the chamber air, as shown in Table 1. The table is separated into two parts, displaying the core instrumentation, which is permanently fixed at



**Figure 2.** Time series (mean  $\pm 1\sigma$ ,  $n = 3$ ) of O<sub>3</sub> (a), NO<sub>x</sub> (b), particle number (c), VOC ( $\alpha$ -pinene; d), and particle mass (e) from three identical experiments conducted in the MAC. Annotations provide information of the related process occurring in the chamber at each time point, normalised to the injection time of the reactants. Cleaning process duration is  $\sim 2$  h, while subsequently the chamber is left with clean air for about 1 h prior to the addition of the reactants (“clean chamber”). After the addition of the reactants, the chamber is stabilised in the dark for another hour (“dark stabilisation”) before the lights are turned on.

the chamber, as well as the additional instrumentation, which can be coupled to the chamber and used on demand. All the instruments sample from a number of ports in the manifolds, equipped with stainless steel or PTFE tubing extending to the middle of the chamber.

NO and NO<sub>2</sub> are measured using a NO<sub>x</sub> Thermo 42i chemiluminescence analyser. O<sub>3</sub> is measured by an Thermo 49C analyser. Both NO<sub>x</sub> and O<sub>3</sub> analysers are regularly calibrated using certified cylinders and an ozone calibrator, respectively. Water-based condensation particle counters (wCPCs; model 3785 and 3786) have been selected as core instrumentation operating in the chamber room to avoid the interference of the volatile working fluid (e.g. butanol), usually found on other CPC units, diffusing into the chamber. A wCPC is being used to measure the total particle con-

centration in the chamber, and the other is coupled to a differential mobility analyser (DMA; Brechtel Inc) as part of a custom-built differential mobility particle sizer (DMPS) system to measure particle size distributions in the 40–600 nm range. The DMA uses filtered chamber air as sheath flow to maintain the gas–particle equilibrium during the measurements.

The chamber is equipped with a removable 47 mm filter holder, which is located at the flushing line of the chamber (see Fig. 1) and can be loaded with the desired substrate and enable the sampling of the entire contents of the chamber at the end of each experiment at a high flow rate ( $3 \text{ m}^3 \text{ min}^{-1}$ ). In such a way, adequate amounts of particulate mass can be collected for subsequent off-line analysis.

A selection of additional instrumentation that is shared within the Centre for Atmospheric Sciences (CAS) group at the University of Manchester is potentially available to be used on demand. Briefly, oxygenated VOCs are measured using a high-resolution time-of-flight chemical ionisation mass spectrometer (CIMS; Aerodyne/Tofware) using iodide as a reagent ion. Non-refractory  $\text{PM}_{10}$  composition is measured using a high-resolution time-of-flight aerosol mass spectrometer (HR-ToF-AMS; Aerodyne), while oxygenated particulate organic composition is measured using the filter inlet for gases and aerosols (FIGAERO) when coupled to a CIMS. Total organic and elemental carbon concentrations are measured using a semi-continuous carbon aerosol analyser (OC/EC, Sunset Laboratory, Model 4). Selection of particles based on their mass or their aerodynamic size can be achieved using a centrifugal particle mass analyser (Cambustion) and an aerodynamic aerosol classifier (Cambustion), respectively. Particle hygroscopicity and volatility are measured by a custom-built hygroscopicity tandem differential mobility analyser (HTDMA) and thermal denuder (TD), respectively, while cloud condensation nuclei (CCN) activity is measured by a CCN counter (Droplet measurement Technologies). Black carbon concentration and properties can be measured by a three-wavelength photoacoustic spectrometer and single-particle soot photometer (Droplet measurement Tech).

Routinely, additional instruments, such as a gas chromatograph coupled to a mass spectrometer (GC-MS), and a proton transfer reaction (PTR) ionisation scheme were added to the MAC as part of collaborative work to measure VOC concentrations (Alfarra et al., 2013; Wyche et al., 2014, 2015). Similarly, offline particle analysis using liquid chromatography tandem mass spectrometry (LC-MS/MS) and two-dimensional GC-MS (2D-GC-MS) have also been employed occasionally to probe the chemical characteristics of the SOA particles (Hamilton et al., 2011; Wyche et al., 2015).

### 3 MAC characterisation

This section describes the characterisation of each element of the chamber with relevance to the operation and influence on and interpretation of the experimental results.

#### 3.1 Temperature and relative humidity

The temperature in the MAC is controlled by the AC system, which compensates the releasing heat from illumination system. The calibrated dew point hygrometer (EdgeTech sensor) is used as a reference for Sensirion capacitance sensors during dark conditions (no irradiation of the chamber), where there is no influence of temperature gradient caused by the light sources. The dark experiment at a set temperature of  $16^{\circ}\text{C}$  and two photo-oxidation experiments at different set points of relative humidity (40 % and 70 %) and a set tem-

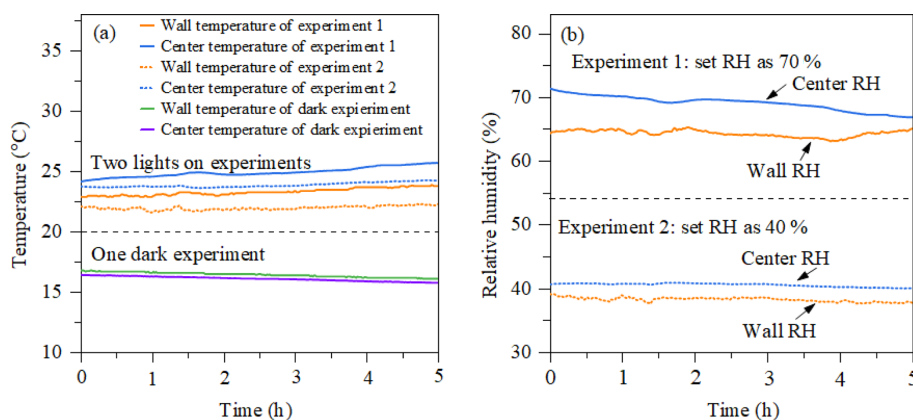
perature of  $25^{\circ}\text{C}$  were conducted to examine the temperature and relative humidity homogeneity of the chamber.

Figure 3a shows the evolution of temperature at the chamber wall and at the centre of the chamber measured by the EdgeTech and one Sensirion sensor, respectively, during dark and photo-oxidation experiments. The temperature accuracy of sensors is  $\pm 0.3$  and  $\pm 0.2^{\circ}\text{C}$  for the Sensirion sensor and EdgeTech sensor at  $25^{\circ}\text{C}$ , respectively. In photo-oxidation experiments, the temperature in the chamber centre ( $24 \pm 1^{\circ}\text{C}$ ) is stable and slightly higher than that in the chamber wall ( $23 \pm 1^{\circ}\text{C}$ ). Such a gradient might be caused by the cooler air between the chamber wall and enclosure and incomplete mixing. The temperature in dark conditions shows good agreement with the two sensors, around  $16^{\circ}\text{C}$ . Figure 3b shows the relative humidity results of the two photo-oxidation experiments measured by the Sensirion and EdgeTech sensors. In the light experiment, the RH in the centre of the chamber measured by the Sensirion capacitance sensor ( $40 \pm 1\%$  and  $70 \pm 1\%$ ) was slightly higher than the RH at the wall of the chamber measured by the EdgeTech hygrometer ( $39 \pm 1\%$  and  $65 \pm 1\%$ ). In the light experiments, it appears that both the temperature and humidity were higher in the centre of the MAC than at the wall, while in the dark experiments these differences were negligible as they were within the uncertainty in our measurement. A likely explanation for this unexpected behaviour in the light experiments can be possibly due to the radiative heating of the sensors in these experiments, which could result in an overestimation of the RH.

#### 3.2 Mixing

$\text{NO}$ ,  $\text{NO}_2$ , and  $\text{NO}_x$  are selected as gas tracers to test the gas-phase mixing time inside the reactor. There are no fans or other equipment inside the chamber; however,  $\text{NO}_x$  is injected as  $\text{NO}_2$  into the  $3\text{ m}^3\text{ min}^{-1}$  ( $= 50\text{ L s}^{-1}$ ) flow through the 50 mm diameter inlet at a velocity of approximately  $25\text{ m s}^{-1}$ , inducing near-instantaneous mixing throughout the chamber. Throughout an experiment, the forceful agitation of the Teflon walls by the AC flow between the enclosure and chamber continuously maintains mixing inside the reactor. As shown in Fig. 2b (for clarity see Fig. S2a in the Supplement), the mixing time for  $\text{NO}$ ,  $\text{NO}_2$ , and  $\text{NO}_x$  gases is on the order of a few minutes. Typically, the mixing time in atmospheric-simulation chambers falls within the range of minutes, for example, 1 min in the CESAM (Multiphase Atmospheric Experimental Simulation) chamber with  $4.2\text{ m}^3$  (Wang et al., 2011) and 2 min in the GIG-CAS chamber  $30\text{ m}^3$  (Wang et al., 2014).

Non-acidic seed particles (ammonium sulfate, AS) were chosen to examine the mixing time of particles in the chamber. Briefly, seed particles were injected into the seed aerosol residence chamber (Fig. 1) and mixed for 1 min and subsequently introduced into the chamber at the flow rate of  $3\text{ m}^3\text{ min}^{-1}$ . Figure 2c (for clarity see Fig. S2b) shows the



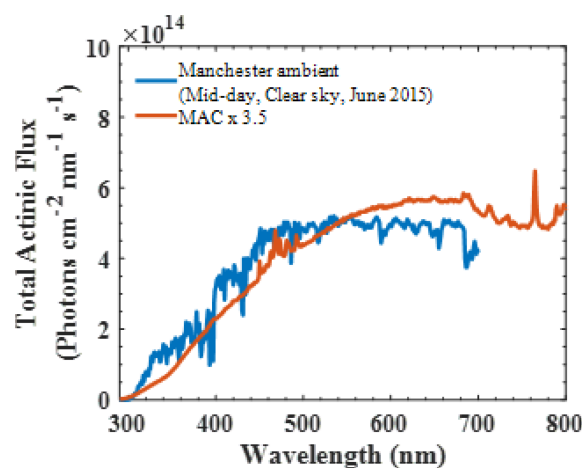
**Figure 3.** (a) Temperature as a function of time measured by the EdgeTech (wall temperature) and Sensirion (centre temperature) in a dark experiment and a photo-oxidation experiment. (b) RH as a function of time in the two photo-oxidation experiments.

number concentration of particles measured by the wCPC as a function of time, which shows that the mixing time for seed particles in the chamber is around 2.5 min. This time is comparable with the gases' mixing time in the chamber. Furthermore, as can be seen, after the addition of  $\text{NO}_x$  and seed aerosol to the chamber and the air condition is turned on, the mixing ratios of  $\text{NO}_x$  remain constant within a few minutes after their injection. Similarly, the number concentration of the seed aerosol shows some fluctuations over the first  $\sim 10$  min, and they appear to stabilise and be subjected to the expected losses to the chamber walls. The stability in the measured concentrations of those tracers provides evidence for the effectiveness of the mixing of the components of the MAC, while the low standard deviations between the experiments (shown as shaded areas) further demonstrate the repeatability that can be achieved in our system.

### 3.3 Light intensity

The artificial radiation in the MAC has a broad radiation distribution owing to the chosen combination of illumination sources, producing irradiation over the wavelength range 290–800 nm to capture all wavelengths of the atmospheric actinic spectrum. Figure 4 shows the total actinic flux measured in the MAC (red line) multiplied by 3.5 compared with the Manchester midday clear-sky measurements on a June day. The total actinic flux in the MAC was measured the centre position of chamber bag (150 cm apart from the arc lamps on both vertical and horizontal axes).

The photolysis rate of  $\text{NO}_2$  ( $j_{\text{NO}_2}$ ) estimated in steady-state actinometry can be used as a confirmation of the light intensity in the chamber (Hu et al., 2014) measured by direct spectral radiometry. Such actinometric measurements were carried out by injecting  $\text{NO}_2$  into the chamber and irradiating for several hours, measuring the concentration of  $\text{NO}$ ,  $\text{NO}_2$ , and  $\text{O}_3$  continuously. A series of  $\text{NO}_2$  actinometry experiments were conducted with  $\sim 70$  ppb  $\text{NO}_2$  injected into



**Figure 4.** Total actinic flux spectrum in the MAC compared to the ambient light spectrum obtained in the city of Manchester (UK) midday with a clear sky in June 2015.

the chamber and irradiated for more than 3 h, with the temperature and humidity maintained at around 25 °C and 50 %, respectively. The photolysis frequency of  $\text{NO}_2$  is calculated from

$$j_{\text{NO}_2} = \frac{k_{\text{NO}+\text{O}_3} \times [\text{NO}] \times [\text{O}_3]}{[\text{NO}_2]}, \quad (1)$$

where  $k_{\text{NO}+\text{O}_3}$  is the rate constant of the reaction of  $\text{O}_3$  and  $\text{NO}$  ( $1.8 \times 10^{-14} \text{ cm}^3 \text{ molec.}^{-1} \text{ s}^{-1}$  at 298 K) (Atkinson et al., 2004).

In the MAC, the photolysis rate of  $\text{NO}_2$  ( $j_{\text{NO}_2}$ ) as derived from our steady-state actinometry experiments was comparable, within our measured variability, with that directly measured from the integrated absorption across the measured wavelengths ( $2.25 \pm 0.4$  vs.  $1.5 \times 10^{-3} \text{ s}^{-1}$ , respectively). Given that the  $j_{\text{NO}_2}$  obtained by the actinometry experiments is an average and is estimated based on the assumption of photostationary state for trace gases in the bag,

while the spectral radiometry is a point measurement in an imperfect integrating sphere, which could not be representative of the whole chamber, these results are in reasonable agreement. The integrated  $j\text{NO}_2$  measured by spectral radiometry in the ambient Manchester on clear sky over the summer was  $7 \times 10^{-3} \text{ s}^{-1}$  but had a comparable light spectrum to that measured in the MAC. The values obtained in the MAC are more similar to those reported previously over the wintertime at Finokalia station, Greece (Gerasopoulos et al., 2012), and are generally comparable with those obtained across the broader simulation chamber community, as shown in Table 2.

### 3.4 Wall loss of gaseous compounds

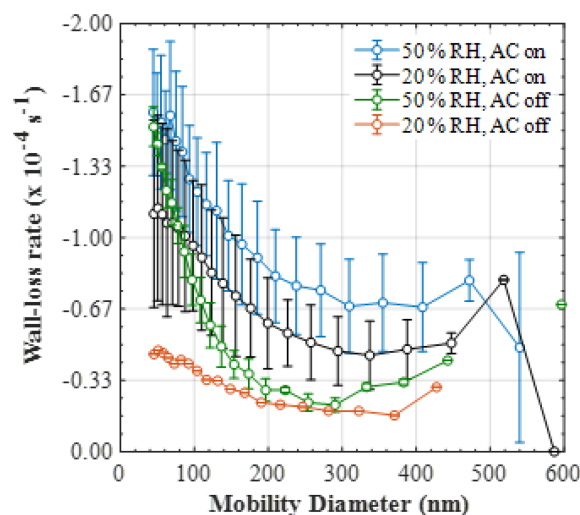
Chamber wall adsorption had been shown to be a substantial source of gas losses inside Teflon bags (Wang et al., 2011) and will influence the gas-phase reactivity and SOA formation. In the MAC, the wall loss rates of  $\text{NO}_2$ ,  $\text{O}_3$ , and several volatile organic compounds ( $\alpha$ -pinene, toluene, 1,3,5-TMB, and limonene) were investigated by injecting known concentrations into the chamber and measuring their concentration decay for an extended period under dark conditions. An approximate 50 ppb concentration of  $\text{NO}_2$  and  $\text{O}_3$  at concentrations ranging from 120 to 350 ppb were injected into the chamber and monitored for 4 h, allowing sufficient time for a measurable decay. Selecting different concentration of  $\text{O}_3$  could assist in investigating the impact of their initial concentration on the wall loss rate in the MAC. For the wall loss experiments of volatile organic species, 50 ppb of each compound was injected into the chamber, with the decay monitored for  $\sim 4$  h. All the wall loss experiments of gaseous species were conducted under a  $T$  and RH of  $\sim 25^\circ\text{C}$  and  $\sim 50\%$ , respectively.

Measured first-order wall loss rates of selected gaseous species were calculated by considering their decay as a first-order process. The wall loss rates of  $\text{NO}_2$  and  $\text{O}_3$  were  $9.40 \pm 7.38 \times 10^{-7}$  and  $2.09 \pm 0.97 \times 10^{-6} \text{ s}^{-1}$ , respectively. Table 2 compares the wall loss rates of  $\text{NO}_2$  and  $\text{O}_3$  between the MAC and other chambers. The  $\text{NO}_2$  decay rate at the MAC was slightly higher than all the other chambers listed, except GIG-CAS, while the  $\text{O}_3$  decay rate of the MAC was higher than the TU and KNU chamber but lower than the GIG-CAS and PSI chamber.

The first-order wall loss rates of the selected anthropogenic and biogenic VOCs were  $2.24 \pm 0.67 \times 10^{-5} \text{ s}^{-1}$  for  $\alpha$ -pinene,  $2.08 \pm 0.54 \times 10^{-5} \text{ s}^{-1}$  for limonene,  $2.06 \pm 1.25 \times 10^{-5} \text{ s}^{-1}$  for toluene, and  $12.22 \pm 0.90 \times 10^{-5} \text{ s}^{-1}$  for 1,3,5-TMB.

### 3.5 Wall losses of particles

Particles are deposited to chamber walls mainly due to natural convection, diffusion, gravitational settling, and electrostatic forces in addition to physical mixing (Crump et



**Figure 5.** Mean ( $\pm 1\sigma$ ) size-resolved wall loss rate ( $\text{s}^{-1}$ ) of particles in the MAC at various relative humidities and mixing conditions (50 % RH and mixing,  $n = 9$ ; 20 % RH and mixing,  $n = 5$ ; 50 % RH and no mixing,  $n = 3$ ; 20 % RH and no mixing,  $n = 1$ ).

al., 1983; Pierce et al., 2008; McMurry and Rader, 1985). Several different approaches have been proposed to determine and account for these losses to the chamber walls that are largely size-dependent (Charan et al., 2019). Most commonly, the particle wall losses are determined by injecting particles with measurable sizes into the chambers and subsequently measuring their size-resolved loss rates by treating the decay as a first-order process (Murphy et al., 2006; Zhang et al., 2007). A series of experiments were conducted to investigate the size-resolved particle lifetimes under various humidity and mixing conditions using AS seed, which was introduced to the chamber and left in the dark at the desired RH and temperature conditions for  $\geq 4$  h. An initial seed concentration of  $50\text{--}100 \mu\text{g m}^{-3}$  was used with a modal diameter of  $\sim 100$  nm. The size-resolved concentration of the AS seed was monitored using a DMPS at  $40\text{--}600$  nm range, with a 10 min scanning time. Here, in line with the literature (Cocker et al., 2001b; Donahue et al., 2012; Gallimore et al., 2017; Smith et al., 2019), the particle wall loss rate was retrieved by fitting an exponential function to the decay of the particle number in each size bin of the DMPS to obtain a size-resolved decay rate coefficient. A comparison between the application of different particle wall loss correction methods is shown in Sect. 3.5.1.

The mean ( $\pm 1\sigma$ ) size-resolved wall loss rates ( $\text{s}^{-1}$ ) of particles in the MAC at various relative humidity and mixing conditions are shown in Fig. 5. The size-resolved particle wall loss rate in all experimental types showed a decreasing trend with particle size. In the size range measured here, such behaviour has been observed previously in chambers with varying volumes (Wang et al., 2018) and was attributed to the high diffusivity of the particles in the range

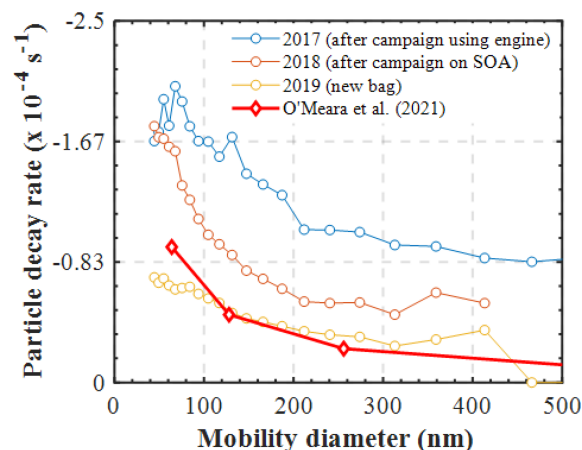


**Table 2.** NO<sub>2</sub> and O<sub>3</sub> wall loss rates as well as  $j_{\text{NO}_2}$  obtained in this study and the literature.

| Chamber   | Wall loss rate (s <sup>-1</sup> ) |                       | $j_{\text{NO}_2}$ ( $\times 10^{-3}$ s <sup>-1</sup> ) | Reference             |
|-----------|-----------------------------------|-----------------------|--|-----------------------|
|           | NO <sub>2</sub>                   | O <sub>3</sub>        |  |                       |
| MAC       | $0.94 \times 10^{-6}$             | $2.09 \times 10^{-6}$ | 2.25   | This study            |
| KNU       | $7.45 \times 10^{-7}$             | $1.08 \times 10^{-6}$ | 2.83   | Babar et al. (2016)   |
| GIG-CAS   | $2.32 \times 10^{-6}$             | $2.18 \times 10^{-6}$ | 8.17   | Wang et al. (2014)    |
| PSI       | $2.17 \times 10^{-7}$             | $4.00 \times 10^{-6}$ | –  | Metzger et al. (2008) |
| TU        | $6.95 \times 10^{-7}$             | $1.02 \times 10^{-8}$ | 3.83   | Wu et al. (2007)      |
| UCR       | –                                 | –                     | 3.17   | Carter et al. (2005)  |
| AIOFM-CAS | –                                 | –                     | 3.50   | Hu et al. (2014)      |

below 100 nm, in addition to the possible contribution of coagulation when particle number concentrations of the small-sized particles are high. Moreover, a considerable scatter in the data obtained under our typical experimental conditions was observed (i.e. at 50% RH and with the AC on). The large deviations in the size-resolved particle wall loss rates can be possibly attributed to the changes in the chamber behaviour, considering that the experiments averaged here were conducted sporadically over a large time period (2017–2019) and under different conditions of the bag. The latter is investigated further in Sect. 5. Alternatively, such deviations could be also attributed to particle and/or chamber charging effects (Charan et al., 2019). More specifically, considering that the AS particles generated in all of our experiments were not neutralised prior to entering the chamber, the potential charge distribution of the particles could have been varying, with consequent implications to the particle losses. Similarly, Teflon chambers are known to acquire charge when in contact with non-conductive surfaces, in turn affecting the particle losses to the walls. In spite of the MAC being suspended and its operators having minimal to no contact with the bag, it is challenging to experimentally assess the potential effects of the chamber charging on the particle wall losses over such a large time period.

However, the combination of our experimental results presented in this study with those presented earlier using our newly developed PyCHAM model (O'Meara et al., 2021) can provide some further insights on the latter matter. Figure 6 shows the measured size-resolved particle decay from several identical wall loss characterisation experiments (i.e. ammonium sulfate seed in the dark), conducted over a span of 3 years and under various conditions of the MAC. Additionally, the size-resolved wall loss rates that were required to reproduce the SOA formation in the limonene nucleation experiment presented in the O'Meara et al. (2021) study are also shown. Evidently, the variation in the measured loss rates of the particles nebulised in a similar manner in the MAC as a function of the chamber bag history can be substantial. Interestingly, the modelled particle losses that required a nucleation experiment to be reproduced, where no induced charge of the particles is expected, are compara-

**Figure 6.** Measured size-dependent particle decay rates (s<sup>-1</sup>) in characterisation experiments (RH = 50%) conducted under different conditions of the bag. The modelled particle losses in a nucleation experiment are shown for comparison (O'Meara et al., 2021).

ble with those measured in a new bag. What is more, the model of McMurry and Rader (1985) suggests that the differences in the wall loss rates of the particles having 0 and +1 charge can be as high as 2 orders of magnitude (or more) for particles of 100 nm in diameter (see Fig. 9 on O'Meara et al., 2021). Here, the observed differences between the potentially charged AS particles in the characterisation experiments were within the same order of magnitude as those modelled for a nucleation experiment, where no particle charge is expected. Therefore, this analysis suggests that neutralising the seed aerosols prior to injection into the MAC would have less of an effect than the usage history of the bag.

In either of the relative humidity conditions (e.g. 20% and 50%), the continuous agitation of the chamber walls due to the air circulation around the chamber from the AC affected the particle wall losses, showing higher wall loss rates compared to those where the AC was disabled. The enhanced particle wall losses when the AC was enabled can be possibly attributed to the turbulence caused by AC as the chamber

walls agitate, causing the particles to deposit at higher rates (Trump et al., 2016).

The amount of the water vapour also affects the particle wall loss rate, with the experiments conducted under drier conditions having lower loss rates compared to those at moderate RH conditions; however the variability was quite high to unambiguously differentiate the results from both conditions. These results suggest that the experimental conditions can have a significant impact on the particle wall loss rates. Therefore, care should be taken when using the retrieved wall loss rates from such experiments to correct the SOA particle mass in experiments conducted under different environmental conditions.

### 3.5.1 Investigation of various particle wall loss correction methods to the SOA formation

As mentioned above, the retrieved size-resolved ammonium sulfate particle loss rates from characterisation experiments are commonly used to correct the SOA particle mass from VOC oxidation experiments (Ng et al., 2007; Fry et al., 2014; Nah et al., 2017). Several alternative numerical approaches have also been proposed (Wang et al., 2018; Pierce et al., 2008). Here, we compare two different approaches to correct the SOA particle mass from a  $\beta$ -caryophyllene photo-oxidation and a limonene ozonolysis experiment. More specifically, we use the size-resolved mass loss rates retrieved from the characterisation experiments (described in Sect. 3.5.) as well as the modelling approach proposed by Verheggen and Mozurkewich (2006). The results are summarised in Fig. 7. It should be noted that our aim here is not to investigate the characteristics of each method but rather to demonstrate their effect when correcting for particle wall losses in atmospheric-simulation chambers.

The different approaches clearly result in substantially different wall-loss-corrected SOA masses (Fig. 7). In all cases, the correction using the ammonium sulfate size-resolved wall loss rates resulted in greater differences compared to the Verheggen and Mozurkewich (2006) model. These differences can be, at least partly, attributed to the parameters accounted for in each method. The size-resolved particle correction applies the measured particle decay rates from the characterisation experiments to the decay of the particles in the SOA experiments. Effectively, in this method it is assumed that the losses of the AS particles in the characterisation experiments (from any loss process) are the same as those formed in the SOA experiments. On the other hand, the Verheggen and Mozurkewich (2006) model employs inverse modelling to simulate the particle wall losses based on diffusion and gravitational settling, while the losses due to coagulation are indirectly inferred, and the eddy diffusion and the turbulent kinetic energy are treated as empirical parameters based on the Crump et al. (1983) model. Therefore, the differences between the two approaches could be partly attributed to the particle losses due to coagulation, which is indirectly

accounted for in the Verheggen and Mozurkewich (2006) model, as opposed to the size-resolved correction. Alternatively, considering that the seed aerosol generated in our experiments was not neutralised, the particle decay rates measured in the characterisation experiments account for any potential influences of the particle charge on the decay rates of the particles, as opposed to the Verheggen and Mozurkewich (2006) model, thereby possibly further contributing to observed discrepancies. Clearly, treating the particle losses to atmospheric-simulation chambers is not a trivial task, and this could have substantial impacts for the reported SOA yields.

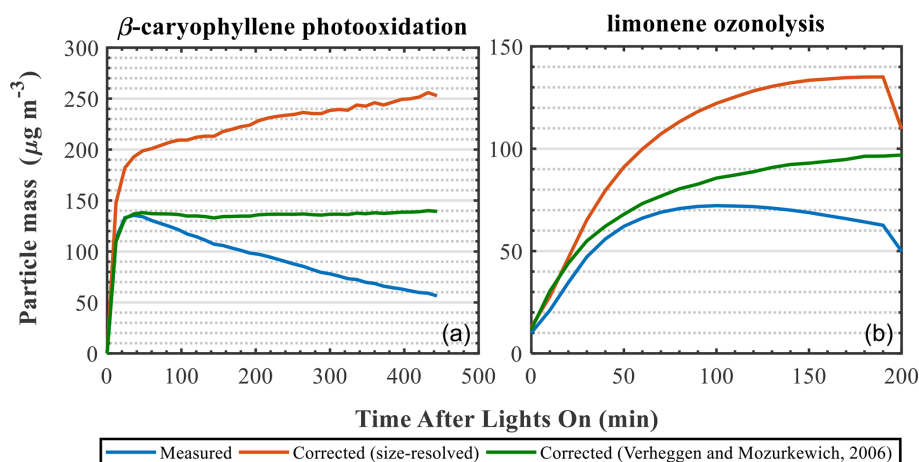
### 3.6 Chamber wall reactivity

The chamber wall reactivity aims to describe the chamber wall activity such that it can be directly used as a data set in future computer modelling to simulate the chamber experiments. A set of experiments were conducted, including simulating clean air and dark decay of  $\text{NO}_2$  and  $\text{O}_3$ . Four non-elementary hypothetical reactions and relevant parameters used in the model are listed in Table 3. The parameters for the  $\text{NO}_2$  and  $\text{O}_3$  formation rate from the Teflon walls were calculated based on the off-gassing experiments under light irradiation conditions for at least 3 h of reaction. The initial concentrations of  $\text{NO}_2$  and  $\text{O}_3$  in the chamber were varied from 0 to 8 ppb. The light-induced formation of  $\text{NO}_2$  and  $\text{O}_3$  from the chamber walls was  $6.95 \pm 1.26 \times 10^{-5}$  and  $8.56 \pm 2.58 \times 10^{-5} \text{ s}^{-1}$ , respectively.

The decrease in  $\text{NO}_2$  and  $\text{O}_3$  in the gaseous phase under dark conditions for the new chamber bag is mentioned in Sect. 3.4. Gas-phase molecules can be lost to the boundary layer of the surface chamber wall by molecular diffusion and macroscopic mixing, while their reactive uptake by the Teflon film and any deposited material is also possible. Teflon film can act as a reservoir for organic vapour deposition during chamber experiments, which may contribute to  $\text{O}_3$  loss by oxidation. Furthermore, the organic compounds deposited can act as absorptive mass, in turn influencing the mass transfer from the gas phase to the walls (Charan et al., 2019).

## 4 Experiment of $\alpha$ -pinene photo-oxidation

To evaluate the chamber facility for the purposes of studying SOA production and transformation,  $\alpha$ -pinene photochemistry experiments were conducted in the MAC. The initial experimental conditions are shown in Table 4. During the experiments, chemical composition ( $\text{NH}_4$ ,  $\text{SO}_4$ ,  $\text{NO}_3$ , OA) in the particle phase and  $\alpha$ -pinene in the gas phase were monitored by the HR-ToF-AMS and semi-continuous GC-MS, respectively. The measured SOA mass by the HR-ToF-AMS was corrected due to the non-unit collection efficiency of the instrument following standard procedures in previous studies



**Figure 7.** Measured and wall-loss-corrected SOA particle mass using two different wall loss correction approaches for a  $\beta$ -caryophyllene photo-oxidation (a) and a limonene ozonolysis (b) experiment.

**Table 3.** Chamber wall activity and rates for chamber-dependent reactions.

| Parameters                           | Gas species     | Rate (mean $\pm$ 1 $\sigma$ )/s <sup>-1</sup> | Experiment  |
|--------------------------------------|-----------------|---|---|
| $(P_{\text{wall,light}})^{\text{a}}$ | NO <sub>2</sub> | $(6.95 \pm 1.26) \times 10^{-5}$              | Direct measurement of NO <sub>2</sub> wall production |
|                                      | O <sub>3</sub>  | $(8.56 \pm 2.58) \times 10^{-5}$              | Direct measurement of NO <sub>2</sub> wall production |
| $(L_{\text{wall,dark}})^{\text{b}}$  | NO <sub>2</sub> | $(9.40 \pm 7.39) \times 10^{-7}$              | Direct measurement of NO <sub>2</sub> wall loss       |
|                                      | O <sub>3</sub>  | $(2.09 \pm 0.9) \times 10^{-6}$               | Direct measurement of O <sub>3</sub> wall loss        |

<sup>a</sup> Production rate of gaseous species from wall under light conditions (P w, l). <sup>b</sup> Loss rate of gaseous species to wall under dark conditions (L w, d).

(Jimenez, 2003; Jayne et al., 2000; Allan et al., 2003, 2004) and chamber wall loss effects (Wang et al., 2018).

To compare with literature data, SOA yield ( $Y$ ) was used as a proxy to evaluate SOA production (Grosjean and Seinfeld, 1989), defined as the SOA mass formation ( $\Delta M_0$ ) from the reactive organic gas ( $\Delta \text{VOC}$ ) consumption as shown in Eq. (2).

$$Y = \frac{\Delta M_0}{\Delta \text{VOC}} \quad (2)$$

Here, the SOA mass is wall-loss-corrected using the size-resolved wall loss rate of ammonium sulfate particles from the nearest characterisation experiment as described in Sect. 3.5.1. Odum et al. (1996) incorporated gas–particle partitioning theory (Pankow, 1994a, b) into SOA formation and calculated SOA yield from individual compounds, shown in Eq. (3).

$$Y = \sum_i Y_i = C_{\text{OA}} \sum_i \left( \frac{\alpha_i K_{\text{p},i}}{1 + K_{\text{p},i} C_{\text{OA}}} \right) \quad (3)$$

Here,  $Y_i$  represents the yield of compound  $i$ ;  $\alpha_i$  is a stoichiometric factor representing the ratio of the molecular weight of product  $i$  to the parent VOC.  $K_{\text{p},i}$  and  $C_{\text{OA}}$  are the partitioning coefficient of product  $i$  and the total absorbing organic mass (the same as  $\Delta M_0$  herein). Furthermore, Odum

et al. (1996) successfully used a two-product model parameterising SOA yield and  $\Delta M_0$  as shown in Eq. (4). The  $\alpha_1$ ,  $\alpha_2$ ,  $K_{\text{p},1}$ , and  $K_{\text{p},2}$  can be fitted upon yield curves.

$$\begin{aligned} Y &= \frac{\Delta M_0}{\Delta \text{VOC}} Y \\ &= \sum_i Y_i \\ &= C_{\text{OA}} \sum_i \left( \frac{\alpha_i K_{\text{p},i}}{1 + K_{\text{p},i} C_{\text{OA}}} \right) Y \\ &= C_{\text{OA}} \left( \frac{\alpha_1 K_{\text{p},1}}{1 + K_{\text{p},1} C_{\text{OA}}} + \frac{\alpha_2 K_{\text{p},2}}{1 + K_{\text{p},2} C_{\text{OA}}} \right) \end{aligned} \quad (4)$$

The yield curves as a function of  $\Delta M_0$  for the three  $\alpha$ -pinene experiments in this study and the comparison with literature data (Saathoff et al., 2009; Cocker et al., 2001a; Eddingsaas et al., 2012; Stirnweis et al., 2017) are shown in Fig. 8 (all yield curves are wall-loss-corrected). As expected from the absorptive partitioning, it can be seen that the SOA yield increased consistently with an increase in absorptive organic mass for the three  $\alpha$ -pinene experiments in this study. Our results are qualitatively and quantitatively comparable with  $\alpha$ -pinene photochemistry experiments conducted under different oxidant conditions (e.g. use of HONO and H<sub>2</sub>O<sub>2</sub>)



**Table 4.** Summary of initial conditions for  $\alpha$ -pinene photochemistry experiments.

| Expiration date | VOC type         | [VOC] <sub>0</sub> (ppbV) | VOC/NO <sub>x</sub> | T (°C) | RH (%) | AS seed concentration ( $\mu\text{g m}^{-3}$ )* |
|-----------------|------------------|---------------------------|---------------------|--------|--------|---|
| 28 Mar 2019     | $\alpha$ -pinene | 309                       | 7.7                 | 26.7   | 50.5   | 60.7  |
| 6 Jul 2019      | $\alpha$ -pinene | 155                       | 6.0                 | 25.9   | 53.1   | 61.3  |
| 13 Jul 2019     | $\alpha$ -pinene | 103                       | 5.7                 | 27.2   | 54.5   | 55.4  |

\* Measured NR-PM (non-refractory particulate matter) mass concentration by HR-ToF-AMS with corrected collection efficiency (30 min average before lights on).

and seed initialisations (no/acidic/neutral) in other chambers. They are also comparable with experiments conducted at different VOC/NO<sub>x</sub> ratios in the range of 0.2 to 25 and AS and ammonium bisulfate (ABS) seed conditions (Stirnweis et al., 2017). Additionally, we use the two-product model to fit the yield curve of the three  $\alpha$ -pinene experiments in this study, and the fitted  $\alpha_1$ ,  $\alpha_2$ ,  $K_{p,1}$ , and  $K_{p,2}$  are 0.03, 0.34,  $3.14 \times 10^6$ , and 0.02, respectively, as shown in Fig. 8 (solid black line). The fitted yield curve for  $\alpha$ -pinene photochemistry with the aqueous AS seed in this study is comparable to the  $\alpha$ -pinene ozonolysis without a seed (Stirnweis et al., 2017; Cocker et al., 2001a) but much higher than the ozonolysis with an aqueous seed (Cocker et al., 2001a).

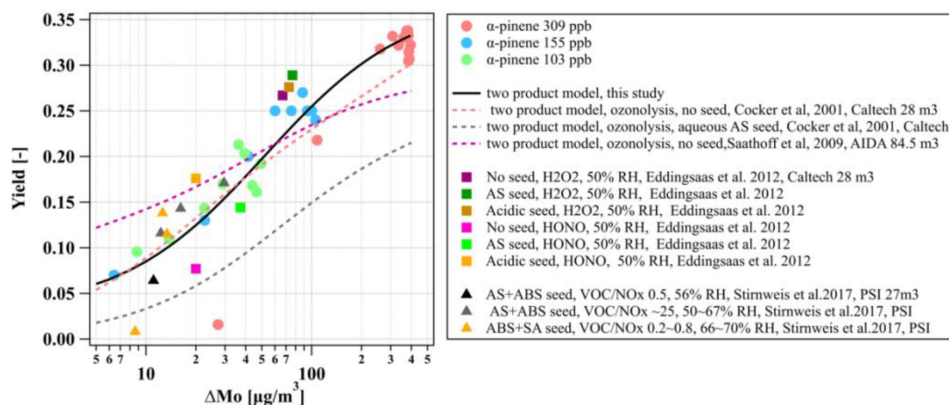
## 5 Effects of contamination on chamber performance

It has been shown that organic vapours can condense on the Teflon chamber walls in a similar manner to the losses of particles (Matsunaga and Ziemann, 2010; Zhang et al., 2014; Krechmer et al., 2020). The deposition of those compounds on the chamber walls can be reversible (Matsunaga and Ziemann, 2010) or quasi-irreversible (Ye et al., 2016) and is proportional to each compound's volatility and chemical characteristics. Similarly, other atmospheric gases, such as HONO, have also been found to condense on chamber walls (Rohrer et al., 2005). The uptake of semi-volatile vapours from the chamber walls has been proven to substantially affect the oxidative chemistry and thereby the reported SOA formation potential (Zhang et al., 2014; Rohrer et al., 2005). It is therefore likely that both gaseous and particle deposition can lead to a build-up of contamination on chamber walls with time (Huang et al., 2018). It is not guaranteed that any cleaning procedures are completely effective, and it is important to consider the experimental history of a chamber when interpreting experimental behaviour (and particularly when comparing experiments conducted in different periods). To assess the effect of contamination from such sources on the chamber performance, we conducted the same characterisation experiments as those described in Sects. 3.3–3.5 in an extensively used Teflon bag after a series of experiments with high concentrations of particles and gases derived from diesel engines.

The photolysis rate of NO<sub>2</sub> (i.e.  $j\text{NO}_2$ ) derived from photostationary-state calculations was found to be lower in

the extensively used bag compared to a newly installed bag ( $1.83 \pm 0.47 \times 10^{-3}$  vs.  $2.25 \pm 0.40 \times 10^{-3} \text{ s}^{-1}$ , respectively). This coincided with a substantial increase in the wall loss rate of NO<sub>2</sub> and O<sub>3</sub> that was observed in the extensively used compared to the newly installed bag ( $7.95 \pm 6.90 \times 10^{-6}$  vs.  $0.93 \pm 0.76 \times 10^{-6} \text{ s}^{-1}$  for the NO<sub>2</sub> and  $2.23 \pm 1.83 \times 10^{-5}$  vs.  $0.20 \pm 0.08 \times 10^{-5} \text{ s}^{-1}$  for the O<sub>3</sub>, respectively). At the same time, the wall production (i.e. off-gassing) of the same gases was decreased ( $0.12$  vs.  $0.19 \pm 0.04 \times 10^{-7} \text{ s}^{-1}$  for the NO<sub>2</sub> and  $0.20$  vs.  $0.24 \pm 0.07 \times 10^{-7} \text{ s}^{-1}$  for the O<sub>3</sub>). Unfortunately, spectral radiometry data are not available for the extensively used bag, which could help to identify whether the reduction in the  $j\text{NO}_2$  is attributed to the transparency of the walls over usage of the bag or the changes in the production and loss of gases from and to the chamber walls. In the absence of such information, we can only speculate that the changes in the  $j\text{NO}_2$  over the bag history could be attributable to the differences in the wall loss rates of these gases.

In addition to the changes in the decay rates of gases, similar changes were observed in the wall losses of particles. Figure 6 shows the measured size-dependent particle decay rates ( $\text{s}^{-1}$ ) in characterisation experiments conducted under different conditions of the bag. More specifically, characterisation experiments conducted in an extensively used bag after a campaign using diesel engine fumes, in a used bag after a campaign of SOA formation, and in a new bag are shown. Clearly, the size-dependent losses of the particles can be substantially affected by the condition and the usage of the bag. Wang et al. (2018) reported significant changes in the wall loss rates of particles after major maintenance activities in the area where the chamber was suspended and attributed those differences to the electrostatic forces caused by friction. In our set-up, the chamber is enclosed in a housing, and the operators have little to no contact with its walls, so it may be unlikely that this is the main cause for the changes in the particle wall losses over the bag usage history. Considering that the correction of the SOA mass and particle yield calculations are strongly dependent on the measured particle loss rates in characterisation experiments, at least for the MAC, it is recommended that more frequent particle and gas loss characterisation experiments be conducted to enable more reliable corrections.



**Figure 8.** Yield curves derived from the photo-oxidation of  $\alpha$ -pinene on aqueous AS seed conducted in this study and from literature data (Cocker et al., 2001a; Saathoff et al., 2009; Eddingsaas et al., 2012; Stirnweis et al., 2017). All experiments are carried out under humid conditions. Lines represent the two-product model fit for yield curves.

## 6 Discussion and conclusions

In this work, the MAC facility was comprehensively described and characterised for the first time. The MAC is a batch reactor and showed good temperature and relative homogeneity, parameters that can influence the SOA formation and partitioning (Cocker et al., 2001a; Saathoff et al., 2009; Stirnweis et al., 2017). Although our reported experiments in this study were performed only under certain conditions, the results shown demonstrate that the MAC can provide controlled temperature and relative humidity conditions, which are important for any systematic chamber study. The MAC is, however, limited to an RH range of 25%–80% and temperature of 15–35°C, owing to the heat generated by the lamps and the capacity of the AC unit.

Due to its explicit set-up, the generated light spectrum mimics the ambient solar radiation spectrum well, comparable to that in Manchester, yet having lower total actinic flux by a factor of  $\sim 3.5$ . Furthermore, fast mixing times are effected by the injection of the reactants at high flow rates, while the air circulation around the chamber housing continuously agitates the chamber walls, resulting in sufficient mixing of its components during the experiments, but enhances wall losses.

The bespoke control system of the MAC allows the generation of automated procedures that can improve the duty cycle and enhance the comparability across experiments. Moreover, due to its design, gases and particles generated via a number of sources can be introduced to the chamber and studied in detail. In addition, its unique capability of transferring the whole contents of the MAC to the MICC provides the grounds for aerosol–cloud interaction studies (e.g. Frey et al., 2018).

Different wall loss rates of  $\text{NO}_2$  were observed between the MAC and other chambers, as shown in Sect. 3.4. Possibly, the wall loss rates of gaseous compounds are affected by experimental conditions (such as temperature and RH), mix-

ing, and chamber sizes (Metzger et al., 2008; Wang et al., 2011). Importantly, we showed that the usage history can influence the wall loss of gases, with a higher wall loss rate of  $\text{NO}_2$  and  $\text{O}_3$ , which may result in the lower  $j_{\text{NO}_2}$  in an extensively used bag, as shown in Sect. 5. Higher particle decay rates were also observed in an extensively used bag after “dirty” experiments compared to a newly installed bag. It is more likely that the contaminated chamber walls may provide additional sinks to absorb more particles and gases irreversibly. Additionally, the various methods for the particle wall loss correction led to different wall-loss-corrected SOA masses, which in turn can have substantial implications for the derived SOA yields (Odum et al., 1996; Wang et al., 2018; Hoffmann et al., 1997), as shown in Sect. 3.5.1. This illustrates that using different approaches or experimental data sets to conduct such corrections may result in bias in the SOA yields (Cocker et al., 2001a; Saathoff et al., 2009; Stirnweis et al., 2017).

Our measured SOA yield curve from the photo-oxidation of  $\alpha$ -pinene in the presence of seed particles appeared to be comparable with other studies that conducted ozonolysis experiments in the absence of seed particles (Cocker et al., 2001b; Stirnweis et al., 2017) but much higher than the ozonolysis with an aqueous seed (Cocker et al., 2001a), as shown in Fig. 8. However, it should be considered that the comparison of yield curves between different laboratories and facilities is quite complicated as there are many factors (seed or no seed, oxidants, relative humidity, VOC/ $\text{NO}_x$  ratios, wall loss correction methods, etc.) that will affect the yields curves. Also, the characterisation parameters of a chamber (e.g. gases and particle wall loss rates) may also play an important role in the SOA formation, as shown in Sect. 3.5.1. and discussed further above. Furthermore, the loss of condensable vapours to the chamber walls can result in a lower SOA formation even for high-seed-concentration conditions (Zhang et al., 2014).

Based on our results, regular characterisation experiments are recommended in order to track the chamber's performance while accounting for any potential changes to the interpretation of the results. Considering that the atmospheric-simulation chambers are composed of various materials, and they come in different designs, sizes, and shapes, in turn affecting their performance and behaviour, the comparability of their results should be a crucial priority of the scientific community. The results presented here highlight the need to develop a set of simple, standardised experiments and/or procedures that can be used for chambers across the globe in an effort to elucidate the characteristics of each facility and the interpretation of their results.

*Data availability.* All the data used in this study are available upon request from the corresponding authors.

*Supplement.* The supplement related to this article is available online at: <https://doi.org/10.5194/amt-15-539-2022-supplement>.

*Author contributions.* GM, MRA, AV, YW, MD and YS conceived the study. GM, MRA and SFT designed the MAC. SPO provided the modelling results. AV, YW, YS and MD conducted the experiments, the data analysis and wrote the manuscript with inputs from all authors.

*Competing interests.* The contact author has declared that neither they nor their co-authors have any competing interests.

*Disclaimer.* Publisher's note: Copernicus Publications remains neutral with regard to jurisdictional claims in published maps and institutional affiliations.

*Special issue statement.* This article is part of the special issue "Simulation chambers as tools in atmospheric research (AMT/ACP/GMD inter-journal SI)". It is not associated with a conference.

*Acknowledgements.* The Manchester Aerosol Chamber was supported by the EUROCHAMP2020 research programme funded by the European Union's Horizon 2020 research and innovation programme under grant agreement no. 730997. Aristeidis Voliotis and Mao Du acknowledge the financial support from the Presidents Doctoral Scholarship from the University of Manchester. Aristeidis Voliotis acknowledges the support by the Natural Environment Research Council (NERC) EAO Doctoral Training Partnership. Yu Wang acknowledges CSC scholarship support. M. Rami Alfarra acknowledges funding support from the Natural Environment Research Council (NERC) through the UK National Centre for Atmospheric Science (NCAS). Instrumentation support was funded

through the NERC Atmospheric Measurement and Observational Facility (AMOF).

*Financial support.* This research has been supported by the Natural Environment Research Council through the Doctoral Training Partnership (grant no. NE/L002469/1).

*Review statement.* This paper was edited by Jean-Francois Doussin and reviewed by two anonymous referees.

## References

- Alfarra, M. R., Hamilton, J. F., Wyche, K. P., Good, N., Ward, M. W., Carr, T., Barley, M. H., Monks, P. S., Jenkin, M. E., Lewis, A. C., and McFiggans, G. B.: The effect of photochemical ageing and initial precursor concentration on the composition and hygroscopic properties of  $\beta$ -caryophyllene secondary organic aerosol, *Atmos. Chem. Phys.*, 12, 6417–6436, <https://doi.org/10.5194/acp-12-6417-2012>, 2012.
- Alfarra, M. R., Good, N., Wyche, K. P., Hamilton, J. F., Monks, P. S., Lewis, A. C., and McFiggans, G.: Water uptake is independent of the inferred composition of secondary aerosols derived from multiple biogenic VOCs, *Atmos. Chem. Phys.*, 13, 11769–11789, <https://doi.org/10.5194/acp-13-11769-2013>, 2013.
- Allan, J. D., Jimenez, J. L., Williams, P. I., Alfarra, M. R., Bower, K. N., Jayne, J. T., Coe, H., and Worsnop, D. R.: Quantitative sampling using an Aerodyne aerosol mass spectrometer 1. Techniques of data interpretation and error analysis, *J. Geophys. Res.-Atmos.*, 108, 4090, <https://doi.org/10.1029/2002jd002358>, 2003.
- Allan, J. D., Delia, A. E., Coe, H., Bower, K. N., Alfarra, M. R., Jimenez, J. L., Middlebrook, A. M., Drewnick, F., Onasch, T. B., Canagaratna, M. R., Jayne, J. T., and Worsnop, D. R.: A generalised method for the extraction of chemically resolved mass spectra from Aerodyne aerosol mass spectrometer data, *J. Aerosol Sci.*, 35, 909–922, <https://doi.org/10.1016/j.jaerosci.2004.02.007>, 2004.
- Atkinson, R., Aschmann, S. M., and Arey, J.: Reactions of hydroxyl and nitrogen trioxide radicals with phenol, cresols, and 2-nitrophenol at  $296 \pm 2$  K, *Environ. Sci. Technol.*, 26, 1397–1403, <https://doi.org/10.1021/es00031a018>, 1992.
- Atkinson, R., Baulch, D. L., Cox, R. A., Crowley, J. N., Hampson, R. F., Hynes, R. G., Jenkin, M. E., Rossi, M. J., and Troe, J.: Evaluated kinetic and photochemical data for atmospheric chemistry: Volume I - gas phase reactions of  $O_x$ ,  $HO_x$ ,  $NO_x$  and  $SO_x$  species, *Atmos. Chem. Phys.*, 4, 1461–1738, <https://doi.org/10.5194/acp-4-1461-2004>, 2004.
- Babar, Z. B., Park, J.-H., Kang, J., and Lim, H.-J.: Characterization of a Smog Chamber for Studying Formation and Physicochemical Properties of Secondary Organic Aerosol, *Aerosol Air Qual. Res.*, 16, 3102–3113, <https://doi.org/10.4209/aaqr.2015.10.0580>, 2016.
- Barnes, I. and Rudzinski, K. J.: *Environmental simulation chambers: Application to atmospheric chemical processes*, Springer Science & Business Media, Zakopane, Poland, 2006.
- Barnes, I., Becker, K. H., and Mihalopoulos, N.: An FTIR product study of the photooxidation of dimethyl disulfide, *J. At-*

- mos. Chem., 18, 267–289, <https://doi.org/10.1007/BF00696783>, 1994.
- Becker, K. H.: Overview on the Development of Chambers for the Study of Atmospheric Chemical Processes, Environmental Simulation Chambers: Application to Atmospheric Chemical Processes, 1–26, Springer, Dordrecht, 2006.
- Behnke, W., Holländer, W., Koch, W., Nolting, F., and Zetzsch, C.: A smog chamber for studies of the photochemical degradation of chemicals in the presence of aerosols, *Atmos. Environ.*, 22, 1113–1120, [https://doi.org/10.1016/0004-6981\(88\)90341-1](https://doi.org/10.1016/0004-6981(88)90341-1), 1988.
- Bianchi, F., Kurtén, T., Riva, M., Mohr, C., Rissanen, M. P., Roldin, P., Berndt, T., Crouse, J. D., Wennberg, P. O., Mentel, T. F., Wildt, J., Junninen, H., Jokinen, T., Kulmala, M., Worsnop, D. R., Thornton, J. A., Donahue, N., Kjaergaard, H. G., and Ehn, M.: Highly Oxygenated Organic Molecules (HOM) from Gas-Phase Autoxidation Involving Peroxy Radicals: A Key Contributor to Atmospheric Aerosol, *Chem. Rev.*, 119, 3472–3509, <https://doi.org/10.1021/acs.chemrev.8b00395>, 2019.
- Bloss, C., Wagner, V., Bonzanini, A., Jenkin, M. E., Wirtz, K., Martin-Reviejo, M., and Pilling, M. J.: Evaluation of detailed aromatic mechanisms (MCMv3 and MCMv3.1) against environmental chamber data, *Atmos. Chem. Phys.*, 5, 623–639, <https://doi.org/10.5194/acp-5-623-2005>, 2005.
- Carlton, A. G., Wiedinmyer, C., and Kroll, J. H.: A review of Secondary Organic Aerosol (SOA) formation from isoprene, *Atmos. Chem. Phys.*, 9, 4987–5005, <https://doi.org/10.5194/acp-9-4987-2009>, 2009.
- Carter, W., Cockeriii, D., Fitz, D., Malkina, I., Bumiller, K., Sauer, C., Pisano, J., Bufalino, C., and Song, C.: A new environmental chamber for evaluation of gas-phase chemical mechanisms and secondary aerosol formation, *Atmos. Environ.*, 39, 7768–7788, <https://doi.org/10.1016/j.atmosenv.2005.08.040>, 2005.
- Carter, W. P. L. and Lurmann, F. W.: Evaluation of a detailed gas-phase atmospheric reaction mechanism using environmental chamber data, *Atmos. Environ. A-Gen.*, 25, 2771–2806, [https://doi.org/10.1016/0960-1686\(91\)90206-m](https://doi.org/10.1016/0960-1686(91)90206-m), 1991.
- Charan, S. M., Kong, W., Flagan, R. C., and Seinfeld, J. H.: Effect of particle charge on aerosol dynamics in Teflon environmental chambers, *Aerosol Sci. Tech.*, 52, 854–871, <https://doi.org/10.1080/02786826.2018.1474167>, 2018.
- Charan, S. M., Huang, Y., and Seinfeld, J. H.: Computational Simulation of Secondary Organic Aerosol Formation in Laboratory Chambers, *Chem. Rev.*, 119, 11912–11944, <https://doi.org/10.1021/acs.chemrev.9b00358>, 2019.
- Cocker, D. R., Clegg, S. L., Flagan, R. C., and Seinfeld, J. H.: The effect of water on gas–particle partitioning of secondary organic aerosol. Part I:  $\alpha$ -pinene/ozone system, *Atmos. Environ.*, 35, 6049–6072, [https://doi.org/10.1016/S1352-2310\(01\)00404-6](https://doi.org/10.1016/S1352-2310(01)00404-6), 2001a.
- Cocker, D. R., Flagan, R. C., and Seinfeld, J. H.: State-of-the-Art Chamber Facility for Studying Atmospheric Aerosol Chemistry, *Environ. Sci. Technol.*, 35, 2594–2601, <https://doi.org/10.1021/es0019169>, 2001b.
- Connolly, P. J., Emersic, C., and Field, P. R.: A laboratory investigation into the aggregation efficiency of small ice crystals, *Atmos. Chem. Phys.*, 12, 2055–2076, <https://doi.org/10.5194/acp-12-2055-2012>, 2012.
- Crump, J. G., Flagan, R. C., and Seinfeld, J. H.: Particle Wall Loss Rates in Vessels, *Aerosol Sci. Tech.*, 2, 303–309, <https://doi.org/10.1080/02786828308958636>, 1983.
- Donahue, N. M., Kroll, J. H., Pandis, S. N., and Robinson, A. L.: A two-dimensional volatility basis set – Part 2: Diagnostics of organic-aerosol evolution, *Atmos. Chem. Phys.*, 12, 615–634, <https://doi.org/10.5194/acp-12-615-2012>, 2012.
- Dunne, E. M., Gordon, H., Kurten, A., Almeida, J., Duplissy, J., Williamson, C., Ortega, I. K., Pringle, K. J., Adamov, A., Baltensperger, U., Barnet, P., Benduhn, F., Bianchi, F., Breitenlechner, M., Clarke, A., Curtius, J., Dommen, J., Donahue, N. M., Ehrhart, S., Flagan, R. C., Franchin, A., Guida, R., Hakala, J., Hansel, A., Heinritzi, M., Jokinen, T., Kangasluoma, J., Kirkby, J., Kulmala, M., Kupc, A., Lawler, M. J., Lehtipalo, K., Makhmutov, V., Mann, G., Mathot, S., Merikanto, J., Miettinen, P., Nenes, A., Onnela, A., Rap, A., Reddington, C. L., Riccobono, F., Richards, N. A., Rissanen, M. P., Rondo, L., Sarnela, N., Schobesberger, S., Sengupta, K., Simon, M., Sipila, M., Smith, J. N., Stozkhov, Y., Tome, A., Trostl, J., Wagner, P. E., Wimmer, D., Winkler, P. M., Worsnop, D. R., and Carslaw, K. S.: Global atmospheric particle formation from CERN CLOUD measurements, *Science*, 354, 1119–1124, <https://doi.org/10.1126/science.aaf2649>, 2016.
- Eddingsaas, N. C., Loza, C. L., Yee, L. D., Chan, M., Schilling, K. A., Chhabra, P. S., Seinfeld, J. H., and Wennberg, P. O.:  $\alpha$ -pinene photooxidation under controlled chemical conditions – Part 2: SOA yield and composition in low- and high-NO<sub>x</sub> environments, *Atmos. Chem. Phys.*, 12, 7413–7427, <https://doi.org/10.5194/acp-12-7413-2012>, 2012.
- Ehn, M., Kleist, E., Junninen, H., Petäjä, T., Lönn, G., Schobesberger, S., Dal Maso, M., Trimborn, A., Kulmala, M., Worsnop, D. R., Wahner, A., Wildt, J., and Mentel, Th. F.: Gas phase formation of extremely oxidized pinene reaction products in chamber and ambient air, *Atmos. Chem. Phys.*, 12, 5113–5127, <https://doi.org/10.5194/acp-12-5113-2012>, 2012.
- Ehn, M., Thornton, J. A., Kleist, E., Sipilä, M., Junninen, H., Pullinen, I., Springer, M., Rubach, F., Tillmann, R., Lee, B., Lopez-Hilfiker, F., Andres, S., Acir, I.-H., Rissanen, M., Jokinen, T., Schobesberger, S., Kangasluoma, J., Kontkanen, J., Nieminen, T., Kurtén, T., Nielsen, L. B., Jørgensen, S., Kjaergaard, H. G., Canagaratna, M., Maso, M. D., Berndt, T., Petäjä, T., Wahner, A., Kerminen, V.-M., Kulmala, M., Worsnop, D. R., Wildt, J., and Mentel, T. F.: A large source of low-volatility secondary organic aerosol, *Nature*, 506, 476–479, <https://doi.org/10.1038/nature13032>, 2014.
- Finlayson-Pitts, B. J. and Pitts, J. N.: Chemistry of the Upper and Lower Atmosphere, Academic Press, San Francisco, USA, 871–942, <https://doi.org/10.1016/B978-012257060-5/50018-6>, 2000.
- Frey, W., Hu, D., Dorsey, J., Alfarra, M. R., Pajunoja, A., Virtanen, A., Connolly, P., and McFiggans, G.: The efficiency of secondary organic aerosol particles acting as ice-nucleating particles under mixed-phase cloud conditions, *Atmos. Chem. Phys.*, 18, 9393–9409, <https://doi.org/10.5194/acp-18-9393-2018>, 2018.
- Fry, J. L., Draper, D. C., Barsanti, K. C., Smith, J. N., Ortega, J., Winkler, P. M., Lawler, M. J., Brown, S. S., Edwards, P. M., Cohen, R. C., and Lee, L.: Secondary organic aerosol formation and organic nitrate yield from NO<sub>3</sub> oxidation of biogenic hydrocarbons, *Environ. Sci. Technol.*, 48, 11944–11953, <https://doi.org/10.1021/es502204x>, 2014.

- Gallimore, P. J., Mahon, B. M., Wragg, F. P. H., Fuller, S. J., Giorio, C., Kourtchev, I., and Kalberer, M.: Multiphase composition changes and reactive oxygen species formation during limonene oxidation in the new Cambridge Atmospheric Simulation Chamber (CASC), *Atmos. Chem. Phys.*, 17, 9853–9868, <https://doi.org/10.5194/acp-17-9853-2017>, 2017.
- Gerasopoulos, E., Kazadzis, S., Vrekoussis, M., Kouvarakis, G., Liakakou, E., Kouremeti, N., Giannadaki, D., Kanakidou, M., Bohn, B., and Mihalopoulos, N.: Factors affecting O<sub>3</sub> and NO<sub>2</sub> photolysis frequencies measured in the eastern Mediterranean during the five-year period 2002–2006, *J. Geophys. Res.*, 117, D22305, <https://doi.org/10.1029/2012JD017622>, 2012.
- Goldstein, A. H. and Galbally, I. E.: Known and Unexplored Organic Constituents in the Earth's Atmosphere, *Environ. Sci. Technol.*, 41, 1514–1521, 2007.
- Good, N., Coe, H., and McFiggans, G.: Instrumentational operation and analytical methodology for the reconciliation of aerosol water uptake under sub- and supersaturated conditions, *Atmos. Meas. Tech.*, 3, 1241–1254, <https://doi.org/10.5194/amt-3-1241-2010>, 2010.
- Gray, H. A., Cass, G. R., Huntzicker, J. J., Heyerdahl, E. K., and Rau, J. A.: Characteristics of atmospheric organic and elemental carbon particle concentrations in Los Angeles, *Environ. Sci. Technol.*, 20, 580–589, <https://doi.org/10.1021/es00148a006>, 1986.
- Grosjean, D. and Seinfeld, J. H.: Parameterization of the formation potential of secondary organic aerosols, *Atmos. Environ.*, 23, 1733–1747, [https://doi.org/10.1016/0004-6981\(89\)90058-9](https://doi.org/10.1016/0004-6981(89)90058-9), 1989.
- Hallquist, M., Wenger, J. C., Baltensperger, U., Rudich, Y., Simpson, D., Claeys, M., Dommen, J., Donahue, N. M., George, C., Goldstein, A. H., Hamilton, J. F., Herrmann, H., Hoffmann, T., Iinuma, Y., Jang, M., Jenkin, M. E., Jimenez, J. L., Kiendler-Scharr, A., Maenhaut, W., McFiggans, G., Mentel, Th. F., Monod, A., Prévôt, A. S. H., Seinfeld, J. H., Surratt, J. D., Szmigielski, R., and Wildt, J.: The formation, properties and impact of secondary organic aerosol: current and emerging issues, *Atmos. Chem. Phys.*, 9, 5155–5236, <https://doi.org/10.5194/acp-9-5155-2009>, 2009.
- Hamilton, J. F., Rami Alfarra, M., Wyche, K. P., Ward, M. W., Lewis, A. C., McFiggans, G. B., Good, N., Monks, P. S., Carr, T., White, I. R., and Purvis, R. M.: Investigating the use of secondary organic aerosol as seed particles in simulation chamber experiments, *Atmos. Chem. Phys.*, 11, 5917–5929, <https://doi.org/10.5194/acp-11-5917-2011>, 2011.
- Hennigan, C. J., Miracolo, M. A., Engelhart, G. J., May, A. A., Presto, A. A., Lee, T., Sullivan, A. P., McMeeking, G. R., Coe, H., Wold, C. E., Hao, W.-M., Gilman, J. B., Kuster, W. C., de Gouw, J., Schichtel, B. A., Collett Jr., J. L., Kreidenweis, S. M., and Robinson, A. L.: Chemical and physical transformations of organic aerosol from the photo-oxidation of open biomass burning emissions in an environmental chamber, *Atmos. Chem. Phys.*, 11, 7669–7686, <https://doi.org/10.5194/acp-11-7669-2011>, 2011.
- Hoffman, E. J. and Duce, R. A.: Organic carbon in marine atmospheric particulate matter: Concentration and particle size distribution, *Geophys. Res. Lett.*, 4, 449–452, <https://doi.org/10.1029/GL004i010p00449>, 1977.
- Hoffmann, T., Odum, J. R., Bowman, F., Collins, D., Klockow, D., Flagan, R. C., and Seinfeld, J. H.: Formation of Organic Aerosols from the Oxidation of Biogenic Hydrocarbons, *J. Atmos. Chem.*, 26, 189–222, <https://doi.org/10.1023/a:1005734301837>, 1997.
- Hohaus, T., Kuhn, U., Andres, S., Kaminski, M., Rohrer, F., Tillmann, R., Wahner, A., Wegener, R., Yu, Z., and Kiendler-Scharr, A.: A new plant chamber facility, PLUS, coupled to the atmosphere simulation chamber SAPHIR, *Atmos. Meas. Tech.*, 9, 1247–1259, <https://doi.org/10.5194/amt-9-1247-2016>, 2016.
- Hu, C.-j., Cheng, Y., Pan, G., Gai, Y.-b., Gu, X.-j., Zhao, W.-x., Wang, Z.-y., Zhang, W.-j., Chen, J., Liu, F.-y., Shan, X.-b., and Sheng, L.-s.: A Smog Chamber Facility for Qualitative and Quantitative Study on Atmospheric Chemistry and Secondary Organic Aerosol, *Chin. J. Chem. Phys.*, 27, 631–639, <https://doi.org/10.1063/1674-0068/27/06/631-639>, 2014.
- Huang, Y., Zhao, R., Charan, S. M., Kenseth, C. M., Zhang, X., and Seinfeld, J. H.: Unified Theory of Vapor–Wall Mass Transport in Teflon-Walled Environmental Chambers, *Environ. Sci. Technol.*, 52, 2134–2142, <https://doi.org/10.1021/acs.est.7b05575>, 2018.
- Jayne, J. T., Leard, D. C., Zhang, X., Davidovits, P., Smith, K. A., Kolb, C. E., and Worsnop, D. R.: Development of an Aerosol Mass Spectrometer for Size and Composition Analysis of Submicron Particles, *Aerosol Sci. Tech.*, 33, 49–70, <https://doi.org/10.1080/027868200410840>, 2000.
- Jenkin, M. E., Wyche, K. P., Evans, C. J., Carr, T., Monks, P. S., Alfarra, M. R., Barley, M. H., McFiggans, G. B., Young, J. C., and Rickard, A. R.: Development and chamber evaluation of the MCM v3.2 degradation scheme for  $\beta$ -caryophyllene, *Atmos. Chem. Phys.*, 12, 5275–5308, <https://doi.org/10.5194/acp-12-5275-2012>, 2012.
- Jimenez, J. L.: Ambient aerosol sampling using the Aerodyne Aerosol Mass Spectrometer, *J. Geophys. Res.*, 108, 8425, <https://doi.org/10.1029/2001jd001213>, 2003.
- Jimenez, J. L., Canagaratna, M. R., Donahue, N. M., Prevot, A. S., Zhang, Q., Kroll, J. H., DeCarlo, P. F., Allan, J. D., Coe, H., Ng, N. L., Aiken, A. C., Docherty, K. S., Ulbrich, I. M., Grieshop, A. P., Robinson, A. L., Duplissy, J., Smith, J. D., Wilson, K. R., Lanz, V. A., Hueglin, C., Sun, Y. L., Tian, J., Laaksonen, A., Raatikainen, T., Rautiainen, J., Vaattovaara, P., Ehni, M., Kulmala, M., Tomlinson, J. M., Collins, D. R., Cubison, M. J., Dunlea, E. J., Huffman, J. A., Onasch, T. B., Alfarra, M. R., Williams, P. I., Bower, K., Kondo, Y., Schneider, J., Drewnick, F., Borrmann, S., Weimer, S., Demerjian, K., Salcedo, D., Cottrell, L., Griffin, R., Takami, A., Miyoshi, T., Hatakeyama, S., Shimono, A., Sun, J. Y., Zhang, Y. M., Dzepina, K., Kimmel, J. R., Sueper, D., Jayne, J. T., Herndon, S. C., Trimborn, A. M., Williams, L. R., Wood, E. C., Middlebrook, A. M., Kolb, C. E., Baltensperger, U., and Worsnop, D. R.: Evolution of organic aerosols in the atmosphere, *Science*, 326, 1525–1529, <https://doi.org/10.1126/science.1180353>, 2009.
- Karl, M., Brauers, T., Dorn, H. P., Holland, F., Komenda, M., Poppe, D., Rohrer, F., Rupp, L., Schaub, A., and Wahner, A.: Kinetic Study of the OH-isoprene and O<sub>3</sub>-isoprene reaction in the atmosphere simulation chamber, SAPHIR, *Geophys. Res. Lett.*, 31, L05117, <https://doi.org/10.1029/2003gl019189>, 2004.
- Katsouyanni, K., Touloumi, G., Spix, C., Schwartz, J., Balducci, F., Medina, S., Rossi, G., Wojtyniak, B., Sunyer, J., Bacharova, L., Schouten, J. P., Ponka, A., and Anderson, H. R.: Short-term effects of ambient sulphur dioxide and par-

- ticulate matter on mortality in 12 European cities: results from time series data from the APHEA project. *Air Pollution and Health: a European Approach*, *BMJ*, 314, 1658–1663, <https://doi.org/10.1136/bmj.314.7095.1658>, 1997.
- Kostenidou, E., Kaltsonoudis, C., Tsielikiotou, M., Louvaris, E., Russell, L. M., and Pandis, S. N.: Burning of olive tree branches: a major organic aerosol source in the Mediterranean. *Atmos. Chem. Phys.*, 13, 8797–8811, <https://doi.org/10.5194/acp-13-8797-2013>, 2013.
- Krechmer, J. E., Day, D. A., and Jimenez, J. L.: Always Lost but Never Forgotten: Gas-Phase Wall Losses Are Important in All Teflon Environmental Chambers, *Environ. Sci. Technol.*, 54, 12890–12897, <https://doi.org/10.1021/acs.est.0c03381>, 2020.
- Leone, J. A., Flagan, R. C., Grosjean, D., and Seinfeld, J. H.: An outdoor smog chamber and modeling study of toluene–NO<sub>x</sub> photooxidation, *Int. J. Chem. Kinet.*, 17, 177–216, <https://doi.org/10.1002/kin.550170206>, 1985.
- Leskinen, A., Yli-Pirilä, P., Kuusalo, K., Sippula, O., Jalava, P., Hirvonen, M.-R., Jokiniemi, J., Virtanen, A., Komppula, M., and Lehtinen, K. E. J.: Characterization and testing of a new environmental chamber, *Atmos. Meas. Tech.*, 8, 2267–2278, <https://doi.org/10.5194/amt-8-2267-2015>, 2015.
- Liu, D., Whitehead, J., Alfarra, M. R., Reyes-Villegas, E., Spracklen, Dominick V., Reddington, Carly L., Kong, S., Williams, Paul I., Ting, Y.-C., Haslett, S., Taylor, Jonathan W., Flynn, Michael J., Morgan, William T., McFiggans, G., Coe, H., and Allan, James D.: Black-carbon absorption enhancement in the atmosphere determined by particle mixing state, *Nat. Geosci.*, 10, 184–188, <https://doi.org/10.1038/ngeo2901>, 2017.
- Lohmann, U. and Feichter, J.: Global indirect aerosol effects: a review, *Atmos. Chem. Phys.*, 5, 715–737, <https://doi.org/10.5194/acp-5-715-2005>, 2005.
- Matsunaga, A. and Ziemann, P. J.: Gas-Wall Partitioning of Organic Compounds in a Teflon Film Chamber and Potential Effects on Reaction Product and Aerosol Yield Measurements, *Aerosol Sci. Tech.*, 44, 881–892, <https://doi.org/10.1080/02786826.2010.501044>, 2010.
- McFiggans, G., Artaxo, P., Baltensperger, U., Coe, H., Facchini, M. C., Feingold, G., Fuzzi, S., Gysel, M., Laaksonen, A., Lohmann, U., Mentel, T. F., Murphy, D. M., O’Dowd, C. D., Snider, J. R., and Weingartner, E.: The effect of physical and chemical aerosol properties on warm cloud droplet activation, *Atmos. Chem. Phys.*, 6, 2593–2649, <https://doi.org/10.5194/acp-6-2593-2006>, 2006.
- McFiggans, G., Mentel, T. F., Wildt, J., Pullinen, I., Kang, S., Kleist, E., Schmitt, S., Springer, M., Tillmann, R., Wu, C., Zhao, D., Hallquist, M., Faxon, C., Le Breton, M., Hallquist, A. M., Simpson, D., Bergstrom, R., Jenkin, M. E., Ehn, M., Thornton, J. A., Alfarra, M. R., Bannan, T. J., Percival, C. J., Priestley, M., Topping, D., and Kiendler-Scharr, A.: Secondary organic aerosol reduced by mixture of atmospheric vapours, *Nature*, 565, 587–593, <https://doi.org/10.1038/s41586-018-0871-y>, 2019.
- McMurry, P. H. and Grosjean, D.: Gas and aerosol wall losses in Teflon film smog chambers, *Environ. Sci. Technol.*, 19, 1176–1182, <https://doi.org/10.1021/es00142a006>, 1985.
- McMurry, P. H. and Rader, D. J.: Aerosol Wall Losses in Electrically Charged Chambers, *Aerosol Sci. Tech.*, 4, 249–268, <https://doi.org/10.1080/02786828508959054>, 1985.
- Metzger, A., Dommen, J., Gaeggeler, K., Duplissy, J., Prevot, A. S. H., Kleffmann, J., Elshorbany, Y., Wisthaler, A., and Baltensperger, U.: Evaluation of 1,3,5 trimethylbenzene degradation in the detailed tropospheric chemistry mechanism, MCMv3.1, using environmental chamber data, *Atmos. Chem. Phys.*, 8, 6453–6468, <https://doi.org/10.5194/acp-8-6453-2008>, 2008.
- Murphy, D. M., Cziczo, D. J., Froyd, K. D., Hudson, P. K., Matthew, B. M., Middlebrook, A. M., Peltier, R. E., Sullivan, A., Thomson, D. S., and Weber, R. J.: Single-particle mass spectrometry of tropospheric aerosol particles, *J. Geophys. Res.*, 111, D23S32, <https://doi.org/10.1029/2006JD007340>, 2006.
- Mutzel, A., Poulain, L., Berndt, T., Iinuma, Y., Rodigast, M., Böge, O., Richters, S., Spindler, G., Sipilä, M., Jokinen, T., Kulmala, M., and Herrmann, H.: Highly Oxidized Multifunctional Organic Compounds Observed in Tropospheric Particles: A Field and Laboratory Study, *Environ. Sci. Technol.*, 49, 7754–7761, <https://doi.org/10.1021/acs.est.5b00885>, 2015.
- Nah, T., McVay, R. C., Pierce, J. R., Seinfeld, J. H., and Ng, N. L.: Constraining uncertainties in particle-wall deposition correction during SOA formation in chamber experiments, *Atmos. Chem. Phys.*, 17, 2297–2310, <https://doi.org/10.5194/acp-17-2297-2017>, 2017.
- Ng, N. L., Kroll, J. H., Chan, A. W. H., Chhabra, P. S., Flagan, R. C., and Seinfeld, J. H.: Secondary organic aerosol formation from *m*-xylene, toluene, and benzene, *Atmos. Chem. Phys.*, 7, 3909–3922, <https://doi.org/10.5194/acp-7-3909-2007>, 2007.
- Niedermeier, D., Voigtländer, J., Schmalfuß, S., Busch, D., Schumacher, J., Shaw, R. A., and Stratmann, F.: Characterization and first results from LACIS-T: a moist-air wind tunnel to study aerosol–cloud–turbulence interactions, *Atmos. Meas. Tech.*, 13, 2015–2033, <https://doi.org/10.5194/amt-13-2015-2020>, 2020.
- Odum, J. R., Hoffmann, T., Bowman, F., Collins, D., Flagan, R. C., and Seinfeld, J. H.: Gas/Particle Partitioning and Secondary Organic Aerosol Yields, *Environ. Sci. Technol.*, 30, 2580–2585, <https://doi.org/10.1021/es950943>, 1996.
- O’Meara, S. P., Xu, S., Topping, D., Alfarra, M. R., Capes, G., Lowe, D., Shao, Y., and McFiggans, G.: PyCHAM (v2.1.1): a Python box model for simulating aerosol chambers, *Geosci. Model Dev.*, 14, 675–702, <https://doi.org/10.5194/gmd-14-675-2021>, 2021.
- Pankow, J. F.: An absorption model of gas/particle partitioning of organic compounds in the atmosphere, *Atmos. Environ.*, 28, 185–188, [https://doi.org/10.1016/1352-2310\(94\)90093-0](https://doi.org/10.1016/1352-2310(94)90093-0), 1994a.
- Pankow, J. F.: An absorption model of the gas/aerosol partitioning involved in the formation of secondary organic aerosol, *Atmos. Environ.*, 28, 189–193, 1994b.
- Paulot, F., Crouse John, D., Kjaergaard Henrik, G., Kürten, A., St. Clair Jason, M., Seinfeld John, H., and Wennberg Paul, O.: Unexpected Epoxide Formation in the Gas-Phase Photooxidation of Isoprene, *Science*, 325, 730–733, <https://doi.org/10.1126/science.1172910>, 2009.
- Paulsen, D., Dommen, J., Kalberer, M., Prevot, A. S., Richter, R., Sax, M., Steinbacher, M., Weingartner, E., and Baltensperger, U.: Secondary organic aerosol formation by irradiation of 1,3,5-trimethylbenzene–NO<sub>x</sub>–H<sub>2</sub>O in a new reaction chamber for atmospheric chemistry and physics, *Environ. Sci. Technol.*, 39, 2668–2678, <https://doi.org/10.1021/es0489137>, 2005.

- Pereira, K. L., Dunmore, R., Whitehead, J., Alfarra, M. R., Allan, J. D., Alam, M. S., Harrison, R. M., McFiggans, G., and Hamilton, J. F.: Technical note: Use of an atmospheric simulation chamber to investigate the effect of different engine conditions on unregulated VOC-IVOC diesel exhaust emissions, *Atmos. Chem. Phys.*, 18, 11073–11096, <https://doi.org/10.5194/acp-18-11073-2018>, 2018.
- Pierce, J. R., Engelhart, G. J., Hildebrandt, L., Weitkamp, E. A., Pathak, R. K., Donahue, N. M., Robinson, A. L., Adams, P. J., and Pandis, S. N.: Constraining Particle Evolution from Wall Losses, Coagulation, and Condensation-Evaporation in Smog-Chamber Experiments: Optimal Estimation Based on Size Distribution Measurements, *Aerosol Sci. Tech.*, 42, 1001–1015, <https://doi.org/10.1080/02786820802389251>, 2008.
- Platt, S. M., El Haddad, I., Zardini, A. A., Clairrotte, M., Astorga, C., Wolf, R., Slowik, J. G., Temime-Roussel, B., Marchand, N., Ježek, I., Drinovec, L., Močnik, G., Möhler, O., Richter, R., Barmet, P., Bianchi, F., Baltensperger, U., and Prévôt, A. S. H.: Secondary organic aerosol formation from gasoline vehicle emissions in a new mobile environmental reaction chamber, *Atmos. Chem. Phys.*, 13, 9141–9158, <https://doi.org/10.5194/acp-13-9141-2013>, 2013.
- Pope, C. A., 3rd, Burnett, R. T., Thun, M. J., Calle, E. E., Krewski, D., Ito, K., and Thurston, G. D.: Lung cancer, cardiopulmonary mortality, and long-term exposure to fine particulate air pollution, *JAMA*, 287, 1132–1141, <https://doi.org/10.1001/jama.287.9.1132>, 2002.
- Ren, Y., Grosselin, B., Daële, V., and Mellouki, A.: Investigation of the reaction of ozone with isoprene, methacrolein and methyl vinyl ketone using the HELIOS chamber, *Faraday Discuss.*, 200, 289–311, <https://doi.org/10.1039/C7FD00014F>, 2017.
- Rohrer, F., Bohn, B., Brauers, T., Brüning, D., Johnen, F.-J., Wahner, A., and Kleffmann, J.: Characterisation of the photolytic HONO-source in the atmosphere simulation chamber SAPHIR, *Atmos. Chem. Phys.*, 5, 2189–2201, <https://doi.org/10.5194/acp-5-2189-2005>, 2005.
- Saathoff, H., Naumann, K.-H., Möhler, O., Jonsson, Å. M., Halquist, M., Kiendler-Scharr, A., Mentel, Th. F., Tillmann, R., and Schurath, U.: Temperature dependence of yields of secondary organic aerosols from the ozonolysis of  $\alpha$ -pinene and limonene, *Atmos. Chem. Phys.*, 9, 1551–1577, <https://doi.org/10.5194/acp-9-1551-2009>, 2009.
- Schnitzhofer, R., Metzger, A., Breitenlechner, M., Jud, W., Heinitzi, M., De Menezes, L.-P., Duplissy, J., Guida, R., Haider, S., Kirkby, J., Mathot, S., Minginette, P., Onnela, A., Walther, H., Wasem, A., Hansel, A., and the CLOUD Team: Characterisation of organic contaminants in the CLOUD chamber at CERN, *Atmos. Meas. Tech.*, 7, 2159–2168, <https://doi.org/10.5194/amt-7-2159-2014>, 2014.
- Seakins, P. W.: A brief review of the use of environmental chambers for gas phase studies of kinetics, chemical mechanisms and characterisation of field instruments, *EPJ Web Conf.*, 9, 143–163, <https://doi.org/10.1051/epjconf/201009012>, 2010.
- Seinfeld, J. H. and Pandis, S. N.: *Atmospheric Chemistry and Physics: From Air Pollution to Climate Change*, John Wiley & Sons, Inc., Hoboken, 2016.
- Smith, D. M., Fiddler, M. N., Sexton, K. G., and Bililign, S.: Construction and Characterization of an Indoor Smog Chamber for Measuring the Optical and Physicochemical Properties of Aging Biomass Burning Aerosols, *Aerosol Air Qual. Res.*, 19, 467–483, <https://doi.org/10.4209/aaqr.2018.06.0243>, 2019.
- Smith, H. J.: Nanoparticle growth in the CLOUD chamber, *Science*, 352, 1422–1422, <https://doi.org/10.1126/science.2016.352.6292.twil>, 2016.
- Stirnweis, L., Marcolli, C., Dommen, J., Barmet, P., Frege, C., Platt, S. M., Bruns, E. A., Krapf, M., Slowik, J. G., Wolf, R., Prévôt, A. S. H., Baltensperger, U., and El-Haddad, I.: Assessing the influence of  $\text{NO}_x$  concentrations and relative humidity on secondary organic aerosol yields from  $\alpha$ -pinene photo-oxidation through smog chamber experiments and modelling calculations, *Atmos. Chem. Phys.*, 17, 5035–5061, <https://doi.org/10.5194/acp-17-5035-2017>, 2017.
- Surratt, J. D., Chan, A. W. H., Eddingsaas, N. C., Chan, M., Loza, C. L., Kwan, A. J., Hersey, S. P., Flagan, R. C., Wennberg, P. O., and Seinfeld, J. H.: Reactive intermediates revealed in secondary organic aerosol formation from isoprene, *P. Natl. Acad. Sci. USA*, 107, 6640, <https://doi.org/10.1073/pnas.0911114107>, 2010.
- Taylor, L., Reist, P. C., Boehlecke, B. A., and Jacobs, R. R.: Characterization of an aerosol chamber for human exposures to endotoxin, *Applied Occupational and Environmental Hygiene*, 15, 303–312, <https://doi.org/10.1080/104732200301629>, 2000.
- Thornton, J. A., Shilling, J. E., Shrivastava, M., D'Ambro, E. L., Zawadowicz, M. A., and Liu, J.: A Near-Explicit Mechanistic Evaluation of Isoprene Photochemical Secondary Organic Aerosol Formation and Evolution: Simulations of Multiple Chamber Experiments with and without Added  $\text{NO}_x$ , *ACS Earth and Space Chemistry*, 4, 1161–1181, <https://doi.org/10.1021/acsearthspacechem.0c00118>, 2020.
- Tong, H., Lakey, P. S. J., Arangio, A. M., Socorro, J., Shen, F., Lucas, K., Brune, W. H., Poschl, U., and Shiraiwa, M.: Reactive Oxygen Species Formed by Secondary Organic Aerosols in Water and Surrogate Lung Fluid, *Environ. Sci. Technol.*, 52, 11642–11651, <https://doi.org/10.1021/acs.est.8b03695>, 2018.
- Trump, E. R., Epstein, S. A., Riipinen, I., and Donahue, N. M.: Wall effects in smog chamber experiments: A model study, *Aerosol Sci. Tech.*, 50, 1180–1200, <https://doi.org/10.1080/02786826.2016.1232858>, 2016.
- Turpin, B. J. and Huntzicker, J. J.: Secondary formation of organic aerosol in the Los Angeles basin: A descriptive analysis of organic and elemental carbon concentrations, *Atmos. Environ. A-Gen.*, 25, 207–215, [https://doi.org/10.1016/0960-1686\(91\)90291-e](https://doi.org/10.1016/0960-1686(91)90291-e), 1991.
- Turpin, B. J. and Huntzicker, J. J.: Identification of secondary organic aerosol episodes and quantitation of primary and secondary organic aerosol concentrations during SCAQS, *Atmos. Environ.*, 29, 3527–3544, [https://doi.org/10.1016/1352-2310\(94\)00276-q](https://doi.org/10.1016/1352-2310(94)00276-q), 1995.
- Verheggen, B. and Mozurkewich, M.: An inverse modeling procedure to determine particle growth and nucleation rates from measured aerosol size distributions, *Atmos. Chem. Phys.*, 6, 2927–2942, <https://doi.org/10.5194/acp-6-2927-2006>, 2006.
- Voliotis, A., Wang, Y., Shao, Y., Du, M., Bannan, T. J., Percival, C. J., Pandis, S. N., Alfarra, M. R., and McFiggans, G.: Exploring the composition and volatility of secondary organic aerosols in mixed anthropogenic and biogenic precursor systems, *Atmos. Chem. Phys.*, 21, 14251–14273, <https://doi.org/10.5194/acp-21-14251-2021>, 2021.

- Wagner, R., Bunz, H., Linke, C., Möhler, O., Naumann, K.-H., Saathoff, H., Schnaiter, M., and Schurath, U.: Chamber Simulations of Cloud Chemistry: The AIDA Chamber, Dordrecht, 67–82, [https://doi.org/10.1007/1-4020-4232-9\\_5](https://doi.org/10.1007/1-4020-4232-9_5), 2006
- Wagner, R., Yan, C., Lehtipalo, K., Duplissy, J., Nieminen, T., Kangasluoma, J., Ahonen, L. R., Dada, L., Kontkanen, J., Manninen, H. E., Dias, A., Amorim, A., Bauer, P. S., Bergen, A., Bernhammer, A.-K., Bianchi, F., Brilke, S., Mazon, S. B., Chen, X., Draper, D. C., Fischer, L., Frege, C., Fuchs, C., Garmash, O., Gordon, H., Hakala, J., Heikkinen, L., Heinritzi, M., Hofbauer, V., Hoyle, C. R., Kirkby, J., Kürten, A., Kvashnin, A. N., Laurila, T., Lawler, M. J., Mai, H., Makhmutov, V., Mauldin III, R. L., Molteni, U., Nichman, L., Nie, W., Ojdic, A., Onnela, A., Piel, F., Quéléver, L. L. J., Rissanen, M. P., Sarnela, N., Schallhart, S., Sengupta, K., Simon, M., Stolzenburg, D., Stozhkov, Y., Tröstl, J., Viisanen, Y., Vogel, A. L., Wagner, A. C., Xiao, M., Ye, P., Baltensperger, U., Curtius, J., Donahue, N. M., Flagan, R. C., Gallagher, M., Hansel, A., Smith, J. N., Tomé, A., Winkler, P. M., Worsnop, D., Ehn, M., Sipilä, M., Kerminen, V.-M., Petäjä, T., and Kulmala, M.: The role of ions in new particle formation in the CLOUD chamber, *Atmos. Chem. Phys.*, 17, 15181–15197, <https://doi.org/10.5194/acp-17-15181-2017>, 2017.
- Wang, J., Doussin, J. F., Perrier, S., Perraudin, E., Katrib, Y., Pangui, E., and Picquet-Varrault, B.: Design of a new multi-phase experimental simulation chamber for atmospheric photosmog, aerosol and cloud chemistry research, *Atmos. Meas. Tech.*, 4, 2465–2494, <https://doi.org/10.5194/amt-4-2465-2011>, 2011.
- Wang, M., Kong, W., Marten, R., He, X. C., Chen, D., Pfeifer, J., Heitto, A., Kontkanen, J., Dada, L., Kurten, A., Yli-Juuti, T., Manninen, H. E., Amanatidis, S., Amorim, A., Baalbaki, R., Baccarini, A., Bell, D. M., Bertozzi, B., Brakling, S., Brilke, S., Murillo, L. C., Chiu, R., Chu, B., De Menezes, L. P., Duplissy, J., Finkenzeller, H., Carracedo, L. G., Granzin, M., Guida, R., Hansel, A., Hofbauer, V., Krechmer, J., Lehtipalo, K., Lamkadam, H., Lampimäki, M., Lee, C. P., Makhmutov, V., Marie, G., Mathot, S., Mauldin, R. L., Mentler, B., Müller, T., Onnela, A., Partoll, E., Petaja, T., Philippov, M., Pospisilova, V., Ranjithkumar, A., Rissanen, M., Rorup, B., Scholz, W., Shen, J., Simon, M., Sipilä, M., Steiner, G., Stolzenburg, D., Tham, Y. J., Tome, A., Wagner, A. C., Wang, D. S., Wang, Y., Weber, S. K., Winkler, P. M., Wlasits, P. J., Wu, Y., Xiao, M., Ye, Q., Zauner-Wieczorek, M., Zhou, X., Volkamer, R., Riipinen, I., Dommen, J., Curtius, J., Baltensperger, U., Kulmala, M., Worsnop, D. R., Kirkby, J., Seinfeld, J. H., El-Haddad, I., Flagan, R. C., and Donahue, N. M.: Rapid growth of new atmospheric particles by nitric acid and ammonia condensation, *Nature*, 581, 184–189, <https://doi.org/10.1038/s41586-020-2270-4>, 2020.
- Wang, N., Jorga, S. D., Pierce, J. R., Donahue, N. M., and Pandis, S. N.: Particle wall-loss correction methods in smog chamber experiments, *Atmos. Meas. Tech.*, 11, 6577–6588, <https://doi.org/10.5194/amt-11-6577-2018>, 2018.
- Wang, X., Liu, T., Bernard, F., Ding, X., Wen, S., Zhang, Y., Zhang, Z., He, Q., Lü, S., Chen, J., Saunders, S., and Yu, J.: Design and characterization of a smog chamber for studying gas-phase chemical mechanisms and aerosol formation, *Atmos. Meas. Tech.*, 7, 301–313, <https://doi.org/10.5194/amt-7-301-2014>, 2014.
- Wang, Y., Voliotis, A., Shao, Y., Zong, T., Meng, X., Du, M., Hu, D., Chen, Y., Wu, Z., Alfarra, M. R., and McFiggans, G.: Phase state of secondary organic aerosol in chamber photo-oxidation of mixed precursors, *Atmos. Chem. Phys.*, 21, 11303–11316, <https://doi.org/10.5194/acp-21-11303-2021>, 2021.
- Wu, S., Lu, Z., Hao, J., Zhao, Z., Li, J., Takekawa, H., Minoura, H., and Yasuda, A.: Construction and characterization of an atmospheric simulation smog chamber, *Adv. Atmos. Sci.*, 24, 250–258, <https://doi.org/10.1007/s00376-007-0250-3>, 2007.
- Wyche, K. P., Ryan, A. C., Hewitt, C. N., Alfarra, M. R., McFiggans, G., Carr, T., Monks, P. S., Smallbone, K. L., Capes, G., Hamilton, J. F., Pugh, T. A. M., and MacKenzie, A. R.: Emissions of biogenic volatile organic compounds and subsequent photochemical production of secondary organic aerosol in mesocosm studies of temperate and tropical plant species, *Atmos. Chem. Phys.*, 14, 12781–12801, <https://doi.org/10.5194/acp-14-12781-2014>, 2014.
- Wyche, K. P., Monks, P. S., Smallbone, K. L., Hamilton, J. F., Alfarra, M. R., Rickard, A. R., McFiggans, G. B., Jenkin, M. E., Bloss, W. J., Ryan, A. C., Hewitt, C. N., and MacKenzie, A. R.: Mapping gas-phase organic reactivity and concomitant secondary organic aerosol formation: chemometric dimension reduction techniques for the deconvolution of complex atmospheric data sets, *Atmos. Chem. Phys.*, 15, 8077–8100, <https://doi.org/10.5194/acp-15-8077-2015>, 2015.
- Ye, P., Ding, X., Hakala, J., Hofbauer, V., Robinson, E. S., and Donahue, N. M.: Vapor wall loss of semi-volatile organic compounds in a Teflon chamber, *Aerosol Sci. Tech.*, 50, 822–834, <https://doi.org/10.1080/02786826.2016.1195905>, 2016.
- Zhang, Q., Jimenez, J. L., Canagaratna, M. R., Allan, J. D., Coe, H., Ulbrich, I., Alfarra, M. R., Takami, A., Middlebrook, A. M., Sun, Y. L., Dzepina, K., Dunlea, E., Docherty, K., DeCarlo, P. F., Salcedo, D., Onasch, T., Jayne, J. T., Miyoshi, T., Shimojo, A., Hatakeyama, S., Takegawa, N., Kondo, Y., Schneider, J., Drewnick, F., Borrmann, S., Weimer, S., Demerjian, K., Williams, P., Bower, K., Bahreini, R., Cottrell, L., Griffin, R. J., Rautiainen, J., Sun, J. Y., Zhang, Y. M., and Worsnop, D. R.: Ubiquity and dominance of oxygenated species in organic aerosols in anthropogenically-influenced Northern Hemisphere midlatitudes, *Geophys. Res. Lett.*, 34, L13801, <https://doi.org/10.1029/2007GL029979>, 2007.
- Zhang, X., Cappa, C. D., Jathar, S. H., McVay, R. C., Ensberg, J. J., Kleeman, M. J., and Seinfeld, J. H.: Influence of vapor wall loss in laboratory chambers on yields of secondary organic aerosol, *P. Natl. Acad. Sci. USA*, 111, 5802–5807, <https://doi.org/10.1073/pnas.1404727111>, 2014.



## **4.2 Paper 2: Chamber investigation of the formation and transformation of secondary organic aerosol in mixtures of biogenic and anthropogenic volatile organic compounds**

This paper is under review in the journal of “*Atmospheric Chemistry and Physics*” and can be found on: <https://acp.copernicus.org/preprints/acp-2021-1080/>

### **4.2.1 Paper introduction**

This paper aims to present an overview in the respect of mixed systems studies and to address the 2<sup>nd</sup> objective of this project.

It was found that the observed average SOA yields in descending order were found for the  $\alpha$ -pinene (32±7%),  $\alpha$ -pinene/o-cresol (28±9%),  $\alpha$ -pinene at ½ initial reactivity (21±5%),  $\alpha$ -pinene/isoprene (16±1%),  $\alpha$ -pinene at ⅓ initial reactivity (15±4%), o-cresol (13±3%),  $\alpha$ -pinene/o-cresol/isoprene (11±4%), o-cresol at ½ initial reactivity (11±3%), o-cresol/isoprene (6±2%) and isoprene systems (0±0%). Online and offline chemical composition and SOA particle volatility, water uptake and “phase” behaviour measurements were utilized to interpret the SOA formation and behaviour, however, that information is introduced briefly in this paper and detailed in other papers.

### **4.2.2 Contribution to the joint authorship**

The author has contributed the following:

I and other co-authors designed and carried out the experiments. I was mainly responsible for the instruments of FIGAERO-CIMS and LC-MS data analysis and corresponding text writing. I also acted as one of the editors to ensure fluency and consistency among sections and grammar checking.

### **4.2.3 Supplemental information**

Paper 2 is shown below.



## Chamber investigation of the formation and transformation of secondary organic aerosol in mixtures of biogenic and anthropogenic volatile organic compounds

Aristeidis Voliotis<sup>1,\*</sup>, Mao Du<sup>1,\*</sup>, Yu Wang<sup>1,\*</sup>, Yunqi Shao<sup>1,\*</sup>, M. Rami Alfarra<sup>1,2,‡</sup>, Thomas J. Bannan<sup>1</sup>, Dawei Hu<sup>1</sup>, Kelly L. Pereira<sup>3</sup>, Jaqueline F. Hamilton<sup>3</sup>, Mattias Hallquist<sup>4</sup>, Thomas F. Mentel<sup>5</sup>, Gordon McFiggans<sup>1</sup>

<sup>1</sup>Centre for Atmospheric Science, Department of Earth and Environmental Sciences, School of Natural Sciences, University of Manchester, Manchester, M13 9PL, UK

<sup>2</sup>National Centre for Atmospheric Science (NCAS), University of Manchester, Manchester, M13 9PL, UK

<sup>3</sup>Wolfson Atmospheric Chemistry Laboratories, Department of Chemistry, University of York, York, YO10 5DD, UK

<sup>4</sup>Department of Chemistry and Molecular Biology, Atmospheric Science, University of Gothenburg, Gothenburg SE-412 96, Sweden

<sup>5</sup>Institut für Energie und Klimaforschung, IEK-8, Forschungszentrum Jülich, Jülich, Germany

‡ now at Environment & Sustainability Center, Qatar Environment & Energy Research Institute, Doha, Qatar

\* These authors all made equal contributions to the work and manuscript

Correspondence to: Gordon McFiggans (g.mcfiggans@manchester.ac.uk)

### Abstract.

A comprehensive investigation of the photochemical secondary organic aerosol (SOA) formation and transformation in mixtures of anthropogenic (o-cresol) and biogenic ( $\alpha$ -pinene and isoprene) volatile organic compound (VOC) precursors in the presence of NO<sub>x</sub> and inorganic seed particles was conducted. Initial iso-reactivity was used to enable direct comparison across systems, adjusting the initial concentration of the systems towards the assumed dominant oxidant (OH). Comparing experiments conducted in single precursor systems at various initial reactivity levels (referenced to a nominal base case VOC reactivity) and their binary and ternary mixtures, we show that the molecular interactions from the mixing of the precursors can be investigated and discuss limitations in their interpretation. The observed average SOA yields in descending order were found for the  $\alpha$ -pinene (32±7%),  $\alpha$ -

pinene/o-cresol ( $28\pm 9\%$ ),  $\alpha$ -pinene at  $\frac{1}{2}$  initial reactivity ( $21\pm 5\%$ ),  $\alpha$ -pinene/isoprene ( $16\pm 1\%$ ),  $\alpha$ -pinene at  $\frac{1}{3}$  initial reactivity ( $15\pm 4\%$ ), o-cresol ( $13\pm 3\%$ ),  $\alpha$ -pinene/o-cresol/isoprene ( $11\pm 4\%$ ), o-cresol at  $\frac{1}{2}$  initial reactivity ( $11\pm 3\%$ ), o-cresol/isoprene ( $6\pm 2\%$ ) and isoprene systems ( $0\pm 0\%$ ). We find a clear suppression of the SOA yield from  $\alpha$ -pinene when it is mixed with isoprene, whilst the addition of isoprene to o-cresol may enhance the mixture's SOA formation potential, however, the difference was too small to be unequivocal. The  $\alpha$ -pinene/o-cresol system yield appeared to be increased compared to that calculated based on the additivity, whilst in the  $\alpha$ -pinene/o-cresol/isoprene system the measured and predicted yield were comparable. However, in mixtures where more than one precursor contributes to the SOA mass, it is unclear whether changes in the SOA formation potential are attributable to physical or chemical interactions since the reference basis for the comparison is complex. Online and offline chemical composition and SOA particle volatility, water uptake and "phase" behaviour measurements that were used to interpret the SOA formation and behaviour are introduced and detailed elsewhere.

## 1. Introduction

The fine fraction of particulate matter (PM) plays the dominant role in the impact of air pollution on human health and of aerosol on climate through direct radiative effects and cloud adjustments. Ambient PM<sub>2.5</sub> was the fifth-ranking global mortality risk factor in 2015, with exposure to it causing 4.2 million deaths and 103.1 million disability-adjusted life-years (DALYs), 7.6% of total global deaths and 4.2% of global DALYs (Cohen et al., 2017). Moreover, fine PM is responsible for the aerosol effects that make the single greatest contributory uncertainty to radiative forcing (IPCC, 2013).

Organic material makes a major contribution to the mass of fine PM in the atmosphere (Jimenez et al., 2009) and secondary organic aerosol (SOA) is the major contributor (Hallquist et al., 2009). Nonetheless, our ability to predict the atmospheric burden and hence impacts of fine secondary aerosol particles (Kanakidou et al., 2005; Tsigaridis and Kanakidou, 2018) has been limited by a basic understanding of the formation of this organic component (Hallquist et al., 2009). Photochemistry dictates the levels of NO<sub>2</sub>, O<sub>3</sub> and the SOA fraction of PM. Whilst it is relatively straightforward to understand and control primary pollutants, these secondary pollutants make a substantial contribution to air quality degradation that is set to become increasingly important as primary pollutants are cleaned up. However, understanding the rate

and extent of SOA formation in the real atmosphere presents a number of challenges. There are tens of thousands of isolated organic compounds in the atmosphere, ranging across more than 12 orders of magnitude in volatility (Goldstein and Galbally, 2007) with possible oxidation products running to many millions (Aumont et al., 2005). They have extensive biogenic and anthropogenic sources and are spatially heterogeneous. Their reactivity ranges over many orders of magnitude and their lifetimes at ambient oxidant levels consequently range from less than a second to several years. An unknown but substantial proportion of the organic compounds have the potential to act as SOA precursors and the degree to which this is influenced by the complex atmospheric mixture is unclear.

It has long been established that prediction of the formation of secondary gaseous pollutants in the troposphere requires knowledge of the nature of the mixture of volatile organic compounds (VOC), their abundance and the chemical regime (e.g. VOC: NO<sub>x</sub> ratio) and air mass history. In contrast, the formation of SOA in the real atmosphere is conventionally considered less mechanistically. Against the backdrop of the near unimaginable complexity of the atmospheric mixture of SOA precursors, the basis for our understanding of SOA formation has been primarily derived from experimental investigations of single component systems (Thornton et al., 2020; Donahue et al., 2012; Jenkin et al., 2012). A wealth of literature derived from chamber experiments on biogenic (Thornton et al., 2020; Carlton et al., 2009) and anthropogenic (Schwantes et al., 2017; Nakao et al., 2012) precursors under a range of chemical environments combined with fundamental kinetic studies (Ziemann and Atkinson, 2012; Cash et al., 2016) has enabled numerous representations of atmospheric SOA at varying levels of detail (Shrivastava et al., 2017; Charan et al., 2019). There have additionally been studies of SOA formation in source-oriented mixtures from diesel (Weitkamp et al., 2007; Nakao et al., 2011) and gasoline (Nordin et al., 2013; Platt et al., 2013) exhaust, woodburning (Tiitta et al., 2016), cooking (Reyes-Villegas et al., 2018; Kaltsonoudis et al., 2017) and from macroalgal (McFiggans et al., 2004) and plant (Joutsensaari et al., 2005; VanReken et al., 2006; Pinto et al., 2007; Mentel et al., 2009; Hao et al., 2009; Wyche et al., 2014) emissions. Building on a well-established framework first suggested by Pankow (1994) to account for absorptive partitioning of mixtures of organic components in the atmosphere, attempts have been made to provide empirically constrained and mechanistically augmented conceptual frameworks of organic aerosol (Donahue et al., 2006; Donahue et al., 2011; Schervish and Donahue, 2020), but there is currently no universally accepted mechanistic basis for SOA understanding in the

complex atmosphere.

Evidence suggests that it is necessary to take a more mechanistic approach in order to capture the observed behaviour of SOA formation in mixtures. It was established that the scavenging of the OH radical by the addition of isoprene significantly inhibits new particle formation in plant chamber studies (Kiendler-Scharr et al., 2009), though the atmospheric implication was questioned by Berndt et al. (2018) since OH will likely not be controlled by isoprene. More recent studies have indicated that the mass and yield of SOA formed from individual precursors may similarly be influenced by the presence of other VOC (McFiggans et al., 2019). In addition to the observed suppression of particle mass and yield from  $\alpha$ -pinene being attributed to the established scavenging of oxidant by the lower SOA yield isoprene, it was found that the C<sub>5</sub> peroxy radical isoprene oxidation products scavenged highly oxygenated C<sub>10</sub> peroxy radicals that would otherwise form extremely low volatility condensable compounds. This had also been reported by Berndt et al. (2018) who demonstrated similar scavenging of C<sub>10</sub> radical products in the presence of ethylene. McFiggans et al. (2019) further reported such product scavenging and consequent reduction in  $\alpha$ -pinene SOA yield by CO and CH<sub>4</sub>. Such interactions should be no surprise, given our understanding of peroxy radical cross-reactions and termination fates in controlling the production of secondary gaseous pollutants. Moreover, the existence of such interactions in mixtures is somewhat obvious in the light of the understanding that has emerged over recent years (e.g., Bianchi et al., 2019) of the roles of atmospheric autoxidation of VOC producing highly oxygenated organic molecules (HOM). Following the early postulations of the role of autoxidation in atmospheric VOC degradation (Crouse et al., 2013), the importance of HOM in SOA formation has been widely established and quantified in monoterpene oxidation (Ehn et al., 2012; Ehn et al., 2014; Jokinen et al., 2015; Berndt et al., 2016; Berndt et al., 2018; Bianchi et al., 2019). The termination of the RO<sub>2</sub> formed via autoxidation (“HOM-RO<sub>2</sub>”) will depend on the chemical conditions (the abundance of NO<sub>x</sub>, HO<sub>2</sub> and the numerous other RO<sub>2</sub> species present in the mixture) as well as the formation rate of the HOM-RO<sub>2</sub>. Schervish and Donahue (2020) provide a discussion of the determinants of the fate of HOM-RO<sub>2</sub> and potential consequences on the distribution of low, extremely low and ultra-low volatility organic compound (LVOC, ELVOC and ULVOC respectively) products and hence on SOA formation in  $\alpha$ -pinene oxidation. Autoxidation is widespread, in atmospheric systems, is unlikely to be restricted to monoterpenes (though unsaturated compounds may be expected to be more susceptible). Indeed, the application of recently

developed mass spectrometric techniques has revealed the presence of HOM in the oxidation of aromatic compounds (Wang et al., 2017; Wang et al., 2020; Molteni et al., 2018; Tsiligiannis et al., 2019; Garmash et al., 2020; Mehra et al., 2020; Priestley et al., 2021). The degree to which the HOM distribution results from direct autoxidation or from multigenerational pathways is unclear, though the prevalence of HOM-RO<sub>2</sub> during aromatic oxidation is clear. The attention on aromatic compounds has been driven by their relevance as anthropogenic VOC emissions, making significant manmade contributions to the VOC burden in the polluted troposphere. Given the prevalence and diversity of autoxidation mechanisms, it is probable that HOM would be detected on the application of modern mass spectrometry to the investigation of many classes of atmospheric VOC. The recent focus on interactions via autoxidation in mixtures has added to more well-established mechanistic linkages in the oxidation of VOCs for understanding gas phase photochemistry. The implications on production of aerosol particle precursors are less well studied. Since the fractional contribution of HOM to particle mass is unclear, the role of autoxidation and influences of interactions on the HOM contributions to SOA mass formation in mixtures is unquantified. It is therefore important to additionally maintain a focus on influences of the non-HOM components on SOA formation in oxidation of VOC mixtures.

Given the potential diversity in VOC sources contributing to the pollutant mixture in the ambient atmosphere, it is important to establish the experimental basis for an understanding of SOA formation beyond the recently studied “simple” biogenic mixed systems (Berndt et al., 2018; McFiggans et al., 2019; Shilling et al., 2019). The importance of establishing a framework to understand interactions in systems of mixed anthropogenic and biogenic VOC stretches well beyond speculative curiosity. Such a framework may be a key to explaining observed non-linearities when natural and manmade pollution mixes (Spracklen et al., 2011; Emanuelsson et al., 2013). Using such considerations as motivation, a series of experiments was conceived to explore SOA formation from typical biogenic and anthropogenic VOC precursors and their binary and ternary mixtures. The binary  $\alpha$ -pinene/isoprene system reported elsewhere was used as a biogenic mixture with established mechanistic interactions in its photo-oxidation. *o*-cresol was chosen as a representative anthropogenic VOC, being both emitted as a primary pollutant and formed through oxidation of other aromatic compounds. The construction of the study is detailed in the methodology section below. The experiments were conducted in the 18m<sup>3</sup> Manchester Aerosol Chamber (MAC), a photochemical chamber

operating in batch mode. The design of experiments on mixed VOCs is complex and requires consideration of aspects not encountered in single VOC experiments. This paper explores many of these elements and associated challenges to inform best practices in their planning and executions. The objectives were broad and diverse and aimed to:

i) establish the suitability of the experimental design for investigating SOA formation in VOC mixtures;

ii) establish the suitability of conventionally reported metrics such as SOA mass yield for quantifying SOA formation in VOC mixtures;

iii) using these metrics, quantify any interactions in VOC mixtures leading to changes in the SOA formation from that may be expected based on single precursor experiments;

iv) using a suite of online and offline measurements of chemical and physical properties, to probe the chemistry and physics leading to these interactions and the properties of particles resulting from them, of potential atmospheric significance.

This paper will address the first three of these and provide an introduction to the findings related to the fourth, which will be detailed in a number of companion manuscripts. It is envisaged that the programme will act as a springboard to investigate the detailed mechanisms of interactions in mixtures of VOC involved in ambient SOA formation.

Importantly, this paper aims to explore whether SOA experiments using multiple VOC precursors can reveal aspects of the multiphase atmospheric systems inaccessible to experiments using a single precursor species.

## **2. Experimental design**

The mixture of atmospheric VOCs and variability in prevailing oxidising environment is so complex that the choice of precursors, concentrations and experimental conditions makes a comprehensive programme intractable. Besides challenges associated with representativeness of atmospheric complexity and concentrations in the multiphase system, numerous infrastructural considerations and measurement challenges must be considered. There are additional conflicts in the requirements needed to fully address the specific objectives of the study. In this section, these criteria and the bounds placed on the study are addressed and the

approaches to experimental design in response to these restrictions and requirements are discussed along with the choices made. Finally, the capabilities and likely consequences and compromises inherent in these choices are listed, before outlining the methodology employed.

## **2.1 VOC mixture and oxidant “representativeness”**

Of the tens of thousands (or perhaps millions) of atmospheric organic compounds present in the vapour phase, only a handful have been studied in previous chamber SOA experiments and fewer in mixtures. The selection of compounds for the study of mixed SOA precursors is simultaneously simple and complex; simple, insofar as study of a random mixture will yield novel results, but complex, in that care is required to maximise their importance. Disregarding chlorine atoms and the Criegee radicals as “exotic”, the dominant oxidants at night are the nitrate radical ( $\text{NO}_3$ ) and ozone and during the day, the hydroxyl radical (OH) and ozone. Whilst arguments (such as likely/possible dominance of daytime oxidising capacity and pathways to SOA over night-time) can be used to select the oxidant combination of interest, this is fairly arbitrary and open, and we have selected daytime oxidation conditions for the present study.

Similarly arbitrary is the selection of  $\text{NO}_x$  regime. Whilst VOC: $\text{NO}_x$  ratio dependence of SOA formation from some precursors has been well studied (e.g. Pullinen et al. 2020), this is not the case for mixtures of VOC. It is established for certain systems that SOA formation pathways in low and high  $\text{NO}_x$  regimes change dramatically and consequently influence SOA particle mass yield (e.g. Sarrafzadeh et al. 2016). Challenges associated with the comparability of experimental configurations and conditions lead to apparently conflicting findings and controversies remain surrounding the influence of  $\text{NO}_x$  on SOA formation, requiring unambiguous mechanistic resolution. Truly low  $\text{NO}_x$  regimes probably do not occur widely in the ambient atmosphere, at least not in the perturbed northern hemisphere. Moreover, in light of selection (see below) of an anthropogenic SOA precursor in the mixture, it would be unreasonable to expect there to be a complete absence of  $\text{NO}_x$ . For reasons outlined below (sections 2.4 and 2.5) related to the chosen concentrations and contributions to reactivity, this study uses moderate VOC:  $\text{NO}_x$  ratios (between roughly 3 and 8) broadly corresponding to a perturbed background chemical regime (Wyche et al., 2015; Pereira and Amiridis, 1995).

The reactivity of gaseous VOCs towards ambient oxidants spans several orders of magnitude and the ratio of reactivity towards each oxidant varies substantially. In particular,



reactivity towards ozone will be negligible for saturated VOCs but can lead to lifetimes of a few minutes for reactive sesquiterpenes (Atkinson, 2000). For each VOC in a mixture to contribute significantly to the distribution of oxidation products in a chamber experiment and thereby influence the pathways to, and potential for, SOA formation, it is desirable for them to have comparable reactivity towards the available oxidants. In such a mixture, similar concentrations of each VOC might be reasonably expected to provide a comparable rate of change of oxidation products into the mix and hence contribute to SOA production pathways. Our approach to this is outlined in section 2.4.

As with reactivity, the SOA particle formation potential of VOCs can vary widely, from unmeasurably low to having particle mass yields of several tens of percent. Intuitively, the presence of a higher yield VOC might be expected to contribute more mass than a lower yield VOC and consequently increase the yield of the mixture. What is less clear is the degree to which a lower yield component might reduce the yields of a higher yield VOC and vice versa – i.e. how strongly is the chemistry coupled and how do such interactions influence SOA particle formation? More fundamentally, the reference for and calculation of yields in VOC mixtures is a challenge depending on the often arbitrary selected definition (see results and discussion sections 4 and 5).

A final consideration is the sort of atmosphere that the experiment aims to represent. McFiggans et al (2019), in their choice of  $\alpha$ -pinene and isoprene, have looked at binary mixtures of abundant biogenically-emitted VOCs (as did Jaoui and Kamens, 2003, previously, in looking at mixtures of  $\alpha$ - and  $\beta$ -pinene). Much of the global atmosphere is perturbed by anthropogenic pollutants and contributions from natural and manmade sources at any location or time will depend upon the mixture and strength of, and distance from, upwind sources (amongst a multitude of other factors). This study builds on previous insight from the binary mixture of low and high yield biogenic SOA precursors to add a moderate yield anthropogenic VOC. Studies could equally be focused on a range of high, low or moderate SOA yield manmade VOCs or numerous other combinations. Indeed, such extension and broadening of the current approach will be of substantial interest.

## **2.2 Infrastructural and instrumental considerations**

This study employs a mixture of VOCs as SOA precursors – i.e., compounds almost entirely in the vapour phase under normal temperate surface atmospheric conditions. This

straightforwardly takes advantage of the heated glass bulb arrangement in the MAC for the injection of small amounts of liquid organic components and enables comparability with other studies using conventional SOA precursors. Future work could readily use materials from solid stock for studies of “unconventional” SOA precursors that have had much recent attention, such as those falling into the intermediate volatility (IVOC) and semi-volatile (SVOC) classes.

All experiments employed ammonium sulphate (AS) seed particles. The presence of AS seeds was primarily to enable greater reproducibility by providing sufficient particulate mass to act as a condensation sink for partitioning compounds, suppressing nucleation and its attendant stochastic elements. In chamber experiments, there is a competition for condensable vapours between the walls and any existing particles such that seeded experiments enable the earlier formation of SOA particle mass. Moreover, detection of this particle mass and determination of their composition and properties are more straightforward with instruments that require particles to be greater than a certain size. Whilst we previously pioneered the technique of generation of SOA particle seeds for use in chamber experiments (Hamilton et al., 2011), the use of ammonium sulphate avoids the additional complication of the chemistry by residual VOC oxidation products. Ammonium sulphate is nebulised into a stainless-steel retaining drum prior to entrainment into the final fill cycle for the experiment (see methods section 3, below). It is recognised that inorganic seeds may not present the most effective absorptive medium for condensational uptake of organic vapours, but the seed generation process is highly reproducible and an implicit assumption of the likelihood of comparable efficiency as an absorptive medium across the systems of choice is made. Acidic seeds are not accessible in the MAC, because uptake of background ambient  $\text{NH}_3$  leads to neutralisation of  $\text{H}^+$  at any reasonable seed mass loading.

Instrumental detection limits and sampling requirements dictate the accessible range of concentrations for the experiments (see table 2). State-of-the-science sampling and measurement techniques are employed throughout. Many are capable of very high precision and time resolution measurement at low concentrations. Some are capable of single particle detection or particle ensemble measurement by number concentration. Most of the approaches employ online, or semi-continuous, operation and low concentrations could be readily accommodated by increasing instrument integration times. Filters are collected for molecular determination of SOA particle composition by the evacuation of the entire chamber through

pre-fired quartz filters (section 3). Collection of sufficient mass provides a lower limit to the mass concentration loadings and dictates moderately high injected VOC concentration (dependent on the particle mass yield of the mixture). The consequences of higher-than-ambient VOC and PM mass loadings are discussed in section 5.

Very low  $\text{NO}_x$  studies are not accessible in the MAC, owing to variable and sometimes elevated  $\text{NO}_x$  concentrations in our chamber laboratory in the centre of Manchester. Such conditions limit the ability of our Purafil scrubber to completely remove  $\text{NO}_x$  at our high inlet flow and may potentially lead to the increase in  $\text{NO}_x$  by diffusion through the Teflon film. Such effects would be non-negligible when attempting sub-ppbv  $\text{NO}_x$  experiments but present modest challenges at higher  $\text{NO}_x$  conditions, unnoticeable under the chosen VOC concentrations and moderate VOC:  $\text{NO}_x$  ratios of the current programme.

The chemical conditions in all experiments were controlled by photo-oxidation under a simulated solar spectrum at a moderate VOC:  $\text{NO}_x$  ratio, with  $\text{NO}_x$  injected as  $\text{NO}_2$ . In all experiments, neutral ammonium sulphate was injected to provide a condensation sink sufficiently large to compete effectively with the wall for condensable vapours. Table 1 shows the initial conditions of all experiments.

### **2.3 Ideal, desirable and realistic objectives**

It is not the intention to quantitatively establish the extent and nature of interactions between VOC precursors in the photochemical processes leading to SOA particle formation in ambient mixtures and the consequent impacts on SOA composition and properties in the real atmosphere. The VOC mixtures and set of experimental conditions is a small sample across a large chemical and physical space. The current programme aims to reveal examples of the behaviours in mixed systems and provide indicative quantifications of potential interactions and consequences. A focus is placed on the physical properties and chemical composition of the evolving particle distribution throughout the photochemistry driving its formation and transformation. Less emphasis is placed on the quantification of the radical chemistry and oxidative environment although some characterisation of the transformations of the oxidation products in the gas phase and their influence on the particle formation is attempted. The experimental design and instrumental payload are used to address the objectives outlined in section 1.

**Table 1:** List of initial experimental conditions for all the experiments in the campaign.

| Exp. No        | Exp. Type | VOC                        | NO <sub>x</sub> (ppb) | VOC (ppb) <sup>a</sup> | VOC/NO <sub>x</sub> (ppb/ppb) | Seed (μg m <sup>-3</sup> ) | SOA mass (μg m <sup>-3</sup> ) |
|----------------|-----------|----------------------------|-----------------------|------------------------|-------------------------------|----------------------------|--------------------------------|
| <b>Single</b>  |           |                            |                       |                        |                               |                            |                                |
| 1              |           | α-pinene                   | 40                    | 309                    | 7.7                           | 72.6                       | 273.2                          |
| 2              |           | α-pinene                   | 43                    | 309                    | 7.2                           | 67.6                       | 283.1                          |
| 3              |           | α-pinene                   | 50                    | 309                    | 6.2                           | 39.4                       | -                              |
| 4              |           | α-pinene                   | 26                    | 155                    | 6.0                           | 45.7                       | 68.6                           |
| 5              |           | α-pinene                   | 35                    | 155                    | 4.4                           | 47.8                       | 109.5                          |
| 6              |           | α-pinene                   | 18                    | 103                    | 5.7                           | 51.0                       | 31.5                           |
| 7              |           | o-cresol                   | 98                    | 400                    | 4.1                           | 50.8                       | 28.2                           |
| 8              |           | o-cresol                   | 44                    | 400                    | 9.1                           | 47.8                       | 56.0                           |
| 9              |           | o-cresol                   | 71                    | 400                    | 5.6                           | 36.0                       | -                              |
| 10             |           | o-cresol                   | 40                    | 200                    | 5.0                           | 51.3                       | 22.8                           |
| 11             |           | isoprene                   | 24                    | 164                    | 6.8                           | 64.1                       | 0.0                            |
| 12             |           | isoprene                   | 23                    | 164                    | 7.1                           | 101.9                      | 0.0                            |
| 13             |           | isoprene                   | 14                    | 55                     | 3.9                           | 42.2                       | 0.0                            |
| <b>Binary</b>  |           |                            |                       |                        |                               |                            |                                |
| 14             |           | o-cresol/isoprene          | 34                    | 282 (200/82)           | 8.3                           | 49.6                       | 11.2                           |
| 15             |           | o-cresol/isoprene          | -                     | 282 (200/82)           | -                             | 57.0                       | 9.4                            |
| 16             |           | α-pinene/o-cresol          | 52                    | 355 (155/200)          | 6.8                           | 48.3                       | 122.3                          |
| 17             |           | α-pinene/o-cresol          | 65                    | 355 (155/200)          | 5.5                           | 72.9                       | -                              |
| 18             |           | α-pinene/o-cresol          | -                     | 355 (155/200)          | -                             | 42.5                       | 130.1                          |
| 19             |           | α-pinene/isoprene          | 33                    | 237 (155/82)           | 7.2                           | 63.7                       | 96.6                           |
| 20             |           | α-pinene/isoprene          | 39                    | 237 (155/82)           | 6.1                           | 62.0                       | 100.9                          |
| 21             |           | α-pinene/isoprene          | 24                    | 237 (155/82)           | 9.9                           | 50.5                       | 75.2                           |
| <b>Ternary</b> |           |                            |                       |                        |                               |                            |                                |
| 22             |           | α-pinene/o-cresol/isoprene | 80                    | 291 (103/133/55)       | 3.6                           | 45.6                       | 55.5                           |
| 23             |           | α-pinene/o-cresol/isoprene | 60                    | 291 (103/133/55)       | 4.9                           | 49.0                       | 51.4                           |
| 24             |           | α-pinene/o-cresol/isoprene | 78                    | 291 (103/133/55)       | 3.7                           | 45.8                       | 58.0                           |

<sup>a</sup>All nominal reported initial VOC concentrations have a  $\pm 15\%$  measurement uncertainty. The individual VOC concentration in the binary and ternary mixtures shown in brackets correspond to the precursor VOC listing. A dash indicates missing data owing to instrument problems.

## 2.4 Concept behind the experimental design

Taking into account the constraints and challenges outlined above, the programme was constructed to investigate a single ternary system comprising one anthropogenic and two biogenic VOCs. The biogenic VOCs were chosen as α-pinene and isoprene to enable comparison of batch reactor experiments with the previous flowtube (Berndt et al., 2018), well-mixed continuously stirred tank reactor (McFiggans et al., 2019) or flow-through chamber

studies (Shilling et al., 2019). The anthropogenic aromatic OVOC *o*-cresol was chosen for its fairly rapid rate constant with OH ( $4.1 \times 10^{-11} \text{ cm}^3\text{molec}^{-1}\text{s}^{-1}$ ), such that it would exhibit comparable reactivity towards OH as a similar concentration of  $\alpha$ -pinene or isoprene. A concept of “initial isoreactivity” towards OH was employed to select ratios of the initial concentrations of the VOCs. This meant that the initial mixing ratios were injected at an  $\alpha$ -pinene: isoprene: *o*-cresol ratio of 309 : 164 : 400 based on the ratios of the inverse of their IUPAC-recommended rate constants at 298K (Atkinson et al., 2006; Mellouki et al., 2021). In order to construct a systematic investigation of the single precursor, binary and ternary mixtures, individual VOC experiments were conducted at full-, half- and third-reactivity for comparison of SOA particle mass, composition and properties. Using previously reported values for the SOA particle mass yields, it was expected that an initial full-reactivity mixing ratio in the 100s ppbv range would provide the 10 to a few 100  $\mu\text{gm}^{-3}$  required to provide enough particle mass on the filter at the end of an experiment (at a final chamber volume of around 10  $\text{m}^3$ ) for molecular characterisation.

## 2.5 Compromises in the experimental plan and consequences

OH is only one of the likely oxidants under the chosen photo-oxidation conditions, and the unsaturated biogenic compounds will each react with ozone with appreciable reactivity. *o*-cresol exhibits negligible reactivity towards ozone. Ozone is the first oxidant to be formed through photolysis of  $\text{NO}_2$ , and there will be appreciable formation of biogenic oxidation products prior to the formation of those from *o*-cresol (see section 4).

In addition to the differential reactivity towards the two dominant oxidants, there will be differences in the product formation rates in the single VOC experiments with varying concentrations owing to the use of a single VOC:  $\text{NO}_x$  ratio. This will result from the reduced  $\text{NO}_x$  at reduced VOC, which will lead to reduced OH concentration owing to a reduction in the  $\text{NO} + \text{HO}_2$  flux. Though there will also be a reduced rate of production of ozone in these experiments, non-linearity will lead to changes in the  $\text{O}_3$ : OH ratio and hence changes in the contributions of the oxidation pathways for the biogenic VOCs. There may be less expected influence on the pathways for *o*-cresol oxidation, though the rate of oxidation will nevertheless be slowed.

Ambient atmospheric OH reactivity can be estimated from the quantification of VOC

abundance or direct measurements of OH lifetime. Using the latter, Whalley et al. (2016) reported central London diurnal average morning peaks of around  $27 \text{ s}^{-1}$  and a campaign maximum of around  $116 \text{ s}^{-1}$ . Our full reactivity experiments have an OH reactivity around  $465 \text{ s}^{-1}$ , some 4 times higher with only one, two or three VOCs for single precursor, binary or ternary experiments respectively. It would be desirable to work with lower concentrations. In addition to challenges associated with maintaining oxidant levels at such high VOC concentrations, there is a likelihood that the chemical regime, particularly with respect to radical concentrations may introduce biases in observed system behaviour. In our systems, OH reactivity is provided by C<sub>5</sub>, C<sub>7</sub> and C<sub>10</sub> VOC compounds (in addition to that provided by NO<sub>2</sub> and VOC oxidation products formed by the oxidation). This will lead to a high abundance of relatively large peroxy-radical, RO<sub>2</sub>, species. OH reactivity in the ambient atmosphere is likely to be distributed amongst a high diversity of small (including CO and CH<sub>4</sub>) and larger components (including carbonyls and other oxygenates). The distribution of RO<sub>2</sub> and the ratio of RO<sub>2</sub>:HO<sub>2</sub> may be substantially different. Nonetheless, it is not the intention or objective of the current study to mimic the atmospheric chemical regime, more to explore the potential for mixed VOC systems to reveal interactions in SOA formation processes.

A further consideration is the selection of neutral seed experiments. The systems studied will more reflect direct partitioning of gaseous oxidation products rather than accounting for products of condensed phase, particularly acid catalysed, reactions. Again, the intention is not to comprehensively mimic the atmosphere and this is recognised in the interpretation and discussed in further detail in section 5.

### **3. Methodology**

All experiments were performed in the MAC; a 18m<sup>3</sup> FEP Teflon bag mounted on three pairs of rectangular extruded aluminium frames and housed in an air-conditioned enclosure. In the MAC, ground-level solar illumination is simulated using two 6 kW Xenon arc lamps and a bank of halogen lamps, mounted on the inner aluminium wall of the enclosure which is lined with reflective “space blanket” material to maximise and homogenise the light intensity across the chamber. Removal of unwanted heat from the lamps is provided by the temperature and RH conditioned air introduced between the bag and the enclosure at  $3 \text{ m}^3 \text{ s}^{-1}$  and active water cooling of the mounting bars of the halogen lamps and the filter in front of the arc lamps. In addition to removing the heat from the arc lamp, the water in the filters removes unwanted IR

radiation and the 4mm quartz plates forming the filter windows remove all UV radiation below 290 nm and increasingly transmit light up to a 100% transmission above 305 nm. The inlet comprises a high flowrate blower, feeding dried laboratory air through 50 mm diameter stainless steel pipework to a series of high-capacity filters and variously via a series of two- and three-way electropneumatic valves to a humidifier, ozoniser and aerosol generation drum before delivering it to the chamber through a Teflon manifold. This is mounted on the top frame of the central rigidly fixed pair of frames. The upper and lower pairs of frames are counter-weighted and free to track vertically, allowing the bag to expand and collapse as it is filled and flushed, by switching the valve positioning.

All controls are automated, and a series of pre- and post-experimental procedures have been programmed, comprising repeatable, characterised sequences of filling and flushing. The pre-experiment sequence is conducted prior to each experiment to ensure an adequately low background of indicative particulate and gaseous contaminants, monitored by CPC, NO<sub>x</sub> and O<sub>3</sub> analysers. A one-hour long chamber background characterisation procedure, following the pre-experiment sequence, is conducted to ensure that a baseline contamination level has been established. This is followed by injection of the VOCs, NO<sub>x</sub> and seed particles and a one-hour collection of data from the experimental background in the dark, during which the chamber conditions and all instrumentation are stabilised. A post-experiment sequence is conducted after each experiment to flush the chamber of all residual contaminants and leave a clean bag for the next experiment. The final fill of the post-experiment sequence contains ppm levels of ozone which is used to soak the chamber overnight between subsequent experiments. A weekly vigorous clean is conducted with full illumination with no UV filter on the arc lamps and ppm levels of ozone at high RH for maximum OH production.

Ammonium sulphate seed particles are atomised into a 50L stainless steel drum for pre-concentration prior to injection into the chamber. The seed concentration in the chamber is controlled by altering the injection time into the drum and the concentration of the stock solution (0.01 g/ml). After the final pre-experiment flush cycle, the fill flow is diverted through the drum. Liquid  $\alpha$ -pinene, isoprene and *o*-cresol are injected as required through the septum of a heated glass bulb and evaporated into an N<sub>2</sub> carrier flow into this final fill along with NO<sub>x</sub> as NO<sub>2</sub> from a cylinder, also carried by N<sub>2</sub>. Photochemistry is initiated by irradiating the VOC at a moderate VOC / NO<sub>x</sub> ratio using the lamps as described above. Online instrumentation is

used to continuously monitor the concentration of NO<sub>x</sub>, O<sub>3</sub>, particle number and mass throughout each experiment. It should be noted that *o*-cresol was found to interfere with O<sub>3</sub> measurement as a result of its UV absorption. The decay of CIMS-measured *o*-cresol was used to correct the O<sub>3</sub> data in all *o*-cresol containing experiments. The dark *o*-cresol measured before the introduction of O<sub>3</sub> into the MAC was used to calibrate the O<sub>3</sub> analyser signal for absorption by *o*-cresol. The decay rate of the CIMS *o*-cresol signal was used to correct the O<sub>3</sub> measurements during the experiment. It should be noted that any UV absorption from the oxidation products of *o*-cresol cannot be captured and O<sub>3</sub> is thus reported as an upper limit in *o*-cresol containing systems.

**Table 2:** List of instrumentation employed throughout the study

| Instrument   | Model  | Measured parameter                                  | LOD/ range  |
|--|--|---|---|
| Dew point hygrometer                                 | Edgetech (DM-C1-DS2-MH-13)                               | Dew point   | -20 – 90± 0.2 °C  |
| NO <sub>x</sub> analyser                             | Thermo 42i   | NO, NO <sub>2</sub>                                 | 0.5 to 1000 ppb   |
| O <sub>3</sub> analyser                              | Thermo 49C   | O <sub>3</sub>                                      | 0-0.05 to 200 ppm   |
| Water-based condensation particle counter            | TSI 3786   | Particle number                                     | <10 <sup>7</sup> p/cc                                     |
| Differential mobility particle sizer                 | Custom.built <sup>a</sup>                                | Particle size                                       | 40-600 nm   |
| Filter collector                                     | Custom.built <sup>b</sup>                                | Particle collection for offline analysis            |   |
| Condensation particle counter                        | TSI 3776   | Particle number                                     | <10 <sup>7</sup> p/cc                                     |
| Scanning mobility particle sizer                     | TSI 3081   | Particle size                                       | 10-1000 nm  |
| High-resolution aerosol mass spectrometer            | Aerodyne   | PM <sub>1</sub> non.refractory particle composition | >0.05 µg m <sup>-3</sup>                                  |
| Iodide chemical ionisation mass spectrometer         | Aerodyne/Tofware   | Oxygenated VOC                                      | LOD >60 ppt; Mass resolution 4000 Th/Th                   |
| Filter Inlet for Gases and AEROSols                  | Aerodyne/Tofware   | Particle composition                                | >10 <sup>2</sup> ng                                       |
| Semi-continuous gas-chromatograph mass spectrometer  | 6850 and 5975C Agilent                                   | VOC concentration                                   | >0.4 ppb  |
| Liquid chromatograph – orbitrap mass spectrometry    | Dionex 3000, Orbitrap QExactive, ThermoFisher Scientific | Particle composition                                |   |
| Hygroscopicity tandem differential mobility analyser | Custom.built <sup>c</sup>                                | Hygroscopicity                                      | 20-350 nm   |
| Cloud condensation nuclei counter                    | Droplet measurement Tech (model CCN-100)                 | CCN activity  | >6 x 10 <sup>3</sup> particles cm <sup>-3</sup> atSS:0.2% |
| Thermal denuder                                      | Custom.built <sup>d</sup>                                | Volatility  | Temperature range: ambient – 200°C                        |



|                           |                           |                 |   |
|---------------------------|---------------------------|-----------------|---|
| Three arm bounce impactor | Custom.built <sup>e</sup> | Particle bounce | 20-500 nm, < 10 <sup>4</sup> particles<br>cm <sup>3</sup> |
|---------------------------|---------------------------|-----------------|---|

<sup>a</sup>Alfarra et al. (2012) <sup>b</sup>Hamilton et al. (2011) <sup>c</sup>Good et al. (2010) <sup>d</sup>Voliotis et al. (2021a)

<sup>e</sup>Liu et al. (2017)

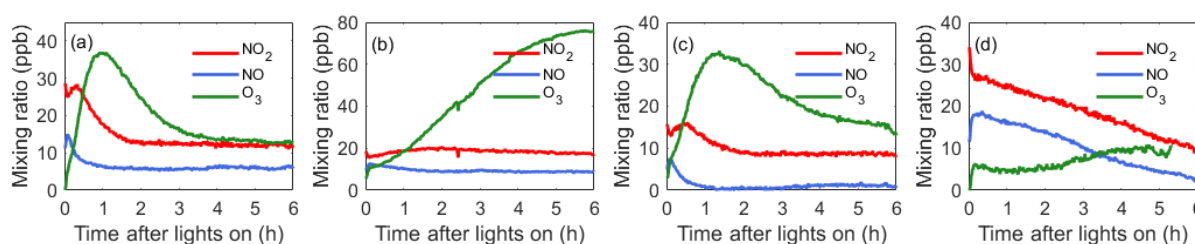
A high-resolution time-of-flight Aerosol Mass Spectrometer (HR-ToF-AMS; Aerodyne Inc.) is used to measure particle composition by mass. The AMS ionization efficiency was calibrated using ammonium nitrate and ammonium sulfate before the experimental campaigns, and the value was used across experiments. A real-time collection efficiency (CE) was utilized to the data of each experiment by comparing the HR-ToF-AMS total mass with the total mass from the SMPS multiplied by an effective density, based on the organic/inorganic ratio from the HR-ToF-AMS, assuming densities of 1.77 and 1.4 g cm<sup>-3</sup> for the inorganic and organic fraction, respectively. The CE for ammonium sulfate, determined in the “dark unreactive” period was found to be ~0.3-0.5, in line with previous findings (Alfarra et al.,2004), and the more SOA condensed the CE increased to reach almost unity (i.e., ~0.9-1.1), also in line with previous of observations (Matthew et al., 2008). A Filter Inlet for Gases and Aerosols coupled to an iodide chemical ionisation mass spectrometer (FIGAERO-I-CIMS; Aerodyne Inc.) for gas and particle phase oxygenated component measurement, a scanning mobility particle sizer (SMPS; TSI Inc.) for particle size distribution retrieval, a home-built hygroscopicity tandem differential mobility analyser (HTDMA) for hygroscopic growth factor determination, a cloud condensation nucleus counter (CCN; DMT Inc.) for cloud droplet potential evaluation and a home-built three-arm bounce impactor for particle rebound determination. Some of the online instrumentation was switched after several hours to cycle between sampling after a home-built thermodenuder (TD) and directly from the chamber. Finally, a semi-continuous 2-trap Gas Chromatograph with Mass Spectrometric detection (GC-MS; Agilent) was used to monitor VOC concentrations. Table 2 provides a list of all instrumentation employed throughout the programme. At the end of each 6-hour experiment, the entire remaining contents of the bag are flushed through a Whatman Quartz microfibre filter (pre-fired at 550°C for 5.5 hours) to collect the particles. The filters were then wrapped in foil and stored at -18°C prior to analysis by LC-electrospray Orbitrap MS.

Actinometry and off-gassing experiments were conducted regularly through the programme in order to establish the consistency of the chamber’s performance, evaluate the effectiveness of the cleaning procedure and confirm the cleanliness of the chamber. Background filters were collected from the actinometry and off-gassing experiments.

## 4. Results

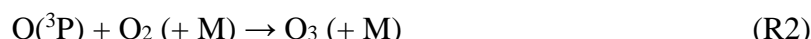
### 4.1 Concentrations of VOCs, NO<sub>x</sub> (NO and NO<sub>2</sub>) and O<sub>3</sub>

To provide the photochemical context for example systems, Figure 1 shows the time series of NO<sub>2</sub>, NO and O<sub>3</sub> from experiments in the following 4 systems: *α*-pinene, isoprene, *α*-pinene/isoprene and *o*-cresol. Note that, in the presence of *o*-cresol, O<sub>3</sub> measurement by UV absorption was influenced by UV absorption by *o*-cresol and Figure 1(d) is corrected as explained in the methods section. Figure S1 shows the NO<sub>2</sub>, NO and O<sub>3</sub> for all systems, similarly corrected for *o*-cresol containing systems.



**Figure 1:** NO<sub>2</sub>, NO and O<sub>3</sub> time series in example single and mixed VOC experiments (a) *α*-pinene, (b) isoprene, (c) *α*-pinene/isoprene, (d) *o*-cresol.

O<sub>3</sub> will move towards photo-stationary state (PSS) with NO and NO<sub>2</sub> according to reactions R1, R2 and R3:



Some insight into the trajectory towards PSS across the systems can be gained by an inspection of Supplementary Figure S2, which provides a comparative summary of the Leighton Ratio (Leighton 1961) for all systems and the O<sub>3</sub> calculated assuming PSS, i.e. Leighton Ratio of 1, shown for the *o*-cresol containing systems. The Leighton Ratio is given by

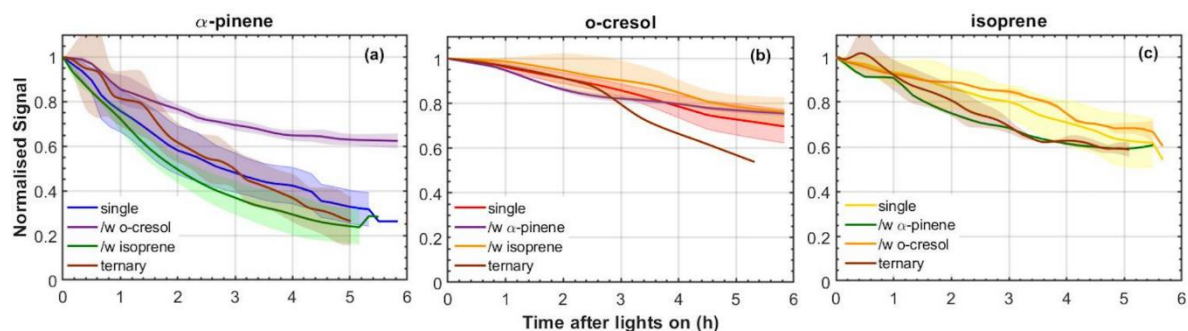
$$\varphi = j_{\text{NO}_2} [\text{NO}_2] / k_{\text{O}_3+\text{NO}} [\text{O}_3] [\text{NO}] \quad (1)$$

In the polluted high-NO<sub>x</sub> atmosphere, PSS universally applies and  $\varphi$  is unity. In moderately polluted conditions, radical reactions are increasingly important in the conversion

of NO to NO<sub>2</sub> and typically  $\phi > 1$ . This is because HO<sub>2</sub> and RO<sub>2</sub> will compete with the O<sub>3</sub> reaction for NO (R3) according to reactions (R4 and R5):



where RO<sub>2</sub> arise from biogenic VOC or *o*-cresol. Note that, in the ambient atmosphere, RO<sub>2</sub> can stem from a very wide pool of VOCs. Further deviation from PSS and consequent increase in  $\phi$  will occur when O<sub>3</sub> loss processes other than R3 become important. These can include reactions of O<sub>3</sub> with NO<sub>2</sub>, alkenes and radicals. In our chamber systems, the O<sub>3</sub> reactions with  $\alpha$ -pinene and isoprene and radical reactions with NO, are competitive and provide a substantial deviation from PSS. The NO<sub>x</sub> and O<sub>3</sub> trajectories in the various systems can be seen to vary substantially. Nevertheless, in all systems, illumination of the chamber leads to the expected onset of significant photochemistry to initiate the VOC photo-oxidation.



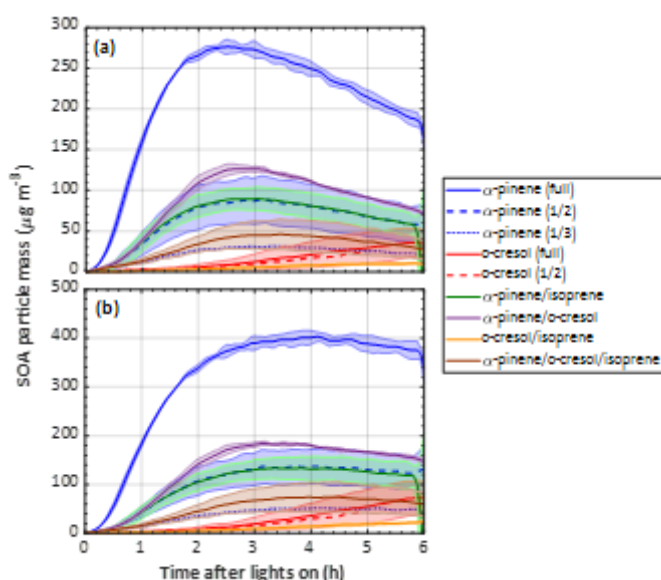
**Figure 2:** Decay rates of each VOC across all mixtures; a)  $\alpha$ -pinene, b) isoprene and c) *o*-cresol. All lines (and shaded areas) containing blue correspond to experiments including  $\alpha$ -pinene, containing red to those including *o*-cresol and yellow to isoprene. For example, purple lines correspond to an  $\alpha$ -pinene /*o*-cresol binary mixture and brown to the ternary mixture. The shaded areas represent 1 standard deviation around the solid line mean value of all experiments.

From Figure 2, it can be seen that the rate of decay is not the same in each experiment, despite the attempt at initial isoreactivity, as explained in section 2.5. Oxidation products from each VOC will nevertheless be present in appreciable quantities in each experiment, satisfying the objectives of the design to enable the exploration of interactions of oxidation products in SOA particle formation.

## 4.2 SOA yields

Figure 3 shows the time series of SOA particle mass in all experiments (with shading

representing  $\pm 1\sigma$  of the measurement across all experiments) in all precursor systems studied. It can be seen that the greatest SOA mass was generated in  $\alpha$ -pinene containing systems, which is unsurprising, given the known efficiency with which it forms particle mass. It was found that *o*-cresol and *o*-cresol containing mixtures were the next most efficient at producing particle mass. This might be expected with its reported moderate SOA particle producing potential. Negligible SOA particles were formed in all single VOC isoprene experiments. Only when isoprene was in a mixture was any mass formed and, in all cases, this was lower than the mass formed from the other VOC alone. Again, this is not too surprising, given the low or negligible particle mass yield reported for isoprene on neutral particle seeds. As seen in Figure 2, not all VOC was consumed in all experiments and it can be seen that the particle mass may not have fully peaked in all *o*-cresol and *o*-cresol / isoprene experiments. Nevertheless, the mass peak was observed in most experiments before they were completed, and the chamber contents were flushed through the filter for compositional analysis. Panel b) in Figure 3 shows the SOA particle mass corrected for the losses of particles to the chamber walls. This was conducted by calculating the exponential decay of particles of each size from a targeted ammonium sulphate wall loss correction experiment performed close to the experiment of interest. Details of the wall loss correction can be found in Shao et al. (2021a).



**Figure 3:** SOA particle mass (mean  $\pm 1\sigma$  as shaded areas) in each system, a) raw measurements and b) particle wall-loss corrected mass. Note that this is organic mass determined from AMS measurements and so does not include the ammonium sulphate seed particles. The same colour scheme is used as in Figure 2.

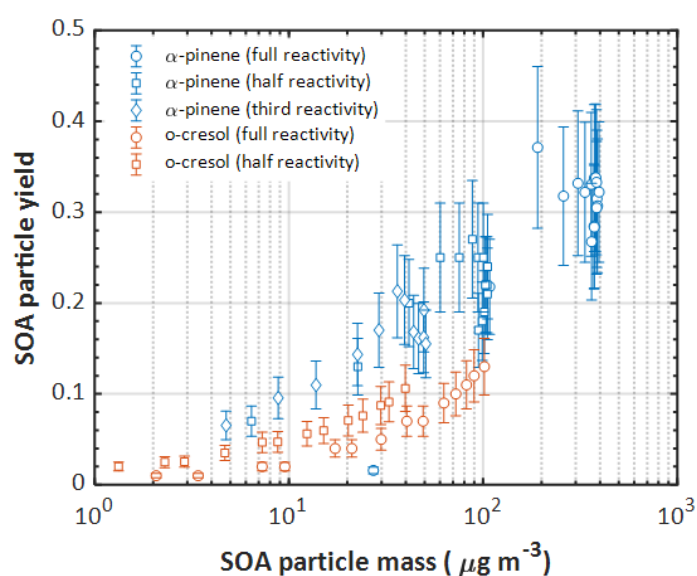
Figure S3 shows the total particle wall loss corrected particle component mass ratios in each system indicating the inorganic and organic component evolution as measured by AMS. As shown in panel a), the mass ratio of organic to inorganic seed follows the production of SOA particle mass and the loss of total particle mass to the walls. In the wall loss correction, the size-resolved loss of multi-component organic-inorganic aerosol particles is assumed to be the same as that for size-resolved ammonium sulphate seeds loss rate measured in dedicated experiments (see methodology). The decrease in  $\text{SO}_4^{2-}/\text{NO}_3^-$  shown in panel b) follows the wall loss of total particle mass (and hence  $\text{SO}_4^{2-}$ ) and simultaneous oxidation of  $\text{NO}_2$  by OH to form  $\text{HNO}_3$  (and hence particulate  $\text{NO}_3^-$ ).  $\text{NH}_4^+$  was found to be in ion balance with the sum of  $\text{NO}_3^-/\text{SO}_4^{2-}$  in all experiments.

Particle mass yield is a widely used metric that aims to represent the effectiveness of a VOC in forming SOA particle mass. In single precursor systems it is relatively straightforward the particle mass formed per unit of VOC consumed:

$$Y = \frac{\Delta[\text{SOA}]}{\Delta[\text{VOC}]} \quad (2)$$

Frequently the yield is reported as a single number and this may be taken from measurements at maximum SOA particle mass formed in the experiment, at the maximum VOC consumed, or perhaps more arbitrarily, at the end of an experiment. Such approaches may be reasonably applied for comparisons between precursors in identical oxidation conditions in the same chamber. Owing to significant particle losses to chamber walls, it can be seen from Figure 3 that it is important to correct the particle mass formed in the yield calculations for such losses. It is noted that the yields need to be corrected for VOC or OVOC product losses to the walls, too as discussed in section 5. Table 3 shows the calculated yields for all individual VOC and mixture experiments. The first 9 rows show the yields for single VOC experiments. Following the particle mass plots shown in Figure 3, it is clear that the efficiency in forming particle mass is in the order  $\alpha$ -pinene > *o*-cresol > isoprene, with no mass yield observed in isoprene oxidation though appreciable isoprene consumption was observed as shown in Figure 2. For  $\alpha$ -pinene and *o*-cresol, it can be seen that the yield increased with increasing initial concentration. The *o*-cresol and *o*-cresol / isoprene experiments were not continued to the point of maximum mass formation (as shown in Figure 3) and so the maximum VOC consumption and mass formation both correspond to the end of the experiments in these systems. Figure 4

shows the yield plotted against SOA particle mass for  $\alpha$ -pinene and *o*-cresol for all individual VOC experiments, indicating that the yield increases monotonically with particle mass within propagated experimental uncertainties. Such behaviour is expected and is consistent with absorptive partitioning considerations. Note that organic mass formation in the “full reactivity” (i.e. 309 ppb  $\alpha$ -pinene) experiment is so rapid that VOC data are only available for yield calculation beyond  $100 \mu\text{g m}^{-3}$ . Supplementary Figure S4 alternatively shows the SOA particle mass yield plotted against the total particle mass in the chamber, including the ammonium sulphate seed particles that provide a condensation sink for the condensable vapours produced by VOC oxidation.



**Figure 4:** SOA particle mass yield as a function of mass formed in the single precursor  $\alpha$ -pinene and *o*-cresol experiments at all initial concentrations. Error bars represent the propagated uncertainties in all measurements and the particle wall loss corrections applied.

Since there is no SOA particle mass formed from isoprene, Table 3 additionally presents yield data omitting the consumption of isoprene in the denominator of equation 2, accordingly increasing the yield. Figure 5 shows the yield curves for typical experiments in all systems. The yield curves allow comparison between the systems, both including and excluding isoprene in the denominator of equation 2. The two-product model (Odum et al., 1996) was used to fit the yield curves for  $\alpha$ -pinene and *o*-cresol. These are included to guide the eye. Here, the two-product model parameterised the relation of overall SOA yield and the adsorptive mass assuming only two products to exist in the system. The equation of the two-product model is shown in eq.3.  $\alpha$ ,  $K_p$  and  $C_{OA}$  represent the stoichiometric factor, the partitioning coefficient of

product and the total absorbing organic mass, respectively. The  $\alpha_1$ ,  $\alpha_2$ ,  $K_{p,1}$ ,  $K_{p,2}$  can be fitted from the yield curves.

**Table 3:** Measured and particle wall-loss corrected SOA particle mass yields for all systems calculated at maximum particle mass and maximum VOC consumed. For mixtures containing isoprene, which had zero yield on the neutral seeds injected, the yields were calculated excluding the consumption of isoprene in the system allowing them to be referenced to the mixtures without isoprene. Yield was calculated with the density of organic matter of  $1.4\mu\text{g m}^{-3}$ . The maximum mass used in the yield at maximum mass calculation is given in Table 1. The uncertainties in SOA particle mass yield was calculated by propagating the  $\pm 1\sigma$  uncertainties of measured  $\Delta\text{SOA}$  and  $\Delta\text{VOC}$ .

|   | Reactivity | Yield at max. mass | Yield at max. VOC consumed | Yield at max. mass (Isoprene excluded) | Yield at max. VOC consumed (Isoprene excluded) |
|---|------------|--------------------|----------------------------|--|--|
| $\alpha$ -pinene                            | Full       | $0.32 \pm 0.08$    | $0.27 \pm 0.06$            |  |  |
|   | 1/2        | $0.21 \pm 0.05$    | $0.17 \pm 0.04$            |  |  |
|   | 1/3        | $0.16 \pm 0.04$    | $0.13 \pm 0.03$            |  |  |
| isoprene                                    | Full       | 0                  | 0                          |  |  |
|   | 1/2        | -                  | -                          |  |  |
|   | 1/3        | 0                  | 0                          |  |  |
| <i>o</i> -cresol                            | Full       | $0.13 \pm 0.03$    | $0.13 \pm 0.03$            |  |  |
|   | 1/2        | $0.11 \pm 0.03$    | $0.11 \pm 0.03$            |  |  |
|   | 1/3        | -                  | -                          |  |  |
| $\alpha$ -pinene/isoprene                   | Full       | $0.16 \pm 0.05$    | $0.13 \pm 0.04$            | $0.19 \pm 0.05$                        | $0.16 \pm 0.04$                                |
|   | Full       | $0.29 \pm 0.09$    | $0.22 \pm 0.07$            |  |  |
| $\alpha$ -pinene/ <i>o</i> -cresol          | Full       | $0.29 \pm 0.09$    | $0.22 \pm 0.07$            |  |  |
|   | Full       | $0.06 \pm 0.02$    | $0.06 \pm 0.02$            | $0.08 \pm 0.02$                        | $0.07 \pm 0.02$                                |
| <i>o</i> -cresol/isoprene                   | Full       | $0.06 \pm 0.02$    | $0.06 \pm 0.02$            | $0.08 \pm 0.02$                        | $0.07 \pm 0.02$                                |
|   | Full       | $0.11 \pm 0.04$    | $0.08 \pm 0.03$            | $0.12 \pm 0.04$                        | $0.08 \pm 0.03$                                |
| $\alpha$ -pinene/ <i>o</i> -cresol/isoprene | Full       | $0.11 \pm 0.04$    | $0.08 \pm 0.03$            | $0.12 \pm 0.04$                        | $0.08 \pm 0.03$                                |
|   | Full       | $0.11 \pm 0.04$    | $0.08 \pm 0.03$            | $0.12 \pm 0.04$                        | $0.08 \pm 0.03$                                |

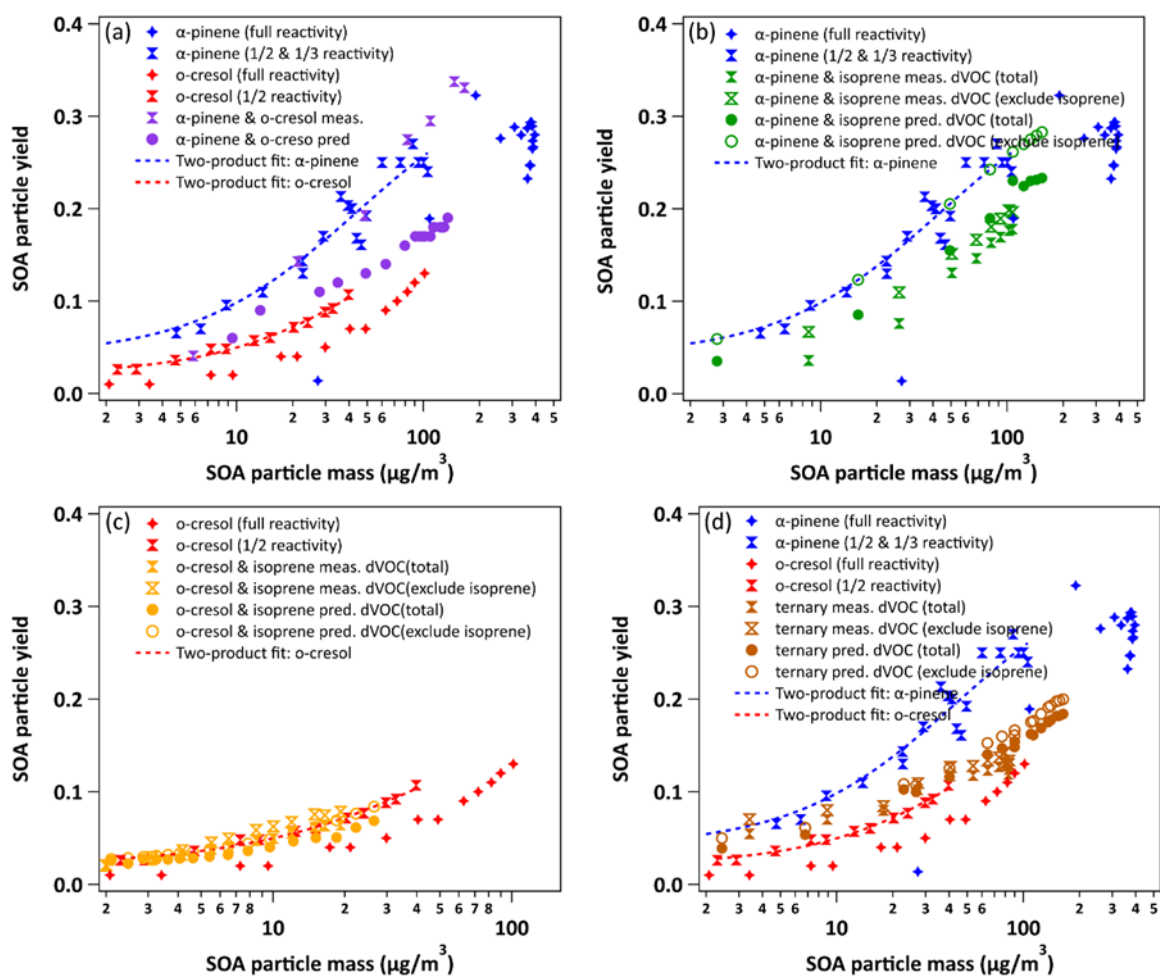
In addition to the measured points, Figure 5 shows “predicted” yields for the mixtures, based on the organic mass at the same VOC consumption measured in the single VOC experiments and additively combining them according to:

$$Yield = C_{OA} \left( \frac{\alpha_1 K_{p,1}}{1 + K_{p,1} C_{OA}} + \frac{\alpha_2 K_{p,2}}{1 + K_{p,2} C_{OA}} \right) \quad (3)$$

and

$$Yield_{pred.} = \frac{\Delta m_{\Delta VOC1} + \Delta m_{\Delta VOC2} + \Delta m_{\Delta VOC3}}{\Delta VOC1 + \Delta VOC2 + \Delta VOC3} \quad (4)$$

Where the  $\Delta m$  is the measured yields from half-reactivity and third-reactivity experiments of  $\alpha$ -pinene, isoprene and *o*-cresol;  $\Delta_{VOC1}$ ,  $\Delta_{VOC2}$ ,  $\Delta_{VOC3}$  represent the measured changes for the concentrations of  $\alpha$ -pinene, isoprene and *o*-cresol. The parameters for the two-product fit from the single VOC half- and third-reactivity experiments were used to generate a yield-mass- $\Delta$ VOC look-up-table. This was then used to calculate the particle mass formed from each precursor at the consumption of the VOC at each point in the binary and ternary systems.



**Figure 5:** Yield data for selected representative experiments in all systems (with 2-product yield curves for  $\alpha$ -pinene and *o*-cresol single VOC experiments). Panel a) shows the binary  $\alpha$ -pinene / *o*-cresol mixture and its constituents, b) the binary  $\alpha$ -pinene / isoprene mixture, c) the *o*-cresol / isoprene mixture (expanded y-axis plot shown in Figure S5) and d) the ternary  $\alpha$ -pinene / *o*-cresol / isoprene mixture. Yields “predicted” from the linear combination of yields from the individual VOC experiments using equation 4 are shown for each mixture.

Using this look-up table, the predicted yield from the binary  $\alpha$ -pinene / *o*-cresol mixture photo-oxidation is below that measured in the  $\alpha$ -pinene / *o*-cresol mixture experiment and slightly higher than that in the individual *o*-cresol experiment at 50% reactivity. Indeed, the

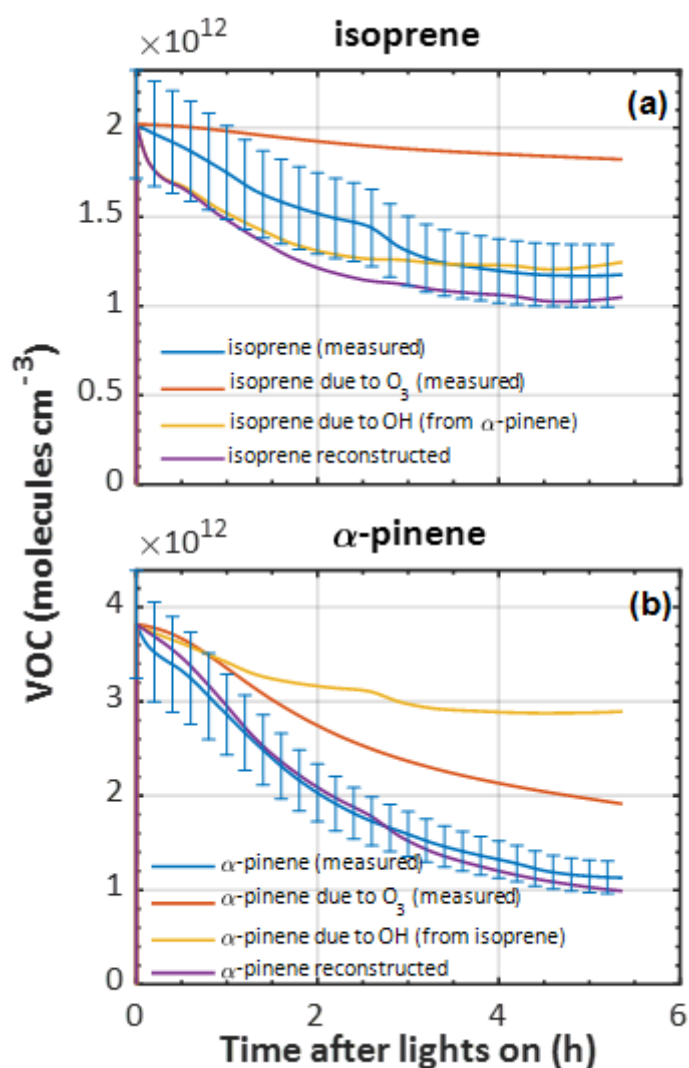


yield measured in the mixture is comparable to that of  $\alpha$ -pinene at one half and one third reference reactivity. For the isoprene-containing binary mixtures, the predicted yield excluding isoprene in the denominator is identical to that of the 2-product curve fitted to the single VOC experiment derived yield of other components in the mixtures. In the  $\alpha$ -pinene / isoprene system, the predicted yield accounting for the consumption of both  $\alpha$ -pinene and isoprene is higher than that measured but, as shown in Tables 3 and 4, comparable to the measured yield referenced only to the consumption of  $\alpha$ -pinene. In the *o*-cresol / isoprene system, the predicted yield accounting for the consumption of both *o*-cresol and isoprene is lower than that measured (at higher mass loadings), there is little difference within uncertainty at a lower mass. The predicted yield accounting for the consumption of *o*-cresol alone is lower than that measured when referenced to the same total VOC consumption but comparable to the measured yield referenced to the consumption of both *o*-cresol and isoprene. Finally, in the ternary system, the predicted yield excluding isoprene consumption is similarly (and obviously) higher than that including its consumption, but both predictions are between the yields of single  $\alpha$ -pinene and *o*-cresol experiment measurements. The measured yields accounting for only  $\alpha$ -pinene and *o*-cresol consumption in the ternary mixture are also similarly (and obviously) higher than that including isoprene consumption. There is insufficient difference between the measurements or the predictions to state whether inclusion or exclusion of isoprene consumption gives a much better agreement, though there is an indication that the predicted yields show a steeper gradient with SOA particle mass than the measured slope, which more closely follows that of the *o*-cresol than that of  $\alpha$ -pinene. Table 4 distills the predictions based on the yield from single VOC experimental data at the same consumption as in the mixtures into single values predicted at maximum SOA particle mass, maximum VOC consumption, both with and without isoprene decay in the calculation. To explore the likely fate of the parent VOCs in the MAC, we used the measured O<sub>3</sub> concentrations and VOC decay rates and exploited the differential reactivities of the VOCs to investigate the decay attributable to each oxidant and also overcome measurement difficulties encountered in the experiments. For example, knowing that *o*-cresol has a negligible rate of reaction with O<sub>3</sub>, we can calculate the OH concentration from the *o*-cresol decay curve. This can then be used to attribute the fraction of the decay of isoprene and  $\alpha$ -pinene to OH and O<sub>3</sub> in their binary mixtures with *o*-cresol. This is important since the measurement of O<sub>3</sub> by UV absorption in the presence of *o*-cresol is challenging and requires correction for the additional absorption by *o*-cresol. In systems without *o*-cresol, the decremental decay attributable to O<sub>3</sub> can be constructed for  $\alpha$ -pinene and isoprene using the O<sub>3</sub>

measurements and (reaction rates of  $9.6$  and  $1.28 \times 10^{-17} \text{ cm}^3 \text{ molecules}^{-1} \text{ s}^{-1}$ , respectively; Cox et al., 2020), by comparing with the actual  $\alpha$ -pinene and isoprene, the residual decay can be attributed to OH. An example of this oxidant reconciliation is shown in Figure 6 for the binary  $\alpha$ -pinene / isoprene system.

**Table 4** SOA predicted yield for the 4 mixtures at maximum SOA particle mass produced and maximum VOC consumed. The uncertainties in SOA particle mass yield were calculated by propagating the  $\pm 1\sigma$  uncertainties of predicted  $\Delta\text{SOA}$  and measured  $\Delta\text{VOC}$ .

| <b>Predicted Yield at:</b>                  |                                       |                                 |  |  |
|---|---------------------------------------|---------------------------------|--|--|
|   | <b>Max. SOA<br/>particle<br/>mass</b> | <b>Max. VOC<br/>consumption</b> | <b>Max. SOA<br/>particle mass<br/>excl. isoprene</b> | <b>Max. VOC<br/>consumption<br/>excl. isoprene</b> |
| $\alpha$ -pinene/isoprene                   | $0.19 \pm 0.08$                       | $0.15 \pm 0.06$                 | $0.21 \pm 0.08$                                      | $0.17 \pm 0.06$                                    |
| $\alpha$ -pinene/ <i>o</i> -cresol          | $0.17 \pm 0.07$                       | $0.14 \pm 0.05$                 | $0.17 \pm 0.07$                                      | $0.14 \pm 0.05$                                    |
| isoprene/ <i>o</i> -cresol                  | $0.10 \pm 0.04$                       | $0.09 \pm 0.04$                 | $0.11 \pm 0.04$                                      | $0.11 \pm 0.04$                                    |
| $\alpha$ -pinene/isoprene/ <i>o</i> -cresol | $0.13 \pm 0.06$                       | $0.11 \pm 0.05$                 | $0.14 \pm 0.05$                                      | $0.12 \pm 0.05$                                    |

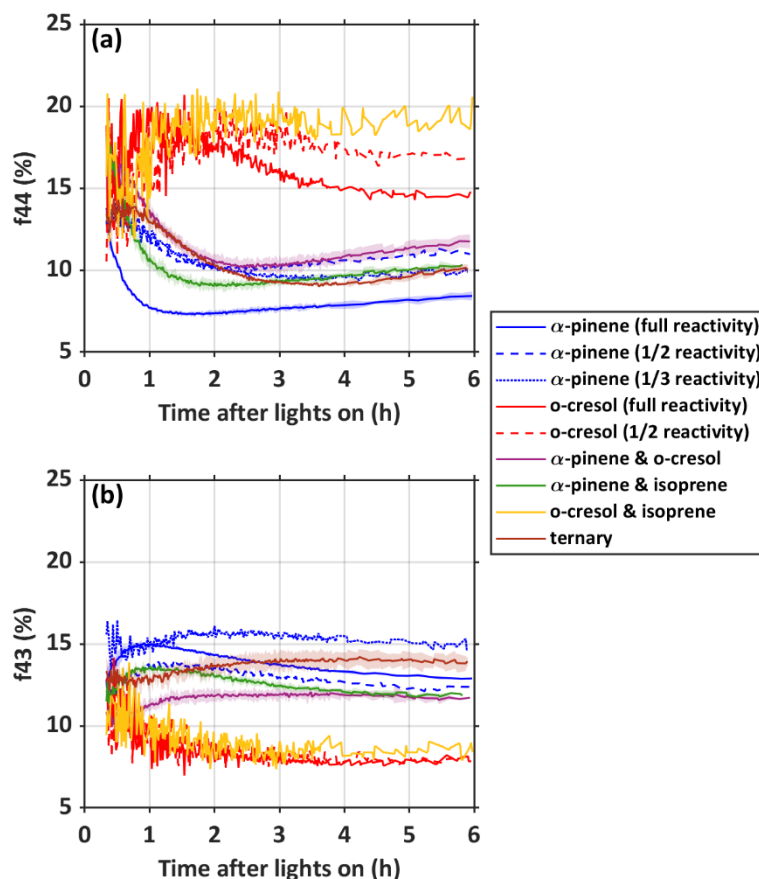


**Figure 6:** Measured ( $\pm 15\%$  error) and reconstructed (a) isoprene and (b)  $\alpha$ -pinene decay in a  $\alpha$ -pinene & isoprene binary experiment. Initially, in each case the decay of the VOC due to ozone was predicted based on the O<sub>3</sub> concentration, the reaction rate of each VOC toward O<sub>3</sub> and the initial VOC concentration. Subsequently, the OH concentration from each VOC was estimated from the difference in the VOC decay attributed to O<sub>3</sub> and the measured VOC decay. Finally, the OH concentration from each precursor was used to reconstruct the decay of the other (i.e., OH from isoprene was used to reconstruct the decay of  $\alpha$ -pinene and vice versa).

In the example shown in Figure 6, it can be seen that roughly twice as much loss of  $\alpha$ -pinene can be attributed to O<sub>3</sub> as to OH and roughly 4 times as much isoprene loss attributed to OH as to O<sub>3</sub>. The inability to control isoreactivity towards all oxidants through controlling the initial VOC concentrations will influence the prediction of SOA particle mass yields owing to the differences in the tendency to condense oxidation products from different oxidants. These aspects are discussed in section 5.

### 4.3 Chemical composition and properties

Differences in the SOA particle oxygenation trajectory between the systems are illustrated in Figure 7 by the percentages of the AMS total signal at  $m/z=44$  ( $f_{44}$ ) and 43 ( $f_{43}$ ) respectively to represent more and less oxygenated contribution to the SOA particle mass.

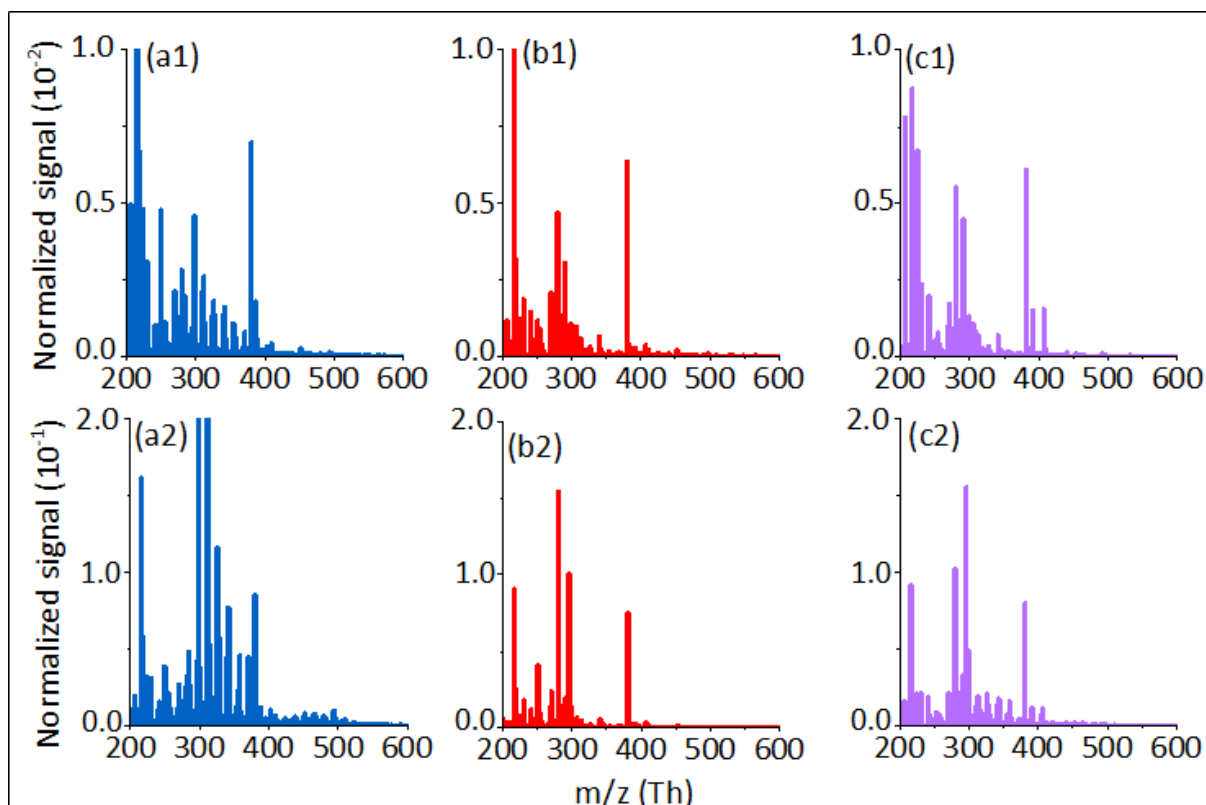


**Figure 7:** Aerosol Mass Spectrometer time series of  $f_{44}$  and  $f_{43}$  in all systems.

With some simplification,  $m/z=44$  is the  $\text{CO}_2^+$  fragment thought to be formed by decarboxylation on the AMS vapouriser and  $m/z=43$  corresponds to the presence of less oxidised components like carbonyls (though with a small contribution from unoxidised alkyl fragment ions that was not subtracted). The full reactivity single VOC  $\alpha$ -pinene experiment has the lowest  $f_{44}$  and highest  $f_{43}$  of all systems. Systems that do not contain  $\alpha$ -pinene can be seen to comprise a persistently higher  $f_{44}$  and lower  $f_{43}$  than all  $\alpha$ -pinene containing systems. This is attributable to a higher contribution of the mass from products of  $\alpha$ -pinene with a lower degree of oxygenation, when it is present in the mixture. However, there is a substantial difference in the fractional contributions of the fragments with a concentration in the single VOC  $\alpha$ -pinene experiments, with higher  $f_{44}$  in the lower concentration experiments forming a lower mass. This

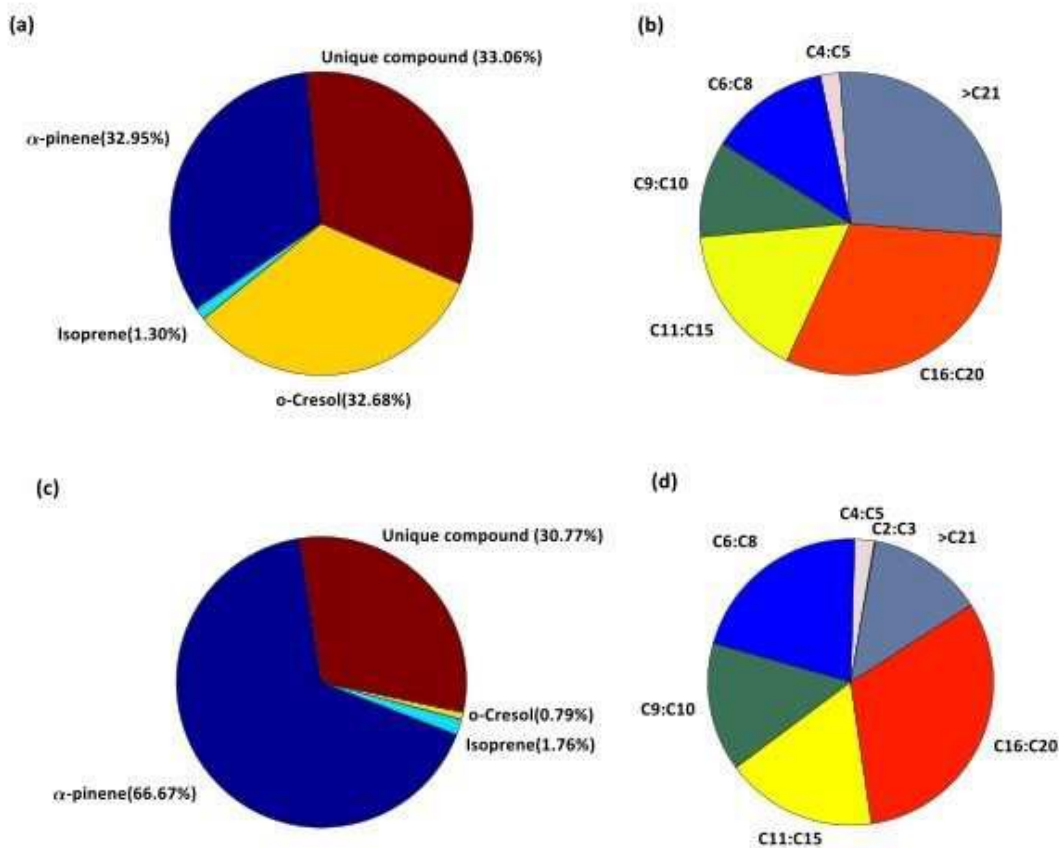
may be partly explained in terms of absorptive partitioning, with lower absorptive mass enabling condensation of only the lower volatility (and more oxidised and higher  $f_{44}$  products). However, such effects would likely be small since the mass reduction is not large. Moreover, the difference between  $f_{44}$  at full and half reactivity might be expected to be smaller than that between half and third reactivity since the mass difference is smaller between the former pair of experiments. However, the reverse is true. The high  $f_{44}$  generated in the *o*-cresol systems and persisting through to high masses later in the experiments is notable and suggests that a high degree of oxygenation is required to enable partitioning of these compounds to the particles (Emanuelsson et al., 2013). Compared with the lower degree of oxygenation required in the  $\alpha$ -pinene systems, it may indicate the requirement for molecules derived from the smaller  $C_7$  precursor to be more oxygenated than those from its  $C_{10}$  counterpart. The attribution of the  $m/z=44$  fragment to di- and polycarboxylic acids are interesting in this context, given the high fractional signal contribution of  $C_7H_7NO_4$  isomers from CIMS and UPLC-Orbitrap MS, see text below and Figure 10. This chemical behaviour has been re-expressed in Figure S6 following the approach first described in Ng et al. (2010). It can be seen that the systems all fall to the right of the delineated triangular area bracketing ambient atmospheric behaviour – a finding frequently observed in many chamber systems (see e.g. Figure 4 in Alfarra et al., 2013). A more thorough analysis of the composition from analysis of the high-resolution AMS data is the subject of a separate manuscript (Shao et al., 2021a, in prep.).

A further illustration of the differences in the chemical trajectories can be provided by the time series of gaseous and particulate components derived from the FIGAERO-I-CIMS instrument. Figure 8 illustrates the changes in particulate mass spectra of single  $\alpha$ -pinene and *o*-cresol experiments and their mixture. These mass spectra have been normalised to the same reagent ion concentration. There is a clear increasing signal in the  $m/z$  range from 200 to 600 (I- adducts) after 5.5-hour reactions in single and mixture systems corresponding to the increase in detected particulate products with the increase in SOA particle mass with time. Additionally, some unique peaks (e.g.,  $m/z$  358, 403, 419, 439, etc) are only detected in the mixture mass spectra. Peak assignment of these mass spectra has been used to attribute signal to the molecular formulae and hence to broad chemical groupings in all single VOC and mixed systems. A full analysis and discussion can be found in Du et al., 2021 (in prep).



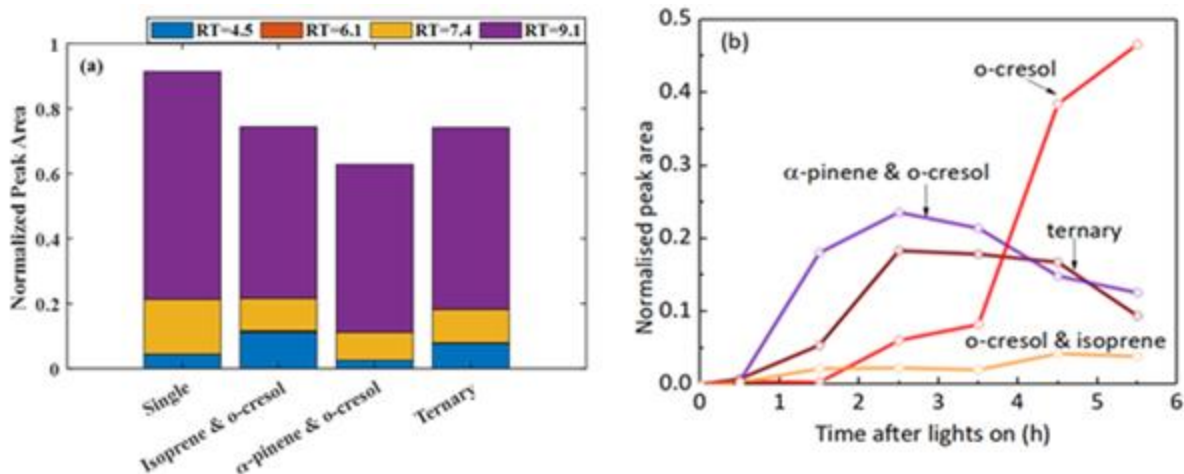
**Figure 8:** FIGAERO-CIMS Mass spectra taken in the single precursor  $\alpha$ -pinene (a1 and a2), *o*-cresol (b1 and b2) and mixed  $\alpha$ -pinene / *o*-cresol system (c1 and c2) at 0.5 hour (a1, b1 and c1) and 5.5 hours (a2,b2 and c2) after the onset of photochemistry in the MAC.

Owing to its separation and accurate mass resolution, the LC-Orbitrap MS analysis of extracts of particles from the filters collected at the end of the experiments provide molecular information to gain insight into interactions in the mixed systems. Figure 9 illustrates the ability to attribute signal in the filter extracts of particles in the ternary *o*-cresol /  $\alpha$ -pinene / isoprene mixture to the individual parent VOC (by matching the attributed formulae to those identified in the individual precursor experiments) and thereby identify molecules found only in the mixture with their associated fractional signal contribution. This is shown for molecules detected in negative, panel a), and positive ionisation mode, c). These “unique-to-mixture” components have been split by contribution to the signal by carbon number in panels b) and d) for negative ion and positive ion mode respectively. These analyses are presented and expanded upon for all mixtures in Shao et al., 2021b (in prep.). Clearly, a substantial fraction of the unique-to-mixture signal is found at carbon number greater than any precursor VOC (in -ve ionisation mode 57% of the signal in 48 individual peaks with  $nC > 10$  and in +ve mode 60% in 115). Whether such components result from gaseous or condensed phase reactions is not accessible from these measurements, but they result from interactions in the mixture.



**Figure 9:** Molecular resolved compounds in the particle phase for the ternary *o*-cresol /  $\alpha$ -pinene / isoprene mixture obtained using UPLC-Orbitrap MS of filter extracts: a) fraction of signal in negative mode, b) fraction of signal by carbon number in the unique-to-mixture compounds, c) fraction of signal in positive mode, d) fraction of signal by carbon number in the unique-to-mixture compounds

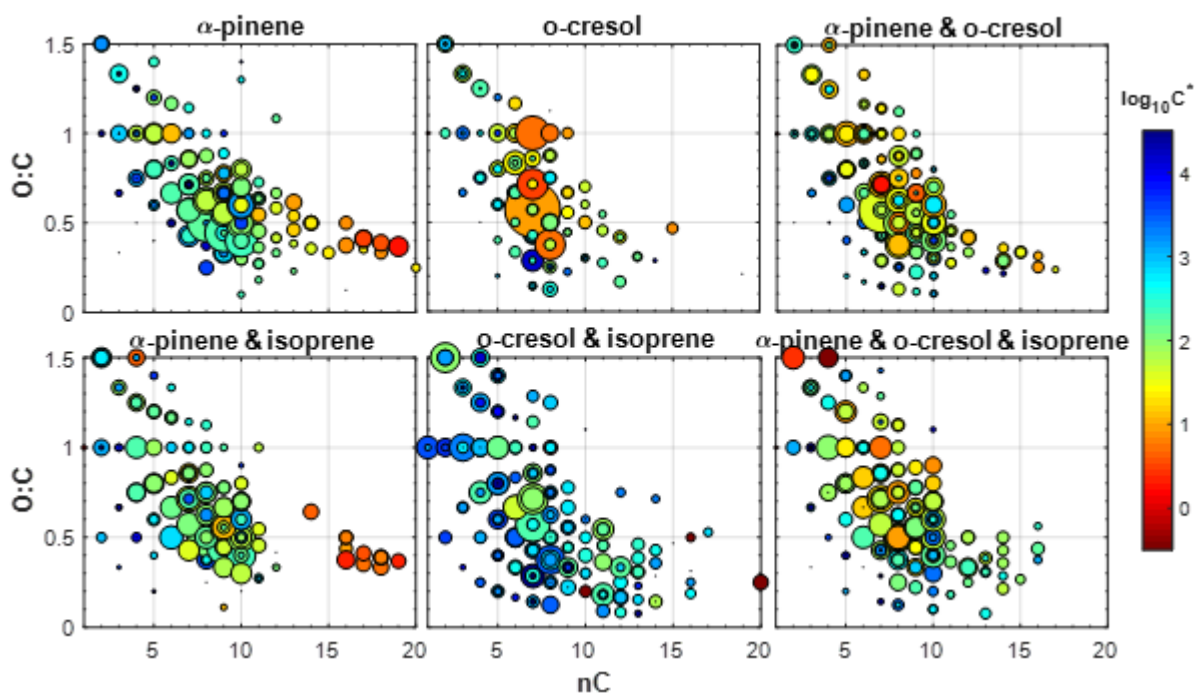
Panel a) in Figure 10 expands on the molecular attribution by LC-Orbitrap MS to demonstrate the ability to separate isomeric contributions to the signal normalised to the total detected signal in single precursor and mixed systems. The example shown is for  $C_7H_7NO_4$  (methyl-nitrocatechol and its isomers) in *o*-cresol containing systems. It can be seen that the isomer at an LC retention time of 9 minutes dominates the signal in all systems, whilst the isomer at a retention time of 6.1 minutes displays negligible signal fractions in all systems. In contrast, the I-CIMS is incapable of separating structural isomers. Panel b) shows the time series of the total signal at  $m/z=296$  (normalised to the total attributed signal) corresponding to the combined signal from all  $C_7H_7NO_4$  isomers in the same systems.



**Figure 10:** a) changes in the isomeric fractions of  $C_7H_7NO_4$  across *o*-cresol containing systems from LC-Orbitrap MS analysis of the filter extracts collected at the end of each experiment; b) time series of particulate  $C_7H_7NO_4$  from FIGAERO-CIMS

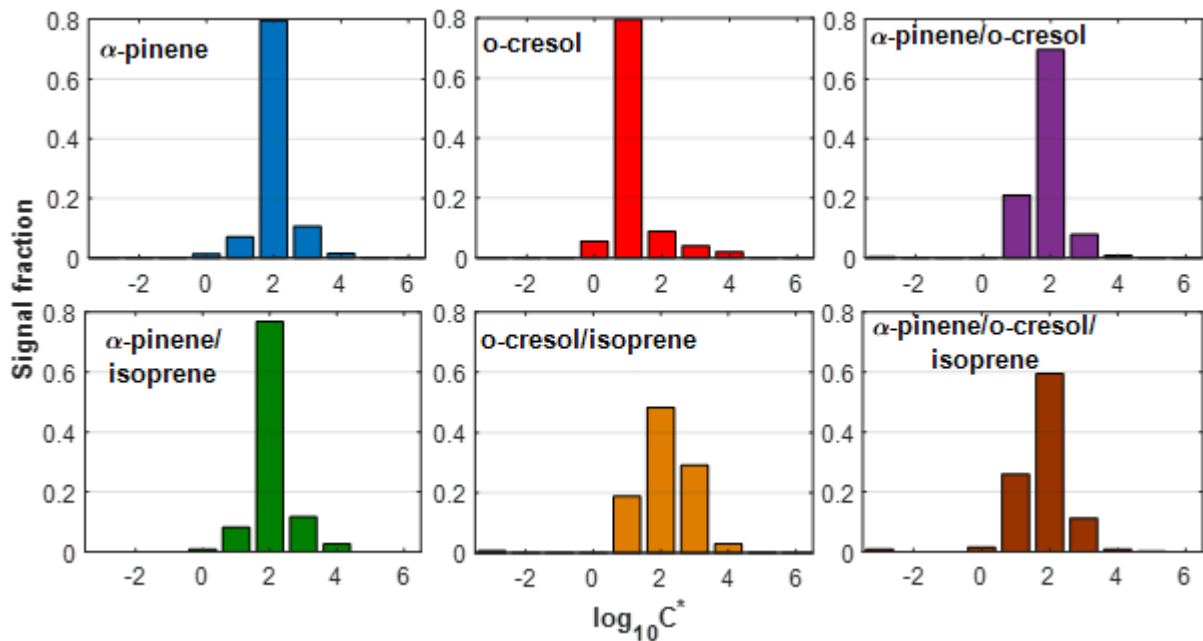
The attribution of elemental composition in the high-resolution FIGAERO-CIMS analysis enables a comprehensive mapping of the particulate oxygen to carbon ratio (O:C) as a function of carbon number, as shown in Figure 11 for each system. It can be seen that the majority of signals in the *o*-cresol single system comprises compounds at the same carbon number,  $C_7$ , as the parent and, on average, with slightly higher O:C ratios than  $C_{10}$ , products dominating the  $\alpha$ -pinene single VOC system. A significant fraction of the signal in all  $\alpha$ -pinene containing systems is found at carbon numbers corresponding to the “dimer” range and these are all found predominantly in the particle phase (showing low volatility). Interestingly, these low volatility products are absent in the mixtures containing  $\alpha$ -pinene and *o*-cresol, suggesting a potential increase of the overall volatility. At the same time, a range of new products appear in mixtures (e.g.  $\alpha$ -pinene / *o*-cresol, *o*-cresol / isoprene) with higher carbon numbers ( $nC=11-16$ ), lower O:C ( $O:C < 0.5$ ) and varying volatility ( $\log_{10}C^* = 1-3$ ), indicating that the molecular interactions influence the overall SOA particle volatility. A more complete discussion of the chemical composition variation across the mixtures in the gas and particle phases can be found in Du et al. (2021, in prep.) and Voliotis et al. (2021b, in prep.).





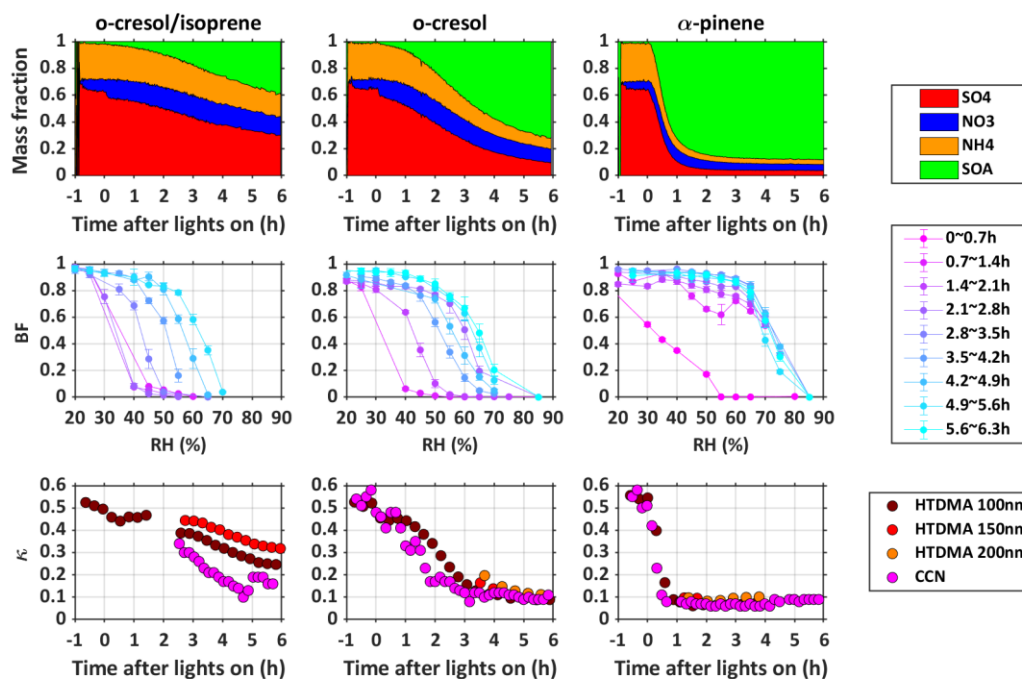
**Figure 11:** Oxygen to carbon ratio (O:C) vs carbon number (nC) of all the products identified by the FIGAERO-I-CIMS in the particle phase at the end of each experiment in characteristic experiments in each system. Dots are sized based on the square root of the contribution of each product to the total signal and coloured according to their effective saturation concentration ( $C^*$ ). The  $C^*$  was calculated using the gas to particle ratio of each ion and absorptive partitioning calculations.

The calculation of the  $C^*$  of all identified formulae by performing partitioning calculations using the gas to particle ratio of the ions (Voliotis et al., 2021a) can be used to assemble the volatility distribution of the products, as shown for the single VOCs, their binary and ternary mixtures in Figure 12. It can be seen that the volatility distributions of particles in the mixture experiments can be similar ( $\alpha$ -pinene / isoprene) or quite different ( $o$ -cresol/isoprene) to those in the experiments using the single precursor. These observations suggest that the effect of mixing precursors can have a varying effect on the resultant particle volatility. A full discussion of the chemical composition and its influence on volatility in all systems can be found in Voliotis et al. (2021b, in prep.)



**Figure 12:** Volatility distributions expressed as effective saturation concentration ( $C^*$ ) in the volatility basis set framework of all the products identified by the FIGAERO-CIMS as a function of the total particle phase signal in example experiments in all systems. The  $C^*$  was calculated using the gas to particle ratio of each ion and absorptive partitioning calculations.

The differences in the evolution of the SOA particle components and the total mass formed directly influences the particle properties as expected. Since the particles are grown on inorganic seeds, the physical properties in all systems are initially dominated by the inorganic components as shown in Figure 13. This shows the relationship between the multicomponent particle composition, the hygroscopic growth factor and the rebound fraction of particles (indicative of their phase state) as the SOA to the inorganic mass fraction of the particles develops in 3 example systems (*o*-cresol / isoprene, *o*-cresol and  $\alpha$ -pinene). The hygroscopicity much more rapidly decreases in systems where organic material is more rapidly formed and the transition to a higher fraction of particles rebounding on a filter at high RH is similarly more rapid. The rate of change of organic to inorganic ratio plays a controlling role in the physical behaviour of the particles. The evolution of both these properties across all systems is discussed in detail in Wang et al. (2021a, b).



**Figure 13:** Top row: AMS chemical composition showing rate of production of SOA and hence rate of increase in organic to inorganic ratio moving from left to right (from *o*-cresol / isoprene to *o*-cresol to  $\alpha$ -pinene); middle row: the corresponding increasingly rapid transition to increased Bounce Fraction (BF) at higher RH; bottom row: the corresponding increasingly rapid reduction in the hygroscopicity parameter,  $k$ .

## 5. Discussion

### 5.1 Experimental conditions and photochemistry

Photolysis of NO<sub>2</sub> under the simulated solar irradiation in the MAC forms O<sub>3</sub> and they rapidly move towards photostationary state with NO. The O<sub>3</sub> is photolysed at wavelengths below 310 nm to yield O(<sup>3</sup>P) and O(<sup>1</sup>D), the latter reacting with available water vapour to form the hydroxyl radical, OH. The O<sub>3</sub> will attack the double bond in unsaturated compounds such as  $\alpha$ -pinene and isoprene, initiating oxidation and yielding secondary OH. The OH will attack all VOCs in the system, either by hydrogen abstraction or OH-addition. Owing to the isoreactivity concept employed in the experiments, the initial VOC destruction rate, and first-generation oxidation product production rate, at a *given* OH concentration will be the same, enabling the opportunity to explore interactions in the mixed systems. However, owing to the indirect method used to produce OH (and hence its production and loss rate and steady-state concentration) the loss rate of each VOC will be different, dependent on the differential reactivity of the VOC towards O<sub>3</sub>, and turnover of products from each will depend on this loss

rate and the reactivity of their oxidation products to the prevailing oxidants. A currently unquantified contribution to the OH concentration will likely be contributed by the release from the walls of HONO, as has been seen in previous studies in Teflon reactors (Rohrer et al., 2005). This is under investigation and will influence the photochemical environment in the MAC, but does not directly change the results reported here.

The control of photochemical conditions in VOC mixtures is challenging. The chemical space is multidimensional and non-linear, and it is unclear how best to define the regime for direct comparison across systems. The approach taken in the current study, to start with concentrations of each VOC isoreactive towards a single oxidant cannot account for the differential reactivity towards the two oxidants, O<sub>3</sub> and OH, present in the system. This is particularly true when the production of oxidants is tightly coupled to the VOC oxidation itself and secondary oxidant production can be at a comparable level to primary production. The combination of oxidants can lead to significantly different VOC decay and hence turnover of oxidants and products. This is an unavoidable feature of VOC mixtures that will occur in the real atmosphere and such differences need to be carefully considered in the interpretation of the results.

It can be seen from Figures 1 and S1 that the time profiles of NO<sub>x</sub> and O<sub>3</sub> vary substantially across the single precursor experiments and the mixtures. This is a characteristic of the method of initiating photochemistry in our experiments, through photolysis of a VOC / NO<sub>x</sub> mixture in the initial absence of O<sub>3</sub>. Within the same single VOC systems, the O<sub>3</sub> concentration temporal profile can vary with VOC concentration at similar VOC/NO<sub>x</sub> values. It is particularly notable in the  $\alpha$ -pinene experiments owing to its reactivity towards O<sub>3</sub>. As expected, there is more ozone production in some systems (notably those containing isoprene). The Leighton ratios shown in Figure S2 indicate a wide variation in the deviation from PSS across the systems, with the high concentration single VOC *o*-cresol experiments and the  $\alpha$ -pinene / *o*-cresol and  $\alpha$ -pinene / isoprene binary mixtures showing the greatest +ve deviation (i.e. greatest ability for RO<sub>2</sub> and HO<sub>2</sub> to compete with O<sub>3</sub> for NO), whereas the single VOC isoprene and  $\alpha$ -pinene, binary isoprene / *o*-cresol and ternary systems all move towards low  $\varphi$ -values.

It was shown in Figure 2 that the turnover of each VOC was different, likely resulting from the differential reactivity of each VOC towards the different oxidants present in the

systems at any one time. However, it can be seen that the turnover of each VOC was comparable across each system (with the notable exceptions of decreased  $\alpha$ -pinene turnover in its binary mixture with *o*-cresol and slightly increased *o*-cresol turnover in the ternary mixture). This may be i) coincidental, ii) indicative that the oxidant regimes remain comparable between experiments or iii) indicative that the turnover is relatively insensitive to the change in oxidant regimes between the mixtures in our experiments. Figures 1 and S1 show the differences in O<sub>3</sub> across systems, so the differences in oxidants are likely to be non-negligible (option ii)). With the turnover to each oxidant in a mixed oxidant system, it should be borne in mind when comparing the results from different studies that results may diverge if the dominant oxidant changes. For example, Figure 6 shows that in the MAC  $\alpha$ -pinene / isoprene experiments, roughly twice as much  $\alpha$ -pinene consumption was due to O<sub>3</sub> reaction as to OH consumption. By contrast, in the experiments in the Julich Plant Aerosol Chamber reported in McFiggans et al. (2019) around 90% of the consumption was estimated to result from OH reaction.

Control of the oxidant regime in chamber experiments is strongly dictated by the goals of the study. It is perhaps most straightforward in a dark system in the absence of NO<sub>x</sub>, where only O<sub>3</sub> is being introduced with a single unsaturated VOC. Even then, the chemical regime can change as the oxidant is consumed and moves from excess to limited. Moreover, the yield of OH from ozonolysis can be non-negligible, such that the VOC consumption from the OH oxidation must be considered. A dark OH source (such as ozonolysis of TME) can be used for oxidation of a saturated VOC to access the OH decay relatively “cleanly”, though the possibility for interaction between the source VOC and SOA precursor derived RO<sub>2</sub> must be remembered. Dark oxidation by continuously injecting NO<sub>3</sub> in the absence of O<sub>3</sub> can also provide a “clean” system with relatively few interfering pathways. NO<sub>3</sub> generated from O<sub>3</sub> reaction with NO<sub>2</sub> starts to become quite complex. The competition between oxidants in establishing the dark consumption of unsaturated VOC will be challenging, though the NO<sub>3</sub> reaction can dominate in systems containing phenolic compounds such as *o*-cresol. In illuminated systems, the oxidant regime becomes complex quite quickly. Photo-oxidation in the absence of NO<sub>x</sub> can access OH consumption of saturated compounds more straightforwardly than for unsaturated VOCs, where ozonolysis (and its associated secondary OH source) must be considered. Photo-oxidation in the presence of NO<sub>x</sub> introduces about as much complexity as can be envisaged. Photo-oxidation of multiple VOCs in the presence of NO<sub>x</sub> multiplies this complexity. The study of McFiggans et al. (2019) avoided many of the

challenges faced in the current study by considering the mixture of biogenic VOCs in the absence of NO<sub>x</sub> and a regime dominated by OH oxidation. This can be considered reasonable since mixtures of these VOCs might exist in the clean troposphere, remote from anthropogenic sources. In studying mixtures of anthropogenic and biogenic VOCs, it might be considered less reasonable since anthropogenic VOCs would seldom exist in the absence of appreciable NO<sub>x</sub>. Related to this, it should also be noted that, whilst maintaining the VOC: NO<sub>x</sub> ratio relatively constant across the systems is desirable, reduced VOC concentrations will lead to reduced NO concentrations. This will inevitably lead to reduced OH concentrations and hence VOC turnover. This is of importance when comparing the single VOC experiments at different concentrations, but less important when considering the initially isoreactive mixtures, since the VOCs have been chosen for their reactivity such that their concentrations are at least comparable magnitude at comparable mixture reactivity.

One feature of chamber experiments using mixtures of VOCs is the ability to exploit their differential reactivity towards the oxidants present in the system to attribute their decay to each of them. This reconciliation of the VOC decay, as shown in Figure 6, is potentially a powerful interpretive tool for diagnosis of the concentration of oxidants in the system and understanding of the turnover of VOCs in the system practice. In our systems when *o*-cresol is present, there are limitations owing to the interference of the direct O<sub>3</sub> measurements owing to absorption of UV by *o*-cresol. However, the reconciliation in these cases can be used to aid validation of the correction based on CIMS measurement of *o*-cresol (see methods section 3). It should be noted any absorption by *o*-cresol oxidation products can still lead to bias in the reconciliation since O<sub>3</sub> will be underestimated. Direct measurement of OH could provide additional confidence in the oxidant field but adequate constraint can be provided by the indirect method described here.

A final consideration relates to the exploratory nature of the current study which aims to establish the suitability of the approach to reveal aspects of SOA formation in mixed VOC atmospheric systems inaccessible to experiments using a single precursor species. The broad suite of analytical techniques employed to investigate these aspects have varying requirements and some compromises have been necessary. Most importantly, the offline filter analyses require a minimum particle mass loading with the corresponding consumption of VOCs with varying yields. This has necessitated the use of initial VOC concentrations above ambient levels. Whilst such concentrations have been commonplace in chamber experiments, they do

introduce limitations. Figure S2 indicates that the deviation from PSS is likely to be significantly affected by the reactions of RO<sub>2</sub> (and/or HO<sub>2</sub>) with NO in some of the binary mixtures. One further important limitation arises from the non-scalability involved with processes that are higher than the first order. Peroxy radical terminations often involve their cross-reaction which will compete with other bimolecular pathways; so, reactions that are second-order in peroxy radical concentration will compete with those that are first order. This will be important in the termination of peroxy radicals formed during autoxidation leading to HOM formation. In particular, the reactions of large HOM-RO<sub>2</sub> with other large peroxy radicals leading to gas-phase formation of accretion products in the “dimer” range may be over-represented at higher concentrations. Under clean ambient conditions, their reaction partners would likely be dominated by HO<sub>2</sub> from CO oxidation or smaller organic peroxy radicals such as CH<sub>3</sub>O<sub>2</sub> from CH<sub>4</sub> oxidation. Under more polluted conditions, the alkoxy pathways from the NO reaction will be competitive or even dominant. Each of these aspects should also be considered when interpreting the interactions in mixed VOC systems.

## 5.2 Yield calculation and reporting

The representation of effectiveness of a VOC to produce SOA particle mass in a given system by its incremental yield is conceptually simple when there is only one VOC being oxidised. Equation (2) can be applied quite straightforwardly, but with consideration of the oxidant regime. There are, however, a number of considerations in the calculation and presentation of yield that should be discussed for single VOC experiments and several more that are of relevance for mixtures.

In Figure 3 we present a summary of the SOA particle mass in the various single VOC systems and their mixtures. It can be seen that the corrections made to account for the losses of particles to the chamber walls are substantial, with peak mass concentrations typically 30 to 40% higher than those measured, and no substantial decay after the peak mass has been formed (as expected). Whilst not without uncertainty, the loss of particles to the walls can be relatively straightforwardly estimated. This is not the case for the interactions of the walls with vapours, which has been the subject of extensive debate (Zhang et al., 2014; Loza et al., 2010; Ye et al., 2016; Krechmer et al., 2020). A full discussion of this subject and characterisation of vapour interaction with the Teflon chamber walls is not provided here (fluxes to and from the chamber walls). We acknowledge that these effects will likely be substantial and that these are

unquantified in our reported SOA particle mass corrections and yields. In the comparisons between different systems in our chamber, it must therefore be noted that we are implicitly assuming the vapour-wall interactions are comparable. This will introduce unquantifiable errors since there will likely be significant vapour pressure differences between products and vapour pressure dependencies of wall interactions. Most importantly, it means that whilst the comparisons may (or may not) be valid across systems in our chamber, our reported yields are very likely not comparable with those in other chambers without further considerations. More broadly, any comparison of yields between chambers should be approached with extreme caution without full confidence that the vapour interactions with the walls of the specific chamber for the specific system have been well quantified.

Single value yields presented in Table 3 calculated at maximum SOA particle mass and maximum VOC consumed can provide useful classifications for comparisons of systems where temporal and mass dependence of yields are comparable. The mass-dependent curves shown in Figures 4 and 5 capture further details of the behaviour throughout the experiments and fitting the “Odum” curves to the single VOC experiments enables the “predictions” of the yields presented in the figures and as single values in Table 4 (as described in results section 4). There are a number of considerations when assessing whether it should be expected that such predictions will be valid. The first of these is the inclusion of the decay of all VOCs in the yield calculation. Whether the consumption of all VOCs in a mixture should be considered in calculating the mixed yield will depend on the question being addressed. It may be inappropriate to consider the consumption of a VOC that would not contribute to the formation of SOA particles when investigating the change in yield of a VOC mixture. In the present study, and consistent with previous work, isoprene was consistently found to generate no measurable SOA particles above the background chamber concentration ( $<1 \mu\text{g m}^{-3}$ ) at any initial isoprene concentration and hence exhibited negligible yield. Therefore, under the conditions of our experiments, when replacing half the reactivity of a higher yield VOC with isoprene in a binary mixture, it may be considered obvious that the SOA particle mass will be reduced. This is the case in the  $\alpha$ -pinene / isoprene and *o*-cresol / isoprene mixtures. Instead, it may be more insightful to consider whether the yield of the  $\alpha$ -pinene and *o*-cresol in the binary mixtures is reduced in the presence of isoprene, using their single VOC system yields as reference. This follows the approach for neutral seeded experiments in McFiggans et al. (2019).



As reported in Table 4 and shown in Figure 5b), the measured binary yield is indeed below that of  $\alpha$ -pinene alone (either including or excluding isoprene in the calculation). For the *o*-cresol / isoprene mixture, the effect is more ambiguous, mainly because the SOA mass had not finished increasing after the experiments, but also because the yields are lower and deviations between the yields more difficult to measure. It should be mentioned that the particle mass yield of isoprene has been measured to be substantial in the presence of acidic seeds (which were not used in our experiments) and cannot be ignored. This raises an interesting question: should there be a threshold below which the reference for mixture yield should exclude a component? A zero SOA yield component such as CO or CH<sub>4</sub> would not be expected to contribute any particle mass in a mixture and would be expected to reduce the overall mixture yield when replacing reactivity of a non-negligible yield SOA precursor. In such cases, and in the case of isoprene with a neutral seed, it appears to make sense to inspect the yield at the consumption of a known SOA precursor regarding that of the precursor for any enhancement or suppression. In mixtures of multiple VOCs with non-negligible individual particle mass yields, it makes sense to compare the particle mass yield of the mixture to the linear combination of the individual precursor's yields at the same VOC consumption.

The “prediction” based on the individual precursor experimental yields is lower than the measurement in the  $\alpha$ -pinene / *o*-cresol binary mixture, possibly indicating enhancement of the mass in the mixed experiment above that which would result from the yields of the individual VOCs. The “predictions” with and without isoprene consumption are comparable to the measurements in the ternary mixture. Without additional composition measurements, this could be interpreted as no interactions taking place, or possibly as the suppression of yield by the presence of isoprene offsetting the enhancement of the mass resulting from the combined oxidation of  $\alpha$ -pinene and *o*-cresol. However, such predictions may be oversimplistic. The oxidation conditions vary significantly across the mixtures (as seen from Figure 1 and S1) and the differences in the chemical trajectories and the time series of the ratios of oxidants between the systems give reason to question the validity of the yield predictions. This is likely to be important in  $\alpha$ -pinene containing systems. Here the particle mass yield from ozonolysis and OH consumption has been reported to differ substantially and Figure 6 shows that about twice as much  $\alpha$ -pinene results from consumption by O<sub>3</sub> as that by OH in the  $\alpha$ -pinene / isoprene system. In the single VOC  $\alpha$ -pinene system, the consumption by each oxidant was found to comprise roughly 50% of the total, based on the assumption that the consumption not

attributable to the measured O<sub>3</sub> was attributable to OH (not shown).

A final consideration when reporting yields relates to the use of seeds as absorptive mass. Conventionally, SOA particle yield curves are plotted against absorptive mass which, in nucleation experiments, is equivalent to the SOA particle mass. In the seeded experiments in the current study, the seeds are used to provide a condensation sink to suppress nucleation, to compete effectively with the walls for condensable vapour and to facilitate measurement by ensuring particles are of a detectable size for composition measurement from early in the experiments. The seeds are nebulised from solution and introduced (and presumably maintained) as metastable aqueous electrolyte solution aerosol at the RH of the experiment. They act as an absorptive mass, since organic mass is observed early in the experiments by AMS (Figure 7 and S5) and they are internally mixed throughout the experiments, as evidenced by HTDMA measurements (shown in Figure 13). Whether the total inorganic mass should be included when interpreting yield data is not clear. Figure S4 depicts the yield behaviour with the inclusion of inorganic seed in the total particle mass, assuming it acts as an effective mass for absorptive partitioning. The added insight provided by such a plot is unclear, though there is a strong argument for dependence on total absorptive mass in the representation of absorptive partitioning even if this is reduced by a factor (analogous to a mass-based activity coefficient to account for non-ideal mixing effects). Note here that inorganic nitrate formation from OH oxidation of NO<sub>2</sub> and subsequent neutralisation of the HNO<sub>3</sub> by available NH<sub>3</sub> leads to the changes in inorganic components throughout the experiments as shown in the top panels of Figure 13. Effects of changing inorganic seed composition could usefully provide the subject of future studies.

### 5.3 Chemical composition

The addition of measurements of particle chemical composition will provide important insights into the development of photo-oxidation in mixtures and the resulting particle yields. Online measurements by AMS in Figures 7 and S5 indicate that single VOC *o*-cresol and its binary mixture with isoprene rapidly exhibit, and then maintain through to significant particle mass production, a higher degree of oxygenation than the other systems as represented by the  $f_{44}$ . This contrasts sharply with the lower  $f_{44}$  of all  $\alpha$ -pinene-containing systems. Since  $\alpha$ -pinene frequently dominates the mass owing to its high yield, this may offset any *o*-cresol-derived high  $f_{44}$  in systems containing both  $\alpha$ -pinene and *o*-cresol. Clearly a less coarse diagnostic of

composition is required to interrogate the reasons for the observed differences, though Shao et al. (2021a) provide more insight from the high-resolution AMS analyses.

The FIGAERO-CIMS data shown in Figure 8 indicate the sorts of analytical products that can aid this interpretation. Whilst the additional analyses presented in Du et al. (2021) can more fully explore the impacts of the mixing of SOA precursors, several features can be directly observed from the mass spectra. First, there is an evident increase in the contribution of higher mass ions with time in the  $\alpha$ -pinene single VOC system that is not observed in either the *o*-cresol single VOC system or their binary mixture. Second, there is clear evidence for signal contributions from components in the mixture that are not present in the individual systems from the beginning of the experiment. This is expanded upon in Figure 9, which shows that much of the signal in analyses of the filters taken at the end of the ternary mixture is not found at masses corresponding to those found in individual component VOC oxidation. Such high-resolution analyses are required to unambiguously identify the specific products resulting from interactions in the system and to postulate mechanisms leading to their formation. It is not yet possible to state whether the “unique-to-mixture” molecules are formed by gas-phase cross-reaction, condensed phase accretion in the particles or on the filter. Neither is it currently possible to unambiguously state that this signal corresponds to the same fraction of the mass, owing to potential differential sensitivity. These aspects are discussed in detail in Shao et al. (2021b). Nonetheless, it can be stated that these compounds are only found in the mixed system. An important challenge with such identification and attributions is the requirement for substantial sampled mass. This may provide a lower limit to the yield and/or initial concentration of precursors that can be studied in this way.

Nevertheless, the power of such analyses is further exploited in separating the isomeric contributions to particle components as shown in Figure 10a). Combining the power of offline and online analyses, this separation of  $C_7H_7NO_4$  isomers in all *o*-cresol-containing systems may be used to interpret the significant differences in the time trends of  $C_7H_7NO_4$  shown in the FIGAERO-CIMS data in Figure 10b). Whilst this may be indicative of mechanistic differences, there will be confounding differences in the rate of SOA particle mass formation between the systems (and hence abundance of absorptive mass) in addition to potential differences in the sensitivity in the different systems and total signal used for the normalisation because of the different FIGAERO filter loadings. These considerations are discussed in detail in Du et al.

(2021) for all systems. Nonetheless, the differences in the fractional isomeric contributions and in the time series reveal substantial changes in the  $C_7H_7NO_4$  contributions between the systems.

#### 5.4 Properties: volatility, water uptake and phase

Figure 11 exploits the high-resolution analysis of the FIGAERO-CIMS data to present the changes in the O:C ratio of detected particle compounds as a function of their carbon number in all systems at the end of the experiments. Combining this with the ratio of the signal in the particle and gas samples is used to indicate likely influences of the mixing of precursors on particle volatility. Whilst there are uncertainties associated with the partitioning, and hence volatility derivations it is evident that changes in the components present in mixtures can lead to change in the volatility and potentially yield, reported in detail in Voliotis et al. (2021a, b). This is extended in Figure 12, which re-expresses the FIGAERO-CIMS data as volatility distributions, further highlighting the differences between the particle volatility in the mixture and that in the single VOC systems. This is complex but is broadly consistent with the observed yield behaviour for most systems. For example, the SOA particle volatility in the single  $\alpha$ -pinene experiment at half reactivity is fairly similar to that measured in the binary system with isoprene, consistent with their comparable yields. Similarly, the measured volatility in the  $\alpha$ -pinene and *o*-cresol binary and the ternary systems appear to be roughly between those obtained in the single precursor experiments, in line with the measured yields that were found to be higher than those in single *o*-cresol but equal or lower than those obtained in the single  $\alpha$ -pinene experiments. Substantial apparent inconsistencies were found in the *o*-cresol and isoprene binary system, where the measured volatility appeared to be substantially higher than that in the single *o*-cresol system, whilst the SOA yields were somewhat comparable. The reason is unclear and additional investigation might focus on the reconciliation of the discrepancies between the volatility and yield behaviour in this system.

Figure 13 shows the behaviour of particle water uptake and the rebound fraction of particles in an impactor in three example systems. These have been chosen for their differences in the rate of formation of SOA particle mass and, in our seeded experiments, the associated organic: inorganic particle mass ratio. The rate of decrease of particle hygroscopicity and increase of rebound fraction at higher RH follows the rate of SOA particle mass increase in the system. This is a clear indication of the influence of the mixing of precursors on the change in particle properties through the change in the rate of formation of condensable material (as

explored in (Wang et al., 2021; Wang et al., 2022). As shown in Figure 2 of Wang et. al (2022), size-resolved chemical composition was observed in all VOC systems, where the smaller particles have a higher size-resolved organic mass fraction ( $MR_{SOA/PM}$ ). To avoid the influences of composition differences on the reconciliation study of sub- and super-saturated water uptake, the synchronized HTDMA and CCN data pairs with a comparable chemical composition were selected according to the size-resolved chemical composition (Wang et al., 2022). Nevertheless, it shows a discrepancy between  $\kappa_{HTDMA}$  and  $\kappa_{CCN}$  varied with the  $MR_{SOA/PM}$  in the process of reconciliation, which is likely caused by the different instrumental differences or the non-ideality of organic-inorganic solutes. It needs further investigation.

## 5.5 Further work

Whilst it is important to explore mixtures including multiple SOA particle precursors under controlled conditions to understand behaviour in the real atmosphere, and measurements in such mixtures can reveal features inaccessible to single VOC experiment, the experimental design will determine their usefulness. Alternative and supplementary methodologies may allow more direct resolution of outstanding questions related to precursor mixing. The effects of mixed and variable oxidant concentrations throughout chamber experiments are both problematic and insightful. Secondary production of oxidants (both OH and ozone) may differentially influence the decay of VOCs in the mixture and it may not be possible to scavenge secondary oxidants, certainly without influencing the oxidation product distribution. In any case, secondary oxidant formation will occur in the real atmosphere and cannot be overlooked. More control over the primary oxidants may be achieved through the use of “cleaner” sources, such as the photolysis of  $H_2O_2$ .

Care is required in the interpretation of condensed phase composition under the high peroxide concentrations required in such experiments, but the avoidance of  $O_3$  from injection or  $NO_2$  photolysis may be advantageous. Nevertheless, secondary  $O_3$  will react with any unsaturated compounds present. Selection of VOCs with low OH yields from ozonolysis may allow isolation of its pathways but will limit the choice of mixtures. Augmentation of broadband illumination with discrete intense light sources such as in the JPAC chamber in the McFiggans et al. (2019) study may push up the OH:  $O_3$  ratio such that the OH channels dominate, though care is necessary to avoid excessively high OH concentrations. Unless conducted at very low  $NO_x$  concentrations, significant VOC consumption in batch mode

chamber experiments will lead to variable VOC: NO<sub>x</sub> ratios. This will lead to a variable production rate of ozone as well as changes in the relative importance of the NO-mediated alkoxy radical pathways. Mechanistic interpretation of such experiments must account for these changes. In any case, isolation of individual mechanistic pathways and probing details of kinetics and product yields may be more suited to more targeted laboratory studies than to chamber experiments. If it is not possible to control the oxidising environment across complex mixtures, then systematic exploration of mixtures with direct and more comprehensive oxidant and peroxy radical measurements would be of benefit. Such well-instrumented studies will be able to take full advantage of the trajectories through chemical space afforded by relatively long batch mode chamber experiments.

Movement towards more atmospherically representative chemical regimes would benefit from lower VOC concentration experiments. However, moving towards a more realistic radical termination regime would present detection limit challenges to composition measurements. More comprehensive coverage of speciated VOC and OVOC measurements using modern online mass spectrometry methods and improved resolution of such temporally resolved instruments may avoid the need to combine online and offline techniques. Whilst they reveal important impacts of the temporal changes in VOC mixtures, the batch reactor experiments in the present study are complex. The use of well-mixed flow reactor experiments to look at multiple steady states can enable the focus of batch reactor experiments on sensitive areas of the chemical regime. The range of potential mixtures is not finite and so there is a need to focus on targeted areas of importance. It is not immediately obvious how this should be done, though it should be remembered that oxidation and SOA formation will occur during both day and night and mixed night-time oxidation by NO<sub>3</sub> should not be forgotten.

## **6. Conclusions**

A comprehensive suite of instrumentation was deployed to investigate the formation of SOA particulate mass on inorganic seeds in chamber photo-oxidation of anthropogenic (*o*-cresol) and biogenic ( $\alpha$ -pinene and isoprene) VOCs and their binary and ternary mixtures in the presence of NO<sub>x</sub>. Whilst compromises were necessary for the experimental design and the complexity of the systems introduced substantial challenges to their interpretation, several important observations were possible.

First, the photochemical trajectory is understandably system dependent and the rates of

consumption of each VOC by each oxidant are consequently variable.

Second, the yield concept typically used for an individual VOC requires careful consideration when adapting it for use with complex mixtures. To account for the dependence of condensed mass on available adsorptive mass, it will be necessary to use the individual component yield at the same mass as in the mixtures. However, in order to compare the mass formed at the same VOC consumption, it is necessary to reference this to the corresponding single precursor experiment at that same VOC consumption and therefore not that calculated at the same adsorptive mass.

In mixtures where the majority of the mass is contributed by only one component precursor, it is possible to identify the existence of and quantify, any interactions in terms of SOA mass or yield. Thus, as shown in Figure 5 there is a clear indication of suppression of the yield of  $\alpha$ -pinene in its mixture with isoprene, but as with the *o*-cresol / isoprene mixture, there is a possible indication of enhancement, though this is too small to be unambiguous.

It is straightforward to make a comparison between the predicted and measured yield in mixtures of precursors both with appreciable yield. It is straightforward to make a comparison between the measured yield of single components with their yield in a mixture with a precursor of zero yields. Where two components with appreciable yield are mixed with another VOC with no yield the reference point for the comparison is complex.

The mixed  $\alpha$ -pinene / *o*-cresol system is measured to have enhanced yield above that expected from the additivity of the individual VOC yield at the same consumption. In such mixtures, where there is a significant contribution to the SOA mass from more than one component precursor, we are unable to unambiguously attribute any discrepancies in predicted and measured mass to physical or chemical interactions. This is because yield and partitioned mass will depend both on available adsorptive mass and upon the rate of consumption of individual VOC and production of condensable oxidation products. In the ternary system, the measured yield is comparable to that calculated from the additivity of the component yields. It is unclear whether this is attributable to cancelling of suppression and enhancement effects, but chemical interactions are evident from the unique-to mixture components.

The trajectories of physical properties such as water uptake and phase behaviour of the particles will depend on the rates of formation of SOA particle mass, so changes in these rates

in mixtures will control changes in particle physical properties.

Mixing experiments are crucial and highly beneficial for our understanding of atmospheric chemical interactions. However, the interpretation quickly becomes complex and both the experimental design and evaluation need to be scrutinised carefully. Here, advanced online and offline compositional measurements can reveal substantial additional information to aid in the interpretation of yield data, including components uniquely found in mixtures and physicochemical property changes in the SOA formed from mixtures of VOCs.

### **Acknowledgements**

The Manchester Aerosol Chamber received funding from the European Union's Horizon 2020 research and innovation programme under grant agreement no. 730997, which supports the EUROCHAMP2020 research programme. AV and MD acknowledge the Presidents Doctoral Scholarship from the University of Manchester and AV, the support from the Natural Environment Research Council (NERC) EAO Doctoral Training Partnership (grant no. NE/L002469/1). YW acknowledges CSC scholarship support. MRA acknowledges funding support from the Natural Environment Research Council (NERC) through the UK National Centre for Atmospheric Science (NCAS). Instrumentational support was funded through the NERC Atmospheric Measurement and Observational Facility (AMOF). We acknowledge Dr. Zhijun Wu from Peking University, China, for providing Bounce behaviour instrument through Trans-National Access (TNA) of EUROCHAMP-2020. MH and TFM acknowledge the strategic research area MERGE, the Swedish Research Council (grant number 2018-04430), the Formas (grant number 2019-586). TFM acknowledges the support from the EU Project FORCeS (grant agreement no. 821205).

### **Competing interests**

The authors declare that they have no conflict of interest

### **Author contributions**

GM, MRA, MH, TFM AV, YW, YS and MD conceived the study. AV, YW, YS and MD conducted the experiments and data analysis. TJB, DH and KP provided on-site support with the instrument deployment and data analysis procedures. JFH provided scientific advice. GM, AV, YW, YS and MD wrote the manuscript with inputs from all co-authors.



## Data Availability

All the data used in this study are available upon request from the corresponding author(s).

## References

Alfarra, M. R., Hamilton, J. F., Wyche, K. P., Good, N., Ward, M. W., Carr, T., Barley, M. H., Monks, P. S., Jenkin, M. E., Lewis, A. C., and McFiggans, G. B.: The effect of photochemical ageing and initial precursor concentration on the composition and hygroscopic properties of  $\beta$ -caryophyllene secondary organic aerosol, *Atmos. Chem. Phys.*, 12, 6417-6436, 10.5194/acp-12-6417-2012, 2012.

Alfarra, M. R., Good, N., Wyche, K. P., Hamilton, J. F., Monks, P. S., Lewis, A. C., and McFiggans, G.: Water uptake is independent of the inferred composition of secondary aerosols derived from multiple biogenic VOCs, *Atmos. Chem. Phys.*, 13, 11769-11789, 10.5194/acp-13-11769-2013, 2013.

Atkinson, R., Baulch, D. L., Cox, R. A., Crowley, J. N., Hampson, R. F., Hynes, R. G., Jenkin, M. E., Rossi, M. J., Troe, J., and Subcommittee, I.: Evaluated kinetic and photochemical data for atmospheric chemistry: Volume II &ndash; gas phase reactions of organic species, *Atmos. Chem. Phys.*, 6, 3625-4055, 10.5194/acp-6-3625-2006, 2006.

Aumont, B., Szopa, S., and Madronich, S.: Modelling the evolution of organic carbon during its gas-phase tropospheric oxidation: development of an explicit model based on a self generating approach, *Atmos. Chem. Phys.*, 5, 2497-2517, 10.5194/acp-5-2497-2005, 2005.

Bannan, T. J., Le Breton, M., Priestley, M., Worrall, S. D., Bacak, A., Marsden, N. A., Mehra, A., Hammes, J., Hallquist, M., Alfarra, M. R., Krieger, U. K., Reid, J. P., Jayne, J., Robinson, W., McFiggans, G., Coe, H., Percival, C. J., and Topping, D.: A method for extracting calibrated volatility information from the FIGAERO-HR-ToF-CIMS and its experimental application, *Atmos Meas Tech*, 12, 1429-1439, 10.5194/amt-12-1429-2019, 2019.

Berndt, T., Richters, S., Jokinen, T., Hyttinen, N., Kurtén, T., Otkjær, R. V., Kjaergaard, H. G., Stratmann, F., Herrmann, H., Sipilä, M., Kulmala, M., and Ehn, M.: Hydroxyl radical-induced formation of highly oxidized organic compounds, *Nature Communications*, 7, 13677, 10.1038/ncomms13677, 2016.

Berndt, T., Mentler, B., Scholz, W., Fischer, L., Herrmann, H., Kulmala, M., and Hansel, A.: Accretion Product Formation from Ozonolysis and OH Radical Reaction of  $\alpha$ -Pinene: Mechanistic Insight and the Influence of Isoprene and Ethylene, *Environmental Science & Technology*, 52, 11069-11077, 10.1021/acs.est.8b02210, 2018.

Bianchi, F., Kurten, T., Riva, M., Mohr, C., Rissanen, M. P., Roldin, P., Berndt, T., Crouse, J. D., Wennberg, P. O., Mentel, T. F., Wildt, J., Junninen, H., Jokinen, T., Kulmala, M., Worsnop, D. R., Thornton, J. A., Donahue, N., Kjaergaard, H. G., and Ehn, M.: Highly Oxygenated Organic Molecules (HOM) from Gas-Phase Autoxidation Involving Peroxy Radicals: A Key Contributor to Atmospheric Aerosol, *Chem Rev*, 119, 3472-3509, 10.1021/acs.chemrev.8b00395, 2019.

Carlton, A. G., Wiedinmyer, C., and Kroll, J. H.: A review of Secondary Organic Aerosol (SOA) formation from isoprene, *Atmos. Chem. Phys.*, 9, 4987-5005, 10.5194/acp-9-4987-2009, 2009.

- Cash, J. M., Heal, M. R., Langford, B., and Drewer, J.: A review of stereochemical implications in the generation of secondary organic aerosol from isoprene oxidation, *Environmental Science: Processes & Impacts*, 18, 1369-1380, 10.1039/C6EM00354K, 2016.
- Charan, S. M., Huang, Y., and Seinfeld, J. H.: Computational Simulation of Secondary Organic Aerosol Formation in Laboratory Chambers, *Chem Rev*, 119, 11912-11944, 10.1021/acs.chemrev.9b00358, 2019.
- Cohen, A. J., Brauer, M., Burnett, R., Anderson, H. R., Frostad, J., Estep, K., Balakrishnan, K., Brunekreef, B., Dandona, L., Dandona, R., Feigin, V., Freedman, G., Hubbell, B., Jobling, A., Kan, H., Knibbs, L., Liu, Y., Martin, R., Morawska, L., Pope, C. A., III, Shin, H., Straif, K., Shaddick, G., Thomas, M., van Dingenen, R., van Donkelaar, A., Vos, T., Murray, C. J. L., and Forouzanfar, M. H.: Estimates and 25-year trends of the global burden of disease attributable to ambient air pollution: an analysis of data from the Global Burden of Diseases Study 2015, *The Lancet*, 389, 1907-1918, 10.1016/S0140-6736(17)30505-6, 2017.
- Cox, R. A., Ammann, M., Crowley, J. N., Herrmann, H., Jenkin, M. E., McNeill, V. F., Mellouki, A., Troe, J., and Wallington, T. J.: Evaluated kinetic and photochemical data for atmospheric chemistry: Volume VII – Criegee intermediates, *Atmos. Chem. Phys.*, 20, 13497–13519, <https://doi.org/10.5194/acp-20-13497-2020>, 2020
- Crouse, J. D., Nielsen, L. B., Jørgensen, S., Kjaergaard, H. G., and Wennberg, P. O.: Autoxidation of Organic Compounds in the Atmosphere, *The Journal of Physical Chemistry Letters*, 4, 3513-3520, 10.1021/jz4019207, 2013.
- Donahue, N. M., Robinson, A. L., Stanier, C. O., and Pandis, S. N.: Coupled partitioning, dilution, and chemical aging of semivolatile organics, *Environmental Science & Technology*, 40, 2635-2643, 2006.
- Donahue, N. M., Epstein, S. A., Pandis, S. N., and Robinson, A. L.: A two-dimensional volatility basis set: 1. organic-aerosol mixing thermodynamics, *Atmos. Chem. Phys.*, 11, 3303-3318, 10.5194/acp-11-3303-2011, 2011.
- Donahue, N. M., Henry, K. M., Mentel, T. F., Kiendler-Scharr, A., Spindler, C., Bohn, B., Brauers, T., Dorn, H. P., Fuchs, H., Tillmann, R., Wahner, A., Saathoff, H., Naumann, K.-H., Möhler, O., Leisner, T., Müller, L., Reinnig, M.-C., Hoffmann, T., Salo, K., Hallquist, M., Frosch, M., Bilde, M., Tritscher, T., Barmet, P., Praplan, A. P., DeCarlo, P. F., Dommen, J., Prévôt, A. S. H., and Baltensperger, U.: Aging of biogenic secondary organic aerosol via gas-phase OH radical reactions, 109, 13503-13508, 10.1073/pnas.1115186109 %J Proceedings of the National Academy of Sciences, 2012.
- Du, M., Voliotis, A., Shao, Y., Wang, Y., Bannan, T. J., Pereira, K., Hamilton J. F., Percival C. J., Alfarra, M. R., McFiggans, G.: Combined application of on-line FIGAERO-CIMS and off-line Orbitrap LC-MS to characterize the chemical composition of SOA in smog chamber studies. In preparation for *Atmos. Chem. Phys. Discuss.*, 2021a
- Ehn, M., Kleist, E., Junninen, H., Petäjä, T., Lönn, G., Schobesberger, S., Dal Maso, M., Trimborn, A., Kulmala, M., Worsnop, D. R., Wahner, A., Wildt, J., and Mentel, T. F.: Gas phase formation of extremely oxidized pinene reaction products in chamber and ambient air, *Atmos. Chem. Phys.*, 12, 5113-5127, 10.5194/acp-12-5113-2012, 2012.
- Ehn, M., Thornton, J. A., Kleist, E., Sipilä, M., Junninen, H., Pullinen, I., Springer, M., Rubach, F., Tillmann, R., Lee, B., Lopez-Hilfiker, F., Andres, S., Acir, I.-H., Rissanen, M., Jokinen, T., Schobesberger, S., Kangasluoma, J., Kontkanen, J., Nieminen, T., Kurtén, T., Nielsen, L. B.,

Jørgensen, S., Kjaergaard, H. G., Canagaratna, M., Maso, M. D., Berndt, T., Petäjä, T., Wahner, A., Kerminen, V.-M., Kulmala, M., Worsnop, D. R., Wildt, J., and Mentel, T. F.: A large source of low-volatility secondary organic aerosol, *Nature*, 506, 476-479, 10.1038/nature13032, 2014.

Emanuelsson, E. U., Hallquist, M., Kristensen, K., Glasius, M., Bohn, B., Fuchs, H., Kammer, B., Kiendler-Scharr, A., Nehr, S., Rubach, F., Tillmann, R., Wahner, A., Wu, H. C., and Mentel, T. F.: Formation of anthropogenic secondary organic aerosol (SOA) and its influence on biogenic SOA properties, *Atmos. Chem. Phys.*, 13, 2837-2855, 10.5194/acp-13-2837-2013, 2013.

Garmash, O., Rissanen, M. P., Pullinen, I., Schmitt, S., Kausiala, O., Tillmann, R., Zhao, D., Percival, C., Bannan, T. J., Priestley, M., Hallquist, Å. M., Kleist, E., Kiendler-Scharr, A., Hallquist, M., Berndt, T., McFiggans, G., Wildt, J., Mentel, T. F., and Ehn, M.: Multi-generation OH oxidation as a source for highly oxygenated organic molecules from aromatics, *Atmos. Chem. Phys.*, 20, 515-537, 10.5194/acp-20-515-2020, 2020.

Goldstein, A. H., and Galbally, I. E.: Known and unexplored organic constituents in the earth's atmosphere, *Environmental Science & Technology*, 41, 1514-1521, 2007.

Good, N., Coe, H., and McFiggans, G.: Instrumentational operation and analytical methodology for the reconciliation of aerosol water uptake under sub- and supersaturated conditions, *Atmos. Meas. Tech.*, 3, 1241-1254, 10.5194/amt-3-1241-2010, 2010.

Hallquist, M., Wenger, J. C., Baltensperger, U., Rudich, Y., Simpson, D., Claeys, M., Dommen, J., Donahue, N. M., George, C., Goldstein, A. H., Hamilton, J. F., Herrmann, H., Hoffmann, T., Iinuma, Y., Jang, M., Jenkin, M. E., Jimenez, J. L., Kiendler-Scharr, A., Maenhaut, W., McFiggans, G., Mentel, T. F., Monod, A., Prévôt, A. S. H., Seinfeld, J. H., Surratt, J. D., Szmigielski, R., and Wildt, J.: The formation, properties and impact of secondary organic aerosol: current and emerging issues, *Atmos. Chem. Phys.*, 9, 5155-5236, 10.5194/acp-9-5155-2009, 2009.

Hamilton, J. F., Alfarra, M. R., Wyche, K. P., Ward, M. W., Lewis, A. C., McFiggans, G. B., Good, N., Monks, P. S., Carr, T., White, I. R., and Purvis, R. M.: Investigating the use of secondary organic aerosol as seed particles in simulation chamber experiments, *Atmospheric Chemistry and Physics*, 11, 5917-5929, 10.5194/acp-11-5917-2011, 2011.

Hao, L. Q., Yli-Pirilä, P., Tiitta, P., Romakkaniemi, S., Vaattovaara, P., Kajos, M. K., Rinne, J., Heijari, J., Kortelainen, A., Miettinen, P., Kroll, J. H., Holopainen, J. K., Smith, J. N., Joutsensaari, J., Kulmala, M., Worsnop, D. R., and Laaksonen, A.: New particle formation from the oxidation of direct emissions of pine seedlings, *Atmos. Chem. Phys.*, 9, 8121-8137, 10.5194/acp-9-8121-2009, 2009.

IPCC: Climate Change 2013: The Physical Science Basis. Contribution of Working Group I to the Fifth Assessment Report of the Intergovernmental Panel on Climate Change, Cambridge University Press, Cambridge, United Kingdom and New York, NY, USA, 1535 pp., 2013.

IPCC: Global Warming of 1.5°C

IPCC, 2018: Summary for Policymakers. In: Global warming of 1.5°C. An IPCC Special Report on the impacts of global warming of 1.5°C above pre-industrial levels and related global greenhouse gas emission pathways, in the context of strengthening the global response to the threat of climate change, sustainable development, and efforts to eradicate poverty, World Meteorological Organization, 2018.

Jaoui, M., and Kamens, R. M.: Gaseous and Particulate Oxidation Products Analysis of a

Mixture of  $\alpha$ -pinene +  $\beta$ -pinene/O<sub>3</sub>/Air in the Absence of Light and  $\alpha$ -pinene +  $\beta$ -pinene/NO<sub>x</sub>/Air in the Presence of Natural Sunlight, *Journal of Atmospheric Chemistry*, 44, 259-297, 10.1023/A:1022977427523, 2003.

Jenkin, M. E., Wyche, K. P., Evans, C. J., Carr, T., Monks, P. S., Alfarra, M. R., Barley, M. H., McFiggans, G. B., Young, J. C., and Rickard, A. R.: Development and chamber evaluation of the MCM v3.2 degradation scheme for  $\beta$ -caryophyllene, *Atmos. Chem. Phys.*, 12, 5275-5308, 10.5194/acp-12-5275-2012, 2012.

Jokinen, T., Berndt, T., Makkonen, R., Kerminen, V.-M., Junninen, H., Paasonen, P., Stratmann, F., Herrmann, H., Guenther, A. B., Worsnop, D. R., Kulmala, M., Ehn, M., and Sipilä, M.: Production of extremely low volatile organic compounds from biogenic emissions: Measured yields and atmospheric implications, 112, 7123-7128, 10.1073/pnas.1423977112 %J Proceedings of the National Academy of Sciences, 2015.

Joutsensaari, J., Loivamäki, M., Vuorinen, T., Miettinen, P., Nerg, A. M., Holopainen, J. K., and Laaksonen, A.: Nanoparticle formation by ozonolysis of inducible plant volatiles, *Atmos. Chem. Phys.*, 5, 1489-1495, 10.5194/acp-5-1489-2005, 2005.

Kaltsonoudis, C., Kostenidou, E., Louvaris, E., Psychoudaki, M., Tsiligiannis, E., Florou, K., Liangou, A., and Pandis, S. N.: Characterization of fresh and aged organic aerosol emissions from meat charbroiling, *Atmos. Chem. Phys.*, 17, 7143-7155, 10.5194/acp-17-7143-2017, 2017.

Kanakidou, M., Seinfeld, J. H., Pandis, S. N., Barnes, I., Dentener, F. J., Facchini, M. C., Van Dingenen, R., Ervens, B., Nenes, A., Nielsen, C. J., Swietlicki, E., Putaud, J. P., Balkanski, Y., Fuzzi, S., Horth, J., Moortgat, G. K., Winterhalter, R., Myhre, C. E. L., Tsigaridis, K., Vignati, E., Stephanou, E. G., and Wilson, J.: Organic aerosol and global climate modelling: a review, *Atmos. Chem. Phys.*, 5, 1053-1123, 10.5194/acp-5-1053-2005, 2005.

Kiendler-Scharr, A., Wildt, J., Maso, M. D., Hohaus, T., Kleist, E., Mentel, T. F., Tillmann, R., Uerlings, R., Schurr, U., and Wahner, A.: New particle formation in forests inhibited by isoprene emissions, *Nature*, 461, 381-384, 10.1038/nature08292, 2009.

Krechmer, J. E., Day, D. A., and Jimenez, J. L.: Always Lost but Never Forgotten: Gas-Phase Wall Losses Are Important in All Teflon Environmental Chambers, *Environmental Science & Technology*, 54, 12890-12897, 10.1021/acs.est.0c03381, 2020.

Leighton, P. A.: Photochemistry of air pollution, 9, *Phys. Chem.*, 300 pp., 1961.

Liu, Y., Wu, Z., Wang, Y., Xiao, Y., Gu, F., Zheng, J., Tan, T., Shang, D., Wu, Y., Zeng, L., Hu, M., Bateman, A. P., and Martin, S. T.: Submicrometer Particles Are in the Liquid State during Heavy Haze Episodes in the Urban Atmosphere of Beijing, China, *Environ Sci Tech Lett*, 4, 427-432, 10.1021/acs.estlett.7b00352, 2017.

Loza, C. L., Chan, A. W. H., Galloway, M. M., Keutsch, F. N., Flagan, R. C., and Seinfeld, J. H.: Characterization of Vapor Wall Loss in Laboratory Chambers, *Environmental Science & Technology*, 44, 5074-5078, 10.1021/es100727v, 2010.

McFiggans, G., Coe, H., Burgess, R., Allan, J., Cubison, M., Alfarra, M. R., Saunders, R., Saiz-Lopez, A., Plane, J. M. C., Wevill, D., Carpenter, L., Rickard, A. R., and Monks, P. S.: Direct evidence for coastal iodine particles from *Laminaria* macroalgae – linkage to emissions of molecular iodine, *Atmos. Chem. Phys.*, 4, 701-713, 10.5194/acp-4-701-2004, 2004.

McFiggans, G., Mentel, T. F., Wildt, J., Pullinen, I., Kang, S., Kleist, E., Schmitt, S., Springer,

- M., Tillmann, R., Wu, C., Zhao, D., Hallquist, M., Faxon, C., Le Breton, M., Hallquist, A. M., Simpson, D., Bergstrom, R., Jenkin, M. E., Ehn, M., Thornton, J. A., Alfarra, M. R., Bannan, T. J., Percival, C. J., Priestley, M., Topping, D., and Kiendler-Scharr, A.: Secondary organic aerosol reduced by mixture of atmospheric vapours, *Nature*, 565, 587-593, 10.1038/s41586-018-0871-y, 2019.
- Mehra, A., Wang, Y., Krechmer, J. E., Lambe, A., Majluf, F., Morris, M. A., Priestley, M., Bannan, T. J., Bryant, D. J., Pereira, K. L., Hamilton, J. F., Rickard, A. R., Newland, M. J., Stark, H., Croteau, P., Jayne, J. T., Worsnop, D. R., Canagaratna, M. R., Wang, L., and Coe, H.: Evaluation of the chemical composition of gas- and particle-phase products of aromatic oxidation, *Atmos. Chem. Phys.*, 20, 9783-9803, 10.5194/acp-20-9783-2020, 2020.
- Mellouki, A., Ammann, M., Cox, R. A., Crowley, J. N., Herrmann, H., Jenkin, M. E., McNeill, V. F., Troe, J., and Wallington, T. J.: Evaluated kinetic and photochemical data for atmospheric chemistry: volume VIII – gas-phase reactions of organic species with four, or more, carbon atoms ( $\geq$  C<sub>4</sub>), *Atmos. Chem. Phys.*, 21, 4797-4808, 10.5194/acp-21-4797-2021, 2021.
- Mentel, T. F., Wildt, J., Kiendler-Scharr, A., Kleist, E., Tillmann, R., Dal Maso, M., Fisseha, R., Hohaus, T., Spahn, H., Uerlings, R., Wegener, R., Griffiths, P. T., Dinar, E., Rudich, Y., and Wahner, A.: Photochemical production of aerosols from real plant emissions, *Atmos. Chem. Phys.*, 9, 4387-4406, 10.5194/acp-9-4387-2009, 2009.
- Molteni, U., Bianchi, F., Klein, F., El Haddad, I., Frege, C., Rossi, M. J., Dommen, J., and Baltensperger, U.: Formation of highly oxygenated organic molecules from aromatic compounds, *Atmos. Chem. Phys.*, 18, 1909-1921, 10.5194/acp-18-1909-2018, 2018.
- Nakao, S., Shrivastava, M., Nguyen, A., Jung, H., and Cocker, D.: Interpretation of Secondary Organic Aerosol Formation from Diesel Exhaust Photooxidation in an Environmental Chamber, *Aerosol Sci Tech*, 45, 964-972, 10.1080/02786826.2011.573510, 2011.
- Nakao, S., Liu, Y., Tang, P., Chen, C. L., Zhang, J., and Cocker Iii, D. R.: Chamber studies of SOA formation from aromatic hydrocarbons: observation of limited glyoxal uptake, *Atmos. Chem. Phys.*, 12, 3927-3937, 10.5194/acp-12-3927-2012, 2012.
- Ng, N. L., Canagaratna, M. R., Zhang, Q., Jimenez, J. L., Tian, J., Ulbrich, I. M., Kroll, J. H., Docherty, K. S., Chhabra, P. S., Bahreini, R., Murphy, S. M., Seinfeld, J. H., Hildebrandt, L., Donahue, N. M., DeCarlo, P. F., Lanz, V. A., Prévôt, A. S. H., Dinar, E., Rudich, Y., and Worsnop, D. R.: Organic aerosol components observed in Northern Hemispheric datasets from Aerosol Mass Spectrometry, *Atmos. Chem. Phys.*, 10, 4625-4641, 10.5194/acp-10-4625-2010, 2010.
- Nordin, E. Z., Eriksson, A. C., Roldin, P., Nilsson, P. T., Carlsson, J. E., Kajos, M. K., Hellén, H., Wittbom, C., Rissler, J., Löndahl, J., Swietlicki, E., Svenningsson, B., Bohgard, M., Kulmala, M., Hallquist, M., and Pagels, J. H.: Secondary organic aerosol formation from idling gasoline passenger vehicle emissions investigated in a smog chamber, *Atmos. Chem. Phys.*, 13, 6101-6116, 10.5194/acp-13-6101-2013, 2013.
- Odum, J. R., Hoffmann, T., Bowman, F., Collins, D., Flagan, R. C., and Seinfeld, J. H.: Gas/Particle Partitioning and Secondary Organic Aerosol Yields, *Environmental Science & Technology*, 30, 2580-2585, 10.1021/es950943+, 1996.
- Pankow, J. F.: An absorption-model of gas-particle partitioning of organic-compounds in the atmosphere, *Atmos. Environ.*, 28, 185-188, 10.1016/1352-2310(94)90093-0, 1994.
- Pinto, D. M., Tiiva, P., Miettinen, P., Joutsensaari, J., Kokkola, H., Nerg, A.-M., Laaksonen,

- A., and Holopainen, J. K.: The effects of increasing atmospheric ozone on biogenic monoterpene profiles and the formation of secondary aerosols, *Atmos Environ*, 41, 4877-4887, 10.1016/j.atmosenv.2007.02.006, 2007.
- Platt, S. M., El Haddad, I., Zardini, A. A., Clairotte, M., Astorga, C., Wolf, R., Slowik, J. G., Temime-Roussel, B., Marchand, N., Ježek, I., Drinovec, L., Močnik, G., Möhler, O., Richter, R., Barmet, P., Bianchi, F., Baltensperger, U., and Prévôt, A. S. H.: Secondary organic aerosol formation from gasoline vehicle emissions in a new mobile environmental reaction chamber, *Atmos. Chem. Phys.*, 13, 9141-9158, 10.5194/acp-13-9141-2013, 2013.
- Priestley, M., Bannan, T. J., Le Breton, M., Worrall, S. D., Kang, S., Pullinen, I., Schmitt, S., Tillmann, R., Kleist, E., Zhao, D., Wildt, J., Garmash, O., Mehra, A., Bacak, A., Shallcross, D. E., Kiendler-Scharr, A., Hallquist, Å. M., Ehn, M., Coe, H., Percival, C. J., Hallquist, M., Mentel, T. F., and McFiggans, G.: Chemical characterisation of benzene oxidation products under high- and low-NO<sub>x</sub> conditions using chemical ionisation mass spectrometry, *Atmos. Chem. Phys.*, 21, 3473-3490, 10.5194/acp-21-3473-2021, 2021.
- Pullinen, I., Schmitt, S., Kang, S., Sarrafzadeh, M., Schlag, P., Andres, S., Kleist, E., Mentel, T. F., Rohrer, F., Springer, M., Tillmann, R., Wildt, J., Wu, C., Zhao, D., Wahner, A., and Kiendler-Scharr, A.: Impact of NO<sub>x</sub> on secondary organic aerosol (SOA) formation from  $\alpha$ -pinene and  $\beta$ -pinene photooxidation: the role of highly oxygenated organic nitrates, *Atmos. Chem. Phys.*, 20, 10125–10147, <https://doi.org/10.5194/acp-20-10125-2020>, 2020.
- Reyes-Villegas, E., Bannan, T., Le Breton, M., Mehra, A., Priestley, M., Percival, C., Coe, H., and Allan, J. D.: Online Chemical Characterization of Food-Cooking Organic Aerosols: Implications for Source Apportionment, *Environmental Science & Technology*, 52, 5308-5318, 10.1021/acs.est.7b06278, 2018.
- Rohrer, F., Bohn, B., Brauers, T., Brüning, D., Johnen, F. J., Wahner, A., and Kleffmann, J.: Characterisation of the photolytic HONO-source in the atmosphere simulation chamber SAPHIR, *Atmos. Chem. Phys.*, 5, 2189-2201, 10.5194/acp-5-2189-2005, 2005.
- Sarrafzadeh, M., Wildt, J., Pullinen, I., Springer, M., Kleist, E., Tillmann, R., Schmitt, S. H., Wu, C., Mentel, T. F., Zhao, D., Hastie, D. R., and Kiendler-Scharr, A.: Impact of NO<sub>x</sub> and OH on secondary organic aerosol formation from  $\beta$ -pinene photooxidation, *Atmos. Chem. Phys.*, 16, 11237–11248, 10.5194/acp-16-11237-2016, 2016.
- Schervish, M., and Donahue, N. M.: Peroxy radical chemistry and the volatility basis set, *Atmos. Chem. Phys.*, 20, 1183-1199, 10.5194/acp-20-1183-2020, 2020.
- Schwantes, R. H., Schilling, K. A., McVay, R. C., Lignell, H., Coggon, M. M., Zhang, X., Wennberg, P. O., and Seinfeld, J. H.: Formation of highly oxygenated low-volatility products from cresol oxidation, *Atmospheric Chemistry and Physics*, 17, 3453-3474, 10.5194/acp-17-3453-2017, 2017.
- Shao, Y., Wang, Y., Du, M., Voliotis, A., Alfarra, M. R., Turner, S. F., and McFiggans, G.: Characterisation of the Manchester Aerosol Chamber facility, *Atmos. Meas. Tech. Discuss.*, 2021, 1-50, 10.5194/amt-2021-147, 2021a.
- Shao, Y., Voliotis, A., Du, M., Wang, Y., Pereira, K., Hamilton, J., Alfarra, M. R., McFiggans, G.: Chemical composition of secondary organic aerosol particles formed from mixtures of anthropogenic and biogenic precursors. In preparation for *Atmos. Chem. Phys. Discuss.*, 2021b.
- Shao, Y., Voliotis, A., Du, M., Wang, Y., Pereira, K., Hamilton, J., Alfarra, M. R., McFiggans, G.: Characterisation of the oxidation state of secondary organic aerosols in mixed precursor

systems. In preparation for Atmos. Chem. Phys. Discuss., 2021c.

Shilling, J. E., Zawadowicz, M. A., Liu, J. M., Zaveri, R. A., and Zelenyuk, A.: Photochemical Aging Alters Secondary Organic Aerosol Partitioning Behavior, *Acs Earth Space Chem*, 3, 2704-2716, 10.1021/acsearthspacechem.9b00248, 2019.

Shrivastava, M., Cappa, C. D., Fan, J., Goldstein, A. H., Guenther, A. B., Jimenez, J. L., Kuang, C., Laskin, A., Martin, S. T., Ng, N. L., Petaja, T., Pierce, J. R., Rasch, P. J., Roldin, P., Seinfeld, J. H., Shilling, J., Smith, J. N., Thornton, J. A., Volkamer, R., Wang, J., Worsnop, D. R., Zaveri, R. A., Zelenyuk, A., and Zhang, Q.: Recent advances in understanding secondary organic aerosol: Implications for global climate forcing, 55, 509-559, 10.1002/2016rg000540, 2017.

Spracklen, D. V., Jimenez, J. L., Carslaw, K. S., Worsnop, D. R., Evans, M. J., Mann, G. W., Zhang, Q., Canagaratna, M. R., Allan, J., Coe, H., McFiggans, G., Rap, A., and Forster, P.: Aerosol mass spectrometer constraint on the global secondary organic aerosol budget, *Atmos. Chem. Phys.*, 11, 12109-12136, 10.5194/acp-11-12109-2011, 2011.

Thornton, J. A., Shilling, J. E., Shrivastava, M., D'Ambro, E. L., Zawadowicz, M. A., and Liu, J.: A Near-Explicit Mechanistic Evaluation of Isoprene Photochemical Secondary Organic Aerosol Formation and Evolution: Simulations of Multiple Chamber Experiments with and without Added NO<sub>x</sub>, *Acs Earth Space Chem*, 4, 1161-1181, 10.1021/acsearthspacechem.0c00118, 2020.

Tiitta, P., Leskinen, A., Hao, L., Yli-Pirilä, P., Kortelainen, M., Grigonyte, J., Tissari, J., Lamberg, H., Hartikainen, A., Kuusalo, K., Kortelainen, A. M., Virtanen, A., Lehtinen, K. E. J., Komppula, M., Pieber, S., Prévôt, A. S. H., Onasch, T. B., Worsnop, D. R., Czech, H., Zimmermann, R., Jokiniemi, J., and Sippula, O.: Transformation of logwood combustion emissions in a smog chamber: formation of secondary organic aerosol and changes in the primary organic aerosol upon daytime and nighttime aging, *Atmos. Chem. Phys.*, 16, 13251-13269, 10.5194/acp-16-13251-2016, 2016.

Tsigaridis, K., and Kanakidou, M.: The Present and Future of Secondary Organic Aerosol Direct Forcing on Climate, *Current Climate Change Reports*, 4, 84-98, 10.1007/s40641-018-0092-3, 2018.

Tsiligiannis, E., Hammes, J., Salvador, C. M., Mentel, T. F., and Hallquist, M.: Effect of NO<sub>x</sub> on 1,3,5-trimethylbenzene (TMB) oxidation product distribution and particle formation, *Atmos. Chem. Phys.*, 19, 15073-15086, 10.5194/acp-19-15073-2019, 2019.

VanReken, T. M., Greenberg, J. P., Harley, P. C., Guenther, A. B., and Smith, J. N.: Direct measurement of particle formation and growth from the oxidation of biogenic emissions, *Atmos. Chem. Phys.*, 6, 4403-4413, 10.5194/acp-6-4403-2006, 2006.

Voliotis, A., Wang, Y., Shao, Y., Du, M., Bannan, T. J., Percival, C. J., Pandis, S. N., Alfarra, M. R., and McFiggans, G.: Exploring the composition and volatility of secondary organic aerosols in mixed anthropogenic and biogenic precursor systems, *Atmos. Chem. Phys.*, 21, 14251-14273, 2021a

Voliotis, A., Wang, Y., Shao, Y., Du, M., Bannan, T. J., Percival, C. J., Pandis, S. N., Alfarra, M. R., and McFiggans, G.: The influence of the addition of a reactive low SOA yield VOC on the volatility of particles formed from photo-oxidation of anthropogenic – biogenic mixtures, in prep for Atmos. Chem. Phys. Discuss., 2021b

Wang, S., Wu, R., Berndt, T., Ehn, M., and Wang, L.: Formation of Highly Oxidized Radicals and Multifunctional Products from the Atmospheric Oxidation of Alkylbenzenes,

- Environmental Science & Technology, 51, 8442-8449, 10.1021/acs.est.7b02374, 2017.
- Wang, Y., Mehra, A., Krechmer, J. E., Yang, G., Hu, X., Lu, Y., Lambe, A., Canagaratna, M., Chen, J., Worsnop, D., Coe, H., and Wang, L.: Oxygenated products formed from OH-initiated reactions of trimethylbenzene: autoxidation and accretion, *Atmos. Chem. Phys.*, 20, 9563-9579, 10.5194/acp-20-9563-2020, 2020.
- Weitkamp, E. A., Sage, A. M., Pierce, J. R., Donahue, N. M., and Robinson, A. L.: Organic Aerosol Formation from Photochemical Oxidation of Diesel Exhaust in a Smog Chamber, *Environmental Science & Technology*, 41, 6969-6975, 10.1021/es070193r, 2007.
- Whalley, L. K., Stone, D., Bandy, B., Dunmore, R., Hamilton, J. F., Hopkins, J., Lee, J. D., Lewis, A. C., and Heard, D. E.: Atmospheric OH reactivity in central London: observations, model predictions and estimates of in situ ozone production, *Atmos. Chem. Phys.*, 16, 2109-2122, 10.5194/acp-16-2109-2016, 2016.
- Wyche, K. P., Ryan, A. C., Hewitt, C. N., Alfarra, M. R., McFiggans, G., Carr, T., Monks, P. S., Smallbone, K. L., Capes, G., Hamilton, J. F., Pugh, T. A. M., and MacKenzie, A. R.: Emissions of biogenic volatile organic compounds and subsequent photochemical production of secondary organic aerosol in mesocosm studies of temperate and tropical plant species, *Atmos. Chem. Phys.*, 14, 12781-12801, 10.5194/acp-14-12781-2014, 2014.
- Ye, P., Ding, X., Hakala, J., Hofbauer, V., Robinson, E. S., and Donahue, N. M.: Vapor wall loss of semi-volatile organic compounds in a Teflon chamber, *Aerosol Sci Tech*, 50, 822-834, 10.1080/02786826.2016.1195905, 2016.
- Zhang, X., Cappa, C. D., Jathar, S. H., Mcvay, R. C., Ensberg, J. J., Kleeman, M. J., and Seinfeld, J. H.: Influence of vapor wall loss in laboratory chambers on yields of secondary organic aerosol, *P Natl Acad Sci USA*, 111, 5802-5807, 10.1073/pnas.1404727111, 2014.
- Ziemann, P. J., and Atkinson, R.: Kinetics, products, and mechanisms of secondary organic aerosol formation, *Chemical Society Reviews*, 41, 6582-6605, 10.1039/C2CS35122F, 2012.
- Atkinson, R.: Atmospheric chemistry of VOCs and NOx, *Atmospheric Environment*, 34, 2063-2101, 10.1016/s1352-2310(99)00460-4, 2000.
- Matthew, B. M., Middlebrook, A. M., and Onasch, T. B.: Collection Efficiencies in an Aerodyne Aerosol Mass Spectrometer as a Function of Particle Phase for Laboratory Generated Aerosols, *Aerosol Science and Technology*, 42, 884-898, 10.1080/02786820802356797, 2008.
- Pereira, C. J. and Amiridis, M. D.: NOx Control from Stationary Sources Overview of Regulations, Technology, and Research Frontiers, *ACS Symposium Series*, 587, 10.1021/bk-1995-0587.ch001, 1995.
- Wang, Y., Voliotis, A., Hu, D., Shao, Y., Du, M., Chen, Y., Alfarra, M. R., and McFiggans, G.: On the evolution of sub- and super-saturated water uptake of secondary organic aerosol in chamber experiments from mixed precursors, *Atmospheric Chemistry and Physics Discussions*, 10.5194/acp-2021-577, 2022.
- Wang, Y., Voliotis, A., Shao, Y., Zong, T., Meng, X., Du, M., Hu, D., Chen, Y., Wu, Z., Alfarra, M. R., and McFiggans, G.: Phase state of secondary organic aerosol in chamber photo-oxidation of mixed precursors, *Atmospheric Chemistry and Physics*, 21, 11303-11316, 10.5194/acp-21-11303-2021, 2021.



Wyche, K. P., Monks, P. S., Smallbone, K. L., Hamilton, J. F., Alfarra, M. R., Rickard, A. R., McFiggans, G. B., Jenkin, M. E., Bloss, W. J., Ryan, A. C., Hewitt, C. N., and MacKenzie, A. R.: Mapping gas-phase organic reactivity and concomitant secondary organic aerosol formation: chemometric dimension reduction techniques for the deconvolution of complex atmospheric data sets, *Atmospheric Chemistry and Physics*, 15, 8077-8100, 10.5194/acp-15-8077-2015, 2015.

[BLANK PAGE]

### **4.3 Paper 3: Combined application of Online FIGAERO-CIMS and Offline LC-Orbitrap MS to Characterize the Chemical Composition of SOA in Smog Chamber Studies**

**This paper is under review in the journal of “*Atmospheric Measurement Techniques*” and can be found on: <https://amt.copernicus.org/preprints/amt-2021-420/>**

#### **4.3.1 Paper introduction**

This paper aims to illustrate the power of the combination of online FIGAERO-CIMS and LC- Orbitrap MS to investigate the SOA in chamber studies. This paper is to solve the 3<sup>rd</sup> objective of this project.

A combination of online and offline mass spectrometric techniques was used to characterize the chemical composition of secondary organic aerosol (SOA) generated from the photooxidation of  $\alpha$ -pinene in an atmospheric simulation chamber. The filter inlet for gases and aerosols (FIGAERO) coupled with a high-resolution time-of-flight iodide chemical ionization mass spectrometer (I-ToF-CIMS) was employed to track the evolution of gaseous and particulate components. Extracts of aerosol particles sampled onto a filter at the end of each experiment were analyzed using ultra-performance liquid chromatography ultra-high-resolution tandem mass spectrometry (LC-Orbitrap MS). It was found that the particle-phase oxidation between the online FIGAERO-CIMS and offline LC-Orbitrap MS negative mode analysis are broadly consistent, while an increased abundance of high carbon number ( $nC \geq 16$ ) compounds additionally containing nitrogen (CHON group) was detected in the LC-Orbitrap MS positive ionisation mode, indicating a fraction missed by the negative mode and CIMS measurements. Additionally, complementary information can be provided by the two instruments. For example, time series of gas-phase and particle-phase oxidation products provided by online measurements allowed investigation of the gas-phase chemistry of those products by hierarchical clustering analysis to assess the phase partitioning of individual molecular compositions.

#### **4.3.2 Contribution to the joint authorship**

The author has contributed the following:

- (1) Developing the main concept for this paper (80%)

(2) Carried out the experiments and collected experimental data for all experiments (25%)

(3) Preparation of tables and carried out the data analysis for FIGAERO-CIMS measurements and data visualization (100%)

(4) Carried out the data analysis for LC- Orbitrap MS and data visualization (50%)

(5) Paper writing (90%).

### **4.3.3 Supplemental information**

Paper 3 is shown below.



## Combined application of Online FIGAERO-CIMS and Offline LC-Orbitrap MS to Characterize the Chemical Composition of SOA in Smog Chamber Studies

Mao Du<sup>1</sup>, Aristeidis Voliotis<sup>1</sup>, Yunqi Shao<sup>1</sup>, Yu Wang<sup>1</sup>, Thomas J. Bannan<sup>1</sup>, Kelly L. Pereira<sup>3,†</sup>, Jacqueline F. Hamilton<sup>3</sup>, Carl J. Percival<sup>4</sup>, M. Rami Alfarra<sup>1,2,‡</sup>, Gordon McFiggans<sup>1,\*</sup>

<sup>1</sup>Centre for atmospheric science, Department of Earth and Environmental Science, School of Natural Sciences, The University of Manchester, Oxford Road, M13 9PL, Manchester, UK

<sup>2</sup>National Centre for Atmospheric Science, Department of Earth and Environmental Science, School of Natural Sciences, The University of Manchester, Oxford Road, M13 9PL, Manchester, UK

<sup>3</sup>Wolfson Atmospheric Chemistry Laboratories, Department of Chemistry, University of York, York, YO10 5DD, UK

<sup>4</sup>NASA Jet Propulsion Laboratory, California Institute of Technology, 4800 Oak Grove Drive, Pasadena, CA 91109, USA.

<sup>†</sup>Now at Department of Life and Environmental Sciences, Bournemouth University, Dorest, BH12 5BB, UK.

<sup>‡</sup> Now at Environment & Sustainability Center, Qatar Environment & Energy Research Institute, 34110, Doha, Qatar

\*Correspondence to: Gordon McFiggans (g.mcfiggans@manchester.ac.uk)

### Abstract.

A combination of online and offline mass spectrometric techniques was used to characterize the chemical composition of secondary organic aerosol (SOA) generated from the photooxidation of  $\alpha$ -pinene in an atmospheric simulation chamber. The filter inlet for gases and aerosols (FIGAERO) coupled with a high-resolution time-of-flight iodide chemical ionization mass spectrometer (I-ToF-CIMS) was employed to track the evolution of gaseous and particulate components. Extracts of aerosol particles sampled onto a filter at the end of each experiment were analyzed using ultra-performance liquid chromatography ultra-high-resolution tandem mass spectrometry (LC-Orbitrap MS). This paper explores the insight brought to the interpretation of SOA chemical composition by the combined application of online FIGAERO-CIMS and offline LC-Orbitrap MS analytical techniques. Both techniques

were used to investigate the major SOA elemental group contributions in each system. The online CIMS particle-phase measurements show that organic species containing exclusively carbon, hydrogen and oxygen (CHO group) dominate the contribution to the ion signals from the SOA products, broadly consistent with the LC-Orbitrap MS negative mode analysis which was better able to identify the sulphur-containing fraction. An increased abundance of high carbon number ( $nC \geq 16$ ) compounds additionally containing nitrogen (CHON group) was detected in the LC-Orbitrap MS positive ionisation mode, indicating a fraction missed by the negative mode and CIMS measurements. Time series of gas-phase and particle-phase oxidation products provided by online measurements allowed investigation of the gas-phase chemistry of those products by hierarchical clustering analysis to assess the phase partitioning of individual molecular compositions. The particle-phase clustering was used to inform the selection of components for targeted structural analysis of the offline samples. Saturation concentrations derived from near-simultaneous gaseous and particulate measurements of the same ions by FIGAERO-CIMS were compared with those estimated from the molecular structure based on the LC-Orbitrap MS measurements to interpret the component partitioning behaviour.

## **1. Introduction**

Secondary organic aerosol (SOA) makes a significant contribution to atmospheric aerosols, which have an important influence on climate and adverse impact on human health and air quality (Hallquist et al., 2009; Kroll and Seinfeld, 2008; Nel, 2005). It is important to understand the formation, composition and behaviour of SOA due to their contribution to many important atmospheric processes, such as cloud formation (Hallquist et al., 2009). There are more than 10,000 individual organic species in the atmosphere and those almost entirely in the vapour phase. Volatile organic compounds (VOCs) are known to be important in tropospheric ozone and SOA formation (Goldstein and Galbally, 2007). Biogenic volatile organic compounds (BVOCs) emitted from plants (such as monoterpenes) and anthropogenic volatile organic compounds (AVOCs) (such as aromatics), undergo atmospheric oxidation processes to generate SOA, leading to the formation of a large number of oxidized products (Goldstein and Galbally, 2007; Guenther et al., 2012; Hoyle et al., 2009; Iinuma et al., 2010; Mcfiggans et al., 2019). As a result of the various VOCs involved and the complexity of the oxidation processes, oxidation products span a wide range of molecular composition and physiochemical

properties (Mentel et al., 2015; Ma et al., 2008; Mohr et al., 2019; Mutzel et al., 2015; Laj et al., 2009). Such chemical complexity poses a major challenge in the molecular characterization of SOA.

Atmospheric simulation chambers play a key role in the study of chemical processes that affect the composition of the atmosphere, enhancing mechanistic understanding of atmospheric chemistry at a molecular level (Cocker et al., 2001; Rohrer et al., 2005; Wang et al., 2011; Burkholder et al., 2017; Ren et al., 2017). In recent years, new developments in the techniques and design of laboratory experiments have been carried out to investigate the chemical composition of SOA generated from the biogenic and anthropogenic sources under various well-controlled conditions, exploring the particle properties, identifying tracers and SOA formation pathways (Winterhalter et al., 2003; Ng et al., 2006; Nguyen et al., 2010; Chhabra et al., 2011; Zhang et al., 2015; Schwantes et al., 2017; Lopez-Hilfiker et al., 2014). Although some progress has been made in characterising sources and formation pathways from some biogenic or anthropogenic precursors, there are still significant gaps remaining in our understanding of the chemical properties of SOA.

Since there is currently no perfect instrument capable of providing a detailed chemical characterisation of SOA (Hallquist et al., 2009; Calvo et al., 2013), various analytical techniques have been established to better characterize SOA chemical composition. Mass spectrometric techniques have been widely employed both online and offline, using a wide range of sample introduction techniques, ionization methods, and mass analyzers (Hallquist et al., 2009; Nizkorodov et al., 2011; Laskin et al., 2012). Liquid chromatography coupled with electrospray ionization orbitrap mass spectrometry (LC-Orbitrap MS) can probe the chemical composition of individual polar and non-polar particle-phase products with accurate mass measurement (Perry et al., 2008; Banerjee and Mazumdar, 2012; Mutzel et al., 2021). LC-MS has been extensively used for the chemical characterization of organic aerosols, quantifying targeted tracers and characterising using tandem MS to determine the molecular identity of ambient SOA (Samy and Hays, 2013; Inuma et al., 2007; Parshintsev et al., 2015; Chen et al., 2020; Hamilton et al., 2013) and laboratory-produced SOA (Winterhalter et al., 2003; Pereira et al., 2014; Mutzel et al., 2021; Mehra et al., 2020a).

Online collection of aerosol samples followed by fast and automated analysis has more recently been developed to overcome some limitations of offline measurements (such as

sampling time integration, evaporation, adsorption and potential filter contamination during transportation or storage). One such technique, the Filter Inlet for Gases and AEROSols combined with a soft chemical ionization method and mass spectrometer (FIGAERO-CIMS; Tofwerk A.G. / Aerodyne Research Inc.), collects filter samples for subsequent thermal desorption to investigate the SOA particle-phase chemical composition (Lopez-Hilfiker et al., 2014). The FIGAERO-CIMS has been coupled to different reagent ions to study the chemical properties of aerosols such as the evolution of gas or particle-phase composition and the volatility of components in laboratory studies and fieldwork (Wang and Hildebrandt Ruiz, 2018; Stark et al., 2017; Bannan et al., 2019; Lee et al., 2020; Lopez-Hilfiker et al., 2016b; Hammes et al., 2019; Thornton et al., 2020). Other online instruments such as particle into liquid sampler (PILS) coupled with ion chromatography (Bateman et al., 2010) and chemical analysis of aerosol online (CHARON) particle inlet coupled to proton-transfer-reaction time-of-flight mass spectrometry (PTR-TOFMS) instruments (Gkatzelis et al., 2018) can also be employed for collection and near real-time analysis of chemical compounds in aerosols. Recently, multiple online analytical techniques have been combined to investigate the chemical properties of atmospheric organic carbon, such as the combination of CIMS, PTR-MS and aerosol mass spectrometer (AMS) (Isaacman-Vanwertz et al., 2017; Isaacman-Vanwertz et al., 2018). There are notable overlaps and differences in the chemical information provided from those online measurements. Nevertheless, few studies have combined offline LC-Orbitrap MS and online FIGAERO-CIMS to study the molecular composition of SOA (Mehra et al., 2020b). By combining both techniques, the detailed molecular composition can be obtained with time evolution/profiling, offering enhanced mechanistic insights.

The purpose of this paper is to explore the benefits of combinatorial LC-Orbitrap MS and FIGAERO-CIMS analytical techniques to investigate SOA chemical composition, demonstrating the power of this combination from a technical perspective. To show this experimentally,  $\alpha$ -pinene ( $C_{10}H_{16}$ ), as one of the most abundant monoterpenes (emitted in substantial amounts by vegetation, e.g., many coniferous trees, notable pine) was selected to generate SOA in the presence of  $NO_x$  in the Manchester Aerosol Chamber (MAC). First, both online and offline analyses were used to retrieve the major elemental group contributions to the SOA in the  $\alpha$ -pinene system. Second, temporal profiles of individual components in gas and particle phases provided by online measurement enabled observation of the evolution of identified components. Third, hierarchical clustering analysis (HCA) was employed to reduce



the dimensionality of the complex composition measurements by grouping compounds with similar chemical properties. Finally, saturation concentrations of targeted compounds derived from the partitioning theory in the FIGAERO-CIMS were compared with those derived from the structural information determined using the LC-Orbitrap MS measurements.

## **2. Instruments and methodology**

### **2.1 Chamber description and experimental design**

Experiments were performed in the Manchester Aerosol Chamber located at the University of Manchester to investigate SOA formation using a broad suite of instrumentation. A full description of the MAC and its characterization can be found in Shao et al. (2021). Briefly, the chamber has a volume of 18 m<sup>3</sup> (3m (L) × 2m (W) × 3m (H)) and consists of a fluorinated ethylene Teflon bag which is suspended in the enclosure and supported by three rectangular aluminum frames. The central frame is fixed, while the upper and lower ones are allowed to move freely to expand and collapse the chamber when sample airflow is introduced to or extracted from the chamber. Relative humidity (RH) and temperature were controlled by the humidifier and air conditioning and were measured at a few points throughout the chamber by a dewpoint hygrometer and a cross-calibrated capacitive sensor. Two 6 kW Xenon arc lamps and 112 halogen lamps (Solux 50W/4700K, Solux MR16, USA, 16 × 7 rows) are mounted on the wall of the enclosure to provide uniform illumination. The experiments reported here used two arc lamps with quartz glass filters in front of them and 5 rows of halogen lamps to simulate the solar spectra over the wavelength range of 290-800 nm (Alfarra et al., 2012). The reported calculated photolysis rate of NO<sub>2</sub> ( $j_{\text{NO}_2}$ ), investigated from the steady-state actinometry experiments, was ~ 0.11-0.18 min<sup>-1</sup> (Shao et al., 2021).

The purified dry air was supplied to the chamber by the laboratory air through a dryer (ML180, Munters) and three filters (Purafil (Purafil Inc., USA), charcoal and HEPA (Donaldson Filtration) filters). The chamber was cleaned by a series of automatic fill/flush cycles with purified air (3 m<sup>3</sup> min<sup>-1</sup>) before each experiment and by overnight oxidation at a high concentration of O<sub>3</sub> (~1ppm) at end of each experiment. An extra 4-5-hour harsh cleaning experiment under strong ultraviolet photolysis was performed weekly with a high concentration of O<sub>3</sub> (~1ppm) to remove the reactive compounds in the chamber. Liquid VOC precursors ( $\alpha$ -pinene in this study; Sigma Aldrich, GC grade  $\geq 99.99\%$  purity) are fed into the chamber via

injecting into a heated glass bulb (max: 80°C), vaporized immediately and flushed into the chamber by continuous high purity nitrogen (ECD grade, 99.998 % purity N<sub>2</sub>). The required concentration of NO<sub>x</sub> (self-made NO<sub>x</sub> cylinder, 10% (v/v) NO<sub>2</sub> and 90% (v/v) N<sub>2</sub>) is controlled by the injection of NO<sub>2</sub> from a cylinder into the charge line. Seed particles were generated from aqueous solutions using ammonium sulfate (AS, Puratonic, 99.999% purity) by nebulizing via an aerosol generator (Topaz model ATM 230) and introduced into the chamber. During injections, the seed particles and gases are fed into the chamber with continuous purified air at flowrate 3 m<sup>3</sup> min<sup>-1</sup>, ensuring the rapid and well-mixed in the chamber. The relative humidity in the chamber will be adjusted by the custom-built humidifier which comprises a 50L tank fed with ultra-pure water (resistivity ≥ 18.2 MΩ-cm), generating water vapour using an immersion heater that heats the water to ~80°C.

In this work, we will focus on the application of offline and online techniques for the chemical characterization of gaseous and particulate components formed from the photo-oxidation of  $\alpha$ -pinene in three repeat experiments. To obtain sufficient particulate mass on the filter at end of each experiment, an initial reference concentration of  $\alpha$ -pinene was targeted at 309 ppb for each experiment, with an initial VOC: NO<sub>x</sub> ratio ranging from 6 to 8. The  $\alpha$ -pinene studies were part of a series of experiments investigating SOA formation in mixtures and the rationale behind the experimental design is detailed elsewhere (Voliotis et al., 2021). The O<sub>3</sub> concentration was zero at the beginning of each experiment and no additional O<sub>3</sub> was added during experiments. Ammonium sulfate seed aerosol (1g AS dissolving in 100ml deionized water, ~53±12  $\mu\text{g m}^{-3}$ ) was added to enable more controllable and uniform condensation of the gas-phase products and suppress their nucleation. VOCs, NO<sub>x</sub> and seed particles were injected into the clean chamber. All experiments were performed under similar conditions (temperature ~ 25°C, relative humidity ~ 50%, 6-h photooxidation reactions). A 1-hour stabilization period was utilized for measurement of the background conditions in the chamber after injection of the precursors and seed particles but before illumination of the chamber and the onset of photooxidation. At the end of each daily experiment, aerosol sample filters were collected through the 47mm embedded filter holder located at the flushing line of the chamber by pre-processed filters (Quartz filter: 2.2  $\mu\text{m}$  pore size) at the flowrate of 3m<sup>3</sup> min<sup>-1</sup>, before storage in a freezer at -20°C for subsequent extraction and analysis. Filters were pre-baked at 550°C for 5.5 h to remove potential contaminants. Table 1 summarises the initial experimental conditions and instrument availability.

Table 1. The initial experimental conditions and instrument availability.

| Exp No | VOC (type)       | Seeds | VOC (ppb) | $\frac{VOC}{NOx}$ | Seed concentration ( $\mu\text{g m}^{-3}$ ) | FIGAERO-CIMS availability | LC-Orbitrap MS availability |
|--------|------------------|-------|-----------|-------------------|---|---------------------------|-----------------------------|
| 1      | $\alpha$ -pinene | AS    | 309       | 8.4               | <i>n.a</i>                                  | ×                         | ✓                           |
| 2      | $\alpha$ -pinene | AS    | 309       | 7.7               | 60.7  | ✓                         | ✓                           |
| 3      | $\alpha$ -pinene | AS    | 309       | 7.2               | 88.4  | ✓                         | ✓                           |

Note: *n.a* represents no data due to the instrumental issues. The reported initial VOC concentrations in this table have a  $\pm 15\%$  measurement uncertainty.

The repeat experiments were used to evaluate the reproducibility of our experimental system, our data processing and provide a quantification of our confidence in the processes leading to the differences in composition. Data differences can arise from a range of sources: control of experimental conditions, instrumental errors and operational differences, data processing and error propagation. The treatment of the data from the three experiments from the different measurement techniques is described in their respective data processing sections.

## 2.2 On-line FIGAERO-CIMS

### 2.2.1 Instrumentation and operation

We employed a FIGAERO-CIMS (Aerodyne Research Inc.) with iodide (I<sup>-</sup>) as the reagent ion to measure the gas and particle phase oxidized species produced from photooxidation reactions of the experiments. This instrument has been described in detail previously (Reyes-Villegas et al., 2018; Bannan et al., 2019) and was operated at a  $\sim 4000$ (Th/Th) resolving power. Gas-phase species are sampled via a 0.5 m  $\frac{1}{4}$ " I.D. PFA tubing at 1 standard litre per minute (SLM) from the chamber and characterized for 30 mins. Meanwhile, particles are collected simultaneously in a separate FIGAERO inlet on a polytetrafluoroethylene (PFTE) filter (Zefluor, 2.0  $\mu\text{m}$  pore size) at the flow rate 1SLM. After 30-min collection, the filter undergoes thermal desorption (15-min temperature ramp to 200 °C, 10 mins holding time and 8 mins cooling down to room temperature). Six gas phase and particle phase cycles were carried out during each experiment. The sample blanks were collected by two additional gas and particle-phase cycles before the initiation of photooxidation, with the first cycle in the cleaned chamber condition and followed by the second cycle after all species (VOC, seeds and NO<sub>x</sub>) injection. To remove the influence of the seed particles, the particle-phase data collected in the second cycle were used as the particle-phase background correction.

The gas-phase data were collected in the first cycle was employed for the gas-phase chamber background. The instrument was flushed with ultra-high purity nitrogen (UHP, 99.999% purity, N<sub>2</sub>) for 0.2 min every 2 min during each gas-phase measurement, which acted as the gas-phase instrumental background.

### 2.2.2 Data processing

Data analysis was performed on the Tofware package (version 3.1.2) using the Igor Pro 7.0.8 (WaveMetrics, OR, USA) environment (Stark et al., 2015). Mass spectra were mass calibrated using the known masses (I<sup>-</sup>, CH<sub>2</sub>O<sub>2</sub>I<sup>-</sup>, I<sub>2</sub><sup>-</sup> and I<sub>3</sub><sup>-</sup> and), after which the high-resolution peaks were fit via the multi-peak fitting algorithm. The exact mass of the multiple peaks is then matched with the most likely elemental formula, with mass errors less than  $\pm 6$  ppm. Assigned peaks were fitted through the iterative peak assignment method outlined in Stark et. al (Stark et al., 2015). In this study, the  $m/z$  of the ion adducts with I<sup>-</sup> range from 200 to 550 was selected to investigate the oxidation products as signals in this range contribute more than 80% of the total signal (exclude the reagent ions, I<sup>-</sup>, IH<sub>2</sub>O<sup>-</sup>, I<sub>2</sub><sup>-</sup> and I<sub>3</sub><sup>-</sup>). All identified molecular formulae were thereafter expressed as C<sub>x</sub>H<sub>y</sub>O<sub>z</sub>N<sub>m</sub>.

Substantial challenges remain in quantifying all identified compounds owing to a lack of standards. The total signal of identified peaks in the range of  $m/z$  200-550 (excluded the reagent ions, I<sub>2</sub><sup>-</sup>:  $m/z$  253.809492 and I<sub>3</sub><sup>-</sup>:  $m/z$  380.713964) was used to normalise the ion signal, expressing the relative contribution of each identified compound with an implicit assumption of uniform sensitivity (Isaacman-Vanwertz et al., 2018). The gas- and particle-phase dataset undergoes post-processing in MATLAB (R2017a) code in different ways. For the gas phase, the averaged gas-phase measurement signal of ion  $i$  was corrected by subtracting the average clean chamber background value and instrumental background value.

For the particle phase, the signal in the first 60 - 90s with relatively low and stable signals was considered as the instrumental background, enabling interference between the gas and particle mode switching to be removed (Voliotis et al., 2021). All the measured signals were corrected by subtracting the average background value of each ion, after which the temperature and the corresponding signal of ion counts  $i$  was integrated to estimate the normalized signal. The thermogram desorption of one compound may have more than one maximum desorption temperature or enhanced tailing even during the temperature ramp period. This can be caused by the fragments from higher molecular weight compounds or the presence of isomers with

different saturation concentrations (Lopez-Hilfiker et al., 2015; Lopez-Hilfiker et al., 2016a; Lutz et al., 2019; Stark et al., 2017). These complex thermogram desorption features for one compound (e.g., two thermogram profiles or enhanced tailing) can be addressed by a custom nonlinear least-squares peak-fitting routine (Stark et al., 2017; Lopez-Hilfiker et al., 2016b; Lopez-Hilfiker et al., 2015). A non-linear iterative curve fitting method was deployed to fit the peaks (O'haver, 2021). First, the highest signal was found corresponding to the first maximum desorption temperature ( $T_{max}$ ) of the ion. The peak width was set based on the full width at half maximum (FWHM) and the shape followed by Gaussian distribution. The number of desorption peaks, the location and the amplitude of each peak were optimized to fit the total shape of the desorption profile and used to retrieve the total ions for each peak. Figure 1 shows an example of desorption peaks of two compounds, which are consistently measured as major components of the detected  $\alpha$ -pinene derived SOA particles. Typically, the results show that the second peak has a  $T_{max}$  between 20 °C and 90 °C higher than the first peak which is caused by the thermally decomposed accretion products from higher molecular weight rather than isomers (Lopez-Hilfiker et al., 2015). Thus, the first desorption peak was considered as the monomer generated from the precursor oxidation, and its related integrated ion counts were employed for normalized signal and partitioning calculations.

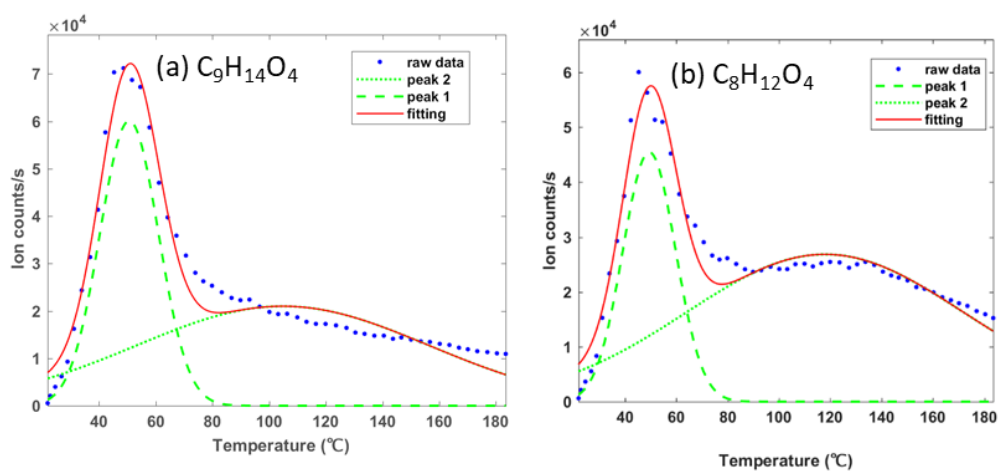


Figure 1. Two examples of an ion with more than a single desorption peak in the FIGAERO-CIMS. Here the peaks at the lower desorption temperature were assigned to monomer  $C_9H_{14}O_4$  (a) and  $C_8H_{12}O_4$  (b) generated from  $\alpha$ -pinene directly and the broader higher temperature peaks being a fragment of another ion at the same mass.

Since a confident peak list is used for two experiments, the normalised fractional CIMS signal for the repeat experiments can be reported as averages along with the associated

variability (as in Figures 2 and 4) or as values from one representative experiment without variability (e.g., Figures 3, 5 and 6) associated with supplementary figures representing another experiment as appropriate.

### 2.2.3 Hierarchical clustering analysis

Hierarchical clustering analysis (HCA) is an analytical method that is used to group or cluster datasets with a large number of individual observations based on the similarity of their behaviour over time. It is used here to investigate the time series of gaseous and particulate oxidation products measured by CIMS and FIGAERO-CIMS. Generally, there are two main hierarchical clustering analysis methods: divisive hierarchical clustering (working in a top-down method) which describes if a cluster needs to be split and agglomerative hierarchical clustering (working from the bottom-up) which describes if clusters should be combined (Nielsen, 2016; Bar-Joseph et al., 2001; Müllner, 2011). Compared to divisive hierarchical clustering, agglomerative hierarchical clustering is commonly used to cluster measurements with distinct time-series behaviours from mass spectrometry datasets and describe the degree of similarity between any two measurements, reducing the dimensionality of mass spectrometry datasets and improving understanding of bulk properties of the chemical processes (Sánchez-López et al., 2014; Rosati et al., 2019; Koss et al., 2020; Priestley et al., 2021). HCA is independent of calibration or instrumental sensitivity since it relies on the relative differences between time series shapes. The final number of clusters is decided based on the distance between the objects and is decided by the user. In this study, we illustrate how HCA can be implemented to reduce the complexity of a dataset while retaining the chemical information by investigating the oxidation processes or product properties from the photooxidation of  $\alpha$ -pinene.

First, to observe the time-series trend changes of each ion and remove the effect of the differences caused by the absolute signal intensity, all measurements are normalized to the highest signal in each time series of each ion. Second, the Euclidean distance between each pair of points of ion A and ion B was calculated (Eq. 1). The sum of the distance for each pair of observations was considered as the distance metric since this approach is most reproducible and least sensitive to outlier points in the time series (Koss et al., 2020).

$$d_{A,B} = \sum_t \text{abs}(A_t - B_t) \quad \text{Eq 1}$$

Third, the average linkage criterion was selected to determine the distance between sets of measurements as this criterion gave more similar or understandable results. The algorithm starts with the distances between all observations. As a first step, the lowest distance between observations A and B is identified and is assigned a new cluster  $x$ . The two observations of A and B are removed from the distance dataset and the new cluster  $x$  is added into the dataset. Then the distance set between the new cluster  $x$  and the remaining observations (named  $y$ ) was calculated as the average of the distances between each of  $n$  individual members of  $x$  and  $m$  individual members of  $y$  over all points  $i$  in cluster  $x$  and points  $j$  in cluster  $y$ , as shown in Eq. 2. The smallest distance between those observations is then found and made up into a new cluster iteratively until only one cluster remains. Finally, the dendrogram tree is deployed to display the relationships between each measurement and cluster. The whole process is carried out in MATLAB (MathWorks, Inc.).

$$d_{x,y} = \sum_{i,j} \frac{d_{(x_i, y_j)}}{m \times n} \quad \text{Eq. 2}$$

## 2.3 Off-line LC-Orbitrap MS

### 2.3.1 Sample preparation

The sample preparation method described in Bryant et al., (2020) was modified for our experimental conditions. Briefly, 4 ml methanol was added to a cleaned and dried extraction vial containing half a filter cut into small pieces and left at room temperature for 2h before sonicating for 30 mins. The extractant was then filtered through a 0.22  $\mu\text{m}$  filter (Thermo Fisher Scientific) using a syringe (1mL, BD PLASTIC PAK, STERILE) into another sample vial, which was evaporated to dryness using a vacuum solvent evaporator (Biotage, Sweden). The sample was reconstituted in 1ml of 10: 90 methanol: water (optima LC-MS grade, Thermo Fisher Scientific) for analysis.

### 2.3.2 LC- Orbitrap MS analysis

The samples were analyzed using ultra-performance liquid chromatography ultra-high-resolution mass spectrometry (Dionex 3000, Orbitrap QExactive, Thermo Fisher Scientific). Compound separation was achieved using a reverse-phase  $\text{C}_{18}$  column (aQ Accucore, Thermo Fisher Scientific) with the following dimensions: 100 mm (length)  $\times$  2.1 mm (width) and 2.6  $\mu\text{m}$  particle size. The column was held at 40°C during analysis and the samples were stored in

the autosampler at 4°C. Gradient elution was used, starting at 90 % with a 1-minute post-injection hold, decreasing to 10 % at 26 minutes, returning to the starting mobile phase conditions at 28 minutes, with a 2-minute hold to re-equilibrate the column, and the total running time was 30 minutes for each sample. The flow rate was set to 0.3 ml/min with a sample injection volume of 2 µl. Heated electrospray ionization was used, with the following parameters: capillary and auxiliary gas temperature of 320 °C, sheath gas flow rate of 70 (arb.) and auxiliary gas flow rate of 3 (arb.). The mass spectrometer was operated in negative and positive ionization mode with a scan range of  $m/z$  85 to 750 and mass resolving power of 70000 (Th/Th). Tandem mass spectrometry was performed using higher-energy collision dissociation with a normalized collision energy of 65, 115.

### 2.3.3 Data processing

Data were analyzed by two complementary approaches. The conventional approach for LC-MS analysis entailed extracting fragments and structural information of targeted compounds using the XCalibur software 4.3. A more recent automated non-targeted approach extracts all detected chromatographic peaks from the sample data set, removing any compounds which do not satisfy a set criterion (see below). The molecular formula is automatically assigned for each compound via a bespoke method designed in the analysis platform, Compound Discoverer version 2.1 (Thermo Fisher Scientific). Full details of the methodology can be found (Pereira et al., 2021). Briefly, molecular formulae assignments were allowed unlimited C, H, O atoms, up to 2 S atoms and 5 N atoms, plus > 2 Na atoms and 1 K atom in positive ionization mode. Compounds with a mass error < 3 ppm and signal-to-noise ratio > 3, a hydrogen-to-carbon ratio of 0.5 to 3 and an oxygen-to-carbon ratio of 0.05 to 2 were included in the data set. Any compounds detected in the procedural (control sample, *i.e.*, blank pre-conditioned filter subjected to the same extraction procedure) and solvent blanks (instrumental blanks) with the same molecular formula and a retention time difference within 0.1 min were removed from the sample data. Furthermore, any compounds detected in the chamber background filter with the same molecular formula and a retention time difference within 0.1 min and the ratio of signal intensities between the sample data and chamber background lower than 3 were removed from the sample data. As with online FIGAERO-CIMS, since quantification for all identified compounds using standards is not possible, all compounds were normalized to the total signal to express the relative contributions, implicitly ignoring differential sensitivity in comparison between the two instruments.



The peak list for the LC-Orbitrap MS is not identical for all experiments since some peaks were not detected in all experiments. The uncertainty as to whether such peaks are truly representative of particle-phase oxidation products is captured by classifying the peaks as “confident” (appear in all repeat experiments) and “inconclusive” (in one specific experiment or appear in two of all experiments) and then by expressing their contribution on average across the experiments with the uncertainty across each in Figure 2. In some cases, the results from one representative experiment are used, such as in Figure 3.

## 2.4 Elemental grouping of identified compounds

The identified species from FIGAERO-CIMS mass spectra and the automated method for LC-Orbitrap MS analysis described above were grouped according to their elements. Compounds containing only carbon, hydrogen, oxygen and nitrogen were categorized as the CHON subgroup. Components containing only carbon, hydrogen and oxygen were classed as CHO subgroup. Similarly, compounds containing carbon, hydrogen, oxygen and sulfur or containing carbon, hydrogen, oxygen, nitrogen and sulfur fell into CHOS or CHONS subgroups respectively. Compounds were additionally classed according to the numbers of carbon atoms in their molecular formulae: C<sub>2</sub> to C<sub>7</sub>, C<sub>8</sub> to C<sub>10</sub>, C<sub>11</sub> to C<sub>15</sub>, ≥C<sub>16</sub>. Given the selectivity and sensitivity of the ionization methods, not all ions were equally observed in the two instruments, and thus only the dominant contribution of identified compounds included in the CHO and CHON groups are discussed in this paper. The minor contribution of CHOS and CHONS groups are not attributed in the FIGAERO-CIMS measurement as it is difficult to identify the two species reliably within the trusted error ( $\pm 6$  ppm). Previous studies also showed difficulties in the identification of isoprene-derived organosulfate compounds from CIMS measurements unambiguously due to the low mass resolution or thermal desorption of organosulfate compounds (D'ambro et al., 2019; Xu et al., 2016). Compounds in the two groups may be included in the unassigned category or may misattribute their signals to the CHO and CHON for the online measurement. The unassigned fractions in the FIGAERO-CIMS measurements (less than 20% of total signal) represent the peaks that are difficult to identify, caused by either the poor signal-to-noise ratios ( $S/N \leq 2$ , ~40-50%) or inaccessible formulae within the trusted error.

## 2.5 Calculation of average carbon oxidation state ( $\overline{OS}_C$ )

The average carbon oxidation state is commonly deployed to describe the degree of oxidation within a complex oxidation reaction (Kroll et al., 2011). The elemental ratios of oxygen-to-carbon (O:C), hydrogen-to-carbon (H: C) and nitrogen-to-carbon (N: C) are used to calculate the  $\overline{OS}_C$ . For the CHON compounds, we assume nitrogen is in the form of nitrate where the oxidation state of N ( $OS_N$ ) is +5 if the oxygen number of the molecule is equal to 3 or more than 3. The nitrogen is in the form of nitrite where the  $OS_N$  is +3 if the oxygen number of the molecule is less than 3. In the FIGAERO-CIMS, the  $\overline{OS}_C$  for the CHOS and CHONS compounds is not considered because of the associated challenges in quantifying S-containing compounds (see above). In the LC-Orbitrap MS analysis, the total signal fractions of CHONS and CHOS groups make low contributions to the total signal, accounting for  $\sim 10 \pm 2\%$  in the confident peaklist in both modes and for  $12.4\% \pm 2.7\%$  and  $28.5\% \pm 2.5\%$  in the inconclusive peaklist for negative mode and positive mode, respectively. It is also impossible to assess if the structure of a compound in the CHONS should be assigned as nitrooxy-OSs with both  $-OSO_3H$  and  $-ONO_2$  groups or as other combinations (e.g.  $-NO_2$  and  $-SO_3H$ ,  $-NO_2$  and  $-OSO_3H$  etc). Given the two considerations, the calculation of  $\overline{OS}_C$  for the CHOS and CHONS compounds is simplified to the equation of  $\overline{OS}_C \approx 2 \times O/C - H/C$  here. The uncertainty of this assumption on the calculated  $\overline{OS}_C$  for CHOS and CHONS species is further discussed in Supplementary Information. The modification of the  $\overline{OS}_C$  is shown in Eq. 3.

$$\overline{OS}_C \approx 2 \times O/C - H/C - (OS_N \times N: C) \quad \text{Eq. 3}$$

Where  $OS_N = 0$  if  $nN = 0$ ; This is for CHO compounds, and CHOS and CHONS compounds for LC-Orbitrap MS analysis;  $OS_N = +3$  if  $nO < 3$ ;  $OS_N = +5$  if  $nO \geq 3$ .

## 2.6 Estimation of component properties

Data from both techniques can be used to investigate the gas-to-particle partitioning behaviour of the targeted compounds in the  $\alpha$ -pinene precursor system. Saturation concentration ( $C_{i,Fp}^*$ ), the concentration at which 50% of a component,  $i$ , is in the vapour phase and 50% is condensed, can be estimated based on the partitioning method from particle-phase fractions ( $F_p$ ) from FIGAERO-CIMS. Although the homologous series of polyethylene glycols (PEG;  $(H-(O-CH_2-CH_2)_n-OH)$  for  $n=3$  to  $n=8$ ) were performed to calibrate the vapour pressures in the FIGAERO-CIMS, useful polyethylene glycols (PEG;  $(H-(O-CH_2-CH_2)_n-OH)$  for  $n=3$  to  $n=8$ ) calibrations are not accessible for interpretation of

this dataset (see Voliotis et al. (2021) for a full discussion). The thermogram method for the online measurements is therefore not accessible to this study and the partitioning method is applied here. Additionally, saturation concentration of a component,  $i$ , ( $C_i^*$ ) was estimated based on the structural information independently obtained from LC-Orbitrap MS.

### 2.6.1 Partitioning Method

$F_p$  is calculated for a given species  $i$  by equation 4, from  $P_i$  and  $G_i$ ; the total signals are corrected by the sampling volume in the particle and gas phase, respectively. Some instrumental factors can affect the gas to particle partitioning process and thus affect the  $F_p$  and  $C^*$  calculated in this way, such as the deposited mass of the component on the filter (Thornton et al., 2020), gas-particle phase equilibrium on the filter, reactions on the surface or in the bulk, or diffusion of the gas to the particle-phase surface or the bulk (Mai et al., 2015; Huang et al., 2018; Yli-Juuti et al., 2017).

$$F_{pi} = \frac{P_i}{P_i + G_i} \quad \text{Eq 4}$$

$C^*$  can be estimated by applying partitioning theory using the equation

$$C_{i,Fp}^* = OA \times \left( \frac{1}{F_p} - 1 \right) = OA \times \frac{G}{P} \quad \text{Eq 5}$$

Where OA is the suspended organic aerosol concentration in the chamber, which is calculated based on the AMS measurement,  $\mu\text{g m}^{-3}$ .

### 2.6.2 Molecular structural method

The structure of targeted compounds is identified using the LC- Orbitrap MS, after which vapor pressure is estimated using the EVAPORATION method (Compernelle et al., 2011) in the UManSysProp tool developed by Topping et al. (Topping et al., 2016). The EVAPORATION method has been assessed as more accurate than other vapor pressure estimation methods for the vapor pressure of individual organic compounds (O'meara et al., 2014), though significant uncertainties persist, particularly for multifunctional compounds. The  $C^*$  is calculated using equation 4 modified by Donahue et al. (2006) based on the earlier absorptive partitioning theory (Pankow, 1994). Errors in the estimation of  $C^*$  attributable to the uncertainties of vapor pressure estimation are extensively discussed in the literature (Barley and Mcfiggans, 2010; Bilde et al., 2015), and are not further discussed here. Additional

uncertainties related to the activity coefficient in mixtures of components – implicit in the derivation of  $C^*$  from CIMS and explicitly assumed as unity for the LC-Orbitrap MS.

$$C_i^* = \frac{M_i 10^6 P_{L,i}^\circ}{RT} \quad \text{Eq 6}$$

Where  $M_i$ : molecular weight of species  $i$ , g/mol;

$P_{L,i}^\circ$ : saturation vapor pressure of pure compound  $i$  at temperature  $T$ , Pa; here  $T$  is 298.15K;

$R$ : gas constant,  $8.314 \text{ m}^3 \text{ Pa K}^{-1} \text{ mol}^{-1}$ .

### 3. Results and discussion

We used the data processing method described in Sections 2.2 and 2.3 to generate the full formula list from FIGAERO-CIMS and LC-Orbitrap MS measurements, respectively. Assigned chromatographic/mass spectral peaks are used to explore the molecular formulae and broad chemical groupings in the  $\alpha$ -pinene photooxidation system. Common capabilities of the two techniques will be illustrated in section 3.1. Additional capabilities of each technique and the strength of their combination are shown in sections 3.2, 3.3 and 3.4, respectively.

#### 3.1 Overview of SOA elemental composition

Chemical composition from the offline filters characterized by LC-Orbitrap MS is shown in Fig 2 from negative and positive ionization mode alongside the final gas and particle-phase measurements by the CIMS, 5.5 hours into the photochemistry experiment. In the LC-Orbitrap MS, the confident compounds in all experiments account for  $\sim 74\% \pm 2.5\%$  in the negative mode and  $\sim 59\% \pm 8.5\%$  in the positive mode, as shown in Figure 2.

General observations can be drawn from the CIMS analysis (see Fig 2a), including i) there are smaller molecules ( $nC < 8$ ) and fewer larger ones ( $nC > 15$ ) in the gas phase than that in the particle phase, ii) compounds in the CHO group dominate the particle phase, and iii) compounds with between 8 and 10 carbon atoms dominate both gas and particle phases.

From the CIMS particle-phase and the LC-Orbitrap MS confident compounds data, the results show that i) the majority of particle-phase signals come from the compounds with 8 to 10 carbon numbers in the CHO group; ii) a small proportion ( $4\% \pm 0.8\%$ ) of high carbon number compounds ( $C_{11}$ - $C_{20}$ ) is observed in the particle phase; iii) the CHO group is shown to account for around  $76\% \pm 2.7\%$  of the total contribution in the CIMS particle-phase signal and

~55%  $\pm$ 1.4% of the total contribution in the LC-Orbitrap MS negative mode; iv) the CIMS particle-phase fractional signal contribution shows high similarity for the C<sub>8</sub>-C<sub>10</sub> and C<sub>11</sub>-C<sub>15</sub> range to the LC-Orbitrap MS negative mode; v) LC-Orbitrap MS negative and positive mode measure a higher fractional signal from compounds with carbon number greater than 16 than the CIMS particle phase, most likely as a result of the higher mass resolution; vi) in contrast, more small molecules with low carbon numbers (C<sub>2</sub>-C<sub>7</sub>) are observed from the CIMS particle-phase measurement, which may be due to the thermal decomposition of low-volatility molecules into smaller fragments (Lopez-Hilfiker et al., 2015; Isaacman-Vanwertz et al., 2016; Thornton et al., 2020). The fractional particle-phase contributions to the CHO and CHON groupings were comparable between the techniques, though a higher fraction of larger molecules was observed particularly in the CHON fraction in the LC-MS negative mode measurement.

From the LC-Orbitrap MS confident compounds alone (see Fig 2a), the results suggest that the positive ionisation mode shows that the CHO and CHON groups contribute to around 48% $\pm$ 7% of the total peak area of all detected compounds. A large fraction (~11% $\pm$ 2.6%) of compounds in the CHON group was observed to contain a high carbon number ( $\geq$ C<sub>16</sub>), showing more formulae with high molecular weight in the positive mode. Signals in the CHO group in both the positive and negative modes are dominated by the C<sub>8-10</sub> ions.

The inconclusive compounds in all experiments from the LC-Orbitrap MS are distributed in the four groups (grey bar in Figure 2a), accounting for 26.1%  $\pm$  6.6% and 40.6%  $\pm$  6.1% in both modes. As shown in Figure 2b, 56%  $\pm$  4.8% of the inconclusive compounds are with high carbon number ( $\geq$ C<sub>16</sub>) in the negative mode, and the compounds with nC = 8-10 and nC  $\geq$  C<sub>16</sub> make large fractions in the positive mode, accounting for ~ 43%  $\pm$  4.4% and 33%  $\pm$  3.4% to the total inconclusive compounds, respectively. The results suggest that the largest fractions of compounds with high carbon numbers are found in the inconclusive compounds, although the existence of those compounds may result from some uncertain factors, such as control of experimental conditions, instrumental errors and operational differences or data processing. Irrespective of the consideration of the inconclusive compounds, a higher fraction of the signal is found in compounds with high carbon numbers in the LC-Orbitrap MS measurements than in the CIMS particle measurements.

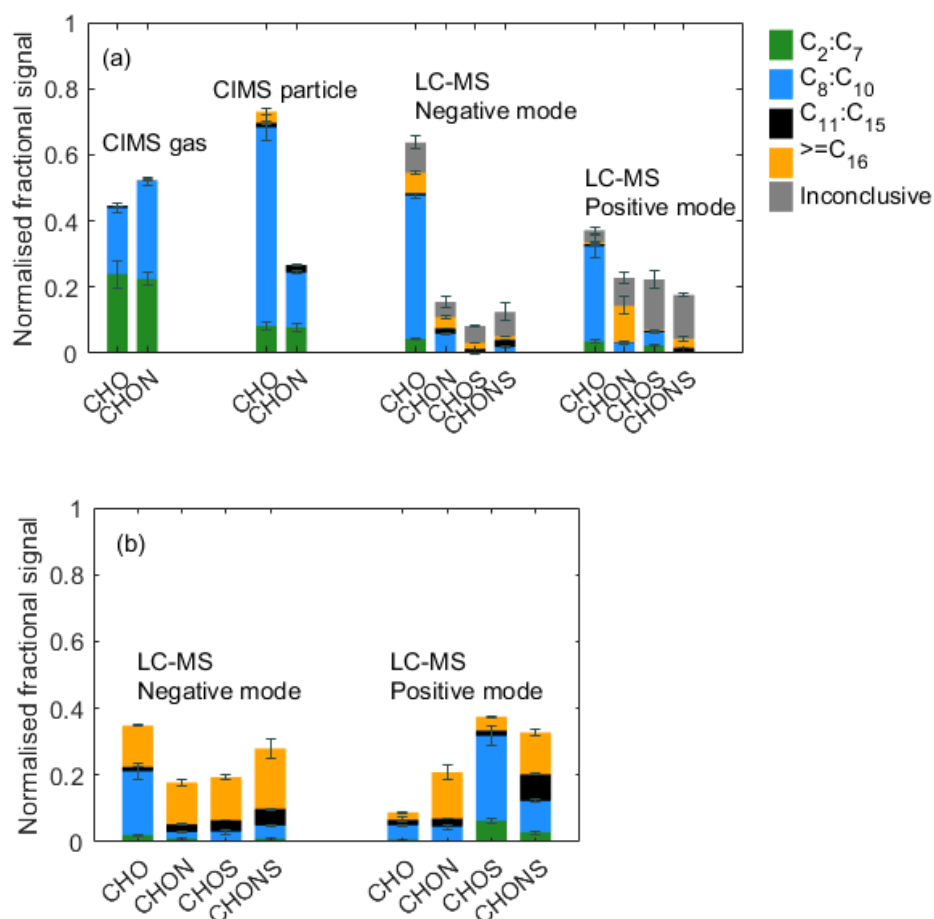


Figure 2. (a) Elemental grouping from CIMS gas phase measurement, CIMS particle-phase measurement, LC-Orbitrap MS in the  $\alpha$ -pinene system. The signal of each compound is normalized to all compounds. (b) Elemental grouping for LC-Orbitrap MS inconclusive compounds. The signal of each compound is normalized to the total inconclusive compounds. The colors correspond to the ones in (a). Standard deviations ( $n=2$  for CIMS and  $n=3$  for LC-Orbitrap MS) are indicated by error bars

Measurements of the oxidation products from both techniques in one representative experiment can be represented in terms of three different chemical spaces as shown in Figure 3. Figure 3a shows that more compounds with higher carbon numbers ( $>10$ ) are observed in the CIMS particle phase compared to that in the gas phase. In the particle phase, Figures 3a and 3b display that the results from LC-Orbitrap MS in both ionisation modes show more molecules with higher carbon numbers ( $C \geq 16$ ) and higher oxygen number molecules ( $O \geq 15$ ) than the results from CIMS particle measurement, though with some of them are from inconclusive compounds. More compounds with lower carbon numbers ( $<5$ ) are mostly detected by the CIMS particle measurements; likely owing to high molecules thermally desorption into small molecules in the online particle-phase measurements or the inability to measure high volatility compounds using LC-Orbitrap MS.

To explore the chemical properties of those compounds and avoid the overlapped formulae with the same carbon number and oxygen number but different hydrogen number, such as the  $C_{10}H_xO_4$ , carbon number vs  $\overline{OS}_C$  and O:C vs H:C are shown in Figures 3c - 3f. Figure 3c and 3d display that some molecules with low carbon number ( $C < 5$ ) and high  $\overline{OS}_C$  ( $\overline{OS}_C > 0$ ) are detected by the CIMS, while molecules with  $10 < nC < 20$  and  $\overline{OS}_C > 0$  and molecules with high carbon number ( $C > 20$ ) are only measured by the LC-MS techniques, although some of them are inconclusive compounds. Figures 3e and 3f show that the results from the two instruments are dominated by formulae with  $1.3 < H/C < 1.8$  and  $0.3 < O/C < 0.7$  which show in the center of the diagram with high density. The majority of compounds in the left bottom of the diagram with a low H: C ratio ( $< 1$ ) and O: C ratio ( $< 0.3$ ) are compounds in the S-containing subgroups, which are only identified by LC-Orbitrap MS. Some highly oxidized (O: C  $> 1$ ) compounds are detected by both techniques.

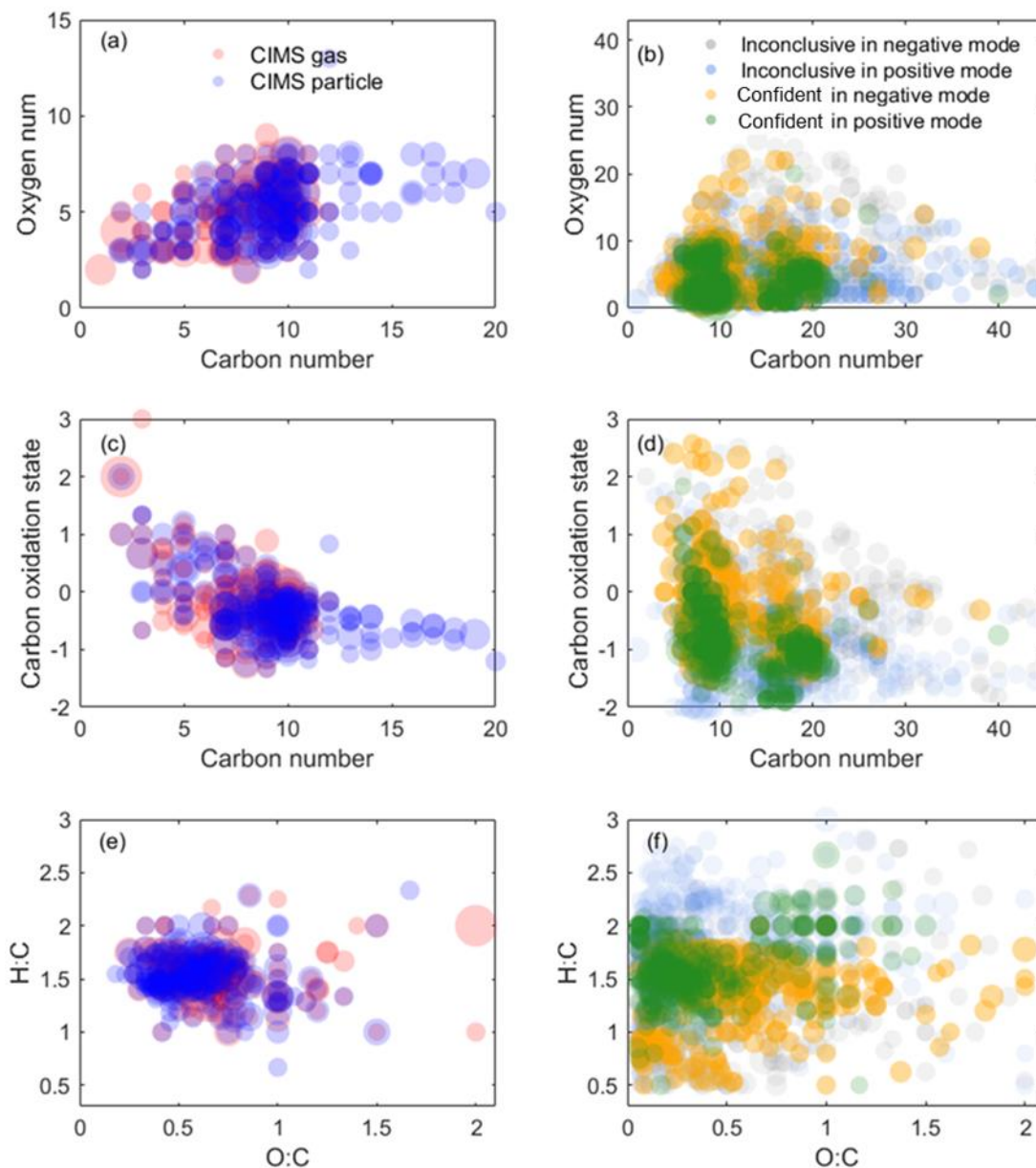


Figure 3. Oxidation products distribution from the representative experiment was detected by the CIMS measurement and LC-Orbitrap MS negative and positive mode. (a), (c) and (e) are for the CIMS measurements. (b), (d) and (f) are for LC-orbitrap MS measurement. The symbol size is proportional to the square root of the ion's signal intensity.

The results suggest that challenges remain in the identification of SOA products using only one technique owing to different capabilities and preferences of instruments. For example, the electrospray ionisation used in the LC-Orbitrap MS has different ionisation efficiencies and sensitivity to molecules, i.e. more sensitive to carbonyl species in positive mode and carboxylic acid or other polar species in negative mode (Mehra et al., 2020a). The iodide-adduct ToF-CIMS is more sensitive to the polar molecules and sensitivity increases with the addition of a



polar functional group in the order of keto-, hydroxy and acid groups (Lee et al., 2014). Thus, the benefits of using combinatorial analytical techniques enable different insights into components found in SOA particles.

### 3.2 Temporal change in elemental composition

The evolution of gas- and particle-phase oxidation products grouped according to their elemental formulae and carbon numbers is shown in Fig 4. Figure 4a shows that the gas-phase products are initially dominated by CHON species at the beginning, with a decreasing trend in relative contribution over time, while CHO species are dominant in the particle phase, increasing over time in relative contribution, plateauing after 2.5-h into photooxidation. The  $\text{NO}_2/\text{NO}$  ratio increases to a maximum value after 1 hour and then decreases (Figure S2a), suggesting the CHON species are mostly generated at the beginning with high NO conditions. In the gas phase, the  $\text{C}_{8-10}$  ions dominate the CHO and CHON groups. The fraction of  $\text{C}_{8-10}$  ions in the CHO group increases over time, whereas the fraction of  $\text{C}_{8-10}$  ions in the CHON group decreases with time. For the particulate oxidation products (Fig 4b), there is a rapid increase to a constant maximum  $\text{C}_{8-10}$  CHO signal (~42%) and a smaller and slightly reducing  $\text{C}_{8-10}$  CHON (~15%) over time. There is a significant early increasing signal contribution from compounds with carbon numbers greater than 15 in the CHO group. The slight increasing fraction of high carbon number compounds ( $\text{C} \geq 16$ ) is investigated in the particle phase over time. It is not possible to confirm whether compounds with high carbon numbers are generated from either gas-phase chemistry reactions or particle-phase reactions in this study.

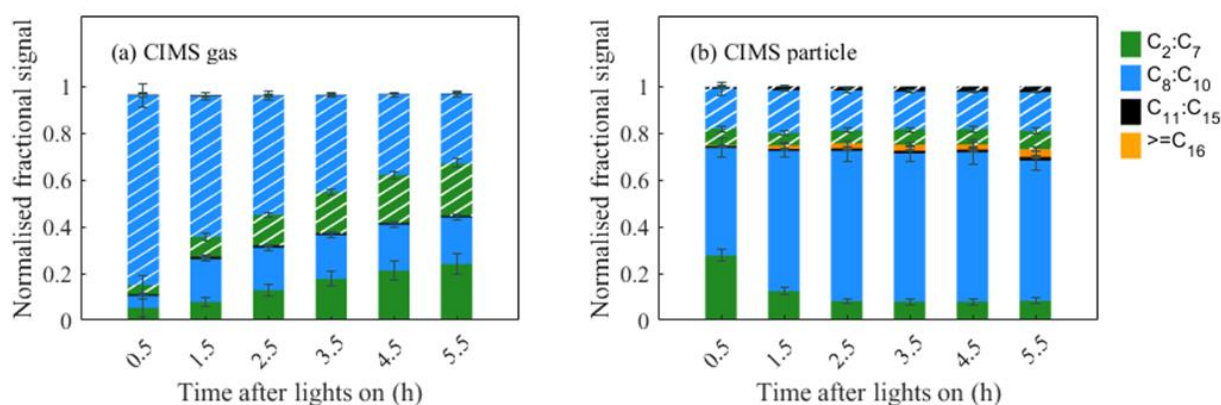


Figure 4. Evolution of chemical compounds in the gas phase and particle phase. Unhatched bars are the CHO group species; hatched bars are the CHON group species. (a) CIMS gas phase; (b) CIMS particle phase. Standard deviations ( $n = 2$ ) are indicated by error bars.

### 3.3 Clustering of the oxidation products from FIGAERO-CIMS

The application of HCA to cluster the top 100 CIMS gas-phase and CIMS particle-phase oxidation products (accounting for more than 96% of the total assigned peaks' signals) is shown in Figure 5 and Figure 6, respectively. Since the data are normalized to the highest intensity of each ion, the results are not sensitive to the intensity of raw ion signals. A dendrogram tree is applied to isolate the clusters (Figure S3 for gas phase and Figure S5 for particle phase). The number of clusters is determined according to whether it already adequately describes the temporal variation and the degree of similarity between clusters. Here, five clusters are chosen for the gas phase and six clusters are chosen for the particle phase according to these criteria. Figure 5a and Figure 6a display the average time series of each cluster calculated by averaging the signals of all ions in every measurement. The time series of ions in each cluster in the gas and particle phase are shown in Figure S4 and Figure S6 respectively, and formulae information in each cluster is provided in Table S2 and Table S3 respectively. It can be seen that the ions with similar time-series trends are mostly clustered together. The matrix showing the relative Euclidean distance between each cluster pair is provided in Figure 5b and Figure 6b, showing a clear distinction between the clusters, with low similarity and high confidence in the quality of the clusters.

In the gas-phase HCA, cluster 5 with the highest cluster contribution peaks at the beginning of the experiments (around 1 hour) before reaching a sharp maximum followed by a more gradual decrease until the end of the experiment. The majority of the ions in this cluster are nitrogen-containing. Cluster 4 (containing  $C_{10}H_{15}NO_5$  and  $C_{10}H_{15}NO_8$ ) and cluster 5 display similar rates to their peak values, but different rates of decrease after 1 hour. The temporal profiles of cluster 5 and cluster 4 show similar temporal profiles to the  $NO_2/NO$  ratio in Fig S2a. This suggests that these early-generation products are likely formed from the reaction of the OH or  $O_3$  initiated peroxy radical with NO rather than with  $RO_2$  or  $HO_2$  (Eddingsaas et al., 2012a). As shown in Fig 5c and d, cluster 4 and cluster 5 have higher weighted average oxygen numbers and weighted average carbon number and carbon oxidation state than other clusters. The high number of oxygen atoms presents indicates these species may have formed via isomerisation of the peroxy radical or secondary OH or  $O_3$  chemistry.

Cluster 3 is the second cluster to peak and is dominated by the CHO species, suggesting significant termination by  $RO_2$  with  $HO_2$  or  $RO_2$  at this stage. The lower nC and nO might be

caused by C-C bond scission during secondary photooxidation reactions over time (e.g.  $C_9H_{14}O_5$ ,  $C_8H_{12}O_5$ , etc), while the higher  $\overline{OS}_C$  in cluster 3 is likely caused by the dominant non-nitrogen-containing compounds (or by the fragmentation leading to a lower carbon number whilst retaining oxygen). Cluster 2 is the third cluster to peak and increase over time, consistent with a later generation of products (Eddingsaas et al., 2012b). The weighted average nC, nO and  $\overline{OS}_C$  values exhibit the lowest nC and nO, as shown in Fig 5c and d. Some carbon-hydrogen species (CHO) appear in this cluster, as shown in Table S2, likely produced from the reactions of  $RO_2$  with  $HO_2$  or  $RO_2$ . Some nitrogen-containing ions (CHON) with  $nC \leq 8$  are in this cluster, suggesting they have undergone a higher degree of fragmentation. Cluster 1 shows the slowest formation rate and lowest cluster contribution suggesting they are likely later generation products.

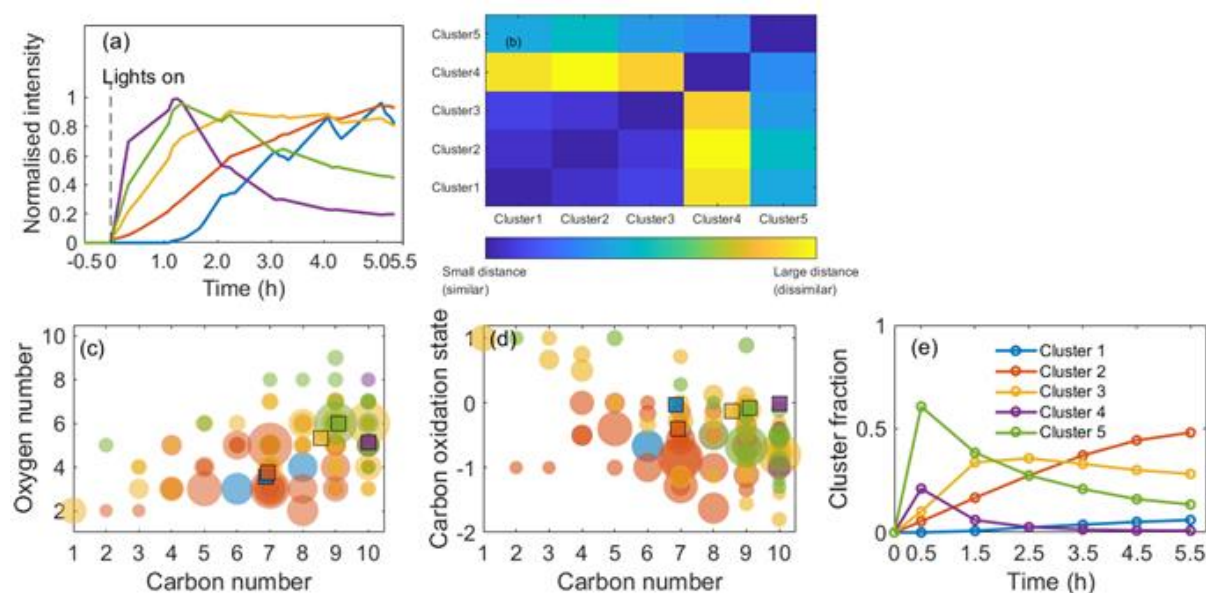


Figure 5. Hierarchical clustering of gas-phase oxidation products from CIMS for the representative  $\alpha$ -pinene system. (a) Time series of each cluster normalized to the highest ions' intensity between 0 and 1. (b) Matrix showing the relative distance between clusters. (c) Carbon number vs oxygen number for each cluster. (d) Carbon number vs oxidation state for each cluster. (e) Time series of the sum of ions' normalized signal fractions to the total signal in each cluster. Note that the square symbols represent the contribution weighted average carbon numbers, oxygen numbers or and  $\overline{OS}_C$  in each cluster. The colors correspond to the ones in (a).

Particle-phase HCA results are shown in Figure 6, and the formulae in each cluster are listed in Table S3. Cluster 5 exhibits the highest contribution to the total identified peaks signals. It shows a continuous increase and slight decrease at the end of experiments, suggesting its constituent ions continuously increase in concentration in the particle phase. The majority of

ions in cluster 5 are non-nitrogen-containing with 7 or 10 carbon atoms, and which may partition from the gas phase directly (Zhang et al., 2015). Several dimers (e.g., ion  $C_{19}H_{28}O_7$ , ion  $C_{18}H_{26}O_7$ , ion  $C_{17}H_{26}O_7$ , etc) contribute to cluster 5, which is expected from further accretion reactions (Kristensen et al., 2014; Zhang et al., 2015). The similar temporal profiles between cluster 5 and SOA mass (Figure S2b) indicate cluster 5 contains the most species with SOA mass. Cluster 4 has the second-highest contribution to the total identified peaks signals. The majority of the ions in this cluster are  $C_{9-10}$ , suggesting less C-C bond cleavage happened in this cluster. The remaining clusters (cluster 1-3 and cluster 4) show sufficiently different temporal profiles to warrant distinct clusters, but each contains few ions and their cluster contributions to the total signals of identified peaks are lower than 5%.

Many of the top 100 gas-phase oxidation products are also found in the top 100 particle-phase ions. Some ions in the same gas-phase HCA cluster may be distributed into different clusters in the particle phase. For example, ions  $C_{10}H_{16}O_3$  and  $C_{10}H_{16}O_4$  in the gas-phase cluster 5 are in the particle-phase cluster 2 and cluster 3, respectively. Different clustering between gas- and particle phases indicate that the particle components time-series trend does not unambiguously relate to the time trend of the corresponding gas-phase ion. Additionally, some ions with high carbon numbers ( $nC \geq 16$ , e.g., ion  $C_{19}H_{28}O_7$ , ion  $C_{18}H_{26}O_7$ , ion  $C_{17}H_{26}O_7$ , etc) in the particle phase are not included in the top 100 gas-phase ions.

Whilst a confident peak-list is used for CIMS data, the HCA is conducted for individual experiments and a single representative experiment is presented here. The effects on clustering of the variability of concentrations and temporal evolution are not straightforward to understand and present as uncertainty that allows ready interpretation. More than 85 ions are the same in the top 100 for the repeat experiment in both gas and particle phases, accounting for 92% - 99% of the top 100 ions. Gas and particle-phase HCA results for the repeat experiment are provided in Figure S7- S10 and Table S4-S5. The generated cluster name from the *MATLAB* code differs between experiments (e.g., gas-phase cluster 4 in the representative experiment corresponding to cluster 3 in the repeat experiment), even though their time-series trends and chemical properties are highly similar. In order to easily compare the two experiments, the time-series trends and clusters' fraction in the representative experiment were considered as the benchmark to adjust the cluster name in the repeat experiment for the gas and particle phase, respectively. The cluster fraction was taken as the particle-phase HCA reference

since only six values (peak areas from six particle-phase desorptions) were used to do the particle-phase HCA and the particle-phase temporal profiles will therefore exhibit greater uncertainties than those in the gas phase owing to their lower temporal resolution.

Comparing Figure S7 to Figure 5, it can be seen in the gas phase, cluster 3 in the repeat experiment contains fewer ions than that in the representative experiment, while cluster 1 in the repeat experiment contains more ions. Figures S7c and d show the different average  $nC$  (9.23 vs 8.55) but comparable  $nO$  (5.54 vs 5.31) and  $\overline{OS}_C$  (-0.12 vs -0.13) in cluster 3 and the different average  $nC$  (6.87 vs 7.18) but comparable  $nO$  (3.57 vs 3.34) and  $\overline{OS}_C$  (-0.03 vs -0.1) in cluster 1 for the repeat and representative experiments, respectively. In the particle phase (see in Figure S9), the chemical characteristics ( $\overline{nC}$ ,  $\overline{nO}$  and  $\overline{OS}_C$ ) are comparable for clusters with the highest and second-highest contributions between the two experiments, while the time-series profiles for the second-highest contribution clusters are slightly different, decreasing after 1 hour and after 2.5 hours, respectively. The different clustering results for some ions with low normalized signal contributions between the two experiments may indicate that those ions are likely sensitive to the experimental conditions (e.g., injected  $\alpha$ -pinene concentration or seed concentrations), leading to different time-series trends in different experiments. The results suggest that the HCA is a powerful approach to separate ion's time-series behaviour. The chemical characteristics for clusters between the two experiments are comparable, although some individual ions differ in the time-series trend between the two experiments, resulting in different numbers of compounds in clusters. The differences do not affect the conclusions from the representative experiment due to the low contribution of those ions.

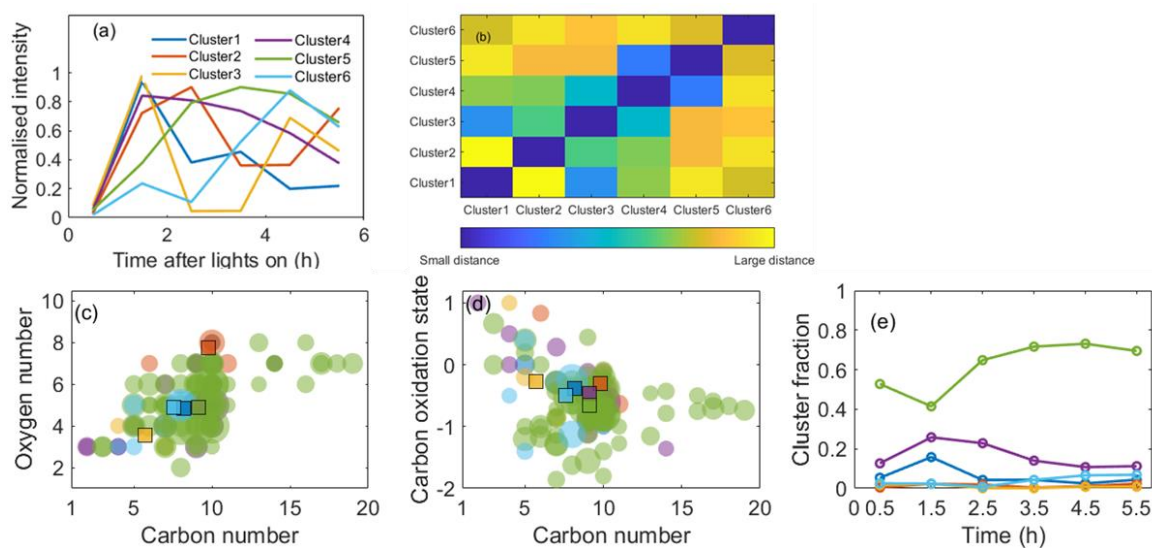


Figure 6. Hierarchical clustering of particle-phase oxidation products for the representative  $\alpha$ -pinene system. (a) Average time series of each cluster normalized to the highest ions' intensity between 0 and 1; (b) Matrix showing the relative distance between clusters. (c) Carbon number vs oxygen number for each cluster. (d) Carbon number vs oxidation state for each cluster. (e) Time series of the sum of ions' normalized signal fractions to the total signal in each cluster. Note that the square symbols represent the contribution weighted average carbon numbers, oxygen numbers or and  $\overline{OS}_c$  in each cluster. The colors correspond to the ones in (a).

### 3.4 Major contributing ions and their properties

#### 3.4.1 Isomeric contributions and evolution in gas and particle phase

The representative oxidation products with relatively high contributions (normalised fractional signal > 0.5%) from the above HCA particle-phase results were selected to investigate their isomeric contributions, evolution and saturation concentrations in order to elucidate the mechanisms of their potential partitioning to the particle phase during SOA formation from  $\alpha$ -pinene photochemistry.

A specific capability of the LC-Orbitrap MS is the ability to separate isomers and quantify their contributions, not possible with the current CIMS technique. Figure 7a shows all molecular formulae with a relative contribution more than 1%, demonstrating the separation of isomers with different retention times by LC-Orbitrap MS. Commonly, one isomer dominates the relative contribution at a particular mass, most likely due to the limited formation routes when a single VOC is oxidised. For example, the contribution of formula  $C_9H_{14}O_4$  at RT= 5.977 min is much higher than the isomer at RT= 13.126 min (21.6% vs 0.5%). In the  $\alpha$ -pinene system, the dominant contribution of only one isomer in one  $m/z$  in offline measurement can support the FIGAERO-CIMS molecular assignment, although the isomers cannot be separated by the FIGAERO-CIMS.

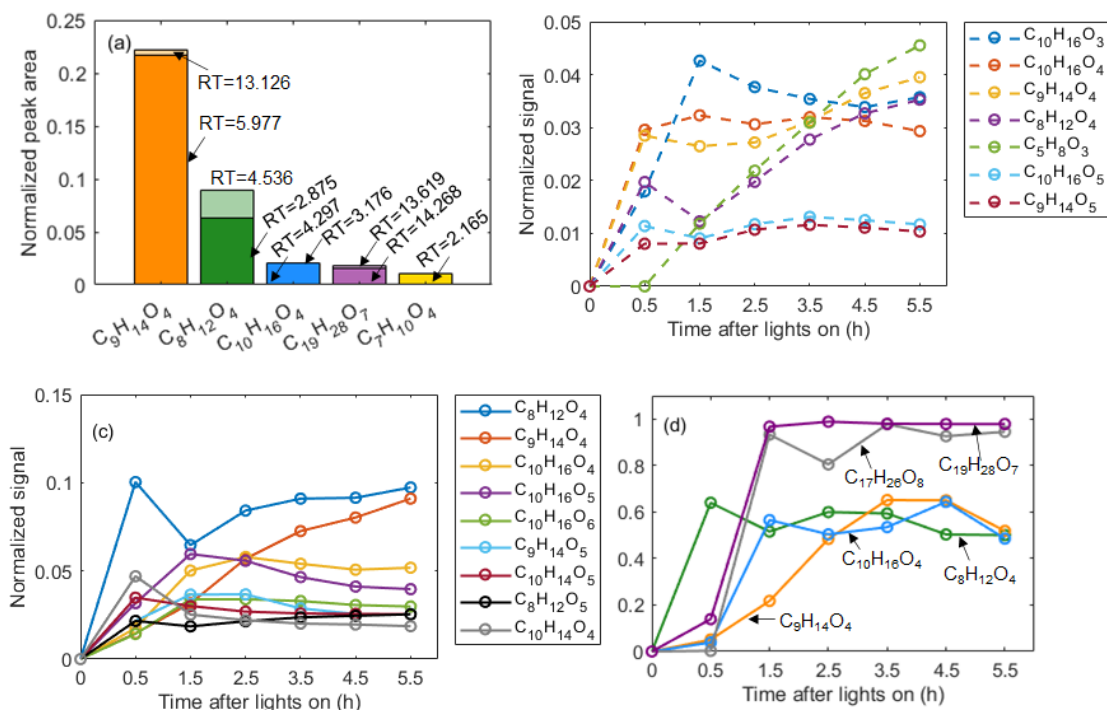


Figure 7. (a) Isomeric fractions of ions from LC-Orbitrap MS analysis; (b) Time series of compounds in the gas phase from CIMS gas-phase measurements. (c) Time series of compounds in the particle phase from CIMS particle-phase measurements. (d) Temporal profiles of particle fractions for a few identified organic molecules generated from  $\alpha$ -pinene photooxidation reactions.

The FIGAERO-CIMS can semi-simultaneously quantify the evolution of the molecular composition of compounds in the vapor and the condensed phase as shown in Fig 7b and 7c, allowing investigation of gas-to-particle conversion processes. The partitioning behaviour of these compounds was explored by investigating their time series of particle fractions,  $F_p$ , as shown in Figure 7d and Figure S11. Distinct temporal profiles were observed in each case. For example,  $F_p$  increases to maximum stable values for  $C_9H_{14}O_4$  after 3.5 hours following initiation of photochemistry, and for  $C_{19}H_{28}O_7$  and  $C_{17}H_{26}O_8$  after 1.5 hours, but with  $C_8H_{12}O_4$  reducing after a rise in the initial 1.5 hours of photochemistry. As expected, the two compounds in the “dimer” range ( $C_{19}H_{28}O_7$  and  $C_{17}H_{26}O_8$ ) have higher particle-phase fractions (almost 1) than those of the “monomer” range oxidation products ( $C_8H_{12}O_4$  and  $C_9H_{14}O_4$ ) as shown in Figure 8.

### 3.4.2 Saturation concentrations

The final  $F_p$  values from the online measurements were used to calculate the  $C^*$  as shown in Table 2. The LC-Orbitrap MS chromatography and mass spectrum of compounds are shown

in Figure S12. The structural information and estimated  $C_i^*$  based on the LC-Orbitrap MS data are also displayed in Table 2.

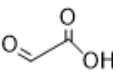
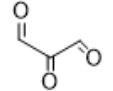
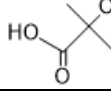
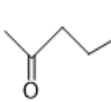
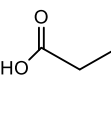

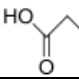
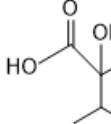
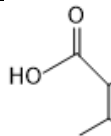
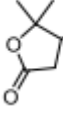
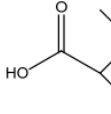
The  $C^*$  calculated from the FIGAERO-CIMS measured  $F_p$  was generally within around 2 orders of magnitude of that estimated from the LC-Orbitrap MS-derived molecular structure for most compounds and sometimes much closer. Such agreement could be used to assign classification into the somewhat broad and arbitrarily defined volatility categories (such as semi-volatile, low volatility, intermediate volatility etc) but such utility is questionable. Moreover, clear discrepancies were noticed for the lowest and highest volatility compounds, as shown in Table 2. It appears that the structural assignment of  $C_2H_2O_3$  and  $C_3H_2O_3$  using the MCM provides unreasonable estimates of high volatility, such that such components could not reasonably be expected to be found in the particle phase. The ions detected at this  $m/z$  in the FIGAERO-CIMS are likely from desorption fragments of larger ions as their desorption  $T_{max}$  are around  $83^\circ\text{C}$  and  $105^\circ\text{C}$  for  $C_2H_2O_3$  and  $C_3H_2O_3$ , respectively. In any case, the physical meaning of their existence in the particle sample is questionable. The accurate determination of the  $F_p$  for compounds with a large number of carbon atoms ( $C_{17}H_{26}O_8$  and  $C_{19}H_{28}O_7$ ) may be limited by the detection limit and signal to noise ratio in the gas phase measurements (Stark et al., 2017; Lopez-Hilfiker et al., 2016b). In addition to the difficulties in measuring partitioning behaviour, challenges remain in its prediction from molecular structure, owing to the acknowledged problems with vapour pressure (and hence  $C^*$ ) estimation, particularly for multifunctional compounds (O'meara et al., 2014; Bilde et al., 2015).

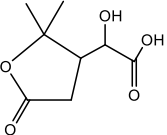
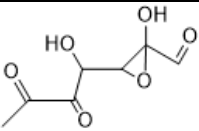
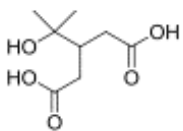
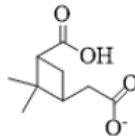
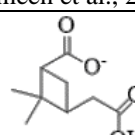
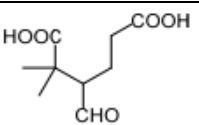
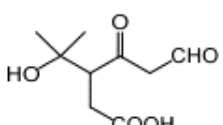
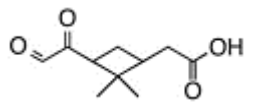
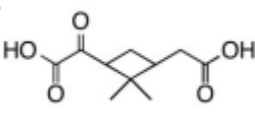
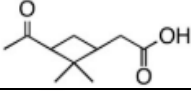
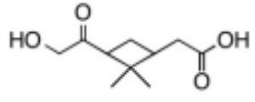
Although the  $C^*$  estimation from the two instruments provides valuable cross confirmation for  $C^*$  of the targeted compounds, the results suggest that accurate measurement for  $C^*$  of compounds remains challenging. The differences in the estimation  $C^*$  of a compound between the two instruments may be attributable to the different estimation methods. The structural information-based method relies on knowledge of the input of the molecular structure to the vapor pressure estimation model, while the partitioning method is dependent on accurate experimental measurements in the gas-to-particle partitioning process. For the partitioning approach, the measured particle fraction is likely biased owing to the thermal desorption of larger ions from the filter (Lopez-Hilfiker et al., 2015), or the gas-phase signals of compounds can be over measured owing to the signal-to-noise limitations (Stark et al., 2017; Lopez-

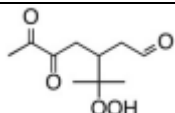
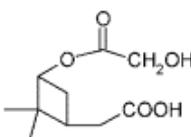
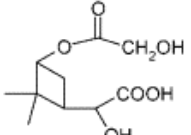
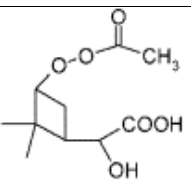
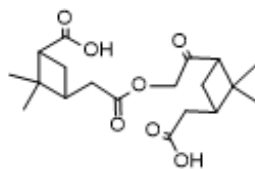
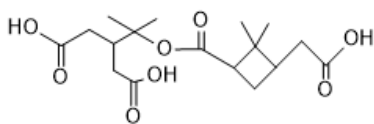


Hilfiker et al., 2016b). The current gaps between the two methods require much work to further investigate the  $C^*$  of compounds in the aerosol particles.

Table 2. Molecular information, being ordered in carbon number, and estimated  $C^*$  of compounds obtained from partitioning theory method and structural information method. The uncertainty of the  $\text{Log}C^*$  from the partitioning theory method was from the uncertainty of measured  $F_p$  and was propagated 1 standard deviation.

| Formula        | MW  | RT (min) | Tentative structure and chemical name   | Log $C^*$ ( $\mu\text{g m}^{-3}$ ) <sup>1</sup> | Log $C_{Fp}^*$ ( $\mu\text{g m}^{-3}$ ) <sup>2</sup> |
|----------------|-----|----------|---|---|--|
| $C_2H_2O_3$    | 74  | n.a      |    | 6.76  | 2.48±0.46  |
| $C_3H_2O_3$    | 86  | n.a      |    | 8.36  | 2.62±0.13  |
| $C_4H_8O_4$    | 120 | 0.858    |    | 2.48  | 3.92±0.05  |
| $C_5H_8O_3$    | 116 | 2.122    |    | 4.68  | 5.51±0.05  |
| $C_5H_8O_5$    | 148 | 0.951    |   | 0.96  | 2.38±0.18  |
| $C_7H_{10}O_4$ | 158 | 2.165    |    | 5.63  | 3.04±0.65  |
| $C_7H_{12}O_4$ | 160 | 1.623    |    | 0.86  | 3.2±0.48   |
| $C_7H_{12}O_5$ | 176 | 1.398    | <br>(Zhang et al., 2018)                         | 1.15  | 2.08± 0.38   |
| $C_7H_{12}O_5$ | 176 | 2.254    |    | 0.46  |  |
| $C_8H_{12}O_4$ | 172 | 2.875    | <br>Terpenylic Acid<br>(Claeys et al., 2009)     | 3.52  | 2.63±0.42  |
| $C_8H_{12}O_4$ | 172 | 4.536    | <br>Norpinic acid<br>(Winterhalter et al., 2003) | 1.80  |  |

|                   |     |        |  |      |            |
|-------------------|-----|--------|--|------|------------|
| $C_8H_{12}O_5$    | 188 | 1.326  |   | 1.26 | 2.09±0.37  |
| $C_8H_{12}O_5$    | 188 | 1.782  |   | 4.55 |            |
| $C_8H_{14}O_5$    | 190 | 1.94   |   | 0.47 | 2.58 ±0.19 |
| $C_9H_{14}O_4$    | 186 | 5.977  | <br>(Yasmeen et al., 2011)                              | 1.34 | 2.4±0.32   |
| $C_9H_{14}O_4$    | 186 | 13.126 | <br>carboxylic acid<br>(Yasmeen et al., 2011)           | 1.34 |            |
| $C_9H_{14}O_5$    | 202 | 2.916  |   | 0.49 | 2.24±0.75  |
| $C_9H_{14}O_5$    | 202 | 4.272  |   | 1.16 |            |
| $C_{10}H_{14}O_4$ | 198 | 2.958  |   | 1.58 | 2.4±0.32   |
| $C_{10}H_{14}O_5$ | 214 | 3.432  |   | 2.21 | 2.11±0.28  |
| $C_{10}H_{16}O_3$ | 184 | 7.935  |   | 3.85 | 3.09±0.45  |
| $C_{10}H_{16}O_4$ | 200 | 4.297  | <br>Hydroxy-pinonic acid<br>(Kristensen et al., 2014) | 3.91 | 2.57±0.41  |
| $C_{10}H_{16}O_5$ | 216 | 5.717  |  | 0.93 |            |

|  |     |        |  |       |           |
|--|-----|--------|--|-------|-----------|
|  |     |        |   |       | 1.82±0.64 |
| C <sub>10</sub> H <sub>16</sub> O <sub>5</sub> | 216 | 4.948  |   | 1.21  |           |
| C <sub>10</sub> H <sub>16</sub> O <sub>6</sub> | 232 | 3.463  |   | -0.91 |           |
| C <sub>10</sub> H <sub>16</sub> O <sub>6</sub> | 232 | 6.189  |   | 2.07  | 1.73±0.48 |
| C <sub>17</sub> H <sub>26</sub> O <sub>8</sub> | 358 | 12.167 | <br>(Kristensen et al., 2014;<br>Demarque et al., 2016) | -2.64 | 1.17±0.38 |
| C <sub>19</sub> H <sub>28</sub> O <sub>7</sub> | 368 | 14.268 | <br>(Kristensen et al., 2014)                        | -0.55 | 1.09±0.33 |

Note: <sup>1</sup>Log C\* estimated from the molecular structural information-based approach. <sup>2</sup>Log C\* estimated from the partitioning theory approach.

#### 4. Conclusions

The characterization of SOA chemical composition in the gas and particle phases is an important but complex process, containing potentially thousands of oxidation products. This study demonstrates the capabilities of the combination of FIGAERO-CIMS and LC-Orbitrap MS in the investigation of SOA chemical compositions and their properties in the  $\alpha$ -pinene photooxidation reactions.

The distribution of particle-phase products is broadly similar between the FIGAERO-CIMS and LC-Orbitrap MS negative ionisation mode for the  $\alpha$ -pinene SOA products. The LC-Orbitrap MS positive ionisation mode provides additional information, with more detected molecular formulae with higher carbon and oxygen numbers. Different insights into components in SOA particles can be gained from the combination of the two techniques.

The gas and particle time-series data from the FIGAERO-CIMS measurement time-series were separated by the hierarchical clustering analysis (HCA), an approach that does not rely on mass calibration. HCA was able to derive cluster properties in terms of average carbon number, oxygen number, oxidation states, for example, enabling interpretation in terms of possible termination pathways of peroxy radicals in the  $\alpha$ -pinene photooxidation reactions.

There is substantial uncertainty in the accurate estimation of saturation concentration of compounds.  $C^*$  estimation from the partitioning method using FIGAERO-CIMS measurements and molecular structure-based method from LC-orbitrap MS enables comparison of the volatility of the targeted compounds. The differences resulting from the two approaches indicates that further work is required to investigate whether the  $C^*$  determined for the compounds are consistent with our understanding of the processes determining the time evolution of phase partitioning.

There are additional questions that remain to be addressed in future work. First, instrumental sensitivity needs more effort in order to have a better understanding of SOA chemical composition. Second, future work will utilize the analytical approaches from the two instruments to explore SOA oxidation products and their chemical properties from complex systems, such as anthropogenic VOCs or biogenic and anthropogenic mixed VOCs, in the chamber experiments. As this study only assessed a single  $\alpha$ -pinene photooxidation system, more work is needed to evaluate how those analytical methods from the two instruments perform with other systems.

### **Data availability**

The dataset of this study is available on the open dataset of EUROCHAMP programme (<https://data.eurochamp.org/data-access/chamber-experiments/>).

### **Author contributions**

GM, MRA, MD, AV, YW and YS conceived the study. MD, AV, YW, and YS conducted the experiments. TJB provided on-site help deploying the FIGAERO-CIMS. KLP and JFH offered help on the LC-orbitrap MS analysis. MD conducted the data analysis and wrote the manuscript with inputs from all co-authors.

### **Competing interests**

The authors declare that they have no conflict of interest.

## Acknowledgements

The Manchester Aerosol Chamber received funding from the European Union's Horizon 2020 research and innovation programme under grant agreement no. 730997, which supports the EUROCHAMP2020 research programme. The financial support received by MD in the form of a President Doctoral Scholarship award (PDS award) by the University of Manchester is gratefully acknowledged. M.R.A. acknowledges support by UK National Centre for Atmospheric Sciences (NACS) funding. Instrumentational support was funded through the NERC Atmospheric Measurement and Observational Facility (AMOF). The Orbitrap MS was funded by a capital grant from NERC (CC090). We acknowledge funding for the COMPLEX-OA project funded by NERC (NE/S010467/1).

## References

- Alfarra, M. R., Hamilton, J. F., Wyche, K. P., Good, N., Ward, M. W., Carr, T., Barley, M. H., Monks, P. S., Jenkin, M. E., Lewis, A. C., and McFiggans, G. B.: The effect of photochemical ageing and initial precursor concentration on the composition and hygroscopic properties of  $\beta$ -caryophyllene secondary organic aerosol, *Atmospheric Chemistry and Physics*, 12, 6417-6436, 10.5194/acp-12-6417-2012, 2012.
- Banerjee, S. and Mazumdar, S.: Electrospray ionization mass spectrometry: a technique to access the information beyond the molecular weight of the analyte, *Int J Anal Chem*, 2012, 282574, 10.1155/2012/282574, 2012.
- Bannan, T. J., Le Breton, M., Priestley, M., Worrall, S. D., Bacak, A., Marsden, N. A., Mehra, A., Hammes, J., Hallquist, M., Alfarra, M. R., Krieger, U. K., Reid, J. P., Jayne, J., Robinson, W., McFiggans, G., Coe, H., Percival, C. J., and Topping, D.: A method for extracting calibrated volatility information from the FIGAERO-HR-ToF-CIMS and its experimental application, *Atmospheric Measurement Techniques*, 12, 1429-1439, 10.5194/amt-12-1429-2019, 2019.
- Bar-Joseph, Z., Gifford, D. K., and Jaakkola, T. S. J. B.: Fast optimal leaf ordering for hierarchical clustering, 17, S22-S29, 2001.
- Barley, M. H. and McFiggans, G.: The critical assessment of vapour pressure estimation methods for use in modelling the formation of atmospheric organic aerosol, *Atmospheric Chemistry and Physics*, 10, 749-767, 10.5194/acp-10-749-2010, 2010.
- Bateman, A. P., Nizkorodov, S. A., Laskin, J., and Laskin, A.: High-resolution electrospray ionization mass spectrometry analysis of water-soluble organic aerosols collected with a particle into liquid sampler, *Anal Chem*, 82, 8010-8016, 10.1021/ac1014386, 2010.
- Bilde, M., Barsanti, K., Booth, M., Cappa, C. D., Donahue, N. M., Emanuelsson, E. U.,

McFiggans, G., Krieger, U. K., Marcolli, C., Topping, D., Ziemann, P., Barley, M., Clegg, S., Dennis-Smith, B., Hallquist, M., Hallquist, A. M., Khlystov, A., Kulmala, M., Mogensen, D., Percival, C. J., Pope, F., Reid, J. P., Ribeiro da Silva, M. A., Rosenoern, T., Salo, K., Soonsin, V. P., Yli-Juuti, T., Prisle, N. L., Pagels, J., Rarey, J., Zardini, A. A., and Riipinen, I.: Saturation vapor pressures and transition enthalpies of low-volatility organic molecules of atmospheric relevance: from dicarboxylic acids to complex mixtures, *Chem Rev*, 115, 4115-4156, 10.1021/cr5005502, 2015.

Burkholder, J. B., Abbatt, J. P., Barnes, I., Roberts, J. M., Melamed, M. L., Ammann, M., Bertram, A. K., Cappa, C. D., Carlton, A. G., Carpenter, L. J., Crowley, J. N., Dubowski, Y., George, C., Heard, D. E., Herrmann, H., Keutsch, F. N., Kroll, J. H., McNeill, V. F., Ng, N. L., Nizkorodov, S. A., Orlando, J. J., Percival, C. J., Picquet-Varrault, B., Rudich, Y., Seakins, P. W., Surratt, J. D., Tanimoto, H., Thornton, J. A., Tong, Z., Tyndall, G. S., Wahner, A., Weschler, C. J., Wilson, K. R., and Ziemann, P. J.: The Essential Role for Laboratory Studies in Atmospheric Chemistry, *Environ Sci Technol*, 51, 2519-2528, 10.1021/acs.est.6b04947, 2017.

Calvo, A. I., Alves, C., Castro, A., Pont, V., Vicente, A. M., and Fraile, R.: Research on aerosol sources and chemical composition: Past, current and emerging issues, *Atmospheric Research*, 120-121, 1-28, 10.1016/j.atmosres.2012.09.021, 2013.

Chen, Y., Zhang, Y., Lambe, A. T., Xu, R., Lei, Z., Olson, N. E., Zhang, Z., Szalkowski, T., Cui, T., Vizueté, W., Gold, A., Turpin, B. J., Ault, A. P., Chan, M. N., and Surratt, J. D.: Heterogeneous Hydroxyl Radical Oxidation of Isoprene-Epoxydiol-Derived Methyltetrol Sulfates: Plausible Formation Mechanisms of Previously Unexplained Organosulfates in Ambient Fine Aerosols, *Environmental Science & Technology Letters*, 7, 460-468, 10.1021/acs.estlett.0c00276, 2020.

Chhabra, P. S., Ng, N. L., Canagaratna, M. R., Corrigan, A. L., Russell, L. M., Worsnop, D. R., Flagan, R. C., and Seinfeld, J. H.: Elemental composition and oxidation of chamber organic aerosol, *Atmospheric Chemistry and Physics*, 11, 8827-8845, 10.5194/acp-11-8827-2011, 2011.

Claeys, M., Iinuma, Y., Szmigielski, R., Surratt, J. D., Blockhuys, F., Van Alsenoy, C., Boge, O., Sierau, B., Gomez-Gonzalez, Y., Vermeylen, R., Van der Veken, P., Shahgholi, M., Chan, A. W., Herrmann, H., Seinfeld, J. H., and Maenhaut, W.: Terpenylic acid and related compounds from the oxidation of alpha-pinene: implications for new particle formation and growth above forests, *Environ Sci Technol*, 43, 6976-6982, 10.1021/es9007596, 2009.

Cocker, D. R., 3rd, Flagan, R. C., and Seinfeld, J. H.: State-of-the-art chamber facility for studying atmospheric aerosol chemistry, *Environ Sci Technol*, 35, 2594-2601, 10.1021/es0019169, 2001.

Compernelle, S., Ceulemans, K., and Müller, J. F.: EVAPORATION: a new vapour pressure estimation method for organic molecules including non-additivity and intramolecular interactions, *Atmospheric Chemistry and Physics*, 11, 9431-9450, 10.5194/acp-11-9431-2011, 2011.

D'Ambro, E. L., Schobesberger, S., Gaston, C. J., Lopez-Hilfiker, F. D., Lee, B. H., Liu, J., Zelenyuk, A., Bell, D., Cappa, C. D., Helgestad, T., Li, Z., Guenther, A., Wang, J., Wise, M.,

Caylor, R., Surratt, J. D., Riedel, T., Hyttinen, N., Salo, V.-T., Hasan, G., Kurtén, T., Shilling, J. E., and Thornton, J. A.: Chamber-based insights into the factors controlling epoxydiol (IEPOX) secondary organic aerosol (SOA) yield, composition, and volatility, *Atmospheric Chemistry and Physics*, 19, 11253-11265, 10.5194/acp-19-11253-2019, 2019.

Demarque, D. P., Crotti, A. E., Vessecchi, R., Lopes, J. L., and Lopes, N. P.: Fragmentation reactions using electrospray ionization mass spectrometry: an important tool for the structural elucidation and characterization of synthetic and natural products, *Nat Prod Rep*, 33, 432-455, 10.1039/c5np00073d, 2016.

Donahue, N. M., Robinson, A. L., Stanier, C. O., and Pandis, S. N.: Coupled partitioning, dilution, and chemical aging of semivolatile organics, *Environ Sci Technol*, 40, 2635-2643, 10.1021/es052297c, 2006.

Eddingsaas, N. C., Loza, C. L., Yee, L. D., Seinfeld, J. H., and Wennberg, P. O.:  $\alpha$ -pinene photooxidation under controlled chemical conditions – Part 1: Gas-phase composition in low- and high-NO<sub>x</sub> environments, *Atmospheric Chemistry and Physics*, 12, 6489-6504, 10.5194/acp-12-6489-2012, 2012a.

Eddingsaas, N. C., Loza, C. L., Yee, L. D., Chan, M., Schilling, K. A., Chhabra, P. S., Seinfeld, J. H., and Wennberg, P. O.:  $\alpha$ -pinene photooxidation under controlled chemical conditions – Part 2: SOA yield and composition in low- and high-NO<sub>x</sub> environments, *Atmospheric Chemistry and Physics*, 12, 7413-7427, 10.5194/acp-12-7413-2012, 2012b.

Gkatzelis, G. I., Hohaus, T., Tillmann, R., Gensch, I., Müller, M., Eichler, P., Xu, K.-M., Schlag, P., Schmitt, S. H., Yu, Z., Wegener, R., Kaminski, M., Holzinger, R., Wisthaler, A., and Kiendler-Scharr, A.: Gas-to-particle partitioning of major biogenic oxidation products: a study on freshly formed and aged biogenic SOA, *Atmospheric Chemistry and Physics*, 18, 12969-12989, 10.5194/acp-18-12969-2018, 2018.

Goldstein, A. H. and Galbally, I. E.: Known and unknown organic constituents in the Earth's atmosphere, *Environ Sci Technol*, 41, 1514-1521, 10.1021/es072476p, 2007.

Guenther, A. B., Jiang, X., Heald, C. L., Sakulyanontvittaya, T., Duhl, T., Emmons, L. K., and Wang, X.: The Model of Emissions of Gases and Aerosols from Nature version 2.1 (MEGAN2.1): an extended and updated framework for modeling biogenic emissions, *Geoscientific Model Development*, 5, 1471-1492, 10.5194/gmd-5-1471-2012, 2012.

Hallquist, M., Wenger, J. C., Baltensperger, U., Rudich, Y., Simpson, D., Claeys, M., Dommen, J., Donahue, N. M., George, C., Goldstein, A. H., Hamilton, J. F., Herrmann, H., Hoffmann, T., Iinuma, Y., Jang, M., Jenkin, M. E., Jimenez, J. L., Kiendler-Scharr, A., Maenhaut, W., McFiggans, G., Mentel, T. F., Monod, A., Prévôt, A. S. H., Seinfeld, J. H., Surratt, J. D., Szmigielski, R., and Wildt, J.: The formation, properties and impact of secondary organic aerosol: current and emerging issues, *Atmospheric Chemistry and Physics*, 9, 5155-5236, 10.5194/acp-9-5155-2009, 2009.

Hamilton, J. F., Alfarra, M. R., Robinson, N., Ward, M. W., Lewis, A. C., McFiggans, G. B., Coe, H., and Allan, J. D.: Linking biogenic hydrocarbons to biogenic aerosol in the Borneo rainforest, *Atmospheric Chemistry and Physics*, 13, 11295-11305, 10.5194/acp-13-11295-

2013, 2013.

Hammes, J., Lutz, A., Mentel, T., Faxon, C., and Hallquist, M.: Carboxylic acids from limonene oxidation by ozone and hydroxyl radicals: insights into mechanisms derived using a FIGAERO-CIMS, *Atmospheric Chemistry and Physics*, 19, 13037-13052, 10.5194/acp-19-13037-2019, 2019.

Hoyle, C. R., Myhre, G., Berntsen, T. K., and Isaksen, I. S. A.: Anthropogenic influence on SOA and the resulting radiative forcing, *Atmospheric Chemistry and Physics*, 9, 2715-2728, 10.5194/acp-9-2715-2009, 2009.

Huang, W., Saathoff, H., Pajunoja, A., Shen, X., Naumann, K.-H., Wagner, R., Virtanen, A., Leisner, T., and Mohr, C.:  $\alpha$ -Pinene secondary organic aerosol at low temperature: chemical composition and implications for particle viscosity, *Atmospheric Chemistry and Physics*, 18, 2883-2898, 10.5194/acp-18-2883-2018, 2018.

Inuma, Y., Boge, O., Grafe, R., and Herrmann, H.: Methyl-nitrocatechols: atmospheric tracer compounds for biomass burning secondary organic aerosols, *Environ Sci Technol*, 44, 8453-8459, 10.1021/es102938a, 2010.

Inuma, Y., Muller, C., Berndt, T., Boge, O., Claeys, M., and Herrmann, H.: Evidence for the existence of organosulfates from beta-pinene ozonolysis in ambient secondary organic aerosol, *Environ Sci Technol*, 41, 6678-6683, 10.1021/es070938t, 2007.

Isaacman-VanWertz, G., Massoli, P., O'Brien, R. E., Nowak, J. B., Canagaratna, M. R., Jayne, J. T., Worsnop, D. R., Su, L., Knopf, D. A., Misztal, P. K., Arata, C., Goldstein, A. H., and Kroll, J. H.: Using advanced mass spectrometry techniques to fully characterize atmospheric organic carbon: current capabilities and remaining gaps, *Faraday Discuss*, 200, 579-598, 10.1039/c7fd00021a, 2017.

Isaacman-VanWertz, G., Massoli, P., O'Brien, R., Lim, C., Franklin, J. P., Moss, J. A., Hunter, J. F., Nowak, J. B., Canagaratna, M. R., Misztal, P. K., Arata, C., Roscioli, J. R., Herndon, S. T., Onasch, T. B., Lambe, A. T., Jayne, J. T., Su, L., Knopf, D. A., Goldstein, A. H., Worsnop, D. R., and Kroll, J. H.: Chemical evolution of atmospheric organic carbon over multiple generations of oxidation, *Nat Chem*, 10, 462-468, 10.1038/s41557-018-0002-2, 2018.

Isaacman-VanWertz, G., Yee, L. D., Kreisberg, N. M., Wernis, R., Moss, J. A., Hering, S. V., de Sa, S. S., Martin, S. T., Alexander, M. L., Palm, B. B., Hu, W., Campuzano-Jost, P., Day, D. A., Jimenez, J. L., Riva, M., Surratt, J. D., Viegas, J., Manzi, A., Edgerton, E., Baumann, K., Souza, R., Artaxo, P., and Goldstein, A. H.: Ambient Gas-Particle Partitioning of Tracers for Biogenic Oxidation, *Environ Sci Technol*, 50, 9952-9962, 10.1021/acs.est.6b01674, 2016.

Koss, A. R., Canagaratna, M. R., Zaytsev, A., Krechmer, J. E., Breitenlechner, M., Nihill, K. J., Lim, C. Y., Rowe, J. C., Roscioli, J. R., Keutsch, F. N., and Kroll, J. H.: Dimensionality-reduction techniques for complex mass spectrometric datasets: application to laboratory atmospheric organic oxidation experiments, *Atmos Chem Phys*, 20, 1021-1041, 10.5194/acp-20-1021-2020, 2020.

Kristensen, K., Cui, T., Zhang, H., Gold, A., Glasius, M., and Surratt, J. D.: Dimers in  $\alpha$ -pinene secondary organic aerosol: effect of hydroxyl radical, ozone, relative humidity and aerosol



acidity, *Atmospheric Chemistry and Physics*, 14, 4201-4218, 10.5194/acp-14-4201-2014, 2014.

Kroll, J. H. and Seinfeld, J. H.: Chemistry of secondary organic aerosol: Formation and evolution of low-volatility organics in the atmosphere, *Atmospheric Environment*, 42, 3593-3624, 10.1016/j.atmosenv.2008.01.003, 2008.

Kroll, J. H., Donahue, N. M., Jimenez, J. L., Kessler, S. H., Canagaratna, M. R., Wilson, K. R., Altieri, K. E., Mazzoleni, L. R., Wozniak, A. S., Bluhm, H., Mysak, E. R., Smith, J. D., Kolb, C. E., and Worsnop, D. R.: Carbon oxidation state as a metric for describing the chemistry of atmospheric organic aerosol, *Nature Chemistry*, 3, 133-139, 10.1038/nchem.948, 2011.

Laj, P., Klausen, J., Bilde, M., Plaß-Duelmer, C., Pappalardo, G., Clerbaux, C., Baltensperger, U., Hjorth, J., Simpson, D., Reimann, S., Coheur, P. F., Richter, A., De Mazière, M., Rudich, Y., McFiggans, G., Tørseth, K., Wiedensohler, A., Morin, S., Schulz, M., Allan, J. D., Attié, J. L., Barnes, I., Birmili, W., Cammas, J. P., Dommen, J., Dorn, H. P., Fowler, D., Fuzzi, S., Glasius, M., Granier, C., Hermann, M., Isaksen, I. S. A., Kinne, S., Koren, I., Madonna, F., Maione, M., Massling, A., Moehler, O., Mona, L., Monks, P. S., Müller, D., Müller, T., Orphal, J., Peuch, V. H., Stratmann, F., Tanré, D., Tyndall, G., Abo Rizeq, A., Van Roozendaal, M., Villani, P., Wehner, B., Wex, H., and Zardini, A. A.: Measuring atmospheric composition change, *Atmospheric Environment*, 43, 5351-5414, 10.1016/j.atmosenv.2009.08.020, 2009.

Laskin, A., Laskin, J., and Nizkorodov, S. A.: Mass spectrometric approaches for chemical characterisation of atmospheric aerosols: critical review of the most recent advances, *Environmental Chemistry*, 9, 10.1071/en12052, 2012.

Lee, B. H., Lopez-Hilfiker, F. D., Mohr, C., Kurten, T., Worsnop, D. R., and Thornton, J. A.: An iodide-adduct high-resolution time-of-flight chemical-ionization mass spectrometer: application to atmospheric inorganic and organic compounds, *Environ Sci Technol*, 48, 6309-6317, 10.1021/es500362a, 2014.

Lee, B. H., D'Ambro, E. L., Lopez-Hilfiker, F. D., Schobesberger, S., Mohr, C., Zawadowicz, M. A., Liu, J., Shilling, J. E., Hu, W., Palm, B. B., Jimenez, J. L., Hao, L., Virtanen, A., Zhang, H., Goldstein, A. H., Pye, H. O. T., and Thornton, J. A.: Resolving ambient organic aerosol formation and aging pathways with simultaneous molecular composition and volatility observations, *ACS Earth Space Chem*, 4, 391-402, 10.1021/acsearthspacechem.9b00302, 2020.

Lopez-Hilfiker, F. D., Iyer, S., Mohr, C., Lee, B. H., and Ambro, E. L., Kurtén, T., and Thornton, J. A.: Constraining the sensitivity of iodide adduct chemical ionization mass spectrometry to multifunctional organic molecules using the collision limit and thermodynamic stability of iodide ion adducts, *Atmospheric Measurement Techniques*, 9, 1505-1512, 10.5194/amt-9-1505-2016, 2016a.

Lopez-Hilfiker, F. D., Mohr, C., Ehn, M., Rubach, F., Kleist, E., Wildt, J., Mentel, T. F., Lutz, A., Hallquist, M., Worsnop, D., and Thornton, J. A.: A novel method for online analysis of gas and particle composition: description and evaluation of a Filter Inlet for Gases and AEROSols (FIGAERO), *Atmospheric Measurement Techniques*, 7, 983-1001, 10.5194/amt-7-983-2014, 2014.

Lopez-Hilfiker, F. D., Mohr, C., Ehn, M., Rubach, F., Kleist, E., Wildt, J., Mentel, T. F., Carrasquillo, A. J., Daumit, K. E., Hunter, J. F., Kroll, J. H., Worsnop, D. R., and Thornton, J.

A.: Phase partitioning and volatility of secondary organic aerosol components formed from  $\alpha$ -pinene ozonolysis and OH oxidation: the importance of accretion products and other low volatility compounds, *Atmospheric Chemistry and Physics*, 15, 7765-7776, 10.5194/acp-15-7765-2015, 2015.

Lopez-Hilfiker, F. D., Mohr, C., D'Ambro, E. L., Lutz, A., Riedel, T. P., Gaston, C. J., Iyer, S., Zhang, Z., Gold, A., Surratt, J. D., Lee, B. H., Kurten, T., Hu, W. W., Jimenez, J., Hallquist, M., and Thornton, J. A.: Molecular Composition and Volatility of Organic Aerosol in the Southeastern U.S.: Implications for IEPOX Derived SOA, *Environ Sci Technol*, 50, 2200-2209, 10.1021/acs.est.5b04769, 2016b.

Lutz, A., Mohr, C., Le Breton, M., Lopez-Hilfiker, F. D., Priestley, M., Thornton, J. A., and Hallquist, M.: Gas to Particle Partitioning of Organic Acids in the Boreal Atmosphere, *ACS Earth and Space Chemistry*, 3, 1279-1287, 10.1021/acsearthspacechem.9b00041, 2019.

Ma, Y., Russell, A. T., and Marston, G.: Mechanisms for the formation of secondary organic aerosol components from the gas-phase ozonolysis of alpha-pinene, *Phys Chem Chem Phys*, 10, 4294-4312, 10.1039/b803283a, 2008.

Mai, H., Shiraiwa, M., Flagan, R. C., and Seinfeld, J. H.: Under What Conditions Can Equilibrium Gas-Particle Partitioning Be Expected to Hold in the Atmosphere?, *Environ Sci Technol*, 49, 11485-11491, 10.1021/acs.est.5b02587, 2015.

McFiggans, G., Mentel, T. F., Wildt, J., Pullinen, I., Kang, S., Kleist, E., Schmitt, S., Springer, M., Tillmann, R., Wu, C., Zhao, D., Hallquist, M., Faxon, C., Le Breton, M., Hallquist, A. M., Simpson, D., Bergstrom, R., Jenkin, M. E., Ehn, M., Thornton, J. A., Alfarra, M. R., Bannan, T. J., Percival, C. J., Priestley, M., Topping, D., and Kiendler-Scharr, A.: Secondary organic aerosol reduced by mixture of atmospheric vapours, *Nature*, 565, 587-593, 10.1038/s41586-018-0871-y, 2019.

Mehra, A., Wang, Y., Krechmer, J. E., Lambe, A., Majluf, F., Morris, M. A., Priestley, M., Bannan, T. J., Bryant, D. J., Pereira, K. L., Hamilton, J. F., Rickard, A. R., Newland, M. J., Stark, H., Croteau, P., Jayne, J. T., Worsnop, D. R., Canagaratna, M. R., Wang, L., and Coe, H.: Evaluation of the Chemical Composition of Gas and Particle Phase Products of Aromatic Oxidation, *Atmos. Chem. Phys. Discuss.*, 10.5194/acp-2020-161, 2020a.

Mehra, A., Wang, Y., Krechmer, J. E., Lambe, A., Majluf, F., Morris, M. A., Priestley, M., Bannan, T. J., Bryant, D. J., Pereira, K. L., Hamilton, J. F., Rickard, A. R., Newland, M. J., Stark, H., Croteau, P., Jayne, J. T., Worsnop, D. R., Canagaratna, M. R., Wang, L., and Coe, H.: Evaluation of the chemical composition of gas- and particle-phase products of aromatic oxidation, *Atmospheric Chemistry and Physics*, 20, 9783-9803, 10.5194/acp-20-9783-2020, 2020b.

Mentel, T. F., Springer, M., Ehn, M., Kleist, E., Pullinen, I., Kurtén, T., Rissanen, M., Wahner, A., and Wildt, J.: Formation of highly oxidized multifunctional compounds: autoxidation of peroxy radicals formed in the ozonolysis of alkenes – deduced from structure–product relationships, *Atmospheric Chemistry and Physics*, 15, 6745-6765, 10.5194/acp-15-6745-2015, 2015.

Mohr, C., Thornton, J. A., Heitto, A., Lopez-Hilfiker, F. D., Lutz, A., Riipinen, I., Hong, J.,

Donahue, N. M., Hallquist, M., Petaja, T., Kulmala, M., and Yli-Juuti, T.: Molecular identification of organic vapors driving atmospheric nanoparticle growth, *Nat Commun*, 10, 4442, 10.1038/s41467-019-12473-2, 2019.

Müllner, D. J. a. p. a.: *Modern hierarchical, agglomerative clustering algorithms*, 2011.

Mutzel, A., Zhang, Y., Böge, O., Rodigast, M., Kolodziejczyk, A., Wang, X., and Herrmann, H.: Importance of secondary organic aerosol formation of  $\alpha$ -pinene, limonene, and *m*-cresol comparing day- and nighttime radical chemistry, *Atmospheric Chemistry and Physics*, 21, 8479-8498, 10.5194/acp-21-8479-2021, 2021.

Mutzel, A., Poulain, L., Berndt, T., Iinuma, Y., Rodigast, M., Boge, O., Richters, S., Spindler, G., Sipila, M., Jokinen, T., Kulmala, M., and Herrmann, H.: Highly Oxidized Multifunctional Organic Compounds Observed in Tropospheric Particles: A Field and Laboratory Study, *Environ Sci Technol*, 49, 7754-7761, 10.1021/acs.est.5b00885, 2015.

Nel, A.: Atmosphere. Air pollution-related illness: effects of particles, *Science*, 308, 804-806, 10.1126/science.1108752, 2005.

Ng, N. L., Kroll, J. H., Keywood, M. D., Bahreini, R., Varutbangkul, V., Flagan, R. C., Seinfeld, J. H., Lee, A., and Goldstein, A. H.: Contribution of first- versus second-generation products to secondary organic aerosols formed in the oxidation of biogenic hydrocarbons, *Environ Sci Technol*, 40, 2283-2297, 10.1021/es052269u, 2006.

Nguyen, T. B., Bateman, A. P., Bones, D. L., Nizkorodov, S. A., Laskin, J., and Laskin, A.: High-resolution mass spectrometry analysis of secondary organic aerosol generated by ozonolysis of isoprene, *Atmospheric Environment*, 44, 1032-1042, 10.1016/j.atmosenv.2009.12.019, 2010.

Nielsen, F.: *Introduction to HPC with MPI for Data Science*, Springer. pp.2016.

Nizkorodov, S. A., Laskin, J., and Laskin, A.: Molecular chemistry of organic aerosols through the application of high resolution mass spectrometry, *Phys Chem Chem Phys*, 13, 3612-3629, 10.1039/c0cp02032j, 2011.

O'Haver, T.: *A Pragmatic Introduction to Signal Processing With applications in scientific measurement*, 2021.

O'Meara, S., Booth, A. M., Barley, M. H., Topping, D., and McFiggans, G.: An assessment of vapour pressure estimation methods, *Phys Chem Chem Phys*, 16, 19453-19469, 10.1039/c4cp00857j, 2014.

Pankow, J. F.: An absorption model of the gas/aerosol partitioning involved in the formation of secondary organic aerosol, *Atmospheric Environment*, 28, 189-193, 10.1016/1352-2310(94)90094-9, 1994.

Parshintsev, J., Vaikkinen, A., Lipponen, K., Vrkoslav, V., Cvacka, J., Kostianen, R., Kotiaho, T., Hartonen, K., Riekkola, M. L., and Kauppila, T. J.: Desorption atmospheric pressure photoionization high-resolution mass spectrometry: a complementary approach for the chemical analysis of atmospheric aerosols, *Rapid Commun Mass Spectrom*, 29, 1233-1241,

10.1002/rcm.7219, 2015.

Pereira, K. L., Ward, M. W., Wilkinson, J. L., Sallach, J. B., Bryant, D. J., Dixon, W. J., Hamilton, J. F., and Lewis, A. C.: An Automated Methodology for Non-targeted Compositional Analysis of Small Molecules in High Complexity Environmental Matrices Using Coupled Ultra Performance Liquid Chromatography Orbitrap Mass Spectrometry, *Environ Sci Technol*, 55, 7365-7375, 10.1021/acs.est.0c08208, 2021.

Pereira, K. L., Hamilton, J. F., Rickard, A. R., Bloss, W. J., Alam, M. S., Camredon, M., Muñoz, A., Vázquez, M., Borrás, E., and Ródenas, M.: Secondary organic aerosol formation and composition from the photo-oxidation of methyl chavicol (estragole), *Atmospheric Chemistry and Physics*, 14, 5349-5368, 10.5194/acp-14-5349-2014, 2014.

Perry, R. H., Cooks, R. G., and Noll, R. J.: Orbitrap mass spectrometry: instrumentation, ion motion and applications, *Mass Spectrom Rev*, 27, 661-699, 10.1002/mas.20186, 2008.

Priestley, M., Bannan, T. J., Le Breton, M., Worrall, S. D., Kang, S., Pullinen, I., Schmitt, S., Tillmann, R., Kleist, E., Zhao, D., Wildt, J., Garmash, O., Mehra, A., Bacak, A., Shallcross, D. E., Kiendler-Scharr, A., Hallquist, Å. M., Ehn, M., Coe, H., Percival, C. J., Hallquist, M., Mentel, T. F., and McFiggans, G.: Chemical characterisation of benzene oxidation products under high- and low-NO<sub>x</sub> conditions using chemical ionisation mass spectrometry, *Atmospheric Chemistry and Physics*, 21, 3473-3490, 10.5194/acp-21-3473-2021, 2021.

Ren, Y., Grosselin, B., Daele, V., and Mellouki, A.: Investigation of the reaction of ozone with isoprene, methacrolein and methyl vinyl ketone using the HELIOS chamber, *Faraday Discuss*, 200, 289-311, 10.1039/c7fd00014f, 2017.

Reyes-Villegas, E., Bannan, T., Le Breton, M., Mehra, A., Priestley, M., Percival, C., Coe, H., and Allan, J. D.: Online Chemical Characterization of Food-Cooking Organic Aerosols: Implications for Source Apportionment, *Environ Sci Technol*, 52, 5308-5318, 10.1021/acs.est.7b06278, 2018.

Rohrer, F., Bohn, B., Brauers, T., Brüning, D., Johnen, F. J., Wahner, A., and Kleffmann, J.: Characterisation of the photolytic HONO-source in the atmosphere simulation chamber SAPHIR, *Atmos. Chem. Phys.*, 5, 2189-2201, 10.5194/acp-5-2189-2005, 2005.

Rosati, B., Teiwes, R., Kristensen, K., Bossi, R., Skov, H., Glasius, M., Pedersen, H. B., and Bilde, M.: Factor analysis of chemical ionization experiments: Numerical simulations and an experimental case study of the ozonolysis of  $\alpha$ -pinene using a PTR-ToF-MS, *Atmospheric Environment*, 199, 15-31, 10.1016/j.atmosenv.2018.11.012, 2019.

Samy, S. and Hays, M. D.: Quantitative LC-MS for water-soluble heterocyclic amines in fine aerosols (PM<sub>2.5</sub>) at Duke Forest, USA, *Atmospheric Environment*, 72, 77-80, 10.1016/j.atmosenv.2013.02.032, 2013.

Sánchez-López, J. A., Zimmermann, R., and Yeretdzian, C.: Insight into the Time-Resolved Extraction of Aroma Compounds during Espresso Coffee Preparation: Online Monitoring by PTR-ToF-MS, *Analytical Chemistry*, 86, 11696-11704, 10.1021/ac502992k, 2014.

Schwantes, R. H., Schilling, K. A., McVay, R. C., Lignell, H., Coggon, M. M., Zhang, X., Wennberg, P. O., and Seinfeld, J. H.: Formation of highly oxygenated low-volatility products from cresol oxidation, *Atmospheric Chemistry and Physics*, 17, 3453-3474, 10.5194/acp-17-3453-2017, 2017.

Shao, Y., Wang, Y., Du, M., Voliotis, A., Alfarra, M. R., Turner, S. F., and McFiggans, G.: Characterisation of the Manchester Aerosol Chamber facility, *Atmospheric measurement techniques*, 10.5194/amt-2021-147, 2021.

Stark, H., Yatavelli, R. L. N., Thompson, S. L., Kimmel, J. R., Cubison, M. J., Chhabra, P. S., Canagaratna, M. R., Jayne, J. T., Worsnop, D. R., and Jimenez, J. L.: Methods to extract molecular and bulk chemical information from series of complex mass spectra with limited mass resolution, *International Journal of Mass Spectrometry*, 389, 26-38, 10.1016/j.ijms.2015.08.011, 2015.

Stark, H., Yatavelli, R. L. N., Thompson, S. L., Kang, H., Krechmer, J. E., Kimmel, J. R., Palm, B. B., Hu, W., Hayes, P. L., Day, D. A., Campuzano-Jost, P., Canagaratna, M. R., Jayne, J. T., Worsnop, D. R., and Jimenez, J. L.: Impact of Thermal Decomposition on Thermal Desorption Instruments: Advantage of Thermogram Analysis for Quantifying Volatility Distributions of Organic Species, *Environ Sci Technol*, 51, 8491-8500, 10.1021/acs.est.7b00160, 2017.

Thornton, J. A., Mohr, C., Schobesberger, S., D'Ambro, E. L., Lee, B. H., and Lopez-Hilfiker, F. D.: Evaluating Organic Aerosol Sources and Evolution with a Combined Molecular Composition and Volatility Framework Using the Filter Inlet for Gases and Aerosols (FIGAERO), *Acc Chem Res*, 53, 1415-1426, 10.1021/acs.accounts.0c00259, 2020.

Topping, D., Barley, M., Bane, M. K., Higham, N., Aumont, B., Dingle, N., and McFiggans, G.: UManSysProp v1.0: an online and open-source facility for molecular property prediction and atmospheric aerosol calculations, *Geoscientific Model Development*, 9, 899-914, 10.5194/gmd-9-899-2016, 2016.

Voliotis, A., Wang, Y., Shao, Y., Du, M., Bannan, T. J., Percival, C. J., Pandis, S. N., Alfarra, M. R., and McFiggans, G.: Exploring the composition and volatility of secondary organic aerosols in mixed anthropogenic and biogenic precursor systems, *Atmospheric Chemistry and Physics*, 21, 14251-14273, 10.5194/acp-21-14251-2021, 2021.

Wang, D. S. and Hildebrandt Ruiz, L.: Chlorine-initiated oxidation of n-alkanes under high-NO<sub>x</sub> conditions: insights into secondary organic aerosol composition and volatility using a FIGAERO-CIMS, *Atmospheric Chemistry and Physics*, 18, 15535-15553, 10.5194/acp-18-15535-2018, 2018.

Wang, J., Doussin, J. F., Perrier, S., Perraudin, E., Katrib, Y., Pangu, E., and Picquet-Varrault, B.: Design of a new multi-phase experimental simulation chamber for atmospheric photo-smog, aerosol and cloud chemistry research, *Atmospheric Measurement Techniques*, 4, 2465-2494, 10.5194/amt-4-2465-2011, 2011.

Winterhalter, R., Van Dingenen, R., Larsen, B. R., Jensen, N. R., and Hjorth, J.: LC-MS analysis of aerosol particles from the oxidation of  $\alpha$ -pinene by ozone and OH-radicals, *Atmospheric Chemistry and Physics Discussions*, 3, 1-39, 10.5194/acpd-3-1-2003, 2003.

Xu, L., Middlebrook, A. M., Liao, J., de Gouw, J. A., Guo, H., Weber, R. J., Nenes, A., Lopez-Hilfiker, F. D., Lee, B. H., Thornton, J. A., Brock, C. A., Neuman, J. A., Nowak, J. B., Pollack, I. B., Welti, A., Graus, M., Warneke, C., and Ng, N. L.: Enhanced formation of isoprene-derived organic aerosol in sulfur-rich power plant plumes during Southeast Nexus, *Journal of Geophysical Research: Atmospheres*, 121, 11,137-111,153, 10.1002/2016jd025156, 2016.

Yasmeen, F., Szmigielski, R., Vermeylen, R., Gomez-Gonzalez, Y., Surratt, J. D., Chan, A. W., Seinfeld, J. H., Maenhaut, W., and Claeys, M.: Mass spectrometric characterization of isomeric terpenoic acids from the oxidation of alpha-pinene, beta-pinene, d-limonene, and Delta3-carene in fine forest aerosol, *J Mass Spectrom*, 46, 425-442, 10.1002/jms.1911, 2011.

Yli-Juuti, T., Pajunoja, A., Tikkanen, O. P., Buchholz, A., Faiola, C., Vaisanen, O., Hao, L., Kari, E., Perakyla, O., Garmash, O., Shiraiwa, M., Ehn, M., Lehtinen, K., and Virtanen, A.: Factors controlling the evaporation of secondary organic aerosol from alpha-pinene ozonolysis, *Geophys Res Lett*, 44, 2562-2570, 10.1002/2016GL072364, 2017.

Zhang, H., Yee, L. D., Lee, B. H., Curtis, M. P., Worton, D. R., Isaacman-VanWertz, G., Offenberg, J. H., Lewandowski, M., Kleindienst, T. E., Beaver, M. R., Holder, A. L., Lonneman, W. A., Docherty, K. S., Jaoui, M., Pye, H. O. T., Hu, W., Day, D. A., Campuzano-Jost, P., Jimenez, J. L., Guo, H., Weber, R. J., de Gouw, J., Koss, A. R., Edgerton, E. S., Brune, W., Mohr, C., Lopez-Hilfiker, F. D., Lutz, A., Kreisberg, N. M., Spielman, S. R., Hering, S. V., Wilson, K. R., Thornton, J. A., and Goldstein, A. H.: Monoterpenes are the largest source of summertime organic aerosol in the southeastern United States, *Proc Natl Acad Sci U S A*, 115, 2038-2043, 10.1073/pnas.1717513115, 2018.

Zhang, X., McVay, R. C., Huang, D. D., Dalleska, N. F., Aumont, B., Flagan, R. C., and Seinfeld, J. H.: Formation and evolution of molecular products in alpha-pinene secondary organic aerosol, *Proc Natl Acad Sci U S A*, 112, 14168-14173, 10.1073/pnas.1517742112, 2015.

[BLANK PAGE]

## **4.4 Paper 4: Chemical characterization and clustering behaviour of oxidation products generated from the mixed anthropogenic and biogenic VOCs in chamber studies**

**This paper is going to be submitted in the journal of “*Atmospheric Chemistry and Physics*” soon.**

### **4.4.1 Paper introduction**

This paper aims to investigate the chemical composition of SOA in the mixed systems using the online FIGAERO-CIMS and offline LC- Orbitrap MS. This paper is to address the 4<sup>th</sup> objective of this project.

It was found that the major chemical components of the SOA differ from each system. In the gas phase, the compounds in the CHON group accounted for greater fractions in  $\alpha$ -pinene, isoprene,  $\alpha$ -pinene/isoprene,  $\alpha$ -pinene/*o*-cresol and ternary systems, while compounds in the CHO group contributed more in *o*-cresol and *o*-cresol/isoprene, dominated by C<sub>6</sub>-C<sub>7</sub>. The online particle-phase measurements exhibited that the oxidation products were dominated by CHO species in the  $\alpha$ -pinene-containing and *o*-cresol/isoprene systems, whereas the oxidation products were dominated by C<sub>6</sub>-C<sub>7</sub> CHON species in the single *o*-cresol system. The results from the negative mode LC- Orbitrap MS were comparable with those from the online particle-phase measurements in the  $\alpha$ -pinene and  $\alpha$ -pinene/isoprene systems. *o*-cresol containing systems were dominated by the CHON signal fraction (>60%). More compounds with high carbon numbers ( $C \geq 16$ ) were detected in LC- Orbitrap MS positive mode for all systems. Molecular interactions were investigated in the mixed VOC systems, supported by the formation of unique-to-the-mixture products in the gas and particle phases. However, more work is needed to get insight into the mechanisms of such interactions in the mixture.

### **4.4.2 Contribution to the joint authorship**

- (1) Developing the main concept for this paper (90%)
- (2) Carried out the experiments and collected experimental data for all experiments (50%).



(3) Preparation of tables and carried out the data analysis for FIGAERO-CIMS measurements and data visualization (100%)

(4) Carried out the data analysis for LC- Orbitrap MS and data visualization (50%)

(5) Paper writing (90%).

#### **4.4.3 Supplemental information**

Paper 4 is shown below.

# Chemical composition and clustering behaviour of oxidation products generated from the mixed anthropogenic and biogenic VOCs in chamber studies

Mao Du<sup>1</sup>, Aristeidis Voliotis<sup>1</sup>, Yunqi Shao<sup>1</sup>, Yu Wang<sup>1</sup>, Thomas J. Bannan<sup>1</sup>, Kelly L. Pereira<sup>3,†</sup>, Jacqueline F. Hamilton<sup>3</sup>, Carl J. Percival<sup>4</sup>, M. Rami Alfarra<sup>1,3,‡</sup>, Gordon McFiggans<sup>1</sup>

<sup>1</sup>Centre for atmospheric science, Department of Earth and Environmental Science, School of Natural Sciences, The University of Manchester, Oxford Road, M13 9PL, Manchester, UK

<sup>2</sup>National Centre for Atmospheric Science, Department of Earth and Environmental Science, School of Natural Sciences, The University of Manchester, Oxford Road, M13 9PL, Manchester, UK

<sup>3</sup>Wolfson Atmospheric Chemistry Laboratories, Department of Chemistry, University of York, York, YO10 5DD, UK

<sup>4</sup>NASA Jet Propulsion Laboratory, California Institute of Technology, 4800 Oak Grove Drive, Pasadena, CA 91109, USA.

<sup>†</sup>Now at: Department of Life and Environmental Sciences, Bournemouth University, Dorest, BH12 5BB, UK.

<sup>‡</sup> Now at Environment & Sustainability Center, Qatar Environment & Energy Research Institute, 34110, Doha, Qatar

**Correspondence to:** Gordon McFiggans (g.mcfiggans@manchester.ac.uk)

## Abstract

This study reports the results of a series of experiments using anthropogenic VOC (*o*-cresol) and biogenic VOCs ( $\alpha$ -pinene and isoprene) as parent precursors in the presence of NO<sub>x</sub> and seeds designed to investigate the evolution of products formed in the oxidation of mixed VOC systems. Near real-time gaseous and particulate oxidation products were monitored by the online FIGAERO-CIMS instrument and filters sampled at the end of each experiment were characterized by offline LC- Orbitrap MS. The results show that the major chemical components of the SOA differ from each system. In the gas phase, the compounds in the CHON group account for greater fractions in  $\alpha$ -pinene, isoprene,  $\alpha$ -pinene/isoprene,  $\alpha$ -pinene/*o*-cresol and ternary systems, while compounds in the CHO group contribute more in *o*-cresol and *o*-cresol/isoprene, dominated by C<sub>6</sub>-C<sub>7</sub>. The online particle-phase measurements show that the oxidation products are dominated by CHO species in the  $\alpha$ -pinene-containing and *o*-cresol/isoprene systems, whereas the oxidation products are dominated by C<sub>6</sub>-C<sub>7</sub> CHON species in the single *o*-cresol system. The negative mode LC- Orbitrap MS composition is comparable to that from online particle-phase measurements in the  $\alpha$ -pinene and  $\alpha$ -pinene/isoprene systems. However, *o*-cresol containing systems are dominated by the CHON

signal fraction (>60%). More number of compounds with high carbon numbers ( $C \geq 16$ ) is detected in all systems in LC- Orbitrap MS positive mode compared with those from the negative mode and online measurements in those VOC experiments. Gas-phase clustering results illustrate that the time-series profiles of  $\alpha$ -pinene/isoprene are more similar to that in the single  $\alpha$ -pinene experiment, with signal fraction dominated by the rapidly formed CHON species. The temporal profiles of *o*-cresol/isoprene show a high similarity to that in the single *o*-cresol experiment, with the signal dominated by the CHO species initially. The temporal profiles of ternary and  $\alpha$ -pinene/*o*-cresol are complex, neither completely similar to that in single  $\alpha$ -pinene nor *o*-cresol. Molecular interactions are investigated in the mixed systems, supported by the formation of unique-to-the-mixture products in the gas and particle phases. However, more work is needed to get insight into the mechanisms of such interactions in the mixture.

## 1. Introduction

Secondary organic aerosol (SOA) from the oxidation of various volatile organic compounds (VOCs) makes a significant contribution to the total organic aerosols, profoundly impacting air quality, human health and climate (Hallquist et al., 2009; Ipcc, 2013; Poschl, 2005). It is estimated that 10 000 to 100 000 different organic compounds have been measured in the atmosphere (Goldstein and Galbally, 2007). According to their sources, the VOCs can be divided into anthropogenic VOCs (AVOCs) and Biogenic VOCs (BVOCs). AVOCs (e.g., aromatic compounds) are emitted from human activities (e.g., vehicle emissions, industrial activities, biomass burning, etc) (Henze et al., 2008; Forstner et al., 1997). BVOCs, including isoprene, monoterpenes and sesquiterpenes primarily produced from vegetations (~1000 Tg C/yr), vastly outweigh anthropogenic emissions on the global scale (Guenther et al., 2012). Field observations and laboratory experiments showed that oxidation products from either AVOCs or BVOCs precursors initiated by oxidants and their subsequent nucleation or condensation are critical sources of SOA in the atmosphere (Brege et al., 2018; Aljawhary et al., 2016; Claeys et al., 2009; Lopez-Hilfiker et al., 2016; Langford et al., 2010; Chen et al., 2019; Fuzzi et al., 2006). Thus, it is important to understand the SOA formation from AVOCs and BVOCs to help improvements in atmospheric SOA control.

The gas-phase chemistry of VOCs degradation has received considerable attention in the past decades. Generally, the mechanism of the oxidative organic compounds is considered as

three steps which are to be: i) initiated by the H abstraction by OH or chlorine atom or OH addition or NO<sub>3</sub> addition to the unsaturated VOCs; ii) subsequently formed the peroxy radicals (RO<sub>2</sub>) by addition of O<sub>2</sub>; iii) terminated by reactions of these peroxy radicals with one of NO, NO<sub>2</sub>, HO<sub>2</sub> or other RO<sub>2</sub> or even decomposition (Atkinson and Arey, 2003; Hallquist et al., 2009). The oxidation products from AVOCs have been widely explored in laboratory studies (e.g., benzene, toluene and xylene) under different conditions (Ng et al., 2007a; Sato et al., 2007; Borrás and Tortajada-Genaro, 2012; Sato et al., 2017; Hurley et al., 2001). The substituted aromatic hydrocarbons have been recently proved to play important roles in the SOA formation, such as cresol isomers (Schwantes et al., 2017; Mehra et al., 2020; Mutzel et al., 2021). Meanwhile, BVOCs have also been extensively studied in laboratory experiments due to their large SOA formation potentials, such as the most abundant  $\alpha$ -pinene and isoprene (Aschmann, 2002; Ma et al., 2008; Eddingsaas et al., 2012b; Zhang et al., 2015). Fundamental mechanisms of those VOCs have been included in the Master Chemical Mechanism website.

Recently, a class of highly oxygenated organic molecules with extremely low volatilities has been proved to exhibit the potential to the SOA formation (Pye et al., 2019; Zhang et al., 2017; Crouse et al., 2013; Mentel et al., 2015). They have been identified in terpenes (Zhang et al., 2017; Pye et al., 2019; Steimer et al., 2018; Wang et al., 2018) and aromatic precursors (Mehra et al., 2020; Priestley et al., 2021). Those products are generated through autoxidation formation pathway where RO<sub>2</sub> undergoes a few rounds of intramolecular hydrogen-shift and O<sub>2</sub> addition and usually have six or more than six oxygen numbers, defined as HOMs (Bianchi et al., 2019; Crouse et al., 2013). This mechanism is distinct from the traditional atmospheric chemistry (Atkinson, 2000; Atkinson and Arey, 2003). It can be seen because of the various types of oxidations products with distinct structures and functional groups and the complex atmospheric conditions, the detailed oxidation mechanisms are generally insufficiently understood and represented in the atmospheric chemical models, particularly for larger and complex molecules (Goldstein and Galbally, 2007; Spracklen et al., 2011).

Compared to a single VOC precursor, multiple VOCs precursor systems are much less known in the gas-phase chemistry and SOA formation. In those years, there is an increasing interest in the studies of VOCs mixtures via laboratory studies or field observations due to the observed potential interactions in the SOA formation between VOCs emissions (Hoyle et al., 2011; Lee et al., 2016; Kiendler-Scharr et al., 2009; Kanawade et al., 2011). Emanuelsson et

al. (2013) found an anthropogenic enhancement in the volume fraction remaining after adding toluene to a mixture of  $\alpha$ -pinene and limonene. Shilling et al. (2013) showed that anthropogenic and biogenic emissions could enhance organic aerosols production from biogenic species in the field measurements. A few studies found that isoprene could inhibit the new particle formations in forests (Kiendler-Scharr et al., 2009; Kanawade et al., 2011; Lee et al., 2016). Recently, Mcfiggans et al. (2019) demonstrated that isoprene reduces the  $\alpha$ -pinene SOA yields by the scavenging from oxidants and isoprene-derived oxidation products in the mixture, revealing the mechanisms of suppression in the  $\alpha$ -pinene/isoprene mixture. Although progress has been achieved in the mixture studies, to our knowledge, no SOA mixture experiments are carried out to investigate the role of isoprene in the chemical properties of anthropogenic VOCs in the laboratory. There are still many uncertainties in the understanding of the chemical properties of gas-phase and particle-phase oxidation products formed in the mixture.

In this study, the anthropogenic VOCs *o*-cresol, which is from the oxidation of toluene, particularly in anthropogenic polluted areas (Seinfeld and Pandis, 2016), and the abundant biogenic VOCs ( $\alpha$ -pinene and isoprene) (Guenther et al., 2012) are chosen as the VOC precursors. The OH-initiated photooxidation reactions of mixed  $\alpha$ -pinene/isoprene,  $\alpha$ -pinene/*o*-cresol, *o*-cresol/isoprene, ternary ( $\alpha$ -pinene/*o*-cresol/isoprene), and single precursors ( $\alpha$ -pinene, isoprene and *o*-cresol) in the presence of NO<sub>x</sub> were carried out in the Manchester Aerosol Chamber (MAC). The purpose of this study is to i) explore the chemical compositions in the mixed experiments by the combination of online FIGAERO-CIMS and offline LC-Orbitrap MS measurements; ii) to identify the similarities and differences of oxidation products between individual and mixture experiments by hierarchical clustering analysis and explore the controlling factors for their cluster behaviours.

## **2. Materials and methods**

### **2.1 Manchester Aerosol Chamber (MAC) description**

Experiments were performed in the MAC with the 18 m<sup>3</sup> Teflon bag, running as a batch reactor. Details of the chamber facilities and characterization have been described in Shao et al. (2021)). Briefly, two 6 kW Xenon arc lamps (XBO 6000 W/HSLA OFR, Osram) and 5 rows of halogen lamps (Solux 50W/4700K, Solux MR16, USA) were used to simulate the solar spectra over the wavelength range of 290-800 nm (Alfarra et al., 2012). The reported calculated photolysis rate of NO<sub>2</sub> ( $j_{\text{NO}_2}$ ), investigated from the steady-state actinometry experiments, was

$\sim 0.11$ - $0.18 \text{ min}^{-1}$  (Shao et al., 2021). The experimental conditions such as temperature, relative humidity (RH), concentrations of  $\text{NO}_x$  ( $\text{NO}_2$  and  $\text{NO}$ ) and  $\text{O}_3$  can be controlled and continuously monitored in the chamber. The purified air was employed via being filtered and dried by three filters: Purafil (Purafil Inc., USA), charcoal and HEPA (Donaldson Filtration) filters, and a drier (ML180, Munters) before being flushed into the chamber. A high concentration of  $\text{O}_3$  ( $\sim 1 \text{ ppm}$ ) was added into the chamber for overnight oxidation after the contaminants are flushed from the chamber at end of each day experiment, and several fill/flush cycles using purified air were carried out before each experiment to ensure a low chamber background with particle concentrations  $< 15 \text{ particles cm}^{-3}$ , particle mass concentration  $\sim 0 \mu\text{g m}^{-3}$ ,  $\text{O}_3$  concentrations  $\sim 0 \text{ ppb}$  and  $\text{NO}_x$  concentration  $< 10 \text{ ppb}$  ( $\text{NO} < 8 \text{ ppb}$  and  $\text{NO}_2 < 2 \text{ ppb}$ ). Additionally, extra harsh cleaning experiments ( $\text{O}_3$ :  $\sim 1 \text{ ppm}$ ,  $\sim 4$ -hour UV irradiation) were conducted weekly to remove potential contaminants in the chamber.

## 2.2 Experimental design and procedure

Experiments were conducted under modest  $\text{NO}_x$  conditions. The initial OH source was primarily from the photolysis of  $\text{NO}_2$  ( $\text{NO}_2 + \text{O}_2 + \text{M} \rightarrow \text{O}_3 + \text{NO} + \text{M}$ ,  $\text{O}_3 + h\nu \rightarrow \text{O}_2 + \text{O}(^1\text{D})$ ,  $\text{O}(^1\text{D}) + \text{H}_2\text{O} \rightarrow 2\text{OH}$ ) under the irradiation of lamps. No additional  $\text{O}_3$  was added into the chamber initially and the  $\text{O}_3$  was generated from the photolysis of  $\text{NO}_2$  during the experiments. The overview and details about the rational theory of the experimental design can be found in the previous study (Voliotis et. al 2021b, ACPD). Briefly, owing to the fastest rate coefficient of the reaction of OH + isoprene at 298 K and the negligible oxidation products from *o*-cresol ozonolysis, the initial concentrations of *o*-cresol and  $\alpha$ -pinene were designed based on the isoprene OH reactivity (call it iso-reactivity in this study). All experiments were designed under the concept of initial iso-reactivity. To ensure an appreciable SOA mass for offline analysis at the end of each experiment, the initial concentration of isoprene in the single experiment was designed to be higher than that in the ambient (nominal concentration of isoprene as 164 ppb, corresponding to the concentrations of  $\alpha$ -pinene and *o*-cresol 309ppb and 400ppb, respectively). In the binary mixture experiments, the concentrations of parent precursors were half in their single experiments and third in the single experiments for the ternary. Additionally, ammonium sulphate particles were injected as seeds for SOA condensation considering its abundance in the atmosphere (Seinfeld and Pandis, 2016).

The corresponding liquid parent precursors ( $\alpha$ -pinene or isoprene or *o*-cresol; Sigma Aldrich, GC grade  $\geq 99.99\%$  purity) were injected into the cleaned chamber via a heated glass bulb ( $\sim 80\text{ }^\circ\text{C}$ ) and flushed into the chamber by a flow of  $\sim 0.5$  bar nitrogen with electron capture device (ECD grade,  $99.998\%$   $\text{N}_2$ ). Meanwhile,  $\text{NO}_2$  (a self-made cylinder,  $90\%/10\%$  v/v  $\text{N}_2/\text{NO}_2$ ) controlled by a mass flow controller and ammonium sulfate seed particles (Puratronic,  $99.999\%$  purity) generated from the nebulizer (Topaz model ATM 230) were fed into the chamber. The initial concentration of VOCs:  $\text{NO}_x$  ratios range from 4 to 12. The water vapour generated from a custom-built humidifier using ultra-pure water (UP; i.e., the resistivity of  $\geq 18.2\text{ M}\Omega\text{-cm}$ ) was flushed into the chamber to alter the experimental RH conditions. The cooling system (including Air Conditioning, a chiller and recirculating water system) was employed to control the chamber temperature. In all experiments, the temperature and RH in the chamber were controlled at around  $25 \pm 2\text{ }^\circ\text{C}$  and  $50 \pm 5\%$  over the entire experiment. Before initiating the 6-hour reactions, a 1-hour dark stabilization period with the clean air in the chamber was used to measure the chamber background, and another 1-hour dark stabilization period with VOCs and seeds was used to ensure the adequate mixing in the chamber and to measure the injected concentrations of gases (VOC precursors and  $\text{NO}_x$ ) and seed particles. At end of each experiment, the sample was collected through the 47mm embedded filter holder located at the flushing line of the chamber using pre-processed (baked at  $550\text{ }^\circ\text{C}$  for 5.5 hours) filters (Quartz filter:  $2.2\text{ }\mu\text{m}$  pore size) at the flowrate of  $3\text{ m}^3\text{ min}^{-1}$  and stored in a freezer ( $-20\text{ }^\circ\text{C}$ ) for subsequent offline LC- Orbitrap MS data analysis. Several instruments were deployed to monitor the physical and chemical properties of gases (VOCs,  $\text{NO}_x$ ,  $\text{O}_3$  and gas-phase oxidation products) and particles. The details of core instruments used in this study are described in section 2.3. A list of all initial experimental conditions is displayed in Table 1.

**Table 1.** Initial experimental conditions in various single and mixed VOC systems in the presence of ammonium sulphate (AS) seeds.

| Exp. No | VOC (type)                        | VOC (ppb) | VOC/ $\text{NO}_x$ | C(seed) ( $\mu\text{g m}^{-3}$ ) |
|---------|-----------------------------------|-----------|--------------------|----------------------------------|
| 01      | $\alpha$ -pinene                  | 309       | 8.4                | <i>n.a.</i>                      |
| 02      | $\alpha$ -pinene                  | 309       | 7.7                | 60.7                             |
| 03      | $\alpha$ -pinene                  | 309       | 7.2                | 88.4                             |
| 04      | $\alpha$ -pinene (1/2 reactivity) | 155       | 6.2                | 30.1                             |
| 05      | $\alpha$ -pinene (1/3 reactivity) | 103       | 5.7                | 55.4                             |
| 06      | Isoprene                          | 164       | 6.8                | 52.8                             |
| 07      | Isoprene                          | 164       | 7.1                | <i>n.a.</i>                      |
| 08      | <i>o</i> -cresol                  | 400       | 7.1                | 71.4                             |
| 09      | <i>o</i> -cresol                  | 400       | 9.1                | 70.8                             |

|    |   |                  |             |      |
|----|---|------------------|-------------|------|
| 10 | <i>o</i> -cresol (1/2 reactivity)           | 200              | 5.6         | 47.2 |
| 11 | $\alpha$ -pinene + isoprene                 | 237 (155,82)     | 6.1         | 56.6 |
| 12 | $\alpha$ -pinene + isoprene                 | 237 (155,82)     | 9.9         | 50.5 |
| 13 | <i>o</i> -cresol + isoprene                 | 282(200,82)      | 8.3         | 50.7 |
| 14 | $\alpha$ -pinene + isoprene                 | 237 (155,82)     | 7.2         | 66.5 |
| 15 | <i>o</i> -cresol + isoprene                 | 282(200,82)      | <i>n.a.</i> | 59.4 |
| 16 | $\alpha$ -pinene + <i>o</i> -cresol         | 355 (155,200)    | <i>n.a.</i> | 43.0 |
| 17 | $\alpha$ -pinene + <i>o</i> -cresol         | 355 (155,200)    | 11.8        | 64.4 |
| 18 | $\alpha$ -pinene + <i>o</i> -cresol         | 355 (155,200)    | 6.8         | 62.1 |
| 19 | $\alpha$ -pinene/ <i>o</i> -cresol/isoprene | 291 (103/133/55) | 3.6         | 45.6 |
| 20 | $\alpha$ -pinene/ <i>o</i> -cresol/isoprene | 291 (103/133/55) | 4.9         | 49.0 |
| 21 | $\alpha$ -pinene/ <i>o</i> -cresol/isoprene | 291 (103/133/55) | 3.7         | 45.8 |

*Note* <sup>1</sup>All nominal reported initial VOC concentrations have a  $\pm 15\%$  measurement uncertainty. <sup>2</sup>The nominal individual VOC concentration in the binary and ternary mixtures shown in brackets correspond to the precursor VOC listing

<sup>3</sup>*n.a.* represents no available data due to instrument issues.

## 2.3 Instrumentation and data analysis

### 2.3.1 Online FIGAERO-CIMS

A high-resolution time-of-flight iodide chemical ionization mass spectrometer (CIMS) (Lee et al., 2014) coupled with a filter inlet for gas and aerosols (FIGAERO) (Lopez-Hilfiker et al., 2014) was deployed to investigate the gas- and particle-phase chemical composition. The details about the FIGAERO-CIMS are provided in previous studies (Reyes-Villegas et al., 2018; Bannan et al., 2019). The experimental setup was described in the previous study (Du et al. 2021, AMTD). Briefly, this instrument was operated at a  $\sim 4000$ (Th/Th) resolving power in this study. Reagent ions were generated by flowing a mixture of CH<sub>3</sub>I and ultra-high purity nitrogen (UHP, 99.999% purity, N<sub>2</sub>) through a Po-210 source. The gas was sampled through a piece of 0.5 m length  $\frac{1}{4}$  I.D. PFA tubing from the chamber at a flow rate of 1 standard litre per minute (slpm) from one inlet, meanwhile, the particles were collected onto a polytetrafluoroethylene filter (PFTE, Zefluor, 2.0  $\mu$ m pore size) through a tube (a 0.5 m  $\frac{1}{4}$  I.D) at a flowrate 1 slpm from the FIGAERO.

During the 6-hour photooxidation reactions, each experiment experienced six gas- and particle-phase measurements cycles, of which each cycle consists of 30-min gas-phase measurement (collecting particles simultaneously in this period) and 35-min particle-phase measurement (15-min ramp to  $\sim 200$  °C, 10-min holding period at this temperature and 10-min cooling down to the room temperature). Additionally, two more additional gas- and particle phases cycles were performed before the onset of the 6-hour photooxidation. The first cycle



was carried out in the cleaned chamber condition, and the second cycle was conducted after all species (VOC, NO<sub>x</sub>, and seed particles) were injected (1-hour dark stabilization period mentioned in 2.2). Gas-phase data collected in the first cycle are considered as the chamber background. To remove the influence of seeds, the particle data collected in the second cycle are considered as the particle-phase chamber background. The instrument was flushed with UHP N<sub>2</sub> for 0.2 min every 2 min during each gas-phase measurement, acting as the gas-phase instrumental background. The signal in the first 60-90s in the 15-min ramp period with relatively low and stable signals was considered as the instrumental background for the particle phase (Voliotis et al., 2021).

Data analysis of online FIGAERO-CIMS was performed on the Tofware package (version 3.1.0) based on the Igor Pro 7.08 environment (Stark et al., 2015). The detailed data analysis was described in the previous study (Du et al. 2021, AMTD). Briefly,  $m/z$  in the range of 200-550 was chosen to observe the oxidation products as signals in this range contribute more than 80% of the total signals (exclude the reagent ions, I<sup>-</sup>, IH<sub>2</sub>O<sup>-</sup>, I<sub>2</sub><sup>-</sup> and I<sub>3</sub><sup>-</sup>). Mass spectra were mass calibrated firstly, after which the high-resolution peaks were fit via the multi-peak fitting algorithm. The exact mass of the multiple peaks is then matched with the most likely elemental formula, within trusted mass errors  $\pm 6$  ppm. Assigned peaks were fitted through the iterative peak assignment method outlined in Stark et. al (Stark et al., 2015). All identified molecular formulae were thereafter expressed as C<sub>x</sub>H<sub>y</sub>O<sub>z</sub>N<sub>m</sub>.

The pure signals of identified ions in the gas and particle phases were obtained by post-processing in *MATLAB* code, subtracting the corresponding chamber background and instrumental background values for each peak. For each gas phase, the averaged gas-phase measurement signal of ion  $i$  was corrected by removing the averaged values from the chamber background and instrumental background period. For each particle phase, all measured signals were corrected by subtracting the average instrumental background value of each ion (first 60-90s in the 15-min ramp period), after which the temperature of ion counts  $i$  was integrated to get the peak area for each ion. Due to the difficulties in calibrating all identified ions, we assume the uniform sensitivity of each identified ion and normalize it to total identified signals to express the relative contribution of an ion (Wang and Hildebrandt Ruiz, 2018; Chen et al., 2020). Eventually, around 85% of the high-resolution peaks have been assigned with proper formulae, with the residual signal of the unidentified signals being either the result of poor

signal to noise (30-50% with  $S/N \leq 2$ ) or inaccessible formulae within in trust error, resulting in difficulty in identification. Since the same peak list is used for the same type of experiments, the normalised fractional CIMS signal for the repeat experiments can be reported as averages along with the associated variability (as in Figures 1) or as values from one representative experiment without variability.

To further observe the temporal evolution of the gas-phase and particle-phase chemistry, the corrected dataset undergoes hierarchical clustering analysis (HCA), which merges the compounds into different clusters according to their similar time-series behaviour observed from the online CIMS measurements. Details about this method are introduced in previous studies (Koss et al., 2020; Du et al., 2021). Briefly, to focus on observing the time-series trends of each ion and remove the effect of the differences caused by the absolute signals, all time-series measurements are normalized to the highest signal for each ion. Then, the Euclidean distance is employed to calculate the distance between each pair of points of ion A and ion B, after which the average linkage criterion is chosen to cluster the sets of measurements. Thus, this method is independent of calibration and only considers the time-series trends.

### **2.3.2 Offline LC- Orbitrap MS**

Ultra-performance liquid chromatography ultra-high resolution mass spectrometry (Dionex 3000, Orbitrap QExactive, Thermo Fisher Scientific) (LC- Orbitrap MS) was deployed for offline analysis of collected filters. The sample preparation and operation methods of the LC- Orbitrap MS technique have been reported in the studies (Du et al., 2021, AMTD). Briefly, a sample filter being cut into small pieces was transferred into a cleaned and dry extraction vial. Then, 4ml methanol was added to the vial, left at room temperature for 2h before 30-min sonication. After that, the extracted solution was filtered into another cleaned vial via a 0.22  $\mu\text{m}$  filter (Thermo Fisher Scientific) by a syringe (1mL, BD PLASTIC PAK, STERILE). This solution was evaporated to dryness using a vacuum solvent evaporator (Biotage, Sweden). Finally, the dried sample was reconstituted to prepare for LC- Orbitrap MS analysis by adding in a solution with 1ml of 10:90 methanol (A): water (B) (optima orbitrap LC-MS grade water, Thermo Fisher Scientific) solution.

Data were analyzed by a conventional approach, containing fragments and structural information of targeted compounds using the XCalibur software 4.3, and a recent self-customed automated approach which was detailed in the previous study (Pereira et al., 2021).

Briefly, molecular formulae assignments were allowed unlimited C, H, O atoms, up to 2 S atoms and 5 N atoms, plus  $> 2$  Na atoms and 1 K atom in positive ionization mode. Only compounds with a mass error  $< 3$  ppm and signal-to-noise ratio  $> 3$ , the hydrogen-to-carbon ratio of 0.5 to 3 and the oxygen-to-carbon ratio of 0.05 to 2 were included in the data set. Any compounds detected in the procedural (control sample, *i.e.*, blank pre-conditioned filter subjected to the same extraction procedure) and solvent blanks (instrumental blanks) with the same molecular formula and a retention time difference within 0.1 min were removed from the sample data. Furthermore, any compounds detected in the chamber background filter with the same molecular formula and a retention time difference within 0.1 min and the ratio of signal intensities between the sample data and chamber background lower than 3 were removed from the sample data. Same with online FIGAERO-CIMS measurements, it is impractical to quantify all identified compounds using standards, so all compounds were normalized to the total signals to express the relative contribution, implicitly ignoring differential sensitivity in comparison between the two instruments.

The peak list for the LC-Orbitrap MS is not identical for all experiments since some peaks were not detected in all experiments. The uncertainty as to whether such peaks are truly representative of particle-phase oxidation products is captured by classifying the peaks as “confident” (can find in all repeat experiments) and “inconclusive” (in one specific experiment or appear in two of all experiments) and then by expressing their contribution on average across the experiments with the uncertainty across each in Figure 2.

### 2.3.3 Elemental grouping of compounds

To visualize the fractional contribution of those oxidation products to the SOA, the identified molecules from the online and offline measurements were divided into four groups according to their elements C, H, N, O, and S: CHO, CHON, CHOS and CHONS. The molecules are further split into seven groups by the carbon number: C<sub>2</sub>-C<sub>3</sub>, C<sub>4</sub>-C<sub>5</sub>, C<sub>6</sub>-C<sub>7</sub>, C<sub>8</sub>-C<sub>10</sub>, C<sub>11</sub>-C<sub>15</sub>, C<sub>16</sub>-C<sub>20</sub>, and C<sub>>=21</sub>. Note that S-containing compounds are not attributed to the online CIMS measurements within the trusted error ( $\pm 6$ ppm) in this study. Previous studies also showed difficulty in the identification of isoprene-derived organosulfur compounds from CIMS measurements unambiguously due to the low mass resolution of the instrument or thermal desorption of organosulfur compounds (Xu et al., 2016; D'ambro et al., 2019).

## 3. Results

## 3.1 Overview of gas-phase and particle-phase species

### 3.1.1 $\alpha$ -pinene and $\alpha$ -pinene/isoprene

In the  $\alpha$ -pinene,  $\frac{1}{2}$  reactivity  $\alpha$ -pinene and  $\frac{1}{3}$  reactivity  $\alpha$ -pinene single precursor experiments (see left panels of Fig 1a, 1b and 1c), the compounds in the CHON species show slightly higher signal fractions than those in the CHO species for the gas-phase oxidation products. Compounds with C<sub>8-10</sub> and C<sub>6-7</sub> in the CHO and CHON groups make almost equal contributions in the three systems, with greater than 80% of the total signal. In the  $\alpha$ -pinene/isoprene system, a large percentage of the signal in the CHO ( $\sim 10\% \pm 1.1\%$ ) and CHON ( $34\% \pm 1.8\%$ ) groups are from C<sub>4-5</sub> compounds (e.g., C<sub>5</sub>H<sub>10</sub>O<sub>3</sub>, C<sub>5</sub>H<sub>9</sub>NO<sub>4</sub> and C<sub>5</sub>H<sub>7</sub>NO<sub>6</sub>), indicative of the fractional contribution of isoprene oxidation products.

From the CIMS particle-phase measurements (see right panels of Fig 1a, 1b and 1c), compounds in the CHO group play a dominant role in all identified compounds, dominated by the C<sub>8-10</sub> ions. In the  $\alpha$ -pinene/isoprene, a lower fraction of compounds in the CHO species are detected than that in the  $\alpha$ -pinene or  $\frac{1}{2}$  reactivity  $\alpha$ -pinene system ( $\sim 73\% \pm 1.2\%$ , 73%, 52%  $\pm 5.2\%$  to the total signals for the  $\alpha$ -pinene,  $\frac{1}{2}$  reactivity  $\alpha$ -pinene and mixture, respectively), whereas a higher fraction of CHON species is investigated in the mixture ( $\sim 26\% \pm 1.2\%$ , 27%, 43%  $\pm 5.2\%$  to the total signals for the  $\alpha$ -pinene,  $\frac{1}{2}$  reactivity  $\alpha$ -pinene and mixture, respectively). Compared to the gas phase, more compounds with nC<sub>>10</sub> are detected in the particle phase in the three systems.

The results of confident compounds from the offline negative mode show comparable with the online particle-phase measurements in the  $\alpha$ -pinene,  $\frac{1}{2}$  reactivity  $\alpha$ -pinene and  $\alpha$ -pinene/isoprene (Fig 2a, 2b and 2f), although more numbers of compounds with higher carbon number compounds (nC<sub>≥16</sub>) are investigated from the offline measurements (see Figure S1 and S2). The results from the positive mode provide that more numbers of compounds with high carbon numbers (nC<sub>≥16</sub>) are detected in the CHON group either in the confident compounds or inconclusive category, although those inconclusive compounds may have resulted from uncertain factors (e.g., experimental differences, data processing, etc).

### 3.1.2 Isoprene

In the gas phase (left panel of Figure 1f), compounds with C<sub>4-5</sub> in the CHO and CHON groups make large contributions in the isoprene system, accounting for  $\sim 92 \pm 3.8\%$  of the total signal. A large percentage of C<sub>4-5</sub> compounds are detected in each of the CHO (e.g., C<sub>5</sub>H<sub>10</sub>O<sub>2,3</sub>, C<sub>5</sub>H<sub>8</sub>O<sub>3</sub>, etc) and CHON (e.g., C<sub>5</sub>H<sub>9</sub>NO<sub>4</sub>, C<sub>5</sub>H<sub>7</sub>NO<sub>6</sub>, C<sub>5</sub>H<sub>10</sub>NO<sub>3</sub>, etc) categories. The results are indicative of the extent of gas-phase photooxidation in the isoprene system under our experimental conditions.

The amount of SOA particle mass formed in the isoprene system was not significantly above the background mass in the chamber and, under our neutral seeded experiments, the isoprene particle mass yield was not found to be statistically significantly above zero in any experiment. Nevertheless, a sufficient mass of individual components could be collected on the FIGAERO and LC-Orbitrap MS filters in every isoprene experiment to confidently attribute them to the isoprene system when they were not observed on the filters from background experiments.

In the particle phase from the CIMS particle measurements (right panel of Figure 1f), oxidation products in the single isoprene system are dominated by compounds with nC<sub>≤5</sub> in the CHO group. The presence of small compounds with only 2 or 3 carbon atoms in the particle phase is difficult to explain, owing to their likely high volatility, and they are therefore likely to result from the decomposition of compounds with a higher molecular weight (Lopez-Hilfiker et al., 2016) during the thermal desorption.

From the offline LC-orbitrap MS (Fig 2e), compounds confidently attributed to isoprene products account for  $\sim 21\% \pm 2.8\%$  in the negative mode and  $12\% \pm 3.2\%$  in the positive mode. In the “confident” peaklist,  $\sim 74.8\% \pm 2.1\%$  of signals compose of nC<sub>5</sub> for negative mode, primarily from the CHO species. More compounds with high carbon number compounds (nC<sub>≥8</sub>) are detected in the positive mode, either in the “confident” peaklist or “inconclusive” peaklist (see Figure S2e).

### 3.1.3 *o*-cresol and *o*-cresol/isoprene

Gas-phase oxidation products in the *o*-cresol (left panel of Fig 1d) and ½ reactivity *o*-cresol (left panel of Fig 1e), are dominated by CHO species. The larger signal fraction is from compounds with 6 and 7 carbon numbers, with the highest contribution compound being C<sub>7</sub>H<sub>8</sub>O<sub>2</sub> which is a major first-generation product from the *o*-cresol and OH reaction

(Schwantes et al., 2017). In the *o*-cresol/isoprene system, as shown in Fig 1h, compounds with  $nC_{4-5}$  in the CHO and CHON groups (e.g.,  $C_5H_{10}O_3$ ,  $C_5H_9NO_4$  and  $C_5H_7NO_6$ ) make large contributions, accounting for  $\sim 58\% \pm 4.2\%$  to the total signal, suggesting a substantial signal contribution of isoprene derived oxidation products.

In the particle phase from the CIMS particle measurements, the compounds are dominated by the CHON species with a larger fraction from the compounds with  $C_{6-7}$ . In the *o*-cresol and  $\frac{1}{2}$  reactivity *o*-cresol (Fig 1d and 1e right panels), product  $C_7H_7NO_4$  makes greater signal contributions to the products with 6 to 7 carbon numbers. In the *o*-cresol/isoprene system, as shown in Fig 1h, a higher signal fraction of compounds with  $C_{11-15}$  in the CHO group and with  $C_{4-5}$  in the CHON group are observed compared with those in the single *o*-cresol systems.

The results from LC-Orbitrap MS negative mode (left panels of Fig 2c, 2d and 2g) show that larger signal fractions are from CHON species ( $>85\%$  of the total signals for the three systems), with most of them from the products  $C_7H_7NO_4$  and  $C_7H_7NO_3$ . This observation may hint at the over-reliance of nitrophenol on the negative ionisation mode of LC-Orbitrap MS (John D. Roberts, 1977). In the positive mode (left panels of Fig 2c, 2d and 2g), more numbers of compounds with higher carbon numbers ( $nC \geq 16$ ) are investigated in those systems compared to the negative mode (Figure S3). A significantly higher fraction of compounds with  $nC \geq 21$  is detected in the positive mode in the  $\frac{1}{2}$  reactivity *o*-cresol.

### 3.1.4 $\alpha$ -pinene/*o*-cresol

In the gas phase (left bars of Figure 1i), CHON species exhibit a higher signal fraction than those in the CHO species ( $\sim 56\% \pm 1.2\%$  vs  $44\% \pm 1.8\%$ ), with a great fraction from the  $nC_{6-7}$  in both groups and a second higher fraction from compounds with  $nC_{8-10}$ . Compounds with  $nC_{8-10}$  such as  $C_9H_{14}O_4$ ,  $C_8H_{12}O_{4-5}$ ,  $C_{10}H_{14-16}O_{3-5}$ , from  $\alpha$ -pinene derived oxidation products and monomers ( $C_{6-7}$ ) from the *o*-cresol oxidation products such as  $C_7H_8O_2$ ,  $C_7H_7NO_3$  and  $C_7H_8O_{3-5}$  are detected in the CHO species. The online particle-phase measurements show that CHO species dominate the signal, with a greater fraction from  $nC_{8-10}$ . The CHON group is dominated by compounds with  $nC_{6-7}$  (such as  $C_7H_7NO_4$ ), which are likely produced from the *o*-cresol oxidation products.

Similar to other *o*-cresol containing systems, the offline LC-orbitrap MS negative mode measurements show a greater signal fraction in the CHON species ( $\sim 92\% \pm 1.1\%$  to total signal),

as shown in Fig 2h. A higher fraction of compounds with  $nC \geq 16$  in the CHON group is detected in the positive mode compared to that in the individual  $\alpha$ -pinene and *o*-cresol systems.

### 3.1.5 $\alpha$ -pinene/*o*-cresol/isoprene (Ternary)

In Fig 1j, gas-phase oxidation products are dominated by CHON species ( $\sim 70\% \pm 1.2\%$  to the total signal), with a higher fraction in the products with  $nC_{4-5}$  and an almost equal fraction for compounds with  $nC_{6-7}$  and  $nC_{8-10}$ . The CHO group contains more compounds with  $nC_{4-5}$  and  $nC_{8-10}$ .

In the online particle-phase measurements, products in the CHO group dominate all the oxidation products ( $\sim 54\% \pm 1.1\%$  to the total signal), with the highest signal fraction in the  $C_{8-10}$  group and the second-highest fraction from products with  $nC_{4-5}$ . A small fraction ( $\sim 5\% \pm 0.8\%$ ) of compounds with  $nC_{6-7}$  are detected in the CHO group. Products with  $nC_{6-7}$  and  $nC_{8-10}$  make almost equal contributions to the CHON species.

From the offline measurements, as shown in Fig 2i, a large fraction of compounds in the CHON species ( $\sim 59\% \pm 3.8\%$ ) is also observed in the negative mode, although it shows a lower signal fraction than those in other *o*-cresol containing systems.  $\sim 20\% \pm 2.1\%$  of the total signal are found in the CHO group, most of them with  $nC_{8-10}$ . A higher fraction of products with  $nC \geq 16$  in the CHON group is observed in the positive mode.

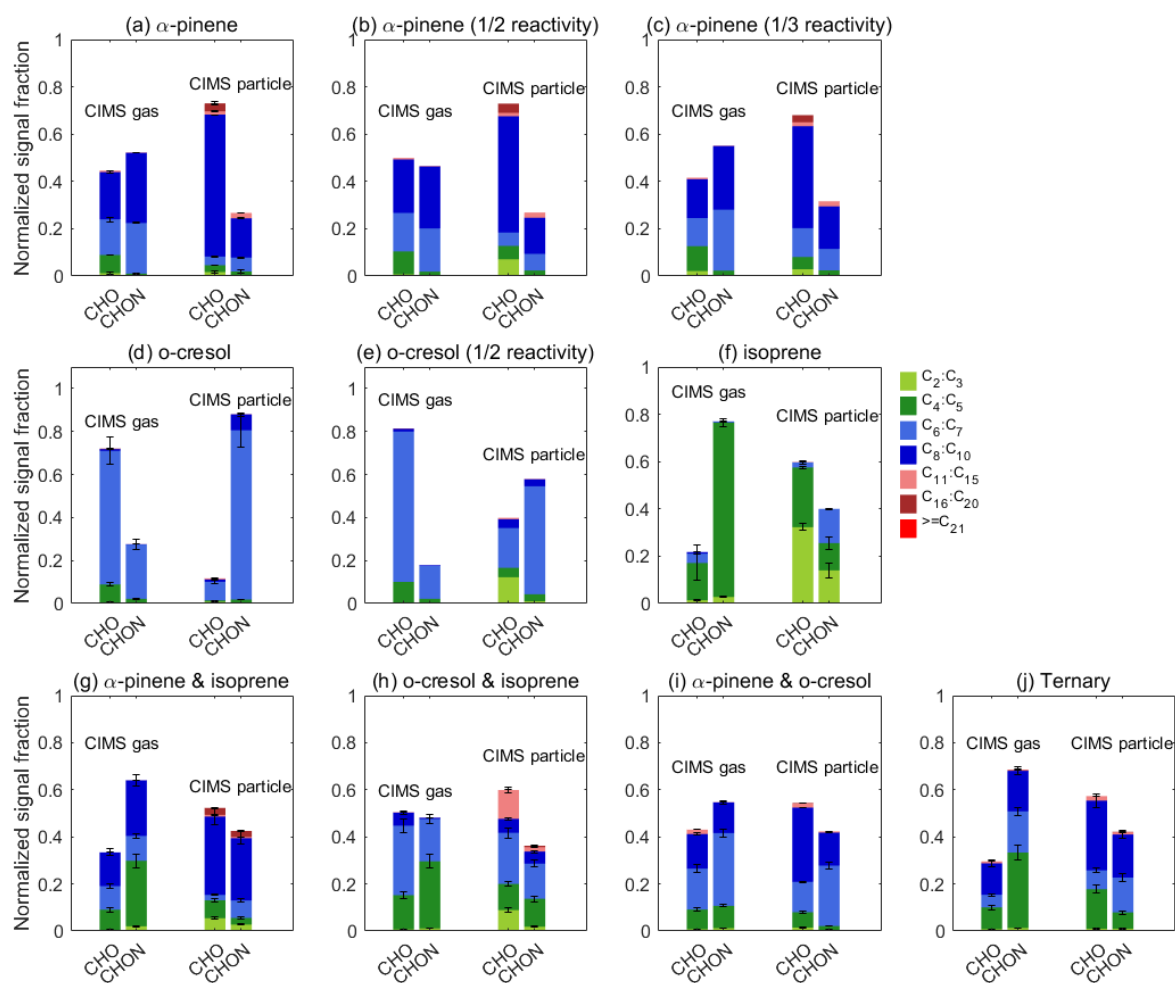


Figure 1. Elemental groups from online FIGAERO-CIMS. Left panels of each subplot are the gas-phase components detected by CIMS gas-phase measurements. The right panels of each subplot are the particle-phase components detected by CIMS particle-phase measurements. Standard deviations are indicated by error bars ( $n=2$  or  $3$ ) for the repeated experiments. Note that results for  $\frac{1}{2}$  reactivity  $\alpha$ -pinene and *o*-cresol, and  $\frac{1}{3}$  reactivity  $\alpha$ -pinene are from one experiment due to no repeated experiments performed.



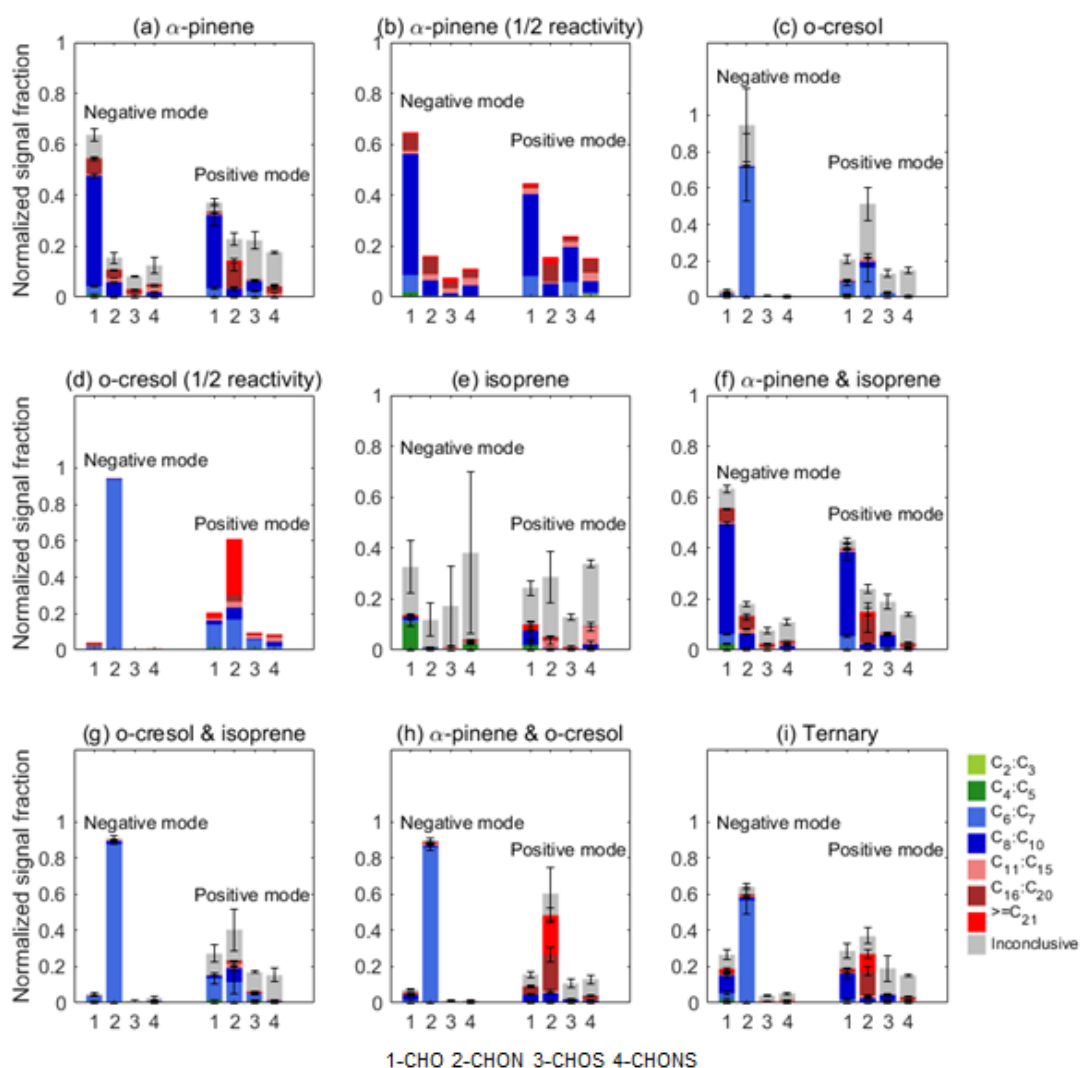


Figure 2. Elemental groups from orbitrap LC- Orbitrap MS negative mode and positive mode measurements. Left panels of each subplot are from the negative mode measurements. The right panels of each subplot are for positive mode measurements. Note that results for  $\frac{1}{2}$  reactivity  $\alpha$ -pinene and  $\frac{1}{2}$  reactivity *o*-cresol are from one experiment due to no repeated experiments performed.  $\frac{1}{3}$  reactivity  $\alpha$ -pinene is not available owing to a lack of background corrections. Standard deviations are indicated by error bars ( $n=2$  or  $3$ ) for the repeated experiments.

### 3.2 Clustering behaviour of oxidation products from FIGAERO-CIMS

The HCA clustering of the top 100 gas-phase and particle-phase oxidation products (accounting for  $> 90\%$  of all identified compounds signals) in all systems are presented in Figure 3 to Figure 12. The numbers of cluster are determined based on whether the averaged time-series trends between clusters are separated well for each experiment. Here, five clusters are chosen for gas-phase analysis and six clusters are selected for particle phase for those systems in this study. It can be seen there are good separations between clusters in terms of average time-series trends.

The generated cluster name from the *MATLAB* code is different among experiments, even though the time-series trends are similar between experiments. In order to compare between single precursor and mixed systems easily, in the gas phase, the time-series trends of  $\alpha$ -pinene are taken as the reference for the half reactivity  $\alpha$ -pinene,  $\alpha$ -pinene/isoprene and  $\alpha$ -pinene/*o*-cresol systems due to their high similarity in the time-series trends. The time-series trends of *o*-cresol are considered as the benchmark for half *o*-cresol and *o*-cresol/isoprene systems. The original cluster names of isoprene and ternary are retained, as their temporal profiles differ from any other system. In the particle-phase HCA, the cluster fractions of single  $\alpha$ -pinene are considered as references for other systems, since the particle-phase time-series trends exhibit lower time resolution (30 min) and greater uncertainties resulting from the use of only six values for each ion in the particle-phase HCA. Gas-phase and particle-phase HCA results for  $\alpha$ -pinene have been discussed extensively in Du et.al (2021) which are shown in the SI here.

### 3.2.1 Gas-phase hierarchical clustering analysis (HCA)

#### 3.2.1.1 Isoprene

In the gas phase HCA, cluster 4 with 21 compounds displays the fastest formation rate and time-series trend continuously increases over time (see Fig 3a). 9 of the 21 compounds are in the CHO category, on average across the experiment comprising 8.6% of the signal and 12 in the CHON comprising an average of 0.9 %, as shown in Fig 3c and 3d. Cluster 4 shows the lowest average oxygen number of all clusters, as probably expected from early-generation products. Cluster 5 exhibits the second-fastest formation rate, with a continuous rise over time, containing 39 ions, 19 in the CHO category (average 6.6% of the signal) and 20 CHON compounds (with an average of 48% of the signal). The nitrogen-containing ions (e.g.,  $C_5H_9NO_4$ ,  $C_4H_7NO_4$ , etc) dominating the cluster 5 signal are produced from the reactions of  $RO_2 + NO_2$  or  $RO_2 + NO$  under the high  $NO_x$  conditions (Paulot et al., 2009; Jenkin et al., 2015). Compounds with  $nC_{4-8}$  in the CHO group appear in this cluster, suggesting the reaction of  $RO_2 + HO_2$  involved simultaneously (Jenkin et al., 2015). Cluster 2 exhibits a slower formation rate, with continuous growth over time, and includes 10 CHO and 11 CHON compounds comprising an average of 3.6% and 12.6% of the signal respectively. Nitrogen-containing compounds with two nitrooxy groups (e.g.,  $C_5H_8N_2O_6$  and  $C_5H_8N_2O_7$ ) appear in this cluster. The average carbon number and oxygen number are 4.76 and 6, respectively, suggesting compounds of this cluster have undergone more fragmentation. Cluster 1 has the slowest formation rate, composed of

compounds with  $nC \leq 5$  and comprising 17 compounds (5 CHO with an average 4.6% of the signal and 12 products CHON with 14.4 % of the signal). The higher average oxygen numbers in cluster 1 and cluster 2 may reflect an increase in the degree of oxidation of the products.

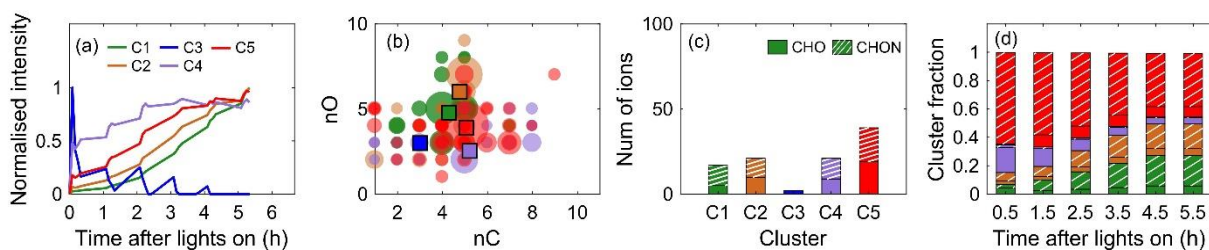


Figure 3. Hierarchical clustering of gas-phase oxidation products in the isoprene system. (a) The average time series of each cluster. Each ion is normalized to the highest intensity itself. (b) Carbon number vs oxygen number. The mean values are marked as squares. (c) The number of ions in each cluster. (d) the sum of ions' signal fractions in each cluster. The color scheme is the same as in (a). In (c) and (d), shaded areas and no shaded area represent ions in the CHON group and CHO group, respectively, with the same meaning in the following figures for the clustering results.

### 3.2.1.2 $\frac{1}{2}$ reactivity $\alpha$ -pinene and $\alpha$ -pinene/isoprene

The overall time series trends of  $\alpha$ -pinene/isoprene (Fig 4 e) are similar to that in the  $\frac{1}{2}$  reactivity  $\alpha$ -pinene (Fig 4 a), although there are different  $\text{NO}_2$ : NO ratios and number of ions in the corresponding cluster between the two systems. In both systems, cluster 4 shows the most rapidly to the peak value with a steeper decrease after reaching the maximum. This cluster contains 1 CHON ion ( $\text{C}_{10}\text{H}_{15}\text{NO}_8$ ) with  $\sim 2\%$  of total signal in the  $\frac{1}{2}$  reactivity  $\alpha$ -pinene and 2 CHON plus 1 CHO ions with a maximum  $\sim 8\%$  in the mixture. Cluster 5 exhibits the second-fastest rate to peak, with a less extent decrease after reaching the maximum (see Fig 4a and 4b). This cluster is composed of 7 CHO ions with an average of 6.4% and 11 CHON ions with an average of 26% of the total signal in the  $\frac{1}{2}$  reactivity  $\alpha$ -pinene system, while it includes 3 CHON ions with an average of 3% in the  $\alpha$ -pinene/isoprene mixture, expected of the early-generation products. Cluster 5 overlaps with cluster 4 initially but they show good separation after 1-hour reactions in the  $\alpha$ -pinene/isoprene experiment.

Cluster 3 shows the third rate to peak value after the onset of photooxidation, expected of the later-generation products. In the  $\alpha$ -pinene/isoprene, the time-series trend of cluster 3 initially overlaps with that in cluster 4 and cluster 5 but they separate well after 1-hour reactions

owing to distinct decreasing trends. Cluster 3 includes most of the ions, with 41 products (24 CHO ions and 17 CHON ions comprising an average of 6.5% and 27.4% of the signal respectively) in the  $\frac{1}{2}$  reactivity  $\alpha$ -pinene system and 45 products (16 CHO comprising an average of 6.9% and 29 CHON compounds with 48.6% of the signal) in the  $\alpha$ -pinene/isoprene system. CHO and CHON species are dominated by C<sub>8-10</sub> and nC<sub>9-10</sub> with lower carbon numbers, respectively. A low signal fraction of products (~6%) is detected as the unique compounds to the mixture system, as shown in Fig 4i. Ions, such as C<sub>9</sub>H<sub>13</sub>NO<sub>6</sub>, C<sub>10</sub>H<sub>16</sub>NO<sub>6</sub>, C<sub>10</sub>H<sub>15</sub>NO<sub>7</sub> in cluster 5 of individual  $\alpha$ -pinene are found in cluster 3 of the  $\alpha$ -pinene/isoprene system. Isoprene-derived compounds (e.g., C<sub>5</sub>H<sub>9</sub>NO<sub>4</sub>, C<sub>5</sub>H<sub>10</sub>O<sub>3</sub> and C<sub>5</sub>H<sub>7</sub>NO<sub>6</sub>) (Carlton et al., 2009) appear in this cluster in the mixture, resulting in a lower averaged carbon number in the mixture compared with that in the individual  $\alpha$ -pinene.

Cluster 2 exhibits the fourth rate to peak with continuous growth over time. This cluster contains 39 products (28 CHO species with an average of 19.9 % and 11 CHON with an average of 5.8% to the total signals) in the  $\frac{1}{2}$  reactivity  $\alpha$ -pinene and 47 products (22 CHO species and 25 CHON with an average of 14.6% and 17.6% to the total signals, respectively) in the  $\alpha$ -pinene/isoprene system. In the  $\alpha$ -pinene/isoprene, some ions with lower carbon numbers (nC<sub>4-5</sub>) from the isoprene-derived compounds (e.g., C<sub>5</sub>H<sub>8</sub>O<sub>3,4</sub>, C<sub>5</sub>H<sub>9</sub>NO<sub>5</sub>, C<sub>4</sub>H<sub>7</sub>NO<sub>5</sub>, etc) are in this cluster. The lower carbon number in the mixture than the ones in the individual  $\alpha$ -pinene is resulted by part of unique ions and isoprene-derived ions. Cluster 1 with a few compounds and lowest signal contributions (~3%) exhibits the slowest rates to peaks in both systems, expected much later generation products in the corresponding systems.

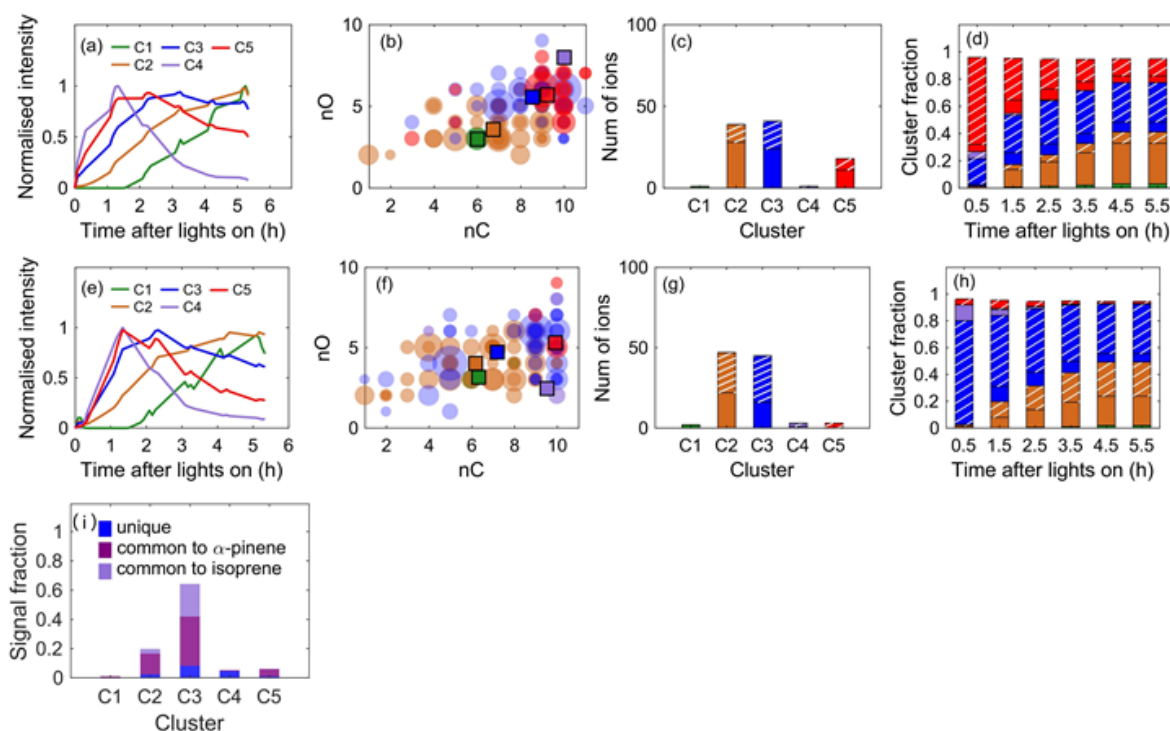


Figure 4. Hierarchical clustering of gas-phase oxidation products in the  $\frac{1}{2}$  reactivity  $\alpha$ -pinene (a-d) and  $\alpha$ -pinene/isoprene (e-i) systems. (a) and (e) The average time series of each cluster. Each ion is normalized to the highest intensity itself. (b) and (f) Carbon number vs oxygen number. The mean values are marked as squares. (c) and (g) The number of ions in each cluster. (d) and (h) the sum of ions' signal fractions in each cluster. The color scheme is the same as in (a). (i) The separation of ions in the  $\alpha$ -pinene/isoprene mixture in each cluster. 'unique' in (i) represents those ions appear in the mixture alone.

### 3.2.1.3 *o*-cresol and *o*-cresol/isoprene systems

Figure 5 depicts the gas-phase HCA results for  $\frac{1}{2}$  reactivity *o*-cresol, *o*-cresol and *o*-cresol/isoprene systems. Cluster 5 with the highest cluster fractions shows the fastest formation rate and continuous growth over time in the three systems. This cluster is composed of 20 ions (13 CHO and 7 CHON compounds with an average of 72% and 0.1% of the total signals respectively) in the  $\frac{1}{2}$  reactivity *o*-cresol experiment, 35 ions (19 CHO and 16 CHON compounds with an average of 60.3% and 25% to the total signals respectively) in the *o*-cresol experiment and 20 ions (10 CHO and 10 CHON compounds with an average of 42.7% and 1.2% to the total signals respectively) in the *o*-cresol/isoprene system, dominated by compounds with 6 and 7 carbon numbers and expected of the early-generation products. The major first-generation compound  $C_7H_8O_2$  generated from *o*-cresol oxidation (Schwantes et al., 2017) is allocated in this cluster in the three systems. However, its percentages to the total signals differ from systems, with a lower fraction in the *o*-cresol/isoprene system (See Figure S7). The

relatively higher average carbon number and lower oxygen number in this cluster illustrate the less oxidized compounds are formed initially in the three systems.

Cluster 2 exhibits the second-fastest formation rate and keeps increasing until the end of the experiments. Signal in the CHON species dominates the products of this cluster. 24 CHO (~2.8% of total signal) and 18 CHON (11.4 % of total signal) ions of 42 are observed in the ½ reactivity *o*-cresol. 31 ions (19 CHO and 12 CHON ions with 3.2% and 2.4% to the total signals respectively) and 70 ions (40 CHO and 30 CHON ions with an average of 14% and 33% to the total signals respectively) are found in the *o*-cresol and *o*-cresol/isoprene systems, respectively. The majority of ions are with  $nC \leq 7$  in those systems. In the *o*-cresol/isoprene, 13 isoprene-derived ions accounting for 19% of the total signal (e.g.,  $C_5H_9NO_4$ ,  $C_4H_7NO_{4,5}$ ) and 27 unique ions accounting for 5% of the total signal (e.g.,  $C_7H_7NO_2$ ,  $C_4H_{10}O_6$ ,  $C_6H_8O_3$ , etc) appear in this cluster, leading to a lower average carbon number. The higher oxygen number in cluster 2 than the results of cluster 5 may be indicative of a higher degree of oxidation of the products.

Cluster 1 with a low signal fraction (~15%) shows the slowest formation rate in the *o*-cresol and ½ reactivity *o*-cresol systems, expected as the later-generation products. 20 and 28 products are investigated in the ½ reactivity *o*-cresol and *o*-cresol systems respectively. However, no such temporal profiles appear in the *o*-cresol/isoprene system. Part of those ions in the *o*-cresol of cluster 1 is detected in cluster 2 in the *o*-cresol/isoprene system. Most of the compounds are with lower carbon numbers ( $nC=4-6$ ) in the individual *o*-cresol systems, suggesting a higher degree of fragmentation which is supported by the lowest average carbon number of this cluster. Cluster 3 and cluster 4 display negligible contributions to the signals (see Fig 5d, 5h and 5l) and contain 6 ions in the two clusters in the three systems.

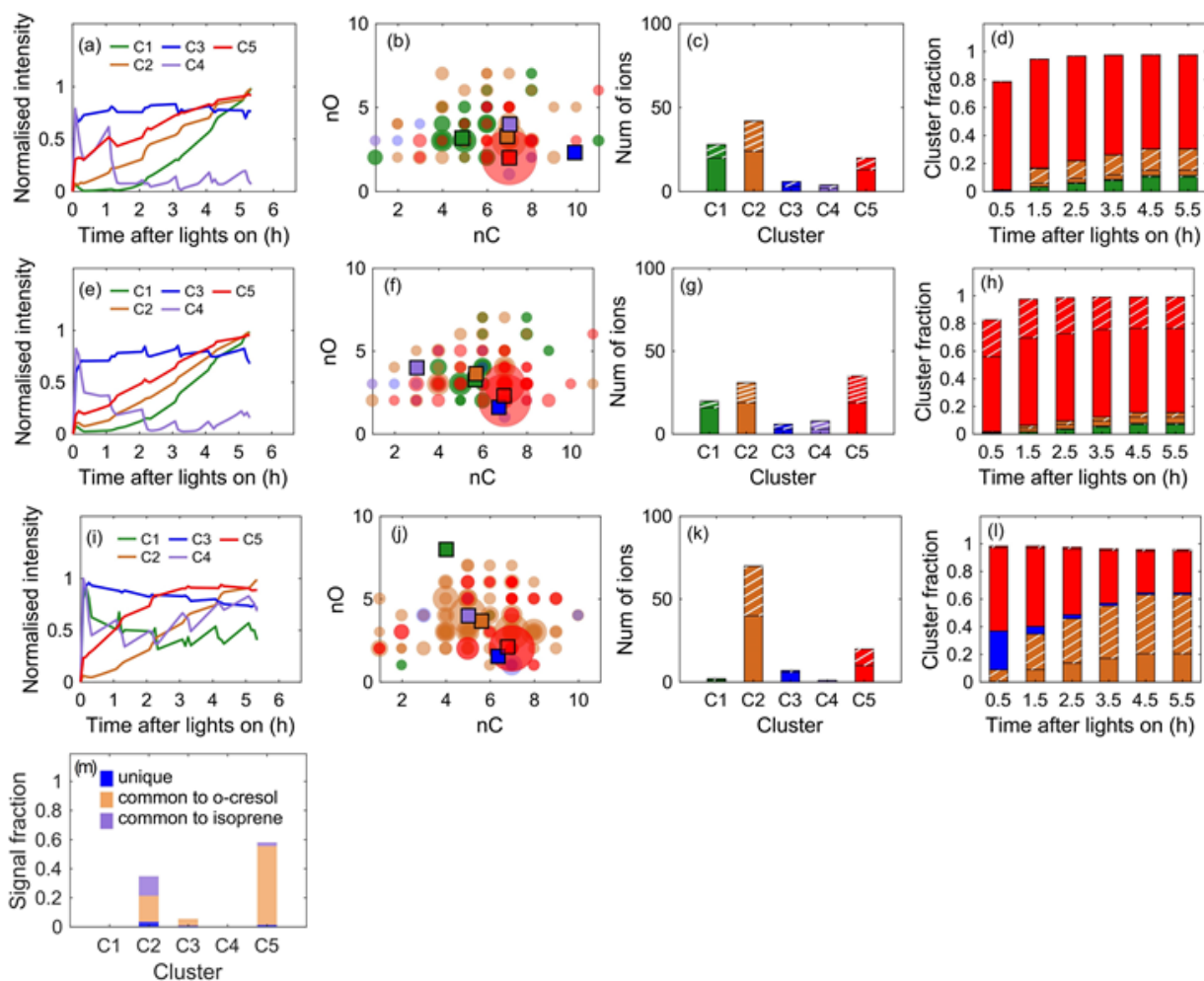


Figure 5. Hierarchical clustering of gas-phase oxidation products in the *o*-cresol (a-d),  $\frac{1}{2}$  reactivity *o*-cresol (e-h) and *o*-cresol/isoprene (i-m) systems. (m) The separation of ions in the *o*-cresol/isoprene mixture in each cluster. ‘unique’ in (m) represents those ions that appear in the mixture alone.

### 3.2.1.4 $\alpha$ -pinene/*o*-cresol

Figure 6a shows the time series trends in the  $\alpha$ -pinene/*o*-cresol, which are more similar to the trends in the single  $\alpha$ -pinene. Cluster 4 increases most rapidly to its peak value, with a quick increase to a maximum followed by a fast decrease, as shown in Fig 6a. 4 ions with a dominant signal from the critical *o*-cresol derived first-generation compound  $C_7H_8O_2$  are found in this cluster, thus the signal fraction of this cluster has a higher contribution from CHO species at the beginning ( $\sim 60\%$  of the total signal), as shown in Fig 6d.

Cluster 5 and cluster 3 overlap at the beginning of the experiment, followed by a good separation after 2-hour reactions due to distinct decrease trends. Cluster 5 contains 13 compounds (6 CHON and 7 CHO compounds comprising an average of 4.5% and 11.1% to the total signals respectively), with the dominated  $\alpha$ -pinene derived ions such as  $C_9H_{13}NO_6$  and a small portion of unique ions (Fig 6e). The average nC and nO exhibit the highest values among clusters, suggesting less C-C cleavage at this stage. Cluster 3 contains 42 ions with ~40% of the total signal, composed of 27 CHO ions (with an average of 8.8% to the total signal) and 15 CHON ions (with an average of 21.7% to the total signal). Some *o*-cresol derived ions (e.g.,  $C_7H_8O_3$ ,  $C_7H_7NO_3$ , and  $C_6H_8O_3$ , etc) with nC<sub>5-7</sub> are detected in this cluster. This leads to the lower average carbon number and oxygen number in the  $\alpha$ -pinene/*o*-cresol system than the one in the  $\alpha$ -pinene.

Cluster 2 in the  $\alpha$ -pinene/*o*-cresol increases fourth most rapidly to its peak value in the system, with 40 ions (20 CHO ions with an average of 9% and 20 CHON ions with an average of 12.7% to the total signals) in this cluster and continuous growth over time (see Fig 6a), expected later formation compounds. It is dominated by nC<10 from the combination of  $\alpha$ -pinene derived ions, *o*-cresol derived ions (e.g.,  $C_7H_7NO_4$ ,  $C_7H_5NO_4$ ,  $C_6H_{10}NO_3$ , etc) and unique ions, with an average nC 6 and nO 4.3. One compound  $C_6H_{10}O_3$  is in cluster 1 in the  $\alpha$ -pinene/*o*-cresol, which also appears in cluster 1 of other  $\alpha$ -pinene-containing systems, expected much later generation compound.

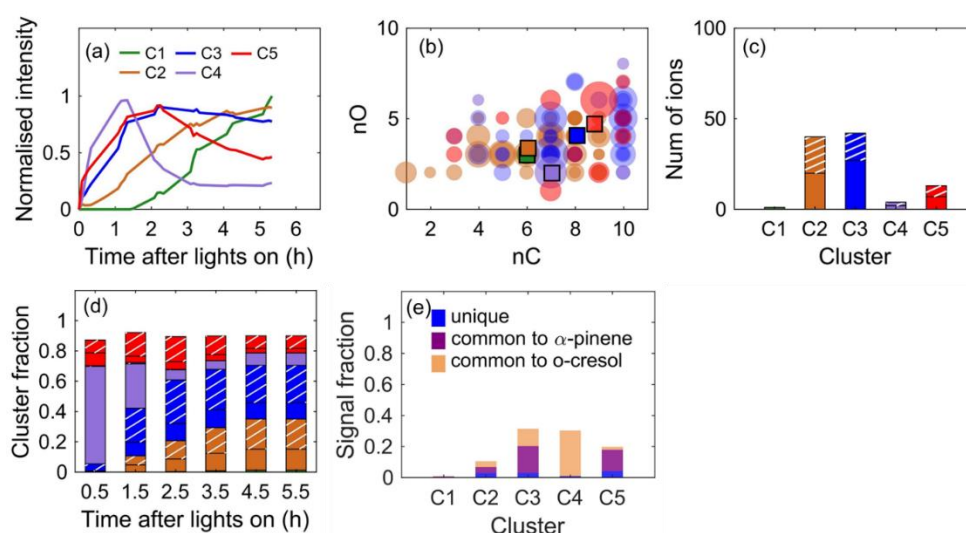


Figure 6 Hierarchical clustering of gas-phase oxidation products in the  $\alpha$ -pinene/*o*-cresol system. (a) The average time series of each cluster. Each ion is normalized to the highest intensity itself. (b) Carbon number vs oxygen number. The mean values are marked as squares. (c) The number of ions in each



cluster. (d) the sum of ions' signal fractions in each cluster. (e) The separation of ions in the *o*-cresol/isoprene mixture in each cluster. 'unique' in (e) represents those ions that appear in the mixture alone.

### 3.2.1.5 Ternary

In the 1/3 reactivity  $\alpha$ -pinene, cluster 3 increases most rapidly to the peak value and contains 78 ions (39 CHO ions with an average of 25% to the total signal and 37 CHON ions with an average of 51.5% to the total signal). Cluster 2 exhibits a slower starting formation time, with 6 compounds included accounting for around 8% of the total signal. Cluster 1 shows the slowest formation time, with 8 CHO compounds in this cluster and accounting for ~15% of the cluster fraction. Clusters 4 and 5 including 10 ions with less than 3% of the total signal have fluctuant time-series patterns. Generally, the overall time-series trends in the 1/3 reactivity  $\alpha$ -pinene are distinct to those in the  $\alpha$ -pinene and 1/2 reactivity  $\alpha$ -pinene. However, insufficient repeatable experiments for 1/3 reactivity  $\alpha$ -pinene makes it difficult to conclude whether the differences are caused by either the randomly experimental errors or real gas-phase chemistry changes owing to the initial concentration of  $\alpha$ -pinene. More effort is needed to investigate the chemical composition in the 1/3 reactivity  $\alpha$ -pinene.

The overall cluster behaviours in the ternary are neither completely similar to that in the individual  $\alpha$ -pinene nor the ones in the individual *o*-cresol systems. Cluster 5 increases most rapidly to the peak value, with a quick increase to a maximum and a decrease after 1.5 hours. 4 ions are included in this cluster and the signal fraction is dominated by the *o*-cresol derived first-generation compound  $C_7H_8O_2$  (~ 52% to the total signal). Cluster 2 shows the second fastest rate of increase, containing 8 ions with a lower signal fraction (~ 2%). Cluster 1 contains the greatest ions (84 ions) and largest signal fractions (rising from 22% to ~ 90% to the total signal), showing the third rate to the peak and continuous growth until 4.5-hour reactions. The majority of those ions are nitrogen-containing compounds, with a broad range of nC in those compounds, nC<sub>2-10</sub>, from mixed three precursors derived ions and unique ions (see Fig 7e) and the signal fraction is dominated by the isoprene derived oxidation products (e.g., ions nC<sub>4-5</sub>:C<sub>5</sub>H<sub>9</sub>NO<sub>4,5</sub>, C<sub>4</sub>H<sub>7</sub>NO<sub>4</sub>, etc). Meanwhile, ions nC<sub>6-7</sub> such as C<sub>7</sub>H<sub>7</sub>NO<sub>3</sub> from *o*-cresol derived compounds and ions nC<sub>8-10</sub> such as C<sub>9</sub>H<sub>13</sub>NO<sub>6</sub>, C<sub>10</sub>H<sub>16</sub>O<sub>3</sub>, C<sub>8</sub>H<sub>12</sub>O<sub>4</sub>, etc from  $\alpha$ -pinene derived products are found in this cluster. More information on the formula is provided in SI. Cluster 3 with 2 ions and cluster 4 with 1 ion carry a very low signal fraction to the total signal.

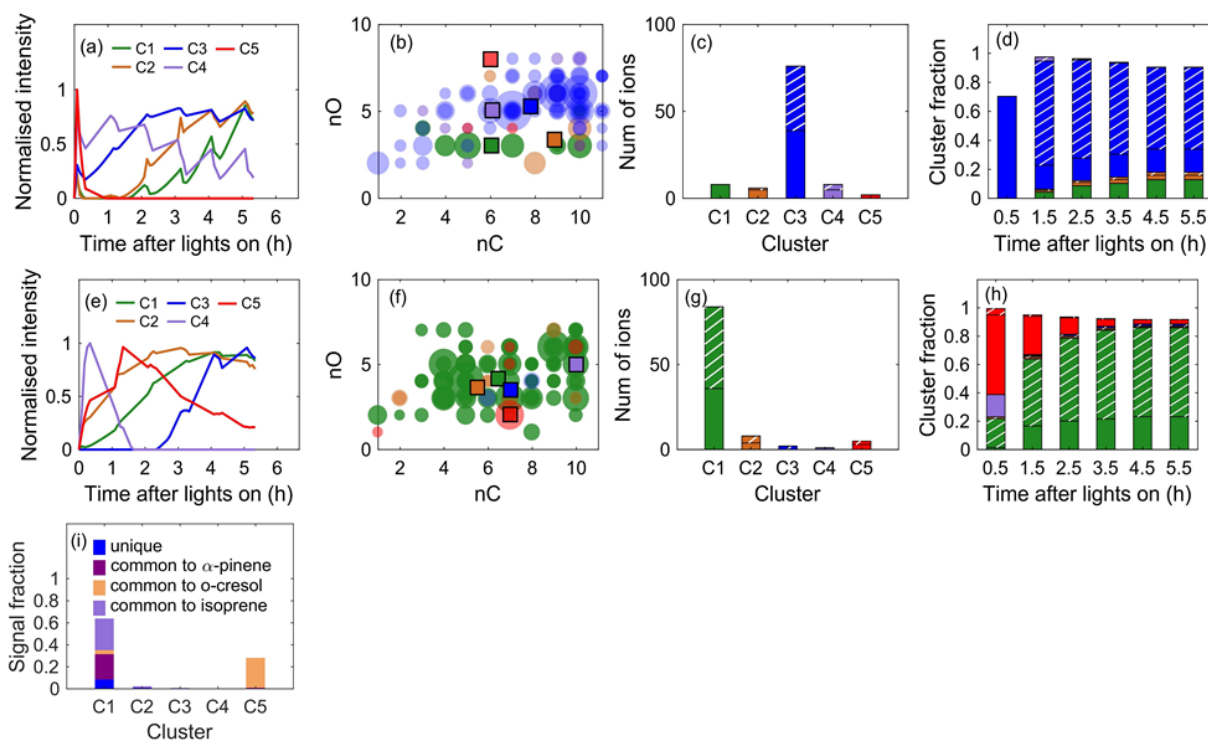


Figure 7 Hierarchical clustering of gas-phase oxidation products in the 1/3 reactivity  $\alpha$ -pinene (a-d) and ternary (e-i) systems. (a) and (e) The average time series of each cluster. Each ion is normalized to the highest intensity itself. (b) and (f) Carbon number vs oxygen number. The mean values are marked as squares. (c) and (g) The number of ions in each cluster. (d) and (h) the sum of ions' signal fractions in each cluster. (i) The separation of ions in the *o*-cresol/isoprene mixture in each cluster. 'unique' in (i) represents those ions that appear in the mixture alone.

### 3.2.2 Particle-phase hierarchical clustering analysis (HCA)

In the isoprene (Fig 8), cluster 5 with 26 ions exhibits an increase after 3.5 hours, dominated by ions with  $nC \leq 5$ , such as  $C_5H_8O_{3-4}$ ,  $C_5H_{12}NO_4$  etc. Cluster 4 with 17 ions displays an increase at the beginning of photooxidation reactions. Ions such as  $C_3H_6O_4$ ,  $C_4H_8O_6$ ,  $C_{12}H_{16}O_5$ , etc are divided in this cluster. The temporal profiles of other clusters show chaos, which can be explained by the near chamber background particle mass in our experiments, resulting in the greater variability in the thermogram of collected components on the filter (Voliotis, et. al (2021, ACPD)) or the lower time resolution of particle phase.

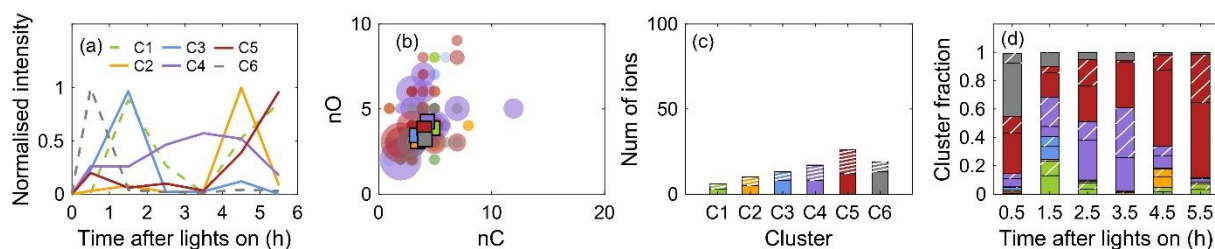


Figure 8. Hierarchical clustering of gas-phase oxidation products in the isoprene system. (a) The average time series of each cluster. Each ion is normalized to the highest intensity itself. (b) Carbon number vs oxygen number. The mean values are marked as squares. (c) The number of ions in each cluster. (d) the sum of ions' signal fractions in each cluster. The color scheme is the same as in (a).

In the  $\frac{1}{2}$  reactivity  $\alpha$ -pinene and  $\alpha$ -pinene/isoprene systems, as shown in Fig 9a, the time-series trend of cluster 5 shows a continuous increase to maximums after  $\sim 2.5$ -hour reactions, followed by stabilization until the end of experiments. The average signal fractions across the experiments of this cluster account for  $\sim 40\%$  ( $\sim 28\%$  for CHO ions) and  $49\%$  ( $34\%$  for CHO ions) to the total signal in  $\frac{1}{2}$  reactivity  $\alpha$ -pinene and  $\alpha$ -pinene/isoprene systems separately. In the  $\alpha$ -pinene/isoprene mixture, more numbers of ions are included in the  $\alpha$ -pinene/isoprene than that in the  $\frac{1}{2}$  reactivity  $\alpha$ -pinene, as shown in Fig 9c and 9g. In the mixture, this cluster composes of 24  $\alpha$ -pinene derived ions (signal fraction increasing from 21% to 44% to the total signal), 29 unique ions (signal fraction increasing from 6% to 17% to the total signal) and 6 isoprene-derived ions (with an average of 3% to the total signal). The CHO species are dominated by  $nC_{7-10}$  and CHON species are dominated by ions with higher oxygen numbers ( $nO \geq 4$ ). The average carbon numbers and oxygen numbers are comparable between the two systems.

Cluster 4 exhibits the second highest signal contribution in the two systems, with an increase initially within 3.5-hour reactions. Fewer ions and lower cluster signal fractions are found in the mixture compared to those in the individual  $\alpha$ -pinene. Most of ions in cluster 4 are with  $nC=7-10$  in all systems. 7 unique ions appear in this cluster of  $\alpha$ -pinene/isoprene experiment, such as  $C_{16}H_{24}N_2O_6$  and  $C_{18}H_{26}NO_{6-7}$ . The weighted average  $nC$  and  $nO$  in the  $\alpha$ -pinene/isoprene mixture ( $nC$ :  $\sim 9.6$  and  $nO$ :  $\sim 4.9$ ) is slightly higher than the values in the individual  $\alpha$ -pinene.

Cluster 6 makes  $\sim 20\%$  to the total signal in the  $\alpha$ -pinene/isoprene system and less than 5% to total signals in individual  $\alpha$ -pinene. In the  $\alpha$ -pinene/isoprene system, seven  $\alpha$ -pinene derived products with dominated signal fractions such as  $C_8H_{12}O_4$  and  $C_7H_{12}O_4$  and nitrogen-containing compounds (e.g.,  $C_{10}H_{15}NO_7$ ,  $C_{10}H_{17}NO_8$ ,  $C_7H_{12}NO_4$ , etc) appear in this cluster. Those ions are found in cluster 4 in the individual  $\alpha$ -pinene. Clusters 1, 2 and 3 (total accounting for  $< 8\%$  to the total signals in the  $\alpha$ -pinene/isoprene) show fluctuant temporal profiles over time.

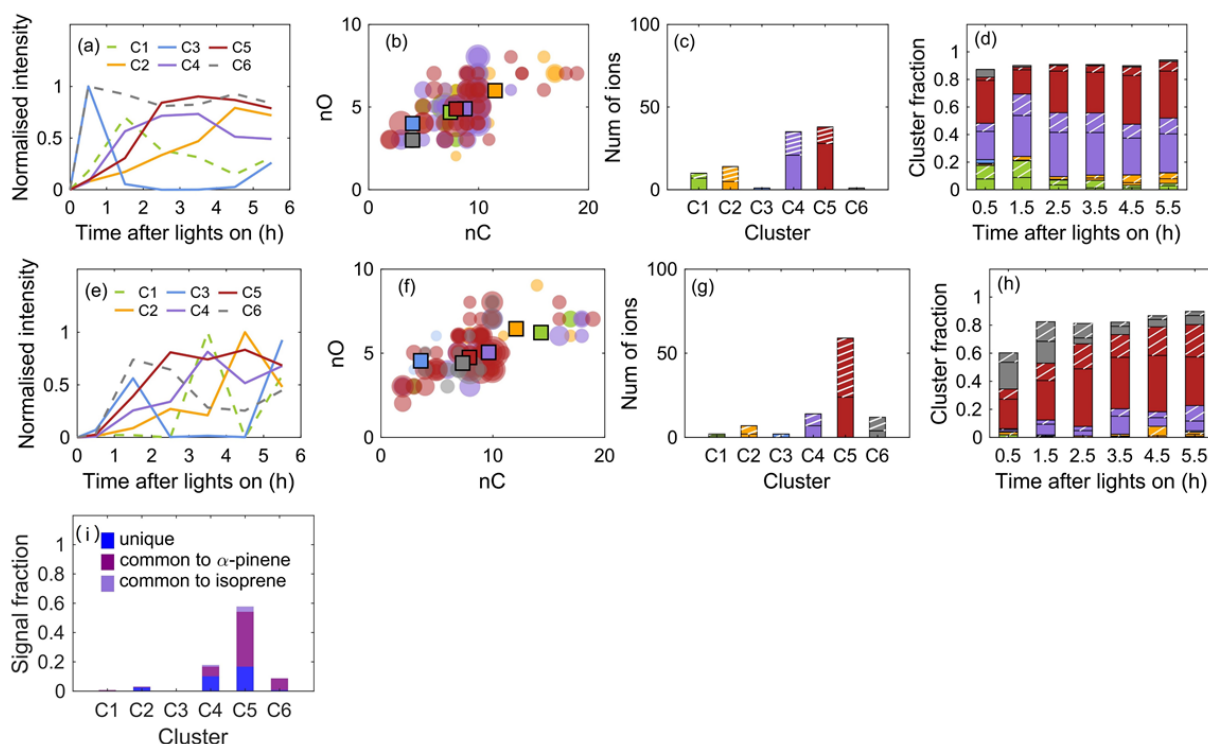


Figure 9. Hierarchical clustering of particle-phase oxidation products in the  $\frac{1}{2}$  reactivity  $\alpha$ -pinene (a-d) and  $\alpha$ -pinene/isoprene (e and i) systems. (a) and (e) The average time series of each cluster. Each ion is normalized to the highest intensity itself. (b) and (f) Carbon number vs oxygen number. The mean values are marked as squares. (c) and (g) The number of ions in each cluster. (d) and (h) the sum of ions' signal fractions in each cluster. The color scheme is the same as in (a). (i) The separation of ions in the  $\alpha$ -pinene/isoprene mixture in each cluster. 'unique' in (i) represents those ions appear in the mixture alone.

In the *o*-cresol and *o*-cresol/isoprene systems, cluster 5 shows the highest contributions at the end of experiments, dominated by the CHON species. The time series trends are generally consistent with the SOA particle mass formation, irrespective of the variability after 3.5 hours in the mixture which is likely caused by the lower time resolution of the dataset. The most abundant compound  $C_7H_7NO_4$  in individual *o*-cresol is allocated in cluster 5 in the three systems, while its signal fraction is lower in the *o*-cresol/isoprene mixture compared to that in the *o*-cresol systems, as shown in Fig S7b. In the *o*-cresol/isoprene system, this cluster is composed of 28 unique ions accounting for an average of 11% of the total signal, 14 *o*-cresol derived ions (with an average of 22% to the total signal) and two isoprene-derived ions (~1% to the total signal). The average carbon number in the mixture is lower than those in the *o*-cresol systems (6.77, 6.87 and 7.08 in the *o*-cresol/isoprene,  $\frac{1}{2}$  reactivity *o*-cresol and *o*-cresol, respectively).

Cluster 4 exhibits the second highest signal contribution in those systems, with continuous growth in the *o*-cresol and fluctuated time-series changes in the ½ reactivity *o*-cresol and *o*-cresol/isoprene system. The signal fraction of this cluster is dominated by the CHO species in the *o*-cresol and *o*-cresol/isoprene systems but dominated by the CHON species in the ½ reactivity *o*-cresol system, as shown in Fig 10d, 10h and 10l. Fewer ions and lower signal fractions are found in the mixture compared to that in the individual *o*-cresol systems.

Cluster 3 exhibits a slower formation rate in the mixture and is composed of 3 *o*-cresol derived ions and 8 unique ions in the mixture, increasing to ~ 7% and 9% of the total signal after 5.5-hour reactions respectively. Cluster 6 containing most of the compounds and higher signal fraction shows a continuous increase over time in the ½ reactivity *o*-cresol, accounting for an average of 10% of the total signal. Cluster 1 displays a continuous increase over time in the *o*-cresol and *o*-cresol/isoprene systems, with an average of 5% to the total signals. 12 unique compounds (~4%) and 4 *o*-cresol derived ions are observed in the mixture. Fluctuant temporal profiles are observed in cluster 2 over time, accounting for <5% of the total signals.

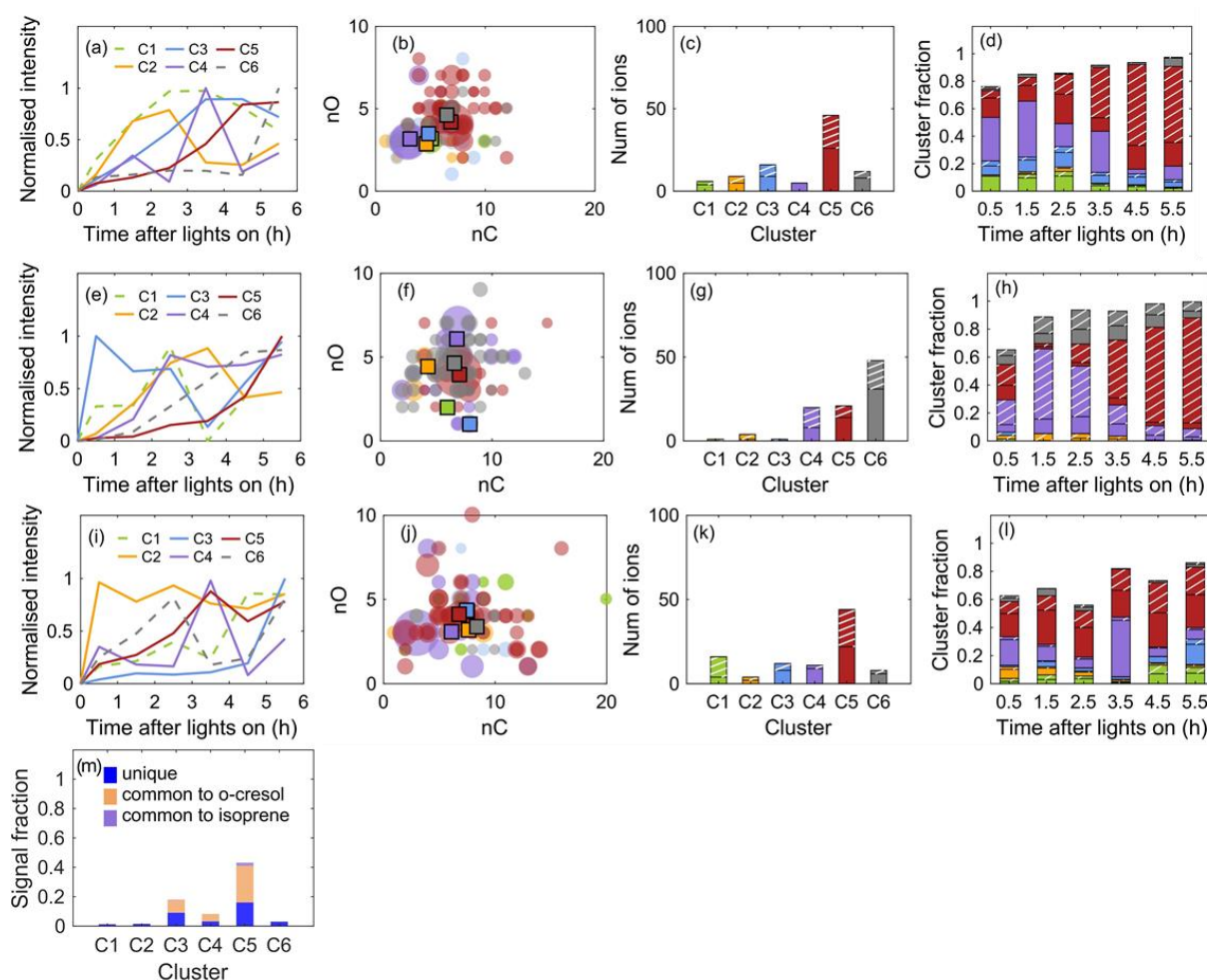


Figure 10. Hierarchical clustering of particle-phase oxidation products in the  $\frac{1}{2}$  reactivity *o*-cresol (a-d), *o*-cresol (e-h) and *o*-cresol/isoprene (i-m) systems. The subplot title is the same as the description of Figure 9. (m) The separation of ions in the *o*-cresol/isoprene mixture in each cluster. ‘unique’ in (m) represents those ions appear in the mixture alone.

In the  $\alpha$ -pinene/*o*-cresol, cluster 5 shows the highest contributions with continuous growth, suggesting continuous particle-phase formation, as shown in Figure 11a. 26 ions from the  $\alpha$ -pinene derived oxidation products (~25% to the total signal), 8 ions from the *o*-cresol derived products (~5% to the total signal) and 29 ions from the unique category (~9% to the total signal) are observed in this cluster. The CHO species dominate this cluster, as shown in Fig 11d. The average carbon number and oxygen number are around 9.2 and 5 respectively.

Cluster 4 exhibits the second highest signal contribution in those systems, with continuous growth until ~2-hour reactions and a decrease then. This cluster is composed of 3  $\alpha$ -pinene derived products, 3 *o*-cresol derived products and 3 unique ions, with an average of 3%, 30% and 1% to the total signal respectively and dominated by the CHON species (mainly  $C_7H_7NO_4$  product).

Cluster 1 contains two  $\alpha$ -pinene derived ions and 4 unique ions, reaching the maximum within 1.5 hours and decreasing then, as shown in Fig 11a. The signal fraction of this cluster increases to the maximum ~18% to the total signal after 0.5-hour reactions followed by a decrease down to 2% to the total signal (see Fig 11d). Other clusters account for less than 5% of total signals with fluctuant temporal profiles over time.

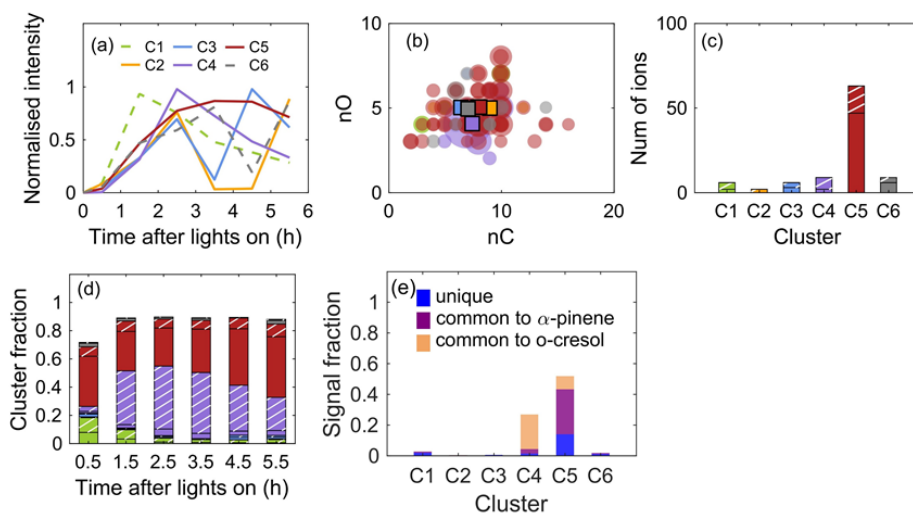


Figure 11. Hierarchical clustering of particle-phase oxidation products in the  $\alpha$ -pinene/*o*-cresol system. (a) The average time series of each cluster. Each ion is normalized to the highest intensity itself. (b) Carbon number vs oxygen number. The mean values are marked as squares. (c) The number of ions in each cluster. (d) the signal fractions in each cluster. The color scheme is the same as in (a). (e) The separation of ions in the *o*-cresol/isoprene mixture in each cluster. ‘unique’ in (i) represents those ions appear in the mixture alone.

In the 1/3 reactivity  $\alpha$ -pinene (see Fig 12a-d), cluster 5 exhibits a continuous increasing time-series trend and includes 60 ions (38 CHO and 22 CHON ions with an average of 40.4% and 19.5% of the total signal respectively). Most of the products are with 7 to 10 carbon numbers and 4 to 8 oxygen numbers, with the average carbon number 8.6 and oxygen number 5. Cluster 4 includes 12 CHO with an average of 8.1% and 7 CHON ions with an average of 2% of the total signal, with an increasing time-series trend. Cluster 6 contains 14 ions and accounts for ~7% of the total signal. Cluster 2 with 3 ions including C<sub>8</sub>H<sub>12</sub>O<sub>4</sub> exhibits an increasing time-series trend at the beginning of experiments, with a cluster signal fraction from ~19% down to 3% eventually. Clusters 1 and 3 have very low signal fractions with 3 ions in the two clusters. In the ternary (see Fig 12e-i), 65 ions are clustered in cluster 5, with an average of 49% for CHO species and 19% for CHON species. There are 24 ions, 5 ions, 7 ions and 29 ions derived from  $\alpha$ -pinene, *o*-cresol, isoprene oxidation products and unique to the mixture products separately, accounting for around 19.5%, 7%, 2% and 31% of the total signal respectively. Figure 12f shows that the ions of this cluster are dominated by ions with 5 to 10



carbon numbers, with an average carbon number of 7.3 and oxygen number 5.4.

Cluster 4 exhibits the second highest signal contribution in those systems, reaching a maximum of around 2-hour reactions. This cluster includes 11 ions from  $\alpha$ -pinene, isoprene, *o*-cresol derived oxidation products and unique ions, accounting for an average of around 11% of the total signal. Cluster 2 and cluster 3 display increasing time-series trends over time, as shown in Fig 12e, with around 8% of the total signal. Other clusters accounting for less than 5% of the total signals show high variability in the temporal profiles.

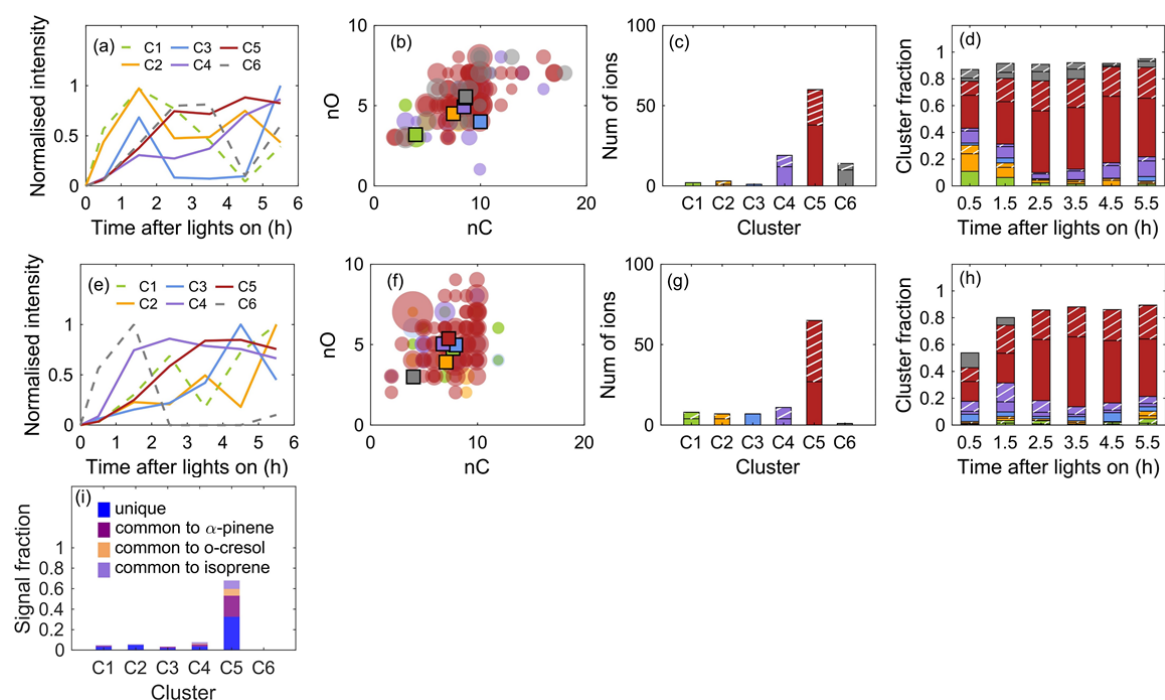


Figure 12. Hierarchical clustering of particle-phase oxidation products in the 1/3 reactivity  $\alpha$ -pinene (a-d) and ternary (e-i) systems. (a) and (e) The average time series of each cluster. Each ion is normalized to the highest intensity itself. (b) and (f) Carbon number vs oxygen number. The mean values are marked as squares. (c) and (g) The number of ions in each cluster. (d) and (h) the signal fractions in each cluster. The color scheme is the same as in (a). (i) The separation of ions in the ternary in each cluster. ‘unique’ in (i) represents those ions appear in the mixture alone.

## 4. Discussion

### 4.1 Comparison of chemical composition from two analytical approaches

The chemical composition was explored by online FIGAERO-CIMS and offline LC-orbitrap MS. Overall, in the  $\alpha$ -pinene and  $\alpha$ -pinene/isoprene experiments, the results from the FIGAERO-CIMS and confident peaklist of LC-Orbitrap MS negative mode are comparable, dominated by compounds with C<sub>8-10</sub> in the CHO species, whilst obvious differences are investigated in other systems between the FIGAERO-CIMS and LC-Orbitrap MS positive



mode and negative mode. Generally, in the  $\alpha$ -pinene/*o*-cresol and ternary systems, compounds in the CHO species with C<sub>6-10</sub> play a dominant role from the online particle-phase measurements. In the *o*-cresol containing systems, there is a larger fraction (>60%) from CHON species (dominated by C<sub>7</sub>H<sub>7</sub>NO<sub>4</sub> or C<sub>7</sub>H<sub>7</sub>NO<sub>3</sub> or the combination of the two products) in the LC-orbitrap MS negative mode, be alike the results from individual *o*-cresol from FIGAERO-CIMS. This is caused by either the real higher yields of the two products or the high instrumental sensitivity of the two species (Voliotis et al., 2021; Kiontke et al., 2016). The high signal contribution of the two products can be supported by the fact that the *o*-cresol precursor is not completely consumed in the course of our experiments (see Fig 2 in Voliotis et al., 2021, ACPD), leading to the continuous formation of the two products over the experiments.

It is clear more compounds with higher carbon numbers (nC>15) were detected by LC-orbitrap MS in both modes for all VOC systems, whereas more compounds with smaller carbon numbers (nC<5) were measured from FIGAERO-CIMS. This is likely caused by the different preferences of instruments, which was discussed in detail in Du et al. (2021). The results highlight the importance of the combinational application of the two instruments to obtain a broad picture of molecular information on the SOA products in the mixture studies.

It can be seen that higher variability was observed in the elemental groupings in the LC-orbitrap MS measurements, which is caused by various factors. The larger differences in the isoprene may result from the unidentical experimental results or data processing or potential contaminates of filters (further reactions on the filter or artificial contamination). It leads to difficulty in the identification of particle-phase components from isoprene reactions due to near chamber background particle mass formation in the isoprene. Differently, the high variability in the *o*-cresol is caused by the unidentical chamber backgrounds during our experimental campaigns. The dominated C<sub>7</sub>H<sub>7</sub>NO<sub>3</sub> compound (~ 39% of total peak areas in single *o*-cresol) was removed from one of the three experiments due to the high signal chamber background, resulting in being split in the inconclusive compounds and thus greater uncertainty in the average values among three experiments. The uncertainty is smaller in the CIMS results due to the same peaklist used for the same experiments but different peaklists regenerated for the LC-Orbitrap MS approach (Pereira et al., 2021). The results from the offline analysis illustrate that molecular level investigation is necessary to identify the cleanness of the chamber in the investigation chemical composition for the chamber experiments in future work, although it is

evident that the repeatable chamber backgrounds were achieved before each experiment after routine cleaning processes and harsh cleaning with high O<sub>3</sub> concentration under strong UV illumination weekly, with particle concentrations <15 particles cm<sup>-3</sup>, particle mass concentration ~0 μg m<sup>-3</sup>, O<sub>3</sub> concentrations ~0 ppb and NO<sub>x</sub> concentration <10 ppb (NO <8 ppb and NO<sub>2</sub> <2 ppb) (Shao et al., 2021).

## 4.2 Connection between clustering results and mechanisms

HCA enables the distinction between oxidation products based on their time-series behaviour, separating chemical regimes and identifying the source and chemical processes for individual systems. This section explores two aspects of SOA formation accessible to our analysis in the mixed systems: namely the roles played by interactions occurring in the systems and the well-established gas-phase oxidation of each precursor.

In all four mixed systems, it can be seen that compounds that are uniquely found in the mixture are generated and are distributed in different clusters in the gas and particle-phase HCA analysis. This suggests that molecular interactions occurred throughout the oxidation in the various system. In the  $\alpha$ -pinene/isoprene system, most of these “unique-to-the-mixture” compounds are included in cluster 3 and cluster 2, suggesting medium to slower formation rates in the system. In the o-cresol/isoprene and  $\alpha$ -pinene/o-cresol systems, most of the gas-phase unique-to-the-mixture compounds are contained in cluster 2, with slower formation rates and an increasing signal fraction over time (see Fig 5m). Most of the unique compounds are in cluster 1 in the ternary, with the third-fastest formation rate. There are several plausible reasons for the differences in gas-phase formation rates. The combination of VOCs will inevitably alter the oxidant regime (see for example Figure S1 in Voliotis et al., 2021) and change the fate of RO<sub>2</sub> derived from other parent precursors or the products formed at any generation of oxidation. Furthermore, the different volatility of products will lead to different mass fractions in the gas and particle phases.

By contrast, the particle-phase clustering analysis shows that the majority of unique-to-mixture compounds are grouped in cluster 5, accounting for ~ 40% of the total signal in the ternary system and ~20% in other binary mixtures. A higher number of unique products with higher carbon numbers are found in the particle phase, which may be generated from the cross-products between the VOC precursors. For example, compound C<sub>16</sub>H<sub>21</sub>NO<sub>5</sub> in the  $\alpha$ -pinene/o-cresol mixture may be generated from C<sub>7</sub>H<sub>7</sub>NO<sub>4</sub> and another compound formed from  $\alpha$ -pinene

reactions. It is not possible to confirm whether such reactions occurred in the gas phase or particle phase without more targeted experiments or measurement techniques. The presence of molecular interaction in the mixture may further influence the chemical properties, such as volatility distribution (Voliotis et. al, in prep.) and SOA yields in the mixture (Voliotis et.al, 2021, ACPD). More effort is needed to investigate the formation of those unique compounds to understand their formation pathways in the mixture.

The oxidation products from individual precursors also play an important role in the mixture. In the gas phase, in the  $\alpha$ -pinene and  $\alpha$ -pinene/isoprene systems, CHON species are produced very quickly and play a dominant role in the signal contributions, as shown in clusters 3, 4 and 5 in the Fig4. The overall time-series trends of clusters 3, 4 and 5 are similar to the time-series trends of  $\text{NO}_2/\text{NO}$  and  $\text{O}_3$  formation in the two systems. It indicates that the formation pathways from OH oxidation of pinonaldehyde followed by termination by  $\text{RO}_2 + \text{NO}_2$  reaction (e.g.,  $\text{C}_9\text{H}_{13}\text{NO}_6$ ,  $\text{C}_{10}\text{H}_{15}\text{NO}_{6-8}$ , etc) (Eddingsaas et al., 2012a) or reactions of ozonolysis-produced  $\text{RO}_2$  radicals +  $\text{NO}/\text{NO}_2$  (e.g.,  $\text{C}_{10}\text{H}_{14,16}\text{NO}_{6-9}$ ) (Johnson and Marston, 2008; Bagchi et al., 2020; Jokinen et al., 2015) or OH initiated isoprene- $\text{RO}_2 + \text{NO}/\text{NO}_2$  (e.g.,  $\text{C}_5\text{H}_9\text{NO}_4$ ) (Xu et al., 2014) are the most important termination pathway at this stage.

In contrast, in the *o*-cresol containing systems, CHO species are formed quickly, dominated by the major first-generation product  $\text{C}_7\text{H}_8\text{O}_2$  in cluster 5 of *o*-cresol, *o*-cresol/isoprene and ternary, and cluster 4 of  $\alpha$ -pinene/*o*-cresol systems. This suggests the OH addition to the aromatic ring (Schwantes et al., 2017) is more competitive than other reactions in the *o*-cresol containing systems, particularly in the *o*-cresol/isoprene system. Another possible explanation for  $\alpha$ -pinene/*o*-cresol and ternary systems is that the more formed gas-phase CHO species from  $\alpha$ -pinene oxidation can partition into particle phase, leading to less fraction of CHO species in the gas phase, which can be supported by the large signals of CHO species in the particle phase in Fig 11 and Fig 12. However, the signal fractions of gas-phase CHO species reduce over time, and the dominant role is taken over by the CHON species from  $\alpha$ -pinene or isoprene-derived products after 1.5-hour reactions for the  $\alpha$ -pinene/*o*-cresol and ternary systems and after 2.5-hour reactions for the *o*-cresol/isoprene system. This is likely resulted by the more reactions of  $\text{C}_7\text{H}_8\text{O}_2 + \text{OH}$  or  $\text{NO}_2$  to form *o*-cresol related CHO species or  $\text{C}_7\text{H}_7\text{NO}_4$  product (Schwantes et al., 2017), leading to the less fraction of gas-phase  $\text{C}_7\text{H}_8\text{O}_2$

and the increasing signal fractions of particle-phase CHO species or  $C_7H_7NO_4$  product in the mixed systems.

Clusters 1 and 2 with slower formation rates and lower average carbon numbers hint those ions undergo more decomposition with C-C cleavage (Ehn et al., 2014; Eddingsaas et al., 2012a). The two clusters exhibit continuous growth over time, indicating the fragmentation that occurred in the course of the experiments. More CHO species in the two clusters of  $\alpha$ -pinene-containing experiments suggest the involvement of the termination pathway by  $RO_2$  with  $HO_2$  or  $RO_2$  at the later stage. The particle-phase HCA results display the majority of compounds related to the SOA formation are generally grouped in two clusters (clusters 4 and 5) in all systems, with continuous growth from the beginning of photooxidation, indicating the continuous formation of SOA particles. However, it is difficult to interpret their formation rates unambiguously due to the lower time resolution (30 min) in the particle phase. In the  $\alpha$ -pinene/isoprene system, most of the gas-phase ions appear in the particle phase, although a small fraction of compounds with small carbon numbers ( $nC < 5$ ) are exclusively in the gas phase and some compounds with high carbon numbers ( $nC > 15$ , e.g., compounds  $C_{18}H_{26}O_7$ ,  $C_{17}H_{26}O_7$ , etc) are detected in the particle phase alone. Generally, the monomers ( $C_{8-10}$ ) in the CHO species from  $\alpha$ -pinene, such as carbonyl acids  $C_9H_{14}O_4$ ,  $C_8H_{12}O_{4-5}$ ,  $C_{10}H_{14-16}O_{3-5}$ ,  $C_7H_{12}O_3$  and  $C_7H_{10}O_4$  dominate the chemical components in the mixed system in both gas and particle phase. It highlights the importance of reactions of the  $RO_2 + HO_2/RO_2$  termination pathway, which enables to further condense onto existing particles or nucleate into particles to produce SOA in the course of experiments (Atkinson, 2000; Atkinson and Arey, 2003). Conversely, in the *o*-cresol/isoprene system, the  $RO_2 + NO/NO_2$  reaction pathway contributes more to particle formation.

### 4.3 Drivers for clustering behaviours

To evaluate the cluster behaviours in those systems, on the one hand, the results between individual precursor and mixed systems are compared. On the other hand, results are compared among clusters in the individual experiment. Generally, there are ultimately four major differences in terms of temporal profiles, the number of ions, cluster signal fractions and chemical characteristics in the clustering behaviours. The temporal profile of each organic product will impact the number of ions in a cluster which can further impact the chemical

characteristics of the cluster, especially for the dominated ions in one system. Multiple factors can contribute to those differences among these systems. These are discussed below.

First, the oxidant regime plays a critical role in the time-series patterns and cluster fractions. The experimental conditions and oxidant controlling are comprehensively discussed in Voliotis, et. al (2021, ACPD). Briefly, although the experiments were initiated based on the iso-reactivity to OH for  $\alpha$ -pinene or *o*-cresol in the mixture to ensure its comparable reactivity towards OH, the further photooxidation reactions probably lead to distinct production of oxidants (OH and O<sub>3</sub>). The results display substantially different time-series of NO<sub>x</sub>, O<sub>3</sub>, Leighton ratios and the VOC decay across systems, as shown in Figure S1 and Figure 3 in the Voliotis, et. al (2021, ACPD). It has been well established that NO<sub>x</sub> levels exert a major influence on SOA formation (Eddingsaas et al., 2012a; Ng et al., 2007b; Schwantes et al., 2017; Carlton et al., 2009; Kroll and Seinfeld, 2008). The NO<sub>x</sub> conditions will impact the fates of peroxy radicals to react with HO<sub>2</sub> or NO or RO<sub>2</sub>, leading to different formation rates of organic compounds and distinct cluster behaviours in different systems. Additionally, the O<sub>3</sub> and OH concentrations can particularly exhibit the influence on the fates of RO<sub>2</sub> in the  $\alpha$ -pinene containing and isoprene systems where can be initiated by the O<sub>3</sub> chemistry (Atkinson, 2000; Atkinson and Arey, 2003).

Generally, the gas-phase clustering results show that there are similar temporal profiles between  $\alpha$ -pinene and  $\alpha$ -pinene/isoprene, although there are differences in the aspect of the number of ions, chemical characteristics and signal fractions. In the  $\alpha$ -pinene/isoprene experiments, the dominated CHON species illustrate that clusters 3, 4 and 5 are highly dependent on the NO<sub>2</sub>/NO and O<sub>3</sub> formation in the  $\alpha$ -pinene/isoprene, while clusters 1 and 2 are independent of the two parameters in both experiments. Another example is that in the single *o*-cresol and *o*-cresol containing binary and ternary experiments, the major first-generation gas-phase compounds C<sub>7</sub>H<sub>8</sub>O<sub>2</sub> and particle-phase C<sub>7</sub>H<sub>7</sub>NO<sub>4</sub> show distinct temporal profiles and signal fractions among those experiments. This can result from different NO<sub>2</sub>/NO ratios in those systems, shown in Figure S3, leading to the reduction of the signal fractions of first-generation *o*-cresol derived product C<sub>7</sub>H<sub>8</sub>O<sub>2</sub> and further impacting the signal fractions of the next-generation C<sub>7</sub>H<sub>7</sub>NO<sub>4</sub> compound in the mixed systems (Fig S7). It can be seen there is lower *o*-cresol decay rates in the binary systems compared to that in the single *o*-cresol

experiment and the lower  $\alpha$ -pinene decay rate in the  $\alpha$ -pinene/*o*-cresol system, as shown in Figure 1 in Shao, et. al (2021, ACPD).

Second, the particle mass (inorganic mass and production of SOA in the chamber) can affect the cluster behaviour by influencing the partitioning behaviours of compounds. The presence of absorptive mass can benefit the fraction of a semivolatile compound partitioning into the particle phase, thus increased absorptive mass will enhance a gas-phase product into the particle phase, resulting in a higher fraction in the particle phase (Kroll and Seinfeld, 2008; Hallquist et al., 2009). There are different SOA levels among those systems, with much higher SOA production in the mixture compared to almost zero SOA mass in the individual isoprene, while the SOA mass shows higher in the single  $\alpha$ -pinene or *o*-cresol experiments compared to binary experiments. It implies that the same volatile or semivolatile may perform different fractions in the gas phase or particle phase in different experiments, which was discussed in detail in Voliotis et al. (2021). In this study, in the single isoprene experiment, the chaotic temporal profiles of particle-phase clusters behaviours can be explained by the near chamber background SOA particle mass in our experiments, resulting in less mass filter loading for thermal desorption and greater variability in the particle phase (Voliotis et al., 2021). However, in the  $\alpha$ -pinene/isoprene, *o*-cresol/isoprene mixture and ternary systems, small fractions of isoprene-derived compounds (e.g.,  $C_5H_8O_4$ ,  $C_5H_9NO_4$ ) are detected with an increasing trend at the beginning of experiments in the particle phase due to more production of SOA in the mixed systems.

Third, the potential interactions of the additional VOCs in the mixed systems possibly act as a factor for the different clustering behaviour, supported by the formation of unique compounds in the mixture. Those unique-to-the-mixture compounds may be derived by the different oxidant regimes or VOC:  $NO_x$  ratios in systems. The presence of unique compounds and oxidation products derived from other precursors can impact the chemical characteristics of clusters, such as the reduced average carbon numbers in cluster 5 in the  $\alpha$ -pinene/isoprene experiment, as shown in Figure 4. Nevertheless, it is impractical to evaluate the reasons for clustering behaviours of all clusters/ions in all systems due to the complex chamber experimental conditions and limitation of our measurements. However, this illustrates the potential for hierarchical cluster analysis to help identify and understand differences between

different SOA systems. Those factors need to be taken into consideration in the different cluster behaviours compared to various systems.

## 5. Conclusions

In this work, we conducted a series of experiments in the smog chamber to characterize the chemical composition from the  $\alpha$ -pinene/isoprene, o-cresol/isoprene,  $\alpha$ -pinene/o-cresol, and ternary mixture and single  $\alpha$ -pinene, o-cresol and isoprene systems in the presence of NO<sub>x</sub> and seeds. The formed gas-phase and particle-phase oxidation products are characterized by nearly real-time online iodide FIGAERO-CIMS, and the particle-phase products at the end of experiments are measured by offline LC-Orbitrap MS negative and positive ionisation modes. Meanwhile, the time-series cluster behaviour of oxidation products was explored in those systems. The following conclusions can be drawn based on our observations.

In the  $\alpha$ -pinene,  $\alpha$ -pinene/isoprene and ternary systems, the results illustrate that CHO species dominated the SOA particle phase under the current experimental conditions, dominated by the compounds with C<sub>8-10</sub>. It highlights the importance of the RO<sub>2</sub> + RO<sub>2</sub>/HO<sub>2</sub> formation pathway in the formation of SOA. Conversely, in the o-cresol and o-cresol/isoprene system, CHON species are the major contributor to the production of SOA, dominated by compounds with C<sub>6-7</sub>, implying the RO<sub>2</sub> + NO/NO<sub>2</sub> reaction pathway plays a major contribution to particle formation. Furthermore, the results from LC-Orbitrap MS display that more oxidation products with higher carbon number and oxygen numbers in all VOCs systems are detected, while the online iodide CIMS enables to measure more compounds with smaller carbon numbers ( $nC \leq 5$ ). The results further demonstrate that the combination of FIGAERO-CIMS and LC-orbitrap MS is important in order to capture the broad information on the SOA particulate components in the mixture studies.

Gas-phase clustering results distinguish that oxidation products of three clusters (clusters 3, 4 and 5) in the  $\alpha$ -pinene and  $\alpha$ -pinene/isoprene dominated by the CHON species show high dependence on the NO<sub>2</sub>/NO and O<sub>3</sub> formation, while clusters 1 and 2 with lower average carbon numbers are independent of the two parameters. In contrast, the gas-phase clustering results show that in the o-cresol containing systems, the cluster with a faster formation rate is dominated by the CHO species. In the individual systems, differences could be highlighted among clusters in respect of time-series patterns. We found the oxidant regimes play an important role in the cluster behaviours of oxidation products. In the  $\alpha$ -pinene/isoprene, clusters

3, 4 and 5 are highly related to the NO<sub>2</sub>/NO ratio and O<sub>3</sub> formation, while clusters 1 and 2 with lower average carbon numbers are independent of the two parameters.

Particle-phase clustering results show that majority of the particle-phase ions are clustered into two clusters (clusters 4 and 5) in all systems, suggesting the particle-phase chemical composition is not unambiguously related to formation rates of gas-phase ions and shows distinct partitioning behaviours among systems. In the  $\alpha$ -pinene/isoprene system, the two clusters are dominated by the CHO species, similar to that in the  $\alpha$ -pinene system, whilst CHON species dominate the products in the *o*-cresol. However, other systems exhibit different clustering results. In cluster 5, CHON species carry larger fractions in *o*-cresol/isoprene systems, whilst CHO species show greater fractions in the  $\alpha$ -pinene/*o*-cresol and ternary systems. In cluster 4, CHO species play a dominant role in the *o*-cresol/isoprene system, whereas products in the CHON group make greater contributions in the  $\alpha$ -pinene/*o*-cresol and ternary systems. Molecular interactions are observed in the mixed systems and the unique-to-the-mixture products are distributed in different clusters, suggesting distinct oxidation rates in various systems. Those products make significant contributions to the particle phase in the mixture. However, more work is required to get insight into the mechanisms of such interactions in the mixture.

With all results taken together, this study gives the foundation for understanding the chemical compositions in the mixed systems under the photooxidation reactions in the presence of NO<sub>x</sub>. The distinct distribution of binary and ternary experiments indicates individual precursor investigation can get insight into the SOA formation mechanisms but the results can not represent the situation of the mixtures. Whilst the results presented here are limited by the used chamber experimental conditions, more effort on the broader ranges of NO<sub>x</sub> and initial precursor concentrations needs to be performed to enable the generalisation of the conclusions of the present study and refine clustering mechanisms of oxidised organic compounds. This study emphasizes the importance and needs of further systematic mixture studies to understand the chemical properties of oxidation products, helping better understand their potential influence on the SOA formation, cloud nuclei and climate changes in the real atmosphere.

## **Acknowledgements**

The Manchester Aerosol Chamber received funding from the European Union's Horizon 2020 research and innovation programme under grant agreement no. 730997, which supports



the EUROCHAMP2020 research programme. MD acknowledges the funding supported by the President Doctoral Scholarship award (PDS award) from the University of Manchester. M.R.A. acknowledges support by UK National Centre for Atmospheric Sciences (NACS) funding. Instrumentational support was funded through the NERC Atmospheric Measurement and Observational Facility (AMOF). The Orbitrap MS was funded by a capital grant from NERC (CC090). We acknowledge funding for the COMPLEX-OA project funded by NERC (NE/S010467/1).

### **Competing interests**

The authors declare that they have no conflict of interest.

### **Data availability**

Data are available on request.

### **Author contributions**

GM, MRA, MD, AV, YW and YS conceived the study. MD, AV, YW, and YS conducted the experiments. TJB provided on-site help deploying the FIGAERO-CIMS. KLP and JFH offered help on the LC-orbitrap MS analysis. MD conducted the data analysis and wrote the manuscript with inputs from all co-authors.

### **References**

Alfarra, M. R., Hamilton, J. F., Wyche, K. P., Good, N., Ward, M. W., Carr, T., Barley, M. H., Monks, P. S., Jenkin, M. E., Lewis, A. C., and McFiggans, G. B.: The effect of photochemical ageing and initial precursor concentration on the composition and hygroscopic properties of  $\beta$ -caryophyllene secondary organic aerosol, *Atmospheric Chemistry and Physics*, 12, 6417-6436, 10.5194/acp-12-6417-2012, 2012.

Aljawhary, D., Zhao, R., Lee, A. K., Wang, C., and Abbatt, J. P.: Kinetics, Mechanism, and Secondary Organic Aerosol Yield of Aqueous Phase Photo-oxidation of alpha-Pinene Oxidation Products, *J Phys Chem A*, 120, 1395-1407, 10.1021/acs.jpca.5b06237, 2016.

Aschmann, S. M.: Products of reaction of OH radicals with  $\alpha$ -pinene, *Journal of Geophysical Research*, 107, 10.1029/2001jd001098, 2002.

Atkinson, R.: Atmospheric chemistry of VOCs and NO<sub>x</sub>, *Atmospheric Environment*, 34, 2063-2101, 10.1016/s1352-2310(99)00460-4, 2000.

Atkinson, R. and Arey, J.: Gas-phase tropospheric chemistry of biogenic volatile organic compounds: a review, *Atmospheric Environment*, 37, 197-219, 10.1016/s1352-

2310(03)00391-1, 2003.

Bagchi, A., Yu, Y., Huang, J. H., Tsai, C. C., Hu, W. P., and Wang, C. C.: Evidence and evolution of Criegee intermediates, hydroperoxides and secondary organic aerosols formed via ozonolysis of alpha-pinene, *Phys Chem Chem Phys*, 22, 6528-6537, 10.1039/c9cp06306d, 2020.

Bannan, T. J., Le Breton, M., Priestley, M., Worrall, S. D., Bacak, A., Marsden, N. A., Mehra, A., Hammes, J., Hallquist, M., Alfarra, M. R., Krieger, U. K., Reid, J. P., Jayne, J., Robinson, W., McFiggans, G., Coe, H., Percival, C. J., and Topping, D.: A method for extracting calibrated volatility information from the FIGAERO-HR-ToF-CIMS and its experimental application, *Atmospheric Measurement Techniques*, 12, 1429-1439, 10.5194/amt-12-1429-2019, 2019.

Bianchi, F., Kurten, T., Riva, M., Mohr, C., Rissanen, M. P., Roldin, P., Berndt, T., Crouse, J. D., Wennberg, P. O., Mentel, T. F., Wildt, J., Junninen, H., Jokinen, T., Kulmala, M., Worsnop, D. R., Thornton, J. A., Donahue, N., Kjaergaard, H. G., and Ehn, M.: Highly Oxygenated Organic Molecules (HOM) from Gas-Phase Autoxidation Involving Peroxy Radicals: A Key Contributor to Atmospheric Aerosol, *Chem Rev*, 119, 3472-3509, 10.1021/acs.chemrev.8b00395, 2019.

Borrás, E. and Tortajada-Genaro, L. A.: Secondary organic aerosol formation from the photo-oxidation of benzene, *Atmospheric Environment*, 47, 154-163, 10.1016/j.atmosenv.2011.11.020, 2012.

Brege, M., Paglione, M., Gilardoni, S., Decesari, S., Facchini, M. C., and Mazzoleni, L. R.: Molecular insights on aging and aqueous-phase processing from ambient biomass burning emissions-influenced Po Valley fog and aerosol, *Atmospheric Chemistry and Physics*, 18, 13197-13214, 10.5194/acp-18-13197-2018, 2018.

Carlton, A. G., Wiedinmyer, C., and Kroll, J. H.: A review of Secondary Organic Aerosol (SOA) formation from isoprene, *Atmospheric Chemistry and Physics*, 9, 4987-5005, 10.5194/acp-9-4987-2009, 2009.

Chen, Y., Takeuchi, M., Nah, T., Xu, L., Canagaratna, M. R., Stark, H., Baumann, K., Canonaco, F., Prévôt, A. S. H., Huey, L. G., Weber, R. J., and Ng, N. L.: Chemical characterization of secondary organic aerosol at a rural site in the southeastern US: insights from simultaneous high-resolution time-of-flight aerosol mass spectrometer (HR-ToF-AMS) and FIGAERO chemical ionization mass spectrometer (CIMS) measurements, *Atmospheric Chemistry and Physics*, 20, 8421-8440, 10.5194/acp-20-8421-2020, 2020.

Chen, Z., Chen, D., Kwan, M.-P., Chen, B., Gao, B., Zhuang, Y., Li, R., and Xu, B.: The control of anthropogenic emissions contributed to 80% of the decrease in PM<sub>2.5</sub> concentrations in Beijing from 2013 to 2017, *Atmospheric Chemistry and Physics*, 19, 13519-13533, 10.5194/acp-19-13519-2019, 2019.

Claeys, M., Iinuma, Y., Szmigielski, R., Surratt, J. D., Blockhuys, F., Van Alsenoy, C., Boge, O., Sierau, B., Gomez-Gonzalez, Y., Vermeylen, R., Van der Veken, P., Shahgholi, M., Chan, A. W., Herrmann, H., Seinfeld, J. H., and Maenhaut, W.: Terpenylic acid and related compounds from the oxidation of alpha-pinene: implications for new particle formation and

growth above forests, *Environ Sci Technol*, 43, 6976-6982, 10.1021/es9007596, 2009.

Crouse, J. D., Nielsen, L. B., Jørgensen, S., Kjaergaard, H. G., and Wennberg, P. O.: Autoxidation of Organic Compounds in the Atmosphere, *The Journal of Physical Chemistry Letters*, 4, 3513-3520, 10.1021/jz4019207, 2013.

D'Ambro, E. L., Schobesberger, S., Gaston, C. J., Lopez-Hilfiker, F. D., Lee, B. H., Liu, J., Zelenyuk, A., Bell, D., Cappa, C. D., Helgestad, T., Li, Z., Guenther, A., Wang, J., Wise, M., Caylor, R., Surratt, J. D., Riedel, T., Hyttinen, N., Salo, V.-T., Hasan, G., Kurtén, T., Shilling, J. E., and Thornton, J. A.: Chamber-based insights into the factors controlling epoxydiol (IEPOX) secondary organic aerosol (SOA) yield, composition, and volatility, *Atmospheric Chemistry and Physics*, 19, 11253-11265, 10.5194/acp-19-11253-2019, 2019.

Du, M., Voliotis, A., Shao, Y., Wang, Y., Bannan, T. J., Pereira, K. L., Hamilton, J. F., Percival, C. J., Alfarra, M. R., and McFiggans, G.: Combined application of Online FIGAERO-CIMS and Offline LC-Orbitrap MS to Characterize the Chemical Composition of SOA in Smog Chamber Studies, *AMTD*, 10.5194/amt-2021-420, 2021.

Eddingsaas, N. C., Loza, C. L., Yee, L. D., Seinfeld, J. H., and Wennberg, P. O.:  $\alpha$ -pinene photooxidation under controlled chemical conditions – Part 1: Gas-phase composition in low- and high-NO<sub>x</sub> environments, *Atmospheric Chemistry and Physics*, 12, 6489-6504, 10.5194/acp-12-6489-2012, 2012a.

Eddingsaas, N. C., Loza, C. L., Yee, L. D., Chan, M., Schilling, K. A., Chhabra, P. S., Seinfeld, J. H., and Wennberg, P. O.:  $\alpha$ -pinene photooxidation under controlled chemical conditions – Part 2: SOA yield and composition in low- and high-NO<sub>x</sub> environments, *Atmospheric Chemistry and Physics*, 12, 7413-7427, 10.5194/acp-12-7413-2012, 2012b.

Ehn, M., Thornton, J. A., Kleist, E., Sipila, M., Junninen, H., Pullinen, I., Springer, M., Rubach, F., Tillmann, R., Lee, B., Lopez-Hilfiker, F., Andres, S., Acir, I. H., Rissanen, M., Jokinen, T., Schobesberger, S., Kangasluoma, J., Kontkanen, J., Nieminen, T., Kurten, T., Nielsen, L. B., Jørgensen, S., Kjaergaard, H. G., Canagaratna, M., Maso, M. D., Berndt, T., Petaja, T., Wahner, A., Kerminen, V. M., Kulmala, M., Worsnop, D. R., Wildt, J., and Mentel, T. F.: A large source of low-volatility secondary organic aerosol, *Nature*, 506, 476-479, 10.1038/nature13032, 2014.

Emanuelsson, E. U., Hallquist, M., Kristensen, K., Glasius, M., Bohn, B., Fuchs, H., Kammer, B., Kiendler-Scharr, A., Nehr, S., Rubach, F., Tillmann, R., Wahner, A., Wu, H. C., and Mentel, T. F.: Formation of anthropogenic secondary organic aerosol (SOA) and its influence on biogenic SOA properties, *Atmospheric Chemistry and Physics*, 13, 2837-2855, 10.5194/acp-13-2837-2013, 2013.

Forstner, H. J. L., Flagan, R. C., and Seinfeld, J. H.: Secondary Organic Aerosol from the Photooxidation of Aromatic Hydrocarbons: Molecular Composition, *Environmental Science & Technology*, 31, 1345-1358, 10.1021/es9605376, 1997.

Fuzzi, S., Andreae, M. O., Huebert, B. J., Kulmala, M., Bond, T. C., Boy, M., Doherty, S. J., Guenther, A., Kanakidou, M., Kawamura, K., Kerminen, V. M., Lohmann, U., Russell, L. M., and Pöschl, U.: Critical assessment of the current state of scientific knowledge, terminology, and research needs concerning the role of organic aerosols in the atmosphere, climate, and

global change, *Atmospheric Chemistry and Physics*, 6, 2017-2038, 10.5194/acp-6-2017-2006, 2006.

Goldstein, A. H. and Galbally, I. E.: Known and unknown organic constituents in the Earth's atmosphere, *Environ Sci Technol*, 41, 1514-1521, 10.1021/es072476p, 2007.

Guenther, A. B., Jiang, X., Heald, C. L., Sakulyanontvittaya, T., Duhl, T., Emmons, L. K., and Wang, X.: The Model of Emissions of Gases and Aerosols from Nature version 2.1 (MEGAN2.1): an extended and updated framework for modeling biogenic emissions, *Geoscientific Model Development*, 5, 1471-1492, 10.5194/gmd-5-1471-2012, 2012.

Hallquist, M., Wenger, J. C., Baltensperger, U., Rudich, Y., Simpson, D., Claeys, M., Dommen, J., Donahue, N. M., George, C., Goldstein, A. H., Hamilton, J. F., Herrmann, H., Hoffmann, T., Iinuma, Y., Jang, M., Jenkin, M. E., Jimenez, J. L., Kiendler-Scharr, A., Maenhaut, W., McFiggans, G., Mentel, T. F., Monod, A., Prévôt, A. S. H., Seinfeld, J. H., Surratt, J. D., Szmigielski, R., and Wildt, J.: The formation, properties and impact of secondary organic aerosol: current and emerging issues, *Atmospheric Chemistry and Physics*, 9, 5155-5236, 10.5194/acp-9-5155-2009, 2009.

Henze, D. K., Seinfeld, J. H., Ng, N. L., Kroll, J. H., Fu, T. M., Jacob, D. J., and Heald, C. L.: Global modeling of secondary organic aerosol formation from aromatic hydrocarbons: high- vs. low-yield pathways, *Atmospheric Chemistry and Physics*, 8, 2405-2420, 10.5194/acp-8-2405-2008, 2008.

Hoyle, C. R., Boy, M., Donahue, N. M., Fry, J. L., Glasius, M., Guenther, A., Hallar, A. G., Huff Hartz, K., Petters, M. D., Petäjä, T., Rosenoern, T., and Sullivan, A. P.: A review of the anthropogenic influence on biogenic secondary organic aerosol, *Atmospheric Chemistry and Physics*, 11, 321-343, 10.5194/acp-11-321-2011, 2011.

Hurley, M. D., Sokolov, O., Wallington, T. J., Takekawa, H., Karasawa, M., Klotz, B., Barnes, I., and Becker, K. H.: Organic aerosol formation during the atmospheric degradation of toluene, *Environ Sci Technol*, 35, 1358-1366, 10.1021/es0013733, 2001.

IPCC: <IPCC 2013.pdf>, 2013.

Jenkin, M. E., Young, J. C., and Rickard, A. R.: The MCM v3.3.1 degradation scheme for isoprene, *Atmospheric Chemistry and Physics*, 15, 11433-11459, 10.5194/acp-15-11433-2015, 2015.

John D. Roberts, M. C. C.: *Basic Principles of Organic Chemistry*, 1977.

Johnson, D. and Marston, G.: The gas-phase ozonolysis of unsaturated volatile organic compounds in the troposphere, *Chem Soc Rev*, 37, 699-716, 10.1039/b704260b, 2008.

Jokinen, T., Berndt, T., Makkonen, R., Kerminen, V. M., Junninen, H., Paasonen, P., Stratmann, F., Herrmann, H., Guenther, A. B., Worsnop, D. R., Kulmala, M., Ehn, M., and Sipila, M.: Production of extremely low volatile organic compounds from biogenic emissions: Measured yields and atmospheric implications, *Proc Natl Acad Sci U S A*, 112, 7123-7128, 10.1073/pnas.1423977112, 2015.

- Kanawade, V. P., Jobson, B. T., Guenther, A. B., Erupe, M. E., Pressley, S. N., Tripathi, S. N., and Lee, S. H.: Isoprene suppression of new particle formation in a mixed deciduous forest, *Atmospheric Chemistry and Physics*, 11, 6013-6027, 10.5194/acp-11-6013-2011, 2011.
- Kiendler-Scharr, A., Wildt, J., Dal Maso, M., Hohaus, T., Kleist, E., Mentel, T. F., Tillmann, R., Uerlings, R., Schurr, U., and Wahner, A.: New particle formation in forests inhibited by isoprene emissions, *Nature*, 461, 381-384, 10.1038/nature08292, 2009.
- Kiontke, A., Oliveira-Birkmeier, A., Opitz, A., and Birkemeyer, C.: Electrospray Ionization Efficiency Is Dependent on Different Molecular Descriptors with Respect to Solvent pH and Instrumental Configuration, *PLoS One*, 11, e0167502, 10.1371/journal.pone.0167502, 2016.
- Koss, A. R., Canagaratna, M. R., Zaytsev, A., Krechmer, J. E., Breitenlechner, M., Nihill, K. J., Lim, C. Y., Rowe, J. C., Roscioli, J. R., Keutsch, F. N., and Kroll, J. H.: Dimensionality-reduction techniques for complex mass spectrometric datasets: application to laboratory atmospheric organic oxidation experiments, *Atmos Chem Phys*, 20, 1021-1041, 10.5194/acp-20-1021-2020, 2020.
- Kroll, J. H. and Seinfeld, J. H.: Chemistry of secondary organic aerosol: Formation and evolution of low-volatility organics in the atmosphere, *Atmospheric Environment*, 42, 3593-3624, 10.1016/j.atmosenv.2008.01.003, 2008.
- Langford, B., Nemitz, E., House, E., Phillips, G. J., Famulari, D., Davison, B., Hopkins, J. R., Lewis, A. C., and Hewitt, C. N.: Fluxes and concentrations of volatile organic compounds above central London, UK, *Atmospheric Chemistry and Physics*, 10, 627-645, 10.5194/acp-10-627-2010, 2010.
- Lee, B. H., Lopez-Hilfiker, F. D., Mohr, C., Kurten, T., Worsnop, D. R., and Thornton, J. A.: An iodide-adduct high-resolution time-of-flight chemical-ionization mass spectrometer: application to atmospheric inorganic and organic compounds, *Environ Sci Technol*, 48, 6309-6317, 10.1021/es500362a, 2014.
- Lee, S.-H., Uin, J., Guenther, A. B., de Gouw, J. A., Yu, F., Nadykto, A. B., Herb, J., Ng, N. L., Koss, A., Brune, W. H., Baumann, K., Kanawade, V. P., Keutsch, F. N., Nenes, A., Olsen, K., Goldstein, A., and Ouyang, Q.: Isoprene suppression of new particle formation: Potential mechanisms and implications, *Journal of Geophysical Research: Atmospheres*, 121, 14,621-614,635, 10.1002/2016jd024844, 2016.
- Lopez-Hilfiker, F. D., Mohr, C., Ehn, M., Rubach, F., Kleist, E., Wildt, J., Mentel, T. F., Lutz, A., Hallquist, M., Worsnop, D., and Thornton, J. A.: A novel method for online analysis of gas and particle composition: description and evaluation of a Filter Inlet for Gases and AEROSols (FIGAERO), *Atmospheric Measurement Techniques*, 7, 983-1001, 10.5194/amt-7-983-2014, 2014.
- Lopez-Hilfiker, F. D., Mohr, C., D'Ambro, E. L., Lutz, A., Riedel, T. P., Gaston, C. J., Iyer, S., Zhang, Z., Gold, A., Surratt, J. D., Lee, B. H., Kurten, T., Hu, W. W., Jimenez, J., Hallquist, M., and Thornton, J. A.: Molecular Composition and Volatility of Organic Aerosol in the Southeastern U.S.: Implications for IEPOX Derived SOA, *Environ Sci Technol*, 50, 2200-2209, 10.1021/acs.est.5b04769, 2016.

Ma, Y., Russell, A. T., and Marston, G.: Mechanisms for the formation of secondary organic aerosol components from the gas-phase ozonolysis of alpha-pinene, *Phys Chem Chem Phys*, 10, 4294-4312, 10.1039/b803283a, 2008.

McFiggans, G., Mentel, T. F., Wildt, J., Pullinen, I., Kang, S., Kleist, E., Schmitt, S., Springer, M., Tillmann, R., Wu, C., Zhao, D., Hallquist, M., Faxon, C., Le Breton, M., Hallquist, A. M., Simpson, D., Bergstrom, R., Jenkin, M. E., Ehn, M., Thornton, J. A., Alfarra, M. R., Bannan, T. J., Percival, C. J., Priestley, M., Topping, D., and Kiendler-Scharr, A.: Secondary organic aerosol reduced by mixture of atmospheric vapours, *Nature*, 565, 587-593, 10.1038/s41586-018-0871-y, 2019.

Mehra, A., Wang, Y., Krechmer, J. E., Lambe, A., Majluf, F., Morris, M. A., Priestley, M., Bannan, T. J., Bryant, D. J., Pereira, K. L., Hamilton, J. F., Rickard, A. R., Newland, M. J., Stark, H., Croteau, P., Jayne, J. T., Worsnop, D. R., Canagaratna, M. R., Wang, L., and Coe, H.: Evaluation of the Chemical Composition of Gas and Particle Phase Products of Aromatic Oxidation, *Atmos. Chem. Phys. Discuss.*, 10.5194/acp-2020-161, 2020.

Mentel, T. F., Springer, M., Ehn, M., Kleist, E., Pullinen, I., Kurtén, T., Rissanen, M., Wahner, A., and Wildt, J.: Formation of highly oxidized multifunctional compounds: autoxidation of peroxy radicals formed in the ozonolysis of alkenes – deduced from structure–product relationships, *Atmospheric Chemistry and Physics*, 15, 6745-6765, 10.5194/acp-15-6745-2015, 2015.

Mutzel, A., Zhang, Y., Böge, O., Rodigast, M., Kolodziejczyk, A., Wang, X., and Herrmann, H.: Importance of secondary organic aerosol formation of  $\alpha$ -pinene, limonene, and *m*-cresol comparing day- and nighttime radical chemistry, *Atmospheric Chemistry and Physics*, 21, 8479-8498, 10.5194/acp-21-8479-2021, 2021.

Ng, N. L., Kroll, J. H., Chan, A. W. H., Chhabra, P. S., Flagan, R. C., and Seinfeld, J. H.: Secondary organic aerosol formation from *m*-xylene, toluene, and benzene, *Atmospheric Chemistry and Physics*, 7, 3909-3922, 10.5194/acp-7-3909-2007, 2007a.

Ng, N. L., Chhabra, P. S., Chan, A. W. H., Surratt, J. D., Kroll, J. H., Kwan, A. J., McCabe, D. C., Wennberg, P. O., Sorooshian, A., Murphy, S. M., Dalleska, N. F., Flagan, R. C., and Seinfeld, J. H.: Effect of NO<sub>x</sub> level on secondary organic aerosol (SOA) formation from the photooxidation of terpenes, *Atmospheric Chemistry and Physics*, 7, 5159-5174, 10.5194/acp-7-5159-2007, 2007b.

Paulot, F., Crounse, J. D., Kjaergaard, H. G., Kroll, J. H., Seinfeld, J. H., and Wennberg, P. O.: Isoprene photooxidation: new insights into the production of acids and organic nitrates, *Atmospheric Chemistry and Physics*, 9, 1479-1501, 10.5194/acp-9-1479-2009, 2009.

Pereira, K. L., Ward, M. W., Wilkinson, J. L., Sallach, J. B., Bryant, D. J., Dixon, W. J., Hamilton, J. F., and Lewis, A. C.: An Automated Methodology for Non-targeted Compositional Analysis of Small Molecules in High Complexity Environmental Matrices Using Coupled Ultra Performance Liquid Chromatography Orbitrap Mass Spectrometry, *Environ Sci Technol*, 55, 7365-7375, 10.1021/acs.est.0c08208, 2021.

Poschl, U.: Atmospheric aerosols: composition, transformation, climate and health effects, *Angew Chem Int Ed Engl*, 44, 7520-7540, 10.1002/anie.200501122, 2005.

Priestley, M., Bannan, T. J., Le Breton, M., Worrall, S. D., Kang, S., Pullinen, I., Schmitt, S., Tillmann, R., Kleist, E., Zhao, D., Wildt, J., Garmash, O., Mehra, A., Bacak, A., Shallcross, D. E., Kiendler-Scharr, A., Hallquist, Å. M., Ehn, M., Coe, H., Percival, C. J., Hallquist, M., Mentel, T. F., and McFiggans, G.: Chemical characterisation of benzene oxidation products under high- and low-NO<sub>2</sub> conditions using chemical ionisation mass spectrometry, *Atmospheric Chemistry and Physics*, 21, 3473-3490, 10.5194/acp-21-3473-2021, 2021.

Pye, H. O. T., D'Ambro, E. L., Lee, B. H., Schobesberger, S., Takeuchi, M., Zhao, Y., Lopez-Hilfiker, F., Liu, J., Shilling, J. E., Xing, J., Mathur, R., Middlebrook, A. M., Liao, J., Welti, A., Graus, M., Warneke, C., de Gouw, J. A., Holloway, J. S., Ryerson, T. B., Pollack, I. B., and Thornton, J. A.: Anthropogenic enhancements to production of highly oxygenated molecules from autoxidation, *Proc Natl Acad Sci U S A*, 116, 6641-6646, 10.1073/pnas.1810774116, 2019.

Reyes-Villegas, E., Bannan, T., Le Breton, M., Mehra, A., Priestley, M., Percival, C., Coe, H., and Allan, J. D.: Online Chemical Characterization of Food-Cooking Organic Aerosols: Implications for Source Apportionment, *Environ Sci Technol*, 52, 5308-5318, 10.1021/acs.est.7b06278, 2018.

Sato, K., Hatakeyama, S., and Imamura, T.: Secondary organic aerosol formation during the photooxidation of toluene: NO<sub>x</sub> dependence of chemical composition, *J Phys Chem A*, 111, 9796-9808, 10.1021/jp071419f, 2007.

Sato, K., Nakashima, Y., Morino, Y., Imamura, T., Kurokawa, J.-i., and Kajii, Y.: Total OH reactivity measurements for the OH-initiated oxidation of aromatic hydrocarbons in the presence of NO<sub>x</sub>, *Atmospheric Environment*, 171, 272-278, 10.1016/j.atmosenv.2017.10.036, 2017.

Schwantes, R. H., Schilling, K. A., McVay, R. C., Lignell, H., Coggon, M. M., Zhang, X., Wennberg, P. O., and Seinfeld, J. H.: Formation of highly oxygenated low-volatility products from cresol oxidation, *Atmospheric Chemistry and Physics*, 17, 3453-3474, 10.5194/acp-17-3453-2017, 2017.

Seinfeld, J. H. and Pandis, S. N.: *Atmospheric chemistry and physics : from air pollution to climate change*, Third edition., John Wiley & Sons, Hoboken, New Jersey 2016.

Shao, Y., Wang, Y., Du, M., Voliotis, A., Alfarra, M. R., Turner, S. F., and McFiggans, G.: Characterisation of the Manchester Aerosol Chamber facility, *Atmospheric measurement techniques*, 10.5194/amt-2021-147, 2021.

Shilling, J. E., Zaveri, R. A., Fast, J. D., Kleinman, L., Alexander, M. L., Canagaratna, M. R., Fortner, E., Hubbe, J. M., Jayne, J. T., Sedlacek, A., Setyan, A., Springston, S., Worsnop, D. R., and Zhang, Q.: Enhanced SOA formation from mixed anthropogenic and biogenic emissions during the CARES campaign, *Atmospheric Chemistry and Physics*, 13, 2091-2113, 10.5194/acp-13-2091-2013, 2013.

Spracklen, D. V., Jimenez, J. L., Carslaw, K. S., Worsnop, D. R., Evans, M. J., Mann, G. W., Zhang, Q., Canagaratna, M. R., Allan, J., Coe, H., McFiggans, G., Rap, A., and Forster, P.: Aerosol mass spectrometer constraint on the global secondary organic aerosol budget,

- Atmospheric Chemistry and Physics, 11, 12109-12136, 10.5194/acp-11-12109-2011, 2011.
- Stark, H., Yatavelli, R. L. N., Thompson, S. L., Kimmel, J. R., Cubison, M. J., Chhabra, P. S., Canagaratna, M. R., Jayne, J. T., Worsnop, D. R., and Jimenez, J. L.: Methods to extract molecular and bulk chemical information from series of complex mass spectra with limited mass resolution, *International Journal of Mass Spectrometry*, 389, 26-38, 10.1016/j.ijms.2015.08.011, 2015.
- Steimer, S. S., Delvaux, A., Campbell, S. J., Gallimore, P. J., Grice, P., Howe, D. J., Pitton, D., Claeys, M., Hoffmann, T., and Kalberer, M.: Synthesis and characterisation of peroxy-pinic acids as proxies for highly oxygenated molecules (HOMs) in secondary organic aerosol, *Atmospheric Chemistry and Physics*, 18, 10973-10983, 10.5194/acp-18-10973-2018, 2018.
- Voliotis, A., Wang, Y., Shao, Y., Du, M., Bannan, T. J., Percival, C. J., Pandis, S. N., Alfarra, M. R., and McFiggans, G.: Exploring the composition and volatility of secondary organic aerosols in mixed anthropogenic and biogenic precursor systems, *Atmospheric Chemistry and Physics*, 21, 14251-14273, 10.5194/acp-21-14251-2021, 2021.
- Wang, D. S. and Hildebrandt Ruiz, L.: Chlorine-initiated oxidation of n-alkanes under high-NO<sub>x</sub> conditions: insights into secondary organic aerosol composition and volatility using a FIGAERO-CIMS, *Atmospheric Chemistry and Physics*, 18, 15535-15553, 10.5194/acp-18-15535-2018, 2018.
- Wang, S., Riva, M., Yan, C., Ehn, M., and Wang, L.: Primary Formation of Highly Oxidized Multifunctional Products in the OH-Initiated Oxidation of Isoprene: A Combined Theoretical and Experimental Study, *Environ Sci Technol*, 52, 12255-12264, 10.1021/acs.est.8b02783, 2018.
- Xu, L., Kollman, M. S., Song, C., Shilling, J. E., and Ng, N. L.: Effects of NO<sub>x</sub> on the volatility of secondary organic aerosol from isoprene photooxidation, *Environ Sci Technol*, 48, 2253-2262, 10.1021/es404842g, 2014.
- Xu, L., Middlebrook, A. M., Liao, J., de Gouw, J. A., Guo, H., Weber, R. J., Nenes, A., Lopez-Hilfiker, F. D., Lee, B. H., Thornton, J. A., Brock, C. A., Neuman, J. A., Nowak, J. B., Pollack, I. B., Welti, A., Graus, M., Warneke, C., and Ng, N. L.: Enhanced formation of isoprene-derived organic aerosol in sulfur-rich power plant plumes during Southeast Nexus, *Journal of Geophysical Research: Atmospheres*, 121, 11,137-111,153, 10.1002/2016jd025156, 2016.
- Zhang, X., McVay, R. C., Huang, D. D., Dalleska, N. F., Aumont, B., Flagan, R. C., and Seinfeld, J. H.: Formation and evolution of molecular products in alpha-pinene secondary organic aerosol, *Proc Natl Acad Sci U S A*, 112, 14168-14173, 10.1073/pnas.1517742112, 2015.
- Zhang, X., Lambe, A. T., Upshur, M. A., Brooks, W. A., Gray Be, A., Thomson, R. J., Geiger, F. M., Surratt, J. D., Zhang, Z., Gold, A., Graf, S., Cubison, M. J., Groessl, M., Jayne, J. T., Worsnop, D. R., and Canagaratna, M. R.: Highly Oxygenated Multifunctional Compounds in alpha-Pinene Secondary Organic Aerosol, *Environ Sci Technol*, 51, 5932-5940, 10.1021/acs.est.6b06588, 2017.



[BLANK PAGE]

## Chapter 5. Conclusions and Perspectives

### 5.1 Conclusions

This thesis explored the SOA formation from the mixed anthropogenic and biogenic VOCs in the presence of NO<sub>x</sub>. The experiments were carried out in the Manchester Aerosol Chamber (MAC).  $\alpha$ -pinene and isoprene were chosen as the representative of biogenic VOCs and *o*-cresol as the representative of anthropogenic VOC. The concept of ‘iso-reactivity’ towards OH was employed to determine the initial concentrations of the parent precursors in the mixtures. All experiments were performed under similar experimental conditions (VOCs: NO<sub>x</sub> ratio ~ 8, AS seed concentration: ~50  $\mu\text{g m}^{-3}$ , RH: 50%, T:25 °C, ~ 6-hour photooxidation reactions). A series of online and offline analytical techniques were utilized to investigate the physical and chemical properties of formed SOA. The results of this work provided a springboard for the scientific community in the SOA formation from the mixtures of VOCs.

The first paper presented the characterization of the MAC and demonstrated the capabilities and limitations of the chamber. MAC can provide controllable temperature and relative humidity conditions which are important for any chamber study. Regular characterization experiments are strongly suggested to track the chamber’s performance in order to well interpret the experimental results, since the bag usage, wall loss rate of gas and particles, etc, will impact the experimental results. The complexity and differences of chamber characterizations highlight the need in developing a set of simple, standardized experiments and/or procedures that can be used from chambers across the globe to elucidate the characteristics of each facility and the interpretation of their results.

The second paper provided a clear suppression of the SOA yield from  $\alpha$ -pinene when it was mixed with isoprene, while the addition of isoprene to *o*-cresol may enhance its SOA formation potential, however, the difference was too small to be univocal. The measured SOA yield in the  $\alpha$ -pinene/*o*-cresol system appeared to be increased compared to that calculated based on the additivity, while in the  $\alpha$ -pinene/*o*-cresol/isoprene system the measured and predicted yield was comparable. However, in mixtures where more than one precursor contributes to the SOA mass, it was unclear to attribute the changes in the SOA formation

potential in physical or chemical interactions as the reference point for the comparison is complex.

The third paper illustrated that the application of the combinational online FIGAERO-CIMS and offline LC-Orbitrap MS measurements can capture broad information on the oxidation products formed from the  $\alpha$ -pinene photooxidation reactions. The gas and particle time-series data from the FIGAERO-CIMS measurement were separated by the hierarchical clustering analysis (HCA), an approach that does not rely on mass calibration. HCA was able to derive cluster properties in terms of average carbon number, oxygen number, oxidation states, for example, enabling interpretation in terms of possible termination pathways of peroxy radicals in the  $\alpha$ -pinene photooxidation reactions. Furthermore, it was found that there was substantial uncertainty in the accurate estimation of saturation concentration of compounds between partitioning theory method from online measurements and molecular structural based approach.

The fourth paper presented that the major chemical components of various systems were different. In the gas phase, the compounds in the CHON group made a greater contribution in the  $\alpha$ -pinene, isoprene,  $\alpha$ -pinene/isoprene,  $\alpha$ -pinene/o-cresol and ternary systems, while compounds in the CHO group contributed more in o-cresol and o-cresol/isoprene, dominated by C<sub>6-7</sub>. The online particle-phase measurements exhibited that the fractions of oxidation products were dominated by the products in the CHO species in the  $\alpha$ -pinene containing and o-cresol/isoprene systems, whereas the fractions of oxidation products were dominated by the products in the CHON species with C<sub>6-7</sub> formulae in the single o-cresol. The outcomes from offline negative mode were comparable to the results from online particle-phase measurements in the  $\alpha$ -pinene and  $\alpha$ -pinene/isoprene systems; however, the o-cresol containing systems were dominated by the CHON signal fraction (>60%). The LC-Orbitrap MS positive mode showed that more compounds with high carbon numbers (C<sub>≥16</sub>) were detected than those from the negative mode and online measurements in all VOC experiments. Unique-to-the-mixture products were investigated in the mixed systems, indicating the molecular interactions in the mixture. However, additional work is needed to get insight into the mechanisms of such interactions in the mixture.

This work highlighted the importance of combinational offline and online measurements in the chemical components of SOA formation. Additionally, molecular interactions were

investigated in the mixed systems, while the formation mechanisms of those unique products are still unclear.

## 5.2 Future work

This thesis has explored the SOA formation from the mixed anthropogenic VOCs and biogenic VOCs in the presence of NO<sub>x</sub> and neutral seeds by the combination of various online and offline analytical techniques. It suggested that the SOA yield and chemical composition in the mixed VOCs are complicated. This work provided the springboard of the mixtures studies for the atmospheric community. However, there are still some open questions that need more effort. Several suggestions help to guide future work and development.

This work found that the bag usage history (e.g. the frequency of usage, types of experiments performed in the bag) can impact the chamber's chemical performance and the different chambers with various facilities can affect the experimental results. Considering that the atmospheric simulation chambers are composed of various materials and they come in different designs, sizes and shapes, in turn affecting their performance and behaviour, the comparability of their results should be a crucial priority of the scientific community. The results from our chamber characterisation highlight the necessity for confirmation of chamber conditions (e.g.  $jNO_2$ , wall loss rates of gases and particles, contaminations, etc) before experiments. The results presented here also stressed the need for the development of a unified framework to characterize the atmospheric simulation chambers globally.

This work found that there is substantial uncertainty in the accurate estimation of saturation concentration of compounds. The  $C^*$  calculated from the FIGAERO-CIMS measured  $F_p$  was generally within around 2 orders of magnitude of that estimated from the LC-Orbitrap MS-derived molecular structure for most compounds and sometimes much closer (less than 1 order of magnitude). Such agreement could be used to assign classification into the somewhat broad and arbitrarily defined volatility categories (such as semi-volatile, low volatility, intermediate volatility etc) but such utility is questionable. Moreover, clear discrepancies were noticed for the lowest and highest volatility compounds. The differences resulting from the two approaches indicates that further work is required to investigate whether the  $C^*$  determined for the compounds are consistent with our understanding of the processes determining the time evolution of phase partitioning. The accurate estimation of  $C^*$  can also

help better understand the gas-to-particle partitioning and volatility distribution in future studies.

This thesis used the online I-CIMS to investigate the SOA chemical composition, which is less sensitive to highly oxygenated molecules. It was reported that isoprene can suppress the formation of HOMs in the  $\alpha$ -pinene/isoprene mixture. It is also illustrated by other studies that HOMs plays an important role in SOA formation in the atmosphere. However, this study suggests that it is challenging to evaluate the HOMs formation and track the contribution and roles of HOMs in the anthropogenic and biogenic mixed systems due to the limitation of iodide reagent ions measurements on HOMs. This is an important consideration for the future development of chemical composition in mixtures studies. And therefore, it suggests that future work should apply online analytical techniques which are capable of measuring HOMs, such as the  $\text{NO}_3$ -CIMS to explore the HOMs formation in the mixture studies. The recent newly found HOMs species illustrate that the gas-phase mechanism from the MCM does not capture the full extent of observed ions, especially from the autooxidation pathways to form the more oxidised molecules. More chamber studies are needed to expand the MCM pathways to get insights into gas-phase chemistry.

This thesis demonstrated the potential interactions in SOA yields, chemical composition formation and their chemical properties in the mixed systems. Such interactions are more complicated than those in the individual precursor. However, it remains many uncertainties in the interpretation of the mechanistic formation in our chamber experiments due to the limitation of measurements. More systematic experiments with more atmospherically relevant combined with other advanced analytical techniques (such as PTR-MS) and flow reactors are necessary to be performed to have a deeper understanding of molecular interactions from the mechanistic insights in the anthropogenic and biogenic VOC mixtures. The OH-initiated photooxidation reactions and mimic the daytime oxidants conditions were studied in this work, but it is still unclear about the SOA formation from the night-time conditions with the  $\text{NO}_3^-$  dominance. Those aspects can be considered in future mixture studies.

Simple experimental conditions were examined and assessed for the mixed systems in this study. However, broader ranges of temperatures, relative humidity,  $\text{NO}_x$  and initial VOCs concentrations in more atmospherically related levels need to be investigated to enable the generalisation of the conclusions of the present study and refine clustering mechanisms of

oxidised organic compounds in order to better model SOA and oxidation products chemistry for more accurate predictions of NO<sub>x</sub> and O<sub>3</sub> budgets.

[BLANK PAGE]

# Appendices

## Supplementary Information for Paper 1

### Characterisation of the Manchester Aerosol Chamber facility

Yunqi Shao<sup>1\*</sup>, Yu Wang<sup>1\*</sup>, Mao Du<sup>1\*</sup>, Aristeidis Voliotis<sup>1\*</sup>, M. Rami Alfarra<sup>1,2,‡</sup>, Simon P. O'Meara<sup>1,2</sup>, S. Fiona Turner<sup>1,†</sup> and Gordon McFiggans<sup>1</sup>

<sup>1</sup> Centre for Atmospheric Science, Department of Earth and Environmental Sciences, School of Natural Sciences, University of Manchester, Manchester, M13 9PL, United Kingdom

<sup>2</sup> National Centre for Atmospheric Science (NCAS), University of Manchester, Manchester, M13 9PL, United Kingdom

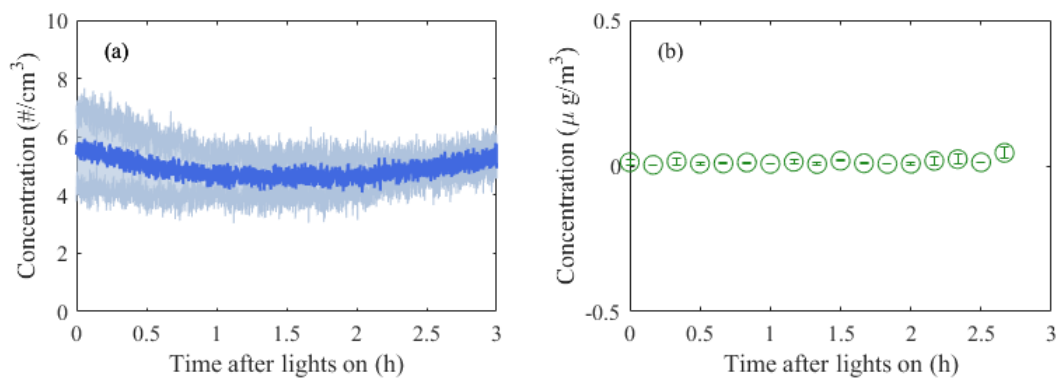
<sup>‡</sup> Now at Environment & Sustainability Center, Qatar Environment & Energy Research Institute, 34110, Doha, Qatar

<sup>†</sup> Now at AMETEK Land, Dronfield, Derbyshire, S18 1DJ, United Kingdom

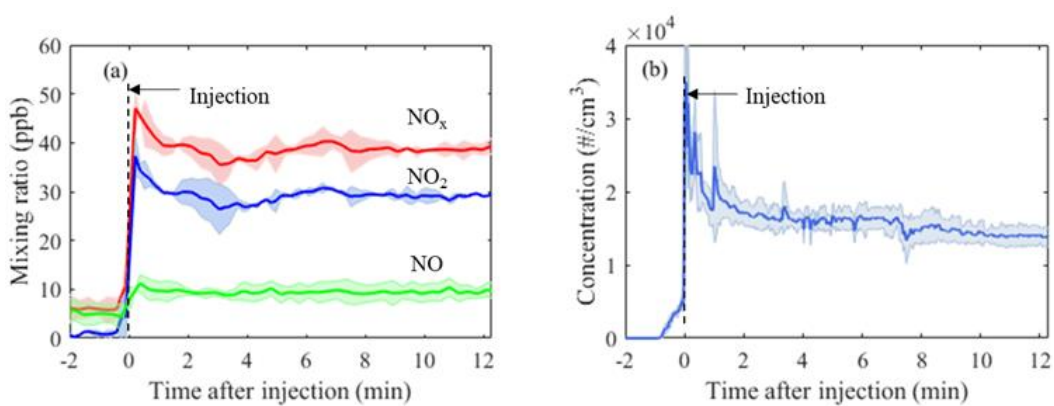
\*These authors all made equal contributions to this work.

*Correspondence to:* G. McFiggans (g.mcfiggans@manchester.ac.uk)





**Figure S1.** Time series (mean  $\pm 1\sigma$ ;  $n=2$ ) of particle number (a) and mass (b) concentrations throughout experiments (i.e., experiments conducted by illuminating the chamber without any reactants added).



**Figure S2.** Mean ( $\pm 1\sigma$ ;  $n=3$ ) (a) gas mixing ratio of NO<sub>x</sub> (ppb) and (b) particle number concentrations (particle  $\text{cm}^{-3}$ ) in three characteristic experiments as a function of their time after their injection to MAC.

## Supplementary Information for Paper 2

### Chamber investigation of the formation and transformation of secondary organic aerosol in mixtures of biogenic and anthropogenic volatile organic compounds

Aristeidis Voliotis<sup>1,\*</sup>, Mao Du<sup>1,\*</sup>, Yu Wang<sup>1,\*</sup>, Yunqi Shao<sup>1,\*</sup>, M. Rami Alfarra<sup>1,2,‡</sup>, Thomas J. Bannan<sup>1</sup>, Dawei Hu<sup>1</sup>, Kelly L. Pereira<sup>3</sup>, Jaqueline F. Hamilton<sup>3</sup>, Mattias Hallquist<sup>4</sup>, Thomas F. Mentel<sup>5</sup>, Gordon McFiggans<sup>1</sup>

<sup>1</sup>Centre for Atmospheric Science, Department of Earth and Environmental Sciences, School of Natural Sciences, University of Manchester, Manchester, M13 9PL, UK

<sup>2</sup>National Centre for Atmospheric Science (NCAS), University of Manchester, Manchester, M13 9PL, UK

<sup>3</sup>Wolfson Atmospheric Chemistry Laboratories, Department of Chemistry, University of York, York, YO10 5DD, UK

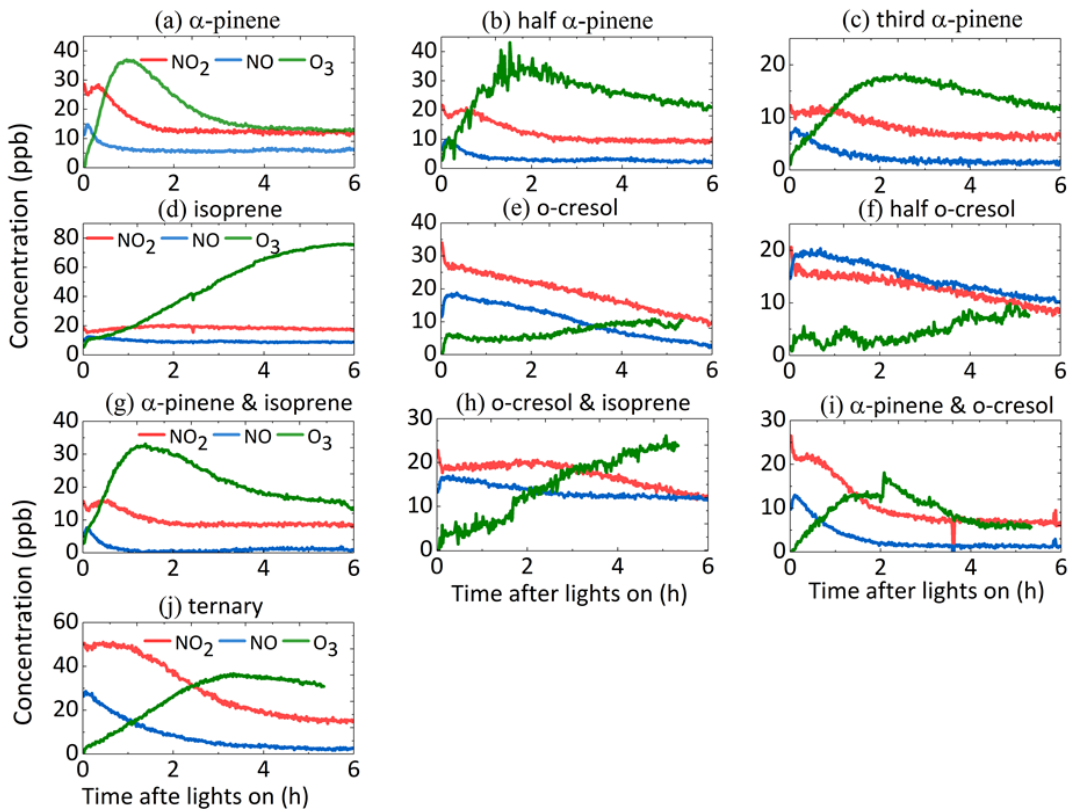
<sup>4</sup>Department of Chemistry and Molecular Biology, Atmospheric Science, University of Gothenburg, Gothenburg SE-412 96, Sweden

<sup>5</sup>Institut für Energie und Klimaforschung, IEK-8, Forschungszentrum Jülich, Jülich, Germany

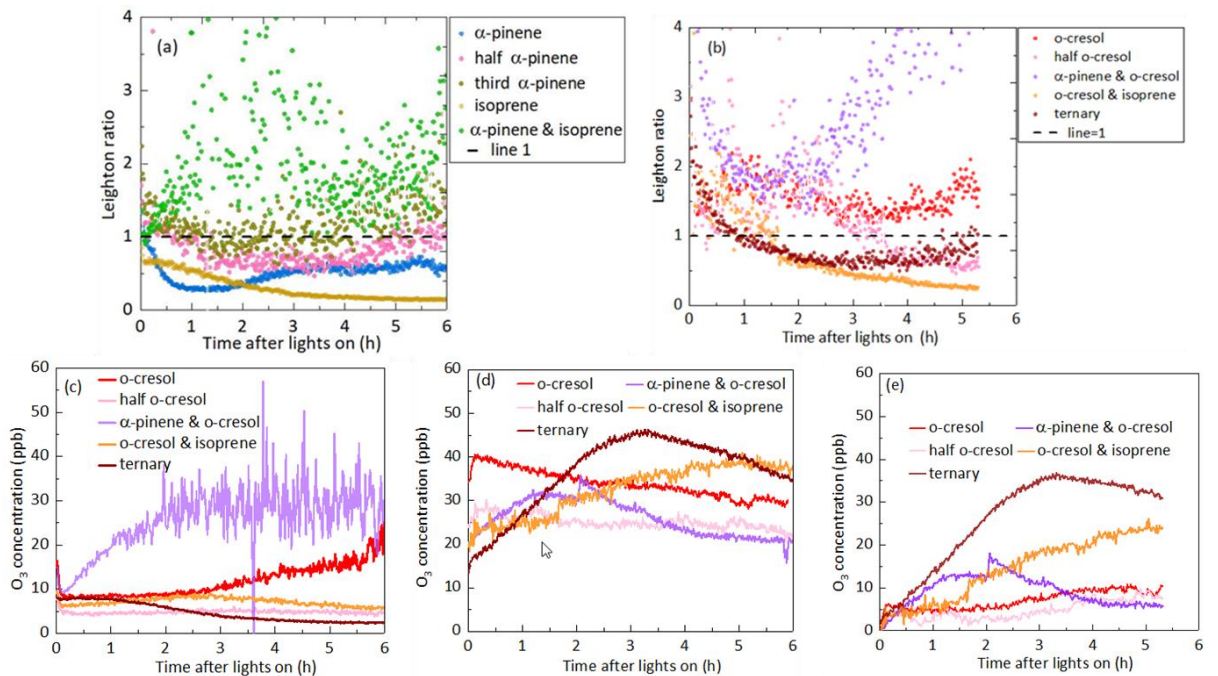
‡ now at Environment & Sustainability Center, Qatar Environment & Energy Research Institute, Doha, Qatar

\* these authors all made equal contribution to the work and manuscript

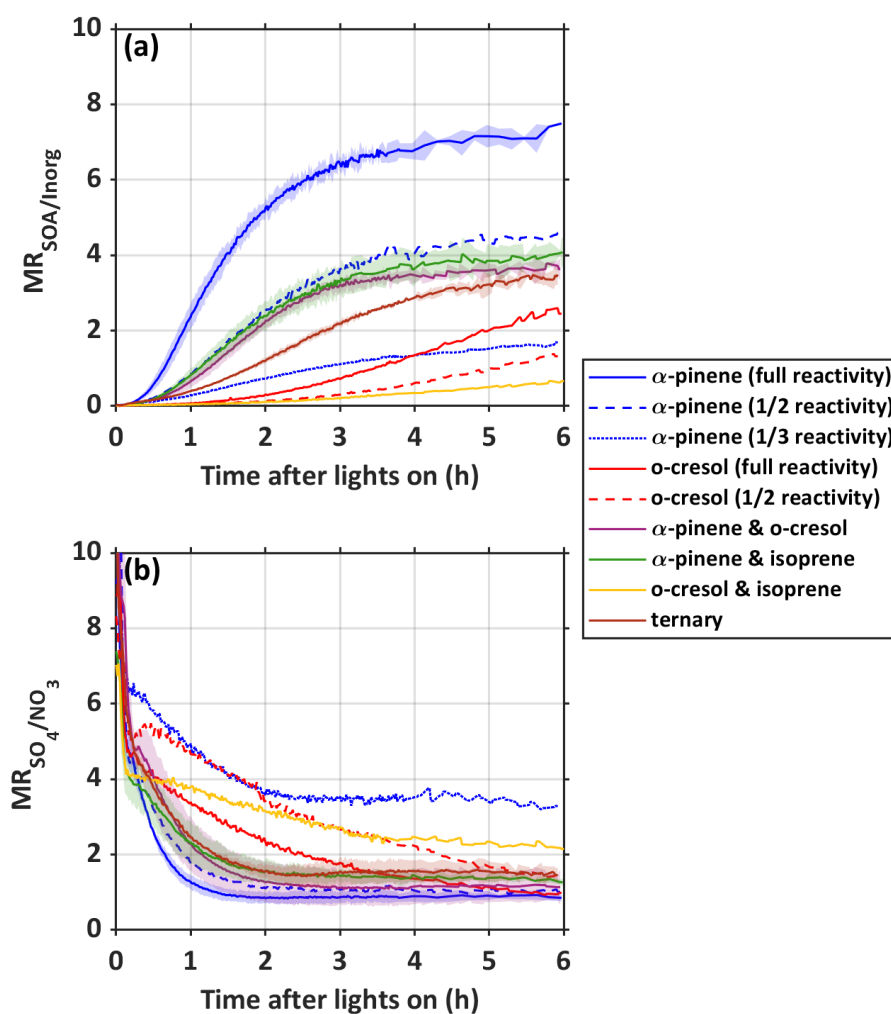
*Correspondence to:* Gordon McFiggans (g.mcfiggans@manchester.ac.uk)



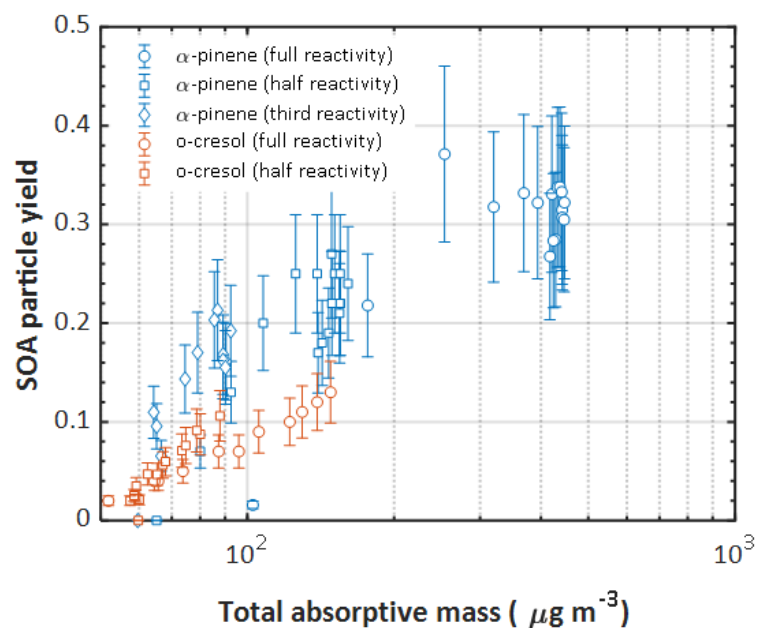
**Figure S1:** NO<sub>2</sub>, NO and O<sub>3</sub> time series in all single and mixed VOC systems (example representative experiments)



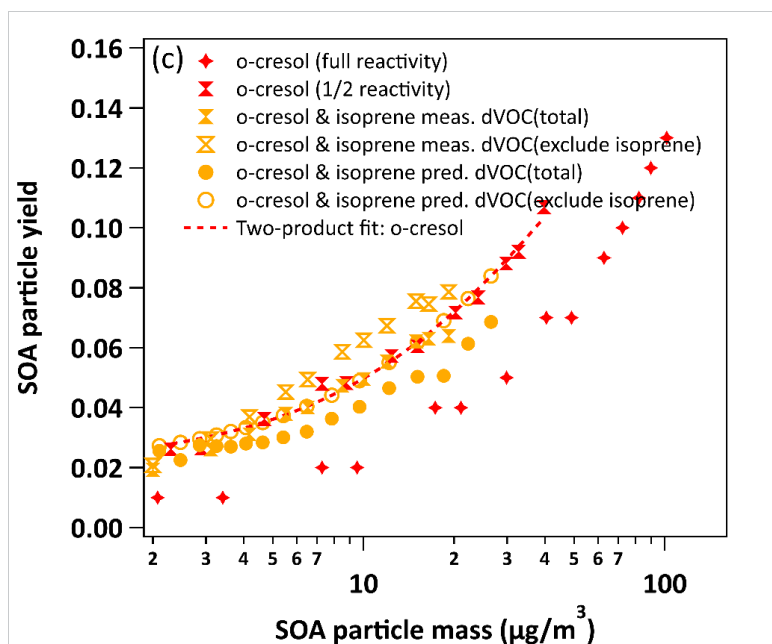
**Figure S2:** Leighton ratios in all systems and O<sub>3</sub> concentrations in all *o*-cresol containing systems. (a) Leighton ratio in all non-*o*-cresol containing systems, (b) Leighton ratio in all *o*-cresol containing systems, (c) O<sub>3</sub> concentrations calculated assuming PSS in the *o*-cresol containing systems, (d) measured O<sub>3</sub> concentrations from O<sub>3</sub> analyser in all *o*-cresol containing systems, (e) corrected O<sub>3</sub> concentrations based on CIMS *o*-cresol signal in all *o*-cresol containing systems.



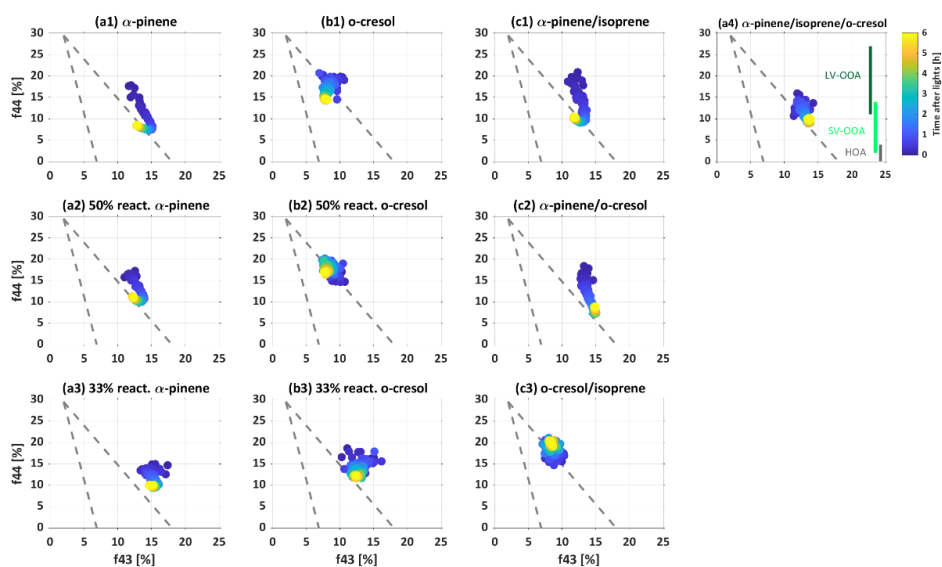
**Figure S3:** Total particle wall loss corrected particle component mass ratios in each system showing inorganic and organic component evolution. Panel a) shows the increase in SOA: inorganic and b) shows the decrease in SO<sub>4</sub><sup>2-</sup>: NO<sub>3</sub><sup>-</sup>, throughout the experiment in each system coloured consistently with Figures 2 and 3. Note that NH<sub>4</sub><sup>+</sup> was found to ion balance the sum of NO<sub>3</sub><sup>-</sup>: SO<sub>4</sub><sup>2-</sup> in all experiments within measurement uncertainty



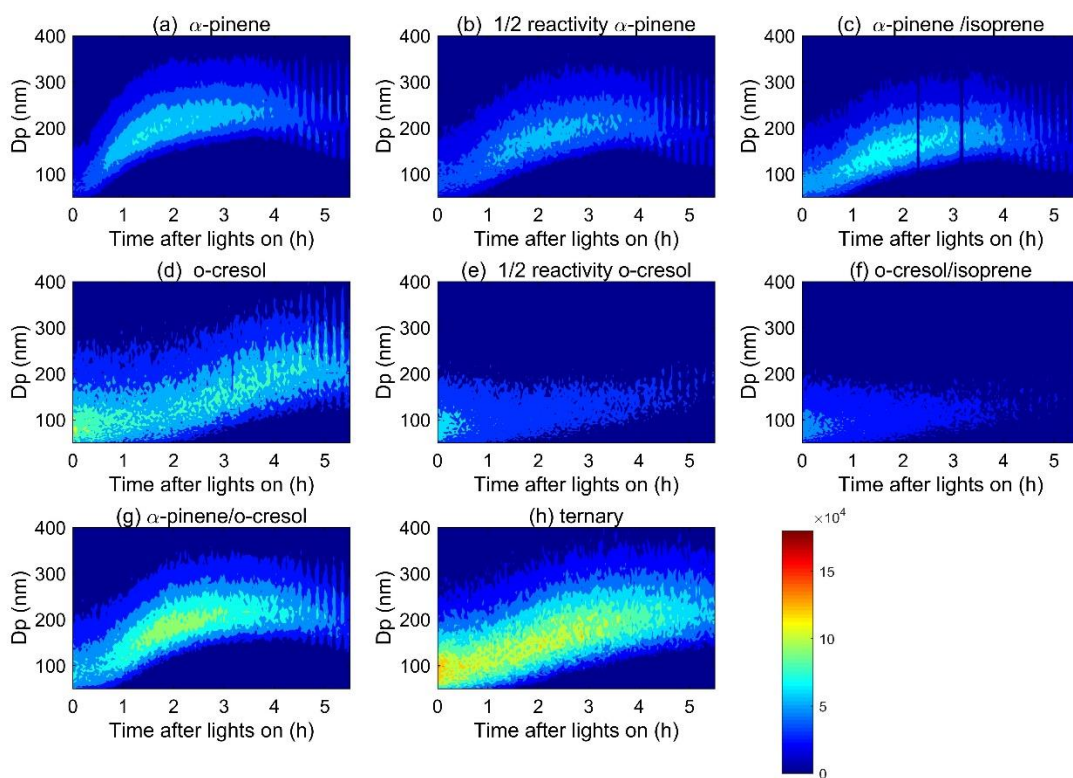
**Figure S4:** SOA particle mass yield as a function of total absorptive mass, including the remaining inorganic seed mass, in the single precursor  $\alpha$ -pinene and *o*-cresol experiments at all initial concentrations. Error bars represent the propagated uncertainties in all measurements and the particle wall loss corrections applied.



**Figure S5:** Expanded plot of yield data for the *o*-cresol / isoprene mixture (with 2-product yield curves *o*-cresol single VOC experiment). Yields “predicted” from the linear combination of yields from the individual VOC experiment using equation 4 are shown for the mixture.



**Figure S6:** Trajectory of AMS  $f_{44}$  vs  $f_{43}$  in all systems.



**Figure S7:** SOA number size distributions from the SMPS measurements.

## Supplementary Information for paper 3

### Combined application of On-line FIGAERO-CIMS and Off-line LC-MS to Characterize the Chemical Composition of SOA in Smog Chamber Studies

Mao Du<sup>1</sup>, Aristeidis Voliotis<sup>1</sup>, Yunqi Shao<sup>1</sup>, Yu Wang<sup>1</sup>, Thomas J. Bannan<sup>1</sup>, Kelly L. Pereira<sup>3,†</sup>, Jacqueline F. Hamilton<sup>3</sup>, Carl J. Percival<sup>4</sup>, M. Rami Alfarra<sup>1,2,‡</sup>, Gordon McFiggans<sup>1,\*</sup>

<sup>1</sup>Centre for atmospheric science, Department of Earth and Environmental Science, School of Natural Sciences, The University of Manchester, Oxford Road, M13 9PL, Manchester, UK

<sup>2</sup>National Centre for Atmospheric Science, Department of Earth and Environmental Science, School of Natural Sciences, The University of Manchester, Oxford Road, M13 9PL, Manchester, UK

<sup>3</sup>Wolfson Atmospheric Chemistry Laboratories, Department of Chemistry, University of York, York, YO10 5DD, UK

<sup>4</sup>NASA Jet Propulsion Laboratory, California Institute of Technology, 4800 Oak Grove Drive, Pasadena, CA 91109, USA.

<sup>†</sup>Now at: Department of Life and Environmental Sciences, Bournemouth University, Dorest, BH12 5BB, UK.

<sup>‡</sup> Now at Environment & Sustainability Center, Qatar Environment & Energy Research Institute, 34110, Doha, Qatar

**\*Correspondence to:** Gordon McFiggans (g.mcfiggans@manchester.ac.uk)

#### 1. Discussion about the calculated $\overline{OS}_C$ for CHOS and CHONS species

In this study, we assumed the carbon oxidation states ( $\overline{OS}_C$ ) for the CHOS and CHONS species was determined by Eq. 1:  $\overline{OS}_C \approx 2 \times O/C - H/C$  (See assumption column in Table S1). In order to confirm the uncertainty of this assumption to the calculated  $\overline{OS}_C$ , for the CHONS species, we assumed N ( $NO_3^-$ ,  $OS_N = +5$ ) and S ( $SO_4^{2-}$ ,  $OS_S = +6$ ) are fully oxidized to obtain the lower limit of calculated  $\overline{OS}_C$  by Eq. 2:  $\overline{OS}_C = 2 \times O/C - H/C - 5 \times N/C - 6 \times S/C$  ( $nO \geq 7$ ). We assumed the N ( $-NO_2^-$ ,  $OS_N = +3$ ) and S ( $SO_3^{2-}$ ,  $OS_S = +4$ ) are reduced, so the upper limit of  $\overline{OS}_C$  was determined by Eq. 3  $\overline{OS}_C = 2 \times O/C - H/C - 3 \times N/C - 4 \times S/C$  ( $nO \geq 5$ ). For the CHOS species, the lower and upper limits of calculated  $\overline{OS}_C$  were determined by Eq. 4:  $\overline{OS}_C = 2 \times O/C - H/C - 6 \times S/C$  ( $nO \geq 4$ ) and Eq. 5:  $\overline{OS}_C = 2 \times O/C - H/C - 4 \times S/C$  ( $nO \geq 3$ ), respectively. The calculated  $\overline{OS}_C$  for other compounds without sufficient oxygen numbers was determined by Eq. 1 in the two groups. The calculated  $\overline{OS}_C$  was weighted to the normalised peak areas and the results are shown in Table S1. The results suggest that the influence of S or NS on the

calculation of  $\overline{OS}_C$  is negligible owing to the low fractions of the two species in the oxidation products. Thus, it is reasonable to calculate the  $\overline{OS}_C$  for CHOS and CHONS species according to Eq. 1 (as shown in Eq. 3 in the paper) in this study.

**Table S1.** Results of calculated  $\overline{OS}_C$  for compounds in the CHOS and CHONS groups.

|   | Unique compounds |             |             | Common compounds |             |             |
|---|------------------|-------------|-------------|------------------|-------------|-------------|
| <b>Negative mode</b>  |                  |             |             |                  |             |             |
|   | Assumption       | Upper limit | Lower limit | Assumption       | Upper limit | Lower limit |
| Sum of CHOS and CHONS   | -0.037           | -0.082      | -0.084      | -0.018           | -0.034      | -0.078      |
| The gap between the assumption and upper limit or lower limit |                  | -0.044      | -0.046      |                  | -0.016      | -0.061      |
| <b>Positive mode</b>  |                  |             |             |                  |             |             |
|   | Assumption       | Upper limit | Lower limit | Assumption       | Upper limit | Lower limit |
| Sum of CHOS and CHONS   | -0.272           | -0.286      | -0.304      | -0.083           | -0.151      | -0.177      |
| The gap between the assumption and upper limit or lower limit |                  | -0.014      | -0.032      |                  | -0.069      | -0.094      |

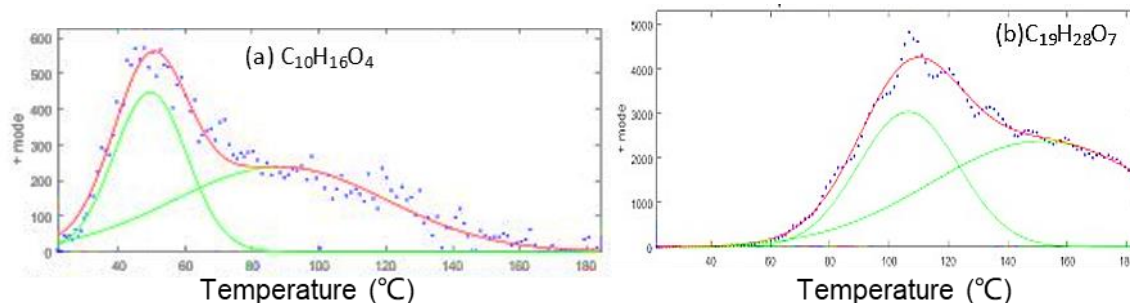


Figure S1. Two examples of an ion having more than a single desorption peak. Here the peaks at the lower desorption temperature were assigned to monomer  $C_{10}H_{16}O_4$  (a) and  $C_{19}H_{28}O_7$  (b) generated from  $\alpha$ -pinene directly and the broader higher temperature peaks being a fragment of another ion at the same mass.



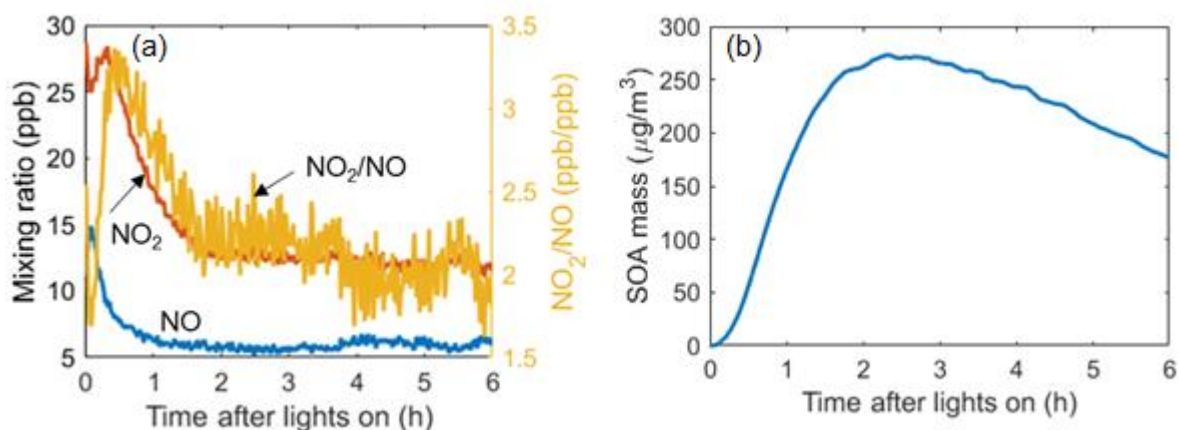


Figure S2. Results from the representative experiment. (a) mixing ratios of NO, NO<sub>2</sub> and NO<sub>2</sub>/NO ratio. (b) SOA mass over time.

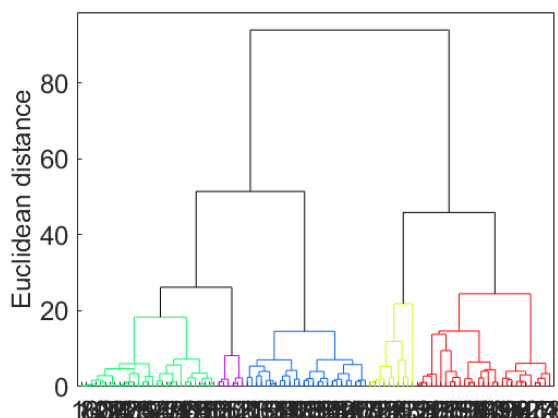


Figure S3. Hierarchical cluster relationship. (Note: the x axis label represents the formula. It is so dense that cannot see them. The formulae are shown in Table S1 in each cluster.)

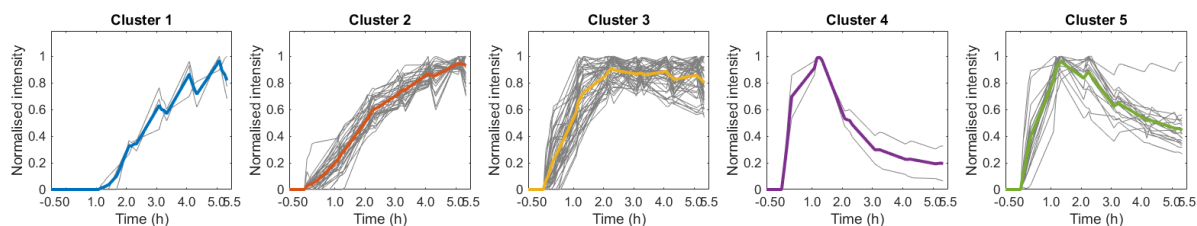


Figure S4. Time series of ions in each cluster in the gas phase.

**Table S2.** Compounds in the gas phase in each cluster for the representative experiment, ranking by ion's contribution in each cluster.

| Cluster 1  |   | Cluster 3  |   | Cluster 4  |   |
|------------|---|------------|---|------------|---|
| MW         | Formula                                       | MW         | Formula   | MW         | Formula   |
| 298.978031 | C <sub>8</sub> H <sub>12</sub> O <sub>4</sub> | 371.994409 | C <sub>10</sub> H <sub>15</sub> NO <sub>6</sub> | 355.999494 | C <sub>10</sub> H <sub>15</sub> NO <sub>5</sub> |
| 256.967466 | C <sub>6</sub> H <sub>10</sub> O <sub>3</sub> | 329.960035 | C <sub>8</sub> H <sub>11</sub> O <sub>6</sub>   | 403.984238 | C <sub>10</sub> H <sub>15</sub> NO <sub>8</sub> |
| 312.944719 | C <sub>7</sub> H <sub>8</sub> NO <sub>5</sub> | 298.806598 | CH <sub>2</sub> O <sub>2</sub>                  |            |   |

| Cluster 2  |  | 214.920516 | C <sub>3</sub> H <sub>4</sub> O <sub>3</sub>                  | Cluster 5  |   |
|------------|--|------------|---|------------|---|
| MW         | Formula  | 317.983844 | C <sub>7</sub> H <sub>13</sub> NO <sub>5</sub>                | MW         | Formula   |
| 315.968194 | C <sub>7</sub> H <sub>11</sub> NO <sub>5</sub> | 343.975685 | C <sub>9</sub> H <sub>13</sub> O <sub>6</sub>                 | 357.978759 | C <sub>9</sub> H <sub>13</sub> NO <sub>6</sub>  |
| 303.968194 | C <sub>6</sub> H <sub>11</sub> NO <sub>5</sub> | 343.963109 | C <sub>8</sub> H <sub>11</sub> NO <sub>6</sub>                | 246.097762 | C <sub>10</sub> H <sub>16</sub> NO <sub>6</sub> |
| 283.006926 | C <sub>8</sub> H <sub>14</sub> NO <sub>2</sub> | 229.107599 | C <sub>11</sub> H <sub>17</sub> O <sub>5</sub>                | 232.082112 | C <sub>9</sub> H <sub>14</sub> NO <sub>6</sub>  |
| 301.96512  | C <sub>7</sub> H <sub>11</sub> O <sub>5</sub>  | 234.073953 | C <sub>9</sub> H <sub>14</sub> O <sub>7</sub>                 | 215.091949 | C <sub>10</sub> H <sub>15</sub> O <sub>5</sub>  |
| 275.936894 | C <sub>4</sub> H <sub>7</sub> NO <sub>5</sub>  | 403.012799 | C <sub>11</sub> H <sub>18</sub> NO <sub>7</sub>               | 289.928735 | C <sub>5</sub> H <sub>7</sub> O <sub>6</sub>    |
| 312.993681 | C <sub>9</sub> H <sub>14</sub> O <sub>4</sub>  | 345.991335 | C <sub>9</sub> H <sub>15</sub> O <sub>6</sub>                 | 387.989324 | C <sub>10</sub> H <sub>15</sub> NO <sub>7</sub> |
| 270.983116 | C <sub>7</sub> H <sub>12</sub> O <sub>3</sub>  | 231.923256 | C <sub>3</sub> H <sub>5</sub> O <sub>4</sub>                  | 373.98625  | C <sub>10</sub> H <sub>15</sub> O <sub>7</sub>  |
| 282.97054  | C <sub>7</sub> H <sub>10</sub> NO <sub>3</sub> | 303.931809 | C <sub>5</sub> H <sub>7</sub> NO <sub>6</sub>                 | 361.98625  | C <sub>9</sub> H <sub>15</sub> O <sub>7</sub>   |
| 242.951816 | C <sub>5</sub> H <sub>8</sub> O <sub>3</sub>   | 317.947459 | C <sub>6</sub> H <sub>9</sub> NO <sub>6</sub>                 | 389.968588 | C <sub>9</sub> H <sub>13</sub> NO <sub>8</sub>  |
| 284.998766 | C <sub>8</sub> H <sub>14</sub> O <sub>3</sub>  | 311.014416 | C <sub>10</sub> H <sub>16</sub> O <sub>3</sub>                | 361.937288 | C <sub>7</sub> H <sub>9</sub> NO <sub>8</sub>   |
| 268.967466 | C <sub>7</sub> H <sub>10</sub> O <sub>3</sub>  | 327.009331 | C <sub>10</sub> H <sub>16</sub> O <sub>4</sub>                | 385.98625  | C <sub>11</sub> H <sub>15</sub> O <sub>7</sub>  |
| 199.92085  | C <sub>2</sub> H <sub>3</sub> NO <sub>2</sub>  | 296.998766 | C <sub>9</sub> H <sub>14</sub> O <sub>3</sub>                 | 341.99642  | C <sub>10</sub> H <sub>15</sub> O <sub>5</sub>  |
| 299.014416 | C <sub>9</sub> H <sub>16</sub> O <sub>3</sub>  | 343.004245 | C <sub>10</sub> H <sub>16</sub> O <sub>5</sub>                | 375.952938 | C <sub>8</sub> H <sub>11</sub> NO <sub>8</sub>  |
| 324.993681 | C <sub>10</sub> H <sub>14</sub> O <sub>4</sub> | 328.988595 | C <sub>9</sub> H <sub>14</sub> O <sub>5</sub>                 | 232.118498 | C <sub>10</sub> H <sub>18</sub> NO <sub>5</sub> |
| 228.936166 | C <sub>4</sub> H <sub>6</sub> O <sub>3</sub>   | 284.962381 | C <sub>7</sub> H <sub>10</sub> O <sub>4</sub>                 | 388.936954 | C <sub>9</sub> H <sub>10</sub> O <sub>9</sub>   |
| 300.981105 | C <sub>7</sub> H <sub>12</sub> NO <sub>4</sub> | 359.994409 | C <sub>9</sub> H <sub>15</sub> NO <sub>6</sub>                | 247.905594 | C <sub>2</sub> H <sub>3</sub> NO <sub>5</sub>   |
| 329.99642  | C <sub>9</sub> H <sub>15</sub> O <sub>5</sub>  | 340.988595 | C <sub>10</sub> H <sub>14</sub> O <sub>5</sub>                | 340.00458  | C <sub>10</sub> H <sub>15</sub> NO <sub>4</sub> |
| 345.019896 | C <sub>10</sub> H <sub>18</sub> O <sub>5</sub> | 314.972945 | C <sub>8</sub> H <sub>12</sub> O <sub>5</sub>                 |            |   |
| 286.978031 | C <sub>7</sub> H <sub>12</sub> O <sub>4</sub>  | 344.012071 | C <sub>10</sub> H <sub>17</sub> O <sub>5</sub>                |            |   |
| 327.98077  | C <sub>9</sub> H <sub>13</sub> O <sub>5</sub>  | 358.99916  | C <sub>10</sub> H <sub>16</sub> O <sub>6</sub>                |            |   |
| 230.951816 | C <sub>4</sub> H <sub>8</sub> O <sub>3</sub>   | 230.915431 | C <sub>3</sub> H <sub>4</sub> O <sub>4</sub>                  |            |   |
| 316.988595 | C <sub>8</sub> H <sub>14</sub> O <sub>5</sub>  | 308.998766 | C <sub>10</sub> H <sub>14</sub> O <sub>3</sub>                |            |   |
| 258.946731 | C <sub>5</sub> H <sub>8</sub> O <sub>4</sub>   | 226.920516 | C <sub>4</sub> H <sub>4</sub> O <sub>3</sub>                  |            |   |
| 302.972945 | C <sub>7</sub> H <sub>12</sub> O <sub>5</sub>  | 388.984573 | C <sub>9</sub> H <sub>14</sub> N <sub>2</sub> O <sub>7</sub>  |            |   |
| 331.975685 | C <sub>8</sub> H <sub>13</sub> O <sub>6</sub>  | 315.009331 | C <sub>9</sub> H <sub>16</sub> O <sub>4</sub>                 |            |   |
| 212.928675 | C <sub>3</sub> H <sub>4</sub> NO <sub>2</sub>  | 345.942374 | C <sub>7</sub> H <sub>9</sub> NO <sub>7</sub>                 |            |   |
| 313.952544 | C <sub>7</sub> H <sub>9</sub> NO <sub>5</sub>  | 390.004974 | C <sub>10</sub> H <sub>17</sub> NO <sub>7</sub>               |            |   |
| 272.998766 | C <sub>7</sub> H <sub>14</sub> O <sub>3</sub>  | 344.98351  | C <sub>9</sub> H <sub>14</sub> O <sub>6</sub>                 |            |   |
| 272.949805 | C <sub>5</sub> H <sub>8</sub> NO <sub>4</sub>  | 356.994743 | C <sub>9</sub> H <sub>14</sub> N <sub>2</sub> O <sub>5</sub>  |            |   |
| 301.030066 | C <sub>9</sub> H <sub>18</sub> O <sub>3</sub>  | 314.001506 | C <sub>9</sub> H <sub>15</sub> O <sub>4</sub>                 |            |   |
| 289.96512  | C <sub>6</sub> H <sub>11</sub> O <sub>5</sub>  | 330.991669 | C <sub>8</sub> H <sub>14</sub> NO <sub>5</sub>                |            |   |
| 288.957295 | C <sub>6</sub> H <sub>10</sub> O <sub>5</sub>  | 341.960035 | C <sub>9</sub> H <sub>11</sub> O <sub>6</sub>                 |            |   |
|            |  | 355.015479 | C <sub>10</sub> H <sub>16</sub> N <sub>2</sub> O <sub>4</sub> |            |   |
|            |  | 261.93382  | C <sub>4</sub> H <sub>7</sub> O <sub>5</sub>                  |            |   |
|            |  | 373.002234 | C <sub>10</sub> H <sub>16</sub> NO <sub>6</sub>               |            |   |
|            |  | 376.0019   | C <sub>10</sub> H <sub>17</sub> O <sub>7</sub>                |            |   |
|            |  | 326.001506 | C <sub>10</sub> H <sub>15</sub> O <sub>4</sub>                |            |   |
|            |  | 331.9393   | C <sub>7</sub> H <sub>9</sub> O <sub>7</sub>                  |            |   |
|            |  | 387.005308 | C <sub>10</sub> H <sub>16</sub> N <sub>2</sub> O <sub>6</sub> |            |   |
|            |  | 338.996755 | C <sub>10</sub> H <sub>14</sub> NO <sub>4</sub>               |            |   |
|            |  | 370.986584 | C <sub>10</sub> H <sub>14</sub> NO <sub>6</sub>               |            |   |

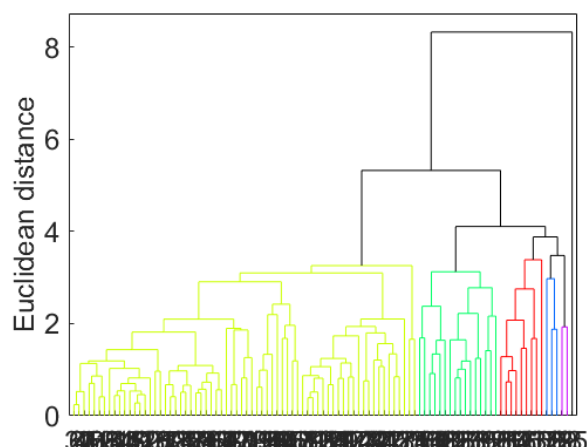


Figure S5. Hierarchical cluster relationship. (Note: the x axis label represents the formula. It is so dense that cannot see them. The formulae are shown in Table S2 in each cluster.)

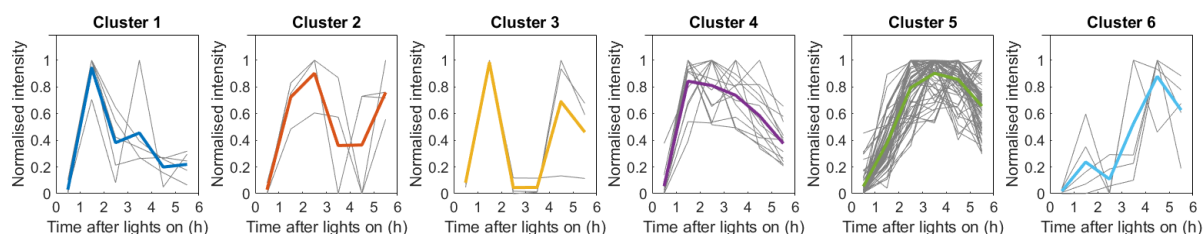


Figure S6. Time series of ions in each cluster in the particle phase.

**Table S3.** Compounds in the particle phase in each cluster for the representative experiment, ranking by ion's contribution in each cluster.

| Cluster 1  |                    | Cluster 5  |                    |
|------------|--------------------|------------|--------------------|
| MW         | Formula            | MW         | Formula            |
| 328.988595 | $C_9H_{14}O_5$     | 312.993681 | $C_9H_{14}O_4$     |
| 284.962381 | $C_7H_{10}O_4$     | 298.978031 | $C_8H_{12}O_4$     |
| 258.946731 | $C_5H_8O_4$        | 327.009331 | $C_{10}H_{16}O_4$  |
| 405.999888 | $C_{10}H_{17}NO_8$ | 358.99916  | $C_{10}H_{16}O_6$  |
| 355.999494 | $C_{10}H_{15}NO_5$ | 371.994409 | $C_{10}H_{15}NO_6$ |
| Cluster 2  |                    | 340.988595 | $C_{10}H_{14}O_5$  |
| MW         | Formula            | 345.019896 | $C_{10}H_{18}O_5$  |
| 403.984238 | $C_{10}H_{15}NO_8$ | 356.994743 | $C_9H_{14}N_2O_5$  |
| 400.997149 | $C_{11}H_{16}NO_7$ | 344.98351  | $C_9H_{14}O_6$     |
| 319.9393   | $C_6H_9O_7$        | 300.981105 | $C_7H_{12}NO_4$    |
| 391.996814 | $C_{10}H_{17}O_8$  | 374.994075 | $C_{10}H_{16}O_7$  |
| Cluster 3  |                    | 302.972945 | $C_7H_{12}O_5$     |
| MW         | Formula            | 300.932143 | $C_5H_6N_2O_5$     |
| 270.983116 | $C_7H_{12}O_3$     | 256.931081 | $C_5H_6O_4$        |
| 268.918505 | $C_5H_4NO_4$       | 328.017156 | $C_{10}H_{17}O_4$  |

|                  |  |            |   |
|------------------|--|------------|---|
| 242.915431       | C <sub>4</sub> H <sub>4</sub> O <sub>4</sub>                 | 314.001506 | C <sub>9</sub> H <sub>15</sub> O <sub>4</sub>                 |
| <b>Cluster 4</b> |  | 330.942708 | C <sub>6</sub> H <sub>8</sub> N <sub>2</sub> O <sub>6</sub>   |
| <b>MW</b>        | <b>Formula</b>   | 282.97054  | C <sub>7</sub> H <sub>10</sub> NO <sub>3</sub>                |
| 343.004245       | C <sub>10</sub> H <sub>16</sub> O <sub>5</sub>               | 469.072325 | C <sub>17</sub> H <sub>26</sub> O <sub>7</sub>                |
| 324.993681       | C <sub>10</sub> H <sub>14</sub> O <sub>4</sub>               | 387.989324 | C <sub>10</sub> H <sub>15</sub> NO <sub>7</sub>               |
| 296.998766       | C <sub>9</sub> H <sub>14</sub> O <sub>3</sub>                | 344.012071 | C <sub>10</sub> H <sub>17</sub> O <sub>5</sub>                |
| 390.004974       | C <sub>10</sub> H <sub>17</sub> NO <sub>7</sub>              | 299.985856 | C <sub>8</sub> H <sub>13</sub> O <sub>4</sub>                 |
| 361.01481        | C <sub>10</sub> H <sub>18</sub> O <sub>6</sub>               | 286.965455 | C <sub>6</sub> H <sub>10</sub> NO <sub>4</sub>                |
| 388.984573       | C <sub>9</sub> H <sub>14</sub> N <sub>2</sub> O <sub>7</sub> | 214.920516 | C <sub>3</sub> H <sub>4</sub> O <sub>3</sub>                  |
| 200.904866       | C <sub>2</sub> H <sub>2</sub> O <sub>3</sub>                 | 359.994409 | C <sub>9</sub> H <sub>15</sub> NO <sub>6</sub>                |
| 316.95221        | C <sub>7</sub> H <sub>10</sub> O <sub>6</sub>                | 316.988595 | C <sub>8</sub> H <sub>14</sub> O <sub>5</sub>                 |
| 361.98625        | C <sub>9</sub> H <sub>15</sub> O <sub>7</sub>                | 495.087975 | C <sub>19</sub> H <sub>28</sub> O <sub>7</sub>                |
| 341.99642        | C <sub>10</sub> H <sub>15</sub> O <sub>5</sub>               | 373.002234 | C <sub>10</sub> H <sub>16</sub> NO <sub>6</sub>               |
| 226.920516       | C <sub>4</sub> H <sub>4</sub> O <sub>3</sub>                 | 372.965849 | C <sub>9</sub> H <sub>12</sub> NO <sub>7</sub>                |
| 228.936166       | C <sub>4</sub> H <sub>6</sub> O <sub>3</sub>                 | 299.014416 | C <sub>9</sub> H <sub>16</sub> O <sub>3</sub>                 |
| 202.920516       | C <sub>2</sub> H <sub>4</sub> O <sub>3</sub>                 | 346.99916  | C <sub>9</sub> H <sub>16</sub> O <sub>6</sub>                 |
| 449.091049       | C <sub>14</sub> H <sub>28</sub> NO <sub>7</sub>              | 342.942708 | C <sub>7</sub> H <sub>8</sub> N <sub>2</sub> O <sub>6</sub>   |
| <b>Cluster 6</b> |  | 332.98351  | C <sub>8</sub> H <sub>14</sub> O <sub>6</sub>                 |
| <b>MW</b>        | <b>Formula</b>   | 216.936166 | C <sub>3</sub> H <sub>6</sub> O <sub>3</sub>                  |
| 314.972945       | C <sub>8</sub> H <sub>12</sub> O <sub>5</sub>                | 312.944719 | C <sub>7</sub> H <sub>8</sub> NO <sub>5</sub>                 |
| 330.991669       | C <sub>8</sub> H <sub>14</sub> NO <sub>5</sub>               | 283.006926 | C <sub>8</sub> H <sub>14</sub> NO <sub>2</sub>                |
| 274.941645       | C <sub>5</sub> H <sub>8</sub> O <sub>5</sub>                 | 315.009331 | C <sub>9</sub> H <sub>16</sub> O <sub>4</sub>                 |
| 256.95489        | C <sub>5</sub> H <sub>8</sub> NO <sub>3</sub>                | 373.98625  | C <sub>10</sub> H <sub>15</sub> O <sub>7</sub>                |
| 230.951816       | C <sub>4</sub> H <sub>8</sub> O <sub>3</sub>                 | 451.070314 | C <sub>13</sub> H <sub>26</sub> NO <sub>8</sub>               |
|                  |  | 370.986584 | C <sub>10</sub> H <sub>14</sub> NO <sub>6</sub>               |
|                  |  | 360.965849 | C <sub>8</sub> H <sub>12</sub> NO <sub>7</sub>                |
|                  |  | 481.072325 | C <sub>18</sub> H <sub>26</sub> O <sub>7</sub>                |
|                  |  | 302.923984 | C <sub>5</sub> H <sub>6</sub> NO <sub>6</sub>                 |
|                  |  | 387.005308 | C <sub>10</sub> H <sub>16</sub> N <sub>2</sub> O <sub>6</sub> |
|                  |  | 439.06176  | C <sub>16</sub> H <sub>24</sub> O <sub>6</sub>                |
|                  |  | 345.991335 | C <sub>9</sub> H <sub>15</sub> O <sub>6</sub>                 |
|                  |  | 288.957295 | C <sub>6</sub> H <sub>10</sub> O <sub>5</sub>                 |
|                  |  | 287.00184  | C <sub>7</sub> H <sub>14</sub> NO <sub>3</sub>                |
|                  |  | 356.947125 | C <sub>9</sub> H <sub>10</sub> O <sub>7</sub>                 |
|                  |  | 427.025375 | C <sub>14</sub> H <sub>20</sub> O <sub>7</sub>                |
|                  |  | 441.028449 | C <sub>14</sub> H <sub>20</sub> NO <sub>7</sub>               |
|                  |  | 467.056675 | C <sub>17</sub> H <sub>24</sub> O <sub>7</sub>                |
|                  |  | 272.949805 | C <sub>5</sub> H <sub>8</sub> NO <sub>4</sub>                 |
|                  |  | 315.968194 | C <sub>7</sub> H <sub>11</sub> NO <sub>5</sub>                |
|                  |  | 471.05159  | C <sub>16</sub> H <sub>24</sub> O <sub>8</sub>                |
|                  |  | 355.015479 | C <sub>10</sub> H <sub>16</sub> N <sub>2</sub> O <sub>4</sub> |
|                  |  | 376.0019   | C <sub>10</sub> H <sub>17</sub> O <sub>7</sub>                |
|                  |  | 317.983844 | C <sub>7</sub> H <sub>13</sub> NO <sub>5</sub>                |
|                  |  | 326.001506 | C <sub>10</sub> H <sub>15</sub> O <sub>4</sub>                |
|                  |  | 399.005308 | C <sub>11</sub> H <sub>16</sub> N <sub>2</sub> O <sub>6</sub> |
|                  |  | 298.006591 | C <sub>9</sub> H <sub>15</sub> O <sub>3</sub>                 |
|                  |  | 303.968194 | C <sub>6</sub> H <sub>11</sub> NO <sub>5</sub>                |
|                  |  | 327.98077  | C <sub>9</sub> H <sub>13</sub> O <sub>5</sub>                 |
|                  |  | 338.972945 | C <sub>10</sub> H <sub>12</sub> O <sub>5</sub>                |

|  |  |            |                    |
|--|--|------------|--------------------|
|  |  | 369.007319 | $C_{11}H_{16}NO_5$ |
|  |  | 397.01481  | $C_{13}H_{18}O_6$  |
|  |  | 296.949805 | $C_7H_8NO_4$       |
|  |  | 308.998766 | $C_{10}H_{14}O_3$  |

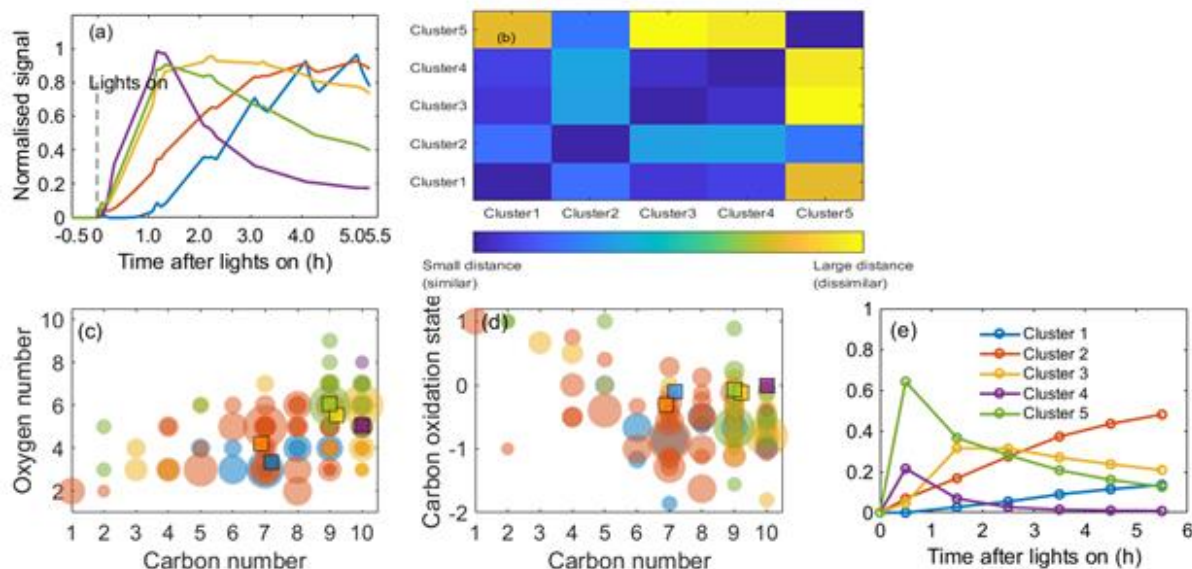


Figure S7. Hierarchical clustering of gas-phase oxidation products for the repeat  $\alpha$ -pinene system. (a) Time series of each cluster normalized to the highest ions' intensity between 0 and 1. (b) Matrix showing the relative distance between clusters. (c) Carbon number vs oxygen number for each cluster. (d) Carbon number vs oxidation state for each cluster. (e) Time series of the sum of ions' normalized fractions to the total signal in each cluster. Note that the square symbols represent the contribution weighted average carbon numbers, oxygen numbers or and  $\overline{OS}_C$  in each cluster. The colors correspond to the ones in (e).

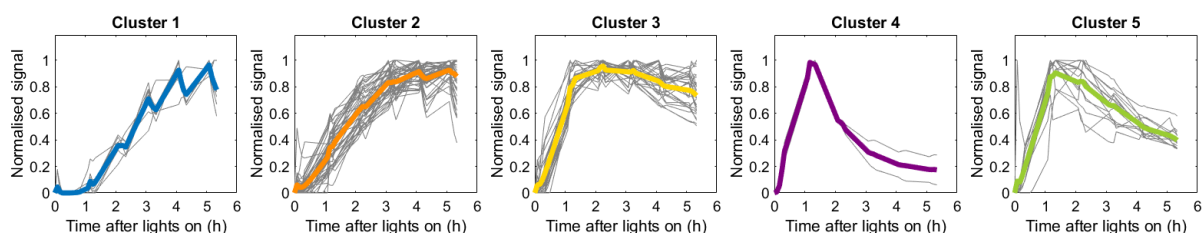


Figure S8. Time series of ions in each cluster in the gas phase for the repeat experiment.

**Table S4.** Compounds in the gas phase in each cluster for the repeat experiment, ranking by ion's contribution in each cluster.

| Cluster 1 |                | Cluster 2 |                 | Cluster 3 |                   |
|-----------|----------------|-----------|-----------------|-----------|-------------------|
| MW        | Formula        | MW        | Formula         | MW        | Formula           |
| 298.978   | $C_8H_{12}O_4$ | 230.9518  | $C_4H_8O_3$     | 214.9205  | $C_3H_4O_3$       |
| 270.9831  | $C_7H_{12}O_3$ | 315.9682  | $C_7H_{11}NO_5$ | 232.0821  | $C_9H_{14}NO_6$   |
| 312.9937  | $C_9H_{14}O_4$ | 298.8066  | $CH_2O_2$       | 234.074   | $C_9H_{14}O_7$    |
| 256.9675  | $C_6H_{10}O_3$ | 329.96    | $C_8H_{11}O_6$  | 229.1076  | $C_{11}H_{17}O_5$ |

|                  |  |          |   |          |   |
|------------------|--|----------|---|----------|---|
| 299.9859         | C <sub>8</sub> H <sub>13</sub> O <sub>4</sub>                | 343.9631 | C <sub>8</sub> H <sub>11</sub> NO <sub>6</sub>  | 403.0128 | C <sub>11</sub> H <sub>18</sub> NO <sub>7</sub>               |
| 345.0199         | C <sub>10</sub> H <sub>18</sub> O <sub>5</sub>               | 317.9838 | C <sub>7</sub> H <sub>13</sub> NO <sub>5</sub>  | 371.9944 | C <sub>10</sub> H <sub>15</sub> NO <sub>6</sub>               |
| 286.9655         | C <sub>6</sub> H <sub>10</sub> NO <sub>4</sub>               | 303.9682 | C <sub>6</sub> H <sub>11</sub> NO <sub>5</sub>  | 311.0144 | C <sub>10</sub> H <sub>16</sub> O <sub>3</sub>                |
| 258.9467         | C <sub>5</sub> H <sub>8</sub> O <sub>4</sub>                 | 296.9988 | C <sub>9</sub> H <sub>14</sub> O <sub>3</sub>   | 327.0093 | C <sub>10</sub> H <sub>16</sub> O <sub>4</sub>                |
| 287.0018         | C <sub>7</sub> H <sub>14</sub> NO <sub>3</sub>               | 282.9705 | C <sub>7</sub> H <sub>10</sub> NO <sub>3</sub>  | 373.0022 | C <sub>10</sub> H <sub>16</sub> NO <sub>6</sub>               |
|                  |  | 283.0069 | C <sub>8</sub> H <sub>14</sub> NO <sub>2</sub>  | 358.9992 | C <sub>10</sub> H <sub>16</sub> O <sub>6</sub>                |
| <b>Cluster 4</b> |  | 343.0042 | C <sub>10</sub> H <sub>16</sub> O <sub>5</sub>  | 359.9944 | C <sub>9</sub> H <sub>15</sub> NO <sub>6</sub>                |
| <b>MW</b>        | <b>Formula</b>   | 242.9518 | C <sub>5</sub> H <sub>8</sub> O <sub>3</sub>    | 341.9964 | C <sub>10</sub> H <sub>15</sub> O <sub>5</sub>                |
| 355.9995         | C <sub>10</sub> H <sub>15</sub> NO <sub>5</sub>              | 343.9757 | C <sub>9</sub> H <sub>13</sub> O <sub>6</sub>   | 312.0222 | C <sub>10</sub> H <sub>17</sub> O <sub>3</sub>                |
| 403.9842         | C <sub>10</sub> H <sub>15</sub> NO <sub>8</sub>              | 284.9988 | C <sub>8</sub> H <sub>14</sub> O <sub>3</sub>   | 230.9154 | C <sub>3</sub> H <sub>4</sub> O <sub>4</sub>                  |
| <b>Cluster 5</b> |  | 268.9675 | C <sub>7</sub> H <sub>10</sub> O <sub>3</sub>   | 340.9886 | C <sub>10</sub> H <sub>14</sub> O <sub>5</sub>                |
| <b>MW</b>        | <b>Formula</b>   | 328.9886 | C <sub>9</sub> H <sub>14</sub> O <sub>5</sub>   | 345.9913 | C <sub>9</sub> H <sub>15</sub> O <sub>6</sub>                 |
| 357.9788         | C <sub>9</sub> H <sub>13</sub> NO <sub>6</sub>               | 199.9209 | C <sub>2</sub> H <sub>3</sub> NO <sub>2</sub>   | 388.9846 | C <sub>9</sub> H <sub>14</sub> N <sub>2</sub> O <sub>7</sub>  |
| 246.0978         | C <sub>10</sub> H <sub>16</sub> NO <sub>6</sub>              | 284.9624 | C <sub>7</sub> H <sub>10</sub> O <sub>4</sub>   | 328.0172 | C <sub>10</sub> H <sub>17</sub> O <sub>4</sub>                |
| 202.9205         | C <sub>2</sub> H <sub>4</sub> O <sub>3</sub>                 | 344.0121 | C <sub>10</sub> H <sub>17</sub> O <sub>5</sub>  | 226.9205 | C <sub>4</sub> H <sub>4</sub> O <sub>3</sub>                  |
| 358.9628         | C <sub>9</sub> H <sub>12</sub> O <sub>7</sub>                | 299.0144 | C <sub>9</sub> H <sub>16</sub> O <sub>3</sub>   | 308.9988 | C <sub>10</sub> H <sub>14</sub> O <sub>3</sub>                |
| 289.9287         | C <sub>5</sub> H <sub>7</sub> O <sub>6</sub>                 | 314.9729 | C <sub>8</sub> H <sub>12</sub> O <sub>5</sub>   | 345.9424 | C <sub>7</sub> H <sub>9</sub> NO <sub>7</sub>                 |
| 215.0919         | C <sub>10</sub> H <sub>15</sub> O <sub>5</sub>               | 329.9964 | C <sub>9</sub> H <sub>15</sub> O <sub>5</sub>   | 341.96   | C <sub>9</sub> H <sub>11</sub> O <sub>6</sub>                 |
| 361.9863         | C <sub>9</sub> H <sub>15</sub> O <sub>7</sub>                | 228.9362 | C <sub>4</sub> H <sub>6</sub> O <sub>3</sub>    | 372.9658 | C <sub>9</sub> H <sub>12</sub> NO <sub>7</sub>                |
| 373.9863         | C <sub>10</sub> H <sub>15</sub> O <sub>7</sub>               | 344.9835 | C <sub>9</sub> H <sub>14</sub> O <sub>6</sub>   | 303.9318 | C <sub>5</sub> H <sub>7</sub> NO <sub>6</sub>                 |
| 356.9947         | C <sub>9</sub> H <sub>14</sub> N <sub>2</sub> O <sub>5</sub> | 316.9886 | C <sub>8</sub> H <sub>14</sub> O <sub>5</sub>   | 355.0155 | C <sub>10</sub> H <sub>16</sub> N <sub>2</sub> O <sub>4</sub> |
| 387.9893         | C <sub>10</sub> H <sub>15</sub> NO <sub>7</sub>              | 300.9811 | C <sub>7</sub> H <sub>12</sub> NO <sub>4</sub>  | 374.9941 | C <sub>10</sub> H <sub>16</sub> O <sub>7</sub>                |
| 389.9686         | C <sub>9</sub> H <sub>13</sub> NO <sub>8</sub>               | 324.9937 | C <sub>10</sub> H <sub>14</sub> O <sub>4</sub>  | 311.9859 | C <sub>9</sub> H <sub>13</sub> O <sub>4</sub>                 |
| 388.937          | C <sub>9</sub> H <sub>10</sub> O <sub>9</sub>                | 314.0015 | C <sub>9</sub> H <sub>15</sub> O <sub>4</sub>   | 361.0148 | C <sub>10</sub> H <sub>18</sub> O <sub>6</sub>                |
| 247.9056         | C <sub>2</sub> H <sub>3</sub> NO <sub>5</sub>                | 298.0066 | C <sub>9</sub> H <sub>15</sub> O <sub>3</sub>   |          |   |
| 385.9863         | C <sub>11</sub> H <sub>15</sub> O <sub>7</sub>               | 312.9447 | C <sub>7</sub> H <sub>8</sub> NO <sub>5</sub>   |          |   |
|                  |  | 327.9808 | C <sub>9</sub> H <sub>13</sub> O <sub>5</sub>   |          |   |
|                  |  | 275.9369 | C <sub>4</sub> H <sub>7</sub> NO <sub>5</sub>   |          |   |
|                  |  | 301.9651 | C <sub>7</sub> H <sub>11</sub> O <sub>5</sub>   |          |   |
|                  |  | 316.9522 | C <sub>7</sub> H <sub>10</sub> O <sub>6</sub>   |          |   |
|                  |  | 330.9917 | C <sub>8</sub> H <sub>14</sub> NO <sub>5</sub>  |          |   |
|                  |  | 302.9729 | C <sub>7</sub> H <sub>12</sub> O <sub>5</sub>   |          |   |
|                  |  | 390.005  | C <sub>10</sub> H <sub>17</sub> NO <sub>7</sub> |          |   |
|                  |  | 313.9525 | C <sub>7</sub> H <sub>9</sub> NO <sub>5</sub>   |          |   |
|                  |  | 256.9311 | C <sub>5</sub> H <sub>6</sub> O <sub>4</sub>    |          |   |
|                  |  | 331.9757 | C <sub>8</sub> H <sub>13</sub> O <sub>6</sub>   |          |   |
|                  |  | 315.0093 | C <sub>9</sub> H <sub>16</sub> O <sub>4</sub>   |          |   |
|                  |  | 317.9475 | C <sub>6</sub> H <sub>9</sub> NO <sub>6</sub>   |          |   |
|                  |  | 326.0015 | C <sub>10</sub> H <sub>15</sub> O <sub>4</sub>  |          |   |
|                  |  | 272.9988 | C <sub>7</sub> H <sub>14</sub> O <sub>3</sub>   |          |   |
|                  |  | 285.9702 | C <sub>7</sub> H <sub>11</sub> O <sub>4</sub>   |          |   |
|                  |  | 261.9338 | C <sub>4</sub> H <sub>7</sub> O <sub>5</sub>    |          |   |
|                  |  | 346.9992 | C <sub>9</sub> H <sub>16</sub> O <sub>6</sub>   |          |   |

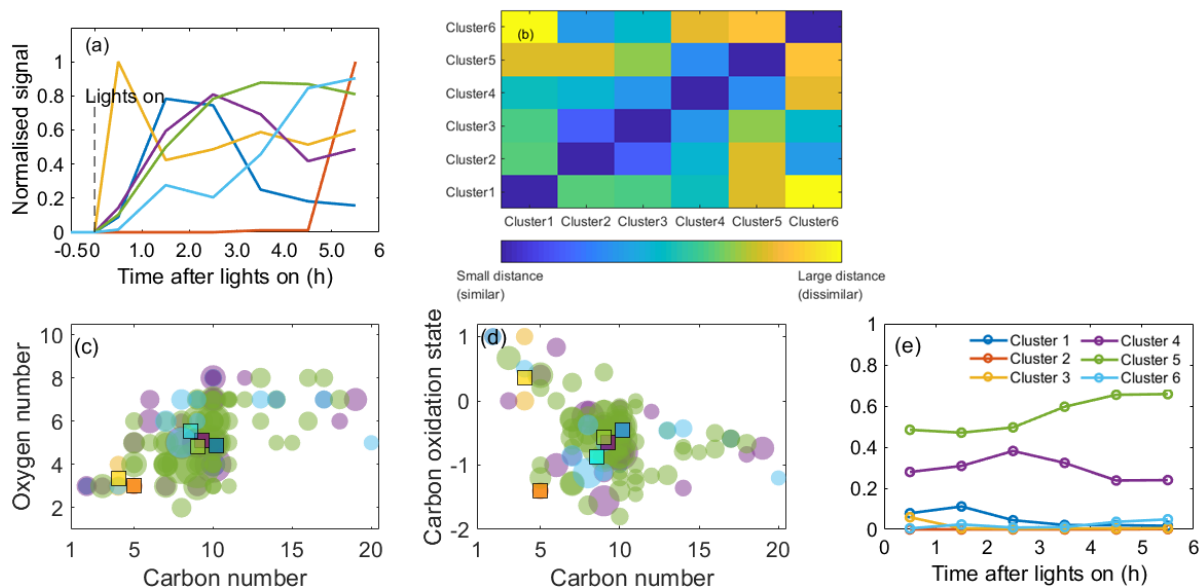


Figure S9. Hierarchical clustering of particle-phase oxidation products for the repeat  $\alpha$ -pinene system. (a) Average time series of each cluster normalized to the highest ions' intensity between 0 and 1; (b) Matrix showing the relative distance between clusters. (c) Carbon number vs oxygen number for each cluster. (d) Carbon number vs oxidation state for each cluster. (e) Time series of the sum of ions' normalized fractions to the total signal in each cluster. Note that the square symbols represent the contribution weighted average carbon numbers, oxygen numbers or and  $\overline{OS}_C$  in each cluster. The colors correspond to the ones in (a).

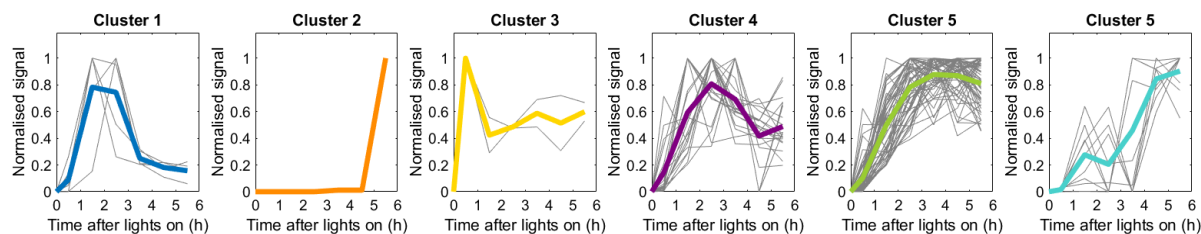


Figure S10. Time series of ions in each cluster in the particle phase for the repeat experiment.

**Table S5.** Compounds in the particle phase in each cluster for the repeat experiment, ranking by ion's contribution in each cluster.

| Cluster 1        |                    | Cluster 4 |                    | Cluster 5 |                    |
|------------------|--------------------|-----------|--------------------|-----------|--------------------|
| MW               | Formula            | MW        | Formula            | MW        | Formula            |
| 324.99368        | $C_{10}H_{14}O_4$  | 327.00933 | $C_{10}H_{16}O_4$  | 312.99368 | $C_9H_{14}O_4$     |
| 467.05668        | $C_{17}H_{24}O_7$  | 314.97295 | $C_8H_{12}O_5$     | 298.97803 | $C_8H_{12}O_4$     |
| 405.99989        | $C_{10}H_{17}NO_8$ | 356.99474 | $C_9H_{14}N_2O_5$  | 343.00425 | $C_{10}H_{16}O_5$  |
| 202.92052        | $C_2H_4O_3$        | 328.9886  | $C_9H_{14}O_5$     | 358.99916 | $C_{10}H_{16}O_6$  |
| 355.99949        | $C_{10}H_{15}NO_5$ | 345.0199  | $C_{10}H_{18}O_5$  | 371.99441 | $C_{10}H_{15}NO_6$ |
| <b>Cluster 2</b> |                    | 403.98424 | $C_{10}H_{15}NO_8$ | 340.9886  | $C_{10}H_{14}O_5$  |
| MW               | Formula            | 330.94271 | $C_6H_8N_2O_6$     | 344.98351 | $C_9H_{14}O_6$     |
| 256.95489        | $C_5H_8NO_3$       | 390.00497 | $C_{10}H_{17}NO_7$ | 296.99877 | $C_9H_{14}O_3$     |
| <b>Cluster 1</b> |                    | 495.08798 | $C_{19}H_{28}O_7$  | 374.99408 | $C_{10}H_{16}O_7$  |

|                  |  |           |   |           |   |
|------------------|--|-----------|---|-----------|---|
| MW               | Formula  | 387.98932 | C <sub>10</sub> H <sub>15</sub> NO <sub>7</sub> | 256.93108 | C <sub>5</sub> H <sub>6</sub> O <sub>4</sub>                  |
| 228.93617        | C <sub>4</sub> H <sub>6</sub> O <sub>3</sub>                 | 274.94165 | C <sub>5</sub> H <sub>8</sub> O <sub>5</sub>    | 302.97295 | C <sub>7</sub> H <sub>12</sub> O <sub>5</sub>                 |
| 242.91543        | C <sub>4</sub> H <sub>4</sub> O <sub>4</sub>                 | 299.01442 | C <sub>9</sub> H <sub>16</sub> O <sub>3</sub>   | 300.98111 | C <sub>7</sub> H <sub>12</sub> NO <sub>4</sub>                |
| <b>Cluster 6</b> |  | 200.90487 | C <sub>2</sub> H <sub>2</sub> O <sub>3</sub>    | 214.92052 | C <sub>3</sub> H <sub>4</sub> O <sub>3</sub>                  |
| MW               | Formula  | 270.98312 | C <sub>7</sub> H <sub>12</sub> O <sub>3</sub>   | 284.96238 | C <sub>7</sub> H <sub>10</sub> O <sub>4</sub>                 |
| 330.99167        | C <sub>8</sub> H <sub>14</sub> NO <sub>5</sub>               | 319.9393  | C <sub>6</sub> H <sub>9</sub> O <sub>7</sub>    | 316.9886  | C <sub>8</sub> H <sub>14</sub> O <sub>5</sub>                 |
| 342.94271        | C <sub>7</sub> H <sub>8</sub> N <sub>2</sub> O <sub>6</sub>  | 216.93617 | C <sub>3</sub> H <sub>6</sub> O <sub>3</sub>    | 282.97054 | C <sub>7</sub> H <sub>10</sub> NO <sub>3</sub>                |
| 360.96585        | C <sub>8</sub> H <sub>12</sub> NO <sub>7</sub>               | 449.09105 | C <sub>14</sub> H <sub>28</sub> NO <sub>7</sub> | 286.97803 | C <sub>7</sub> H <sub>12</sub> O <sub>4</sub>                 |
| 427.02538        | C <sub>14</sub> H <sub>20</sub> O <sub>7</sub>               | 466.08524 | C <sub>18</sub> H <sub>27</sub> O <sub>6</sub>  | 315.00933 | C <sub>9</sub> H <sub>16</sub> O <sub>4</sub>                 |
| 415.02538        | C <sub>13</sub> H <sub>20</sub> O <sub>7</sub>               | 417.00464 | C <sub>12</sub> H <sub>18</sub> O <sub>8</sub>  | 300.93214 | C <sub>5</sub> H <sub>6</sub> N <sub>2</sub> O <sub>5</sub>   |
| 388.98457        | C <sub>9</sub> H <sub>14</sub> N <sub>2</sub> O <sub>7</sub> | 391.99681 | C <sub>10</sub> H <sub>17</sub> O <sub>8</sub>  | 387.00531 | C <sub>10</sub> H <sub>16</sub> N <sub>2</sub> O <sub>6</sub> |
| 226.92052        | C <sub>4</sub> H <sub>4</sub> O <sub>3</sub>                 | 331.97569 | C <sub>8</sub> H <sub>13</sub> O <sub>6</sub>   | 332.98351 | C <sub>8</sub> H <sub>14</sub> O <sub>6</sub>                 |
| 357.97876        | C <sub>9</sub> H <sub>13</sub> NO <sub>6</sub>               |           |   | 373.00223 | C <sub>10</sub> H <sub>16</sub> NO <sub>6</sub>               |
| 481.1451         | C <sub>20</sub> H <sub>34</sub> O <sub>5</sub>               |           |   | 372.96585 | C <sub>9</sub> H <sub>12</sub> NO <sub>7</sub>                |
|                  |  |           |   | 346.99916 | C <sub>9</sub> H <sub>16</sub> O <sub>6</sub>                 |
|                  |  |           |   | 451.07031 | C <sub>13</sub> H <sub>26</sub> NO <sub>8</sub>               |
|                  |  |           |   | 312.94472 | C <sub>7</sub> H <sub>8</sub> NO <sub>5</sub>                 |
|                  |  |           |   | 370.98658 | C <sub>10</sub> H <sub>14</sub> NO <sub>6</sub>               |
|                  |  |           |   | 283.00693 | C <sub>8</sub> H <sub>14</sub> NO <sub>2</sub>                |
|                  |  |           |   | 481.07233 | C <sub>18</sub> H <sub>26</sub> O <sub>7</sub>                |
|                  |  |           |   | 316.95221 | C <sub>7</sub> H <sub>10</sub> O <sub>6</sub>                 |
|                  |  |           |   | 439.06176 | C <sub>16</sub> H <sub>24</sub> O <sub>6</sub>                |
|                  |  |           |   | 441.02845 | C <sub>14</sub> H <sub>20</sub> NO <sub>7</sub>               |
|                  |  |           |   | 485.06724 | C <sub>17</sub> H <sub>26</sub> O <sub>8</sub>                |
|                  |  |           |   | 356.94713 | C <sub>9</sub> H <sub>10</sub> O <sub>7</sub>                 |
|                  |  |           |   | 373.98625 | C <sub>10</sub> H <sub>15</sub> O <sub>7</sub>                |
|                  |  |           |   | 471.05159 | C <sub>16</sub> H <sub>24</sub> O <sub>8</sub>                |
|                  |  |           |   | 399.00531 | C <sub>11</sub> H <sub>16</sub> N <sub>2</sub> O <sub>6</sub> |
|                  |  |           |   | 302.92398 | C <sub>5</sub> H <sub>6</sub> NO <sub>6</sub>                 |
|                  |  |           |   | 355.01548 | C <sub>10</sub> H <sub>16</sub> N <sub>2</sub> O <sub>4</sub> |
|                  |  |           |   | 288.9573  | C <sub>6</sub> H <sub>10</sub> O <sub>5</sub>                 |
|                  |  |           |   | 400.99715 | C <sub>11</sub> H <sub>16</sub> NO <sub>7</sub>               |
|                  |  |           |   | 272.94981 | C <sub>5</sub> H <sub>8</sub> NO <sub>4</sub>                 |
|                  |  |           |   | 397.01481 | C <sub>13</sub> H <sub>18</sub> O <sub>6</sub>                |
|                  |  |           |   | 312.02224 | C <sub>10</sub> H <sub>17</sub> O <sub>3</sub>                |
|                  |  |           |   | 338.97295 | C <sub>10</sub> H <sub>12</sub> O <sub>5</sub>                |
|                  |  |           |   | 376.0019  | C <sub>10</sub> H <sub>17</sub> O <sub>7</sub>                |
|                  |  |           |   | 361.98625 | C <sub>9</sub> H <sub>15</sub> O <sub>7</sub>                 |
|                  |  |           |   | 340.00458 | C <sub>10</sub> H <sub>15</sub> NO <sub>4</sub>               |
|                  |  |           |   | 369.00732 | C <sub>11</sub> H <sub>16</sub> NO <sub>5</sub>               |
|                  |  |           |   | 429.01587 | C <sub>12</sub> H <sub>18</sub> N <sub>2</sub> O <sub>7</sub> |
|                  |  |           |   | 296.94981 | C <sub>7</sub> H <sub>8</sub> NO <sub>4</sub>                 |
|                  |  |           |   | 341.99642 | C <sub>10</sub> H <sub>15</sub> O <sub>5</sub>                |
|                  |  |           |   | 353.01241 | C <sub>11</sub> H <sub>16</sub> NO <sub>4</sub>               |
|                  |  |           |   | 409.0512  | C <sub>15</sub> H <sub>22</sub> O <sub>5</sub>                |
|                  |  |           |   | 311.98586 | C <sub>9</sub> H <sub>13</sub> O <sub>4</sub>                 |



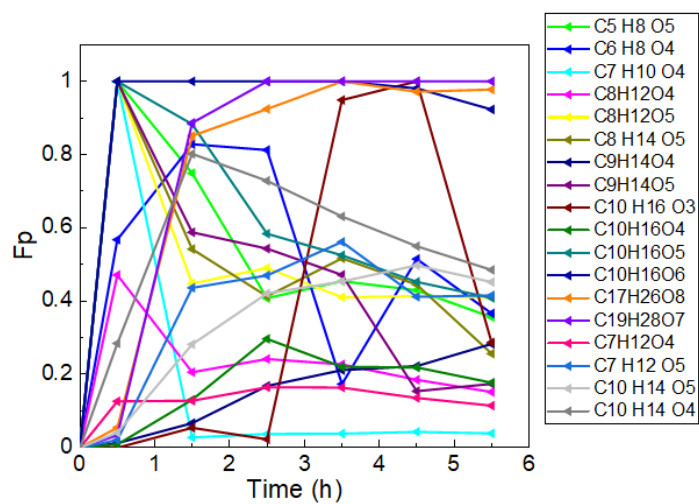
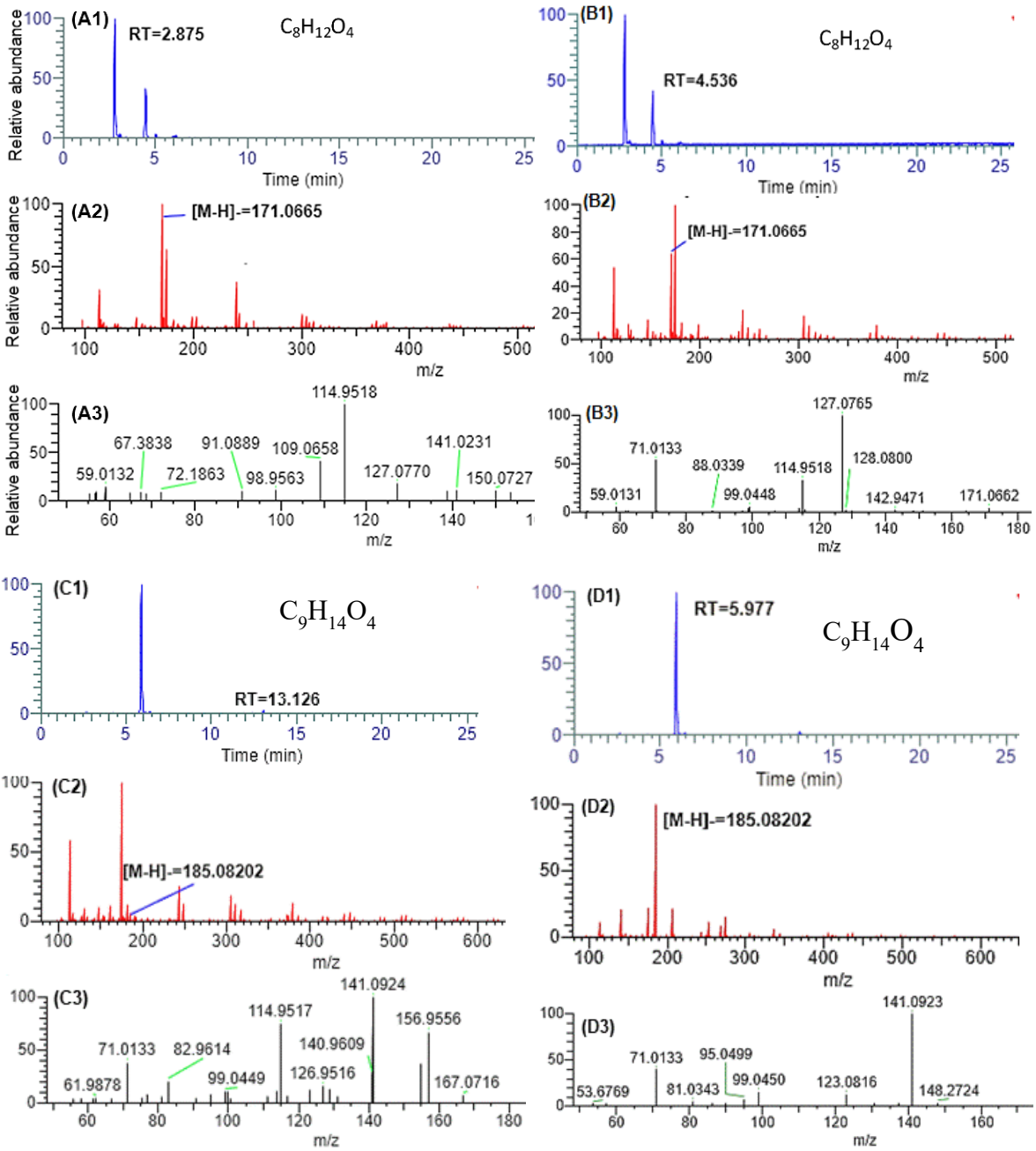
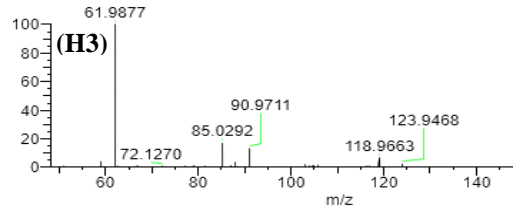
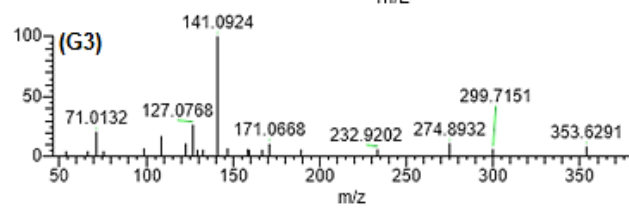
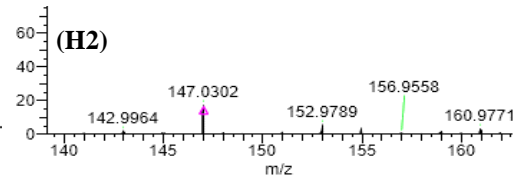
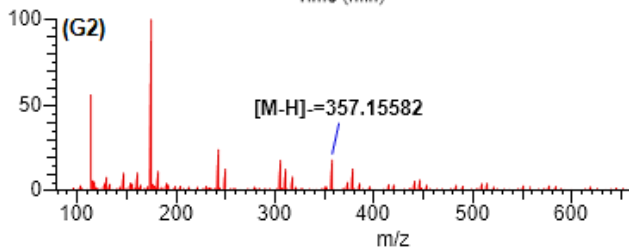
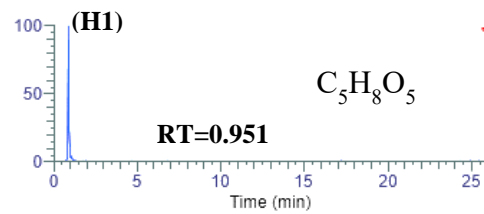
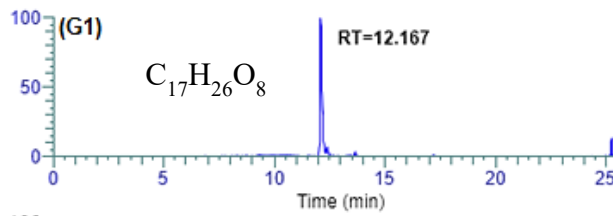
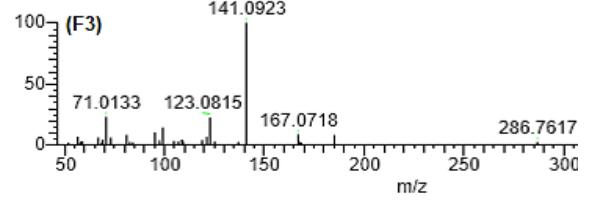
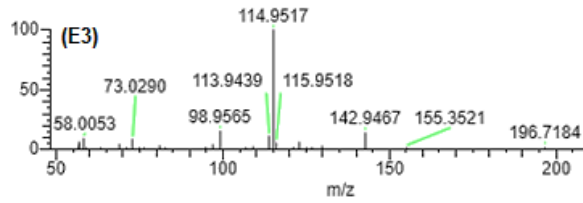
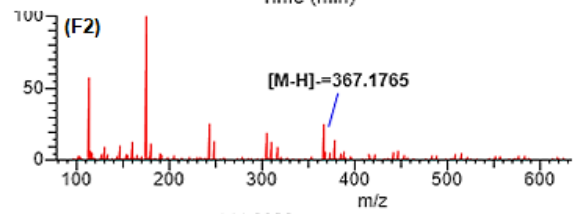
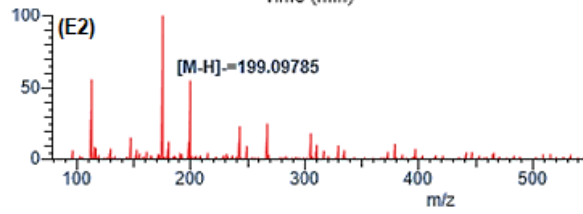
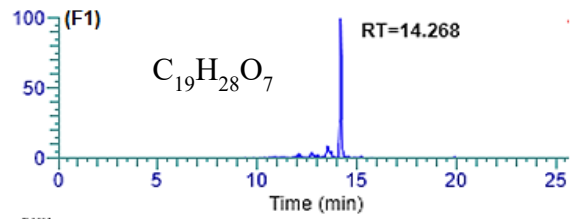
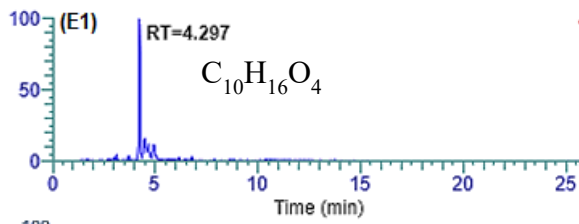
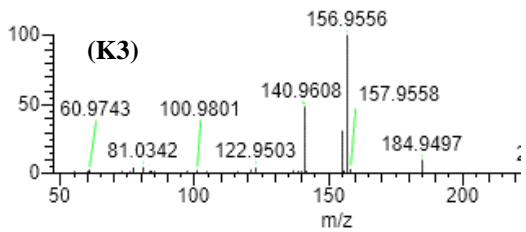
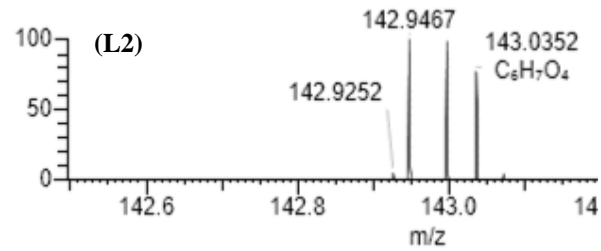
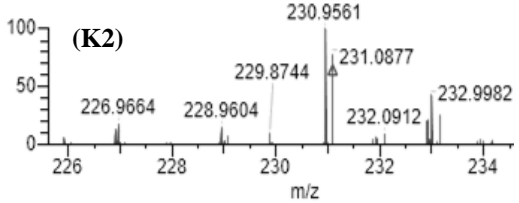
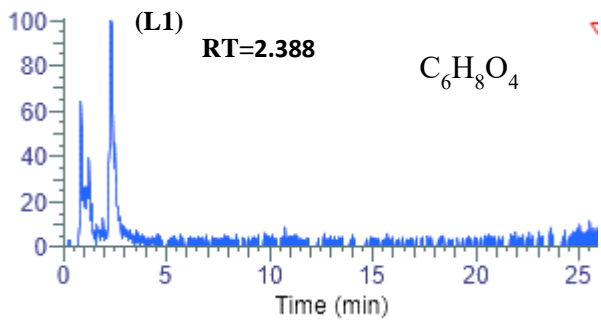
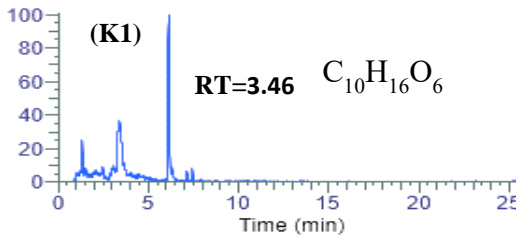
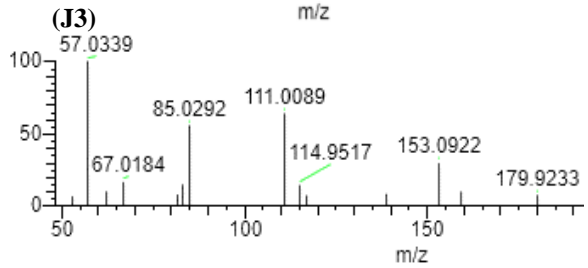
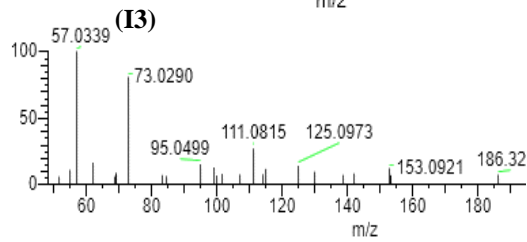
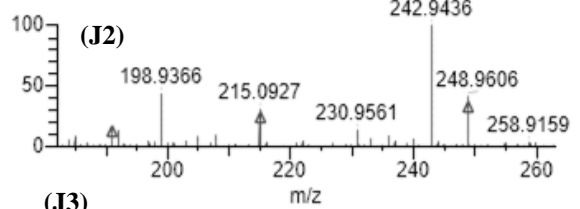
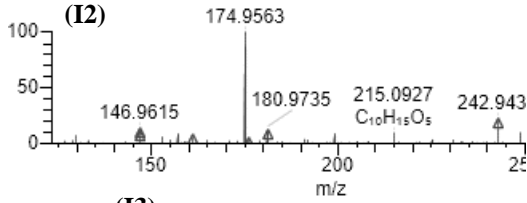
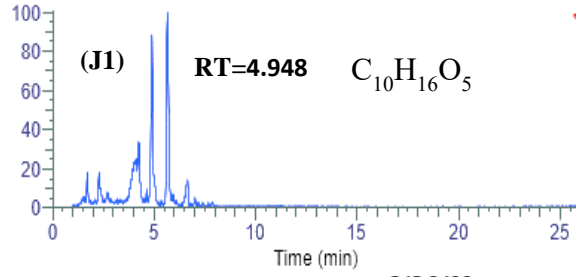
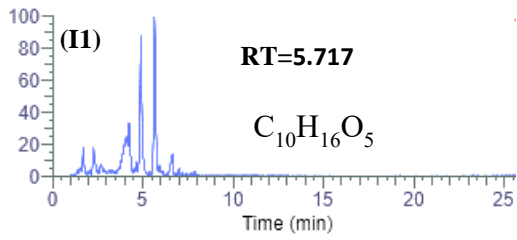
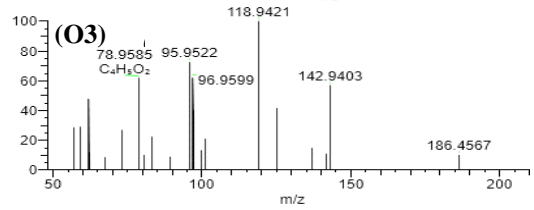
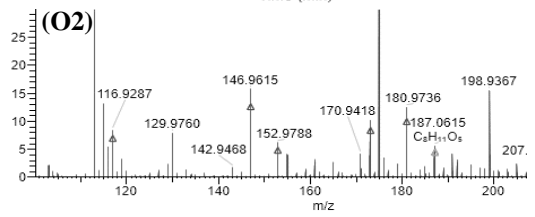
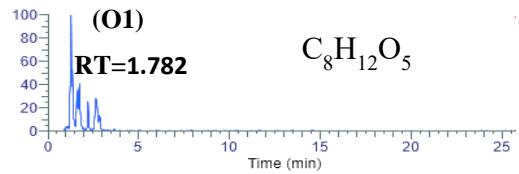
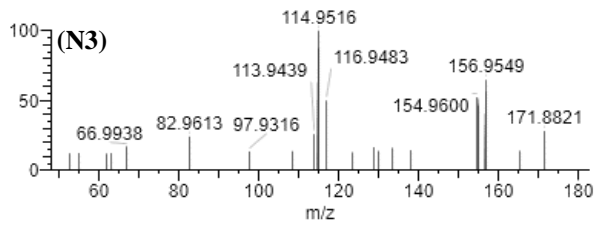
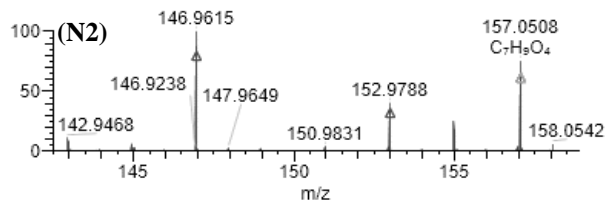
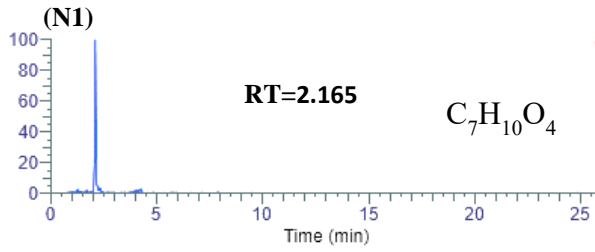
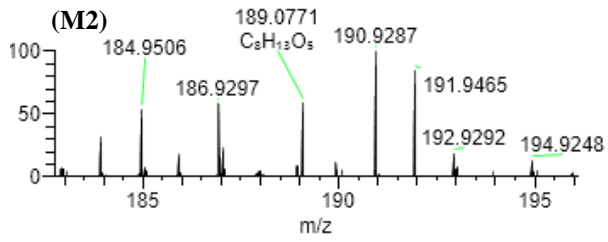
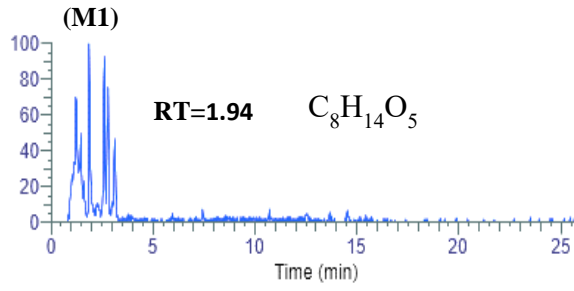


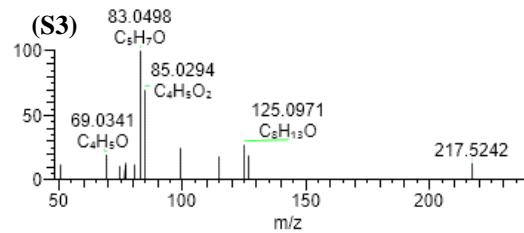
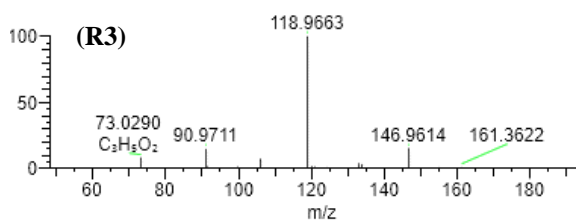
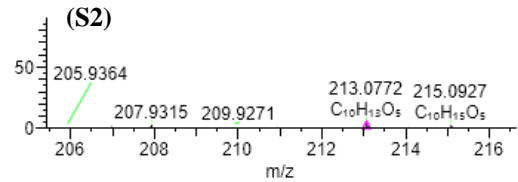
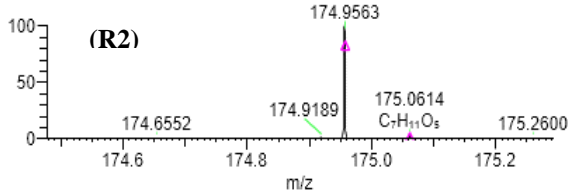
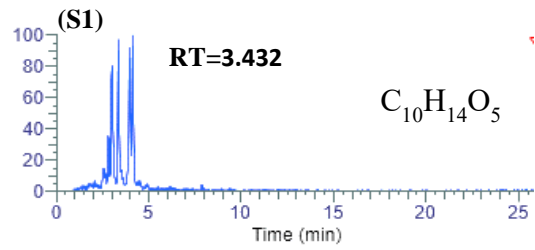
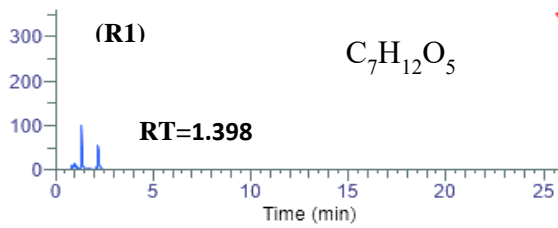
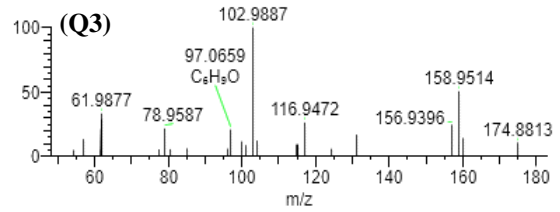
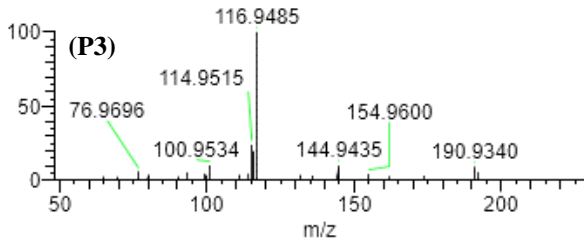
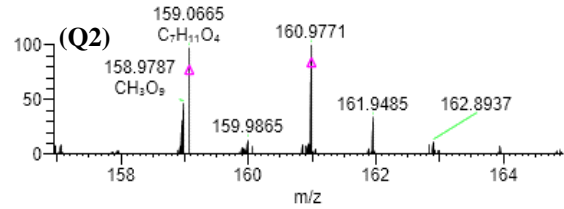
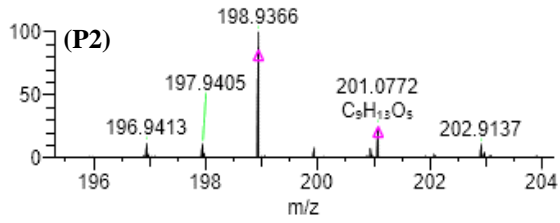
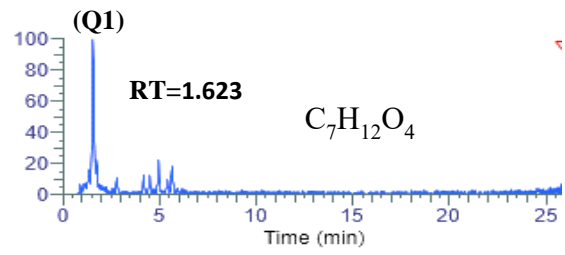
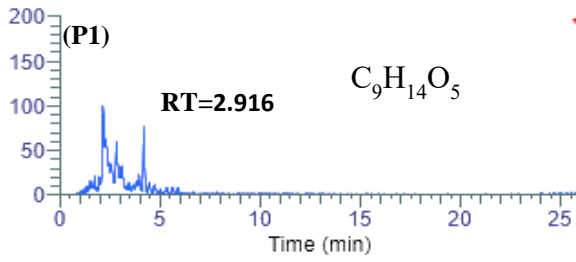
Figure S11. Temporal profiles of particle fractions for the selected identified organic molecules generated from  $\alpha$ -pinene photooxidation reactions.











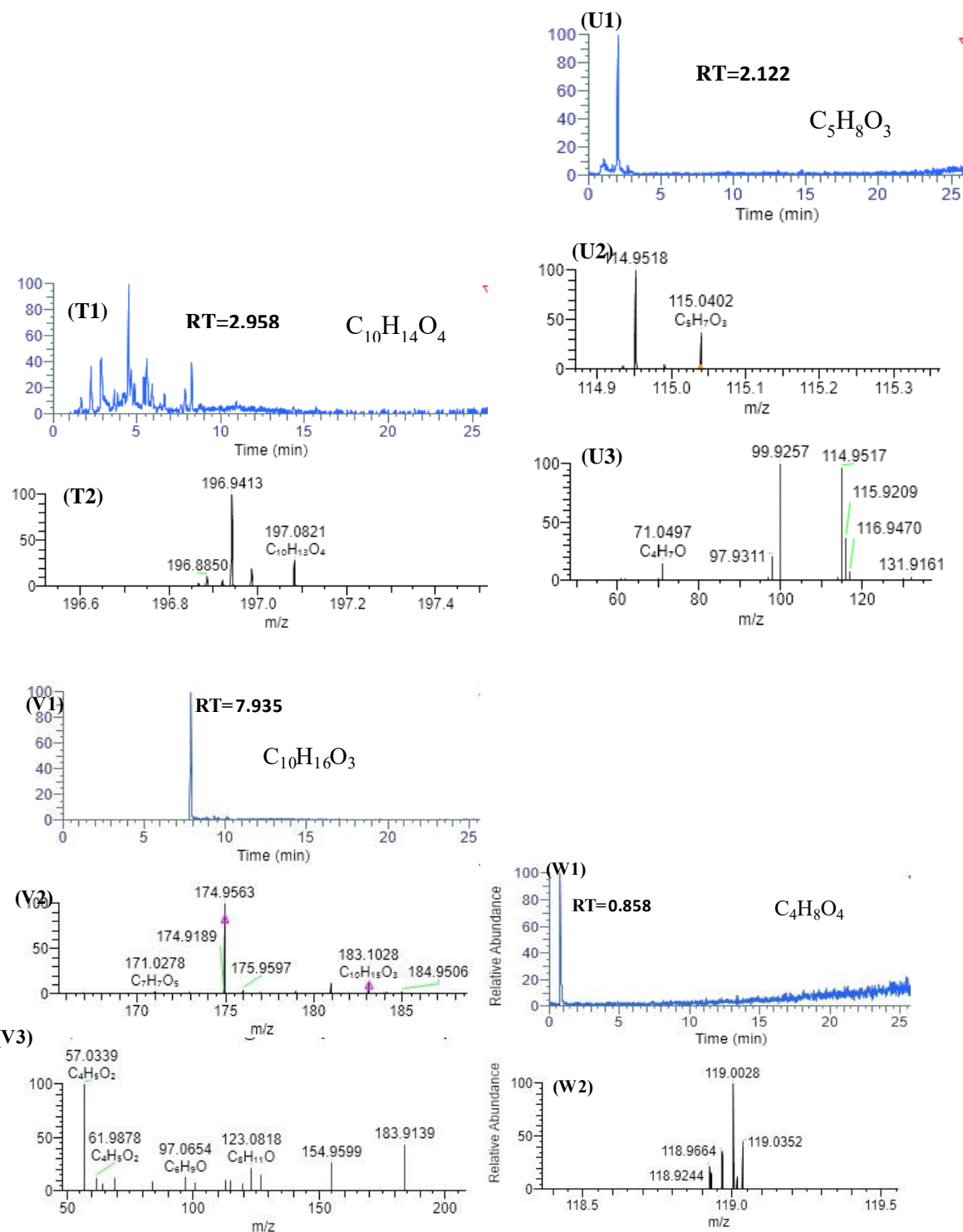


Figure S12 LC-MS chromatography and mass spectrum of particle phase from a-pinene oxidation products. Subplot (A1-W1): the retention time from liquid chromatography for each component; subplot (A2-W2): corresponding mass spectra for the peaks in A1-W1. Ions are detected in the negative mode by the loss of one hydrogen atom ( $[M-H]^-$ ); subplot (A3-W3): corresponding mass spectra for the product ions produced from the parent ions in A2-W2. Note that mass spectra of products generated from their parent ions for a few compounds cannot be identified likely due to their very low concentrations.

## Supplementary Information for paper 4

### Chemical characterization and clustering behaviour of oxidation products generated from the mixed anthropogenic and biogenic VOCs in chamber studies

Mao Du<sup>1</sup>, Aristeidis Voliotis<sup>1</sup>, Yunqi Shao<sup>1</sup>, Yu Wang<sup>1</sup>, Thomas J. Bannan<sup>1</sup>, Kelly L. Pereira<sup>3,†</sup>, Jacqueline F. Hamilton<sup>3</sup>, Carl J. Percival<sup>4</sup>, M. Rami Alfarra<sup>1,3,‡</sup>, Gordon McFiggans<sup>1</sup>

<sup>1</sup>Centre for atmospheric science, Department of Earth and Environmental Science, School of Natural Sciences, The University of Manchester, Oxford Road, M13 9PL, Manchester, UK

<sup>2</sup>National Centre for Atmospheric Science, Department of Earth and Environmental Science, School of Natural Sciences, The University of Manchester, Oxford Road, M13 9PL, Manchester, UK

<sup>3</sup>Wolfson Atmospheric Chemistry Laboratories, Department of Chemistry, University of York, York, YO10 5DD, UK

<sup>4</sup>NASA Jet Propulsion Laboratory, California Institute of Technology, 4800 Oak Grove Drive, Pasadena, CA 91109, USA.

<sup>†</sup>Now at: Department of Life and Environmental Sciences, Bournemouth University, Dorest, BH12 5BB, UK.

<sup>‡</sup> Now at Environment & Sustainability Center, Qatar Environment & Energy Research Institute, 34110, Doha, Qatar

**Correspondence to:** Gordon McFiggans ([g.mcfiggans@manchester.ac.uk](mailto:g.mcfiggans@manchester.ac.uk))



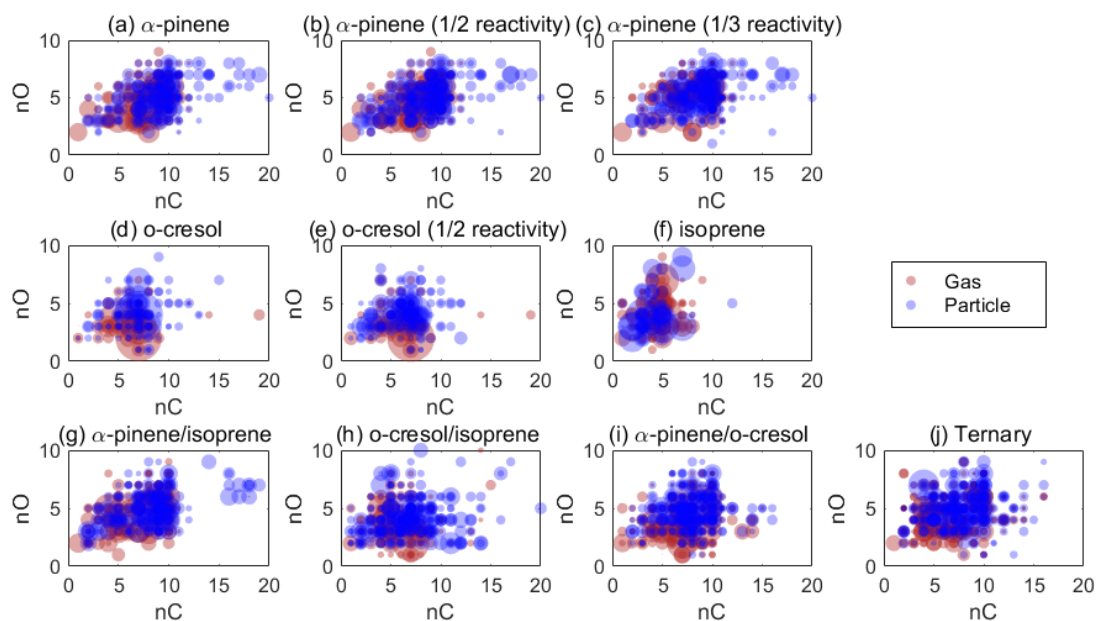


Figure S1. Oxygen numbers as a function of carbon numbers for oxidation products observed by online CIMS measurements. The symbol size represents the square root of the normalised signal of each compound.

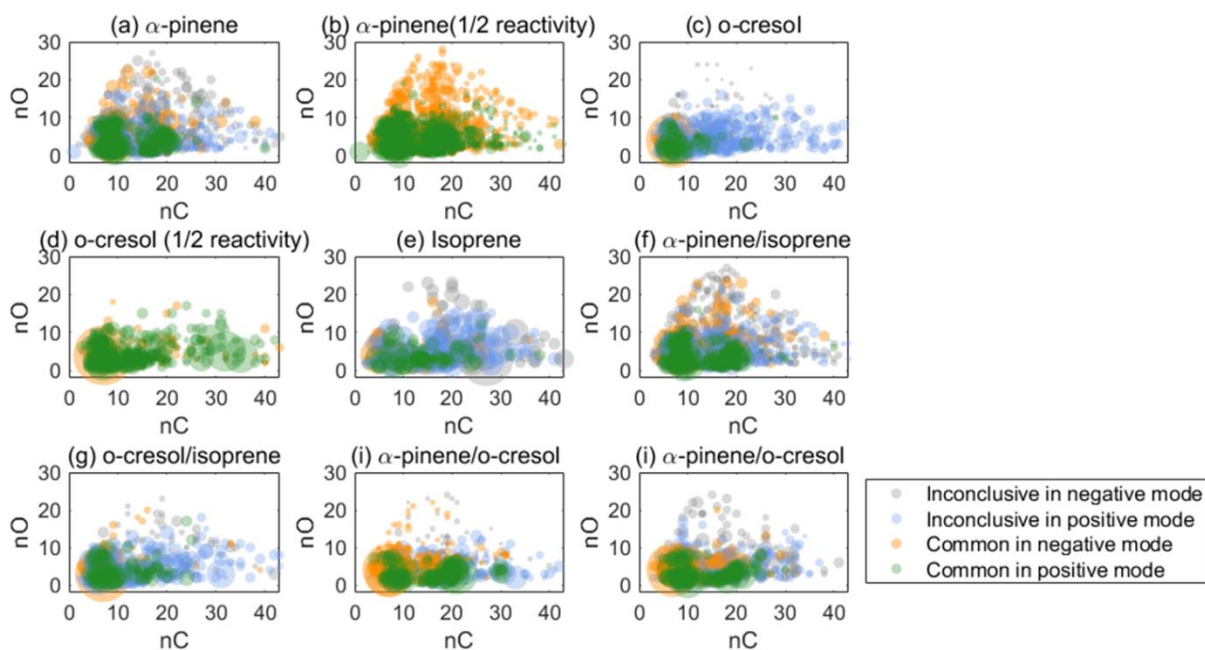


Figure S2. Oxygen numbers as a function of carbon numbers for oxidation products observed by LC-Orbitrap MS measurements. The symbol size represents the square root of a normalised signal of each compound.

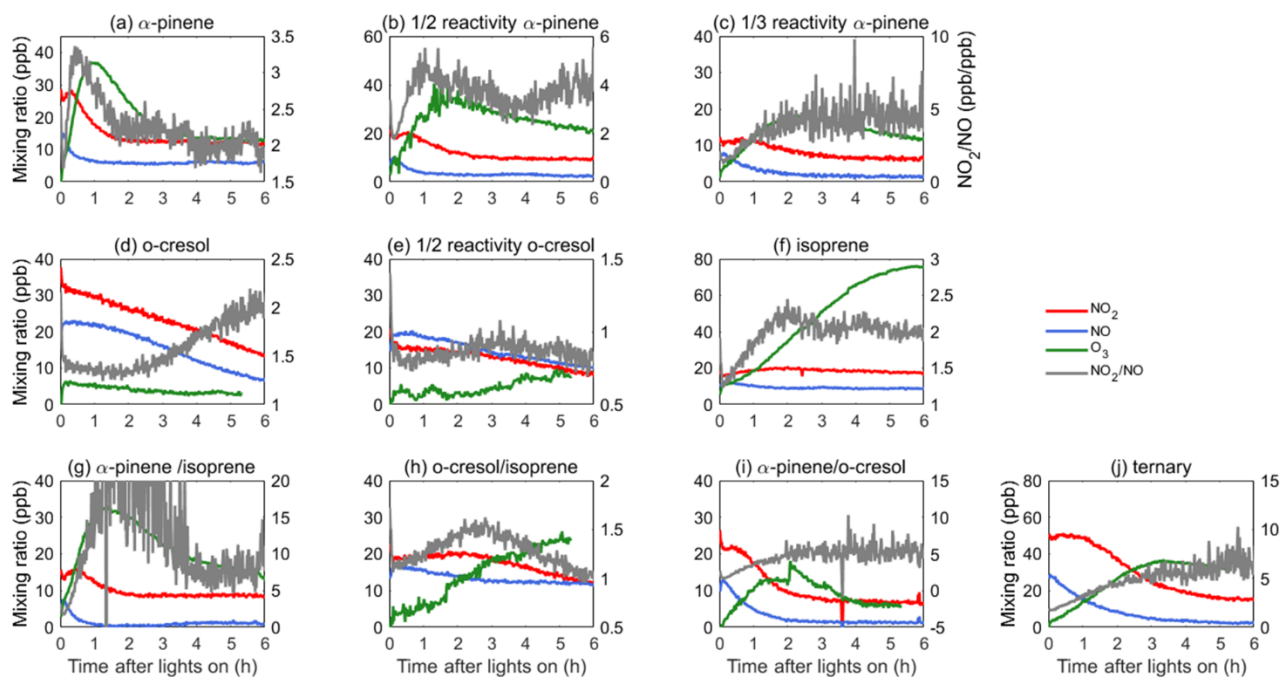


Figure S3. mixing ratios of NO, NO<sub>2</sub>, O<sub>3</sub> and NO<sub>2</sub>/NO ratio from the representative experiment.

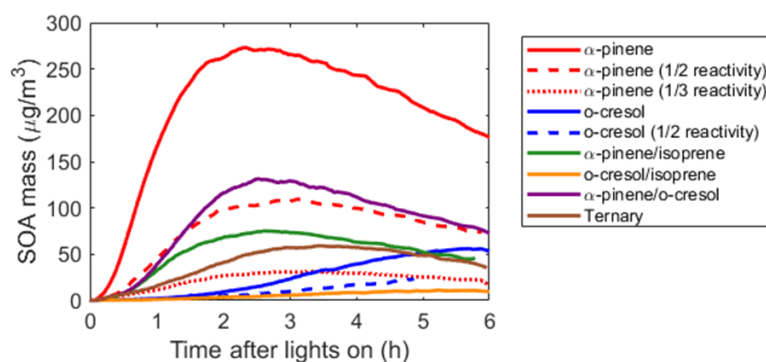


Figure S4. Raw measurements of SOA particle mass over time from the representative experiment. The data are organic mass determined from AMS measurements excluding the mass from the ammonium sulphate seed particles.

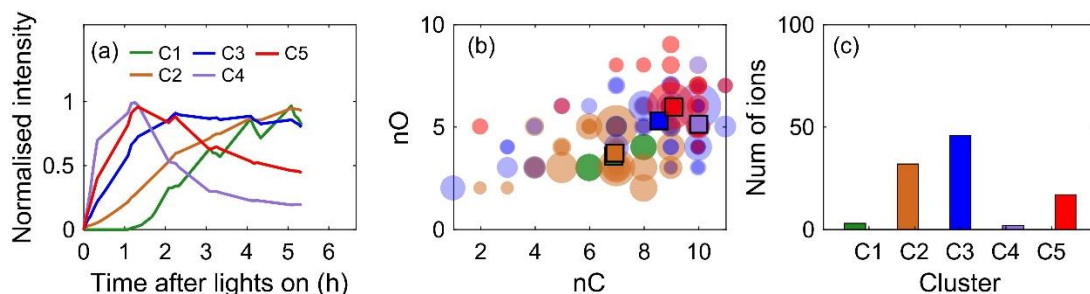


Figure S5 Hierarchical clustering of gas-phase oxidation products in the  $\alpha$ -pinene system. (a) The average time series of each cluster. Each ion is normalized to the highest intensity itself. (b) Carbon number vs oxygen number. The mean values are marked as squares. (c) The number of ions in each cluster.

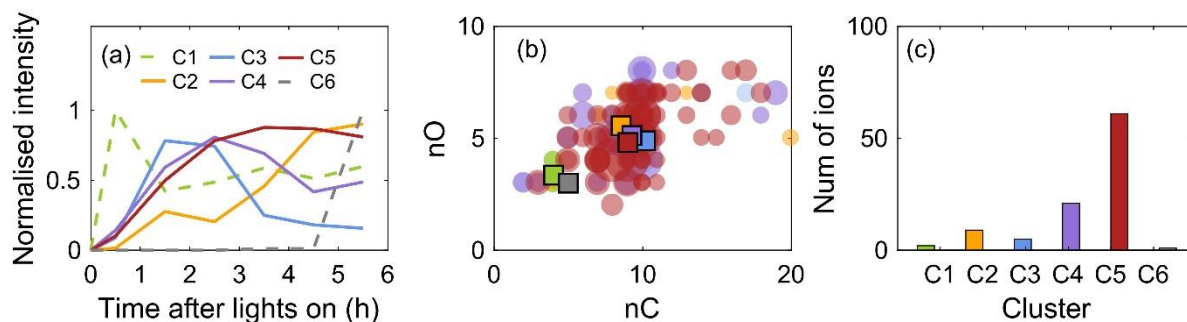


Figure S6 Hierarchical clustering of particle-phase oxidation products in the a-pinene system. (a) The average time series of each cluster. Each ion is normalized to the highest intensity itself. (b) Carbon number vs oxygen number. The mean values are marked as squares. (c) The number of ions in each cluster.

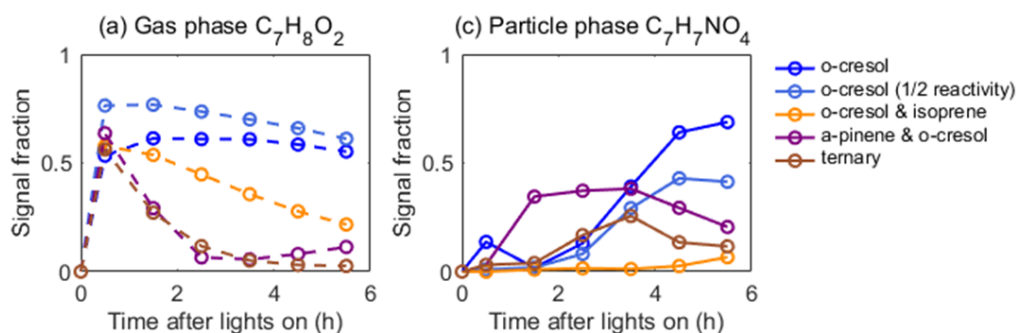


Figure S7. Temporal profiles for compounds  $C_7H_8O_2$  and  $C_7H_7NO_4$  from online measurement. (a) compound  $C_7H_8O_2$  in the gas phase (b) compound  $C_7H_7NO_4$  in the particle phase.